# NOVEL SMALL-MOLECULE AGENTS IN OVERCOMING MULTIDRUG RESISTANCE IN CANCERS

EDITED BY: Qingbin Cui, Yingfang Fan, Qianxiong Zhou, Cong Wang and Leli Zeng

PUBLISHED IN: Frontiers in Oncology, Frontiers in Chemistry and Frontiers in Pharmacology

frontiers Research Topics

ISSN 1664-8714
ISBN 978-2-88976-235-4
DOI 10.3389/978-2-88976-235-4

## About Frontiers

Frontiers is more than just an open-access publisher of scholarly articles: it is a pioneering approach to the world of academia, radically improving the way scholarly research is managed. The grand vision of Frontiers is a world where all people have an equal opportunity to seek, share and generate knowledge. Frontiers provides immediate and permanent online open access to all its publications, but this alone is not enough to realize our grand goals.

## Frontiers Journal Series

The Frontiers Journal Series is a multi-tier and interdisciplinary set of open-access, online journals, promising a paradigm shift from the current review, selection and dissemination processes in academic publishing. All Frontiers journals are driven by researchers for researchers; therefore, they constitute a service to the scholarly community. At the same time, the Frontiers Journal Series operates on a revolutionary invention, the tiered publishing system, initially addressing specific communities of scholars, and gradually climbing up to broader public understanding, thus serving the interests of the lay society, too.

## Dedication to Quality

Each Frontiers article is a landmark of the highest quality, thanks to genuinely collaborative interactions between authors and review editors, who include some of the world's best academicians. Research must be certified by peers before entering a stream of knowledge that may eventually reach the public - and shape society; therefore, Frontiers only applies the most rigorous and unbiased reviews.
Frontiers revolutionizes research publishing by freely delivering the most outstanding research, evaluated with no bias from both the academic and social point of view. By applying the most advanced information technologies, Frontiers is catapulting scholarly publishing into a new generation.

## What are Frontiers Research Topics?

Frontiers Research Topics are very popular trademarks of the Frontiers Journals Series: they are collections of at least ten articles, all centered on a particular subject. With their unique mix of varied contributions from Original Research to Review Articles, Frontiers Research Topics unify the most influential researchers, the latest key findings and historical advances in a hot research area! Find out more on how to host your own Frontiers Research Topic or contribute to one as an author by contacting the Frontiers Editorial Office: frontiersin.org/about/contact

# NOVEL SMALL-MOLECULE AGENTS IN OVERCOMING MULTIDRUG RESISTANCE IN CANCERS

Topic Editors:
**Qingbin Cui,** University of Toledo, United States
**Yingfang Fan,** Zhujiang Hospital Southern Medical University, China
**Qianxiong Zhou,** Technical Institute of Physics and Chemistry (CAS), China
**Cong Wang,** Zhengzhou University, China
**Leli Zeng,** Sun Yat-sen University, China

**Citation:** Cui, Q., Fan, Y., Zhou, Q., Wang, C., Zeng, L., eds. (2022). Novel Small-Molecule Agents in Overcoming Multidrug Resistance in Cancers. Lausanne: Frontiers Media SA. doi: 10.3389/978-2-88976-235-4

# Table of Contents


05 ***Editorial: Novel Small-Molecule Agents in Overcoming Multidrug Resistance in Cancers***
Qingbin Cui, Cong Wang, Leli Zeng, Qian-Xiong Zhou and Ying-Fang Fan

08 ***HMGB1 Promotes Resistance to Doxorubicin in Human Hepatocellular Carcinoma Cells by Inducing Autophagy* via *the AMPK/mTOR Signaling Pathway***
Junhua Li, Wei Zhou, Qiang Mao, Dandan Gao, Lin Xiong, Xinyao Hu, Yongfa Zheng and Ximing Xu

19 ***LY294002 Is a Promising Inhibitor to Overcome Sorafenib Resistance in FLT3-ITD Mutant AML Cells by Interfering With PI3K/Akt Signaling Pathway***
Amin Huang, Peiting Zeng, Yinguang Li, Wenhua Lu and Yaoming Lai

29 ***The PI3K Inhibitor XH30 Enhances Response to Temozolomide in Drug-Resistant Glioblastoma* via *the Noncanonical Hedgehog Signaling Pathway***
Ming Ji, Zhihui Zhang, Songwen Lin, Chunyang Wang, Jing Jin, Nina Xue, Heng Xu and Xiaoguang Chen

41 ***Targeting Mitochondrial Metabolism and RNA Polymerase POLRMT to Overcome Multidrug Resistance in Cancer***
Hui-Jing Yu, Guan-Li Xiao, Yu-Ying Zhao, Xin-Xin Wang and Rongfeng Lan

48 ***The Role of Circular RNAs in the Drug Resistance of Cancers***
Xin-Yuan Liu, Qi Zhang, Jing Guo, Peng Zhang, Hua Liu, Zi-Bin Tian, Cui-Ping Zhang and Xiao-Yu Li

62 ***Anlotinib Reverses Multidrug Resistance (MDR) in Osteosarcoma by Inhibiting P-Glycoprotein (PGP1) Function In Vitro and In Vivo***
Gangyang Wang, Lingling Cao, Yafei Jiang, Tao Zhang, Hongsheng Wang, Zhuoying Wang, Jing Xu, Min Mao, Yingqi Hua, Zhengdong Cai, Xiaojun Ma, Shuo Hu and Chenghao Zhou

74 ***Local Anesthetic Ropivacaine Exhibits Therapeutic Effects in Cancers***
Peng Xu, Shaobo Zhang, Lili Tan, Lei Wang, Zhongwei Yang and Jinbao Li

84 ***Overexpression of ABCB1 Associated With the Resistance to the KRAS-G12C Specific Inhibitor ARS-1620 in Cancer Cells***
Xing-Duo Dong, Meng Zhang, Chao-Yun Cai, Qiu-Xu Teng, Jing-Quan Wang, Yi-Ge Fu, Qingbin Cui, Ketankumar Patel, Dong-Tao Wang and Zhe-Sheng Chen

95 ***Complex Crystal Structure Determination of Hsp90$^{N}$-NVP-AUY922 and* In Vitro *Anti-NSCLC Activity of NVP-AUY922***
Chun-Xia He, You Lv, Meng Guo, Huan Zhou, Wei Qin, Dong Zhao, Hui-Jin Li, Lu Xing, Xin Zhou, Peng-Quan Li, Feng Yu, Jian-Hua He and Hui-Ling Cao

106 ***The Resistance of Cancer Cells to Palbociclib, a Cyclin-Dependent Kinase 4/6 Inhibitor, is Mediated by the ABCB1 Transporter***
Han Fu, Zhuo-Xun Wu, Zi-Ning Lei, Qiu-Xu Teng, Yuqi Yang, Charles R. Ashby, Yixiong Lei, Yuyin Lian and Zhe-Sheng Chen

118 ***A Mini-Review of Flavone Isomers Apigenin and Genistein in Prostate Cancer Treatment***

Xiaozhen Ji, Kai Liu, Qingyue Li, Qun Shen, Fangxuan Han, Qingmei Ye and Caijuan Zheng

127 ***Combining EGFR-TKI With SAHA Overcomes EGFR-TKI-Acquired Resistance by Reducing the Protective Autophagy in Non-Small Cell Lung Cancer***

Peijun Cao, Yongwen Li, Ruifeng Shi, Yin Yuan, Hao Gong, Guangsheng Zhu, Zihe Zhang, Chen Chen, Hongbing Zhang, Minghui Liu, Zhenhua Pan, Hongyu Liu and Jun Chen

138 ***Research Progress on Natural Diterpenoids in Reversing Multidrug Resistance***

Zhuo-fen Deng, Irina Bakunina, Hua Yu, Jaehong Han, Alexander Dömling, Maria-José U Ferreira and Jian-ye Zhang

152 ***Ribociclib Inhibits P-gp-Mediated Multidrug Resistance in Human Epidermoid Carcinoma Cells***

Lei Zhang, Biwei Ye, Yunfeng Lin, Yi-Dong Li, Jing-Quan Wang, Zhuo Chen, Feng-Feng Ping and Zhe-Sheng Chen

162 ***Research Advances on Matrine***

Xiao-Ying Sun, Li-Yi Jia, Zheng Rong, Xin Zhou, Lu-Qi Cao, Ai-Hong Li, Meng Guo, Jie Jin, Yin-Di Wang, Ling Huang, Yi-Heng Li, Zhong-Jing He, Long Li, Rui-Kang Ma, Yi-Fan Lv, Ke-Ke Shao, Juan Zhang and Hui-Ling Cao

182 ***Design, Synthesis, and Biological Evaluation of [1,2,4]triazolo[4,3-a] Pyrazine Derivatives as Novel Dual c-Met/VEGFR-2 Inhibitors***

Xiaobo Liu, Yuzhen Li, Qian Zhang, Qingshan Pan, Pengwu Zheng, Xinyang Dai, Zhaoshi Bai and Wufu Zhu

196 ***Meclofenamic Acid Restores Gefinitib Sensitivity by Downregulating Breast Cancer Resistance Protein and Multidrug Resistance Protein 7* via *FTO/m6A-Demethylation/c-Myc in Non-Small Cell Lung Cancer***

Hui Chen, Bin Jia, Qiang Zhang and Yu Zhang

205 ***Novel MDM2 Inhibitor XR-2 Exerts Potent Anti-Tumor Efficacy and Overcomes Enzalutamide Resistance in Prostate Cancer***

Meng Wu, Jingyi Cui, Huimin Hou, Ying Li, Shengjie Liu, Li Wan, Lili Zhang, Wei Huang, Gaoyuan Sun, Jingchao Liu, Pengfei Jin, Shunmin He and Ming Liu

221 ***Research Advances on Anti-Cancer Natural Products***

Meng Guo, Jie Jin, Dong Zhao, Zheng Rong, Lu-Qi Cao, Ai-Hong Li, Xiao-Ying Sun, Li-Yi Jia, Yin-Di Wang, Ling Huang, Yi-Heng Li, Zhong-Jing He, Long Li, Rui-Kang Ma, Yi-Fan Lv, Ke-Ke Shao and Hui-Ling Cao

238 ***DHW-221, a Dual PI3K/mTOR Inhibitor, Overcomes Multidrug Resistance by Targeting P-Glycoprotein (P-gp/ABCB1) and Akt-Mediated FOXO3a Nuclear Translocation in Non-small Cell Lung Cancer***

Mingyue Liu, Chang Xu, Xiaochun Qin, Wenwu Liu, Deping Li, Hui Jia, Xudong Gao, Yuting Wu, Qiong Wu, Xiangbo Xu, Bo Xing, Xiaowen Jiang, Hongyuan Lu, Yingshi Zhang, Huaiwei Ding and Qingchun Zhao

frontiers | Frontiers in Chemistry

EDITORIAL
published: 04 May 2022
doi: 10.3389/fchem.2022.921985

# Editorial: Novel Small-Molecule Agents in Overcoming Multidrug Resistance in Cancers

*Qingbin Cui[1]*, Cong Wang[2], Leli Zeng[3], Qian-Xiong Zhou[4] and Ying-Fang Fan[5]*

[1]Department of Cell and Cancer Biology, University of Toledo College of Medicine and Life Sciences, Toledo, OH, United States, [2]State Key Laboratory of Esophageal Cancer Prevention and Treatment, School of Pharmaceutical Sciences, Zhengzhou University, Zhengzhou, China, [3]Guangdong Provincial Key Laboratory of Digestive Cancer Research, Scientific Research Center, The Seventh Affiliated Hospital, Sun Yat-sen University, Shenzhen, China, [4]Key Laboratory of Photochemical Conversion and Optoelectronic Materials, Technical Institute of Physics and Chemistry, Chinese Academy of Sciences, Beijing, China, [5]Department of First Hepatobiliary Surgery, Zhujiang Hospital, Southern Medical University, Guangzhou, China

**Keywords: multidrug resistance, mechanism, reversal agents, medicinal chemistry, drug discovery**

## Editorial on the Research Topic

## Novel Small-Molecule Agents in Overcoming Multidrug Resistance in Cancers

Multidrug resistance (MDR) is a term describing the phenomenon that cancer cells show resistant properties to various anticancer drugs of structurally and mechanistically different, accounting for approximate 90% of cancer treatment failures (Chaffer and Weinberg, 2011; Pluchino et al., 2012; Gao et al., 2020; Wang et al., 2021). It is worth noting that even the cutting-edge immunotherapy, is only 10%–20% effective, encountering resistance as well in certain patients (Sabbatino et al., 2018; Bai et al., 2020; Imbert et al., 2020; Bashash et al., 2022). Thus, MDR appears to be one of the major challenges in cancer treatment, which significantly undermines patients' survival and quality of life (Zugazagoitia et al., 2016). The causes of MDR are usually multi-facet (Assaraf et al., 2019; Vasan et al., 2019), rendering it an even tougher challenge to tackle. Therefore, in the current Research Topic "Novel Small-Molecule Agents in Overcoming Multidrug Resistance in Cancers," we attempted to collect the most-recent progress made in identifying new targets and agents in the treatment of drug-resistant cancers. In total, after being peer-reviewed, 20 manuscripts, composed with 13 research articles and seven review articles authored by 187 researchers worldwide, were successfully accepted for publication.

Natural products-derived drug discovery remains a practical and feasible strategy in the term of efficiently finding new hit/lead compounds that can undergo structural modification (Munos, 2009; Newman and Cragg, 2020). Guo et al. reviewed the latest progress of using eight classes of natural products in cancers. In their review, compounds of alkaloids, terpenoids, naturally occurring inorganic salt, phenylpropanoids, flavonoids, quinonoids, saponin and polysaccharides, their derivatives, as well as their research in cancer treatment, and the associated action modes were summarized and discussed. Specially, a separate review by Sun et al. from the same group above focused on matrine, a quinolizidine alkaloid isolated from *Sophora flavescentis*. Pharmacological effects including anticancer of matrine and its derivatives were summarized. In addition, critical structure-activity relationship (SAR) was also presented and discussed. Ji et al. conducted an interesting comparison of the flavones apigenin and genistein, two isomers that show similar yet different activities and mechanisms in prostate cancer. Importantly, genistein has been extensively studied in lab and in clinical trials for many diseases including cancers (Russo et al., 2016; Yu et al., 2021), and it has been used as nutritional supplement on market for decades. Genistein appears to be a more promising drug candidate and lead compound than its counterpart apigenin, since much more combinational regimens were developed and evaluated using genistein as a chemo-sensitizer. Deng et al. presented a systematic review of the recent progress of using

OPEN ACCESS

***Edited and reviewed by:***
*Michael Kassiou,*
*The University of Sydney, Australia*

****Correspondence:***
*Qingbin Cui*
*qingbin.cui@utoledo.edu*

***Specialty section:***
*This article was submitted to Medicinal and Pharmaceutical Chemistry, a section of the journal Frontiers in Chemistry*

***Received:*** *17 April 2022*
***Accepted:*** *20 April 2022*
***Published:*** *04 May 2022*

***Citation:***
*Cui Q, Wang C, Zeng L, Zhou Q-X and Fan Y-F (2022) Editorial: Novel Small-Molecule Agents in Overcoming Multidrug Resistance in Cancers. Front. Chem. 10:921985. doi: 10.3389/fchem.2022.921985*

natural diterpenoids in drug-resistant cancers cells overexpressing ATP-binding cassette (ABC) transporter. Jatrophanes, lathyranes, clerodanes, pimaranes, ingenanes, briaranes, segetane, jatropholane, pseudolaric acid, taxanes and euphoractine were thoroughly reviewed for their bioactivities in killing drug resistant cancer cells, and sensitizing certain chemotherapeutics.

Drug repurposing is another efficient strategy in identifying novel agents by defining new indications (Parvathaneni et al., 2019; Berdigaliyev and Aljofan, 2020; Dinić et al., 2020). Xu et al. summarized the anticancer activity of local anesthetic ropivacaine. Ropivacaine, at either clinic-relevant dose/concentrations or much higher concentrations, could suppress the proliferation, migration of certain drug-resistant cancer cells, including leukemia stem cells, triple-negative breast cancer MDA-MB-231 cells, and it sensitized 1) 5-fluorouracil (5-FU) in breast cancer MDA-MB-468 and SkBr cells, and 2) tumor necrosis factor α (TNFα) in human hepatoma HepG2 cells, human colon cancer HT-29 cells and human leukemic monocyte THP-1 cells. Chen et al. found that non-steroidal anti-inflammatory drug (NSAID) meclofenamic acid was a potential dual inhibitor of breast cancer resistance protein (BCRP) and multidrug resistance protein-7 (MRP-7), two important ABC transporters. Meclofenamic acid and its combination with gefitinib down-regulated the expression of both BCRP and MRP-7 in gefitinib-resistant non-small cell lung cancer (NSCLC) PC9-GR and H292-GR cell, mediated by FTO/m6A-demethylation/c-Myc axis. Meclofenamic acid could increase the intracellular concentration of gefitinib, leading to its re-sensitization.

Several compounds were found to show inhibitory effects toward drug resistant cancer cells, and synergistic effects were achieved when combined with certain chemotherapeutics. Ji et al. reported the recent progress of their novel phosphatidylinositide 3-kinase (PI3K) inhibitor XH30 in the treatment of temozolomide-resistant glioblastoma. XH30 was not only highly toxic toward temozolomide-resistant U251/TMZ and T98G cells *in vitro* and *in vivo*, but also was able to sensitize temozolomide in the U251/TMZ xenograft model, probably mediated by the negative regulation of transcription factor GLI1. In addition to its ability in suppressing brain metastasis (Ji et al., 2022), XH30 represents a promising drug candidate in combating drug resistance in glioblastoma. Liu et al. reported that the dual PI3K/mTOR inhibitor, DHW-221 could act as an inhibitor of P-gp (one of the most important ABC transporters which cause MDR) in resistant NSCLC A549/Taxol cells. DHW-221 was predicted to bind and inhibit P-gp, leading to down-regulated P-gp expression and enhanced cytotoxicity of taxol (a substrate of P-gp) in A549/Taxol cells. DHW-221 appeared to preferably target A549/Taxol cells over sensitive A549 cells, inducing cell death mediated by cell arrest, mitochondrial apoptosis pathway and mitogen-activated protein kinase (MAPK) pathway. More importantly, DHW-221 was able to suppress the migration and invasion of A549/Taxol cells, and it reduced tumor growth in A549/Taxol xenograft model, suggesting its great promise as a chemo-sensitizer and drug candidate. Anlotinib, a vascular endothelial growth factor receptor 2 (VEGFR2) inhibitor, is an approved anticancer drug in China for the treatment of locally advanced or metastatic NSCLC. Wang et al. further validated that it could act as a P-gp inhibitor. Anlotinib inhibited the efflux function of P-gp without altering its expression level and localization, leading to increased accumulation of chemotherapeutics that are P-gp substrates, thereby sensitizing doxorubicin, paclitaxel and vincristine in P-pg overexpressing osteosarcoma cells. In KHOSR2 xenograft model, the combination of anlotinib and docorubicin showed higher inhibitory effects as compared to mono-therapy, and no significant toxic effects were observed. Another drug ribociclib, a CDK4/6 inhibitor, was identified as a P-pg inhibitor by Zhang et al. Different with anlotinib, ribociclib could down-regulate the translation and transcription levels of P-gp, leading to increased concentration of colchicine and doxorubicin in P-gp overexpressing human epidermoid carcinoma KB-C2 cells. Both ribociclib and anlotinib could stimulate the ATPase of P-gp. Huang et al. reported the therapeutic effects of PI3K inhibitor LY294002 in Fms-like tyrosine kinase 3-internal tandem duplication (FLT3-ITD) mutant acute myeloid leukemia (AML) cells that show sorafenib-resistant property. LY294002 inhibited the glycolysis of sorafenib-resistant cells which rely heavily on glycolysis for ATP production, leading to cell apoptosis. Liu et al. designed and evaluated a series of dual c-Met/VEGFR-2 inhibitors based on the core structure triazolopyrazine. Their study yielded a highly potent compound 17l that can suppress the enzymatic activities of c-Met and VEGFR-2, and inhibit the proliferation of A549 cells. Cao et al. found that SAHA, a histone deacetylase inhibitor, when combined with gefitinib or osimertinib, showed synergistic effects in the corresponding resistant NSCLC PC-9/AB2 and H1975OR cells *in vitro* and in animal models (SAHA plus gefitinib), which was mediated by increased enhancer of zeste homolog 2 (EZH2) and decreased autophagy. Heat shock protein 90 (HSP90) inhibitor, NVP-AUY922 was terminated in phase II clinical trials, despite its favorable results in overcoming drug resistance NSCLC cells. He et al. obtained the co-crystallization of NVP-AUY922 with HSP90, which showed detailed binding information that further directed the further drug design. Wu et al. designed and synthesized a novel murine double minute 2 (MDM2) inhibitor, XR-2 that was able to disturb the MDM2-p53 interaction, induce cell cycle arrest and apoptosis of wild-type p53 castration-resistant prostate cancer (CRPC) cell lines. In the enzalutamide-resistant CRPC xenograft model, XR-2 showed a strong synergistic effect with enzalutamide, resulting in a nearly complete inhibition of tumor growth while without showing any toxic effects.

In addition, several potential druggable targets causing drug resistance were also highlighted. Fu et al. found that the overexpression of P-gp can cause resistance of approved drug CDK 4/6 inhibitor palbociclib, whereas the inhibition of the efflux of P-gp by verapamil could restore its sensitivity. Similar phenomenon was also observed by Dong et al. on ARS-1620, a KRAS-G12C inhibitor that is now under clinical trials. Furthermore, Li et al. reported the involvement of high mobility group box protein 1 (HMGB1) in doxorubicin resistance, and its inhibitor ethyl pyruvate that can significantly enhance the sensitivity of doxorubicin in HMGB1 overexpressing hepatocellular carcinoma BEL7402 and SMMC7721 cells. Yu et al. summarized the druggability of mitochondrial DNA-directed RNA polymerase (POLRMT) and its inhibitors in overcoming drug resistance. Liu et al. systematically reviewed circular RNAs (circRNAs) and their roles in inducing drug resistance.

In conclusion, the identified novel small-molecule agents can serve as drug candidates and/or leading compounds that can be further structurally modified. Furthermore, rational designed combinations using these agents should be evaluated in the future to combat drug resistance.

## AUTHOR CONTRIBUTIONS

QC, CW, LZ, Q-XZ, and Y-FF wrote and reviewed this Editorial. All authors reviewed and approved the final version of the manuscript.

## REFERENCES


Assaraf, Y. G., Brozovic, A., Gonçalves, A. C., Jurkovicova, D., Linē, A., Machuqueiro, M., et al. (2019). The Multi-Factorial Nature of Clinical Multidrug Resistance in Cancer. *Drug Resist. Updat.* 46, 100645. Available at: http://www.ncbi.nlm.nih.gov/entrez/query.fcgi?cmd=Retrieve&db=pubmed&dopt=Abstract&list_uids=31585396&query_hl=1. doi:10.1016/j.drup.2019.100645

Bai, R., Chen, N., Li, L., Du, N., Bai, L., Lv, Z., et al. (2020). Mechanisms of Cancer Resistance to Immunotherapy. *Front. Oncol.* 10, 1290. Available at: http://www.ncbi.nlm.nih.gov/entrez/query.fcgi?cmd=Retrieve&db=pubmed&dopt=Abstract&list_uids=32850400&query_hl=1. doi:10.3389/fonc.2020.01290

Bashash, D., Zandi, Z., Kashani, B., Pourbagheri-Sigaroodi, A., Salari, S., and Ghaffari, S. H. (2022). Resistance to Immunotherapy in Human Malignancies: Mechanisms, Research Progresses, Challenges, and Opportunities. *J. Cell. Physiology* 237 (1), 346–372. Available at: http://www.ncbi.nlm.nih.gov/entrez/query.fcgi?cmd=Retrieve&db=pubmed&dopt=Abstract&list_uids=34498289&query_hl=1. doi:10.1002/jcp.30575

Berdigaliyev, N., and Aljofan, M. (2020). An Overview of Drug Discovery and Development. *Future Med. Chem.* 12 (10), 939–947. Available at: http://www.ncbi.nlm.nih.gov/entrez/query.fcgi?cmd=Retrieve&db=pubmed&dopt=Abstract&list_uids=32270704&query_hl=1. doi:10.4155/fmc-2019-0307

Chaffer, C. L., and Weinberg, R. A. (2011). A Perspective on Cancer Cell Metastasis. *Science* 331 (6024), 1559–1564. Available at: http://www.ncbi.nlm.nih.gov/entrez/query.fcgi?cmd=Retrieve&db=pubmed&dopt=Abstract&list_uids=21436443&query_hl=1. doi:10.1126/science.1203543

Dinić, J., Efferth, T., García-Sosa, A. T., Grahovac, J., Padrón, J. M., Pajeva, I., et al. (2020). Repurposing Old Drugs to Fight Multidrug Resistant Cancers. *Drug Resist. Updat.* 52, 100713. Available at: http://www.ncbi.nlm.nih.gov/entrez/query.fcgi?cmd=Retrieve&db=pubmed&dopt=Abstract&list_uids=32615525&query_hl=1. doi:10.1016/j.drup.2020.100713

Gao, H.-L., Gupta, P., Cui, Q., Ashar, Y. V., Wu, Z.-X., Zeng, L., et al. (2020). Sapitinib Reverses Anticancer Drug Resistance in Colon Cancer Cells Overexpressing the ABCB1 Transporter. *Front. Oncol.* 10, 574861. Available at: http://www.ncbi.nlm.nih.gov/entrez/query.fcgi?cmd=Retrieve&db=pubmed&dopt=Abstract&list_uids=33163405&query_hl=1. doi:10.3389/fonc.2020.574861

Imbert, C., Montfort, A., Fraisse, M., Marcheteau, E., Gilhodes, J., Martin, E., et al. (2020). Resistance of Melanoma to Immune Checkpoint Inhibitors is Overcome by Targeting the Sphingosine Kinase-1. *Nat. Commun.* 11 (1), 437. Available at: http://www.ncbi.nlm.nih.gov/entrez/query.fcgi?cmd=Retrieve&db=pubmed&dopt=Abstract&list_uids=31974367&query_hl=1. doi:10.1038/s41467-019-14218-7

Ji, M., Wang, D., Lin, S., Wang, C., Li, L., Zhang, Z., et al. (2022). A Novel PI3K Inhibitor XH30 Suppresses Orthotopic Glioblastoma and Brain Metastasis in Mice Models. *Acta Pharm. Sin. B* 12 (2), 774–786. Available at: http://www.ncbi.nlm.nih.gov/entrez/query.fcgi?cmd=Retrieve&db=pubmed&dopt=Abstract&list_uids=35256946&query_hl=1. doi:10.1016/j.apsb.2021.05.019

Munos, B. (2009). Lessons from 60 Years of Pharmaceutical Innovation. *Nat. Rev. Drug Discov.* 8 (12), 959–968. Available at: http://www.ncbi.nlm.nih.gov/entrez/query.fcgi?cmd=Retrieve&db=pubmed&dopt=Abstract&list_uids=19949401&query_hl=1. doi:10.1038/nrd2961

Newman, D. J., and Cragg, G. M. (2020). Natural Products as Sources of New Drugs Over the Nearly Four Decades from 01/1981 to 09/2019. *J. Nat. Prod.* 83 (3), 770–803. Available at: http://www.ncbi.nlm.nih.gov/entrez/query.fcgi?cmd=Retrieve&db=pubmed&dopt=Abstract&list_uids=32162523&query_hl=1. doi:10.1021/acs.jnatprod.9b01285

Parvathaneni, V., Kulkarni, N. S., Muth, A., and Gupta, V. (2019). Drug Repurposing: A Promising Tool to Accelerate the Drug Discovery Process. *Drug Discov. Today* 24 (10), 2076–2085. Available at: http://www.ncbi.nlm.nih.gov/entrez/query.fcgi?cmd=Retrieve&db=pubmed&dopt=Abstract&list_uids=31238113&query_hl=1. doi:10.1016/j.drudis.2019.06.014

Pluchino, K. M., Hall, M. D., Goldsborough, A. S., Callaghan, R., and Gottesman, M. M. (2012). Collateral Sensitivity as a Strategy against Cancer Multidrug Resistance. *Drug Resist. Updat.* 15 (1-2), 98–105. http://www.ncbi.nlm.nih.gov/entrez/query.fcgi?cmd=Retrieve&db=pubmed&dopt=Abstract&list_uids=22483810&query_hl=1. doi:10.1016/j.drup.2012.03.002

Russo, M., Russo, G. L., Daglia, M., Kasi, P. D., Ravi, S., Nabavi, S. F., et al. (2016). Understanding Genistein in Cancer: The "Good" and the "Bad" Effects: A Review. *Food Chem.* 196, 589–600. Available at: http://www.ncbi.nlm.nih.gov/entrez/query.fcgi?cmd=Retrieve&db=pubmed&dopt=Abstract&list_uids=26593532&query_hl=1. doi:10.1016/j.foodchem.2015.09.085

Sabbatino, F., Marra, A., Liguori, L., Scognamiglio, G., Fusciello, C., Botti, G., et al. (2018). Resistance to Anti-PD-1-Based Immunotherapy in Basal Cell Carcinoma: a Case Report and Review of the Literature. *J. Immunother. Cancer* 6 (1), 126. Available at: http://www.ncbi.nlm.nih.gov/entrez/query.fcgi?cmd=Retrieve&db=pubmed&dopt=Abstract&list_uids=30458852&query_hl=1. doi:10.1186/s40425-018-0439-2

Vasan, N., Baselga, J., and Hyman, D. M. (2019). A View on Drug Resistance in Cancer. *Nature* 575 (7782), 299–309. Available at: http://www.ncbi.nlm.nih.gov/entrez/query.fcgi?cmd=Retrieve&db=pubmed&dopt=Abstract&list_uids=31723286&query_hl=1. doi:10.1038/s41586-019-1730-1

Wang, J.-Q., Yang, Y., Cai, C.-Y., Teng, Q.-X., Cui, Q., Lin, J., et al. (2021). Multidrug Resistance Proteins (MRPs): Structure, Function and the Overcoming of Cancer Multidrug Resistance. *Drug Resist. Updat.* 54, 100743. Available at: http://www.ncbi.nlm.nih.gov/entrez/query.fcgi?cmd=Retrieve&db=pubmed&dopt=Abstract&list_uids=33513557&query_hl=1. doi:10.1016/j.drup.2021.100743

Yu, T., Huang, D., Wu, H., Chen, H., Chen, S., and Cui, Q. (2021). Navigating Calcium and Reactive Oxygen Species by Natural Flavones for the Treatment of Heart Failure. *Front. Pharmacol.* 12, 718496. Available at: http://www.ncbi.nlm.nih.gov/entrez/query.fcgi?cmd=Retrieve&db=pubmed&dopt=Abstract&list_uids=34858167&query_hl=1. doi:10.3389/fphar.2021.718496

Zugazagoitia, J., Guedes, C., Ponce, S., Ferrer, I., Molina-Pinelo, S., and Paz-Ares, L. (2016). Current Challenges in Cancer Treatment. *Clin. Ther.* 38 (7), 1551–1566. Available at: http://www.ncbi.nlm.nih.gov/entrez/query.fcgi?cmd=Retrieve&db=pubmed&dopt=Abstract&list_uids=27158009&query_hl=1. doi:10.1016/j.clinthera.2016.03.026


**Conflict of Interest:** The authors declare that the research was conducted in the absence of any commercial or financial relationships that could be construed as a potential conflict of interest.

frontiers in Oncology

ORIGINAL RESEARCH
published: 27 October 2021
doi: 10.3389/fonc.2021.739145

# HMGB1 Promotes Resistance to Doxorubicin in Human Hepatocellular Carcinoma Cells by Inducing Autophagy *via* the AMPK/mTOR Signaling Pathway

*Junhua Li*[1†], *Wei Zhou*[1†], *Qiang Mao*[2], *Dandan Gao*[3], *Lin Xiong*[4], *Xinyao Hu*[5], *Yongfa Zheng*[5*] and *Ximing Xu*[5*]

[1] Basic and Clinical Medical Research Center, Department of Gastroenterology, The First People's Hospital of Jingmen, Jingmen, China, [2] Department of Statistics, The First People's Hospital of Jingmen, Jingmen, China, [3] Department of Infectious Diseases, The First People's Hospital of Jingmen, Jingmen, China, [4] Department of Pathology, Renmin Hospital of Wuhan University, Wuhan, China, [5] Cancer Center, Renmin Hospital of Wuhan University, Wuhan, China

Chemoresistance remains as a major hindrance in the treatment of hepatocellular carcinoma (HCC). High mobility group box protein 1 (HMGB1) enhances autophagic flux and protects tumor cells from apoptosis, which results in acquired drug resistance. However, the exact mechanisms underlying HMGB1-modulated autophagy in HCC chemoresistance remain to be defined. In the present study, we found that administration of doxorubicin (DOX) significantly promoted HMGB1 expression and induced HMGB1 cytoplasmic translocation in human HCC cell lines BEL7402 and SMMC7721, which enhanced autophagy that contributes to protecting HCC cells from apoptosis and increasing drug resistance. Moreover, we observed HMGB1 translocation and elevation of autophagy in DOX-resistant BEL7402 and SMMC7721 cells. Additionally, inhibition of HMGB1 and autophagy increased the sensitivities of BEL-7402 and SMMC-7721 cells to DOX and re-sensitized their DOX-resistant cells. Subsequently, we confirmed with HMGB1 regulated autophagy by activating the 5′ adenosine monophosphate-activated protein kinase (AMPK)/mTOR pathway. In summary, our results indicate that HMGB1 promotes acquired DOX resistance in DOX-treated BEL7402 and SMMC7721 cells by enhancing autophagy through the AMPK/mTOR signaling pathway. These findings provide the proof-of-concept that HMGB1 inhibitors might be an important targeted treatment strategy for HCC.

**Keywords: HMGB1, autophagy, hepatocellular carcinoma cell, drug resistance, doxorubicin, AMPK/mTOR pathway**

OPEN ACCESS

***Edited by:***
*Qingbin Cui,*
*University of Toledo, United States*

***Reviewed by:***
*Chun-Yu Liu,*
*Taipei Veterans General Hospital, Taiwan*
*Hua Zhu,*
*The Ohio State University, United States*

***Correspondence:**
*Yongfa Zheng*
*zyf0322@126.com*
*Ximing Xu*
*doctorxu120@aliyun.com*

*†These authors have contributed equally to this work*

***Specialty section:***
*This article was submitted to Pharmacology of Anti-Cancer Drugs, a section of the journal Frontiers in Oncology*

***Received:*** *10 July 2021*
***Accepted:*** *12 October 2021*
***Published:*** *27 October 2021*

***Citation:***
*Li J, Zhou W, Mao Q, Gao D, Xiong L, Hu X, Zheng Y and Xu X (2021) HMGB1 Promotes Resistance to Doxorubicin in Human Hepatocellular Carcinoma Cells by Inducing Autophagy via the AMPK/mTOR Signaling Pathway. Front. Oncol. 11:739145. doi: 10.3389/fonc.2021.739145*

## INTRODUCTION

Liver cancer is considered to be the sixth most common cancer (1). The incidence and mortality of it rank the fourth and second among malignant tumors, respectively, which show a continuous upward trend in China (2, 3). Hepatocellular carcinoma (HCC) is the most common type of live cancer, accounting for approximately 75%–85% of cases (1, 4). Chemotherapy remains an indispensable comprehensive treatment for patients with postoperative or unresectable HCC at present (5, 6). Doxorubicin (DOX), a traditional chemotherapeutic agent for a wide variety of tumors, is a standard component for the treatment of advanced HCC. It demonstrates higher efficacy than other agents such as 5-fluorouracil, epirubicin, cisplatin, and etoposide (7, 8). However, the tendency to acquired resistance to DOX severely limits its clinical application in HCC therapy. DOX resistance involves multiple mechanisms, mainly related to drug accumulation (9), decreased DNA damage (10), and apoptosis signaling (11). Recently, the role of autophagy in DOX resistance has attracted a great deal of attention. Some studies have demonstrated that reversing DOX resistance *via* modulation of autophagy is a promising therapeutic strategy (12–14).

Autophagy is an essential cellular process that involves self-degradation of cellular proteins, damaged organelles, and lipid droplets *via* the lysosome, maintaining the energy balance and intracellular homeostasis (15). Recently, it was reported that autophagy is a significant contributor to chemoresistance in osteosarcoma cells and inhibition of autophagy enhances drug sensitivity of osteosarcoma cells (16). Autophagy has also been implicated in modulating sensitivity to oxaliplatin in human colorectal cancer cell lines (17). Some studies have shown that upregulation of autophagy promotes tumor cell survival and probably contributes to chemoresistance in liver cancer therapy (18, 19). These findings suggest that autophagy participates in the development of chemoresistance. However, little is still known about the underlying molecular mechanism of autophagy in regulating the development of chemotherapy resistance in HCC.

High mobility group box protein 1 (HMGB1), a well-known regulator of autophagy, is a highly conserved non-histone nuclear protein that has various biological functions in the nucleus such as DNA replication, recombination, transcription, and repair (20). In addition to its nuclear functions, HMGB1 in the cytoplasm acts as an extracellular signaling molecule that is closely associated with inflammation, cell proliferation and differentiation, and tumor progression (20, 21). Upregulation of HMGB1 expression has been unequivocally observed in various cancers such as HCC and lung cancer (22–24). Cytosolic translocation of HMGB1 and secretion of HMGB1 by tumor cells in response to chemotherapy are major factors in the disordered tumor microenvironment (25, 26). Many reports have demonstrated that subcellular localization and secretion of HMGB1 plays a major role as a positive regulator of autophagy in chemotherapy resistance in various cancers (26–29). However, the exact mechanism of HMGB1-mediated autophagy in the DOX resistance of HCC has not been clearly defined.

In this study, we investigated whether DOX augmented HMGB1 expression and induced HMGB1 translocation, whether the autophagy induced by DOX was regulated by HMGB1, and whether the changes in autophagy and HMGB1 protect HCC cells against DOX and facilitate the development of acquired DOX resistance. BEL7402 and SMMC7721 cells and DOX-resistant BEL7402 and SMMC7721 cells (BEL7402/DOX and SMMC7721/DOX cells, respectively) were used as the cell model. We found that HMGB1 expression and the associated autophagic flux were increased in response to DOX treatment in HCC cells, and autophagy modulated by HMGB1 protected HCC cells from DOX-induced apoptosis. Additionally, BEL7402/DOX and SMMC7721/DOX cells exhibited more autophagy and HMGB1 expression, and inhibition of autophagy and HMGB1 enhanced apoptosis sensitivity of DOX-resistant HCC cells to DOX. Moreover, we found that the 5′ adenosine monophosphate-activated protein kinase (AMPK)/mTOR signaling pathway was involved in these processes. Our data support HMGB1 as a potential molecular therapeutic target to enhance the efficacy of DOX in HCC.

## MATERIALS AND METHODS

### Cell Culture and Establishment of Drug-Resistant Cell Lines

Human HCC cell lines BEL-7402 and SMMC-7721 were purchased from the Cell Bank of the Chinese Academy of Science (Shanghai, China). Cells were cultured in RPMI-1640 medium (Gibco, Invitrogen, CA, USA) supplemented with 10% fetal bovine serum (Thermo Fisher Scientific Inc., Shanghai, China) at 37°C in a humidified atmosphere with 5% $CO_2$. DOX-resistant BEL-7402 and SMMC-7721 cell lines, BEL-7402/DOX and SMMC-7721/DOX, were established in our laboratory by selecting cells for resistance to increasing stepwise concentrations of DOX (Shanghai Shenggong Biological Engineering Co., Ltd., Shanghai, China) over 10 months until the cells survived in 1 μg/mL DOX as described previously (30). The half maximal inhibitory concentration ($IC_{50}$) value was calculated with GraphPad Prism version 7.0 software, and the resistance index (RI) was calculated according to the following formulae: RI = ($IC_{50}$ of drug-resistant cells)/($IC_{50}$ of parental cells), which was used as the relative indicator to evaluate drug resistance.

### Drug Sensitivity Measured by the MTT Assay

The sensitivity of HCC cells to DOX, expressed as the proliferation inhibition rate, was measured using the MTT assay. The cells were seeded at a density of $1 \times 10^5$ cells per well in 96-well plates in 200 μl RPMI (Gibco, Invitrogen, CA, USA) and incubated at 37°C in a humidified atmosphere with 5% $CO_2$ for 24 h. Then, the cells were treated with DOX at increasing concentrations of 0.1, 0.2, 0.4, 0.8, 1.6, and 3.2 μg/mL (five replicates for each concentration). After 48 h of culture at 37°C for adherence, the supernatants were removed and 20 μL per well

MTT (Thermo Fisher Scientific, Shanghai, China) was added to the medium, followed by incubation for 2 h. Then, 150 μL per well of DMSO (Sigma-Aldrich, St. Louis, MO, USA) was added to dissolve the purple crystals. Subsequently, absorbance was determined at 490 nm and $IC_{50}$ values were calculated by Graphpad Prism 7.0 software. The inhibition rate of cells was calculated by the following formula: (1-experimental blank absorbance value/control-blank absorbance value) × 100%. All experiments were repeated three times and the results are expressed as mean values.

## Construction of Vectors, siRNA, and Transfection Into Cells

BEL-7402 and SMMC7721 cells were seeded at $1 \times 10^5$ cells per well in six-well plates and cultured to 80%–90% confluence. HMGB1-overexpressing vector pcDNA3.1-HMGB1 was obtained from Genechem Company (Shanghai, China) and transfected into HCC cells using Lipofectamine™ 2000 (Invitrogen, Carlsbad, CA, USA). Knockdown of HMGB1 was accomplished by specific small interfering RNA (siRNA). HMGB1-siRNA or negative control (NC) siRNA (GenePharma Company, Shanghai, China) were transfected into cell, using Lipofectamine™ 2000 in accordance with the manufacturers' instructions. The siRNA sequences were as follows (31, 32): siHMGB1, sense strand 5′-ccuguccauuggug auguutt-3′ and anti-sense strand 5′-aacaucaccaauggacaggtt-3′; siNC, sense strand 5′-uucuccgaacgugucacgutt-3′ and anti-sense strand 5′-acgugacacguucggagaatt-3′. The working concentration of siRNA was 40 nmol/L. At 48 h after transfection, the culture medium was replaced and the cells were treated with the indicated concentrations of drugs for various periods.

## Western Blot Analysis

Cell lysates were prepared using RIPA lysis buffer containing 1 mM phenylmethylsulfonyl fluoride and 1% phosphatase inhibitor cocktail. The protein concentration was measured with a BCA assay (Beyotime Biotechnology, Shanghai, China). All samples were adjusted to equal protein content before analysis. Samples (20 μg total protein) from each group were separated by 12% sodium dodecyl sulfate-polyacrylamide gel electrophoresis and subsequently transferred onto PVDF membranes (Millipore, Billerica, MA, USA) under a constant current. Then, the membranes were blocked with 5% dry non-fat milk in TBST buffer for 2 hour at room temperature. The membrane was then incubated overnight at 4°C with a primary antibody diluted in TBST. The primary antibodies were as follows: polyclonal rabbit anti-human HMGB1, Beclin 1, LC3B, p62, AMPK, phosphorylated AMPK (p-AMPK), mTOR, phosphorylated mTOR (p-mTOR), and cleaved PARP (Affinity Biosciences, OH, USA), and antibodies against GAPDH (Cell Signaling Technology, Inc., MA, USA) and Lamin B (Boster Biological Technology Co. Ltd., Wuhan, China). After washing three times with TBST for 10 min each wash, the membrane was incubated with corresponding peroxidase-conjugated goat IgG (1:2,000 dilution, Boster Biological Technology Co. Ltd., Wuhan, China) as the secondary antibody for 1 h at room temperature. Enhanced chemiluminescent reagent (Applygen Technologies Inc., Beijing, China) was used for development. Protein bands were quantified and analyzed using the BandScan5.0 system. Each experiment was repeated three times and the results were averaged.

## Flow Cytometric Analysis of Apoptosis

Apoptosis was detected by annexin V-FITC and PI staining using an Apoptosis Detection kit (KeyGEN Bio TECH Co. Ltd., Nanjing, China) in accordance with the manufacturer's instructions. Drug-treated cells were washed, collected, resuspended in PBS, and transferred to a flow cytometer tube after incubation with 500 μl Binding Buffer. Then, 5 μl annexin V-FITC and 5 μl PI were added, followed by incubation in the dark for 15 min at room temperature. Stained cells were analyzed by a CytoFLEX flow cytometer (Beckman Coulter, USA).

## Statistical Analysis

Statistical analyses were performed using SPSS22.0 software (IBM Corp., Armonk, NY, USA). Data are expressed as the mean ± standard deviation. Student's t test was used for continuous variable comparison between two groups, and one-way ANOVA was adopted for multi-group comparison (Dunnett-*t* test or LSD-*t* test were used for multiple comparison). $P < 0.05$ was considered statistically significant.

# RESULTS

## BEL7402/DOX and SMMC7721/DOX Cells Exhibit Stable Drug Resistance

To evaluate drug resistance of BEL7402/DOX and SMMC7721/DOX cells, the DOX $IC_{50}$ of cells was determined by the MTT assay and RI indexes were calculated. The $IC_{50}$ values of BEL7402 and BEL7402/DOX cells were 0.226 ± 0.004 and 4.776 ± 0.128 μg/mL, respectively, and those of SMMC7721 and SMMC7721/DOX cells were 0.175 ± 0.007 and 2.556 ± 0.002 μg/mL, respectively. As shown in **Figure 1A**, the RIs of BEL7402/DOX and SMMC7721/DOX cells were 21.1 and 14.6, respectively, suggesting that BEL7402/DOX and SMMC7721/DOX cells had exhibited stable DOX chemoresistance (33).

## DOX Treatment Promotes HMGB1 Expression and Induces HMGB1 Translocation in HCC Cell Lines

To determine whether HMGB1 expression was related to chemotherapy of HCC cells, we treated BEL-7402 and SMMC-7721 cells, which are commonly used in drug resistance experiments, with the chemotherapeutic drug DOX. DOX exerts anti-cancer effects by intercalating nucleotide bases, which depends on topoisomerase II enzyme, and inducing programmed cell death (34, 35). Here, BEL-7402 and SMMC-7721 cells were exposed to increasing concentrations of DOX or a fixed concentration (3.2 μg/mL, which determined by preliminary experiment) for 0, 12, 24, and 48 h. As shown in **Figure 1B**, western blot analysis revealed that DOX treatment

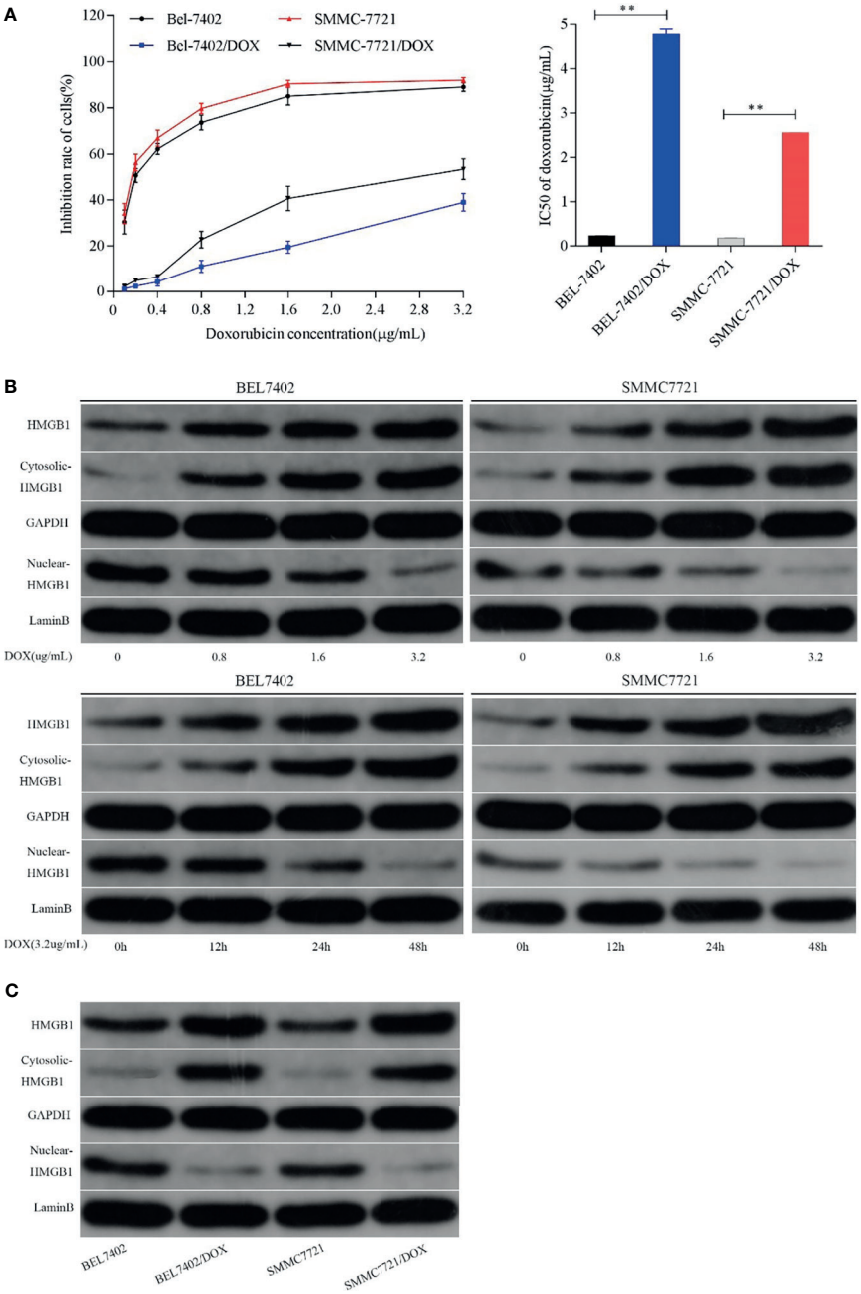


**FIGURE 1** | Chemotherapeutic treatment promotes HMGB1 expression and induces HMGB1 translocation. **(A)** Effect of DOX on the proliferation of BEL7402, BEL7402/DOX, SMMC7721, and SMMC7721/DOX cells, and DOX $IC_{50}$ in these cells. The $IC_{50}$ values of BEL7402/DOX and SMMC7721/DOX cells were higher than those of the parental cells, $^{**}P < 0.01$. **(B)** Treatment with DOX increased the expression of HMGB1 and promoted HMGB1 translocation in a dose- and time-dependent manner. **(C)** Lysates of parental and DOX-resistant HCC cells were prepared to detect HMGB1. Total and cytoplasmic expression of HMGB1 were higher in DOX-resistant HCC cells.

led to a dose- and time-dependent increase in the total level of HMGB1 in both BEL-7402 and SMMC-7721 cells. Moreover, the cytosolic levels of HMGB1 were up-regulated, whereas HMGB1 expression in the nucleus was obviously reduced when the cells treated with DOX. Additionally, BEL-7402/DOX and SMMC-7721/DOX cells, the DOX-resistant sublines, showed relatively higher total and cytosolic levels of HMGB1 compared with parental cells (**Figure 1C**). These results suggested that DOX treatment induced expression and translocation of HMGB1 and that HMGB1 might be associated with drug resistance.

## Suppression of HMGB1 Increases the Sensitivity to DOX in HCC Cells

To investigate the effect of HMGB1 induced by DOX on HCC cells, we analyzed the responses of BEL-7402 and SMMC-7721 cells and their DOX-resistant cells to DOX treatment after inhibition of HMGB1 expression and translocation. The cells were transfected with HMGB1 siRNA (Si-HMGB1) or negative control siRNA (Si-NC). HMGB1 expression was significantly lower in Si-HMGB1 cells than in Si-NC cells (**Figure 2A**). The cells were incubated with various concentrations DOX for 48 h after transfection with HMGB1 siRNA or pretreated with ethyl pyruvate (EP), a pharmacological inhibitor of HMGB1 cytoplasmic translocation (26). The $IC_{50}$ values of cells transfected with HMGB1 siRNA or pretreated with EP were significantly lower than those of NC siRNA-transfected cells (**Figure 2B**), which indicated that the DOX sensitivities of BEL-7402 and SMMC-7721 cells were significantly increased by inhibition of HMGB1 expression and cytoplasmic translocation. Simultaneously, the apoptosis of cells, which were transfected with siRNA-HMGB1/siRNA-NC or pretreated with EP(10mM) 2h and then exposed to doxorubicin(3.2μg/mL) for 48h, was increased significantly after HMGB1 knockdown (**Figure 2C**), which suggested that suppression of HMGB1 enhanced apoptosis sensitivity in BEL-7402 and SMMC-7721

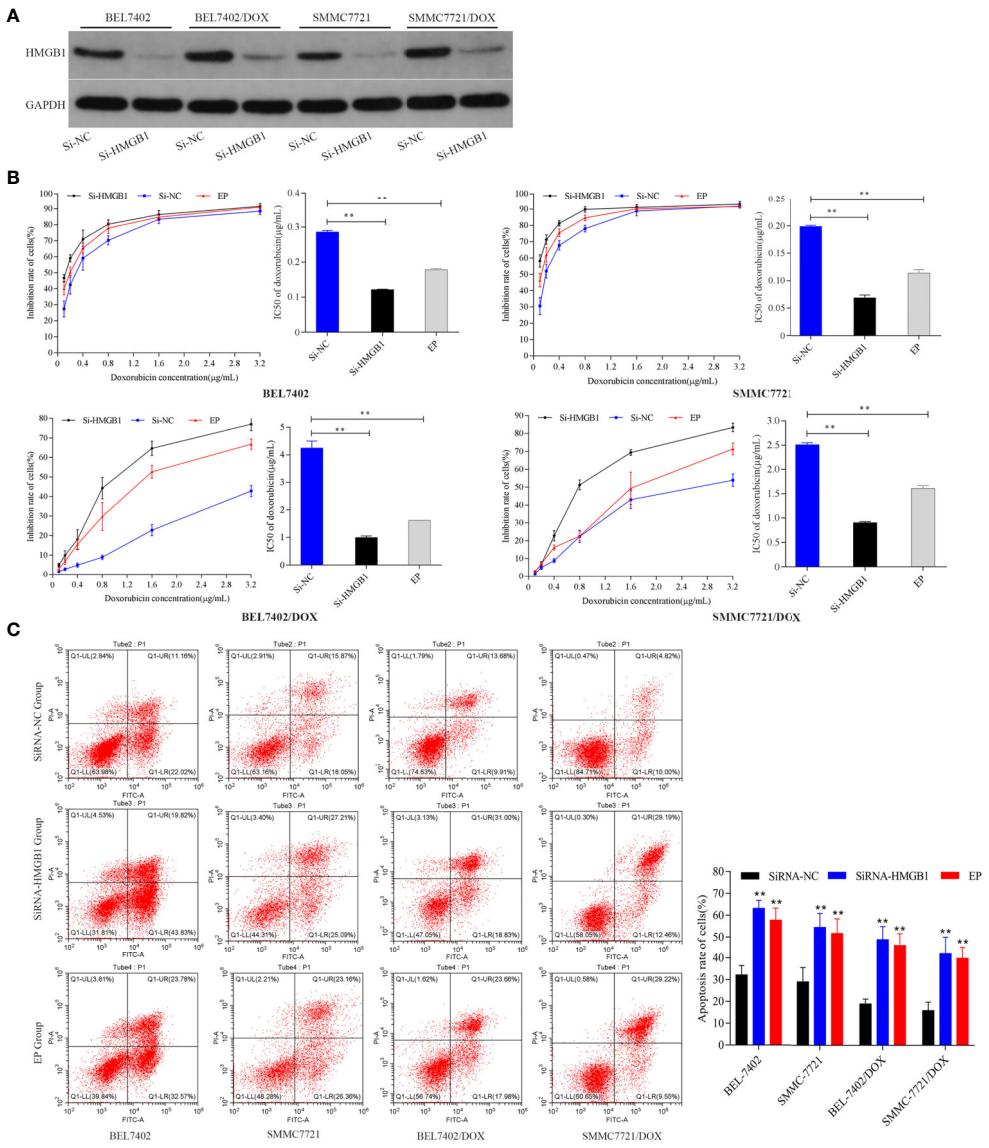


**FIGURE 2** | Inhibition of HMGB1 expression and cytoplasmic translocation increases sensitivity to DOX in HCC cells. **(A)** Compared with Si-NC cells, the level of HMGB1 was significantly decreased in Si-HMGB1 cells. **(B)** Suppression of HMGB1 expression and cytoplasmic translocation in HCC cells decreased the $IC_{50}$ value of DOX. $^{**}P < 0.01$ compared with Si-NC cells. **(C)** Inhibition of HMGB1 expression and cytoplasmic translocation enhanced apoptosis sensitivity of HCC cells to DOX. Apoptosis was analyzed by flow cytometric analysis of annexin-V/PI staining. $^{**}P < 0.01$ compared with Si-NC cells.

cells. Similar to the results in parental cells, transfection of BEL-7402/DOX and SMMC-7721/DOX cells with HMGB1 siRNA and pretreatment with EP rendered them largely more sensitive to DOX as indicated by decreases in $IC_{50}$ values and increased apoptosis (**Figures 2B, C**).

## DOX Induces Autophagy That Protects HCC Cells From Apoptosis

To explore the effect of DOX on autophagy and the role of autophagy in chemotherapeutic drug resistance of HCC cells, we first detected the autophagy-related proteins Beclin 1, LC3-II, and p62, which are reliable markers of autophagy (36), in BEL-7402 and SMMC-7721 cells treated with various concentrations DOX for the indicated periods. As shown in **Figure 3A**, DOX markedly enhanced the levels of Beclin 1 and LC3-II, and reduced p62 expression in a time- and dose-dependent manner in BEL-7402 and SMMC-7721 cells.

These data indicated that treatment with chemotherapeutic drugs induced and increased autophagy in HCC cells.

Next, to determine whether DOX-induced autophagy was involved in drug resistance of HCC cells, we analyzed autophagy activity in two DOX-resistant cell lines: BEL-7402/DOX and SMMC-7721/DOX. Western blot analysis showed that the levels of LC3-II and Beclin 1 were higher and levels of p62 were lower in DOX-resistant cells than in parental cells (**Figure 3A**), which suggested that DOX-resistant HCC cells had an increased capacity for autophagy. Next, the parental and DOX-resistant HCC cells were pretreated with 3-MA (25μM) before incubating with doxorubicin(3.2μg/mL) for 48h. Cell proliferation inhibition rates were performed by MTT assay and IC50 was calculated. We found that the cytotoxicity and apoptosis were increased significantly when autophagy was inhibited by 3-MA in these kinds of cells as indicated by a decrease of $IC_{50}$ and increase of apoptosis (**Figures 3B, C**). Furthermore, the sensitivity of BEL-7402/DOX and SMMC-7721/DOX cells to DOX was enhanced markedly, which indicated that the drug resistance of these cells was reversed by treatment with 3-MA (**Figure 3B**). Both parental and DOX-resistant cell lines showed potentiation of apoptosis after suppression of autophagy (**Figure 3C**).

These findings suggested that treatment with chemotherapeutic drug DOX induced autophagy in HCC cells, which protected HCC cells from DOX-induced apoptosis and contributed to the survival of HCC cells treated with DOX.

## HMGB1 Regulates DOX-Induced Autophagy in HCC Cells

Both HMGB1 and autophagy were induced by chemotherapy, which decreased sensitivity to the drug in HCC cells. Next, we investigated the relationship between them and examined whether HMGB1 is a direct regulator of autophagy. Previous studies have shown that starvation or other stresses facilitate translocation of HMGB1 to the cytoplasm and enhance autophagic flux (20, 37). In this study, BEL7402 and SMMC7721 cells were transfected with pcDNA3.1-control or pcDNA3.1-HMGB1 and then pretreated with or without 3-MA(25μM) for 12h before additional 48h incubated with doxorubicin(3.2μg/mL). HMGB1, Lc3 and P62 levels were assayed by western blot. We found that pcDNA3.1-HMGB1 vector significantly increased HMGB1 protein in the cells (**Figure 4A**). Moreover, western blot analysis showed that overexpression of HMGB1 increased the conversion levels of LC3-I to LC3-II and promoted the degradation of p62 compared with the pcDNA3.1-control group when cells were exposed to DOX. However, the LC3-II elevation and p62 degradation were abrogated by suppression of autophagy with 3-MA (**Figure 4A**). To further verify effect of HMGB1 on autophagy, the cells, BEL7402 and SMMC7721, were transfected with HMGB1 siRNA or negative control and then were treated with 3-MA and doxorubicin. And western blot results showed that inhibition of HMGB1 by transfecting with HMGB1 siRNA could significantly reduce autophagy in cells, which was more obvious when cells pretreated with 3-MA (**Figure 4B**). Furthermore, we observed changes of LC3-II and p62 expression in cells when cytosolic translocation of HMGB1 was inhibited by EP. BEL7402 and SMMC7721 cells were pretreated with or without EP(10mM) for 12h, and then incubated with doxorubicin (3.2μg/mL) for 48h. Nuclear and cytoplasmic HMGB1 and autophagy-related proteins were detected by western blotting. The results demonstrated that pretreatment with EP decreased the levels of LC3-II, but increased the level of p62 in cells before incubation with DOX (**Figure 4C**). Therefore, HMGB1 played an important role in the regulation of autophagy in HCC cells.

## HMGB1-Mediated Autophagy and Downregulated Apoptosis Induced by DOX Involve the AMPK/mTOR Pathway in HCC Cells

AMPK is a highly conserved serine/threonine kinase that is widely distributed in eukaryotic cells, which is typically activated by a high AMP/ATP ratio to maintain energy homeostasis (38). Moreover, AMPK coordinates with many upstream and downstream molecules, such as LKBI, mTOR, 70 kDa ribosomal protein S6 kinase (p70S6K), Akt, and ULKI, and regulates apoptosis and autophagy (39–41). Mammalian rapamycin target protein mTOR —an atypical serine/threonine kinase—is an important downstream protein of AMPK and plays a "gating" role in regulation of autophagy by phosphorylation of p70S6K. Activated AMPK inactivates mTOR and the AMPK/mTOR pathway has been linked to actuation of autophagy (42–44). Thus, to determine whether the AMPK/mTOR pathway was involved in regulation of HMGB1-mediated autophagy in HCC cells, we measured AMPK and mTOR phosphorylation, markers of autophagy, p62, and apoptosis-related protein cleaved PARP in DOX-induced cells with or without AMPK inhibitor Compound C (10 μM) and mTOR inhibitor rapamycin (10 nM) treatments after transfection with the HMGB1 cDNA plasmid or HMGB1 siRNA. As shown in **Figure 5A**, compared with vector control cells, overexpression of HMGB1 significantly increased AMPK phosphorylation and obviously decreased the levels of p-mTOR, p62, and cleaved PARP in both BEL7402 and SMMC7721 cells. However, these effects were abolished by suppression of AMPK with Compound C. These results suggested that AMPK participated in promotion of autophagy by HMGB1, which downregulated apoptosis in HCC cells.

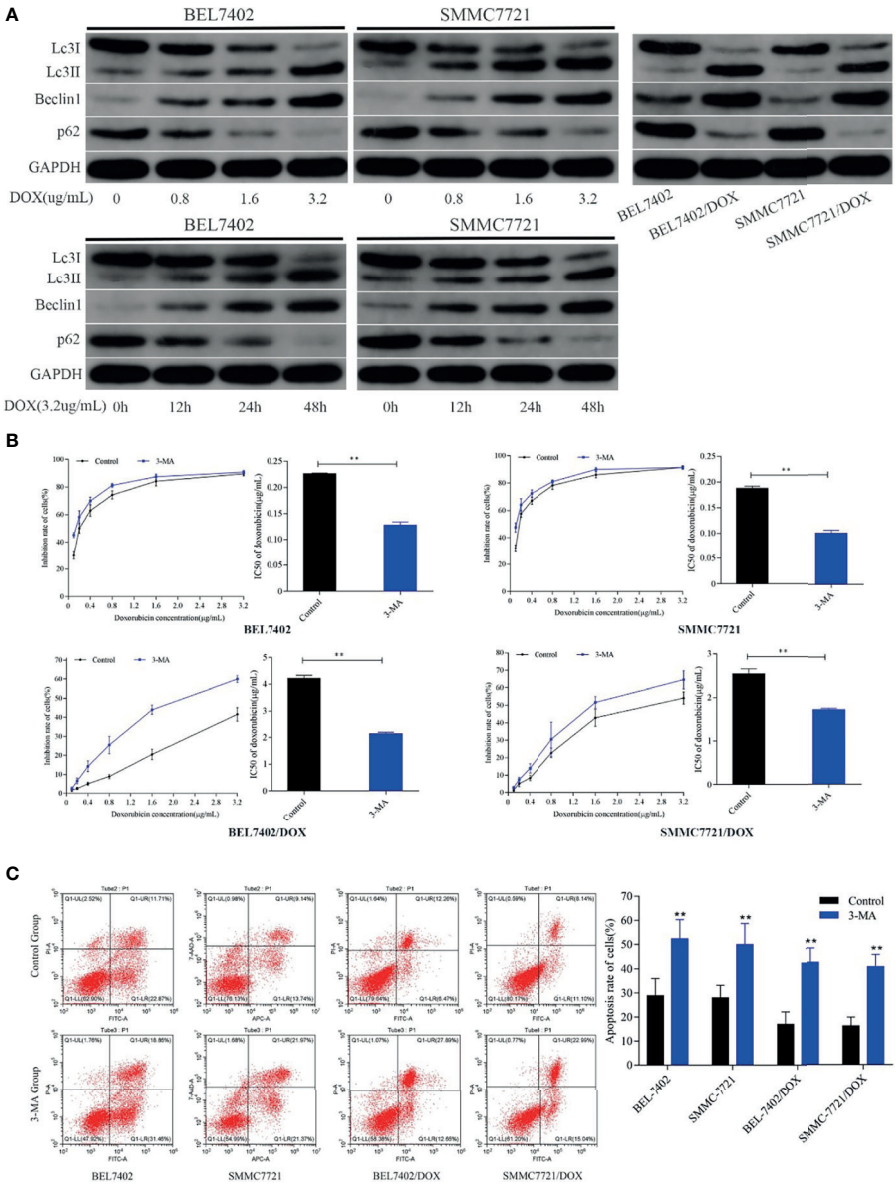


**FIGURE 3** | DOX induces autophagy that protects HCC cells from apoptosis and reduces the sensitivity of HCC cells to DOX. **(A)** Treatment with DOX promoted autophagy in a dose- and time-dependent manner in BEL7402 and SMMC7721 cells. Autophagy was also upregulated in DOX-resistant HCC cells. **(B)** Inhibition of autophagy promoted apoptosis and sensitivity of HCC cells to DOX. The DOX $IC_{50}$ of parental and DOX-resistant HCC cells was significantly decreased by pretreatment with 3-MA. **(C)** Apoptosis rates of cells in the 3-MA group were remarkably higher than those of control cells both in parental and DOX-resistant HCC cells. $^{**}P < 0.01$ compared with control cells.

We also observed the role of mTOR in the abovementioned regulation process. Compared with the siRNA-NC group, depletion of HMGB1 by siRNA notably decreased p-AMPK and increased p-mTOR. Moreover, p62 degradation was weakened and cleaved PARP expression was enhanced in the siRNA-HMGB1 group, which further supported the role of AMPK in HMGB1-mediated autophagy and apoptosis of HCC cells. Additionally, when combined with mTOR inhibitor rapamycin in cells transfected with HMGB1 siRNA, the p-mTOR level was decreased obviously, p62 degradation was enhanced, and apoptosis was reduced significantly (**Figure 5B**). These results indicated that downregulation of p-AMPK after knockdown of HMGB1 did not promote p-mTOR expression, inhibit autophagy, or promote apoptosis when mTOR was blocked by rapamycin, which suggesting that mTOR was a downstream molecule of AMPK. Therefore, HMGB1 may regulate DOX-induced autophagy and reduce apoptosis through the AMPK/mTOR pathway in HCC cells. Similar to the results in parental cells, transfection of BEL7402/DOX and SMMC7721/DOX cells with HMGB1 cDNA plasmid improved activation of AMPK/mTOR

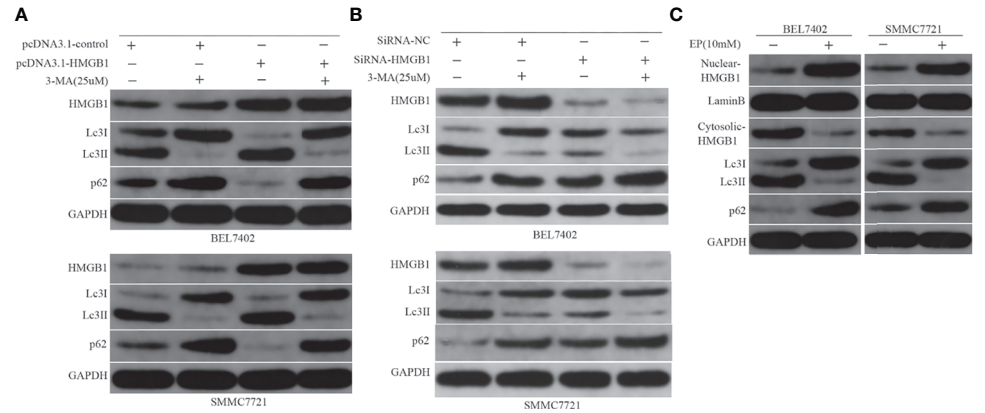


**FIGURE 4** | HMGB1 regulates autophagy in HCC cells. **(A)** Western blot analysis of HMGB1, LC3, and p62 levels in BEL7402 and SMMC7721 cells. **(B)** Western blot results showed inhibition of HMGB1 could significantly reduce autophagy in cells, which was more obvious when cells pretreated with 3-MA. **(C)** Nuclear and cytoplasmic HMGB1 and autophagy-related proteins were detected by western blotting.

pathway and autophagy (**Figure 5C**), and decreased the propensity for apoptosis. And the changes trend of these indexes were just opposite in HMGB1-knockdown DOX-resistant cells (**Figure 5D**). Together with data of the studies, we proposed a model in which doxorubicin induced the cytosolic translocation of HMGB1, which regulated autophagy that decreased apoptosis and increased drug resistance by activating the AMPK/mTOR pathway(**Figure 5E**).

## DISCUSSION

In the present study, we demonstrated that DOX treatment markedly induced cytosolic HMGB1 translocation, HMGB1 expression, and autophagy in HCC cell lines. HMGB1-regulated autophagy contributed to the acquirement of DOX resistance by protecting HCC cells from apoptosis, and inhibition of HMGB1 or suppression of HMGB1 cytosolic translocation attenuated this autophagic protection in response to DOX. Additionally, we showed that activation of the AMPK/mTOR signaling pathway was involved in the process of HMGB1-mediated autophagy.

Acquired resistance is a major hindrance for the application of chemotherapeutic drugs to tumors. Numerous investigations have described that the mechanisms of DOX resistance include upregulation of multidrug resistance efflux pumps, topoisomerase, altered drug targets, and alterations in apoptosis signaling (45–48). However, the molecular mechanism of DOX resistance in HCC has not been fully elucidated. Currently, autophagy is considered as a novel clinical target to reverse DOX resistance. Studies have implied that autophagy is involved in several steps of HCC initiation and progression as well as therapeutic resistance (18, 19). Here, we found that BEL-7402 and SMMC-7721 cells underwent autophagy in a time- and dose-dependent manner when treated with DOX and drug-resistant sublines BEL-7402/DOX and SMMC-7721/DOX had an increased capacity for autophagy. Inhibition of autophagy by 3-MA potentiated the inhibitory effect of DOX on the proliferation of these cells, which was accompanied by significantly increased apoptosis. Additionally, autophagy inhibitor 3-MA partially reversed DOX resistance of BEL-7402/DOX and SMMC-7721/DOX cells by inhibiting autophagy. Our results suggested that DOX-induced autophagy protected HCC cells from apoptosis and was highly related to DOX resistance in these cells. Therefore, revealing the detailed mechanism of autophagy regulation may provide novel therapeutic options to improve chemotherapy efficacy.

HMGB1—a chromatin-associated nuclear protein—is a critical regulator of cell death and survival. Overexpression of HMGB1 is associated with the hallmarks of cancer, which included an unlimited replicative potential, angiogenesis, evasion of apoptosis, insensitivity to inhibitors of growth, inflammation, tissue invasion, and metastasis (20, 21). The activities of HMGB1 are related to its cellular localization. In the nucleus, HMGB1 binds to DNA and regulates nuclear events such as DNA replication, recombination, and repair. It is also actively secreted or passively released under various stimuli, such as injury, necrosis, hypoxia, and endotoxin, in different cell types (16, 20). Both endogenous and exogenous HMGB1 have been suggested to be important regulators of autophagy in tumor cells (49, 50). It was reported that anticancer agents doxorubicin induced HMGB1 upregulation in human osteosarcoma cells, and knockdown of HMGB1 restored the chemosensitivity of osteosarcoma cells *in vivo* and *in vitro* by inducing autophagy, an intracellular self-defense mechanism known to confer drug resistance (51). Pan et al. (26) found that HMGB1 is a crucial regulator of autophagy, which significantly contributes to docetaxel resistance in LAD cells. Wang et al. (50) showed that HMGB1 facilitates autophagic progression and reduces oxidative stress induced by DOX, which is a critical factor for the development of chemoresistance and tumorigenesis. This prompted us to investigate the relationship between HMGB1 and autophagy in chemotherapy resistance of HCC.

Here, we focused on the interaction between intracellular HMGB1 and autophagy in chemotherapy resistance to DOX. We observed that DOX treatment promoted HMGB1 expression and induced HMGB1 translocation in HCC cells and overexpression of HMGB1 by transfection with pcDNA3.1-HMGB1 increased the

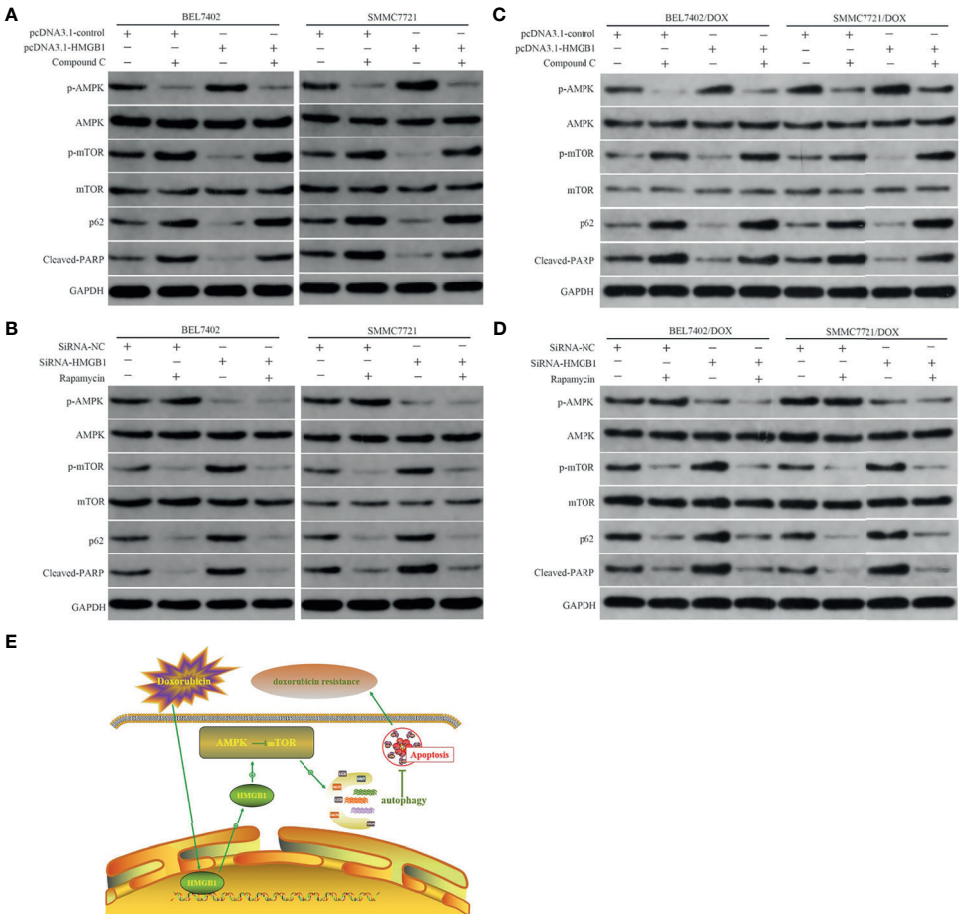


**FIGURE 5** | HMGB1-mediated autophagy that downregulates apoptosis in HCC cells involves the AMPK/mTOR pathway. **(A)** Western blot analysis of p-AMPK, p-mTOR, p62, and apoptosis-related protein cleaved PARP in BEL7402 and SMMC7721 cells transfected with pcDNA3.1-control or pcDNA3.1-HMGB1 and then pretreated with or without AMPK inhibitor Compound C (10μM). **(B)** Western blot analysis of p-AMPK, p-mTOR, p62, and cleaved PARP in BEL7402 and SMMC7721 cells transfected with siRNA-HMGB1 or siRNA-NC and then treated with or without mTOR inhibitor rapamycin(10 nM). **(C)** Western blot analysis of p-AMPK, p-mTOR, p62, and apoptosis-related protein cleaved PARP in DOX-resistant BEL7402 and SMMC7721 cells transfected with pcDNA3.1-control or pcDNA3.1-HMGB1 and then pretreated with or without AMPK inhibitor Compound C. **(D)** Western blot analysis of p-AMPK, p-mTOR, p62, and cleaved PARP in BEL7402/DOX and SMMC7721/DOX cells transfected with siRNA-HMGB1 or siRNA-NC and then treated with or without mTOR inhibitor rapamycin. **(E)** Model depicting the mechanism by which HMGB1 modulates doxorubicin resistance by inducing autophagy. Doxorubicin induces the cytosolic translocation of HMGB1, which promotes autophagy that decreases apoptosis and increases doxorubicin resistance by activating the AMPK/mTOR pathway.

level of autophagy when HCC cells treated with DOX. However, this upregulation of autophagy was abolished by suppression of autophagy with 3-MA. Interestingly, we found that inhibition of autophagy by 3-MA was unable to increase the level of intracellular HMGB1, although autophagy is also regulated by the release of HMGB1 (52). Moreover, we observed that ethyl pyruvate (EP), an inhibitor of HMGB1 cytoplasmic translocation, attenuated DOX-induced autophagy. Our results showed that both HMGB1 upregulation and cytoplasmic translocation of HMGB1 enhanced the level of autophagy, which contributed to resistance against DOX when HCC cells were exposed to DOX. Furthermore, knockdown of HMGB1 or inhibition of HMGB1 cytoplasmic translocation increased sensitivity to DOX in BEL-7402 and SMMC-7721 cells and re-sensitized DOX-resistant BEL-7402/DOX and SMMC7721/DOX cells. Our findings obviously demonstrate that HMGB1 is a positive regulator of autophagy in HCC and mediates DOX resistance.

We further explored the molecular mechanism by which intracellular HMGB1 regulates autophagy. Previous studies have demonstrated the role of AMPK in viability, migration, invasiveness, and apoptosis of HCC cells (43, 53). Moreover, the AMPK/mTOR signaling pathway is involved in autophagy and AMPK negatively regulates mTOR and triggers autophagy flux. Thus, mTOR is suggested to be the predominate regulator of autophagy (42–44). Studies have showed that HMGB1 induced cardiomyocyte autophagy following acute myocardial infarction through activation of AMPK and inhibition of mTORC1 (54). Targeting autophagy enhances heat stress-induced apoptosis *via* the ATP-AMPK-mTOR axis in hepatocellular carcinoma (55). In the present study, we found that transfection with an HMGB1 cDNA plasmid

promoted AMPK phosphorylation and reduced the level of mTOR phosphorylation, which were accompanied by increased autophagy and lower apoptosis. Suppression of AMPK with Compound C facilitated mTOR phosphorylation, inhibited autophagy, and enhanced apoptosis, even in HMGB1-overexpressing cells. These data suggested that AMPK participated in HMGB1-mediated promotion of autophagy, which downregulated apoptosis in HCC cells. Additionally, we observed that downregulation of p-AMPK by depletion of HMGB1 did not enhance p-mTOR expression, inhibit autophagy, or promote apoptosis of HCC cells when mTOR was blocked by rapamycin, which implied that mTOR was a downstream molecule of AMPK in the abovementioned regulation process. Taken together, these results suggest that HMGB1 regulates autophagy by activating the AMPK/mTOR pathway.

In summary, our study showed that both HMGB1 expression and cytoplasmic translocation of HMGB1 are enhanced by chemotherapy with DOX in HCC cell lines, which promotes autophagy that decreases apoptosis and increases drug resistance. HMGB1 facilitates autophagy by activating the AMPK/mTOR pathway. These results demonstrate that HMGB1 could be a potential target for HCC therapy. Further experiments are needed to clarify whether other downstream genes participate in the regulation process and to confirm our hypothesis in animal models *in vivo*.

## DATA AVAILABILITY STATEMENT

The raw data supporting the conclusions of this article will be made available by the authors, without undue reservation.

## AUTHOR CONTRIBUTIONS

All the authors have contributed greatly to this article. YZ and XX contributed to the conception of the study. JL and WZ performed the experiment and wrote the manuscript. DG and LX contributed significantly to analysis and manuscript preparation. QM performed the data analyses. XH helped perform the analysis with constructive discussions. All authors contributed to the article and approved the submitted version.

## FUNDING

This work was supported by the National Natural Science Foundation of China (no. 31971166 to XX) and Key Scientific Project of Jingmen (no. YFZD2017037 to JL).

## REFERENCES

1. Bray F, Ferlay J, Soerjomataram I, Siegel RL, Torre LA, Jemal A. Global Cancer Statistics 2018: GLOBOCAN Estimates of Incidence and Mortality Worldwide for 36 Cancers in 185 Countries. *CA Cancer J Clin* (2018) 68 (6):394–424. doi: 10.3322/caac.21492
2. Zheng RS, Sun KX, Zhang SW, Zeng HM, Zou XN, Chen R, et al. Report of Cancer Epidemiology in China, 2015. *Zhonghua Zhong Liu Za Zhi* (2019) 41 (1):19–28. doi: 10.3760/cma.j.issn.0253-3766.2019.01.005
3. Feng RM, Zong YN, Cao SM, Xu RH. Current Cancer Situation in China: Good or Bad News From the 2018 Global Cancer Statistics? *Cancer Commun (Lond)* (2019) 39(1):22. doi: 10.1186/s40880-019-0368-6
4. Chen W, Zheng R, Baade PD, Zhang S, Zeng H, Bray F, et al. Cancer Statistics in China, 2015. *CA Cancer J Clin* (2016) 66(2):115–32. doi: 10.3322/caac.21338
5. Chen S, Cao Q, Wen W, Wang H. Targeted Therapy for Hepatocellular Carcinoma: Challenges and Opportunities. *Cancer Lett* (2019) 460:1–9. doi: 10.1016/j.canlet.2019.114428
6. Galun D, Srdic-Rajic T, Bogdanovic A, Loncar Z, Zuvela M. Targeted Therapy and Personalized Medicine in Hepatocellular Carcinoma: Drug Resistance, Mechanisms, and Treatment Strategies. *J Hepatocell Carcinoma* (2017) 4:93–103. doi: 10.2147/JHC.S106529
7. Yeo W, Mok TS, Zee B, Leung TW, Lai PB, Lau WY, et al. A Randomized Phase III Study of Doxorubicin Versus Cisplatin/Interferon α-2b/Doxorubicin/Fluorouracil (PIAF) Combination Chemotherapy for Unresectable Hepatocellular Carcinoma. *J Natl Cancer Inst* (2005) 97(20):1532–8. doi: 10.1093/jnci/dji315
8. Manov I, Pollak Y, Broneshter R, Iancu TC. Inhibition of Doxorubicin-Induced Autophagy in Hepatocellular Carcinoma Hep3B Cells by Sorafenib—The Role of Extracellular Signal-Regulated Kinase Counteraction. *FEBS J* (2011) 278 (18):3494–507. doi: 10.1111/j.1742-4658.2011.08271.x
9. Lu YL, Ma YB, Feng C, Zhu DL, Liu J, Chen L, et al. Co-Delivery of Cyclopamine and Doxorubicin Mediated by Bovine Serum Albumin Nanoparticles Reverses Doxorubicin Resistance in Breast Cancer by Down-Regulating P-Glycoprotein Expression. *J Cancer* (2019) 10(10):2357–68. doi: 10.7150/jca.30323
10. Stefanski CD, Keffler K, McClintock S, Milac L, Prosperi JR. APC Loss Affects DNA Damage Repair Causing Doxorubicin Resistance in Breast Cancer Cells. *Neoplasia* (2019) 21(12):1143–50. doi: 10.1016/j.neo.2019.09.002
11. Xiang X, Yuan D, Liu Y, Li J, Wen Q, Kong P, et al. PIM1 Overexpression in T-Cell Lymphomas Protects Tumor Cells From Apoptosis and Confers Doxorubicin Resistance by Upregulating C-Myc Expression. *Acta Biochim Biophys Sin (Shanghai)* (2018) 50(8):800–6. doi: 10.1093/abbs/gmy076
12. Chen C, Lu L, Yan S, Yi H, Yao H, Wu D, et al. Autophagy and Doxorubicin Resistance in Cancer. *Anticancer Drugs* (2018) 29(1):1–9. doi: 10.1097/CAD.0000000000000572
13. Christowitz C, Davis T, Isaacs A, van Niekerk G, Hattingh S, Engelbrecht AM. Mechanisms of Doxorubicin-Induced Drug Resistance and Drug Resistant Tumour Growth in a Murine Breast Tumour Model. *BMC Cancer* (2019) 19 (1):757. doi: 10.1186/s12885-019-5939-z
14. Guo B, Tam A, Santi SA, Parissenti AM. Role of Autophagy and Lysosomal Drug Sequestration in Acquired Resistance to Doxorubicin in MCF-7 Cells. *BMC Cancer* (2016) 16(1):762. doi: 10.1186/s12885-016-2790-3
15. Lohitesh K, Chowdhury R, Mukherjee S. Resistance a Major Hindrance to Chemotherapy in Hepatocellular Carcinoma: An Insight. *Cancer Cell Int* (2018) 18:44. doi: 10.1186/s12935-018-0538-7
16. Huang J, Liu K, Yu Y, Xie M, Kang R, Vernon P, et al. Targeting HMGB1-Mediated Autophagy as a Novel Therapeutic Strategy for Osteosarcoma. *Autophagy* (2012) 8(2):275–7. doi: 10.4161/auto.8.2.18940
17. Yang HZ, Ma Y, Zhou Y, Xu LM, Chen XJ, Ding WB, et al. Autophagy Contributes to the Enrichment and Survival of Colorectal Cancer Stem Cells Under Oxaliplatin Treatment. *Cancer Lett* (2015) 361(1):128–36. doi: 10.1016/j.canlet.2015.02.045
18. Shi YH, Ding ZB, Zhou J, Hui B, Shi GM, Ke AW, et al. Targeting Autophagy Enhances Sorafenib Lethality for Hepatocellular Carcinoma *via* ER Stress-Related Apoptosis. *Autophagy* (2011) 7(10):1159–72. doi: 10.4161/auto.7.10.16818
19. Sheng J, Qin H, Zhang K, Li B, Zhang X. Targeting Autophagy in Chemotherapy-Resistant of Hepatocellular Carcinoma. *Am J Cancer Res* (2018) 8(3):354–65.
20. He SJ, Cheng J, Feng X, Yu Y, Tian L, Huang Q. The Dual Role and Therapeutic Potential of High-Mobility Group Box 1 in Cancer. *Oncotarget* (2017) 8(38):64534–50. doi: 10.18632/oncotarget.17885
21. Tang D, Kang R, Zeh HJ3rd, Lotze MT. High-Mobility Group Box 1 and Cancer. *Biochim Biophys Acta* (2010) 1799(1-2):131–40. doi: 10.1016/j.bbagrm.2009.11.014
22. Ando K, Sakoda M, Ueno S, Hiwatashi K, Iino S, Minami K, et al. Clinical Implication of the Relationship Between High Mobility Group Box-1 and Tumor Differentiation in Hepatocellular Carcinoma. *Anticancer Res* (2018) 38 (6):3411–8. doi: 10.21873/anticanres.12609

23. Zhou J, Yang Y, Gan T, Li Y, Hu F, Hao N, et al. Lung Cancer Cells Release High Mobility Group Box 1 and Promote the Formation of Neutrophil Extracellular Traps. *Oncol Lett* (2019) 18(1):181–8. doi: 10.3892/ol.2019.10290
24. Huang CY, Chiang SF, Chen WT, Ke TW, Chen TW, You YS, et al. HMGB1 Promotes ERK-Mediated Mitochondrial Drp1 Phosphorylation for Chemoresistance Through RAGE in Colorectal Cancer. *Cell Death Dis* (2018) 9(10):1004. doi: 10.1038/s41419-018-1019-6
25. Zhan Z, Li Q, Wu P, Ye Y, Tseng HY, Zhang L, et al. Autophagy-Mediated HMGB1 Release Antagonizes Apoptosis of Gastric Cancer Cells Induced by Vincristine *via* Transcriptional Regulation of Mcl-1. *Autophagy* (2012) 8:109–21. doi: 10.4161/auto.8.1.18319
26. Pan B, Chen D, Huang J, Wang R, Feng B, Song H, et al. HMGB1-Mediated Autophagy Promotes Docetaxel Resistance in Human Lung Adenocarcinoma. *Mol Cancer* (2014) 13:165. doi: 10.1186/1476-4598-13-165
27. Zhang R, Li Y, Wang Z, Chen L, Dong X, Nie X. Interference With HMGB1 Increases the Sensitivity to Chemotherapy Drugs by Inhibiting HMGB1-Mediated Cell Autophagy and Inducing Cell Apoptosis. *Tumour Biol* (2015) 36(11):8585–92. doi: 10.1007/s13277-015-3617-6
28. Chai W, Ye F, Zeng L, Li Y, Yang L. HMGB1-Mediated Autophagy Regulates Sodium/Iodide Symporter Protein Degradation in Thyroid Cancer Cells. *J Exp Clin Cancer Res* (2019) 38(1):325. doi: 10.1186/s13046-019-1328-3
29. Liu W, Zhang Z, Zhang Y, Chen X, Guo S, Lei Y, et al. HMGB1-Mediated Autophagy Modulates Sensitivity of Colorectal Cancer Cells to Oxaliplatin *via* MEK/ERK Signaling Pathway. *Cancer Biol Ther* (2015) 16(4):511–7. doi: 10.1080/15384047.2015.1017691
30. Chen S, Wang Y, Ruan W, Wang X, Pan C. Reversing Multidrug Resistance in Hepatocellular Carcinoma Cells by Inhibiting Extracellular Signal-Regulated Kinase/Mitogen-Activated Protein Kinase Signaling Pathway Activity. *Oncol Lett* (2014) 8(5):2333–9. doi: 10.3892/ol.2014.2521
31. Yue Y, Zhou T, Gao Y, Zhang Z, Li L, Liu L, et al. High Mobility Group Box 1/Toll-Like Receptor 4/Myeloid Differentiation Factor 88 Signaling Promotes Progression of Gastric Cancer. *Tumour Biol* (2017) 39(3):1010428317694312. doi: 10.1177/1010428317694312
32. Cheng P, Ma Y, Gao Z, Duan L. High Mobility Group Box 1 (HMGB1) Predicts Invasion and Poor Prognosis of Glioblastoma Multiforme *via* Activating AKT Signaling in an Autocrine Pathway. *Med Sci Monit* (2018) 24:8916–24. doi: 10.12659/MSM.912104
33. Snow K, Judd W. Characterisation of Adriamycin- and Amsacrine-Resistant Human Leukaemic T Cell Lines. *Br J Cancer* (1991) 63(1):17–28. doi: 10.1038/bjc.1991.7
34. Kudo M. Systemic Therapy for Hepatocellular Carcinoma: 2017 Update. *Oncology* (2017) 93(Suppl 1):135–46. doi: 10.1159/000481244
35. Usmani A, Mishra A, Arshad M, Jafri A. Development and Evaluation of Doxorubicin Self Nanoemulsifying Drug Delivery System With Nigella Sativa Oil Against Human Hepatocellular Carcinoma. *Artif Cells Nanomed Biotechnol* (2019) 47(1):933–44. doi: 10.1080/21691401.2019.1581791
36. Zhang B, Yin X, Sui S. Resveratrol Inhibited the Progression of Human Hepatocellular Carcinoma by Inducing Autophagy *via* Regulating P53 and the Phosphoinositide 3-Kinase/Protein Kinase B Pathway. *Oncol Rep* (2018) 40 (5):2758–65. doi: 10.3892/or.2018.6648
37. Tang D, Kang R, Livesey KM, Cheh CW, Farkas A, Loughran P, et al. Endogenous HMGB1 Regulates Autophagy. *J Cell Biol* (2010) 190(5):881–92. doi: 10.1083/jcb.200911078
38. Lin SC, Hardie DG. AMPK: Sensing Glucose as Well as Cellular Energy Status. *Cell Metab* (2018) 27(2):299–313. doi: 10.1016/j.cmet.2017.10.009
39. Liang P, Jiang B, Li Y, Liu Z, Zhang P, Zhang M, et al. Autophagy Promotes Angiogenesis *via* AMPK/Akt/mTOR Signaling During the Recovery of Heat-Denatured Endothelial Cells. *Cell Death Dis* (2018) 9(12):1152. doi: 10.1038/s41419-018-1194-5
40. Whang YM, Kim MJ, Cho MJ, Yoon H, Choi YW, Kim TH, et al. Rapamycin Enhances Growth Inhibition on Urothelial Carcinoma Cells Through LKB1 Deficiency-Mediated Mitochondrial Dysregulation. *J Cell Physiol* (2019) 234 (8):13083–96. doi: 10.1002/jcp.27979
41. Liu J, Long S, Wang H, Liu N, Zhang C, Zhang L, et al. Blocking AMPK/ULK1-Dependent Autophagy Promoted Apoptosis and Suppressed Colon Cancer Growth. *Cancer Cell Int* (2019) 19:336. doi: 10.1186/s12935-019-1054-0
42. Hu Y, Tao Y, Hu J. Cannabinoid Receptor 2 Deletion Deteriorates Myocardial Infarction Through the Down-Regulation of AMPK-mTOR-P70s6k Signaling-Mediated Autophagy. *Biosci Rep* (2019) 39(4):BSR20180650. doi: 10.1042/BSR20180650
43. Gao L, Lv G, Li R, Liu WT, Zong C, Ye F, et al. Glycochenodeoxycholate Promotes Hepatocellular Carcinoma Invasion and Migration by AMPK/mTOR Dependent Autophagy Activation. *Cancer Lett* (2019) 454:215–23. doi: 10.1016/j.canlet.2019.04.009
44. Suvorova II, Pospelov VA. AMPK/Ulk1-Dependent Autophagy as a Key mTOR Regulator in the Context of Cell Pluripotency. *Cell Death Dis* (2019) 10:260. doi: 10.1038/s41419-019-1501-9
45. Cox J, Weinman S. Mechanisms of Doxorubicin Resistance in Hepatocellular Carcinoma. *Hepat Oncol* (2016) 3(1):57–9. doi: 10.2217/hep.15.41
46. Nies AT, König J, Pfannschmidt M, Klar E, Hofmann WJ, Keppler D. Expression of the Multidrug Resistance Proteins MRP2 and MRP3 in Human Hepatocellular Carcinoma. *Int J Cancer* (2001) 94(4):492–9. doi: 10.1002/ijc.1498
47. Hyuga S, Shiraishi M, Hori A, Hyuga M, Hanawa T. Effects of Kampo Medicines on MDR-1-Mediated Multidrug Resistance in Human Hepatocellular Carcinoma HuH-7/PTX Cells. *Biol Pharm Bull* (2012) 35 (10):1729–39. doi: 10.1248/bpb.b12-00371
48. Ye CG, Wu WK, Yeung JH, Li HT, Li ZJ, Wong CC, et al. Indomethacin and SC236 Enhance the Cytotoxicity of Doxorubicin in Human Hepatocellular Carcinoma Cells via Inhibiting P-Glycoprotein and MRP1 Expression. *Cancer Lett* (2011) 304(2):90–6. doi: 10.1016/j.canlet.2011.01.025
49. Su Z, Wang T, Zhu H, Zhang P, Han R, Liu Y, et al. HMGB1 Modulates Lewis Cell Autophagy and Promotes Cell Survival *via* RAGE-HMGB1-Erk1/2 Positive Feedback During Nutrient Depletion [Published Correction Appears in Immunobiology. 2018 Feb;223(2):258]. *Immunobiology* (2015) 220(5):539–44. doi: 10.1016/j.imbio.2014.12.009
50. Wang L, Zhang H, Sun M, Yin Z, Qian J. High Mobility Group Box 1-Mediated Autophagy Promotes Neuroblastoma Cell Chemoresistance. *Oncol Rep* (2015) 34(6):2969–76. doi: 10.3892/or.2015.4278
51. Huang J, Ni J, Liu K, Yu Y, Xie M, Kang R, et al. HMGB1 Promotes Drug Resistance in Osteosarcoma. *Cancer Res* (2012) 72(1):230–8. doi: 10.1158/0008-5472.CAN-11-2001
52. Tang D, Kang R, Cheh CW, Livesey KM, Liang X, Schapiro NE, et al. HMGB1 Release and Redox Regulates Autophagy and Apoptosis in Cancer Cells. *Oncogene* (2010) 29:5299–310. doi: 10.1038/onc.2010.261
53. Sun Y, Lei B, Huang Q. SOX18 Affects Cell Viability, Migration, Invasiveness, and Apoptosis in Hepatocellular Carcinoma (HCC) Cells by Participating in Epithelial-To-Mesenchymal Transition (EMT) Progression and Adenosine Monophosphate Activated Protein Kinase (AMPK)/Mammalian Target of Rapamycin(mTOR). *Med Sci Monit* (2019) 25:6244–54. doi: 10.12659/MSM.915729
54. Foglio E, Puddighinu G, Germani A, Russo MA, Limana F. HMGB1 Inhibits Apoptosis Following MI and Induces Autophagy *via* Mtorc1 Inhibition. *J Cell Physiol* (2017) 232(5):1135–43. doi: 10.1002/jcp.25576
55. Jiang J, Chen S, Li K, Zhang C, Tan Y, Deng Q, et al. Targeting Autophagy Enhances Heat Stress-Induced Apoptosis *via* the ATP-AMPK-mTOR Axis for Hepatocellular Carcinoma. *Int J Hyperthermia* (2019) 36(1):499–510. doi: 10.1080/02656736.2019.1600052


**Conflict of Interest:** The authors declare that the research was conducted in the absence of any commercial or financial relationships that could be construed as a potential conflict of interest.

**Publisher's Note:** All claims expressed in this article are solely those of the authors and do not necessarily represent those of their affiliated organizations, or those of the publisher, the editors and the reviewers. Any product that may be evaluated in this article, or claim that may be made by its manufacturer, is not guaranteed or endorsed by the publisher.

frontiers in Oncology

ORIGINAL RESEARCH
published: 08 November 2021
doi: 10.3389/fonc.2021.782065

# LY294002 Is a Promising Inhibitor to Overcome Sorafenib Resistance in FLT3-ITD Mutant AML Cells by Interfering With PI3K/Akt Signaling Pathway

*Amin Huang[1*†], Peiting Zeng[2†], Yinguang Li[3], Wenhua Lu[2] and Yaoming Lai[4]*

*[1] Department of Medical Oncology of the East Division, The First Affiliated Hospital, Sun Yat-Sen University, Guangzhou, China, [2] State Key Laboratory of Oncology in Southern China, Sun Yat-Sen University Cancer Center, Guangzhou, China, [3] Department of Obstetrics and Gynecology of the East Division, The First Affiliated Hospital, Sun Yat-Sen University, Guangzhou, China, [4] Department of Rehabilitation, The Fifth Affiliated Hospital of Guangzhou Medical University, Guangzhou, China*

OPEN ACCESS

**Edited by:**
*Qingbin Cui,*
*University of Toledo, United States*

**Reviewed by:**
*Kaiyan Liu,*
*University of Maryland, Baltimore, United States*
*Lisi Zeng,*
*Affiliated Cancer Hospital & Institute of Guangzhou Medical University, China*

***Correspondence:**
*Amin Huang*
*huangam3@mail.sysu.edu.cn*

*[†]These authors share first authorship*

**Specialty section:**
*This article was submitted to Pharmacology of Anti-Cancer Drugs, a section of the journal Frontiers in Oncology*

**Received:** *23 September 2021*
**Accepted:** *13 October 2021*
**Published:** *08 November 2021*

**Citation:**
*Huang A, Zeng P, Li Y, Lu W and Lai Y (2021) LY294002 Is a Promising Inhibitor to Overcome Sorafenib Resistance in FLT3-ITD Mutant AML Cells by Interfering With PI3K/Akt Signaling Pathway. Front. Oncol. 11:782065. doi: 10.3389/fonc.2021.782065*

Internal tandem duplications (ITD) mutation within FMS-like tyrosine kinase 3 (FLT3), the most frequent mutation happens in almost 20% acute myeloid leukemia (AML) patients, always predicts a poor prognosis. As a small molecule tyrosine kinase inhibitor, sorafenib is clinically used for the treatment of advanced renal cell carcinoma (RCC), hepatocellular carcinoma (HCC), and differentiated thyroid cancer (DTC), with its preclinical and clinical activity demonstrated in the treatment of Fms-like tyrosine kinase 3-internal tandem duplication (FLT3-ITD) mutant AML. Even though it shows a rosy future in the AML treatment, the short response duration remains a vital problem that leads to treatment failure. Rapid onset of drug resistance is still a thorny problem that we cannot overlook. Although the mechanisms of drug resistance have been studied extensively in the past years, there is still no consensus on the exact reason for resistance and without effective therapeutic regimens established clinically. My previous work reported that sorafenib-resistant FLT3-ITD mutant AML cells displayed mitochondria dysfunction, which rendered cells depending on glycolysis for energy supply. In my present one, we further illustrated that losing the target protein FLT3 and the continuously activated PI3K/Akt signaling pathway may be the reason for drug resistance, with sustained activation of PI3K/AKT signaling responsible for the highly glycolytic activity and adenosine triphosphate (ATP) generation. PI3K inhibitor, LY294002, can block PI3K/AKT signaling, further inhibit glycolysis to disturb ATP production, and finally induce cell apoptosis. This finding would pave the way to remedy the FLT3-ITD mutant AML patients who failed with FLT3 targeted therapy.

**Keywords: FMS-like tyrosine kinase 3, Internal tandem duplication, LY294002, Drug resistance, Acute myeloid leukemia, PI3K/Akt**

## INTRODUCTION

Internal tandem duplications (ITD) mutation, the most frequent mutation in the juxtamembrane domain of the FMS-like tyrosine kinase 3 (FLT3) gene, was found in almost 20% of all acute myeloid leukemia (AML) patients (1, 2). This mutation leads to constitutive activation of FLT3 and its downstream signaling, including phosphatidylinositol3-kinase (PI3K)/AKT, mitogen-activated protein kinase/extracellular signal-regulated kinase (MAPK/ERK), and signal transducer and activator of transcription5 (STAT5). It also results in cell proliferation and disease progress (3–5). It is demonstrated that FLT3 mutational status, an independent predictor of poor prognosis, was closely associated with chemotherapy efficacy and disease relapse (6, 7). Many inhibitors targeting FLT3 kinase are under development, with some already demonstrating their efficacy in treating FLT3-ITD mutant AML (8–10).

Sorafenib, firstly known for its antiangiogenic effect and approved for treating HCC, RCC and DTC, is found potent in inhibiting FLT3, with a significant anti-tumor effect in the FLT3-ITD mutant AML (11–13). Clinical trials of sorafenib were widely conducted in the first-line induction, relapsed or refractory and post-transplant maintenance period, as a single agent, and in combination with chemotherapy and hypomethylating agents. Farhad et al. reported the combination of sorafenib and chemotherapy (cytarabine and idarubicin) resulted in a higher CR rate in FLT3-mutated patients than that of the FLT3-WT patients (14). However, no significant difference in overall survival (OS) or disease-free survival (DFS) was observed in the final analysis due to the emergence of sorafenib-resistant leukemic clones (15). SORAML, a phase 2 trial, investigated the effect of sorafenib in consolidation therapy and maintenance. Median event-free survival in the sorafenib group was 21months versus 9 months in the placebo group. The combination effect of sorafenib with azacitidine in older patients unsuitable for intensive induction therapy was evaluated. In the 27 patients enrolled, 7 patients reached CR, 12 CRi/CRp, and 2 PR, with an overall response rate, 78% (16). As monotherapy, sorafenib has been proven effective in the salvage therapy for R/R FLT3-ITD AML and maintenance after transplantation by reducing the possibility of relapse and death (17, 18). Besides sorafenib, other FLT3 inhibitors, such as midostaurin, gilteritinib and quizartinib were also approved by Food and Drug Administration (FDA) for treating FLT3 mutant AML (19–22). Both European LeukemiaNet and National Comprehensive Cancer Network guidelines recommend FLT3 genetic testing to predict the prognosis and evaluate the targeted therapy when the disease is diagnosed and relapsed.

Eventhough FLT3 inhibitors are promising in treating FLT3-ITD mutant AML patients, the limitations should not be ignored: drug resistance that often occurs within 1–3 months after initial remission responses, resulting in disease relapse and treatment failure (23). As massive studies have investigated the resistance mechanism, multiple mechanisms have been proposed, including increased efflux of drugs induced by ATP-binding cassette (ABC) proteins, the emergence of new mutations, up-regulation of FLT3 ligand, aberrant activation of pro-survival signaling, rewired metabolic profiles and redox change (24–32). However, there is still no consensus on the precise mechanisms of drug resistance, and more efforts should be taken in clarifying the mechanisms and exploring new strategies to reverse this resistance.

In my previous paper, we established two sorafenib-resistant cell lines and compared the metabolic differences between the resistant cells and their corresponding parental cells. We found the resistant cells were with mitochondria dysfunction and active aerobic glycolysis (30). In my present work, we will further elucidate the relationship between PI3K/Akt signaling and glycolysis and investigate the possibility of overcoming this resistance by interfering PI3K/Akt signaling pathway.

## MATERIALS AND METHODS

### Cell Lines and Cell Culture

Human FLT3-ITD mutant cell line: MV4-11 was ordered from ATCC. BaF3-ITD cell line was established as described previously from mouse hematopoietic progenitor BaF3 cell line (33). All parental cells were cultured in RPMI 1640 with 2.05 mM L-Glutamine (Hyclone, South Logan, UT, USA) and 10% Fetal Bovine Serum (Hyclone, South Logan, UT, USA) in the incubator with 5% CO2 at 37°C.

### Generation of the Drug-Resistant Cell Lines

To generate drug-resistant cell lines, we co-cultured the BaF3-ITD and MV4-11 cells with sorafenib with the initial concentration of 1 nM. When the cells could survive in the present concentration for 3-5 days, the concentration of sorafenib would be improved to a higher dose. Three months later, the resistant cell lines, MV4-11-R and BaF3-ITD-R cell lines could grow in a medium containing 0.5μM sorafenib. The sorafenib-resistant cells were continuously cultured in the RPMI 1640 medium with 0.5 μM sorafenib.

### Chemical Compounds and Biologic Reagents

All small molecule inhibitors were obtained from Selleck Chemicals (Houston, TX, USA), these inhibitors include: Sorafenib tosylate (#S1040), PI3K inhibitors: LY294002 (#S1105), Buparlisib (#S2247), Pictilisib (#S1065), Alpelisib (#S2814) and Akt inhibitors MK2206 (#S1078), Ipatasertib (#S2808), Afuresertib (#S7521). All chemicals formulated by their suppliers' recommendations.

### Antibodies

Antibodies of anti–HK2 (#2867), anti–PKM2 (#4053), anti–P-FLT3 (#3464), anti–FLT3 (#3462), anti–Akt (#4691), anti–P-Akt (#4060), anti–PARP (#9542) were obtained from Cell Signaling Technologies (Beverly, MA, USA); Antibodies of anti–PDK1 (#ab11025), anti–β-actin (#ab8227), goat anti-Rabbit secondary HRP-conjugated antibody (#ab6721), and goat anti-Mouse secondary HRP-conjugated antibody (#ab6789) were supplied by Abcam (Cambridge, UK).

## Cell Proliferation Assays

Cell viability assay was performed using CellTiter 96 AQueous One Solution Reagent (Promega, Madison, WI, USA) according to the manufacturer's recommendations. Briefly, cells were plated in 96-well microplates in triplicate at a density of $3\times10^5$cells/ml and treated as indicated for 72 hrs. Then 20 μl of a tetrazolium compound (MTS) was added to each well for 4 h at 37°C. After incubation, the absorbance was read at a wave length of 490 nm. Accordingly, cell viability is reported as percentage of control (untreated) cells, with the data representing three independent experiments. Error bars represent the standard error of the mean for each data point.

## Western Blot

Protein was extracted by RIPA lysis buffer supplemented with protease inhibitor cocktail set I and phosphatase inhibitor cocktail set II (Calbiochem, Nottingham, England). Equal amounts of protein extracts were resolved in 4%-12% standard SDS-PAGE and transferred to polyvinylidenedifluoride (PVDF) membranes. Membranes were probed with primary antibody overnight at 4°C and Horseradish peroxidase (HRP)-conjugated secondary antibody for 1 h at room temperature, with the protein band visualized by chemiluminescent detection kit with ClarityTM Western ECL Substrate from Bio-Rad Laboratories (Richmond, CA, USA). The images were captured using Bio-Rad ChemiDoc Imaging System.

## Quantitative Real-Time PCR

Ribonucleic acid (RNA) was isolated with TRIzol reagent (Invitrogen, Paisley, United Kingdom), and complementary DNA (cDNA) was generated using PrimeScript RT reagent Kit (Takara Shuzo, Shiga, Japan) according to the manufacturer's recommendation. Quantitative real-time polymerase chain reaction (PCR) was performed with SYBR Premix Ex Taq II (Takara Shuzo, Shiga, Japan) according to the manufacturer's recommendation. The quantitative polymerase chain reaction was carried out in triplicate on a CFX96 multicolor real-time PCR system (Bio-Rad, Richmond, CA).β-actin was used as an internal standard. The PCR primers are listed in **Table 1**.

## Flow Cytometry

Apoptosis detection kit containing Annexin-V-FITC, propidiumiodide (PI) and binding buffer were purchased from Keygen Biotech (Nanjing, China). To detect apoptosis, cells were seeded in a 6-well plate at the density of $3\times10^5$ cells/well and incubated with designated drugs for 48h. The cells were collected and washed with cold phosphate-buffered saline (PBS) three times. Each sample was suspended in 500 μl binding buffer containing 5 μl Annexin-V-FITC, 5 μl PI, and incubated for 15 min in the dark at room temperature. The cells were analyzed by CytoFlex flow cytometry (Becton Dickinson, Heidelberg, Germany) and CytExpert software. The results shown here represent three independent experiments.

## Glucose Uptake and Lactate Production

To determine the cellular glucose uptake and lactate production, cells were collected and seeded in triplicate at the density of $1\sim2\times10^6$ cells/well and treated with certain drugs for indicated times. Culture mediums were removed to analyze glucose and lactate content with the fresh medium as control using a SBA-40C biosensor (Biology institute of Shandong academy of science, Jinan, Shandong province) according to the manufacturer's instruction.

## Statistical Analysis

The statistical analyses were performed with SPSS version 18.0 software (SPSS Inc., Chicago, IL, USA). Comparisons between groups were analyzed by the Student paired t test. Multiple groups were compared using analysis of variance (ANOVA) followed by post-hoc Fisher's least significant difference (LSD) testing when appropriate. Significance was judged when $p<0.05$.

# RESULTS

## Evaluation of the Drug-Resistant Characteristics: Comparison of Proliferation and Apoptosis in the Presence of Sorafenib

Two sorafenib resistant cell lines, MV4-11-R and BaF3-ITD-R, generated from the parental MV4-11 and BaF3-ITD cells should be continuously maintained in the medium containing 0.5 μM sorafenib. When deprived with sorafenib treatment they may lose the drug resistance. After a long time to store in the liquid nitrogen, it's necessary to confirm the drug resistance prior to use. Cell viability and cell apoptosis assays were utilized to evaluate the drug resistance characteristics. Cell viability of MV4-11 and MV4-11-R cells responding to increasing concentrations of sorafenib for 72 h, and that of BaF3-ITD and BaF3-ITD-R were

**TABLE 1** | Specific primer sequences used in this paper (5′-3′).

| | Gene name | Forward | Reverse | Accession number |
|---|---|---|---|---|
| Homo | PKM2 | CCACTTGCAATTATTTGAGGAA | GTGAGCAGACCTGCCAGACT | NM_002654 |
| | HK2 | CAAAGTGACAGTGGGTGTGG | GCCAGGTCCTTCACTGTCTC | NM_000189 |
| | β-actin | AACTCCATCATGAAGTGTGACG | GATCCACATCTGCTGGAAGG | NM_001101 |
| | LDHA | ATCTTGACCTACGTGGCTTGGA | CCATACAGGCACACTGGAATCTC | NM_005566 |
| | GLUT1 | CGGGCCAAGAGTGTGCTAAA | TGACGATACCGGAGCCAATG | NM_006516 |
| | FLT3 | CTTCCCTTTCATCCAAGACAACATC | ATCCACATTCTGATACATCGCTTCT | NM_004119 |
| musculus | β-actin | GTGACGTTGACATCCGTAAAGA | GCCGGACTCATCGTACTCC | NM_007392 |
| | flt3 | TTTCATCCAAGACAACATCTCCTTC | CTAAAAATGAAGTCAGGTTGGGGAA | NM_010229 |

shown in **Figure 1A**. The IC50 values of the two pairs of cells were evaluated. We estimated the IC50 for resistant cell line MV4-11-R and BaF3-ITD-R is 2.43 μM and 1.52 μM, which is significantly higher than 4.35 nM in MV4-11 and 4.85 nM in BaF3-ITD. By analyzing the cell viability, we confirmed the resistant cell lines were resistant to sorafenib treatment.

Furthermore, flow cytometry was used to evaluate apoptosis when cells were treated with sorafenib. As shown in **Figure 1B**, we didn't observe any cell apoptosis after incubation MV4-11-R and BaF3-ITD-R cells with 0.25 μM sorafenib for 48h. However, after incubating the parental cells in 0.25 μM sorafenib for 48h, significant cell apoptosis was observed in MV4-11 and BaF3-ITD cells (31.2% and 40.4%, respectively). When the concentration was increased to 0.5 μM, more apoptosis was detected in the parental cells, and still no apoptosis was observed in the resistant cells. From this figure, we further confirmed the resistant cells kept their drug-resistance characteristics after long time of storing in liquid nitrogen.

## The Significant Restraining of FLT3 Is Concurrent With Sustained Activation of PI3K/Akt Signaling in the Resistant Cells

Sorafenib induced FLT3-ITD mutant AML cell death by targeting FLT3 and downstream signaling, including PI3K/AKT, MAPK/ERK, and STAT5. Firstly, the FLT3 gene expression examined by PCR and then visualized by agarose gel electrophoresis in **Figure 2A** indicated that FLT3 gene expression was dramatically inhibited by sorafeinb in the resistant cells. Corresponding to the gene expression, FLT3 and phosphorylated FLT3 protein expression were not observed in the sorafenib-resistant cells compared with the parental cells (**Figure 2B**). However, the phosphorylated Akt was remarkablely activated (**Figure 2C**), indicating the lost target protein may be responsible for drug resistance to FLT3 inhibitors. However, PI3K/Akt signaling's sustained activation may provide survival advantages for the resistant cells.

## The Resistant Cells Rely on Glucose for Proliferation

The activation of the PI3K/Akt signaling pathway is known to regulate cell death and survival, and enhance glycolytic activity and metabolism (34). Plentiful work had shown that increased Akt activation could directly phosphorylate a number of glycolytic enzymes such as hexokinase 2 (HK2) (35). Based on the hyper-activation of PI3K/Akt signaling, we firstly examined glycolytic genes, including HK2, pyruvate kinase isozyme M2 (PKM2), lactate dehydrogenase A (LDHA), and glucose transporter type 1 (GLUT1), found HK2, PKM2 and GLUT1 genes were over-expressed in varying degrees in the resistant cells. Western blotting further confirmed the up-regulation of HK2, PKM2 and 3-phosphoinositide dependent kinase-1 (PDK1) in protein level, as shown in **Figures 3A, B**. When the glucose in the medium was

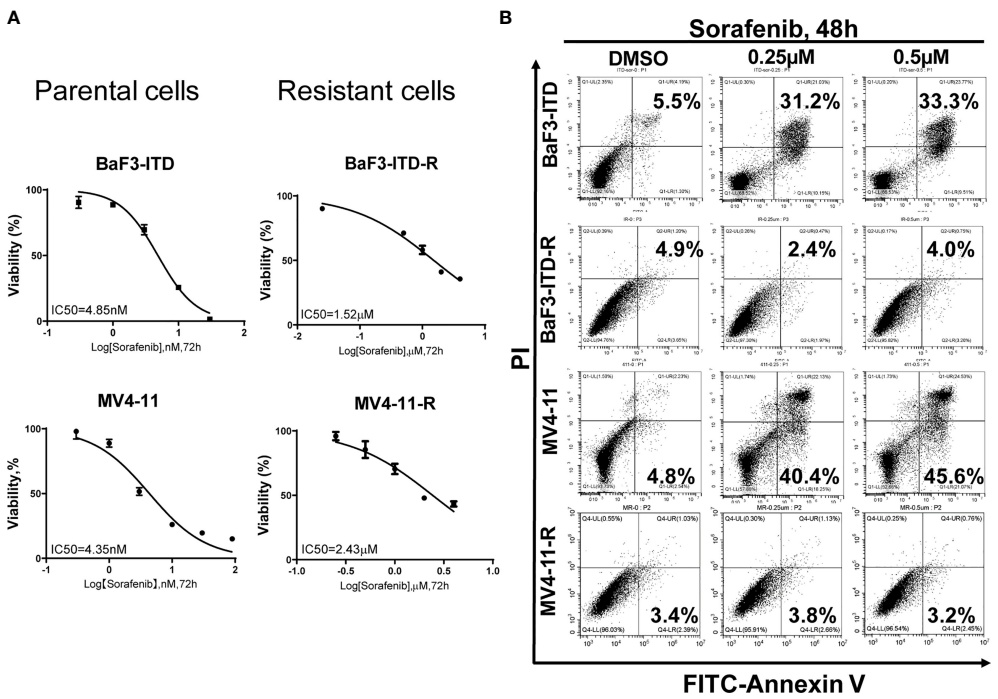


**FIGURE 1** | Comparison of the cell proliferation and apoptosis of the parental and sorafenib-resistant cell lines in the presence of sorafenib. **(A)** The sorafenib-resistant cells, MV4-11-R and BaF3-ITD-R, and parental BaF3-ITD and MV4-11 cells were incubated with increasing concentrations of sorafenib for 72 hours. Cell viability (%) was compared. Data represent three independent experiments. **(B)** Cells were exposed to sorafenib at the indicated concentrations for 48 hours. The apoptotic cells were stained with Annexin-V and propidium iodide (PI) for 15 mins and detected by flow cytometry in one hour. Data represent three independent experiments.

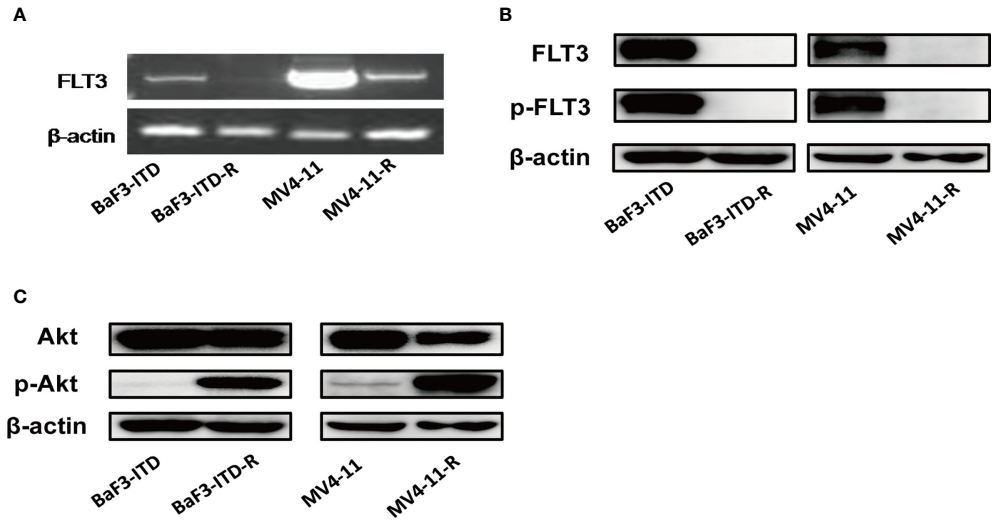


**FIGURE 2** | FLT3 and PI3K/Akt signaling were detected. **(A)** PCR product of FLT3 gene was applied to agarose gel electrophoresis. β-actin was used as an internal control. **(B, C)** The protein level of total FLT3, phosphorylated-FLT3, total Akt, phosphorylated-Akt in BaF3-ITD, BaF3-ITD-R, MV4-11, MV4-11-R cells were evaluated by immunoblotting, with β-actin used as aloading control.

deprived, the proliferation of resistant cells was inhibited more significantly than that of the corresponding parental cells, especially for MV4-11 cells, so deprivation of glucose indeed inhibited cells growth from 24h to 72h. However, this inhibition didn't show any statistical significance ($P>0.05$). However, this difference was more apparent for the MV4-11-R cells, with the cell growth suppressed significantly from 48h, as shown in **Figure 3C** ($P<0.001$). For BaF3-ITD and BaF3-ITD-R cell lines, same phenomenon was observed, as shown in **Figure 3D**, the inhibition effect was more apparent for the resistant cells at 48 h, 72 h, and 96h. That means the resistant cells are more dependent on glucose for cell proliferation and energy supply. Glycolysis is the major way of adenosine triphosphate (ATP) production for the resistant cells since mitochondria dysfunction was reported in my previous work (26). Intracellular ATP was measured when the enzymes relevant to glucose metabolism were interfered. By treating the resistant cells with 10 μM oxamate, a competitive LDHA inhibitor, for 6 hrs, we observed the ATP production was reduced to 62.8% and 60.7% for MV4-11-R and BaF3-ITD-R respectively ($P<0.001$). 2-deoxy-d-glucose (2-DG), a derivative of glucose, can be phosphorylated by hexokinase and interfere with glucose uptake. Similar phenomenon was observed when cells were treated with 10μM 2-DG for 6 hrs, with ATP production significantly reduced to 83.7% and 74.7% for MV4-11-R and BaF3-ITD-R, respectively ($P<0.05$) (**Figure 3E**). These results mean the resistant cells depended on glycolysis for survival and ATP production.

## PI3K/Akt Signaling Was Responsible for the Highly Activated Glycolytic Activity

To illustrate whether the highly expressed glycolytic enzymes were associated with retained activation of PI3K signaling, a pan-PI3K inhibitor, LY294002 was applied to treat the resistant cells. The real-time quantitative polymerase chain reaction (PCR) revealed that when the cells were treated with 20 μM LY294002 for 48 h, gene expression of HK2, PKM2 and Glut1 were obviously depleted (**Figure 4A**). Western Blot also verified the protein expression inhibition of glycolytic enzymes induced by LY294002 (**Figure 4B**). As the concentration of LY294002 increased, HK2 were significantly suppressed in both MV4-11-R and BaF3-ITD-R cells, however PDK1 and PKM2 level were not apparently influenced by LY294002 treatment. Moreover, co-culturing cells with 20 μM LY294002 for only 6 hrs, glucose uptake could be reduced to 72.8% and 73.5% for BaF3-ITD-R and MV4-11-R, respectively ($P<0.01$), with their lactate production inhibited to 89.2% and 85.3% ($P<0.05$) (**Figure 4C**). Thus, we speculate activation of PI3K/Akt axis maybe the incentive factor for the highly glycolysis of the drug-resistant cells and the crucial pathway for cell survival and proliferation. This leads us to investigate further whether blocking this pathway could be the potential therapeutic regimen to conquer drug-resistance.

## The Resistant Cells Were More Sensitive to PI3K Inhibitor LY294002

As a highly glycolytic activity of resistant cells is promoted by the activation of PI3K/Akt signaling, interfering with this signaling pathway can suppress glycolysis and cell growth. So, we speculated PI3K inhibitor could selectively induce resistant cell death and reverse drug resistance. To verify this hypothesis, the pan PI3K inhibitor LY294002 was adopted to treat drug-resistant cells. LY294002 could induce cell apoptosis for both the drug-resistant and the parental cells in a dose-dependent manner, but the apoptosis was more significant in the resistant cells. As illustrated in **Figure 5A**, in the presence of 40 μM LY294002 for 24h, the apoptotic rate of BaF3-ITD-R cells was 26.5%, while

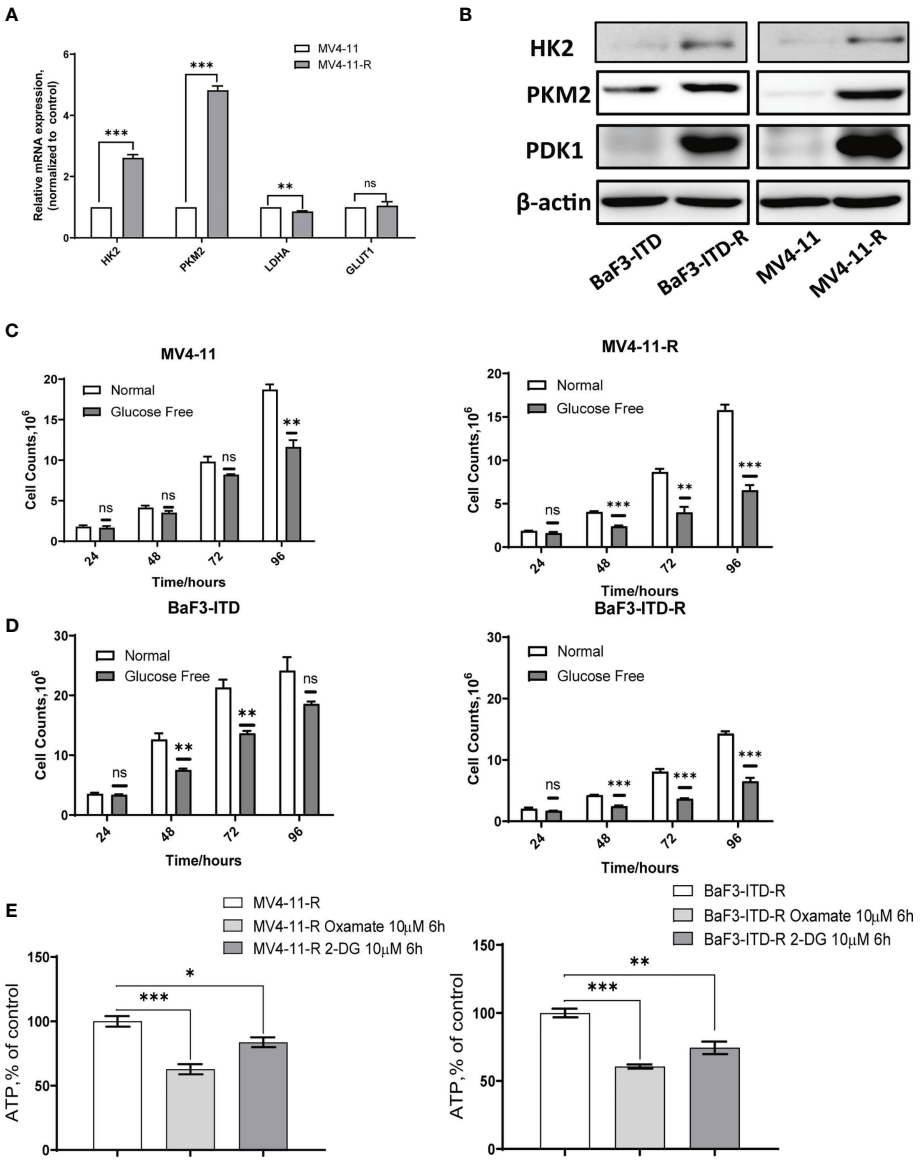


**FIGURE 3** | Sorafenib-resistant cells rely on glucose for proliferation and ATP generation. **(A)** Real-time quantitative PCR was used to compare the gene expression of glycolytic enzymes. **(B)** Western blot analysis of glycolytic enzyme HK2, PKM2 and PDK1. β-actin was shown as a loading control. **(C, D)** Cell counts were compared for the two pairs of cells after incubating with the normal and glucose-free medium for indicated times. **(E)** ATP production rate of the resistant cells was detected when treated with 10 μM Oxamate and 10 μM 2-DG, respectively, for 6 hours. *p < 0.05, **p < 0.01, ***p < 0.001, NS, No significance.

for the BaF3-ITD cells, the value was only 17.3%. When the concentration reached to 80 μM, 57.6% of apoptosis was observed in the resistant cell BaF3-ITD-R. However, the value was only 31.6% for the BaF3-ITD cells. The same phenomenon was observed in MV4-11 and MV4-11-R cells, with LY294002 inducing more apoptosis in the resistant cells than parental cells. Poly-ADP-ribose polymerase (PARP) and cleaved PARP were detected by western blotting to confirm the cell apoptosis induced by LY294002. As shown in **Figure 5B**, inhibition of PI3K by LY294002 induced the appearance of cleaved PARP in a dose-dependent manner. Treatment of BaF3-ITD and BaF3-ITD-R cells with 20 μM LY294002 for 24h witnessed prominent up-regulation of cleaved PARP in the BaF3-ITD-R cells, yet no obvious change was observed until the concentration comes to 80 μM, only slight change was detected for the BaF3-ITD cells. Similar results were observed in the MV4-11 and MV4-11-R cells. When cells were treated with 80 μM LY294002 for 24h, more apparent cleaved PARP was detected in the MV4-11-R cell line than that of MV4-11 cells. These results mean that the drug-resistant cells were much more sensitive to PI3K inhibitor, and LY294002 is promising in overcoming FLT3 inhibitor induced drug-resistance. We also evaluated the drug sensitivity of the other

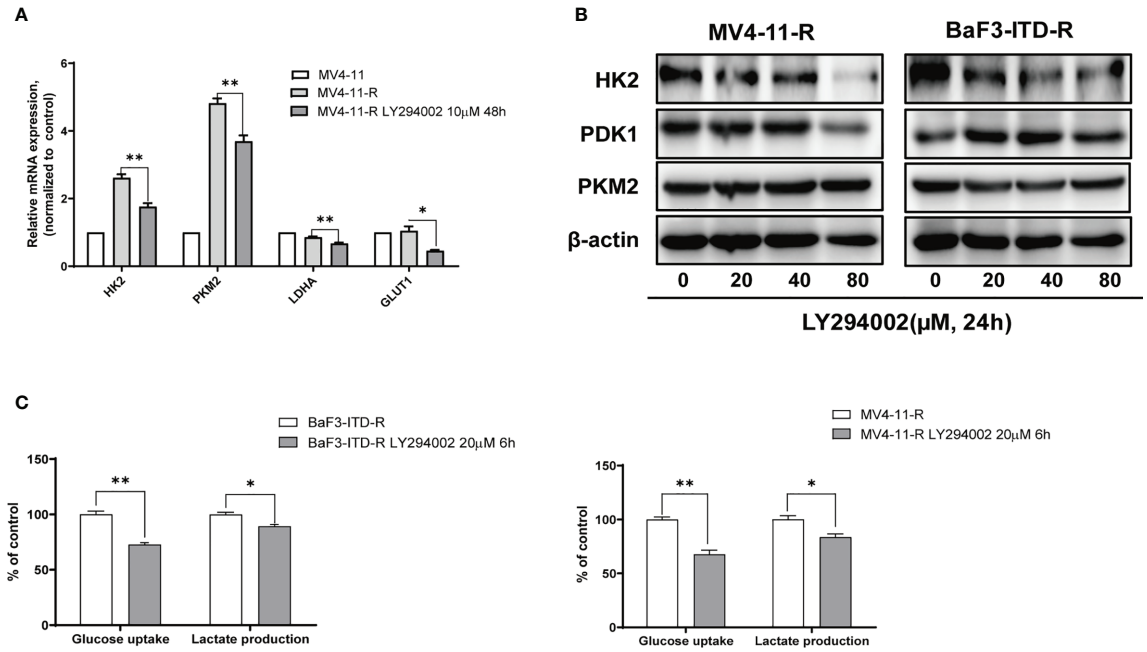


**FIGURE 4** | Gene expression of glycolytic enzymes and ATP generation were diminished by LY294002 in the resistant cells. **(A)** Incubating the MV4-11-R cells with 10 μM LY294002 for 48 hours, and messenger ribonucleic acid (mRNA) level of HK2, PKM2, LDHA, GLUT1 were compared. **(B)** The sorafenib-resistant cells, MV4-11-R and BaF3-ITD-R, were incubated with increasing concentrations of LY294002 for 24 hours, with the protein expression of HK2, PDK1 and PKM2 were evaluated by western blotting. β-actin was used as a loading control. **(C)** Glucose uptake and lactate production were evaluated when resistant cells were treated with 10μM LY294002 for 6 hours.*$p < 0.05$, **$p < 0.01$.

PI3K and Akt inhibitor, as shown in **Supplementary Figure 1**, we found the drug resistance cells showed resistant to all these inhibitors in different degrees. This means that it's not all the PI3K/Akt pathway inhibitors could overcome the drug resistance. As a PI3K inhibitor, LY294002 has its special function and mechanism that deserve further investigation.

## DISCUSSION

Internal tandem duplication of FLT3, the predictor of poor prognosis, occurs in a subset of patients with AML. Although various FLT3 inhibitors have been developed, with several applied to clinical practices, the development of drug resistance remains a major challenge. The mechanisms of drug resistance have been extensively studied, and efforts are underway to develop new strategies to overcome this resistance. However, no effective treatment procedure is found and approved clinically.

In this paper, we established two sorafenib-resistant cells by culturing BaF3-ITD and MV4-11 cells with increasing concentrations of sorafenib for almost three months. By comparing the resistant cells with their parental ones, we tried to investigate mechanisms of sorafenib resistance in human leukemic cell lines. The drug-resistance was firstly determined by calculating the IC50 value and detecting the cell apoptosis in the presence of sorafenib, with the resistant cells confirmed, highly resistant to sorafenib treatment. FLT3 is the target of FLT3 inhibitors. Western blot analysis revealed that prolonged sorafenib treatment resulted in significant down-regulation of total and phosphorylated FLT3 with the retained downstream signaling PI3K/Akt activated. My previous study also reported the resistant cells were cross-resistant to FLT3 inhibitor, protein kinase C 412 (PKC412) and tandutinib (MLN518) (30). That means the lost target protein FLT3 leads to ineffective of FLT3 inhibitors. However, sustained activation of PI3K/Akt pathway resulted in cell proliferation and survival. These together possibly explain the underlying mechanism for drug resistance.

The PI3K/Akt signaling pathway plays a vital role in regulating cell proliferation, survival, and apoptosis (36). Moreover, it is closely relevant to aerobic glycolysis through interacting with glycolytic enzymes. As the enzyme controlling glucose uptake into cells, GLUT1, regulated by Akt, can enhance glucose uptake. HK2, the rate-limiting enzyme in glycolysis, sequesters glucose inside the cells by phosphorylating it to glucose-6-phosphate, with Akt activation promoting HK2 localized to mitochondria. This process leads to rapid mitochondria-derived ATP production and sustained HK2-mediated glucose phosphorylation (35, 37). The downstream effector of Akt, mammalian target of rapamycin (mTOR), was reported to enhance PKM2 expression by simulating HIF1α expression (38). Besides, PI3K/Akt could also stimulate the

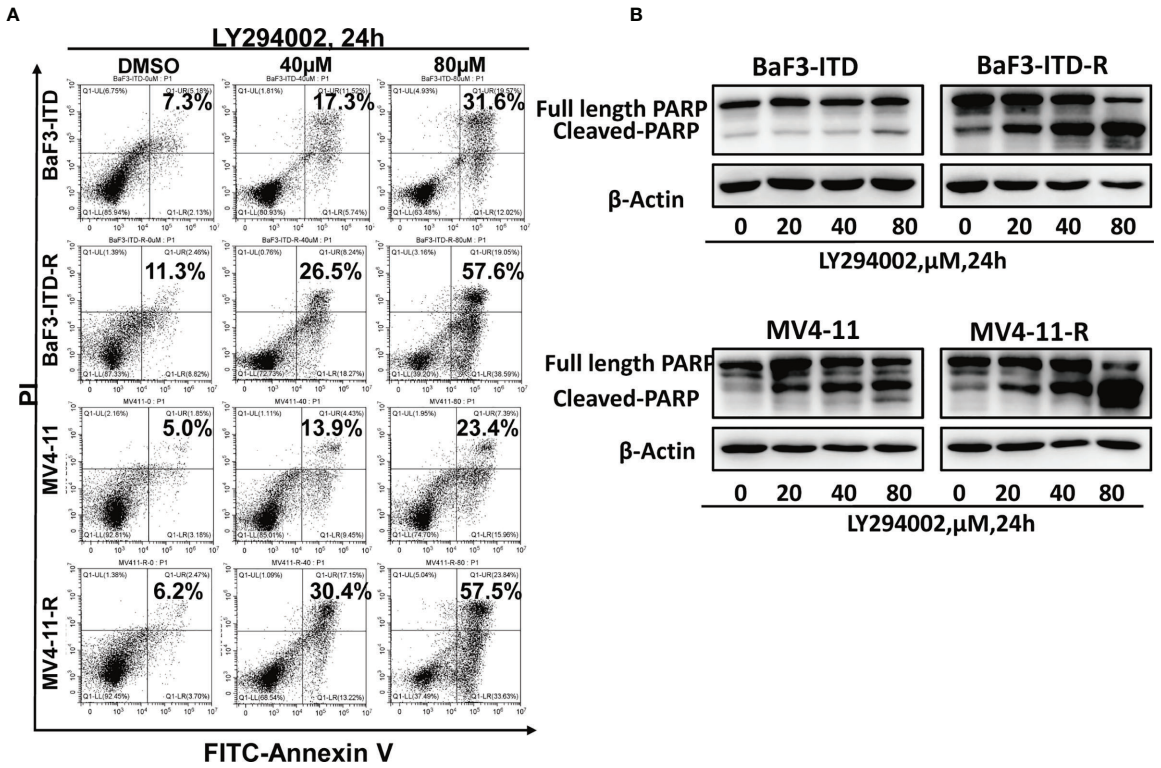


**FIGURE 5** | Drug-resistant cells are more sensitive to LY294002. **(A)** Comparison of the apoptotic effect induced by LY294002 in two pairs of cell lines. Cells were exposed to LY294002 at the indicated concentrations for 24 hours, and the apoptotic cells were stained with Annexin-V and PI for 15 mins and detected by flow cytometry in one hour. Data represent three independent experiments. **(B)** Cells were treated with LY294002 for increasing concentrations, with PARP and cleaved PARP detected by western blotting. β-actin was used as a loading control.

activity of other enzymes such as phosphofructokinase 1 (PFK1) and PDK1 (36, 39).

Based on this, we speculated the resistant cells with highly activated PI3K/Akt signaling may have more active glycolytic activity. By qRT-PCR and western blotting, we found the resistant panels were over-expressed with PKM2 and HK2. Furthermore, when culturing cells in the medium deprived of glucose, more significant growth inhibition were observed in the drug-resistant cells than the parental. That means the resistant cells were more dependent on glucose for proliferation. Blocking the glycolytic pathway, with 2-DG and oxamate could sharply shrink ATP production and cell survival.

To further illustrate the relationship between PI3K/Akt signaling and glycolysis, PI3K inhibitor, LY294002, was adopted to treat cells. The discovered suppression of glycolytic enzymes, glucose uptake and lactate production represent the inhibition of the glycolytic pathway. Cell apoptosis assay and PARP cleavage detected by western blotting further verified the cytotoxicity of LY294002.

In summary, through prolonged exposure to sorafenib, we established two pairs of drug-resistant cells. We demonstrated that drug-resistant cells, losing the target protein FLT3, lead to resistance to TKI inhibitors. The continuous activation of PI3K/Akt signaling, the major downstream signaling of FLT3, led to highly glycolytic activity that provides ATP production and cell survival advantages. As PI3K/Akt signaling is the initiator for metabolic changes and cell survival, we hypothesized that blocking this pathway with PI3K inhibitors may selectively induce cell death and conquer drug resistance. Further experiments confirmed this speculation, and PI3K inhibitor LY294002 may provide a new therapeutic regimen to combat sorafenib-induced drug resistance. In the meanwhile, the other PI3K and Akt inhibitors were tested for their drug sensitivities, the result showed the BaF3-ITD-R cells were resistant to all these inhibitors. This leads us to speculate that besides inhibiting PI3K, LY294002 may have other mechanisms to interfere with the survival of resistant cells. The underlying mechanisms need further investigations. Moreover, the anti-tumor effect of LY294002 should be investigated in animal experiments and possibly in clinical trials in future.

## DATA AVAILABILITY STATEMENT

The original contributions presented in the study are included in the article/**Supplementary Material**. Further inquiries can be directed to the corresponding author.

## AUTHOR CONTRIBUTIONS

AH designed the research study. AH, WL, PZ, and YLi conducted the cell experiments. AH, YLi, and YLai were involved in data analysis. AH was responsible for writing the manuscript. All authors contributed to the article and approved the submitted version.

## FUNDING

This work was supported by National Natural Science Foundation of China (No.81900150), Medical Scientific Research Foundation of Guangdong Province, China (No. A2019451), The Science and Technology Planning Project of Guangzhou, China (No. 202102020741).

## ACKNOWLEDGMENTS

We thank Dr. Donald Small for providing the BaF3-ITD cells, we also thank Dr. Yumin Hu and Prof. Heping Li for the instruction on the research work.

## SUPPLEMENTARY MATERIAL

The Supplementary Material for this article can be found online at: https://www.frontiersin.org/articles/10.3389/fonc.2021.782065/full#supplementary-material

**Supplementary Figure 1 |** Effect of the other PI3K and Akt inhibitor in the proliferation of BaF3-ITD and BaF3-ITD-R cells. BaF3-ITD and BaF3-ITD-R cells were incubated with increasing concentrations of the other PI3K inhibitor: buparlisib, pictilisib, alpelisib and Akt inhibitors: afuresertib, MK2206, ipatasertib for 72 hours. Cell viability (%) was detected by MTS method.

## REFERENCES

1. Thiede C, Steudel C, Mohr B, Schaich M, Schäkel I, Mohr B, et al. Analysis of FLT3-Activating Mutations in 979 Patients With Acute Myelogenous Leukemia: Association With FAB Subtypes and Identification of Subgroups With Poor Prognosis. *Blood* (2002) 99(12):4326–35. doi: 10.1182/blood.V99.12.4326
2. Nakao M, Yokota S, Iwai T, Kaneko H, Horiike S, Kashima K, et al. Internal Tandem Duplication of the Flt3 Gene Found in Acute Myeloid Leukemia. *Leukemia* (1996) 10:1911–8.
3. Hayakawa F, Towatari M, Kiyoi H, Tanimoto M, Kitamura T, Saito H, et al. Tandem-Duplicated Flt3 Constitutively Activates STAT5 and MAP Kinase and Introduces Autonomous Cell Growth in IL-3-Dependent Cell Lines. *Oncogene* (2000) 19:624–31. doi: 10.1038/sj.onc.1203354
4. Mizuki M, Fenski R, Halfter H, Matsumura I, Schmidt R, Müller C, et al. Flt3 Mutations From Patients With Acute Myeloid Leukemia Induce Transformation of 32D Cells Mediated by the Ras and STAT5 Pathways. *Blood* (2000) 96:3907–14. doi: 10.1182/blood.V96.12.3907
5. Brandts CH, Sargin B, Rode M, Biermann C, Lindtner B, Schwäble J, et al. Constitutive Activation of Akt by Flt3 Internal Tandem Duplications Is Necessary for Increased Survival, Proliferation, and Myeloid Transformation. *Cancer Res* (2005) 65:9643–50. doi: 10.1158/0008-5472.CAN-05-0422
6. Kottaridis PD, Gale RE, Frew ME, Harrison G, Langabeer SE, Belton AA, et al. The Presence of a FLT3 Internal Tandem Duplication in Patients With Acute Myeloid Leukemia (AML) Adds Important Prognostic Information to Cytogenetic Risk Group and Response to the First Cycle of Chemotherapy: Analysis of 854 Patients From the United Kingdom Medical Research Council AML 10 and 12 Trials. *Blood* (2001) 98:1752–9. doi: 10.1182/blood.v98.6.1752
7. Kiyoi H, Naoe T, Nakano Y, Yokota S, Minami S, Miyawaki S, et al. Prognostic Implication of FLT3 and N-RAS Gene Mutations in Acute Myeloid Leukemia. *Blood* (1999) 93:3074–80. doi: 10.1182/blood.V93.9.3074
8. Perl AE. Availability of FLT3 Inhibitors: How do We Use Them. *Blood* (2019) 134:741–5. doi: 10.1182/blood.2019876821
9. Antar AI, Otrock ZK, Jabbour E, Mohty M, Bazarbachi A. FLT3 Inhibitors in Acute Myeloid Leukemia: Ten Frequently Asked Questions. *Leukemia* (2020) 34:682–96. doi: 10.1038/s41375-019-0694-3
10. Wu M, Li C, Zhu X. FLT3 Inhibitors in Acute Myeloid Leukemia. *J Hematol Oncol* (2018) 11:133. doi: 10.1186/s13045-018-0675-4
11. Abdelgalil AA, Alkahtani HM, Al-Jenoobi FI. Sorafenib. *Profiles Drug Subst Excip Relat Methodol* (2019) 44:239–66. doi: 10.1016/bs.podrm.2018.11.003
12. Zhang W, Konopleva M, Shi YX, McQueen T, Harris D, Ling X, et al. Mutant FLT3: A Direct Target of Sorafenib in Acute Myelogenous Leukemia. *J Natl Cancer Inst* (2008) 100:184–98. doi: 10.1093/jnci/djm328
13. Auclair D, Miller D, Yatsula V, Pickett W, Carter C, Chang Y, et al. Antitumor Activity of Sorafenib in FLT3-Driven Leukemic Cells. *Leukemia* (2007) 21:439–45. doi: 10.1038/sj.leu.2404508
14. Ravandi F, Cortes JE, Jones D, Faderl S, Garcia-Manero G, Konopleva MY, et al. Phase I/II Study of Combination Therapy With Sorafenib, Idarubicin, and Cytarabine in Younger Patients With Acute Myeloid Leukemia. *J Clin Oncol* (2010) 28:1856–62. doi: 10.1200/JCO.2009.25.4888
15. Ravandi F, Arana Yi C, Cortes JE, Levis M, Faderl S, Garcia-Manero G, et al. Final Report of Phase II Study of Sorafenib, Cytarabine and Idarubicin for Initial Therapy in Younger Patients With Acute Myeloid Leukemia. *Leukemia* (2014) 28:1543–5. doi: 10.1038/leu.2014.54
16. Röllig C, Serve H, Hüttmann A, Noppeney R, Müller-Tidow C, Krug U, et al. Addition of Sorafenib Versus Placebo to Standard Therapy in Patients Aged 60 Years or Younger With Newly Diagnosed Acute Myeloid Leukaemia (SORAML): A Multicentre, Phase 2, Randomised Controlled Trial. *Lancet Oncol* (2015) 16:1691–9. doi: 10.1016/S1470-2045(15)00362-9
17. Burchert A, Bug G, Fritz LV, Finke J, Stelljes M, Röllig C, et al. Sorafenib Maintenance After Allogeneic Hematopoietic Stem Cell Transplantation for Acute Myeloid Leukemia With FLT3-Internal Tandem Duplication Mutation (SORMAIN). *J Clin Oncol* (2020) 38:2993–3002. doi: 10.1200/JCO.19.03345
18. Xuan L, Wang Y, Huang F, Fan Z, Xu Y, Sun J, et al. Sorafenib Maintenance in Patients With FLT3-ITD Acute Myeloid Leukaemia Undergoing Allogeneic Haematopoietic Stem-Cell Transplantation: An Open-Label, Multicentre, Randomised Phase 3 Trial. *Lancet Oncol* (2020) 21:1201–12. doi: 10.1016/S1470-2045(20)30455-1
19. Levis M. Midostaurin Approved for FLT3-Mutated AML. *Blood* (2017) 129:3403–6. doi: 10.1182/blood-2017-05-782292
20. Kim ES. Midostaurin: First Global Approval. *Drugs* (2017) 77:1251–9. doi: 10.1007/s40265-017-0779-0
21. Dhillon S. Gilteritinib: First Global Approval. *Drugs* (2019) 79:331–9. doi: 10.1007/s40265-019-1062-3
22. Kucukyurt S, Eskazan AE. New Drugs Approved for Acute Myeloid Leukaemia in 2018. *Br J Clin Pharmacol* (2019) 85:2689–93. doi: 10.1111/bcp.14105
23. Pratz KW, Cortes J, Roboz GJ, Rao N, Arowojolu O, Stine A, et al. A Pharmacodynamic Study of the FLT3 Inhibitor KW-2449 Yields Insight Into the Basis for Clinical Response. *Blood* (2009) 113:3938–46. doi: 10.1182/blood-2008-09-177030
24. Zhou J, Chng WJ. Resistance to FLT3 Inhibitors in Acute Myeloid Leukemia: Molecular Mechanisms and Resensitizing Strategies. *World J Clin Oncol* (2018) 9:90–7. doi: 10.5306/wjco.v9.i5.90
25. Weisberg E, Sattler M, Ray A, Griffin JD. Drug Resistance in Mutant FLT3-Positive AML. *Oncogene* (2010) 29:5120–34. doi: 10.1038/onc.2010.273
26. You X, Jiang W, Lu W, Zhang H, Yu T, Tian J, et al. Metabolic Reprogramming and Redox Adaptation in Sorafenib-Resistant Leukemia Cells: Detected by Untargeted Metabolomics and Stable Isotope Tracing Analysis. *Cancer Commun (Lond)* (2019) 39:171–13. doi: 10.1186/s40880-019-0362-z

27. Lam S, Leung A. Overcoming Resistance to FLT3 Inhibitors in the Treatment of FLT3-Mutated AML. *Int J Mol Sci* (2020) 21(*4*):1537. doi: 10.3390/ijms21041537
28. Scholl S, Fleischmann M, Schnetzke U, Heidel FH. Molecular Mechanisms of Resistance to FLT3 Inhibitors in Acute Myeloid Leukemia: Ongoing Challenges and Future Treatments. *Cells* (2020) 9. doi: 10.3390/cells9112493
29. Ghiaur G, Levis M. Mechanisms of Resistance to FLT3 Inhibitors and the Role of the Bone Marrow Microenvironment. *Hematol Oncol Clin North Am* (2017) 31:681–92. doi: 10.1016/j.hoc.2017.04.005
30. Huang A, Ju HQ, Liu K, Zhan G, Liu D, Wen S, et al. Metabolic Alterations and Drug Sensitivity of Tyrosine Kinase Inhibitor Resistant Leukemia Cells With a FLT3/ITD Mutation. *Cancer Lett* (2016) 377:149–57. doi: 10.1016/j.canlet.2016.04.040
31. Cui Q, Wang JQ, Assaraf YG, Ren L, Gupta P, Wei L, et al. Modulating ROS to Overcome Multidrug Resistance in Cancer. *Drug Resist Update* (2018) 41:1–25. doi: 10.1016/j.drup.2018.11.001
32. Wang JQ, Yang Y, Cai CY, Teng QX, Cui Q, Lin J, et al. Multidrug Resistance Proteins (MRPs): Structure, Function and the Overcoming of Cancer Multidrug Resistance. *Drug Resist Update* (2021) 54:100743. doi: 10.1016/j.drup.2021.100743
33. Schmidt-Arras DE, Böhmer A, Markova B, Choudhary C, Serve H, Böhmer FD. Tyrosine Phosphorylation Regulates Maturation of Receptor Tyrosine Kinases. *Mol Cell Biol* (2005) 25:3690–703. doi: 10.1128/MCB.25.9.3690-3703.2005
34. Revathidevi S, Munirajan AK. Akt in Cancer: Mediator and More. *Semin Cancer Biol* (2019) 59:80–91. doi: 10.1016/j.semcancer.2019.06.002
35. Roberts DJ, Tan-Sah VP, Smith JM, Miyamoto S. Akt Phosphorylates HK-II at Thr-473 and Increases Mitochondrial HK-II Association to Protect Cardiomyocytes. *J Biol Chem* (2013) 288:23798–806. doi: 10.1074/jbc.M113.482026
36. Hoxhaj G, Manning BD. The PI3K-AKT Network at the Interface of Oncogenic Signalling and Cancer Metabolism. *Nat Rev Cancer* (2020) 20:74–88. doi: 10.1038/s41568-019-0216-7
37. Gottlob K, Majewski N, Kennedy S, Kandel E, Robey RB, Hay N. Inhibition of Early Apoptotic Events by Akt/PKB Is Dependent on the First Committed Step of Glycolysis and Mitochondrial Hexokinase. *Genes Dev* (2001) 15:1406–18. doi: 10.1101/gad.889901
38. Sun Q, Chen X, Ma J, Peng H, Wang F, Zha X, et al. Mammalian Target of Rapamycin Up-Regulation of Pyruvate Kinase Isoenzyme Type M2 is Critical for Aerobic Glycolysis and Tumor Growth. *Proc Natl Acad Sci USA* (2011) 108:4129–34. doi: 10.1073/pnas.1014769108
39. DeBerardinis RJ, Lum JJ, Hatzivassiliou G, Thompson CB. The Biology of Cancer: Metabolic Reprogramming Fuels Cell Growth and Proliferation. *Cell Metab* (2008) 7:11–20. doi: 10.1016/j.cmet.2007.10.002

**Conflict of Interest:** The authors declare that the research was conducted in the absence of any commercial or financial relationships that could be construed as a potential conflict of interest.

The reviewer LZ declared a shared parent affiliation with one of the authors, YLa, to the handling editor at time of review.

frontiers in Pharmacology

ORIGINAL RESEARCH
published: 26 November 2021
doi: 10.3389/fphar.2021.749242

# The PI3K Inhibitor XH30 Enhances Response to Temozolomide in Drug-Resistant Glioblastoma *via* the Noncanonical Hedgehog Signaling Pathway

*Ming Ji[1,2†], Zhihui Zhang[3†], Songwen Lin[1], Chunyang Wang[3], Jing Jin[1,2], Nina Xue[1]*, Heng Xu[1]* and Xiaoguang Chen[1,3]**

[1]State Key Laboratory of Bioactive Substances and Functions of Natural Medicines, Institute of Materia Medica, Chinese Academy of Medical Sciences and Peking Union Medical College, Beijing, China, [2]Beijing Key Laboratory of Non-Clinical Drug Metabolism and PK/PD Study, Institute of Materia Medica, Chinese Academy of Medical Sciences and Peking Union Medical College, Beijing, China, [3]Beijing Key Laboratory of New Drug Mechanisms and Pharmacological Evaluation Study, Institute of Materia Medica, Chinese Academy of Medical Sciences and Peking Union Medical College, Beijing, China

OPEN ACCESS

**Edited by:**
Qingbin Cui,
University of Toledo, United States

**Reviewed by:**
Roberto Würth,
German Cancer Research Center (DKFZ), Germany
Mounir Tilaoui,
Waterford Institute of Technology, Ireland

***Correspondence:**
Nina Xue
angelnina@imm.ac.cn
Heng Xu
xuheng@imm.ac.cn
Xiaoguang Chen
chxg@imm.ac.cn

[†]These authors have contributed equally to this work

**Specialty section:**
This article was submitted to Pharmacology of Anti-Cancer Drugs, a section of the journal Frontiers in Pharmacology

**Received:** 29 July 2021
**Accepted:** 03 November 2021
**Published:** 26 November 2021

**Citation:**
Ji M, Zhang Z, Lin S, Wang C, Jin J, Xue N, Xu H and Chen X (2021) The PI3K Inhibitor XH30 Enhances Response to Temozolomide in Drug-Resistant Glioblastoma via the Noncanonical Hedgehog Signaling Pathway. Front. Pharmacol. 12:749242. doi: 10.3389/fphar.2021.749242

Glioblastoma multiforme (GBM) is the most common malignant tumor of the central nervous system. Temozolomide (TMZ)–based adjuvant treatment has improved overall survival, but clinical outcomes remain poor; TMZ resistance is one of the main reasons for this. Here, we report a new phosphatidylinositide 3-kinase inhibitor, XH30; this study aimed to assess the antitumor activity of this compound against TMZ-resistant GBM. XH30 inhibited cell proliferation in TMZ-resistant GBM cells (U251/TMZ and T98G) and induced cell cycle arrest in the G1 phase. In an orthotopic mouse model, XH30 suppressed TMZ-resistant tumor growth. XH30 was also shown to enhance TMZ cytotoxicity both *in vitro* and *in vivo*. Mechanistically, the synergistic effect of XH30 may be attributed to its repression of the key transcription factor GLI1 via the noncanonical hedgehog signaling pathway. XH30 reversed sonic hedgehog–triggered GLI1 activation and decreased GLI1 activation by insulin-like growth factor 1 via the noncanonical hedgehog signaling pathway. These results indicate that XH30 may represent a novel therapeutic option for TMZ-resistant GBM.

**Keywords: glioblastoma, TMZ, PI3K, hedgehog, GLI1**

## INTRODUCTION

Glioblastoma multiforme (GBM) is the most aggressive tumor of the central nervous system in adults (DeAngelis, 2001). Despite recent research focusing on various glioblastoma therapies, the clinical benefit from treatment for people with GBM remains unsatisfactory (Touat et al., 2017; Castresana and Melendez, 2021; Liau, 2021). Mean overall survival is currently estimated to be only 9.7 months after primary treatment.

Temozolomide (TMZ) chemotherapy is still recommended as the standard care for GBM. However, GBM recurs in most people with this tumor type after primary treatment. The development of resistance to TMZ is often the primary limiting factor for treatment success (Bocangel et al., 2002; Lee, 2016; Dymova et al., 2021). Many factors contribute to TMZ

resistance, such as overexpression of O6-methylguanine methyltransferase (MGMT), lack of a DNA repair pathway, activation of the hedgehog signaling pathway, the presence of glioma stem cells, and metabolic dysfunction (Happold and Weller, 2015; Perazzoli et al., 2015; Yun et al., 2020; Chien et al., 2021; Zheng et al., 2021). The hedgehog signaling pathway has been a focus of research in this area recently (Melamed et al., 2018; Avery et al., 2021). The glioma-associated oncogene GLI, a zinc finger protein, is a key component in this pathway. Pharmacological inhibition of GLI-1 has been shown to enhance the cytotoxicity of TMZ in GBM and overcome TMZ resistance (Li J. et al., 2016; Ji et al., 2018).

The phosphatidylinositide 3-kinase (PI3K) pathway is frequently overactivated in glioblastoma due to PIK3CA mutations, loss of phosphotase and tensin homolog (*PTEN*) gene function, and amplification of epidermal growth factor receptor (*EGFR*) gene expression (Sami and Karsy, 2013; Langhans et al., 2017; Colardo et al., 2021). PI3K is an attractive therapeutic target for glioblastoma (Li X. et al., 2016; Colardo et al., 2021). In animal models, PI3K inhibitors have been shown to have substantial antitumor activity against GBM (Zhao et al., 2017). The effects of PI3K inhibitors, such as paxalisib, have been tested in patients with newly diagnosed GBM (Wen et al., 2019). Preliminary data have shown encouraging survival outcomes in these patients. In addition, PI3K inhibitors have also been shown to enhance TMZ cytotoxicity in GBM via distinct mechanisms, such as downregulation of ATP-binding cassette subfamily E member 1, inhibition of autophagy, promotion of apoptosis, and inhibition of DNA double-strand break repair (Gil del Alcazar et al., 2014; Radoul et al., 2016; Zhang et al., 2018; Zajac et al., 2021). However, the antitumor activity of PI3K inhibitors in patients with TMZ-resistant GBM currently remains unclear (Hainsworth et al., 2019).

Many studies have reported crosstalk between the PI3K and hedgehog signaling pathways (Ranjan and Srivastava, 2017). The PI3K signaling pathway is a crucial non-canonical activator of GLI1 (Riobo et al., 2006; Zhou et al., 2016; Liang et al., 2017; Ranjan and Srivastava, 2017). Activation of this pathway has been found to enhance GLI1 protein stability because the serine/threonine kinase in this pathway, AKT, can extend the half-life of GLI proteins in the cells by alleviating the inhibitory effect of protein kinase A, thus facilitating nuclear translocation (Singh et al., 2017). Meanwhile, PI3K signaling activates GLI1 via its downstream effector, ribosomal S6 kinase (p70S6K) (Wang et al., 2012). Activated p70S6K promotes GLI1 disassociation from suppressor of fused homolog (SUFU) by phosphorylating GLI1 at Ser84 and enhancing GLI1 transcriptional activity. In addition, p70S6K2 has been shown to inhibit glycogen synthase kinase (GSK3) by phosphorylating GLI1 at Ser9, leading to a decrease in GSK3β-mediated GLI1 degradation (Mizuarai et al., 2009).

XH30 is a PI3K inhibitor that can cross the blood–brain barrier (Lin et al., 2018). XH30 has previously been demonstrated to have robust antitumor activity in GBM and brain metastases of lung cancer *in vivo* (Lin et al., 2018; Ji et al., 2021). In this study, we aimed to assess the capacity of XH30 to inhibit the growth of GBM cells with natural or TMZ-induced drug resistance both *in vitro* and *in vivo*, in an orthotopic mouse model. We also explored the underlying mechanisms of the antitumor effects of XH30.

# MATERIALS AND METHODS

## Cell Lines

Two cell lines were used in this study. The T98G human glioma tumor cell line was purchased from ATCC (Manassas, VA, United States); this is a naturally TMZ-resistant cell line with elevated levels of MGMT. The U251/TMZ cell line was a gift from Dr. Yuhui Zou of General Hospital of Guangzhou Military Command of People's Liberation Army, as previously reported (Ji et al., 2018); this line has acquired TMZ resistance, with overactivated hedgehog signaling. Both cell lines were cultured in Dulbecco's modified eagle medium (Gibco, TX, United States) with 10% (v/v) fetal bovine serum (Gibco), penicillin (100 units/ml), and streptomycin (100 units/ml) in a humidified atmosphere of 5% $CO_2$ at 37°C.

## Antibodies and Reagents

XH30 was synthesized in house as described previously (Lin et al., 2018). PI3K inhibitor PF-04691502 was purchased from Selleck Chemicals (Houston, TX, United States). TMZ was purchased from J&K Scientific (Beijing, China). All antibodies [AKT, phosphor-AKT (S473), phosphor-AKT (T308), mammalian target of rapamycin (mTOR), phosphor-mTOR (S2448), GSK3β, phosphor-GSK3β (S9), proline-rich AKT substrate of 40 kDa (PRAS40), phosphor-PRAS40 (T246), p70S6K, phosphor-p70S6K (T389), S6 ribosomal protein (S6RP), phosphor-S6RP (S240/244), smoothened (SMO), cyclin D1, and anti-cyclin–dependent kinase (CDK2)] were purchased from Cell Signaling Technology (Danvers, MA, United States). Anti-GLI1 and anti–β-actin antibodies were purchased from Abcam (Cambridge, United Kingdom) and Santa Cruz Biotechnology (Dallas, TX, United States), respectively.

## Cell Viability Assay

Cell viability was assessed using the Cell Counting Kit-8 (CCK-8; Solarbio, Beijing, China). Briefly, 2,000 cells per well were seeded into a 96-well plate. After incubation overnight, the cells were treated with different concentrations (0.0512, 0.256, 1.28, 6.4, 32, 160, 800, 4,000, and 20,000 nM) of XH30 or PF-04691502 with three replicates for 72 h. Then, CCK-8 solution was added and incubated for 3 h, after which, absorbance values were measured at 450 nM using a microplate reader (BioTek Instruments, Inc., United States). The half-maximal inhibitory concentration ($IC_{50}$) was calculated using GraphPad Prism v8.0.1 (La Jolla, CA, United States).

## Colony Formation Assay

U251/TMZ and T98G cells were seeded at a density of 200 cells per well into six-well plates. After 24 h, the cells were treated with indicated concentrations (4, 20, 100, and 500 nM) of XH30 with

three replicates. The culture medium with test compound was replaced every 3 days. After cell colonies formed, cells were washed with phosphate-buffered saline (PBS) and fixed with 4% paraformaldehyde for 15 min, then stained with crystal violet for 30 min, and washed with PBS. Finally, colonies were recorded with a photograph and measured by a microplate reader (BioTek).

## Cell Cycle Analysis

Flow cytometry assays were used to analyze the cell cycle distribution as previously reported (Ji et al., 2018). In brief, U251/TMZ and T98G cells were dispensed into six-well plates at a density of 50,000 cells per well. After growing overnight in a humidified atmosphere of 5% $CO_2$ at 37°C, cells were treated with indicated concentrations (4, 20, 100, and 500 nM) of XH30 for 24 h. Then, cells were harvested and fixed ice cold 70% ethanol overnight at −20°C, washed with PBS, and stained with propidium iodide (PI) solution containing PI (20 mg/ml) and RNase A (20 mg/ml) in PBS for 30 min. DNA contents were measured using the BD fluorescence-activated cell sorting verse flow cytometer (BD Biosciences, NJ, United States), and the cell cycle distribution was analyzed.

## Immunoblotting Analysis

Cells or mice tumor tissues were collected and lysed in RIPA lysate buffer supplemented with 1% protease inhibitor cocktail and 1% phosphatase inhibitor cocktail (Solarbio, Beijing, China). Lysates were then centrifuged at 12,000 g for 30 min. Proteins were quantified using a bicinchoninic acid assay kit (Solarbio, Beijing, China). Resultant samples containing equal amounts of proteins were subjected to sodium dodecylsulfate–polyacrylamide gel electrophoresis and transferred to a polyvinylidene fluoride membrane (Millipore, Darmstadt, Germany). The membrane was blocked with TBST buffer containing 5% non-fat milk for 30 min and incubated with appropriate primary antibodies (1: 1,000 dilution) in TBST at 4°C overnight. After washing with TBST, the membrane was incubated with horseradish peroxidase–conjugated secondary antibodies (1:2,000 dilution; Cell Signaling Technologies, Boston, MA) for 1 h at room temperature. Bound proteins were visualized using enhanced chemiluminescence and detected using ImageQuant LAS 4000 software.

## Quantitative Real-Time Polymerase Chain Reaction Analysis

Total RNA from XH30-treated U251/TMZ or T98G cells was isolated using TRIzol reagent (Bioteke Corporation, China) according to the recommended procedures of the manufacturer. First-strand cDNA was synthesized from 1 μg of total RNA using the ReverTra Ace® qPCR RT Master Mix with gDNA Remover (Toyobo, Japan). Real-time polymerase chain reaction (PCR) was performed using the Analytikjena qTOWER detection system and the SYBR® Green RT-PCR master mix (Toyobo). Target sequences were amplified at 95°C for 1 min, followed by 40 cycles at 95°C for 15 s, 60°C for 15 s, and 72°C for 45 s. Fold changes in *GLI1*, paired box protein 6 (*PAX6*), and O6-methylguanine-DNA-MGMT (*MGMT*) gene expression were calculated according to the 2−ΔΔCt method. The primers sequences used to amplify specific regions of the indicated genes were as follows: *GLI1* forward, ATGTTCAACTCGATG ACCCCAC; *GLI1* reverse, CAACTTGACTTCTGTCCCCACA; *MGMT* forward, ATGGAT GTTTGAGCGACACA; *MGMT* reverse, ATAGAGCAAGGGCAGCGTTA; *PAX6* forward, AACGATAACATACCAAGCGTGT; *PAX6* reverse, GGTCTG CCCGTTCAACATC.

## Orthotopic Mouse Tumor Model and Subcutaneous Mouse Tumor Model

Eight- to 10-week-old female Balb/c athymic nude mice (SPF Biotechnology, Beijing, China) were housed in standard facilities. Human U251/TMZ cells in PBS were injected intracranially, 2.0 mm below the skull surface, according to a previously published protocol (Ji et al., 2018). Three days after surgery, mice were randomized to receive one of the four following treatments: a drug vehicle (delivered orally once per day for 9 days). TMZ (50 mg/kg, delivered orally once per day for 5 days), or XH30 (5 mg/kg, delivered orally once per day for 9 days). TMZ and XH30 were dissolved in 0.5% carboxymethylcellulose solution. Tumor volumes were monitored using an animal magnetic resonance imaging (MRI) scanner (PharmaScan 70/16 US, Bruker, Germany). The parameters for the MRI scans were as follows: a T2_TurboRARE, with TR/TE = 5,000/40, 6 averages, 20 × 20 field of view, and 0.5-mm slice thickness. The tumor volume on the basis of MRI was calculated as $V = L \times W \times T$, where L is the maximum length of tumor, W is the maximum width perpendicular to L, and T is the thickness of the tumor slice (set at 0.5 mm).

For the subcutaneous mice tumor model, female Balb/c athymic nude mice (eight to 10 weeks of age) were subcutaneously implanted with $1 \times 10^7$ U251/TMZ cells in 0.2 ml matrigel solution in the right flank. After 2 weeks, tumor issue was harvested sterilely, and tumor cells were extracted from the tissue homogenate. Then, the mice were implanted with $2 \times 10^6$ tumor cells each in the right flank. Seven days later, when the average tumor volumes reached to 100–300 $mm^3$, the mice were randomized into four groups, in which either alone treatment or combination was administered, respectively, using the same dose regime as in the orthotopic model. Tumor volume and body weight were monitored twice a week. Tumor volume was calculated as $V = 1/2 \times L \times W^2$, where L is the maximum length of tumor and W is the maximum width of tumor. The mice were euthanized at day 14, and tumor tissues were collected for immunoblotting.

All procedures were approved by the Ethics Committee for Animal Experiments of the Institute of Materia Medica, Chinese Academy of Medical Sciences and Peking Union Medical College and conducted under the Guidelines for Animal Experiments of Peking Union Medical College.

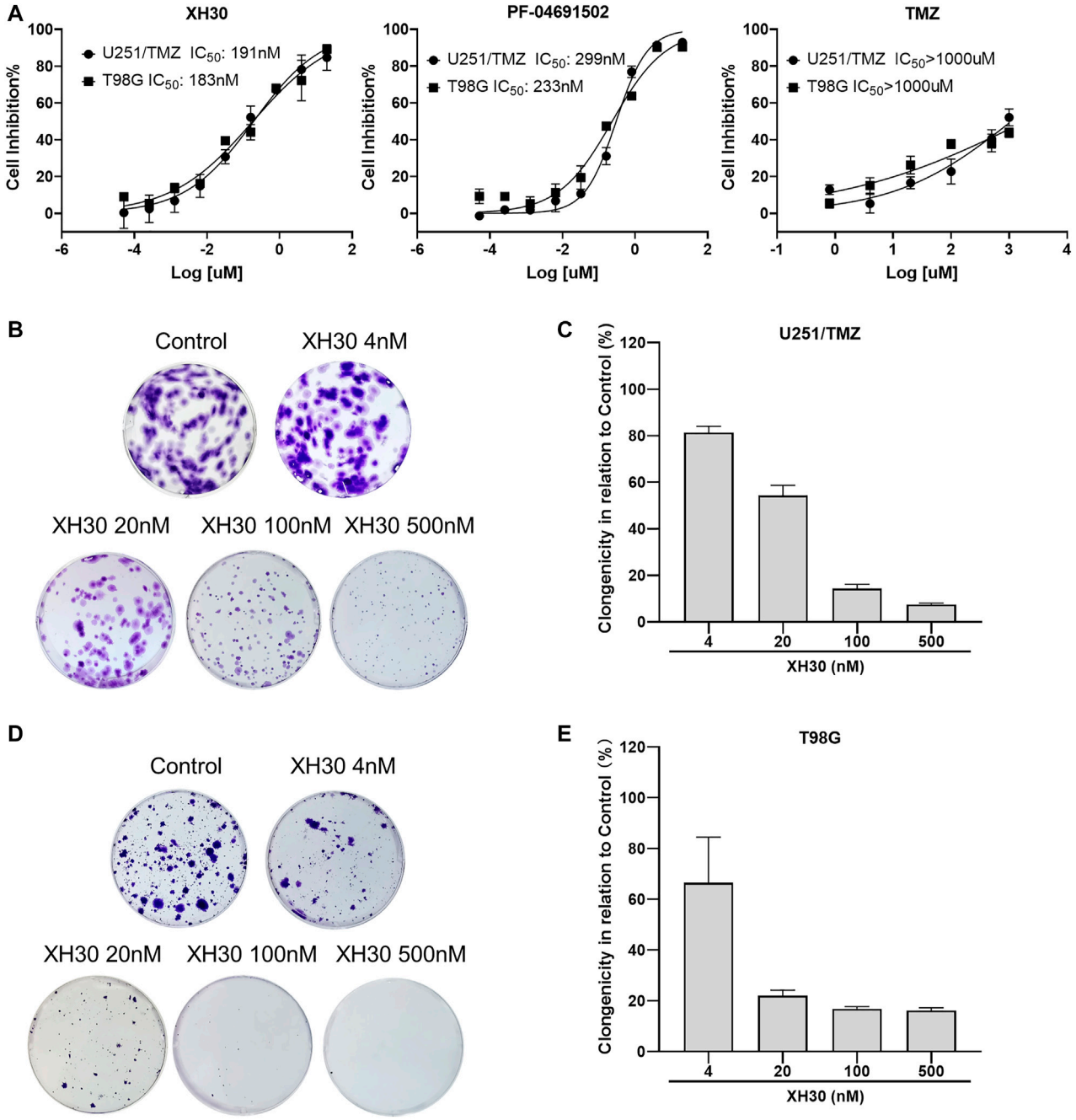


**FIGURE 1 |** The PI3K inhibitor XH30 inhibited cell proliferation in temozolomide (TMZ)–resistant glioblastoma multiforme (GBM) cells. **(A)** The $IC_{50}$ values of XH30, PF-04691502 (control), and TMZ in TMZ-resistant GBM cells over 72 h. Data are presented as means ± SD, $n = 3$. **(B,D)** Colony formation assay of XH30 in TMZ-resistant U251/TMZ and T98G cells, respectively. Representative images are shown for each group. **(C,E)** The inhibition ratio of colony formation assay of XH30 in U251/TMZ and T98G cells, respectively. Data are presented as means ± SD, $n = 3$.

## Statistical Analysis

Most statistical analyses were performed utilizing GraphPad Prism v8.0.1 (La Jolla, CA, United States), and significance levels were evaluated using analysis of variance (ANOVA) or T-tests, as appropriate. In our experiments, we distinguish between three of significance (***$p < 0.001$, **$p < 0.01$, and *$p < 0.05$, respectively).

On the basis of the cell viability assay, the combination index (CI) was calculated using the Chou–Talalay method, with CI = 1, CI < 1 and CI > 1 denoting an additive effect, synergism, and antagonism, respectively. CI = (D)1/(Dx)1 + (D)2/(Dx)2, where (Dx)1 and (Dx)2 represented concentrations of each drug alone to exert x% effect, while (D)1 and (D)2 were concentrations of drugs in combination to elicit the same effect.

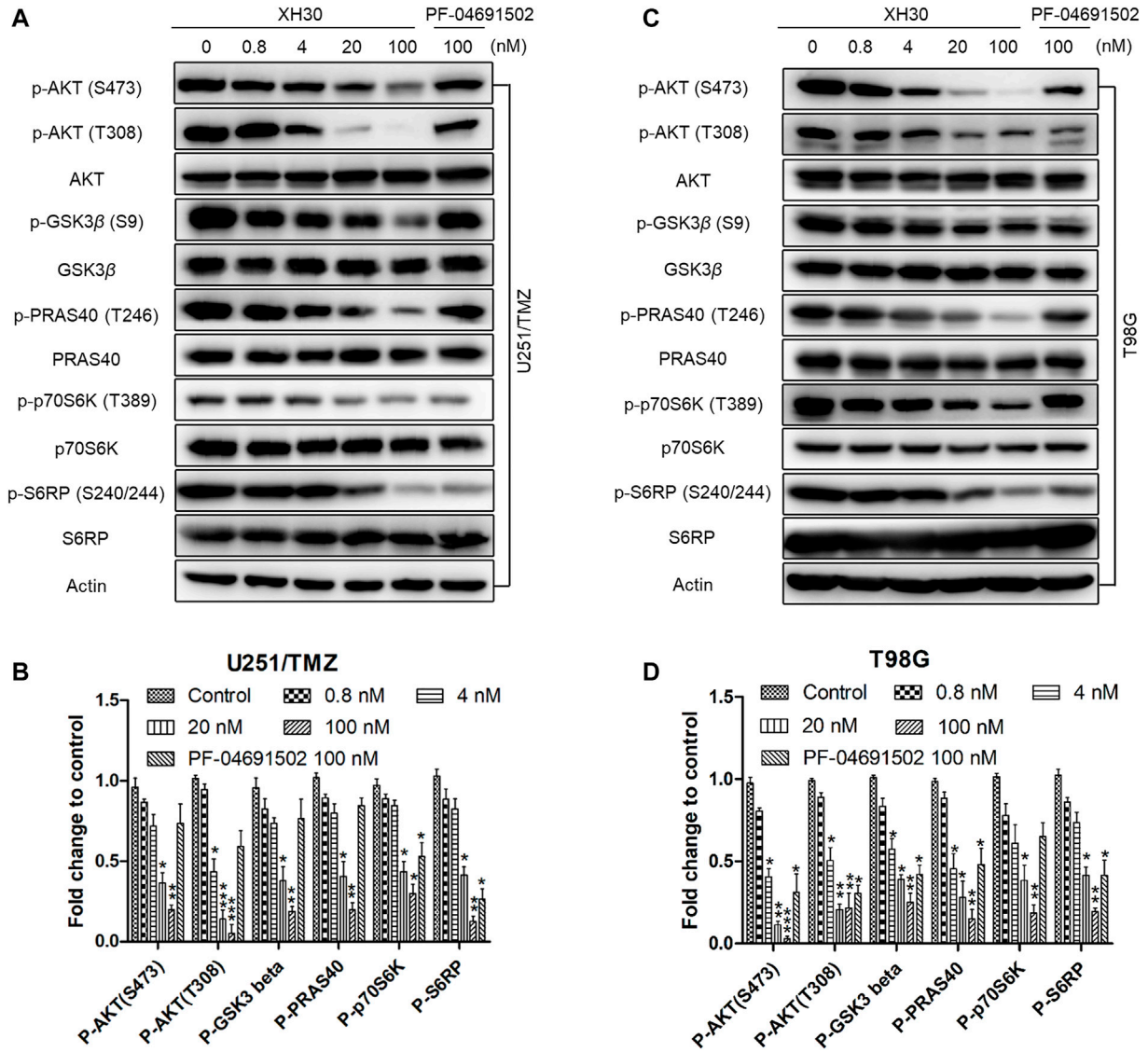


**FIGURE 2 |** The PI3K inhibitor XH30 suppressed the PI3K signaling pathway in TMZ-resistant GBM cells. **(A)** XH30 dose-dependently inhibited PI3K pathway signaling in TMZ-resistant U251/TMZ cells. The cells were incubated with XH30 at indicated concentrations (0.8, 4, 20, and 100 nmol/L) or PF-04691502 (100 nmol/L) as a control for 3 h. The experiment was repeated three times. **(B)** Relative expression levels of the major proteins in **(A)**. Data are presented as means ± SD, $n = 3$. *t*-test, $^{*}p < 0.05$, $^{**}p < 0.01$, and $^{***}p < 0.001$ compared with control. **(C)** XH30 dose-dependently inhibited PI3K pathway signaling in TMZ-resistant T98G cells. The cells were incubated with XH30 at indicated concentrations (0.8, 4, 20, and 100 nmol/L) or PF-04691502 (100 nmol/L) as a control for 3 h. The experiment was repeated three times. **(D)** Relative expression levels of major proteins in **(C)**. Data are presented as means ± SD, $n = 3$. *t*-test, $^{*}p < 0.05$, $^{**}p < 0.01$, and $^{***}p < 0.001$, compared with control.

# RESULTS

## The PI3K Inhibitor XH30 Inhibited TMZ-Resistant GBM Cell Growth *in vitro*

Here, we assessed the anti-tumor activity of XH30 in two TMZ-resistant GBM cell lines: one with acquired TMZ resistance and overactivated hedgehog signaling (U251/TMZ) and one with natural TMZ resistance and elevated MGMT levels (T98G). As shown in **Figure 1A**, TMZ did not exhibit cytotoxicity at the highest concentration of 1,000 μM. XH30 suppressed cell proliferation of both U251/TMZ and T98G cells, with 72 h $IC_{50}$ values of 191 and 183 nM, respectively. The cytotoxic effect was stronger at 72 h than at 24 or 48 h (**Supplementary Figure S1**). The positive control, PF-04691502, also inhibited the proliferation of both cell types. In a colony formation assay, the formation of cell colonies dose-dependently decreased after exposure to XH30 in both U251/TMZ and T98G cells (**Figures 1B–E**). These results indicated that XH30 exhibited strong inhibitory effects on the proliferation of TMZ-resistant GBM cells.

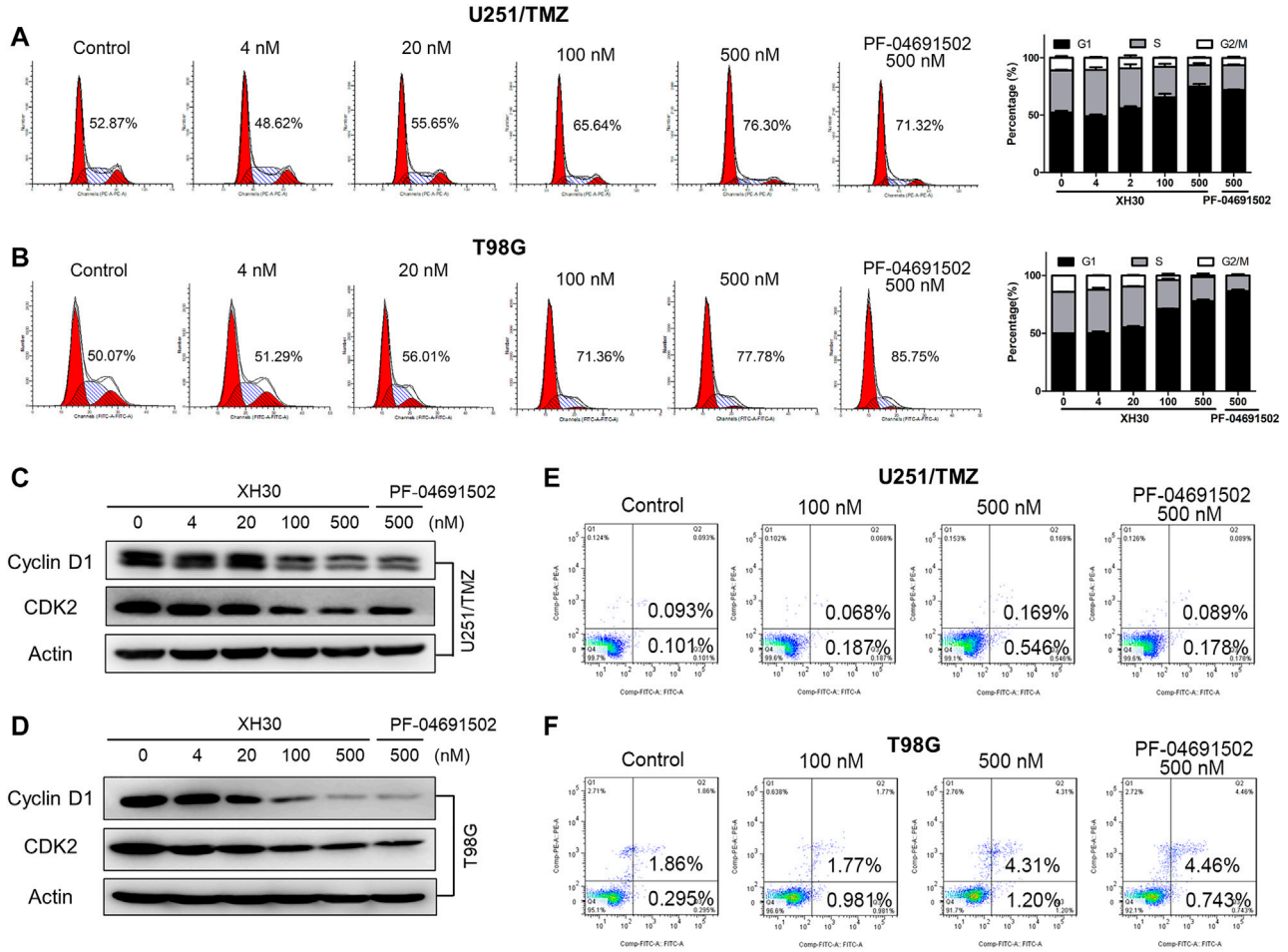


**FIGURE 3 |** XH30 induced G1 cell-cycle arrest in TMZ-resistant GBM cells. **(A, B)** XH30 induced cell cycle arrest in TMZ-resistant U251/TMZ and T98G cells in the G1 phase. Exposure to various concentrations of XH30 at indicated concentrations (4, 20, 100, and 500 nM) or the control, PF-04691502 (500 nM), for 24 h. The cells were stained with propidium iodide (PI) for flow cytometry analysis, $n = 3$. **(C, D)** XH30 downregulated markers of the G1 phase of the cell cycle. The protein levels of cyclin D1 and CDK2 were detected *via* immunoblotting in both U251/TMZ and T98G cells exposed to XH30 for 24 h. **(E, F)** The effect of XH30 on apoptosis in both U251/TMZ and T98G cells exposed to XH30 for 48 h.

## XH30 Reduced Downstream Molecules in the PI3K Signaling Pathway in TMZ-Resistant GBM Cells

We assessed the inhibitory activity of XH30 on the PI3K signaling pathway in both U251/TMZ and T98G cells. XH30 dose-dependently blocked downstream molecules in the PI3K pathway including p-AKT, p-GSK3β, p-PRAS40, p-p70S6K, and p-S6RP (**Figures 2A–D**). At a concentration of 100 nM, XH30 strongly suppressed the phosphorylation of these signaling molecules. This inhibitory activity was more potent than the inhibitory effect of the positive control, PF-04691502, at the same concentrations.

## XH30 Induced Cell Cycle Arrest in TMZ-Resistant GBM Cells

Next, we investigated whether XH30 could induce cell cycle arrest or apoptosis in both TMZ-resistant GBM cell lines. In U251/TMZ cells, both PF-04691502 and XH30 induced cell cycle arrest in the G0/G1 phases. The percentage of G1 phase increased from 48.62% to 76.30% after a concentration titration of XH30 (**Figure 3A**). In T98MG cells, cell cycle arrest was observed during the G1 phase after exposure to XH30. The percentage of G1 phase at a XH30 concentration of 500 nM was increased compared to the control group (77.78% vs. 50.07%) (**Figure 3B**). Moreover, XH30 downregulated the expression of cyclin D1 and CDK2, which are markers of the G1 phase (**Figures 3C,D**). However, apoptosis was not observed in either U251/TMZ or T98G cells after exposure to XH30 for 48 h. These data demonstrated that XH30 induces cell cycle arrest in TMZ-resistant GBM cells (**Figures 3E,F**).

## XH30 Exhibited Antitumor Activity in TMZ-Resistant GBM *in vivo*

To further explore the antitumor activity of XH30 in TMZ-resistant GBM, we used a U251/TMZ orthotopic mouse model.

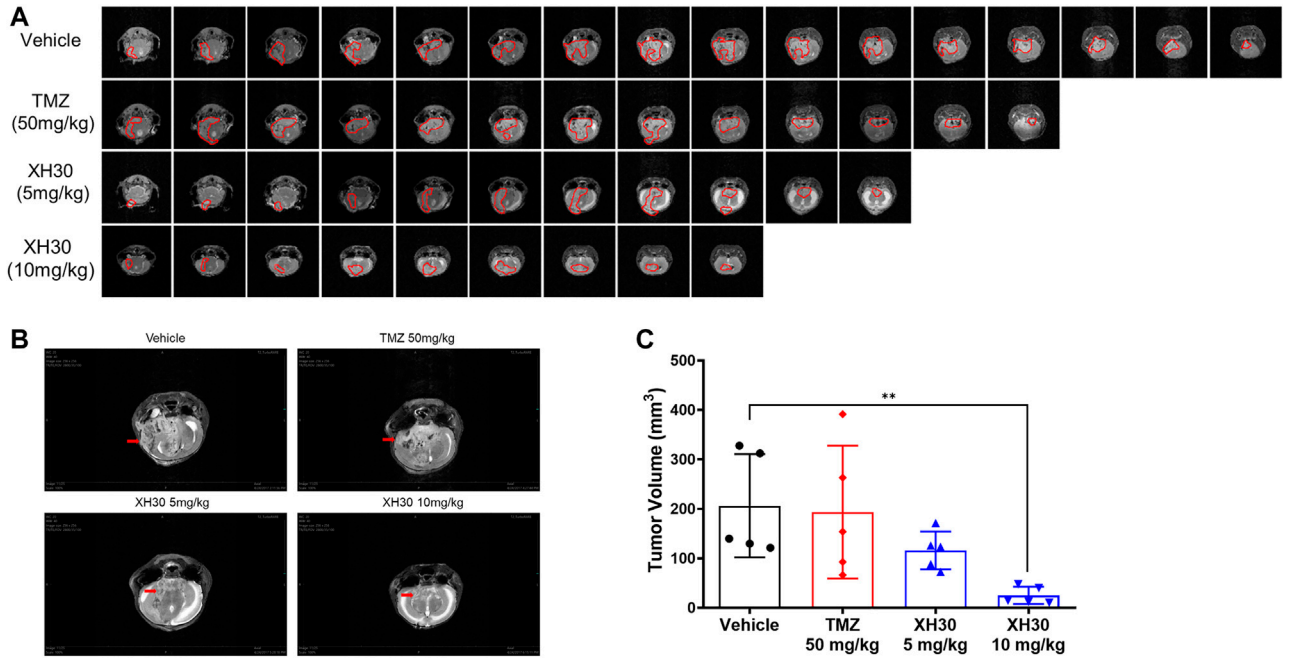


**FIGURE 4 |** XH30 repressed TMZ-resistant GBM growth in a mouse orthotopic xenograft model. **(A)** magnetic resonance imaging (MRI) T2-weighted image of intracranial tumors from the various groups from the U251/TMZ orthotopic model at day 9. Images in each lane show all tumor slices from one representative mouse in each group. The red curves indicate the tumors. **(B)** Representative MRI images from the U251/TMZ orthotopic model at day 9. The red arrows indicate the tumor. **(C)** Tumor volumes in the U251/TMZ orthotopic model at day 9. Data are presented as means ± SD, $n = 5$. ANOVA, $^{**}p < 0.01$ compared with the vehicle control group.

Mice were given TMZ orally at doses of 50 mg/kg/day for 5 days or XH30 at either 5 mg/kg or 10 mg/kg daily for 9 days. In our MRI analysis, the images showed that XH30 suppressed tumor growth in brain (**Figures 4A,B**). At a dose of 10 mg/kg/day, tumor volume was significantly lower compared to the control group that received the drug vehicle ($p < 0.01$; **Figure 4C**; **Supplementary Table S1**). In this model, TMZ did not reduce tumor volume at a dose of 50 mg/kg/day with 6.2% tumor growth inhibition (TGI), whereas the TGI of TMZ at the same dose was 98.4% in a U251 (TMZ sensitive) orthotopic mice model (**Supplementary Figures S3A, B**). During the experiments, the body weight of mice in the XH30 group did not significantly decrease compared to that of the control group (**Supplementary Figure S2A**). Together, these data indicate that XH30 suppressed TMZ-resistant GBM growth *in vivo*.

## XH30 Enhanced TMZ Cytotoxicity in TMZ-Resistant GBM

Because XH30 showed excellent antitumor activity against TMZ-resistant GBM and TMZ resistance is a current barrier to effective treatment in GBM, we investigated whether XH30 could sensitize GBM to TMZ. To do this, XH30 and TMZ were administered together in GBM cells. XH30 at concentrations of 20 and 100 nM enhanced TMZ cytotoxicity in both U251/TMZ and T98G cells (**Figure 5A**). Calculation of the CI gave values of <1 for combined XH30 and TMZ in both cell types, indicating a synergic effect of these drugs (**Supplementary Table S2**). Immunoblotting results showed that the combination of XH30 and TMZ increased the level of the DNA damage marker λH2AX to a greater extent compared with TMZ or XH30 alone, indicating that XH30 increases TMZ cytotoxicity (**Figure 5B**).

We then evaluated whether combining XH30 and TMZ had synergistic antitumor effects *in vivo*. We employed a subcutaneous mouse model implanted with U251/TMZ cells. The groups that received XH30 or a combination of XH30 and TMZ both had significantly delayed tumor growth (**Figure 5C**). Treatment with either TMZ at 50 mg/kg/day or XH30 at 5 mg/kg/day suppressed tumor growth, with TGI values of 58.9% and 69.9%, respectively (**Figures 5D,E**). Combined TMZ and XH30 significantly suppressed tumor growth compared with the groups that received either TMZ or XH30 alone, with a TGI of 90.1%. Although TMZ exhibited antitumor activity, the effect was weaker than in the parent cell line U251 (TMZ sensitive) in the subcutaneous mouse model (58.9% vs. 94.9% TGI, Figure S3C and D). The body weight change with combined TMZ and XH30 treatment was within acceptable limits (**Supplementary Figure S4**). The immunoblotting data also showed that the phosphorylation proteins downstream to PI3K including mTOR, AKT, and S6RP decreased in tumor tissues with XH30 alone and in combination with TMZ (**Figure 5F**).

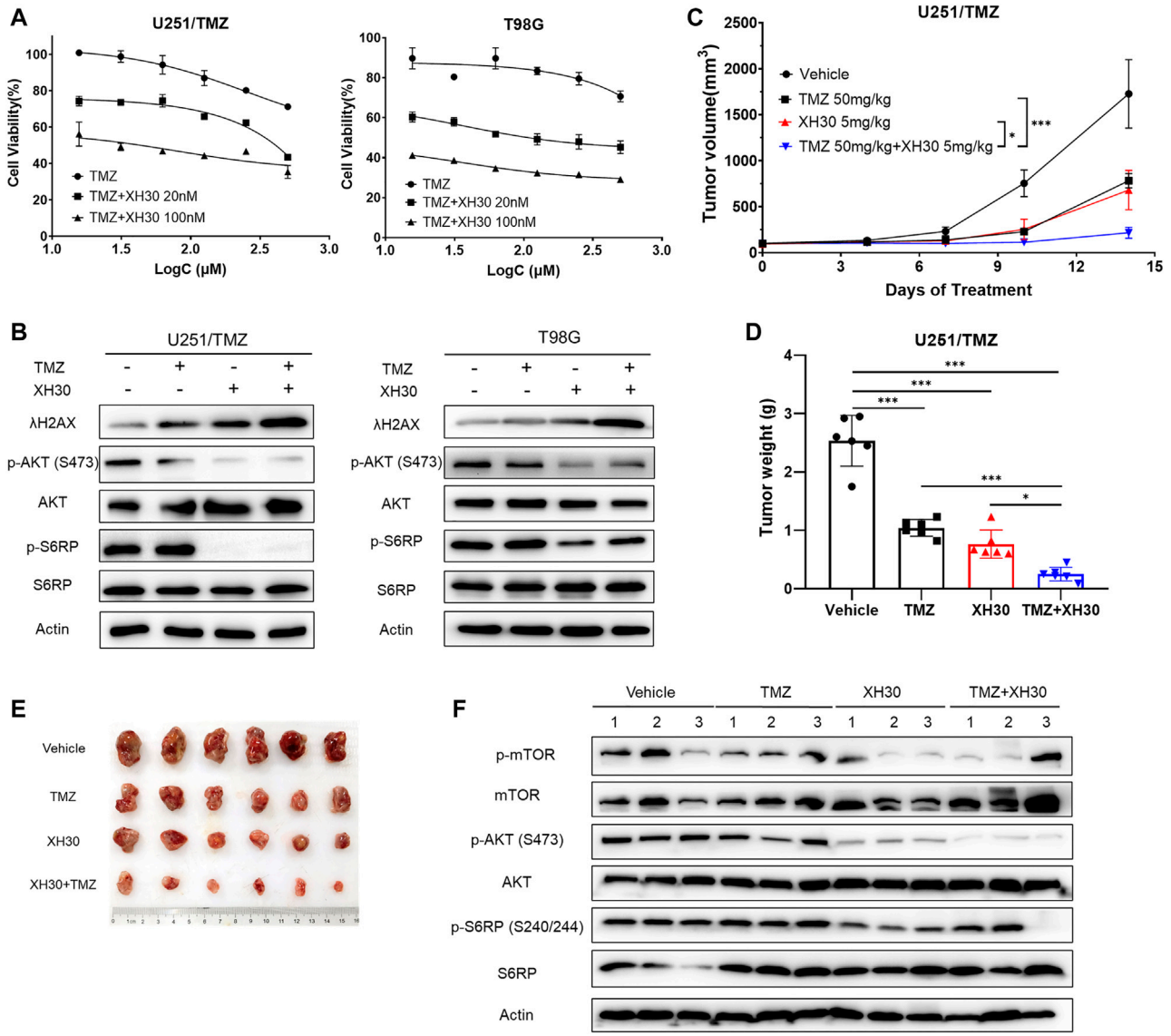


**FIGURE 5 |** XH30 enhanced TMZ response in TMZ-resistant GBM. **(A)** The curve for combined XH30 and TMZ treatment in GBM cells for 72 h. Data are presented as means ± SD, $n = 3$. **(B)** Combination of XH30 with TMZ increased the level of λH2AX. Cells were incubated with XH30 (100 nM) or TMZ (250 μM) for 12 h. **(C)** Antitumor activity of XH30 in an U251/TMZ subcutaneous xenograft model. *t*-test, $^{*}p < 0.05$ and $^{***}p < 0.001$, compared with the TMZ or XH30 group. Data are presented as means ± SD, $n = 6$. **(D)** Tumor weight in an U251/TMZ xenograft model. *t*-test, $^{*}p < 0.05$ and $^{***}p < 0.001$. **(E)** Tumor issues in a U251/TMZ xenograft model. **(F)** Levels of proteins in the PI3K signaling pathway in tumor tissue from the U251/TMZ xenograft mice model.

## XH30 Repressed GLI1 *via* the Noncanonical Hedgehog Signaling Pathway to Increase TMZ Cytotoxicity

The hedgehog signaling pathway has been demonstrated to have a role in TMZ resistance (Li J. et al., 2016; Lee, 2016), and crosstalk between noncanonical hedgehog and PI3K signaling pathways has been documented (Riobo et al., 2006). Previously, we showed that the hedgehog pathway is overactive in both U251/TMZ and T98G cells (Ji et al., 2018). Therefore, we hypothesized that inhibition of PI3K may also inhibit the noncanonical hedgehog pathway to increase the response to TMZ. As shown in **Figure 6A**, the protein levels of GLI1, a key factor in the hedgehog signaling pathway, was dose-dependently decreased in U251/TMZ cells exposed to XH30 in various concentrations, along with decreased levels of phosphorylated AKT. SMO protein levels did not decrease after treatment with XH30. Similar results were also observed in T98G cells. GLI1 target genes, such as *PAX6* and *GLI1* itself, were downregulated in the presence of XH30 at 100 nM (**Figure 6B**), likely because XH30 suppresses noncanonical hedgehog signaling pathway *via* the blockade of PI3K. In T98G cells, another GLI1 target gene, *MGMT*, was also downregulated by XH30. Next, we investigated whether XH30

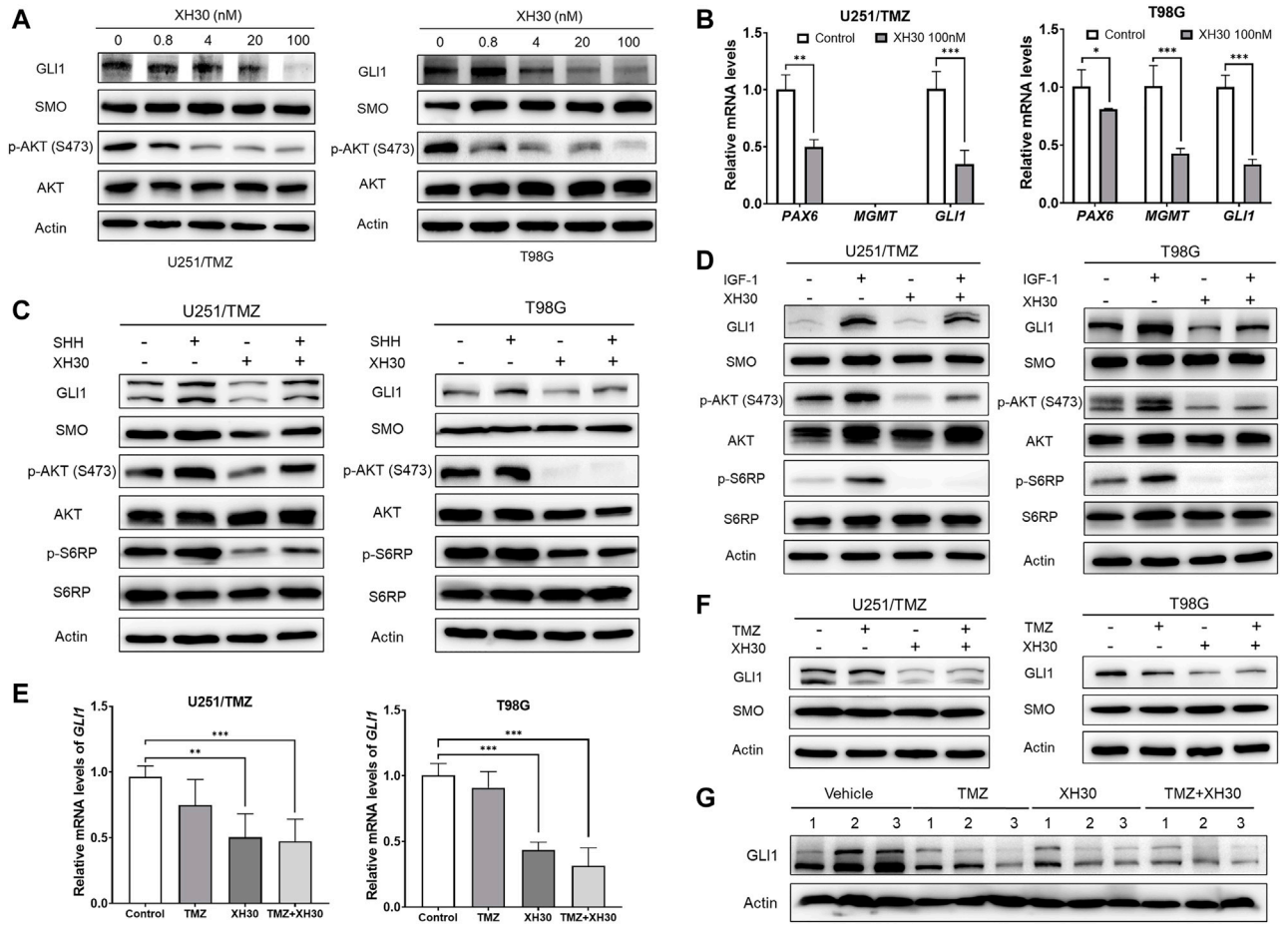


**FIGURE 6 |** XH30 suppressed GLI1 *via* blockade of the noncanonical hedgehog signal pathway. **(A)** XH30 dose-dependently reduced GLI1 protein levels in TMZ-resistant U251/TMZ and T98G cells. Cells were incubated with XH30 at indicated concentrations (0.8, 4, 20, and 100 nmol/L) for 12 h **(B)** XH30 downregulated the GLI1 target gene expression, as indicated by mRNA levels, in both U251/TMZ and T98G cells. Data are presented as means ± SD, $n = 3$. *t*-test, $^{*}p < 0.05$, $^{**}p < 0.01$, and $^{***}p < 0.001$, compared with control. **(C)** XH30 attenuated SHH-triggered GLI1 activation in U251/TMZ and T98G cells. The cells were incubated with XH30 at a concentration of 100 nM in the absence or presence of recombinant SHH (500 ng/ml) for 24 h. **(D)** XH30 reversed GLI1 activation by IGF-1 in U251/TMZ and T98G cells. Cells were incubated with XH30 at a concentration of 100 nM in the absence or presence of recombinant IGF-1 (50 ng/ml) for 12 h. **(E)** XH30 and TMZ in combination maintained lower mRNA levels of *GLI1* in GBM cells. The cells were incubated with XH30 (100 nM) or TMZ (250 μM) for 12 h. *t*-test, $^{**}p < 0.01$ and $^{***}p < 0.001$, compared with control. **(F)** XH30 and TMZ in combination maintained lower protein levels of GLI1 in GBM cells. The cells were incubated with XH30 (100 nM) or TMZ (250 μM) for 12 h. **(G)** Protein levels of GLI1 in tumor tissue from the U251/TMZ xenograft mice model.

was able to block the hedgehog pathway in the presence of the hedgehog ligand SHH (sonic hedgehog). As shown in **Figure 6C**, SHH activated the hedgehog pathway in U251/TMZ and T98G, reflecting upregulated GLI1 expression, whereas XH30 reduced GLI1 expression. In the presence of SHH, XH30 partially reversed SHH-mediated GLI1 activation. The phosphorylation of downstream proteins in the PI3K pathway, including AKT and S6RP, was consistently decreased in cells exposed to XH30. Moreover, insulin-like growth factor 1 (IGF-1), which activates PI3K, also upregulated GLI1 expression, which can be attributed to the crosstalk between the PI3K signaling pathway and GLI1 (**Figure 6D**). In the presence of XH30, IGF-mediated elevation of GLI1 was partially attenuated. There was no obvious change in SMO protein levels. We also observed that XH30 and TMZ in combination maintained lower level of GLI1 expression in both mRNA and protein level in TMZ-resistant GBM cells (**Figures 6E,F**). Immunoblotting results of tumor tissues also showed that the protein levels of GLI1 decreased in XH30 and TMZ combination group compared to vehicle group (**Figure 6G**). Together, our results demonstrate that XH30 suppressed GLI1 *via* blockade of the noncanonical hedgehog signaling pathway.

## DISCUSSION

Glioblastoma is the most aggressive cancer of the brain in adults, and its prevalence is increasing, especially in China (Yang et al., 2013). Standard treatment includes surgery combined with radiotherapy and chemotherapy (Weller et al., 2014). So far, TMZ is the only chemotherapeutic option with confirmed efficacy and an acceptable safety profile in this cancer type (Rajaratnam et al., 2020). In addition, vascular endothelial

growth factor inhibitors and tumor-treating fields have also been approved for the treatment of glioblastoma (Lassman et al., 2020; Seystahl et al., 2020; Zhang et al., 2020). However, patient outcomes from these treatments remain contentious. Clinical trials of immunotherapy with anti-programmed cell death 1 antibodies also did not meet clinical survival endpoints in patients with GBM (Khasraw et al., 2020; Maghrouni et al., 2021). Overactivation of the PI3K pathway occurs frequently in GBM, including in those with TMZ resistance (Sami and Karsy, 2013). In our previous study, XH30 exerted robust antitumor activity against TMZ-sensitive glioblastoma (Lin et al., 2018). Therefore, in this study, we tested this compound in GBM with either natural or acquired TMZ resistance. As expected, XH30 was shown to have acceptable antitumor activity against TMZ-resistant GBM both *in vitro* and *in vivo*, *via* inhibition of PI3K and downstream proteins and induction of cell cycle arrest. Similarly to other pan-PI3K inhibitors, we observed reductions in total white blood cells, neutrophils, and lymphocytes after XH30 treatment in our *in vivo* mouse model (**Supplementary Figure S2B**).

After standard treatment, GMB recurs in most people with this tumor type; TMZ resistance is a primary factor contributing to this process (Bocangel et al., 2002). For recurring tumors, repeated treatment with low doses of TMZ or treatment with lomustine (CCNU) has been recommended (Birzu et al., 2020; Di Nunno et al., 2020; Weller and Le Rhun, 2020). However, the clinical benefits of this approach are limited. The mechanism of TMZ resistance is extremely complex and includes overexpression of MGMT, aberrant activation of the hedgehog signaling pathway, overexpression of P-glycoprotein, and even metabolic reprogramming (Lee, 2016). Many approaches for overcoming TMZ resistance have been assessed (Happold and Weller, 2015), but none have been particularly successful. The hedgehog signal pathway represents an attractive target for glioblastoma treatment; inhibition of this pathway could overcome TMZ resistance (Shahi et al., 2008; Braun et al., 2012). In this context, a particularly interesting finding in our study is that XH30 dose-dependently decreased GLI-1 protein levels and downregulated its target genes including *PAX6* and *GLI1* itself in both U251/TMZ and T98G. In T98G cells, the mRNA level of *MGMT*, which may be regulated by GLI1, was reduced after XH30 treatment as well. This observation triggered us to explore the possible mechanism of XH30 as part of the hedgehog signaling pathway. There have been reports that PI3K signaling pathway is an important non-canonical activator of GLI1 and that targeting the PI3K/AKT pathway *via* GLI inhibition enhances drug sensitivity (Liang et al., 2017). Conversely, GLI1 reduces drug sensitivity *via* direct activation of the PI3K pathway in acute myeloid leukemia (Zhou et al., 2021). In our study, in the presence of SHH, XH30 suppressed the hedgehog pathway and partially reversed GLI1 activation. In addition, when we added IGF-1 to activate the PI3K signaling pathway, we found that GLI1 protein levels increased after IGF-1 stimulation. In the presence of XH30, this GLI1 level increase was partially attenuated. These results provided us with an additional clue that XH30 may play other roles in GBM treatment, which warrants further research.

Previous research has reported that inhibition of hedgehog signal pathway can enhance TMZ cytotoxicity and overcome TMZ resistance (Li J. et al., 2016; Ji et al., 2018). Therefore, we predicted that XH30 may also increase the response to TMZ *via* blockade of the non-canonical hedgehog pathway, allowing direct antitumor activity against TMZ-resistant GBM. In our experiments, XH30 enhanced the cytotoxicity of TMZ in both TMZ-resistant cell types *in vitro*. Treatment with combined XH30 and TMZ increased the level of λH2AX, a marker of DNA damage. Our *in vivo* studies in orthotopic mice also confirmed this synergistic effect. The combination of XH30 with TMZ yielded an improved antitumor activity compared with XH30 or TMZ treatment alone. This suggests that PI3K inhibitors could be tested as adjuvant treatment along with TMZ in patients with recurrent GMB.

In conclusion, the PI3K inhibitor XH30 exhibited robust antitumor activity in TMZ-resistant GBM; this compound is therefore a novel potential therapeutic option for TMZ-resistant GBM.

## DATA AVAILABILITY STATEMENT

The original contributions presented in the study are included in the article/**Supplementary Material**; further inquiries can be directed to the corresponding authors.

## ETHICS STATEMENT

The animal study was reviewed and approved by the Ethics Committee for Animal Experiments of the Institute of Materia Medica, Chinese Academy of Medical Sciences and Peking Union Medical College.

## AUTHOR CONTRIBUTIONS

MJ designed the experiments. MJ, ZZ, and CW conducted all the experiments. SL synthesized the compound. MJ drafted the manuscript. NX, HX, and XC reviewed and edited the manuscript and supervised the entire study. All authors reviewed and approved the final version of the manuscript.

## FUNDING

This work was supported by the Non-Profit Central Research Institute Fund of Chinese Academy of Medical Sciences (Grant 2018PT35003).

## ACKNOWLEDGMENTS

We thank Charlesworth (https://www.cwauthors.com/) for its linguistic assistance during the preparation of this manuscript.

## SUPPLEMENTARY MATERIAL

The Supplementary Material for this article can be found online at: https://www.frontiersin.org/articles/10.3389/fphar.2021.749242/full#supplementary-material

## REFERENCES


Avery, J. T., Zhang, R., and Boohaker, R. J. (2021). GLI1: A Therapeutic Target for Cancer. *Front. Oncol.* 11, 673154. doi:10.3389/fonc.2021.673154

Birzu, C., French, P., Caccese, M., Cerretti, G., Idbaih, A., Zagonel, V., et al. (2020). Recurrent Glioblastoma: From Molecular Landscape to New Treatment Perspectives. *Cancers (Basel)* 13. doi:10.3390/cancers13010047

Bocangel, D. B., Finkelstein, S., Schold, S. C., Bhakat, K. K., Mitra, S., and Kokkinakis, D. M. (2002). Multifaceted Resistance of Gliomas to Temozolomide. *Clin. Cancer Res.* 8, 2725–2734.

Braun, S., Oppermann, H., Mueller, A., Renner, C., Hovhannisyan, A., Baran-Schmidt, R., et al. (2012). Hedgehog Signaling in Glioblastoma Multiforme. *Cancer Biol. Ther.* 13, 487–495. doi:10.4161/cbt.19591

Castresana, J. S., and Melendez, B. (2021). Molecular and Cellular Mechanisms of Glioblastoma. *Cells* 10. doi:10.3390/cells10061456

Chien, C. H., Hsueh, W. T., Chuang, J. Y., and Chang, K. Y. (2021). Dissecting the Mechanism of Temozolomide Resistance and its Association with the Regulatory Roles of Intracellular Reactive Oxygen Species in Glioblastoma. *J. Biomed. Sci.* 28, 18. doi:10.1186/s12929-021-00717-7

Colardo, M., Segatto, M., and Di Bartolomeo, S. (2021). Targeting RTK-Pi3k-mTOR Axis in Gliomas: An Update. *Int. J. Mol. Sci.* 22. doi:10.3390/ijms22094899

Deangelis, L. M. (2001). Brain Tumors. *N. Engl. J. Med.* 344, 114–123. doi:10.1056/NEJM200101113440207

Di Nunno, V., Franceschi, E., Tosoni, A., Di Battista, M., Gatto, L., Lamperini, C., et al. (2020). Treatment of Recurrent Glioblastoma: State-Of-The-Art and Future Perspectives. *Expert Rev. Anticancer Ther.* 20, 785–795. doi:10.1080/14737140.2020.1807949

Dymova, M. A., Kuligina, E. V., and Richter, V. A. (2021). Molecular Mechanisms of Drug Resistance in Glioblastoma. *Int. J. Mol. Sci.* 22. doi:10.3390/ijms22126385

Gil Del Alcazar, C. R., Hardebeck, M. C., Mukherjee, B., Tomimatsu, N., Gao, X., Yan, J., et al. (2014). Inhibition of DNA Double-Strand Break Repair by the Dual PI3K/mTOR Inhibitor NVP-Bez235 as a Strategy for Radiosensitization of Glioblastoma. *Clin. Cancer Res.* 20, 1235–1248. doi:10.1158/1078-0432.CCR-13-1607

Hainsworth, J. D., Becker, K. P., Mekhail, T., Chowdhary, S. A., Eakle, J. F., Wright, D., et al. (2019). Phase I/II Study of Bevacizumab with BKM120, an Oral PI3K Inhibitor, in Patients with Refractory Solid Tumors (Phase I) and Relapsed/refractory Glioblastoma (Phase II). *J. Neurooncol.* 144, 303–311. doi:10.1007/s11060-019-03227-7

Happold, C., and Weller, M. (2015). New Insights into Acquired Temozolomide Resistance in Glioblastoma? *Brain* 138, 3468–3470. doi:10.1093/brain/awv301

Ji, M., Wang, L., Chen, J., Xue, N., Wang, C., Lai, F., et al. (2018). CAT3, a Prodrug of 13A(S)-3-hydroxyl-6,7-dimethoxyphenanthro[9,10-b]-indolizidine, Circumvents Temozolomide-Resistant Glioblastoma via the Hedgehog Signaling Pathway, Independently of O6-Methylguanine DNA Methyltransferase Expression. *Onco. Targets Ther.* 11, 3671–3684. doi:10.2147/OTT.S163535

Ji, M., Wang, D., Lin, S., Wang, C., Li, L., Zhang, Z., et al. (2021). A Novel PI3K Inhibitor XH30 Suppresses Orthotopic Glioblastoma and Brain Metastasis in Mice Models. *Acta Pharm. Sin. B.*

Khasraw, M., Reardon, D. A., Weller, M., and Sampson, J. H. (2020). PD-1 Inhibitors: Do They Have a Future in the Treatment of Glioblastoma? *Clin. Cancer Res.* 26, 5287–5296. doi:10.1158/1078-0432.CCR-20-1135

Langhans, J., Schneele, L., Trenkler, N., Von Bandemer, H., Nonnenmacher, L., Karpel-Massler, G., et al. (2017). The Effects of PI3K-Mediated Signalling on Glioblastoma Cell Behaviour. *Oncogenesis* 6, 398. doi:10.1038/s41389-017-0004-8

Lassman, A. B., Joanta-Gomez, A. E., Pan, P. C., and Wick, W. (2020). Current Usage of Tumor Treating fields for Glioblastoma. *Neurooncol. Adv.* 2, vdaa069. doi:10.1093/noajnl/vdaa069

Lee, S. Y. (2016). Temozolomide Resistance in Glioblastoma Multiforme. *Genes Dis.* 3, 198–210. doi:10.1016/j.gendis.2016.04.007

Li, J., Cai, J., Zhao, S., Yao, K., Sun, Y., Li, Y., et al. (2016a). GANT61, a GLI Inhibitor, Sensitizes Glioma Cells to the Temozolomide Treatment. *J. Exp. Clin. Cancer Res.* 35, 184. doi:10.1186/s13046-016-0463-3

Li, X., Wu, C., Chen, N., Gu, H., Yen, A., Cao, L., et al. (2016b). PI3K/Akt/mTOR Signaling Pathway and Targeted Therapy for Glioblastoma. *Oncotarget* 7, 33440–33450. doi:10.18632/oncotarget.7961

Liang, H., Zheng, Q. L., Fang, P., Zhang, J., Zhang, T., Liu, W., et al. (2017). Targeting the PI3K/AKT Pathway via GLI1 Inhibition Enhanced the Drug Sensitivity of Acute Myeloid Leukemia Cells. *Sci. Rep.* 7, 40361. doi:10.1038/srep40361

Liau, L. M. (2021). Glioblastoma: Molecular Mechanisms and Clinical Trials. *Neurosurg. Clin. N. Am.* 32, xiii. doi:10.1016/j.nec.2021.03.001

Lin, S., Wang, C., Ji, M., Wu, D., Lv, Y., Zhang, K., et al. (2018). Discovery and Optimization of 2-Amino-4-Methylquinazoline Derivatives as Highly Potent Phosphatidylinositol 3-Kinase Inhibitors for Cancer Treatment. *J. Med. Chem.* 61, 6087–6109. doi:10.1021/acs.jmedchem.8b00416

Maghrouni, A., Givari, M., Jalili-Nik, M., Mollazadeh, H., Bibak, B., Sadeghi, M. M., et al. (2021). Targeting the PD-1/pd-L1 Pathway in Glioblastoma Multiforme: Preclinical Evidence and Clinical Interventions. *Int. Immunopharmacol.* 93, 107403. doi:10.1016/j.intimp.2021.107403

Melamed, J. R., Morgan, J. T., Ioele, S. A., Gleghorn, J. P., Sims-Mourtada, J., and Day, E. S. (2018). Investigating the Role of Hedgehog/GLI1 Signaling in Glioblastoma Cell Response to Temozolomide. *Oncotarget* 9, 27000–27015. doi:10.18632/oncotarget.25467

Mizuarai, S., Kawagishi, A., and Kotani, H. (2009). Inhibition of p70S6K2 Down-Regulates Hedgehog/GLI Pathway in Non-small Cell Lung Cancer Cell Lines. *Mol. Cancer* 8, 44. doi:10.1186/1476-4598-8-44

Perazzoli, G., Prados, J., Ortiz, R., Caba, O., Cabeza, L., Berdasco, M., et al. (2015). Temozolomide Resistance in Glioblastoma Cell Lines: Implication of MGMT, MMR, P-Glycoprotein and CD133 Expression. *PLoS One* 10, e0140131. doi:10.1371/journal.pone.0140131

Radoul, M., Chaumeil, M. M., Eriksson, P., Wang, A. S., Phillips, J. J., and Ronen, S. M. (2016). MR Studies of Glioblastoma Models Treated with Dual PI3K/mTOR Inhibitor and Temozolomide:Metabolic Changes Are Associated with Enhanced Survival. *Mol. Cancer Ther.* 15, 1113–1122. doi:10.1158/1535-7163.MCT-15-0769

Rajaratnam, V., Islam, M. M., Yang, M., Slaby, R., Ramirez, H. M., and Mirza, S. P. (2020). Glioblastoma: Pathogenesis and Current Status of Chemotherapy and Other Novel Treatments. *Cancers (Basel)* 12. doi:10.3390/cancers12040937

Ranjan, A., and Srivastava, S. K. (2017). Penfluridol Suppresses Glioblastoma Tumor Growth by Akt-Mediated Inhibition of GLI1. *Oncotarget* 8, 32960–32976. doi:10.18632/oncotarget.16515

Riobó, N. A., Lu, K., Ai, X., Haines, G. M., and Emerson, C. P., Jr. (2006). Phosphoinositide 3-kinase and Akt Are Essential for Sonic Hedgehog Signaling. *Proc. Natl. Acad. Sci. U S A.* 103, 4505–4510. doi:10.1073/pnas.0504337103

Sami, A., and Karsy, M. (2013). Targeting the PI3K/AKT/mTOR Signaling Pathway in Glioblastoma: Novel Therapeutic Agents and Advances in Understanding. *Tumour Biol.* 34, 1991–2002. doi:10.1007/s13277-013-0800-5

Seystahl, K., Hentschel, B., Loew, S., Gramatzki, D., Felsberg, J., Herrlinger, U., et al. (2020). Bevacizumab versus Alkylating Chemotherapy in Recurrent Glioblastoma. *J. Cancer Res. Clin. Oncol.* 146, 659–670. doi:10.1007/s00432-019-03086-9

Shahi, M. H., Lorente, A., and Castresana, J. S. (2008). Hedgehog Signalling in Medulloblastoma, Glioblastoma and Neuroblastoma. *Oncol. Rep.* 19, 681–688. doi:10.3892/or.19.3.681

Singh, R., Dhanyamraju, P. K., and Lauth, M. (2017). DYRK1B Blocks Canonical and Promotes Non-canonical Hedgehog Signaling through Activation of the mTOR/AKT Pathway. *Oncotarget* 8, 833–845. doi:10.18632/oncotarget.13662

Touat, M., Idbaih, A., Sanson, M., and Ligon, K. L. (2017). Glioblastoma Targeted Therapy: Updated Approaches from Recent Biological Insights. *Ann. Oncol.* 28, 1457–1472. doi:10.1093/annonc/mdx106

Wang, Y., Ding, Q., Yen, C. J., Xia, W., Izzo, J. G., Lang, J. Y., et al. (2012). The Crosstalk of mTOR/S6K1 and Hedgehog Pathways. *Cancer Cell* 21, 374–387. doi:10.1016/j.ccr.2011.12.028

Weller, M., and Le Rhun, E. (2020). How Did Lomustine Become Standard of Care in Recurrent Glioblastoma? *Cancer Treat. Rev.* 87, 102029. doi:10.1016/j.ctrv.2020.102029

Weller, M., Van Den Bent, M., Hopkins, K., Tonn, J. C., Stupp, R., Falini, A., et al. (2014). European Association for Neuro-Oncology Task Force on Malignant, GEANO Guideline for the Diagnosis and Treatment of Anaplastic Gliomas and Glioblastoma. *Lancet Oncol.* 15, e395–e403. doi:10.1016/s1470-2045(14)70011-7

Wen, P. Y., Touat, M., Alexander, B. M., Mellinghoff, I. K., Ramkissoon, S., Mccluskey, C. S., et al. (2019). Buparlisib in Patients with Recurrent Glioblastoma Harboring Phosphatidylinositol 3-Kinase Pathway Activation: An Open-Label, Multicenter, Multi-Arm, Phase II Trial. *J. Clin. Oncol.* 37, 741–750. doi:10.1200/JCO.18.01207

Yang, P., Wang, Y., Peng, X., You, G., Zhang, W., Yan, W., et al. (2013). Management and Survival Rates in Patients with Glioma in China (2004-2010): a Retrospective Study from a Single-Institution. *J. Neurooncol.* 113, 259–266. doi:10.1007/s11060-013-1103-9

Yun, E. J., Kim, S., Hsieh, J. T., and Baek, S. T. (2020). Wnt/β-catenin Signaling Pathway Induces Autophagy-Mediated Temozolomide-Resistance in Human Glioblastoma. *Cell Death Dis* 11, 771. doi:10.1038/s41419-020-02988-8

Zając, A., Sumorek-Wiadro, J., Langner, E., Wertel, I., Maciejczyk, A., Pawlikowska-Pawlęga, B., et al. (2021). Involvement of PI3K Pathway in Glioma Cell Resistance to Temozolomide Treatment. *Int. J. Mol. Sci.* 22. doi:10.3390/ijms22105155

Zhang, C., Du, J., Xu, W., Huang, H., and Gao, L. (2020). The Value of Tumor Treating Fields in Glioblastoma. *J. Korean Neurosurg. Soc.* 63, 681–688. doi:10.3340/jkns.2019.0224

Zhang, P., Chen, X. B., Ding, B. Q., Liu, H. L., and He, T. (2018). Down-regulation of ABCE1 Inhibits Temozolomide Resistance in Glioma through the PI3K/Akt/NF-Kb Signaling Pathway. *Biosci. Rep.* 38. doi:10.1042/BSR20181711

Zhao, H. F., Wang, J., Shao, W., Wu, C. P., Chen, Z. P., To, S. T., et al. (2017). Recent Advances in the Use of PI3K Inhibitors for Glioblastoma Multiforme: Current Preclinical and Clinical Development. *Mol. Cancer* 16, 100. doi:10.1186/s12943-017-0670-3

Zheng, Y., Liu, L., Wang, Y., Xiao, S., Mai, R., Zhu, Z., et al. (2021). Glioblastoma Stem Cell (GSC)-derived PD-L1-Containing Exosomes Activates AMPK/ULK1 Pathway Mediated Autophagy to Increase Temozolomide-Resistance in Glioblastoma. *Cell. Biosci.* 11, 63. doi:10.1186/s13578-021-00575-8

Zhou, C., Du, J., Zhao, L., Liu, W., Zhao, T., Liang, H., et al. (2021). GLI1 Reduces Drug Sensitivity by Regulating Cell Cycle through PI3K/AKT/GSK3/CDK Pathway in Acute Myeloid Leukemia. *Cell. Death Dis.* 12, 231. doi:10.1038/s41419-021-03504-2

Zhou, J., Zhu, G., Huang, J., Li, L., Du, Y., Gao, Y., et al. (2016). Non-canonical GLI1/2 Activation by PI3K/AKT Signaling in Renal Cell Carcinoma: A Novel Potential Therapeutic Target. *Cancer Lett.* 370, 313–323. doi:10.1016/j.canlet.2015.11.006

**Conflict of Interest:** The authors declare that the research was conducted in the absence of any commercial or financial relationships that could be construed as a potential conflict of interest.

**Publisher's Note:** All claims expressed in this article are solely those of the authors and do not necessarily represent those of their affiliated organizations or those of the publisher, the editors, and the reviewers. Any product that may be evaluated in this article, or claim that may be made by its manufacturer, is not guaranteed or endorsed by the publisher.

frontiers in Chemistry

MINI REVIEW
published: 16 December 2021
doi: 10.3389/fchem.2021.775226

# Targeting Mitochondrial Metabolism and RNA Polymerase POLRMT to Overcome Multidrug Resistance in Cancer

*Hui-Jing Yu*[1], *Guan-Li Xiao*[1], *Yu-Ying Zhao*[2], *Xin-Xin Wang*[2] *and Rongfeng Lan*[2]*

[1]School of Pharmaceutical Sciences, Shenzhen University Health Science Center, Shenzhen, China, [2]Department of Cell Biology and Medical Genetics, School of Basic Medical Sciences, Shenzhen University Health Science Center, Shenzhen, China

Clinically, the prognosis of tumor therapy is fundamentally affected by multidrug resistance (MDR), which is primarily a result of enhanced drug efflux mediated by channels in the membrane that reduce drug accumulation in tumor cells. How to restore the sensitivity of tumor cells to chemotherapy is an ongoing and pressing clinical issue. There is a prevailing view that tumor cells turn to glycolysis for energy supply due to hypoxia. However, studies have shown that mitochondria also play crucial roles, such as providing intermediates for biosynthesis through the tricarboxylic acid (TCA) cycle and a plenty of ATP to fuel cells through the complete breakdown of organic matter by oxidative phosphorylation (OXPHOS). High OXPHOS have been found in some tumors, particularly in cancer stem cells (CSCs), which possess increased mitochondria mass and may be depends on OXPHOS for energy supply. Therefore, they are sensitive to inhibitors of mitochondrial metabolism. In view of this, we should consider mitochondrial metabolism when developing drugs to overcome MDR, where mitochondrial RNA polymerase (POLRMT) would be the focus, as it is responsible for mitochondrial gene expression. Inhibition of POLRMT could disrupt mitochondrial metabolism at its source, causing an energy crisis and ultimately eradicating tumor cells. In addition, it may restore the energy supply of MDR cells to glycolysis and re-sensitize them to conventional chemotherapy. Furthermore, we discuss the rationale and strategies for designing new therapeutic molecules for MDR cancers by targeting POLRMT.

**Keywords: cancer stem cell, multidrug resisitance, OxPhos, POLRMT, RNA polymerase**

OPEN ACCESS

***Edited by:***
*Youhui Lin,*
*Xiamen University, China*

***Reviewed by:***
*Parmanand Malvi,*
*Yale University, United States*
*Hongli Du,*
*South China University of Technology, China*

***Correspondence:**
*Rongfeng Lan*
*lan@szu.edu.cn*

***Specialty section:***
*This article was submitted to Chemical Biology, a section of the journal Frontiers in Chemistry*

***Received:*** *22 September 2021*
***Accepted:*** *06 December 2021*
***Published:*** *16 December 2021*

***Citation:***
*Yu H-J, Xiao G-L, Zhao Y-Y, Wang X-X and Lan R (2021) Targeting Mitochondrial Metabolism and RNA Polymerase POLRMT to Overcome Multidrug Resistance in Cancer. Front. Chem. 9:775226. doi: 10.3389/fchem.2021.775226*

## INTRODUCTION

Cancer multidrug resistance (MDR) is the development of resistance of tumor cells to drugs with different structures and mechanisms of action after exposure to a particular anticancer drug. This resistance is a unique broad-spectrum phenomenon, acquired by tumor cells, either innately or later in life. The presence of MDR leads to increasingly poor prognosis and failure of chemotherapy in clinical trials (Szakacs et al., 2006). There are three main reasons for the formation of MDR: first, reduced uptake of the drug, which may be due to a reduction or closure of transmembrane channels that transport the drug into the cells. Second, alteration or modification of the drug, which reduces the potency of the drug. Third, efflux of the drug. According to many years of research, members of the ATP-binding cassette (ABC) transporter family, such as the ATP-dependent translocase ABCB1

(also known as multidrug resistance protein 1) (MDR1), multidrug resistance-associated protein 1 (MRP1), and mitoxantrone resistance protein (MXR), are the main causes of increased efflux and resistance to chemotherapy in most tumors (Szakacs et al., 2006; Holohan et al., 2013). These proteins are ATP-dependent transporters that actively pump drugs out of the cells, thereby increasing drug efflux and reducing intracellular accumulation. MDR1 reversal agents, such as verapamil and cyclosporine A, have been developed to inhibit the efflux activity of MDR1 and restore the sensitivity of cancers to chemotherapeutic drugs (Szakacs et al., 2006). However, the results of clinical studies proved to be disappointing, with the aforementioned MDR1 reversal agents struggling to achieve effective concentrations due to their high *in vivo* toxicity, and even the clinical application of MDR1 reversal agents was suboptimal due to the surrogate effects of abundant members of the ABC family. Therefore, there is a great need to rethink how to overcome MDR, especially with new inhibitors designed for new targets in the altered pathways.

Mitochondria are sensitive and versatile organelles that provide a large amount of energy for cellular activities and are the main sites of biological oxidation and energy conversion in living organisms, hence the name "power plant" in eukaryotic cells. The TCA cycle in the mitochondrial matrix completely oxidizes organic matter and releases much more energy than glycolysis via OXPHOS, and also provides intermediates for the biosynthesis of amino acids, porphyrins, pyrimidines, etc. (DeBerardinis and Chandel, 2020). Thus, mitochondria are the hub of cellular metabolism. Changes in mitochondria are associated with important cellular events, such as apoptosis and senescence, and are closely linked to various pathologies, such as mitochondrial encephalopathy, fatigue intolerance, senescence, short stature, and neurological deafness (Olahova et al., 2021). Studies have shown profound changes in cellular metabolism and mitochondria in tumor cells, and glycolysis, TCA cycle and OXPHOS are all thought to play important roles in tumor cells, especially the latter two providing the cells with robust ATP and intermediates for biosynthesis (Fulda et al., 2010). In light of this, it may be important to investigate approaches targeting MDR cancers from new perspectives, such as targeting cellular metabolism, mitochondrial metabolism, and energy conversion (Weinberg and Chandel, 2015). In this paper, we focus on mitochondrial metabolism, specifically POLRMT, which controls the expression of mitochondria-encoded genes. We discuss the rationale for targeting POLRMT in the hope of providing insights and new pathways to overcome MDR.

## Metabolism Reprogramming and Transformation of Energy Supply in Cancer Cells

The main manifestation of tumorigenesis is a failure of cell cycle regulation and, in fact, profound changes in mitochondria. It has long been thought that cancer relies on glycolysis to produce ATP and intermediates for biosynthesis (Warburg effect) (Vander Heiden et al., 2009; DeBerardinis and Chandel, 2020), thus many tumors are addicted to glucose or glutamine. However, tumors are heterogeneous and not as homogenous as previously expected, containing subpopulations of cells strictly dependent on OXPHOS. Indeed, recent reports have shown that the supply of robust ATP and biosynthetic intermediates via mitochondrial metabolism is critical for tumor growth. Studies have shown that upregulation of OXPHOS can be a selective vulnerability for cancer stem cells (CSCs) and MDR cancers (Kuntz et al., 2017; Molina et al., 2018), and consistent with these observations, inhibitors of OXPHOS can be used to eradicate cancer (Crunkhorn, 2021). As a result, mitochondrial metabolism is now becoming a Frontier for cancer therapy (Weinberg and Chandel, 2015; Martinez-Outschoorn et al., 2017). However, tumors are not uniform but heterogeneous and may harbor a subset of CSCs capable of repopulating the entire tumor. Interestingly, CSCs also differ between cancer types, being either glycolytic or OXPHOS dependent (Sancho et al., 2016; Bosc et al., 2017). CSCs contain a range of properties, including undifferentiated state, robust DNA damage response, high antioxidant capacity, and metabolic plasticity, etc. that confer them the ability to escape conventional cancer therapy and achieve a resistant phenotype via permanent cell revolution (Garcia-Mayea et al., 2020). It is also clear that hematological neoplasm and many MDRs are subsequently reprogrammed for energy supply, and they shifted to OXPHOS for the energy supply and biosynthetic intermediates (Sancho et al., 2016; Mukha and Dubrovska, 2020). Unlike non-stem cancer cells, CSCs are relatively quiescent rather than rapidly proliferating, which distinguishes them from cancer cell populations. In addition, CSCs are expected to addicted to mitochondrial metabolism and in some cancers rely on OXPHOS for energy supply (Funes et al., 2007). In Drosophila, OXPHOS is able to drive the immortalization of neural stem cells during tumorigenesis (Bonnay et al., 2020). Even in chemotherapy-resistant acute myeloid leukemia (AML) cells that dot not enriched for CSCs, mitochondrial metabolism with a highly active OXPHOS is still required (Farge et al., 2017). Thus, targeting mitochondrial metabolism may induce an energy shift to low OXPHOS and resensitization to conventional cancer therapy. Interestingly, blocking glucose supply by metformin, a standard diabetic drug, showed specific inhibition of CSCs derived from breast cancers (Vasan et al., 2020). Also, metformin has synergistic effects with conventional chemotherapeutic agents such as doxorubicin to eradicate CSCs and non-stem cancer cells, respectively (Hirsch et al., 2009). Inhibition of mitochondrial electron transport, protein synthesis, or fatty-acid oxidation leads to low OXPHOS and significantly enhanced chemotherapeutic effects (Bosc et al., 2017). Thus, targeting OXPHOS may shift energetic and metabolic to glycolysis and largely enhanced the effects of chemotherapy.

## Rationale for Inhibition Mitochondrial Metabolism to Overcome MDR

While the metabolic properties of CSCs need to be adequately addressed, mitochondrial metabolism is necessary to maintain the properties of CSCs, which mainly contribute to tumor

therapeutic resistance, including ROS resistance, robust DNA damage response, altered microenvironment and metabolism (Martinez-Outschoorn et al., 2017), all of which are associated with mitochondria-mediated antioxidant capacity (Ding et al., 2015). Consistently, increased mitochondrial mass or OXPHOS has been found in multiple tumor types (Lamb et al., 2015). Therefore, by inhibiting OXPHOS, reducing mitochondrial membrane potential, and disrupting mitochondrial biogenesis, i.e., all are effective ways of targeting mitochondria to eradicate tumor cells (Skrtic et al., 2011; Kuntz et al., 2017; Ashton et al., 2018; Shi et al., 2019; Vasan et al., 2020). Gene mutations are probably the most widespread cause of OXPHOS restoration in tumor cells. For example, it has been shown that gene mutations can promote enhanced OXPHOS activity. In *RB1*-deficient MDA-MB-436 breast xenografts, OXPHOS is highly upregulated and can be inhibited by the mitochondrial translation inhibitor tigecycline, which ultimately strongly impairs tumor growth (Jones et al., 2016; Zacksenhaus et al., 2017). Like *RB-1* deletion, depletion of *ATP5H* (a subunit of ATP synthase) confers a resistant and stem-like phenotype to tumor cells by triggering a reprogramming of mitochondrial metabolism (Song et al., 2018). Furthermore, *SMARCA4,* a subunit of the SWI/SNF complex, is frequently inactivated, leading to enhanced OXPHOS and increased sensitivity to OXPHOS inhibition in lung cancer (Lissanu Deribe et al., 2018). Other examples, in AML, they are more reliable to high OXPHOS and mitochondrial metabolism, possibly due to easier access to sufficient oxygen in the circulation. Studies using different types of inhibitors targeting mitochondrial metabolism and even POLRMT have shown effective inhibition of AML (Bralha et al., 2015; Farge et al., 2017; Molina et al., 2018). Inhibition of OXPHOS has the added benefit that leukemic stem cells may not be able to respond to a decrease in OXPHOS by increasing glycolysis. In theory, it is reasonable that strategies targeting mitochondrial metabolism should be broadly applicable to different cancer types that rely on OXPHOS. Furthermore, inhibitors targeting mitochondrial metabolism may play a synergistic anticancer role with conventional chemotherapy (e.g., inhibition of glycolysis or kinases) (Ashton et al., 2018). Interestingly, cancer cells turn more depend on OXPHOS after targeted therapy, due to elevated activity of PGC-1α (peroxisome proliferator-activated receptor gamma coactivator 1-α), a regulator of mitochondrial biogenesis (Haq et al., 2013; Ashton et al., 2018). Thus, by synergizing conventional chemotherapy with mitochondrial targeting, this is a reasonable and novel pathway for cancer treatment. Inhibition of OXPHOS may provide a promising strategy to overcome MDR cancers.

## Rationale for Targeting POLRMT to Undermine ETC and OXPHOS to Overcome MDR

Consistent with the high activity of OXPHOS in CSCs, the mitochondrial transcriptional machinery and subsequent protein translation is upregulated and predicted poor prognosis in patients with AML, breast cancer, or NSCLC, among others. (Skrtic et al., 2011; Wu et al., 2019; Zhou et al., 2021). Therefore, mitochondrial DNA transcription and translation may be a therapeutic target. Among the genes associated with mitochondrial gene expression, POLRMT plays a key role (**Figure 1**). Clinically, pathogenic *POLRMT* variants induce developmental delay, short stature, hypotonia, and neurological disorders, such as mental retardation in childhood (Olahova et al., 2021). The rational for targeting POLRMT is that rapidly dividing cells such as cancer require high OXPHOS, whereas terminally differentiated cells such as heart and muscle show good tolerance to OXPHOS inhibition (Bonekamp et al., 2020) (**Figure 1**). POLRMT is a single subunit and nuclear encoded RNA polymerase that catalyzes the transcription of mitochondrial DNA (mtDNA) into RNA (Hillen et al., 2017). POLRMT shows significant sequence homology with mitochondrial RNA polymerases from lower eukaryotes and several phages (Kuhl et al., 2014). They were closely related in structure, but not to other nuclear RNA polymerases including Pol I, II, or III. Circular mammalian mtDNA encodes 13 core proteins of OXPHOS, 12S and 16S ribosomal RNAs, and 22 transfer RNAs. In addition, all 13 proteins are essential components of the complexes that form mitochondrial ETC and OXPHOS pathways (complexes I, III, IV, and V). Thus, POLRMT is required for the biogenesis of the OXPHOS system, although gene expression in mitochondria is also dependent on hundreds of nuclear genes that encode proteins and RNA components either required for mtDNA replication and translation of mtDNA transcripts (Kuhl et al., 2014; Bonekamp et al., 2020). Furhtermore, POLRMT acts as a primase for mtDNA replication, regulating the transition between replication primer formation and gene expression, suggesting a key role in the maintenance and propagation of the mitochondrial genome (Kuhl et al., 2016).

Because POLRMT is expressed by nuclear-encoded gene, it is a key regulator of nucleo-mitochondrial signaling crosstalk. Inhibition of POLRMT impairs mtDNA replication and mitochondrial biogenesis. Thus, POLRMT is of fundamental importance for both mitochondrial genome expression and replication. Bonekamp et al. identified the first-in-class compound IMT1B (LDC203974) for targeting POLRMT (Bonekamp et al., 2020; Crunkhorn, 2021). Inhibition of POLRMT impairs mitochondrial transcription and OXPHOS protein synthesis, leading to dysfunction of the OXPHOS protein complex and cellular energy crisis, resulting in inhibition of a broad spectrum of cancer cells. Thus, POLRMT inhibitors are promising molecules to overcoming MDR. More importantly, IMT1B treatment was well tolerated in mice for up to 4 weeks and showed no effect on mtDNA in liver and heart and only a slight effect on mitochondrial transcripts compared to the tumors, although germ line cells were not examined (Bonekamp et al., 2020). It can be speculated that the side effects or toxicity of mitochondrial targeting molecules may be focused on tissue and cell types that are proliferating, such as the hematopoietic system, gastrointestinal epithelium, germ cells, hair follicle cells, periodontal cells, liver and spleen cells, and terminal differentiated cells that relay mitochondrial energy supply, such as cardiac and skeletal muscle cells, neurons, etc. Mouse models of conditional knockout of *Tfam* (mitochondrial

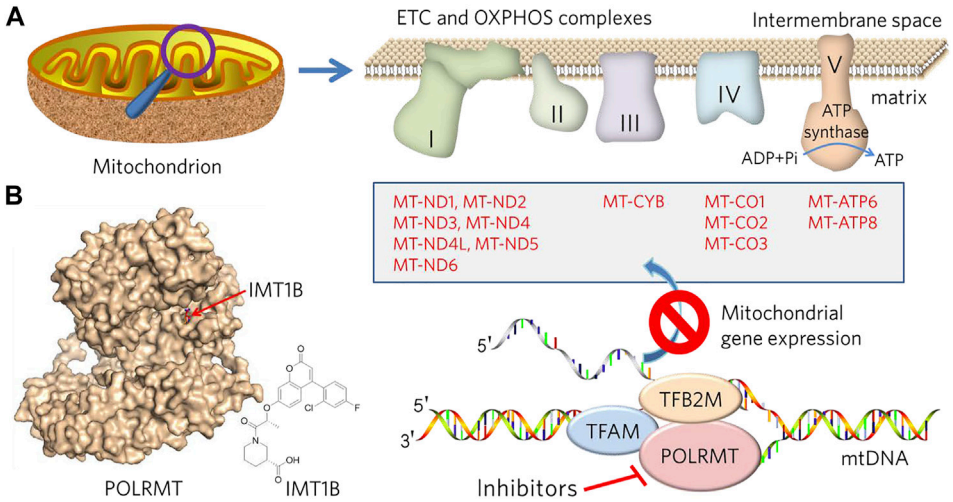


**FIGURE 1 |** Description of the design and rationale for overcoming MDR by targeting mitochondrial metabolism and mtDNA transcription. **(A)** Mitochondria are bilayer membranous organelles. OXPHOS consists of protein complexes located within the innermembrane, of which 13 protein components (list in box) belong to complexes I, III, IV and V, respectively, encoded by the mitochondrial genome and transcribed by POLRMT. Inhibition of POLRMT is thought to shut down the protein source of the OXPHOS system, which may lead to malfunction of the mitochondrial electron transport chain (ETC) and OXPHOS and a subsequent energy crisis. **(B)** POLRMT and its small chemical inhibitor, IMT1B (from PDB: 7A8P).

transcription factor A) in heart or skeletal muscle result in mitochondrial myopathy, suggesting an important role for mitochondrial transcription in these tissues (Wang et al., 1999; Wredenberg et al., 2002). Consistently, clinical manifestations of mitochondrial toxicity were surprised to found associated with the use of nucleoside analog reverse transcriptase inhibitors in HIV patients, leading to myopathy, peripheral neuropathy and lactic acidosis due to off-target inhibition of mitochondrial DNA polymerase $\gamma$ and depletion of mtDNA (Moyle, 2000). However, IMTIB-induced reduction of mtDNA transcript levels in liver and heart was much less extent than that in tumors (Bonekamp et al., 2020). Despite this, anticancer drugs targeting mitochondria are not widely available in the clinic, and there are remains few evidences from experimental cell lines and animals (Ashton et al., 2018). Therefore, mitochondrial metabolism targeted drugs for cancer treatment need more experimental supports from both the bench and clinic, both for their effectiveness and side effects.

## Potential Strategies for Inhibition of POLRMT

Due to the similarity of substrates in RNA synthesis, some nucleoside analogs exhibit inhibitory activities against POLRMT (Ehteshami et al., 2016; Fenaux et al., 2016; Feng et al., 2016; Bergbrede et al., 2017; Ehteshami et al., 2017; Lu et al., 2018). Thus, it is interesting to find that many antiviral agents targeting viral RNA polymerases produce off-target inhibition of POLRMT (Arnold et al., 2012; Young, 2017; Freedman et al., 2018). This could be a first strategy for designing or screening POLRMT inhibitory molecules. In addition, genetic methods including siRNA and CRISPR/Cas9, and chemical approaches such as small inhibitors with non-covalent or covalent binding modes, targeted protein degradation by proteolysis-targeting chimera (PROTAC) are potential approaches to inhibit POLRMT (Bralha et al., 2015; Zhou et al., 2021). Multifunctional molecules with imaging and inhibition activities against POLRMT coupled with light- or heart-induced ligands may also have broad potential. However, precise targeting and corresponding clinical effects should be highly emphasized, as targeting mitochondria may be toxic to germ cells, which require cell duplication to produce generative cells (Larsson et al., 1998). Therefore, in addition to developing compounds with high affinity for POLRMT, increasing the enrichment of compounds in the mitochondrial matrix is a strategy worth considering. It can be speculated that tumor cells are likely to become resistant to POLRMT inhibitors by changing the conformation of the binding site via genetic mutations or by promoting drug efflux, or mitochondrial fission (Saito et al., 2021). Therefore, it is necessary to consider avoiding the emergence of resistance when designing POLRMT inhibitors. One approach is to combine POLRMT inhibitors with other ABC transporter inhibitors in the clinic to completely kill tumor cells in a short period of time without giving them a window of time to adapt and develop tolerance. The second option is to enhance the specific uptake of POLRMT inhibitors by mitochondria (Murphy and Smith, 2007). Since both mitochondrial and cellular membranes have membrane potentials, certain molecules driven by membrane potentials can be considered for transmembrane use (**Figure 2**). For example, POLRMT-targeted molecules can be conjugated to lipophilic compounds such as triphenylphosphonium (TPP), which can effectively penetrate membranes driven by membrane potential (Weinberg and Chandel, 2015). In detail, TPP first penetrates the membrane via the plasma membrane potential and accumulates in the cytoplasm. Subsequently, the mitochondrial membrane potential would drive the accumulation of these molecules into the mitochondria by several hundredfold. If this could be achieved, it would allow for much lower concentrations of

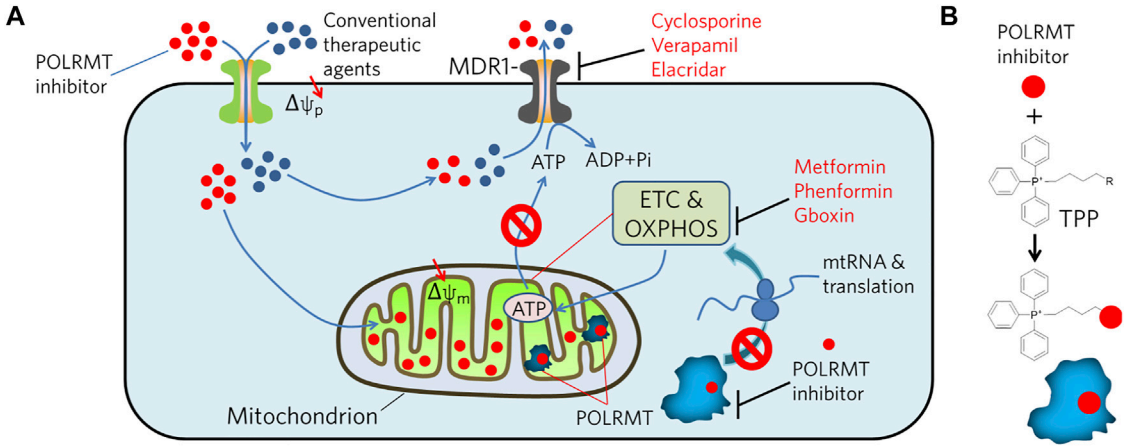


**FIGURE 2 |** Illustration of potential strategies to combat MDR tumors by inhibiting POLRMT in concert with MDR1. **(A)** MDR1 effluxes chemicals, i.e. POLRMT inhibitors and conventional therapeutic agents, from the cytosol out of the cell in an ATP-dependent manner. However, inhibition of POLRMT blocks its mediated transcription of mtDNA, thereby inhibiting translation of the ETC and OXPHOS complexes. As a result, ATP production is compromised and ultimately leads to the inhibition of ATP-dependent chemical efflux by MDR1. **(B)** Conjugation of POLRMT inhibitors to lipophilic TPP is designed to facilitate its permeation to the plasma and mitochondrial membranes driven by the membrane potential ($\Delta\psi$) and accumulates several hundred-fold in the mitochondrial matrix.

the drug used in clinical trials while avoiding the possible side effects of conventional dosing.

And in clinical practice, it is ideal and most important to first distinguish the type of energy metabolism of cancer cells before choosing a drug. POLRMT inhibitors may work well in combination with other chemotherapeutic agents for treatment of resistant and or recurrent tumors (**Figure 2**). That is, POLRMT inhibitors target tumors with high oxygen metabolism in the MDR or relapsed population, while conventional drugs such as cisplatin and docetaxel, i.e., target tumor cells that are highly proliferative or glycolysis-dependent. Therefore, it is expected that this combination may effective in eradicating tumors with mixed types of energy supply. This therapeutic approach will contribute to the selection and formulation of personalized therapies for future tumor treatment and to the development of precision medicine.

## SUMMARY AND OUTLOOK

Tumor therapies targeting mitochondria have not been developed, and in particular, no drugs targeting POLRMT are currently available for clinical cancer treatment. Inhibition of OXPHOS or in combination with other antitumor drugs should be effective in tumors with high OXPHOS activity. This may be particularly important for drug-resistant or relapsed tumors. It also fits right in with the personalized requirement of precision medicine. It is foreseeable that POLRMT-targeted drugs for clinical cancer treatment will emerge in the near future to achieve precise eradication of cancer.

## AUTHOR CONTRIBUTIONS

H-JY and G-LX contributed to the writing of this review. Y-YZ and X-XW drew the figures. RFL supervised and submitted the paper. All authors contributed to the article and approved the submitted version.

## FUNDING

This work was supported by the National Natural Science Foundation of China (21778038).

## REFERENCES

Arnold, J. J., Sharma, S. D., Feng, J. Y., Ray, A. S., Smidansky, E. D., Kireeva, M. L., et al. (2012). Sensitivity of Mitochondrial Transcription and Resistance of RNA Polymerase II Dependent Nuclear Transcription to Antiviral Ribonucleosides. *Plos Pathog.* 8 (11), e1003030. doi:10.1371/journal.ppat.1003030

Ashton, T. M., McKenna, W. G., Kunz-Schughart, L. A., and Higgins, G. S. (2018). Oxidative Phosphorylation as an Emerging Target in Cancer Therapy. *Clin. Cancer Res.* 24 (11), 2482–2490. doi:10.1158/1078-0432.CCR-17-3070

Bergbrede, T., Hoberg, E., Larsson, N.-G., Falkenberg, M., and Gustafsson, C. M. (2017). An Adaptable High-Throughput Technology Enabling the Identification of Specific Transcription Modulators. *SLAS DISCOVERY: Advancing Sci. Drug Discov.* 22 (4), 378–386. doi:10.1177/2472555217690326

Bonekamp, N. A., Peter, B., Hillen, H. S., Felser, A., Bergbrede, T., Choidas, A., et al. (2020). Small-molecule Inhibitors of Human Mitochondrial DNA Transcription. *Nature* 588 (7839), 712–716. doi:10.1038/s41586-020-03048-z

Bonnay, F., Veloso, A., Steinmann, V., Köcher, T., Abdusselamoglu, M. D., Bajaj, S., et al. (2020). Oxidative Metabolism Drives Immortalization of Neural Stem Cells during Tumorigenesis. *Cell* 182 (6), 1490–1507. doi:10.1016/j.cell.2020.07.039

Bosc, C., Selak, M. A., and Sarry, J.-E. (2017). Resistance Is Futile: Targeting Mitochondrial Energetics and Metabolism to Overcome Drug Resistance in Cancer Treatment. *Cel Metab.* 26 (5), 705–707. doi:10.1016/j.cmet.2017.10.013

Bralha, F. N., Liyanage, S. U., Hurren, R., Wang, X., Son, M. H., Fung, T. A., et al. (2015). Targeting Mitochondrial RNA Polymerase in Acute Myeloid Leukemia. *Oncotarget* 6 (35), 37216–37228. doi:10.18632/oncotarget.6129

Crunkhorn, S. (2021). Targeting the Mitochondria to Block Tumour Growth. *Nat. Rev. Drug Discov.* 20 (2), 97. doi:10.1038/d41573-021-00001-1

DeBerardinis, R. J., and Chandel, N. S. (2020). We Need to Talk about the Warburg Effect. *Nat. Metab.* 2 (2), 127–129. doi:10.1038/s42255-020-0172-2

Ding, S., Li, C., Cheng, N., Cui, X., Xu, X., and Zhou, G. (2015). Redox Regulation in Cancer Stem Cells. *Oxidative Med. Cell Longevity* 2015, 1–11. doi:10.1155/2015/750798

Ehteshami, M., Tao, S., Ozturk, T., Zhou, L., Cho, J. H., Zhang, H., et al. (2016). Biochemical Characterization of the Active Anti-hepatitis C Virus Metabolites of 2,6-Diaminopurine Ribonucleoside Prodrug Compared to Sofosbuvir and BMS-986094. *Antimicrob. Agents Chemother.* 60 (8), 4659–4669. doi:10.1128/AAC.00318-16

Ehteshami, M., Zhou, L., Amiralaei, S., Shelton, J. R., Cho, J. H., Zhang, H., et al. (2017). Nucleotide Substrate Specificity of Anti-hepatitis C Virus Nucleoside Analogs for Human Mitochondrial RNA Polymerase. *Antimicrob. Agents Chemother.* 61 (8), e00492–17. doi:10.1128/AAC.00492-17

Farge, T., Saland, E., de Toni, F., Aroua, N., Hosseini, M., Perry, R., et al. (2017). Chemotherapy-resistant Human Acute Myeloid Leukemia Cells Are Not Enriched for Leukemic Stem Cells but Require Oxidative Metabolism. *Cancer Discov.* 7 (7), 716–735. doi:10.1158/2159-8290.CD-16-0441

Fenaux, M., Lin, X., Yokokawa, F., Sweeney, Z., Saunders, O., Xie, L., et al. (2016). Antiviral Nucleotide Incorporation by Recombinant Human Mitochondrial RNA Polymerase Is Predictive of Increased *In Vivo* Mitochondrial Toxicity Risk. *Antimicrob. Agents Chemother.* 60 (12), 7077–7085. doi:10.1128/AAC.01253-16

Feng, J. Y., Xu, Y., Barauskas, O., Perry, J. K., Ahmadyar, S., Stepan, G., et al. (2016). Role of Mitochondrial RNA Polymerase in the Toxicity of Nucleotide Inhibitors of Hepatitis C Virus. *Antimicrob. Agents Chemother.* 60 (2), 806–817. doi:10.1128/AAC.01922-15

Freedman, H., Winter, P., Tuszynski, J., Tyrrell, D. L., and Houghton, M. (2018). A Computational Approach for Predicting Off-Target Toxicity of Antiviral Ribonucleoside Analogues to Mitochondrial RNA Polymerase. *J. Biol. Chem.* 293 (25), 9696–9705. doi:10.1074/jbc.RA118.002588

Fulda, S., Galluzzi, L., and Kroemer, G. (2010). Targeting Mitochondria for Cancer Therapy. *Nat. Rev. Drug Discov.* 9 (6), 447–464. doi:10.1038/nrd3137

Funes, J. M., Quintero, M., Henderson, S., Martinez, D., Qureshi, U., Westwood, C., et al. (2007). Transformation of Human Mesenchymal Stem Cells Increases Their Dependency on Oxidative Phosphorylation for Energy Production. *Proc. Natl. Acad. Sci.* 104 (15), 6223–6228. doi:10.1073/pnas.0700690104

Garcia-Mayea, Y., Mir, C., Masson, F., Paciucci, R., and LLeonart, M. E. (2020). Insights into New Mechanisms and Models of Cancer Stem Cell Multidrug Resistance. *Semin. Cancer Biol.* 60, 166–180. doi:10.1016/j.semcancer.2019.07.022

Haq, R., Shoag, J., Andreu-Perez, P., Yokoyama, S., Edelman, H., Rowe, G. C., et al. (2013). Oncogenic BRAF Regulates Oxidative Metabolism via PGC1α and MITF. *Cancer Cell* 23 (3), 302–315. doi:10.1016/j.ccr.2013.02.003

Hillen, H. S., Morozov, Y. I., Sarfallah, A., Temiakov, D., and Cramer, P. (2017). Structural Basis of Mitochondrial Transcription Initiation. *Cell* 171 (5), 1072–1081. e1010. doi:10.1016/j.cell.2017.10.036

Hirsch, H. A., Iliopoulos, D., Tsichlis, P. N., and Struhl, K. (2009). Metformin Selectively Targets Cancer Stem Cells, and Acts Together with Chemotherapy to Block Tumor Growth and Prolong Remission. *Cancer Res.* 69 (19), 7507–7511. doi:10.1158/0008-5472.CAN-09-2994

Holohan, C., Van Schaeybroeck, S., Longley, D. B., and Johnston, P. G. (2013). Cancer Drug Resistance: an Evolving Paradigm. *Nat. Rev. Cancer* 13 (10), 714–726. doi:10.1038/nrc3599

Jones, R. A., Robinson, T. J., Liu, J. C., Shrestha, M., Voisin, V., Ju, Y., et al. (2016). RB1 Deficiency in Triple-Negative Breast Cancer Induces Mitochondrial Protein Translation. *J. Clin. Invest.* 126 (10), 3739–3757. doi:10.1172/JCI81568

Kühl, I., Kukat, C., Ruzzenente, B., Milenkovic, D., Mourier, A., Miranda, M., et al. (2014). POLRMT Does Not Transcribe Nuclear Genes. *Nature* 514 (7521), E7–E11. doi:10.1038/nature13690

Kühl, I., Miranda, M., Posse, V., Milenkovic, D., Mourier, A., Siira, S. J., et al. (2016). POLRMT Regulates the Switch between Replication Primer Formation and Gene Expression of Mammalian mtDNA. *Sci. Adv.* 2 (8), e1600963. doi:10.1126/sciadv.1600963

Kuntz, E. M., Baquero, P., Michie, A. M., Dunn, K., Tardito, S., Holyoake, T. L., et al. (2017). Targeting Mitochondrial Oxidative Phosphorylation Eradicates Therapy-Resistant Chronic Myeloid Leukemia Stem Cells. *Nat. Med.* 23 (10), 1234–1240. doi:10.1038/nm.4399

Lamb, R., Ozsvari, B., Lisanti, C. L., Tanowitz, H. B., Howell, A., Martinez-Outschoorn, U. E., et al. (2015). Antibiotics that Target Mitochondria Effectively Eradicate Cancer Stem Cells, across Multiple Tumor Types: Treating Cancer like an Infectious Disease. *Oncotarget* 6 (7), 4569–4584. doi:10.18632/oncotarget.3174

Larsson, N.-G., Wang, J., Wilhelmsson, H., Oldfors, A., Rustin, P., Lewandoski, M., et al. (1998). Mitochondrial Transcription Factor A Is Necessary for mtDNA Maintance and Embryogenesis in Mice. *Nat. Genet.* 18 (3), 231–236. doi:10.1038/ng0398-231

Lissanu Deribe, Y., Sun, Y., Terranova, C., Khan, F., Martinez-Ledesma, J., Gay, J., et al. (2018). Mutations in the SWI/SNF Complex Induce a Targetable Dependence on Oxidative Phosphorylation in Lung Cancer. *Nat. Med.* 24 (7), 1047–1057. doi:10.1038/s41591-018-0019-5

Lu, G., Bluemling, G. R., Mao, S., Hager, M., Gurale, B. P., Collop, P., et al. (2018). Simple *In Vitro* Assay to Evaluate the Incorporation Efficiency of Ribonucleotide Analog 5′-Triphosphates into RNA by Human Mitochondrial DNA-dependent RNA Polymerase. *Antimicrob. Agents Chemother.* 62 (2), e01830–17. doi:10.1128/AAC.01830-17

Martinez-Outschoorn, U. E., Peiris-Pagés, M., Pestell, R. G., Sotgia, F., and Lisanti, M. P. (2017). Erratum: Cancer Metabolism: a Therapeutic Perspective. *Nat. Rev. Clin. Oncol.* 14 (2), 113. doi:10.1038/nrclinonc.2017.1

Molina, J. R., Sun, Y., Protopopova, M., Gera, S., Bandi, M., Bristow, C., et al. (2018). An Inhibitor of Oxidative Phosphorylation Exploits Cancer Vulnerability. *Nat. Med.* 24 (7), 1036–1046. doi:10.1038/s41591-018-0052-4

Moyle, G. (2000). Clinical Manifestations and Management of Antiretroviral Nucleoside Analog-Related Mitochondrial Toxicity. *Clin. Ther.* 22 (8), 911–936. doi:10.1016/S0149-2918(00)80064-8

Mukha, A., and Dubrovska, A. (2020). Metabolic Targeting of Cancer Stem Cells. *Front. Oncol.* 10, 537930. doi:10.3389/fonc.2020.537930

Murphy, M. P., and Smith, R. A. J. (2007). Targeting Antioxidants to Mitochondria by Conjugation to Lipophilic Cations. *Annu. Rev. Pharmacol. Toxicol.* 47, 629–656. doi:10.1146/annurev.pharmtox.47.120505.105110

Oláhová, M., Peter, B., Szilagyi, Z., Diaz-Maldonado, H., Singh, M., Sommerville, E. W., et al. (2021). POLRMT Mutations Impair Mitochondrial Transcription Causing Neurological Disease. *Nat. Commun.* 12 (1), 1135. doi:10.1038/s41467-021-21279-0

Saito, K., Zhang, Q., Yang, H., Yamatani, K., Ai, T., Ruvolo, V., et al. (2021). Exogenous Mitochondrial Transfer and Endogenous Mitochondrial Fission Facilitate AML Resistance to OxPhos Inhibition. *Blood Adv.* 5, 4233–4255. doi:10.1182/bloodadvances.2020003661

Sancho, P., Barneda, D., and Heeschen, C. (2016). Hallmarks of Cancer Stem Cell Metabolism. *Br. J. Cancer* 114 (12), 1305–1312. doi:10.1038/bjc.2016.152

Shi, Y., Lim, S. K., Liang, Q., Iyer, S. V., Wang, H.-Y., Wang, Z., et al. (2019). Gboxin Is an Oxidative Phosphorylation Inhibitor that Targets Glioblastoma. *Nature* 567 (7748), 341–346. doi:10.1038/s41586-019-0993-x

Škrtić, M., Sriskanthadevan, S., Jhas, B., Gebbia, M., Wang, X., Wang, Z., et al. (2011). Inhibition of Mitochondrial Translation as a Therapeutic Strategy for Human Acute Myeloid Leukemia. *Cancer Cell* 20 (5), 674–688. doi:10.1016/j.ccr.2011.10.015

Song, K.-H., Kim, J.-H., Lee, Y.-H., Bae, H. C., Lee, H.-J., Woo, S. R., et al. (2018). Mitochondrial Reprogramming via ATP5H Loss Promotes Multimodal Cancer Therapy Resistance. *J. Clin. Invest.* 128 (9), 4098–4114. doi:10.1172/JCI96804

Szakács, G., Paterson, J. K., Ludwig, J. A., Booth-Genthe, C., and Gottesman, M. M. (2006). Targeting Multidrug Resistance in Cancer. *Nat. Rev. Drug Discov.* 5 (3), 219–234. doi:10.1038/nrd1984

Vander Heiden, M. G., Cantley, L. C., and Thompson, C. B. (2009). Understanding the Warburg Effect: the Metabolic Requirements of Cell Proliferation. *Science* 324 (5930), 1029–1033. doi:10.1126/science.1160809

Vasan, K., Werner, M., and Chandel, N. S. (2020). Mitochondrial Metabolism as a Target for Cancer Therapy. *Cel Metab.* 32 (3), 341–352. doi:10.1016/j.cmet.2020.06.019

Wang, J., Wilhelmsson, H., Graff, C., Li, H., Oldfors, A., Rustin, P., et al. (1999). Dilated Cardiomyopathy and Atrioventricular Conduction Blocks Induced by Heart-specific Inactivation of Mitochondrial DNA Gene Expression. *Nat. Genet.* 21 (1), 133–137. doi:10.1038/5089

Weinberg, S. E., and Chandel, N. S. (2015). Targeting Mitochondria Metabolism for Cancer Therapy. *Nat. Chem. Biol.* 11 (1), 9–15. doi:10.1038/nchembio.1712

Wredenberg, A., Wibom, R., Wilhelmsson, H., Graff, C., Wiener, H. H., Burden, S. J., et al. (2002). Increased Mitochondrial Mass in Mitochondrial Myopathy Mice. *Proc. Natl. Acad. Sci.* 99 (23), 15066–15071. doi:10.1073/pnas.232591499

Wu, S., Fahmy, N., and Alachkar, H. (2019). The Mitochondrial Transcription Machinery Genes Are Upregulated in Acute Myeloid Leukemia and Associated with Poor Clinical Outcome. *Metab. Open* 2, 100009. doi:10.1016/j.metop.2019.100009

Young, M. J. (2017). Off-target Effects of Drugs that Disrupt Human Mitochondrial DNA Maintenance. *Front. Mol. Biosci.* 4, 74. doi:10.3389/fmolb.2017.00074

Zacksenhaus, E., Shrestha, M., Liu, J. C., Vorobieva, I., Chung, P. E. D., Ju, Y., et al. (2017). Mitochondrial OXPHOS Induced by RB1 Deficiency in Breast Cancer: Implications for Anabolic Metabolism, Stemness, and Metastasis. *Trends Cancer* 3 (11), 768–779. doi:10.1016/j.trecan.2017.09.002

Zhou, T., Sang, Y.-H., Cai, S., Xu, C., and Shi, M.-h. (2021). The Requirement of Mitochondrial RNA Polymerase for Non-small Cell Lung Cancer Cell Growth. *Cell Death Dis.* 12 (8), 751. doi:10.1038/s41419-021-04039-2

**Conflict of Interest:** The authors declare that the research was conducted in the absence of any commercial or financial relationships that could be construed as a potential conflict of interest.

**Publisher's Note:** All claims expressed in this article are solely those of the authors and do not necessarily represent those of their affiliated organizations, or those of the publisher, the editors and the reviewers. Any product that may be evaluated in this article, or claim that may be made by its manufacturer, is not guaranteed or endorsed by the publisher.

frontiers in Oncology

REVIEW
published: 05 January 2022
doi: 10.3389/fonc.2021.790589

# The Role of Circular RNAs in the Drug Resistance of Cancers

*Xin-Yuan Liu, Qi Zhang, Jing Guo, Peng Zhang, Hua Liu, Zi-Bin Tian, Cui-Ping Zhang and Xiao-Yu Li**

*Department of Gastroenterology, The Affiliated Hospital of Qingdao University, Qingdao, China*

Cancer is a major threat to human health and longevity. Chemotherapy is an effective approach to inhibit cancer cell proliferation, but a growing number of cancer patients are prone to develop resistance to various chemotherapeutics, including platinum, paclitaxel, adriamycin, and 5-fluorouracil, among others. Significant progress has been made in the research and development of chemotherapeutic drugs over the last few decades, including targeted therapy drugs and immune checkpoint inhibitors; however, drug resistance still severely limits the application and efficacy of these drugs in cancer treatment. Recently, emerging studies have emphasized the role of circular RNAs (circRNAs) in the proliferation, migration, invasion, and especially chemoresistance of cancer cells by regulating the expression of related miRNAs and targeted genes. In this review, we comprehensively summarized the potential roles and mechanisms of circRNAs in cancer drug resistance including the efflux of drugs, apoptosis, intervention with the TME (tumor microenvironment), autophagy, and dysfunction of DNA damage repair, among others. Furthermore, we highlighted the potential value of circRNAs as new therapeutic targets and prognostic biomarkers for cancer.

**Keywords: circular RNAs, drug resistance, cancer, chemotherapy, therapeutic targets**

OPEN ACCESS

***Edited by:***
*Qingbin Cui,*
*University of Toledo, United States*

***Reviewed by:***
*Xiu-Yan Huang,*
*Shanghai Jiao Tong University, China*
*Changlong Xu,*
*Second Affiliated Hospital and Yuying Children's Hospital of Wenzhou Medical University, China*

***Correspondence:**
*Xiao-Yu Li*
*lixiaoyu05@163.com*

***Specialty section:***
*This article was submitted to Pharmacology of Anti-Cancer Drugs, a section of the journal Frontiers in Oncology*

***Received:*** *13 October 2021*
***Accepted:*** *13 December 2021*
***Published:*** *05 January 2022*

***Citation:***
*Liu X-Y, Zhang Q, Guo J, Zhang P, Liu H, Tian Z-B, Zhang C-P and Li X-Y (2022) The Role of Circular RNAs in the Drug Resistance of Cancers. Front. Oncol. 11:790589. doi: 10.3389/fonc.2021.790589*

## INTRODUCTION

Cancer is a worldwide public health problem and a leading cause of premature death (1). The main reasons for the high mortality of patients and poor cancer prognosis are late diagnosis, tumor invasion and metastasis, and resistance to chemotherapeutic drugs. Resistance to chemotherapy, which involves intrinsic resistance and acquired resistance, has become a serious obstacle towards cancer therapy (2).

Although recent breakthroughs in treatment have contributed to the decline in cancer mortality, such as combined administration of drugs, checkpoint blockade immunotherapies, and targeted therapies for malignant tumors, tumor cells still exhibit a tendency towards drug resistance (1, 3). This becomes problematic as cancer cells become cross-resistant to several drugs with different anti-tumor mechanisms, causing invalid effects of various combination chemotherapies (4). Immune checkpoint inhibitors including programmed cell death 1 (PD1), PD1 ligand 1 (PD- L1), and cytotoxic T lymphocyte antigen 4 (CTLA4) have been successfully used in clinical applications. However, resistance to immune checkpoint blockade appeared simultaneously. For instance, it has been found that STK11/LKB1 mutations act as the main driver of immune escape and intrinsic

resistance to PD-1 blockade in KRAS-mutant lung adenocarcinoma (LUAD) (5). Additionally, epidermal growth factor receptor (EGFR) tyrosine kinase inhibitors (TKIs) have been extensively studied as key targeted therapies, and within one or two years after treatment with TKIs, patients with activating alterations of the EGFR gene often acquire resistance to TKI therapy (2). Therefore, an insight into the specific molecular mechanisms that mediate drug resistance is crucial for understanding and overcoming drug tolerance in cancers.

Circular RNAs (circRNAs) were first identified in 1976 and belong to a growing list of types of non-coding RNAs, with a circular loop structure (6, 7). Most circRNAs, comprising a single exon or multiple exons, are expressed by known protein-coding genes (8). circRNAs can modulate gene splicing of pre-RNA and transcription, regulate RNA-binding proteins, and act as microRNA (miRNA) "sponges" to play a crucial role in transcriptional regulation (9, 10). Recent studies have revealed that numerous circRNAs are differentially expressed in various cancer patients and are correlated with the tumorigenesis and progression of cancers (11). For example, autophagy-associated circCDYL promotes the malignant progression of breast cancer cells and suppresses the clinical response to chemotherapy in patients with breast cancer (12). Conversely, circ-HuR suppresses the expression of CNBP-facilitated HuR and the progression of gastric cancer, serving as a tumor inhibitor (13). Moreover, accumulating evidence has shown that circRNAs are correlated with tumor chemoresistance and may play a crucial role in the occurrence and regulation of chemoresistance (14). To investigate the emerging role of circRNAs in the drug resistance of cancers, we systematically and comprehensively summarized the major mechanisms of cancer chemoresistance and the molecular mechanisms by which circRNAs enhance or suppress drug resistance in cancers (**Figure 1**), which indicates that circRNAs may function as potential biomarkers and therapeutic targets for cancer.

# MECHANISMS OF DRUG RESISTANCE

## Efflux of Drugs

Drug efflux from cancer cells is a common and important mechanism of resistance or multidrug resistance (MDR), which is inseparable from ATP-binding cassette (ABC) efflux transporters, including MDR-associated protein 2 (MRP2/ABCC2), P-glycoprotein (P-gp/ABCB1), and breast cancer resistance protein (BCRP/ABCG2) (15). ABC efflux transporters, as membrane protein complexes, are often overexpressed in cancer cells and form a defense system against chemotherapeutic drugs as well as a variety of cytotoxic agents, which greatly restricts the effective application of chemotherapy. For example, P-glycoprotein (P-gp) has a wide substrate spectrum that mediates the export of a multitude of drugs, including antibiotics, immunosuppressive agents, and chemotherapeutic drugs (16).

Several researchers have discovered that the function of some circRNAs in drug resistance of cancers is related to ABC efflux transporters. For example, it has been found that circ_0076305 enhances *ABCC1* expression by sponging miR-186-5p, thus regulating cisplatin (CDDP) resistance in non-small cell lung cancer (NSCLC) (17). Similarly, ABCB1 overexpression can reverse the effects of circRNA_103615 silencing on CDDP resistance in NSCLC (18). CircSETD3 upregulates the expression of the ABCG2 transporter by binding to miR-520h, mediating gefitinib to be pumped out of NSCLC cells (19). Both circ_0002060 and circPVT1 contribute to drug resistance in osteosarcoma cells by regulating the expression of *ABCB1* (20, 21). Additionally, the knockdown of circ-CHI3L1.2 downregulates the expression levels of P-gp, *MRP1*, and *GSTP1* and weakens CDDP resistance in osteosarcoma (22). CircPTGR1 and ABCC1 levels are significantly overexpressed in hepatocellular carcinoma (HCC) cells, and circPTGR1 modulates the 5-FU resistance of HCC cells *via* the miR-129-5p/ABCC1 axis (23). Therefore, it is crucial to explore the

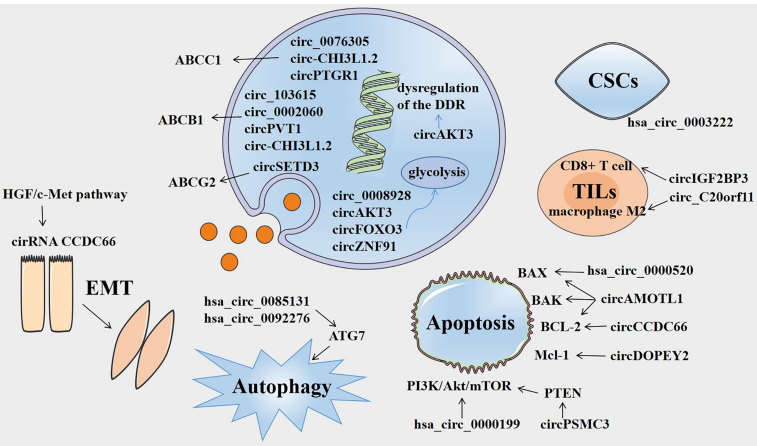


**FIGURE 1** | Overview of the involvement of circRNAs in cancer drug resistance. Several circRNAs are involved in drug resistance by influencing ABC efflux transporters, dysregulation of DNA damage response (DDR), glycolysis, epithelial-mesenchymal transition (EMT), autophagy, apoptosis, tumor-infiltrating lymphocytes (TILs), and cancer stem cells (CSCs).

relationships among circRNAs, ABC efflux transporters, and tolerance to anti-cancer drugs in order to find new therapeutic targets for cancer.

## Apoptosis

The major aim of cancer chemotherapy is to promote the apoptosis of cancer cells and expose them to anti-cancer drugs. The effector phase of apoptosis involves several pro-apoptotic proteins (e.g., BAX, Bak, Bad) and anti-apoptotic proteins (e.g., BCL-2, BCL-XL, BCL-W) (24). However, the genes in cancer cells commonly demonstrate mutations, including apoptotic genes, which often cause dysfunction. This may result in the occurrence of resistance to chemotherapeutics, as any interference that mediates the activation of anti-apoptotic pathways or suppression of pro-apoptotic signal transduction is a potential mechanism of drug resistance (25).

Certain circRNAs have been shown to regulate the apoptosis of drug-resistant cancer cells by modulating pro- or anti-apoptotic proteins. For example, circAMOTL1 can significantly modulate the expression of the Protein Kinase B (AKT) as well as AKT-related pro-apoptotic (BAX and BAK) factors and anti-apoptotic (BCL-2) proteins, thus mediating the paclitaxel (PTX)-resistant effects in breast cancer (26). CircCCDC66 inhibits apoptosis by targeting miR-618 and resists the release of BCL-2, which is an essential regulator of CDDP resistance in gastric cancer (27). Moreover, hsa_circ_0000520 overexpression increases the expression of the BAX protein and reduces the expression of p-PI3K and p-Akt proteins, ultimately reversing the Herceptin resistance of gastric cancer (28). Re-expression of cDOPEY2 decreases the expression of the anti-apoptotic protein Mcl-1 and substantially strengthens the cell lethality of CDDP by augmenting the apoptotic process in CDDP-resistant esophageal squamous cell carcinoma (ESCC) cells (29). The PI3K/Akt/mTOR signaling pathway plays a crucial role in cell cycle regulation, including cell survival, proliferation, and metabolism, and is intimately related to autophagy and apoptosis (30). Based on the existing literature, PI3K-AKT-mTOR signaling is extensively implicated in chemoresistance and drives the process of malignant tumors (31). Silencing of hsa_circ_0000199 deactivates PI3K/Akt/mTOR signaling to promote apoptosis, enhancing triple-negative breast cancer (TNBC) chemosensitivity (32). *PTEN* is an important tumor suppressor gene that encodes a phosphatase protein and resists the PI3K/Akt/mTOR anti-apoptotic pathway as an antagonist (33). It has been reported that *PTEN* expression can be promoted by circPSMC3 by decreasing miR-10a-5p levels, which enhances the esophageal squamous cell carcinoma (ESCC) cells towards gefitinib sensitivity (34).

## TME

TME consists of the stromal cells, immune cells, and extracellular matrix and mounting evidence suggests that the TME plays a crucial role in multiple aspects of tumor progression, particularly in therapeutic resistance (35). Acquired resistance induced by the TME primarily acts as an adaptive response by the host towards pharmacological damage (36). Li et al. explored the combined effects of cancer stem cells (CSCs), circRNA (hsa_circ_0003222), and immune checkpoint blockers in NSCLC malignant behavior as well as drug resistance and found that NSCLC resistance to anti-PD-L1-based therapy could be reduced by silencing hsa_circ_0003222 (37). Additionally, circFGFR1 promotes immune evasion of NSCLC cells and enhances tolerance to anti- PD-1- based therapy by interacting with miR-381-3p and upregulating the expression of C-X-C motif chemokine receptor 4 (CXCR4) (38). Tumor-infiltrating lymphocytes (TILs), an important component of the TME, have attracted increasing attention for therapy resistance in recent years. CircIGF2BP3 expression is negatively associated with the infiltration of $CD8^+$ T cells, which induces immune escape from $CD8^+$ T cell-mediated killing. Mechanistically, PKP3 upregulated by circIGF2BP3 combines with FXR1 to stabilize OTUB1 mRNA, which increases PD-L1 abundance by promoting its deubiquitination (39). A study on ovarian cancer has suggested that silencing of circ_C20orf11 suppresses extracellular vesicle (EV)-induced macrophage M2 polarization and enhances sensitivity to CDDP *in vivo* (40).

In addition, the interactions between cancer cells and TME also play a pivotal role in epithelial-mesenchymal transition (EMT), which has emerged as a significant cancer cell behavior correlated with metastatic potential and chemoresistance (41). The EMT-associated NF-κB/HER2/STAT3 pathway is crucial in radioresistance of breast cancer stem cells (42). However, the relationship between circRNAs and EMT in drug resistance still needs to be investigated. A recent study has found that the HGF/c-Met pathway regulates the expression of circCCDC66 and SAE2 to promote EMT and chemoresistance in lung adenocarcinoma (LADC) cells (43). In order to overcome this resistance, disruption of EMT-related pathways in tumor cells is desirable.

## Other Mechanisms

Many other drug resistance mechanisms of cancers, including autophagy, glycolysis, dysfunction of DNA damage repair, altered drug targets, decreased drug influx, and so forth are known (14). However, the relationship between circRNAs and the above mentioned drug resistance mechanisms are still being investigated. Autophagy plays a crucial role in tumorigenesis, progression, and therapeutic intervention in cancers (44). A previous study has found that the knockdown of autophagy-related genes (*ATG5* and *ATG7*) enhances therapeutic cell killing, indicating that autophagy may promote the acquired resistance of cancer cells to chemotherapeutics (45). Hsa_circ_0085131 and hsa_circ_0092276 serve as competitive endogenous RNAs (ceRNAs) to elevate autophagy-associated factor *ATG7* expression, thus enhancing CDDP resistance in NSCLC and doxorubicin (DOX) resistance in breast cancer (46, 47). Tumor cells often switch to glycolysis, even under aerobic conditions, and components of the glycolytic pathway, including transporters, enzymes, and metabolites, are involved in inducing drug resistance (48). Some circRNAs mediate chemotherapy resistance by modulating glycolysis in tumor cells. For instance, circ_0008928 silencing enhances CDDP sensitivity in CDDP-resistant NSCLC cells and impedes NSCLC progression and glycolysis by upregulating miR-488 expression and downregulating HK2

expression (49). Similarly, the CDDP-resistance mechanism of circAKT3 and circRNA-FOXO3 is involved in disturbing the glycolysis balance (50, 51). CDDP sensitivity is suppressed partly by circAKT3 by modulating the miR-516b-5p/STAT3 axis in lung cancer cells, whereas CDDP sensitivity is promoted by circRNA-FOXO3 *via* the miR-543/Foxo3 axis in NSCLC cells. The hypoxia-induced exosomal circZNF91 transferred to normoxic pancreatic cancer cells can interact with miR-23b-3p and upregulate the expression of the deacetylase sirtuin1 (*SIRT1*), thereby enhancing the deacetylation-dependent stability of HIF-1α, resulting in gemcitabine (GEM) resistance and glycolysis-induced chemoresistance (52). DNA damage is a relatively common and vital cellular event that is implicated in mutations, metabolic dysfunction, cellular or organismic death, and tumorigenesis (53). Upregulation of processes such as DNA damage tolerance (DDT) and DNA damage response (DDR) is advantageous to cancer cells because it allows them to resist damage lesions (54). A large number of processes in cancers activate cellular DDR to remove or repair DNA lesions (54). Dysregulation of DDR is often the route by which tumor cells evade chemotherapy (55). A recent study found that circAKT3 had an impact on DDR in gastric cancer cells and might promote CDDP resistance in gastric cancer through the DDR and PI3K/AKT pathways (56). Alterations in chemotherapeutic targets can have a great influence on drug resistance. Alterations in DNA topoisomerase-II (Topo-II) activity, such as topo-II mutations or downregulation of topo-II protein, can result in resistance to topo-II-targeted drugs, including anthracyclines (57). As for drug influx, the mechanism by which only a small amount of chemotherapeutics enters cells has been elucidated. For instance, methotrexate (MTX), a dihydrofolate reductase (DHFR) inhibitor, enters the cell predominantly *via* the decreased folate carrier (RFC) (58). Decreased expression and inactivating alterations of the RFC are documented mechanisms of MTX resistance (59). Taken together, diverse mechanisms of drug resistance have been discovered, however more detailed mechanisms of chemoresistance are still largely unknown and require further investigation.

## CircRNAs AND DRUG RESISTANCE

### CircRNAs and Lung Cancer Drug Resistance

According to the global cancer statistics of 2020, lung cancer remains a major cause of cancer-related deaths (60). CDDP is one of the most effective anti-cancer drugs and is extensively used in the clinic; however, the development of CDDP resistance seriously hinders the therapeutic effect of cancer (61). The involvement of circRNAs in drug resistance in lung cancer is shown in **Table 1**. Accumulating evidence has demonstrated that circRNAs are implicated in CDDP resistance in lung cancer. Knockdown or silencing of certain circRNAs suppresses CDDP resistance in NSCLC such as circ-RNF121, circ_0076305, circRNA_103615, circ_0008928, hsa_circRNA_103809, circ-PRMT5, and circ_0007385 (17, 18, 49, 62–65). Additionally, circAKT3 inhibits glycolysis balance and enhances CDDP resistance, whereas circRNA-FOXO3 accelerates glycolysis and promotes CDDP sensitivity (50, 51). Both hsa_circ_0014235 and hsa_circ_0096157 overexpression intensifies the CDDP resistance and facilitates the malignancy of NSCLC cells, including proliferation, migration, and invasion (66, 67). circRNA_100565 is correlated with a poor prognosis of NSCLC, and circRNA_100565 deletion mitigates CDDP resistance, which can be attenuated by miR-377-3p inhibition or ADAM28 overexpression (68). circ_PIP5K1A regulates CDDP sensitivity *via* the miR-493-5p/ROCK1 axis, and circ_0085131 enhances NSCLC cell drug resistance by targeting miR-654-5p to upregulate *ATG7* expression (46, 69). Additionally, the sensitivity of CDDP can be promoted by the knockdown of circ-ABCB10 in lung cancer cells (70). However, circ_0000079 overexpression disturbs the formation of the FXR1/PRCKI complex by regulating FXR1, thereby suppressing cell invasion and CDDP resistance in NSCLC (71).

PTX is also an anti-neoplastic agent widely used to treat several solid tumor types, including lung cancer. Knockdown of circ_0001821 and circ_ZFR reduces the proliferation and metastasis ability but enhances PTX sensibility and apoptosis of NSCLC cells by downregulating the expression of GRK5 and KPNA4 by sponging related miRNAs (72, 73). Similarly, circ_0011292 modulates the miR-379-5p/TRIM65 axis to promote tumorigenesis and enhance PTX resistance in NSCLC (74). It has also been found that hsa_circ_0002874 downregulation can reverse the PTX resistance of NSCLC and induce apoptosis by regulating the miR1273f/MDM2/P53 signaling pathway (75). In contrast to the above circRNAs, circ_0030998 and circ_0002483 overexpression decreases the malignant behavior of lung cancer cells and enhances their sensitivity to PTX by targeting miR-558 and miR-182-5p, respectively (76, 77).

Du et al. explored a special circ_0014130-miR-545-3p-YAP1 pathway in the modulation of drug resistance and malignant behaviors of docetaxel (DTX)-resistant NSCLC cells (78). circ_0003998 knockdown suppresses colony formation and facilitates apoptosis and DTX sensitivity by sponging miR-136-5p to control CORO1C expression in DTX-resistant NSCLC cells (79). It has also been found that circ_0005909 knockdown resists the proliferation, metastasis, and drug resistance of NSCLC cells (80). Moreover, a novel protein encoded by circASK1 activates ASK1-dependent apoptosis, thereby ameliorating gefitinib resistance in LUAD (81). It has been shown that circSETD3 overexpression interferes with gefitinib sensitivity, and circSETD3 interacts with miR-520h and ABCG2 to reduce the intracellular concentration of gefitinib (19).

Exosomes are small extracellular vesicles that play essential roles in immunity, signal transduction, tumor treatment, and drug resistance (83). Yang et al. suggested that tumor-derived exosomal circRNA_102481 participated in EGFR-TKI resistance by sponging microRNA-30a-5p to modulate ROR1 in NSCLC (82). As for immune checkpoint inhibitors, hsa_circ_0003222 and circFGFR1 can promote NSCLC resistance to anti-PD-L1-based and anti-PD-1-based therapies, respectively (37, 38). Furthermore, suppression of circIGF2BP3/PKP3 promotes the therapeutic efficacy of anti-PD-1 in a Lewis LADC mouse model (39).

**TABLE 1** | Lung cancer drug resistance related circRNAs.

| CircRNA | Source | Expression | Sponging miRNAs | Targets and Pathways | Resistant Drugs | Cancer Type | Reference |
|---|---|---|---|---|---|---|---|
| circ_0076305 | exosomes | up | miR-186-5p | ABCC1 | cisplatin | NSCLC | (17) |
| circRNA_103615 | N/A | up* | N/A | ABCC1 | cisplatin | NSCLC | (18) |
| circ_0008928 | exosomes | up | miR-488 | HK2 | cisplatin | NSCLC | (49) |
| circ-RNF121 | N/A | up | miR-646 | SOX4 | cisplatin | NSCLC | (62) |
| hsa_circRNA_103809 | N/A | up | miR-377-3p | GOT1 | cisplatin | NSCLC | (63) |
| circ-PRMT5 | N/A | up | miR-4458 | REV3L | cisplatin | NSCLC | (64) |
| circ_0007385 | N/A | up | miR-519d-3p | HMGB1 | cisplatin | NSCLC | (65) |
| circAKT3 | N/A | up* | miR-516b-5p | STAT3 | cisplatin | lung cancer | (50) |
| circRNA-FOXO3 | N/A | up* | microRNA-543 | Foxo3 | cisplatin | NSCLC | (51) |
| hsa_circ_0014235 | exosomes | up* | miR-520a-5p | CDK4 | cisplatin | NSCLC | (66) |
| hsa_circ_0096157 | N/A | up | N/A | N/A | cisplatin | NSCLC | (67) |
| circRNA_100565 | N/A | up | miR-377-3p | ADAM28 | cisplatin | NSCLC | (68) |
| circ_PIP5K1A | N/A | up | miR-493-5p | ROCK1 | cisplatin | NSCLC | (69) |
| hsa_circ_0085131 | N/A | up | miR-654-5p | ATG7 | cisplatin | NSCLC | (46) |
| circ-ABCB10 | N/A | up* | miR-556-3p | AK4 | cisplatin | lung cancer | (70) |
| circ_0000079 | N/A | down | N/A | FXR1 | cisplatin | NSCLC | (71) |
| circ_0001821 | N/A | up* | miR-526b-5p | GRK5 | paclitaxel | NSCLC | (72) |
| circ_ZFR | N/A | up | miR-195-5p | KPNA4 | paclitaxel | NSCLC | (73) |
| circ_0011292 | N/A | up | miR-379-5p | TRIM65 | paclitaxel | NSCLC | (74) |
| hsa_circ_0002874 | N/A | up | miR1273f | MDM2/P53 pathway | paclitaxel | NSCLC | (75) |
| hsa_circ_0030998 | N/A | down | miR-558 | N/A | paclitaxel | lung cancer | (76) |
| circ_0002483 | N/A | down* | miR-182-5p | GRB2, FOXO1, and FOXO3 | Taxol | NSCLC | (77) |
| circ_0014130 | N/A | up | miR-545-3p | YAP1 | docetaxel | NSCLC | (78) |
| circ_0003998 | N/A | up | miR-136-5p | CORO1C | docetaxel | NSCLC | (79) |
| hsa_circ_0005909 | cytoplasm | up* | miRNA-338-3p | SOX4 | adriamycin | NSCLC | (80) |
| circASK1 | N/A | down | ASK1 | N/A, ASK1/JNK/p38 signaling | gefitinib | LUAD | (81) |
| circSETD3 | N/A | up | miR-520h | ABCG2 | gefitinib | NSCLC | (18) |
| circRNA_102481 | exosomes | up | miR-30a-5p | ROR1 | EGFR-TKIs | NSCLC | (82) |
| hsa_circ_0003222 | N/A | up* | miR-527 | N/A | anti-PD-L1 | NSCLC | (37) |
| circFGFR1 | N/A | up* | miR-381-3p | CXCR4 | anti-PD-1 | NSCLC | (38) |
| circIGF2BP3 | N/A | up* | miR-328-3p, miR-3173-5p | PKP3 | anti-PD-1 | NSCLC | (39) |

*N/A, Not Applicable.*

**The expression of circRNA upregulated only in cancer cells, others (without *) upregulated in cancer drug-resistant cells or both.*

## CircRNAs and Breast Cancer Drug Resistance

It was reported that there were 2.3 million new cases of breast cancer in female patients, which became the most generally diagnosed cancer, exceeding lung cancer in 2020 (60). Multiple circRNAs are shown to be correlated with breast cancer resistance (**Table 2**). The resistance to adriamycin (ADM), namely DOX, is closely correlated with therapeutic efficacy in patients with breast cancer and their prognosis (93). The knockdown of circ_0085495, circ_0001667, and circ_0006528 attenuates ADM resistance by related sponging miRNAs, becoming promising therapeutic targets for overcoming ADM resistance in patients with breast cancer (84–86). Similarly, hsa_circ_0092276, which sponges miR-384, regulates *ATG7* expression and promotes DOX resistance in breast cancer (47). Additionally, circUBE2D2 depletion induces a tumor-suppressive effect and suppression in DOX resistance, which has been greatly impaired upon miR512-3p downregulation or CDCA3 overexpression (87).

Lapatinib resistance is promoted by circ-MMP11 in breast cancer cells, and mechanically circ-MMP11 regulates ANLN expression by sponging miR-153-3p (88). CircFAT1 facilitates oxaliplatin (OX) resistance in breast cancer by regulating miR-525-5p/SKA1, and the Notch and Wnt pathways can be activated by SKA1, which has been identified by rescue assays, GSEA, and western blotting (89). Li et al. found that silencing hsa_circ_0000199 contributed to TNBC chemosensitivity to multiple drugs (32). In their study, the TNBC cell lines in the si-hsa_circ_0000199 group are prone to become sensitive to chemotherapeutic drugs, including CDDP, adriamycin, paclitaxel, and gemcitabine (GEM). It has also been found that circ-RNF111 increases PTX resistance in breast cancer by elevating E2F3 *via* sponging miR-140-5p (90). CircAMOTL1 overexpression reduces apoptosis and enhances the invasion of breast cancer cells exposed to PAX (26). Furthermore, 5-FU resistance is promoted by circFBXL5 in breast cancer *via* the miR-216b/HMGA2 axis (91). Additionally, hsa_circ_0025202 overexpression impedes tumor growth and promotes tamoxifen sensitivity, while miR-197-3p overexpression facilitates cell malignancy and TAM resistance in breast cancer (92).

## CircRNA and Gastric Cancer Drug Resistance

Gastric cancer (GC) is the fifth most common malignant tumor and is the fourth leading cause of cancer-related deaths (60, 94). The 5-year survival rate of advanced GC is approximately 20% (95). Platinum is a basic first-line

**TABLE 2 |** Breast cancer drug resistance related circRNAs.

| CircRNA | Source | Expression | Sponging miRNAs | Targets and Pathways | Resistant Drugs | Cancer Type | Reference |
|---|---|---|---|---|---|---|---|
| circ_0085495 | cytoplasm | up | miR-873-5p | integrin β1 | adriamycin | breast cancer | (84) |
| circ_0001667 | N/A | up | miR-4458 | NCOA3 | adriamycin | breast cancer | (85) |
| circ_0006528 | N/A | up | miR-1236-3p | CHD4 | adriamycin | breast cancer | (86) |
| hsa_circ_0092276 | N/A | up | miR-348 | ATG7 | doxorubicin | breast cancer | (47) |
| circUBE2D2 | N/A | up* | miR-512-3p | CDCA3 | doxorubicin | TNBC | (87) |
| circ-MMP11 | exosomes | up | miR-153-3p | ANLN | lapatinib | breast cancer | (88) |
| circFAT1 | N/A | up | miR-525-5p | SKA1, Notch and Wnt pathway | oxaliplatin | breast cancer | (89) |
| hsa_circ_0000199 | unclear | up | miR-613 and miR-206 | PI3K/Akt/mTOR signaling | cisplatin, adriamycin, paclitaxel, gemcitabine | TNBC | (32) |
| circ-RNF111 | N/A | up | miR-140-5p | E2F3 | paclitaxel | breast cancer | (90) |
| circAMOTL1 | N/A | up | N/A | AKT pathway | paclitaxel | breast cancer | (26) |
| circFBXL5 | N/A | up | miR-216b | HMGA2 | 5-fluorouracil | breast cancer | (91) |
| hsa_circ_0025202 | N/A | down | miR-197-3p | HIPK3 | tamoxifen | breast cancer | (92) |

*N/A, Not Applicable.*
**The expression of circRNAs only upregulated in cancer cells, others (without *) upregulated in cancer drug-resistant cells or both.*

chemotherapy drug for advanced GC (95). Studies on the mechanisms of circRNAs and resistance to CDDP are presented in **Table 3**. Exosomal circ-PVT1 regulates invasion, autophagy, and apoptosis and promotes CDDP resistance *via* the miR-30a-5p/YAP1 axis in GC cells, indicating that exosomal circ-PVT1 may be a valuable therapeutic target in GC (96). Additionally, the sensitivity of GC to CDDP is increased by knockdown of circ_ASAP2 or hsa_circ_0081143, which also represses the progression of GC by acting as ceRNAs (97, 98). It has been found that circAKT3 contributes to CDDP resistance in GC by enhancing DNA damage repair and hindering GC cell apoptosis (56). CircCCDC66 and circDONSON have been shown to induce CDDP resistance in GC by targeting the related miRNA and gene (27, 99). All the above studies demonstrate that certain circRNAs are overexpressed in CDDP-resistant GC and may serve as biomarkers for poor prognosis.

In contrast, Zhang et al. illustrated that upregulated expression of circ_0001017 inhibited malignant biological behaviors of GC and promoted CDDP sensitivity of CDDP-resistant GC cells partially *via* the miR-543/PHLPP2 axis (100). Similarly, circCUL2, acting as a tumor suppressor, enhances CDDP sensitivity by miR-142-3p/ROCK2-mediated autophagy (101). Exosomal circ_0032821 facilitates OXA resistance in OXA-sensitive GC cells by sponging miR-515-5p to enhance SOX9 expression (102). In addition, Herceptin resistance of GC cells can be reversed by hsa_circ_0000520 overexpression through inhibition of the PI3K-Akt signaling pathway (28).

**TABLE 3 |** Gastric cancer drug resistance related circRNAs.

| CircRNA | Source | Expression | Sponging miRNAs | Targets | Resistant Drugs | Cancer Type | Reference |
|---|---|---|---|---|---|---|---|
| circ-PVT1 | exosomes | up | miR-30a-5p | YAP1 | cisplatin | GC | (96) |
| circ_ASAP2 | N/A | up | miR-330-3p | NT5E | cisplatin | GC | (97) |
| hsa_circ_0081143 | N/A | up* | miR-646 | CDK6 | cisplatin | GC | (98) |
| circAKT3 | N/A | up | miR-198 | PIK3R1 | cisplatin | GC | (56) |
| circCCDC66 | N/A | up | miR-618 | BCL2 | cisplatin | GC | (27) |
| circDONSON | N/A | up | miR-802 | BMI1 | cisplatin | GC | (99) |
| circ_0001017 | N/A | down | miR-543 | PHLPP2 | cisplatin | GC | (100) |
| circCUL2 | cytoplasm | down | miR-142-3p | ROCK2 | cisplatin | GC | (101) |
| hsa_circ_0032821 | exosomes | up | miR-515-5p | SOX9 | oxaliplatin | GC | (102) |
| hsa_circ_0000520 | N/A | down | N/A | N/A | herceptin | GC | (28) |

*N/A, Not Applicable.*
**The expression of circRNAs only upregulated in cancer cells, others (without *) upregulated in cancer drug-resistant cells or both.*

## CircRNAs and Osteosarcoma Drug Resistance

Osteosarcoma is the most widespread primary bone tumor affecting children and adolescents, and effective chemotherapeutic regimens include the combination of high-dose MTX, DOX, and CDDP (103). As shown in **Table 4**, multiple circRNAs are associated with osteosarcoma drug resistance. Circ_0081001 knockdown promotes MTX sensitivity of osteosarcoma cells through the suppression of miR-494-3p-mediated upregulation of TGM2 (104). Similarly, hsa_circ_0000073 promotes malignant behaviors, including proliferation, invasion, and migration, and facilitates MTX resistance of osteosarcoma cells by sponging miR-145-5p and miR-151-3p to upregulate NRAS (105).

DOX resistance of osteosarcoma is facilitated by hsa_circ_0004674 through the Wnt/β-catenin pathway *via* modulation of the miR-342-3p/FBN1 axis (106). Moreover, some circRNAs potentiate DOX resistance and facilitate the progression of osteosarcomas, such as circ_0001721, circSAMD4A, circ_0002060, and circ_0003496 (20, 107–109). Zhu et al. report that resistance to DOX and CDDP can be weakened by suppressing circPVT1 expression in osteosarcoma cells (21). It has been reported that circ-CHI3L1.2 knockdown promotes apoptosis and attenuates resistance of CDDP-resistant osteosarcoma cells (22). Additionally, exosomal hsa_circ_103801 can intensify the facilitating effect of exosomes on the chemoresistance of osteosarcoma cells to CDDP (110). Similarly, circTADA2A can target miR-129-5p, which is competitively bound to TRPS1 and YAP1, thereby regulating osteosarcoma cell proliferation and CDDP resistance (111).

## CircRNA and Glioma Drug Resistance

Glioma is the most common form of aggressive intracranial tumors and is characterized by a high rate of mortality, metastasis, and drug resistance (112). Here, we summarized the contribution of circRNAs to chemoresistance in glioma patients (**Table 5**). It has been shown that exosomal hsa_circ_0042003, mediated by heparanase transfers from temozolomide (TMZ)-resistant glioma cells to drug-sensitive cells, which contributes to TMZ resistance in glioma (113). In glioma, exosomal circ_0072083 modulates NANOG and ALKBH5 by targeting miR-1252-5p and demethylation to control TMZ resistance (114). Hsa_circ_0110757 and circ_0005198 facilitate TMZ resistance and inhibit glioma cell apoptosis through the miR-1298-5p/ITGA1 and miR-198/TRIM14 axis, respectively (115, 116). Consistent with these findings, downregulation of circ-VPS18, hsa_circ_0000936, circHIPK3, and circ CEP128 improve TMZ sensitivity and repress glioma progression (117–120). The highlight is that circHIPK3 downregulation inhibits the PI3K/AKT signaling pathway partly through the miR-524-5p/KIF2A axis (119). Similarly, in TMZ-resistant glioma, exosomal circ-HIPK3 can regulate the miR-421/ZIC5 axis to promote cell progression and TMZ resistance (123). circASAP1 overexpression promotes glioblastoma cell proliferation and TMZ resistance *via* the circASAP1/miR-502-5p/NRAS regulatory network, indicating that circASAP1 is a potential target for TMZ-resistant glioblastoma therapy (121). circ_0008344 downregulation impedes glioma growth and functions on the miR-433-3p/RNF2 axis to promote radiosensitivity in glioma (122).

## CircRNAs and Ovarian Cancer Drug Resistance

Ovarian cancer is one of the most common gynecologic malignant tumors, and conventional treatment is mainly limited to chemoresistance (124). **Table 6** displays the chemoresistance-related circRNAs in ovarian cancer. Both circ_C20orf11 and circulating exosomal circFoxp1 can confer CDDP resistance in ovarian cancer cells (40, 125). In contrast, Cdr1as improves sensitivity to CDDP in ovarian cancer by modulating the miR-1270/SCAI axis (126).

The downregulation of circRNA_0000735 and upregulation of circRNA_0006404 can suppress the expression of p-GP, causing DTX treatment tolerance (127). Two studies demonstrated that circ_CELSR1 was upregulated in PTX-resistant ovarian cancer cells, and circ_CELSR1 silencing impeded PTX resistance in ovarian cancer *in vivo* (128, 129). Meanwhile, one study revealed that the inhibition of circCELSR1 also resulted in ovarian cancer cell $G_0/G_1$ arrest and the

**TABLE 4** | Osteosarcoma drug resistance related circRNAs.

| CircRNA | Source | Expression | Sponging miRNAs | Targets | Resistant Drugs | Cancer Type | Reference |
|---|---|---|---|---|---|---|---|
| circ_0081001 | N/A | up | miR-494-3p | TGM2 | Methotrexate | osteosarcoma | (104) |
| hsa_circ_0000073 | N/A | up | miR-145-5p and miR-151-3p | NRAS | Methotrexate | osteosarcoma | (105) |
| hsa_circ_0004674 | N/A | up | miR-342-3p | FBN1 | doxorubicin | osteosarcoma | (106) |
| circ_0001721 | N/A | up | miR-758 | TCF4 | doxorubicin | osteosarcoma | (107) |
| circSAMD4A | N/A | up | miR-218-5p | KLF8 | doxorubicin | osteosarcoma | (108) |
| circ_0002060 | N/A | up | miR-198 | ABCB1 | doxorubicin | osteosarcoma | (20) |
| circ_0003496 | N/A | up | miR-370 | KLF12 | doxorubicin | osteosarcoma | (109) |
| circPVT1 | N/A | up | N/A | ABCB1 | doxorubicin and cisplatin | osteosarcoma | (20) |
| circ-CHI3L1.2 | N/A | up | miR-340-5p | LPAATβ | cisplatin | osteosarcoma | (22) |
| hsa_circ_103801 | exosomes | up | N/A | N/A | cisplatin | osteosarcoma | (110) |
| circTADA2A | N/A | up | miR-129-5p | TRPS1, YAPS | cisplatin | osteosarcoma | (111) |

*N/A, Not Applicable.*

**TABLE 5 |** Glioma drug resistance related circRNAs.

| CircRNA | Source | Expression | Sponging miRNAs | Targets | Resistant Drugs | Cancer Type | Reference |
|---|---|---|---|---|---|---|---|
| hsa_circ_0042003 | exosomes | up | N/A | N/A | Temozolomide | glioma | (113) |
| circ_0072083 | exosomes | up | miR-1252-5p | NANOG | Temozolomide | glioma | (114) |
| Hsa_circ_0110757 | N/A | up | miR-1298-5p | ITGA1 | Temozolomide | glioma | (115) |
| circ_0005198 | N/A | up | miR-198 | TRIM14 | Temozolomide | glioma | (116) |
| circ-VPS18 | N/A | up | miR-370 | RUNX1 | Temozolomide | glioma | (117) |
| hsa_circ_0000936 | N/A | up | miR-1294 | N/A | Temozolomide | glioma | (118) |
| circHIPK3 | N/A | up | miR-524-5p | KIF2A | Temozolomide | glioma | (119) |
| circ CEP128 | N/A | up | miR-145-5p | N/A | Temozolomide | glioma | (120) |
| circ-HIPK3 | exosomes | up | miR-421 | ZIC5 | Temozolomide | glioma | (119) |
| circASAP1 | N/A | up | miR-502-5p | NRAS | Temozolomide | glioblastoma | (121) |
| circ_0008344 | N/A | up | miR-433-3p | RNF2 | radiotherapy | glioma | (122) |

*N/A, Not Applicable.*

**TABLE 6 |** Ovarian cancer drug resistance related circRNAs.

| CircRNA | Source | Expression | Sponging miRNAs | Targets | Resistant Drugs | Cancer Type | Reference |
|---|---|---|---|---|---|---|---|
| circ_C20orf11 | N/A | up* | miR-527 | YWHAZ | cisplatin | ovarian cancer | (40) |
| circFoxp1 | exosomes | up | miR-22 and miR-150-3p | CEBPG and FMNL3 | cisplatin | ovarian cancer | (125) |
| circRNA Cdr1as | N/A | down | miR-1270 | SCAI | cisplatin | ovarian cancer | (126) |
| circRNA_0006404 | N/A | down | miR-346 | DKK3 | Docetaxel | ovarian cancer | (127) |
| circRNA_0000735 | N/A | up | miR-526b | DKK4 | Docetaxel | ovarian cancer | (127) |
| circ_CELSR1 | N/A | up | miR-149-5p | SIK2 | paclitaxel | ovarian cancer | (128) |
| circCELSR1 | N/A | up | miR-1252 | FOXR2 | paclitaxel | ovarian cancer | (129) |
| circTNPO3 | N/A | up | miR-1299 | NEK2 | paclitaxel | ovarian cancer | (130) |

*N/A, Not Applicable.*
**The expression of circRNAs only upregulated in cancer cells, others (without *) upregulated in cancer drug-resistant cells or both.*

promotion of apoptosis (129). Similarly, circTNPO3 upregulates NEK2 expression by sponging miR-1299 to enhance PTX resistance in ovarian cancer cells (130).

## CircRNA and Drug Resistance of Other Cancers

We also summarized a number of studies on circRNAs and drug resistance in other cancers, including hepatocellular carcinoma (HCC), colorectal cancer (CRC), esophageal cancer (EC), pancreatic cancer (PC), and some urinary system tumors (**Table 7**). As we all know, tolerance to chemotherapeutics is the pivotal cause of recurrence and poor prognosis in colorectal cancer patients. It has been shown that circ_0000338 knockdown sensitizes 5-FU-resistant CRC cells to 5-FU by promoting apoptosis and hindering proliferation (131). Exosomal circ-FBXW7 leads resistant cells sensitive to OX-induced apoptosis, inhibits OX-induced epithelial-mesenchymal transition, and suppresses OX efflux (132). In contrast, hsa_circ_0005963 is transferred by exosomes from OX-resistant CRC cells to OX-sensitive cells, resulting in glycolysis and drug resistance by enhancing PKM2 expression (133). A recent study suggested that circ_0020095 acts as a miR-487a-3p sponge to promote CDDP resistance by increasing the expression of SOX9 (134). In DOX-resistant CRC cells, circCSPP1 knockdown improves DOX sensitivity, attenuates cell malignant behaviors, and induces apoptosis through the miR-944/FZD7 axis (135).

As for HCC, the knockdown of circPTGR1 and circARNT2 induces apoptosis of HCC cells and inhibits 5-FU and CDDP resistance, respectively (23, 136). Moreover, circRNA, as a ceRNA, suppresses the activity of miR-326 to upregulate RUNX2 expression and enhance CDDP resistance (137). Two studies elaborate the mechanism of circRNA-SORE in sorafenib resistance in HCC from different perspectives. One study reveals that circRNA-SORE inhibits PRP19-mediated YBX1 degradation, thus affecting the expression of downstream gene targets of YBX1, including ERK, AKT, c-Myc, Raf1, and TGF-β1 (138). Another study demonstrates that circRNA-SORE interacts with miR-103a-2-5p and miR-660-3p by serving as a microRNA sponge, thus activating the Wnt/β-catenin pathway and leading to sorafenib resistance (139). In addition, Huang et al. confirm that overexpression of circMET can promote HCC development

**TABLE 7 |** Drug resistance related circRNAs of other cancers.

| CircRNA | Source | Expression | Sponging miRNAs | Targets and Pathways | Resistant Drugs | Cancer Type | Reference |
|---|---|---|---|---|---|---|---|
| circ_0000338 | exosome | up | miR-217 and miR-485-3p | N/A | 5-fluorouracil | CRC | (131) |
| circ-FBXW7 | exosome | down | miR-18b-5p | N/A | oxaliplatin | CRC | (132) |
| hsa_circ_0005963 | exosome | up | miR-122 | PKM2 | oxaliplatin | CRC | (133) |
| circ_0020095 | N/A | up* | miR-487a-3p | SOX9 | cisplatin | colon cancer | (134) |
| circCSPP1 | N/A | up | miR-944 | FZD7 | doxorubicin | CRC | (135) |
| circPTGR1 | N/A | up* | miR-129-5p | ABCC1 | 5-fluorouracil | HCC | (23) |
| circARNT2 | N/A | up | miR-155-5p | PDK1 | cisplatin | HCC | (136) |
| circRNA_102272 | N/A | up* | miR-326 | RUNX2 | cisplatin | HCC | (137) |
| circRNA-SORE | exosomes | up | N/A | YBX1 | sorafenib | HCC | (138) |
| circRNA-SORE | N/A | up | miR-103a-2-5p and miR-660-3p, | Wnt/β-cateninpathway | sorafenib | HCC | (139) |
| two novel circRNAs△ | N/A | up | miR-19a-3p and miR-145-5p | N/A | Gemcitabine | pancreatic cancer | (140) |
| circZNF91 | exosomes | up* | miR-23b-3p | SIRT1 | Gemcitabine | pancreatic cancer | (52) |
| circ_0000337 | exosomes | up | miR-377-3p | JAK2 | cisplatin | esophageal cancer | (141) |
| circRNA-DOPEY2 | N/A | down | N/A | N/A | cisplatin | ESCC | (29) |
| circ_0006168 | N/A | up | miR-194-5p | JMJD1C | Taxol | esophageal cancer | (142) |
| circPSMC3 | N/A | down | miR-10a-5p | PTEN | gefitinib | ESCC | (34) |
| circFNTA | N/A | up* | miR-370-3p | FNTA, KRAS signaling | cisplatin | bladder cancer | (143) |
| circELP3 | cytoplasm | up* | N/A | N/A | cisplatin | bladder cancer | (144) |
| circ0008399 | N/A | up* | WTAP | TNFAIP3 | cisplatin | bladder cancer | (145) |
| hsa_circ_0000285 | N/A | down | N/A | N/A | cisplatin | bladder cancer | (146) |
| hsa_circ_0035483 | N/A | up* | miR-335 | CCNB1 | gemcitabine | RCC | (147) |

*N/A, Not Applicable.*

*△chr14:101402109-101464448+ and chr4:52729603-52780244+.*

**The expression of circRNAs upregulated only in cancer cells, others (without *) upregulated in cancer drug-resistant cells or both.*

and immune tolerance through the miR-30-5p/Snail/DPP4/CXCL10 axis (148).

An increasing number of studies have elucidated the molecular mechanism of circRNAs in the initiation and progression of PC; however, studies on drug resistance mechanisms are in their preliminary exploration stage (149). For example, PC drug-resistant cells (PANC-1-GR) increase sensitivity to GEM after silencing two novel circRNAs (chr14:101402109-101464448+ or chr4:52729603-52780244+) (140). Exosomal circZNF91 transferred to normoxic PC cells can result in GEM and glycolysis chemoresistance (52).

As early as 2016, researchers utilized circRNA microarray to discover that some circRNAs are distinguished in the radioresistant esophageal cell line and the parental cell line, indicating that these dysregulated circRNAs are involved in radiation resistance (150). In esophageal cancer cells, CDDP resistance can be increased by exosomal circ_0000337, which regulates the miR-377-3p/JAK2 axis (141). cDOPEY2 promotes the ubiquitination and degradation of CPEB4 to inhibit CPEB4-mediated Mcl-1 translation, thereby alleviating CDDP resistance (29). Moreover, knockdown of circ_0006168 or JMJD1C plays a crucial role in inhibiting cell proliferation, invasion, and migration and promoting apoptosis, which accelerates the taxol sensitivity of Esophageal squamous cell carcinoma (ESCC) *in vitro* (142). In contrast, circPSMC3 overexpression inhibits miR-10a-5p expression and increases the sensitivity of ESCC cells to gefitinib (34).

Research on circRNAs in the drug resistance of urinary system tumors is also in its initial stages. It is an AR-mediated ADAR2/circFNTA/miR-370-3p/FNTA pathway that stimulates KRAS to change bladder cancer cell invasion and chemosensitivity to CDDP (143). Hypoxia-elevated circELP3 facilitates CDDP resistance in bladder cancer cells (144). circ0008399 promotes the formation of the WTAP/METTL3/METTL14 $m^6A$ methyltransferase complex and increases the expression of TNFAIP3 in an $m^6A$-dependent manner. Additionally, the high expression of circ0008399 and WTAP is correlated with poor prognosis in patients with bladder cancer (145). A study reveals that hsa_circ_0000285 is expressed at significantly lower levels in both bladder cancer tissues and CDDP-resistant patients, but the detailed mechanism of hsa_circ_0000285 in chemosensitivity needs further exploration (146). In addition, hsa_circ_0035483 contributes to GEM-induced autophagy and promotes resistance of renal clear cell carcinoma (RCC) to GEM by regulating the hsa-miR-335/CCNB1 axis (147).

## CONCLUSIONS AND FUTURE PERSPECTIVES

Currently, resistance to chemotherapeutic drugs has become an urgent problem impeding the treatment of various cancers. As a novel RNA class, an increasing number of circRNAs have been confirmed to be related to the chemoresistance of cancers. Most circRNAs function as miRNA sponges and form the circRNAs/miRNAs/mRNAs regulatory axis to regulate drug resistance or sensitivity of cancers. The sensitivity of cancer cells to chemotherapeutic drugs can be enhanced by silencing circRNAs that are upregulated in drug-resistant cancer cells or

by overexpressing circRNAs that are downregulated in drug-resistant cancer cells.

The underlying mechanisms of chemoresistance-related circRNAs include the efflux of drugs, apoptosis, glycolysis, intervention with the TME, autophagy, and dysfunction of DNA damage repair, among others, which still requires further exploration. In addition, multiple pathways are involved in circRNA-modulated drug resistance in cancers including P53 signaling, KRAS signaling, the Wnt/β-catenin pathway, and the PI3K/Akt/mTOR pathway. New challenges owing to different chemotherapies are inevitable, demanding further elucidation of the involved signaling networks.

Taken together, it is still a challenge to select the key target for the treatment of malignancies from a large number of candidate circRNAs. Most studies on circRNAs and drug resistance are limited to *in vitro* and *in vivo* experiments. Therefore, long-term follow-up of patients and analysis of the relationship between circRNAs and drug resistance are warranted in this regard. The drug resistance of cancers may be associated with a systematic and comprehensive regulatory network comprising circRNAs, miRNAs, and target mRNAs. More research is required to elucidate the concrete molecular mechanisms between circRNAs and drug resistance in cancers and to survey the role of circRNAs in clinical practice in the future.

## AUTHOR CONTRIBUTIONS

Xin-YL, QZ, and JG reviewed literature and originally drafted the manuscript. PZ, HL, Z-BT, and C-PZ contributed to editing and embellished the manuscript. Xia-YL approved the final version of the manuscript. All authors contributed to the article and approved the submitted version.

## FUNDING

The study was supported by the National Natural Science Foundation (No. 81802777), the "Clinical medicine + X" scientific research project of Affiliated Hospital of Qingdao University, and Qingdao Chinese Medicine Technology Project (2021-zyym26).

## ACKNOWLEDGMENTS

We would like to thank Editage (www.editage.com) for English language editing. And we thank all the authors for helping with the writing and publication of this article.

## REFERENCES

1. Bray F, Laversanne M, Weiderpass E, Soerjomataram I. The Ever-Increasing Importance of Cancer as a Leading Cause of Premature Death Worldwide. *Cancer* (2021) 127:3029–30. doi: 10.1002/cncr.33587
2. Kuwano M, Sonoda K, Murakami Y, Watari K, Ono M. Overcoming Drug Resistance to Receptor Tyrosine Kinase Inhibitors: Learning From Lung Cancer. *Pharmacol Ther* (2016) 161:97–110. doi: 10.1016/j.pharmthera.2016.03.002
3. Vasan N, Baselga J, Hyman DM. A View on Drug Resistance in Cancer. *Nature* (2019) 575:299–309. doi: 10.1038/s41586-019-1730-1
4. Longley DB, Johnston PG. Molecular Mechanisms of Drug Resistance. *J Pathol* (2005) 205:275–92. doi: 10.1002/path.1706
5. Skoulidis F, Goldberg ME, Greenawalt DM, Hellmann MD, Awad MM, Gainor JF, et al. STK11/LKB1 Mutations and PD-1 Inhibitor Resistance in KRAS-Mutant Lung Adenocarcinoma. *Cancer Discov* (2018) 8:822–35. doi: 10.1158/2159-8290.Cd-18-0099
6. Jeck WR, Sharpless NE. Detecting and Characterizing Circular RNAs. *Nat Biotechnol* (2014) 32:453–61. doi: 10.1038/nbt.2890
7. Sanger HL, Klotz G, Riesner D, Gross HJ, Kleinschmidt AK. Viroids are Single-Stranded Covalently Closed Circular RNA Molecules Existing as Highly Base-Paired Rod-Like Structures. *Proc Natl Acad Sci USA* (1976) 73:3852–6. doi: 10.1073/pnas.73.11.3852
8. Guo JU, Agarwal V, Guo H, Bartel DP. Expanded Identification and Characterization of Mammalian Circular RNAs. *Genome Biol* (2014) 15:409. doi: 10.1186/s13059-014-0409-z
9. Kulcheski FR, Christoff AP, Margis R. Circular RNAs are miRNA Sponges and can be Used as a New Class of Biomarker. *J Biotechnol* (2016) 238:42–51. doi: 10.1016/j.jbiotec.2016.09.011
10. Cheng F, Zheng B, Si S, Wang J, Zhao G, Yao Z, et al. The Roles of CircRNAs in Bladder Cancer: Biomarkers, Tumorigenesis Drivers, and Therapeutic Targets. *Front Cell Dev Biol* (2021) 9:666863. doi: 10.3389/fcell.2021.666863
11. Meng S, Zhou H, Feng Z, Xu Z, Tang Y, Li P, et al. CircRNA: Functions and Properties of a Novel Potential Biomarker for Cancer. *Mol Cancer* (2017) 16:94. doi: 10.1186/s12943-017-0663-2
12. Liang G, Ling Y, Mehrpour M, Saw PE, Liu Z, Tan W, et al. Autophagy-Associated circRNA circCDYL Augments Autophagy and Promotes Breast Cancer Progression. *Mol Cancer* (2020) 19:65. doi: 10.1186/s12943-020-01152-2
13. Yang F, Hu A, Li D, Wang J, Guo Y, Liu Y, et al. Circ-HuR Suppresses HuR Expression and Gastric Cancer Progression by Inhibiting CNBP Transactivation. *Mol Cancer* (2019) 18:158. doi: 10.1186/s12943-019-1094-z
14. Wei L, Sun J, Zhang N, Zheng Y, Wang X, Lv L, et al. Noncoding RNAs in Gastric Cancer: Implications for Drug Resistance. *Mol Cancer* (2020) 19:62. doi: 10.1186/s12943-020-01185-7
15. Chen Z, Shi T, Zhang L, Zhu P, Deng M, Huang C, et al. Mammalian Drug Efflux Transporters of the ATP Binding Cassette (ABC) Family in Multidrug Resistance: A Review of the Past Decade. *Cancer Lett* (2016) 370:153–64. doi: 10.1016/j.canlet.2015.10.010
16. Sharom FJ. The P-Glycoprotein Multidrug Transporter. *Essays Biochem* (2011) 50:161–78. doi: 10.1042/bse0500161
17. Wang X, Wang H, Jiang H, Qiao L, Guo C. Circular RNAcirc_0076305 Promotes Cisplatin (DDP) Resistance of Non-Small Cell Lung Cancer Cells by Regulating ABCC1 Through miR-186-5p. *Cancer Biother Radiopharm* (2021). doi: 10.1089/cbr.2020.4153
18. Liang H, Lin Z, Lin H, Zhao L, Huang W. circRNA_103615 Contributes to Tumor Progression and Cisplatin Resistance in NSCLC by Regulating ABCB1. *Exp Ther Med* (2021) 22:934. doi: 10.3892/etm.2021.10366
19. Huang Y, Dai Y, Wen C, He S, Shi J, Zhao D, et al. Circsetd3 Contributes to Acquired Resistance to Gefitinib in Non-Small-Cell Lung Cancer by Targeting the miR-520h/ABCG2 Pathway. *Mol Ther Nucleic Acids* (2020) 21:885–99. doi: 10.1016/j.omtn.2020.07.027
20. Ji Y, Liu J, Zhu W, Ji J. Circ_0002060 Enhances Doxorubicin Resistance in Osteosarcoma by Regulating the miR-198/ABCB1 Axis. *Cancer Biother Radiopharm* (2020). doi: 10.1089/cbr.2020.4240
21. Kun-Peng Z, Xiao-Long M, Chun-Lin Z. Overexpressed Circpvt1, a Potential New Circular RNA Biomarker, Contributes to Doxorubicin and Cisplatin Resistance of Osteosarcoma Cells by Regulating ABCB1. *Int J Biol Sci* (2018) 14:321–30. doi: 10.7150/ijbs.24360
22. Zhang Z, Zhou Q, Luo F, Zhou R, Xu J, Xiao J, et al. Circular RNA Circ-CHI3L1.2 Modulates Cisplatin Resistance of Osteosarcoma Cells *via* the miR-340-5p/Lpaatβ Axis. *Hum Cell* (2021) 34:1558–68. doi: 10.1007/s13577-021-00564-6
23. Li X, Zhang T. Circular RNA PTGR1 Regulates 5-FU Resistance and Development of Hepatocellular Carcinoma Cells by Modulating miR-129-5p/ABCC1 Axis. *Cell Biol Int* (2021). doi: 10.1002/cbin.11635

24. Lomonosova E, Chinnadurai G. BH3-Only Proteins in Apoptosis and Beyond: An Overview. *Oncogene* (2008) 27 Suppl 1:S2–19. doi: 10.1038/onc.2009.39
25. Kryczka J, Kryczka J, Czarnecka-Chrebelska KH, Brzeziańska-Lasota E. Molecular Mechanisms of Chemoresistance Induced by Cisplatin in NSCLC Cancer Therapy. *Int J Mol Sci* (2021) 22(16):8885. doi: 10.3390/ijms22168885
26. Ma J, Fang L, Yang Q, Hibberd S, Du WW, Wu N, et al. Posttranscriptional Regulation of AKT by Circular RNA Angiomotin- Like 1 Mediates Chemoresistance Against Paclitaxel in Breast Cancer Cells. *Aging (Albany NY)* (2019) 11:11369–81. doi: 10.18632/aging.102535
27. Zhang Q, Miao Y, Fu Q, Hu H, Chen H, Zeng A, et al. CircRNACCDC66 Regulates Cisplatin Resistance in Gastric Cancer *via* the miR-618/BCL2 Axis. *Biochem Biophys Res Commun* (2020) 526:713–20. doi: 10.1016/j.bbrc.2020.03.156
28. Lv X, Li P, Wang J, Gao H, Hei Y, Zhang J, et al. Hsa_Circ_0000520 Influences Herceptin Resistance in Gastric Cancer Cells Through PI3K-Akt Signaling Pathway. *J Clin Lab Anal* (2020) 34:e23449. doi: 10.1002/jcla.23449
29. Liu Z, Gu S, Wu K, Li L, Dong C, Wang W, et al. CircRNA-DOPEY2 Enhances the Chemosensitivity of Esophageal Cancer Cells by Inhibiting CPEB4-Mediated Mcl-1 Translation. *J Exp Clin Cancer Res* (2021) 40:361. doi: 10.1186/s13046-021-02149-5
30. Tewari D, Patni P, Bishayee A, Sah AN, Bishayee A. Natural Products Targeting the PI3K-Akt-mTOR Signaling Pathway in Cancer: A Novel Therapeutic Strategy. *Semin Cancer Biol* (2019). doi: 10.1016/j.semcancer.2019.12.008
31. Burris HA. 3rd. Overcoming Acquired Resistance to Anticancer Therapy: Focus on the PI3K/AKT/mTOR Pathway. *Cancer Chemother Pharmacol* (2013) 71:829–42. doi: 10.1007/s00280-012-2043-3
32. Li H, Xu W, Xia Z, Liu W, Pan G, Ding J, et al. Hsa_circ_0000199 Facilitates Chemo-Tolerance of Triple-Negative Breast Cancer by Interfering With miR-206/613-Led PI3K/Akt/mTOR Signaling. *Aging (Albany NY)* (2021) 13:4522–51. doi: 10.18632/aging.202415
33. Yang SM, Huang C, Li XF, Yu MZ, He Y, Li J. miR-21 Confers Cisplatin Resistance in Gastric Cancer Cells by Regulating PTEN. *Toxicology* (2013) 306:162–8. doi: 10.1016/j.tox.2013.02.014
34. Zhu H, Du F, Cao C. Restoration of Circpsmc3 Sensitizes Gefitinib-Resistant Esophageal Squamous Cell Carcinoma Cells to Gefitinib by Regulating miR-10a-5p/PTEN Axis. *Cell Biol Int* (2021) 45:107–16. doi: 10.1002/cbin.11473
35. Pitt JM, Vetizou M, Daillere R, Roberti MP, Yamazaki T, Routy B, et al. Resistance Mechanisms to Immune-Checkpoint Blockade in Cancer: Tumor-Intrinsic and -Extrinsic Factors. *Immunity* (2016) 44:1255–69. doi: 10.1016/j.immuni.2016.06.001
36. Sun Y. Tumor Microenvironment and Cancer Therapy Resistance. *Cancer Lett* (2016) 380:205–15. doi: 10.1016/j.canlet.2015.07.044
37. Li C, Zhang J, Yang X, Hu C, Chu T, Zhong R, et al. Hsa_Circ_0003222 Accelerates Stemness and Progression of non-Small Cell Lung Cancer by Sponging miR-527. *Cell Death Dis* (2021) 12:807. doi: 10.1038/s41419-021-04095-8
38. Zhang PF, Pei X, Li KS, Jin LN, Wang F, Wu J, et al. Circular RNA Circfgfr1 Promotes Progression and Anti-PD-1 Resistance by Sponging miR-381-3p in non-Small Cell Lung Cancer Cells. *Mol Cancer* (2019) 18:179. doi: 10.1186/s12943-019-1111-2
39. Liu Z, Wang T, She Y, Wu K, Gu S, Li L, et al. N(6)-Methyladenosine-Modified Circigf2bp3 Inhibits CD8(+) T-Cell Responses to Facilitate Tumor Immune Evasion by Promoting the Deubiquitination of PD-L1 in non-Small Cell Lung Cancer. *Mol Cancer* (2021) 20:105. doi: 10.1186/s12943-021-01398-4
40. Yin J, Huang HY, Long Y, Ma Y, Kamalibaike M, Dawuti R, et al. Circ_C20orf11 Enhances DDP Resistance by Inhibiting miR-527/YWHAZ Through the Promotion of Extracellular Vesicle-Mediated Macrophage M2 Polarization in Ovarian Cancer. *Cancer Biol Ther* (2021) 22(7–9):440–54. doi: 10.1080/15384047.2021.1959792
41. Erin N, Grahovac J, Brozovic A, Efferth T. Tumor Microenvironment and Epithelial Mesenchymal Transition as Targets to Overcome Tumor Multidrug Resistance. *Drug Resist Update* (2020) 53:100715. doi: 10.1016/j.drup.2020.100715
42. Nantajit D, Lin D, Li JJ. The Network of Epithelial-Mesenchymal Transition: Potential New Targets for Tumor Resistance. *J Cancer Res Clin Oncol* (2015) 141:1697–713. doi: 10.1007/s00432-014-1840-y
43. Joseph NA, Chiou SH, Lung Z, Yang CL, Lin TY, Chang HW, et al. The Role of HGF-MET Pathway and CCDC66 cirRNA Expression in EGFR Resistance and Epithelial-to-Mesenchymal Transition of Lung Adenocarcinoma Cells. *J Hematol Oncol* (2018) 11:74. doi: 10.1186/s13045-018-0557-9
44. Choi AM, Ryter SW, Levine B. Autophagy in Human Health and Disease. *N Engl J Med* (2013) 368:651–62. doi: 10.1056/NEJMra1205406
45. White E. Deconvoluting the Context-Dependent Role for Autophagy in Cancer. *Nat Rev Cancer* (2012) 12:401–10. doi: 10.1038/nrc3262
46. Kong R. Circular RNA Hsa_Circ_0085131 is Involved in Cisplatin-Resistance of non-Small-Cell Lung Cancer Cells by Regulating Autophagy. *Cell Biol Int* (2020) 44:1945–56. doi: 10.1002/cbin.11401
47. Wang Q, Liang D, Shen P, Yu Y, Yan Y, You W. Hsa_circ_0092276 Promotes Doxorubicin Resistance in Breast Cancer Cells by Regulating Autophagy *via* miR-348/ATG7 Axis. *Transl Oncol* (2021) 14:101045. doi: 10.1016/j.tranon.2021.101045
48. Marcucci F, Rumio C. Glycolysis-Induced Drug Resistance in Tumors-A Response to Danger Signals? *Neoplasia* (2021) 23:234–45. doi: 10.1016/j.neo.2020.12.009
49. Shi Q, Ji T, Ma Z, Tan Q, Liang J. Serum Exosomes-Based Biomarker Circ_0008928 Regulates Cisplatin Sensitivity, Tumor Progression, and Glycolysis Metabolism by miR-488/HK2 Axis in Cisplatin-Resistant Nonsmall Cell Lung Carcinoma. *Cancer Biother Radiopharm* (2021). doi: 10.1089/cbr.2020.4490
50. Xu Y, Jiang T, Wu C, Zhang Y. CircAKT3 Inhibits Glycolysis Balance in Lung Cancer Cells by Regulating miR-516b-5p/STAT3 to Inhibit Cisplatin Sensitivity. *Biotechnol Lett* (2020) 42:1123–35. doi: 10.1007/s10529-020-02846-9
51. Zhang Y, Ge P, Zhou D, Xing R, Bai L. Circular RNA FOXO3 Accelerates Glycolysis and Improves Cisplatin Sensitivity in Lung Cancer Cells. *Via miR-543/Foxo3 Axis Oncol Lett* (2021) 22:839. doi: 10.3892/ol.2021.13100
52. Zeng Z, Zhao Y, Chen Q, Zhu S, Niu Y, Ye Z, et al. Hypoxic Exosomal HIF-1α-Stabilizing Circznf91 Promotes Chemoresistance of Normoxic Pancreatic Cancer Cells via Enhancing Glycolysis. *Oncogene* (2021). doi: 10.1038/s41388-021-01960-w
53. Sancar A, Lindsey-Boltz LA, Unsal-Kaçmaz K, Linn S. Molecular Mechanisms of Mammalian DNA Repair and the DNA Damage Checkpoints. *Annu Rev Biochem* (2004) 73:39–85. doi: 10.1146/annurev.biochem.73.011303.073723
54. Haynes B, Saadat N, Myung B, Shekhar MP. Crosstalk Between Translesion Synthesis, Fanconi Anemia Network, and Homologous Recombination Repair Pathways in Interstrand DNA Crosslink Repair and Development of Chemoresistance. *Mutat Res Rev Mutat Res* (2015) 763:258–66. doi: 10.1016/j.mrrev.2014.11.005
55. Jeggo PA, Pearl LH, Carr AM. DNA Repair, Genome Stability and Cancer: A Historical Perspective. *Nat Rev Cancer* (2016) 16:35–42. doi: 10.1038/nrc.2015.4
56. Huang X, Li Z, Zhang Q, Wang W, Li B, Wang L, et al. Circular RNA AKT3 Upregulates PIK3R1 to Enhance Cisplatin Resistance in Gastric Cancer. *Via miR-198 Suppression Mol Cancer* (2019) 18:71. doi: 10.1186/s12943-019-0969-3
57. Friche E, Danks MK, Schmidt CA, Beck WT. Decreased DNA Topoisomerase II in Daunorubicin-Resistant Ehrlich Ascites Tumor Cells. *Cancer Res* (1991) 51:4213–8.
58. Bertino JR. Karnofsky Memorial Lecture. Ode to Methotrexate. *J Clin Oncol* (1993) 11:5–14. doi: 10.1200/jco.1993.11.1.5
59. Guo W, Healey JH, Meyers PA, Ladanyi M, Huvos AG, Bertino JR, et al. Mechanisms of Methotrexate Resistance in Osteosarcoma. *Clin Cancer Res* (1999) 5:621–7.
60. Sung H, Ferlay J, Siegel RL, Laversanne M, Soerjomataram I, Jemal A, et al. Global Cancer Statistics 2020: GLOBOCAN Estimates of Incidence and Mortality Worldwide for 36 Cancers in 185 Countries. *CA Cancer J Clin* (2021) 71:209–49. doi: 10.3322/caac.21660
61. Shen DW, Pouliot LM, Hall MD, Gottesman MM. Cisplatin Resistance: A Cellular Self-Defense Mechanism Resulting From Multiple Epigenetic and Genetic Changes. *Pharmacol Rev* (2012) 64:706–21. doi: 10.1124/pr.111.005637
62. Liu Y, Zhai R, Hu S, Liu J. Circular RNA Circ-RNF121 Contributes to Cisplatin (DDP) Resistance of non-Small-Cell Lung Cancer Cells by

Regulating the miR-646/SOX4 Axis. *Anticancer Drugs* (2022) 33(1):e186–97. doi: 10.1097/cad.0000000000001184

63. Zhu X, Han J, Lan H, Lin Q, Wang Y, Sun X. A Novel Circular RNA Hsa_circRNA_103809/miR-377-3p/GOT1 Pathway Regulates Cisplatin-Resistance in non-Small Cell Lung Cancer (NSCLC). *BMC Cancer* (2020) 20:1190. doi: 10.1186/s12885-020-07680-w
64. Pang J, Ye L, Zhao D, Zhao D, Chen Q. Circular RNA PRMT5 Confers Cisplatin-Resistance *via* miR-4458/REV3L Axis in non-Small-Cell Lung Cancer. *Cell Biol Int* (2020) 44:2416–26. doi: 10.1002/cbin.11449
65. Ye Y, Zhao L, Li Q, Xi C, Li Y, Li Z. Circ_0007385 Served as Competing Endogenous RNA for miR-519d-3p to Suppress Malignant Behaviors and Cisplatin Resistance of non-Small Cell Lung Cancer Cells. *Thorac Cancer* (2020) 11:2196–208. doi: 10.1111/1759-7714.13527
66. Xu X, Tao R, Sun L, Ji X. Exosome-Transferred Hsa_Circ_0014235 Promotes DDP Chemoresistance and Deteriorates the Development of non-Small Cell Lung Cancer by Mediating the miR-520a-5p/CDK4 Pathway. *Cancer Cell Int* (2020) 20:552. doi: 10.1186/s12935-020-01642-9
67. Lu H, Xie X, Wang K, Chen Q, Cai S, Liu D, et al. Circular RNA Hsa_Circ_0096157 Contributes to Cisplatin Resistance by Proliferation, Cell Cycle Progression, and Suppressing Apoptosis of non-Small-Cell Lung Carcinoma Cells. *Mol Cell Biochem* (2020) 475:63–77. doi: 10.1007/s11010-020-03860-1
68. Zhong Y, Lin H, Li Q, Liu C, Shen J. CircRNA_100565 Contributes to Cisplatin Resistance of NSCLC Cells by Regulating Proliferation, Apoptosis and Autophagy *via* miR-337-3p/ADAM28 Axis. *Cancer biomark* (2021) 30:261–73. doi: 10.3233/cbm-201705
69. Feng N, Guo Z, Wu X, Tian Y, Li Y, Geng Y, et al. Circ_PIP5K1A Regulates Cisplatin Resistance and Malignant Progression in non-Small Cell Lung Cancer Cells and Xenograft Murine Model *via* Depending on miR-493-5p/ROCK1 Axis. *Respir Res* (2021) 22:248. doi: 10.1186/s12931-021-01840-7
70. Wu Z, Gong Q, Yu Y, Zhu J, Li W. Knockdown of Circ-ABCB10 Promotes Sensitivity of Lung Cancer Cells to Cisplatin *via* miR-556-3p/AK4 Axis. *BMC Pulm Med* (2020) 20:10. doi: 10.1186/s12890-019-1035-z
71. Chen C, Zhang M, Zhang Y. Circ_0000079 Decoys the RNA-Binding Protein FXR1 to Interrupt Formation of the FXR1/PRCKI Complex and Decline Their Mediated Cell Invasion and Drug Resistance in NSCLC. *Cell Transplant* (2020) 29:963689720961070. doi: 10.1177/0963689720961070
72. Liu Y, Li C, Liu H, Wang J. Circ_0001821 Knockdown Suppresses Growth, Metastasis, and TAX Resistance of non-Small-Cell Lung Cancer Cells by Regulating the miR-526b-5p/GRK5 Axis. *Pharmacol Res Perspect* (2021) 9:e00812. doi: 10.1002/prp2.812
73. Li J, Fan R, Xiao H. Circ_ZFR Contributes to the Paclitaxel Resistance and Progression of non-Small Cell Lung Cancer by Upregulating KPNA4 Through Sponging miR-195-5p. *Cancer Cell Int* (2021) 21:15. doi: 10.1186/s12935-020-01702-0
74. Guo C, Wang H, Jiang H, Qiao L, Wang X. Circ_0011292 Enhances Paclitaxel Resistance in Non-Small Cell Lung Cancer by Regulating miR-379-5p/TRIM65 Axis. *Cancer Biother Radiopharm* (2020) 33(1):e166–77. doi: 10.1089/cbr.2019.3546
75. Xu J, Ni L, Zhao F, Dai X, Tao J, Pan J, et al. Overexpression of Hsa_Circ_0002874 Promotes Resistance of non-Small Cell Lung Cancer to Paclitaxel by Modulating miR-1273f/MDM2/p53 Pathway. *Aging (Albany NY)* (2021) 13:5986–6009. doi: 10.18632/aging.202521
76. Li X, Feng Y, Yang B, Xiao T, Ren H, Yu X, et al. A Novel Circular RNA, Hsa_Circ_0030998 Suppresses Lung Cancer Tumorigenesis and Taxol Resistance by Sponging miR-558. *Mol Oncol* (2021) 15:2235–48. doi: 10.1002/1878-0261.12852
77. Li X, Yang B, Ren H, Xiao T, Zhang L, Li L, et al. Hsa_circ_0002483 Inhibited the Progression and Enhanced the Taxol Sensitivity of non-Small Cell Lung Cancer by Targeting miR-182-5p. *Cell Death Dis* (2019) 10:953. doi: 10.1038/s41419-019-2180-2
78. Du D, Cao X, Duan X, Zhang X. Blocking Circ_0014130 Suppressed Drug Resistance and Malignant Behaviors of Docetaxel Resistance-Acquired NSCLC Cells *via* Regulating miR-545-3p-YAP1 Axis. *Cytotechnology* (2021) 73:571–84. doi: 10.1007/s10616-021-00478-z
79. Zhang W, Song C, Ren X. Circ_0003998 Regulates the Progression and Docetaxel Sensitivity of DTX-Resistant Non-Small Cell Lung Cancer Cells by the miR-136-5p/CORO1C Axis. *Technol Cancer Res Treat* (2021) 20:1533033821990040. doi: 10.1177/1533033821990040
80. Song HM, Meng D, Wang JP, Zhang XY. circRNA Hsa_Circ_0005909 Predicts Poor Prognosis and Promotes the Growth, Metastasis, and Drug Resistance of Non-Small-Cell Lung Cancer *via* the miRNA-338-3p/SOX4 Pathway. *Dis Markers* (2021) 2021:8388512. doi: 10.1155/2021/8388512
81. Wang T, Liu Z, She Y, Deng J, Zhong Y, Zhao M, et al. A Novel Protein Encoded by Circask1 Ameliorates Gefitinib Resistance in Lung Adenocarcinoma by Competitively Activating ASK1-Dependent Apoptosis. *Cancer Lett* (2021) 520:321–31. doi: 10.1016/j.canlet.2021.08.007
82. Yang B, Teng F, Chang L, Wang J, Liu DL, Cui YS, et al. Tumor-Derived Exosomal circRNA_102481 Contributes to EGFR-TKIs Resistance *via* the miR-30a-5p/ROR1 Axis in non-Small Cell Lung Cancer. *Aging (Albany NY)* (2021) 13:13264–86. doi: 10.18632/aging.203011
83. Pegtel DM, Gould SJ. Exosomes. *Annu Rev Biochem* (2019) 88:487–514. doi: 10.1146/annurev-biochem-013118-111902
84. Xie H, Zheng R. Circ_0085495 Knockdown Reduces Adriamycin Resistance in Breast Cancer Through miR-873-5p/Integrin β1 Axis. *Anticancer Drugs* (2021) 33(1):e166–77. doi: 10.1097/cad.0000000000001174
85. Cui Y, Fan J, Shi W, Zhou Z. Circ_0001667 Knockdown Blocks Cancer Progression and Attenuates Adriamycin Resistance by Depleting NCOA3 via Releasing miR-4458 in Breast Cancer. *Drug Dev Res* (2021). doi: 10.1002/ddr.21845
86. Hao J, Du X, Lv F, Shi Q. Knockdown of Circ_0006528 Suppresses Cell Proliferation, Migration, Invasion, and Adriamycin Chemoresistance *via* Regulating the miR-1236-3p/CHD4 Axis in Breast Cancer. *J Surg Res* (2021) 260:104–15. doi: 10.1016/j.jss.2020.10.031
87. Dou D, Ren X, Han M, Xu X, Ge X, Gu Y, et al. CircUBE2D2 (Hsa_Circ_0005728) Promotes Cell Proliferation, Metastasis and Chemoresistance in Triple-Negative Breast Cancer by Regulating miR-512-3p/CDCA3 Axis. *Cancer Cell Int* (2020) 20:454. doi: 10.1186/s12935-020-01547-7
88. Wu X, Ren Y, Yao R, Zhou L, Fan R. Circular RNA Circ-MMP11 Contributes to Lapatinib Resistance of Breast Cancer Cells by Regulating the miR-153-3p/ANLN Axis. *Front Oncol* (2021) 11:639961. doi: 10.3389/fonc.2021.639961
89. Yao Y, Li X, Cheng L, Wu X, Wu B. Circular RNA FAT Atypical Cadherin 1 (Circfat1)/microRNA-525-5p/Spindle and Kinetochore-Associated Complex Subunit 1 (SKA1) Axis Regulates Oxaliplatin Resistance in Breast Cancer by Activating the Notch and Wnt Signaling Pathway. *Bioengineered* (2021) 12:4032–43. doi: 10.1080/21655979.2021.1951929
90. Zang H, Li Y, Zhang X, Huang G. Circ-RNF111 Contributes to Paclitaxel Resistance in Breast Cancer by Elevating E2F3 Expression. *Via miR-140-5p Thorac Cancer* (2020) 11:1891–903. doi: 10.1111/1759-7714.13475
91. Zhu M, Wang Y, Wang F, Li L, Qiu X. CircFBXL5 Promotes the 5-FU Resistance of Breast Cancer *via* Modulating miR-216b/HMGA2 Axis. *Cancer Cell Int* (2021) 21:384. doi: 10.1186/s12935-021-02088-3
92. Li H, Li Q, He S. Hsa_circ_0025202 Suppresses Cell Tumorigenesis and Tamoxifen Resistance *via* miR-197-3p/HIPK3 Axis in Breast Cancer. *World J Surg Oncol* (2021) 19:39. doi: 10.1186/s12957-021-02149-x
93. Zeng H, Wang L, Wang J, Chen T, Li H, Zhang K, et al. microRNA-129-5p Suppresses Adriamycin Resistance in Breast Cancer by Targeting SOX2. *Arch Biochem Biophys* (2018) 651:52–60. doi: 10.1016/j.abb.2018.05.018
94. Siegel RL, Miller KD, Jemal A. Cancer Statistics, 2020. *CA Cancer J Clin* (2020) 70:7–30. doi: 10.3322/caac.21590
95. Smyth EC, Nilsson M, Grabsch HI, van Grieken NC, Lordick F. Gastric Cancer. *Lancet* (2020) 396:635–48. doi: 10.1016/s0140-6736(20)31288-5
96. Yao W, Guo P, Mu Q, Wang Y. Exosome-Derived Circ-PVT1 Contributes to Cisplatin Resistance by Regulating Autophagy, Invasion, and Apoptosis *Via* miR-30a-5p/YAP1 Axis in Gastric Cancer Cells. *Cancer Biother Radiopharm* (2021) 36:347–59. doi: 10.1089/cbr.2020.3578
97. Sun Y, Ma J, Lin J, Sun D, Song P, Shi L, et al. Circular RNA Circ_ASAP2 Regulates Drug Sensitivity and Functional Behaviors of Cisplatin-Resistant Gastric Cancer Cells by the miR-330-3p/NT5E Axis. *Anticancer Drugs* (2021) 32(9):950–61. doi: 10.1097/cad.0000000000001087
98. Xue M, Li G, Fang X, Wang L, Jin Y, Zhou Q. Hsa_Circ_0081143 Promotes Cisplatin Resistance in Gastric Cancer by Targeting miR-646/CDK6 Pathway. *Cancer Cell Int* (2019) 19:25. doi: 10.1186/s12935-019-0737-x

99. Liu Y, Xu J, Jiang M, Ni L, Ling Y. CircRNA DONSON Contributes to Cisplatin Resistance in Gastric Cancer Cells by Regulating miR-802/BMI1 Axis. *Cancer Cell Int* (2020) 20:261. doi: 10.1186/s12935-020-01358-w
100. Zhang J, Zha W, Qian C, Ding A, Mao Z. Circular RNA Circ_0001017 Sensitizes Cisplatin-Resistant Gastric Cancer Cells to Chemotherapy by the miR-543/PHLPP2 Axis. *Biochem Genet* (2021). doi: 10.1007/s10528-021-10110-6
101. Peng L, Sang H, Wei S, Li Y, Jin D, Zhu X, et al. Circcul2 Regulates Gastric Cancer Malignant Transformation and Cisplatin Resistance by Modulating Autophagy Activation *via* miR-142-3p/ROCK2. *Mol Cancer* (2020) 19:156. doi: 10.1186/s12943-020-01270-x
102. Zhong Y, Wang D, Ding Y, Tian G, Jiang B. Circular RNA Circ_0032821 Contributes to Oxaliplatin (OXA) Resistance of Gastric Cancer Cells by Regulating SOX9 *via* miR-515-5p. *Biotechnol Lett* (2021) 43:339–51. doi: 10.1007/s10529-020-03036-3
103. Isakoff MS, Bielack SS, Meltzer P, Gorlick R. Osteosarcoma: Current Treatment and a Collaborative Pathway to Success. *J Clin Oncol* (2015) 33:3029–35. doi: 10.1200/jco.2014.59.4895
104. Wei W, Ji L, Duan W, Zhu J. Circular RNA Circ_0081001 Knockdown Enhances Methotrexate Sensitivity in Osteosarcoma Cells by Regulating miR-494-3p/TGM2 Axis. *J Orthop Surg Res* (2021) 16:50. doi: 10.1186/s13018-020-02169-5
105. Li X, Liu Y, Zhang X, Shen J, Xu R, Liu Y, et al. Circular RNA Hsa_Circ_0000073 Contributes to Osteosarcoma Cell Proliferation, Migration, Invasion and Methotrexate Resistance by Sponging miR-145-5p and miR-151-3p and Upregulating NRAS. *Aging (Albany NY)* (2020) 12:14157–73. doi: 10.18632/aging.103423
106. Bai Y, Li Y, Bai J, Zhang Y. Hsa_circ_0004674 Promotes Osteosarcoma Doxorubicin Resistance by Regulating the miR-342-3p/FBN1 Axis. *J Orthop Surg Res* (2021) 16:510. doi: 10.1186/s13018-021-02631-y
107. Guan H, Xu H, Chen J, Wu W, Chen D, Chen Y, et al. Circ_0001721 Enhances Doxorubicin Resistance and Promotes Tumorigenesis in Osteosarcoma Through miR-758/TCF4 Axis. *Cancer Cell Int* (2021) 21:336. doi: 10.1186/s12935-021-02016-5
108. Wei W, Ji L, Duan W, Zhu J. CircSAMD4A Contributes to Cell Doxorubicin Resistance in Osteosarcoma by Regulating the miR-218-5p/KLF8 Axis. *Open Life Sci* (2020) 15:848–59. doi: 10.1515/biol-2020-0079
109. Xie C, Liang G, Xu Y, Lin E. Circular RNA Hsa_Circ_0003496 Contributes to Tumorigenesis and Chemoresistance in Osteosarcoma Through Targeting (microRNA) miR-370/Krüppel-Like Factor 12 Axis. *Cancer Manag Res* (2020) 12:8229–40. doi: 10.2147/cmar.S253969
110. Pan Y, Lin Y, Mi C. Cisplatin-Resistant Osteosarcoma Cell-Derived Exosomes Confer Cisplatin Resistance to Recipient Cells in an Exosomal Circ_103801-Dependent Manner. *Cell Biol Int* (2021) 45:858–68. doi: 10.1002/cbin.11532
111. Zhang J, Ma X, Zhou R, Zhou Y. TRPS1 and YAP1 Regulate Cell Proliferation and Drug Resistance of Osteosarcoma *via* Competitively Binding to the Target of Circtada2a - miR-129-5p. *Onco Targets Ther* (2020) 13:12397–407. doi: 10.2147/ott.S276953
112. Gusyatiner O, Hegi ME. Glioma Epigenetics: From Subclassification to Novel Treatment Options. *Semin Cancer Biol* (2018) 51:50–8. doi: 10.1016/j.semcancer.2017.11.010
113. Si J, Li W, Li X, Cao L, Chen Z, Jiang Z. Heparanase Confers Temozolomide Resistance by Regulation of Exosome Secretion and Circular RNA Composition in Glioma. *Cancer Sci* (2021) 112(9):3491–06. doi: 10.1111/cas.14984
114. Ding C, Yi X, Chen X, Wu Z, You H, Chen X, et al. Warburg Effect-Promoted Exosomal Circ_0072083 Releasing Up-Regulates NANGO Expression Through Multiple Pathways and Enhances Temozolomide Resistance in Glioma. *J Exp Clin Cancer Res* (2021) 40:164. doi: 10.1186/s13046-021-01942-6
115. Li H, Liu Q, Chen Z, Wu M, Zhang C, Su J, et al. Hsa_circ_0110757 Upregulates ITGA1 to Facilitate Temozolomide Resistance in Glioma by Suppressing hsa-miR-1298-5p. *Cell Death Dis* (2021) 12:252. doi: 10.1038/s41419-021-03533-x
116. Deng Y, Zhu H, Xiao L, Liu C, Meng X. Circ_0005198 Enhances Temozolomide Resistance of Glioma Cells Through miR-198/TRIM14 Axis. *Aging (Albany NY)* (2020) 13:2198–211. doi: 10.18632/aging.202234
117. Li W, Ma Q, Liu Q, Yan P, Wang X, Jia X. Circ-VPS18 Knockdown Enhances TMZ Sensitivity and Inhibits Glioma Progression by MiR-370/RUNX1 Axis. *J Mol Neurosci* (2021) 71:1234–44. doi: 10.1007/s12031-020-01749-8
118. Hua L, Huang L, Zhang X, Feng H. Downregulation of Hsa_Circ_0000936 Sensitizes Resistant Glioma Cells to Temozolomide by Sponging miR-1294. *J Biosci* (2020) 45:101. doi: 10.1007/s12038-020-00072-z
119. Yin H, Cui X. Knockdown of Circhipk3 Facilitates Temozolomide Sensitivity in Glioma by Regulating Cellular Behaviors Through miR-524-5p/KIF2A-Mediated PI3K/AKT Pathway. *Cancer Biother Radiopharm* (2020) 36(7):556–67. doi: 10.1089/cbr.2020.3575
120. Hua L, Huang L, Zhang X, Feng H, Shen B. Knockdown of Circular RNA CEP128 Suppresses Proliferation and Improves Cytotoxic Efficacy of Temozolomide in Glioma Cells by Regulating miR-145-5p. *Neuroreport* (2019) 30:1231–8. doi: 10.1097/wnr.0000000000001326
121. Wei Y, Lu C, Zhou P, Zhao L, Lyu X, Yin J, et al. EIF4A3-Induced Circular RNA ASAP1 Promotes Tumorigenesis and Temozolomide Resistance of Glioblastoma *via* NRAS/MEK1/ERK1-2 Signaling. *Neuro Oncol* (2021) 23:611–24. doi: 10.1093/neuonc/noaa214
122. Di L, Zhao X, Ding J. Knockdown of Circ_0008344 Contributes to Radiosensitization in Glioma *via* miR-433-3p/RNF2 Axis. *J Biosci* (2021) 46:101. doi: 10.1007/s12038-021-00198-8
123. Han C, Wang S, Wang H, Zhang J. Exosomal Circ-HIPK3 Facilitates Tumor Progression and Temozolomide Resistance by Regulating miR-421/ZIC5 Axis in Glioma. *Cancer Biother Radiopharm* (2020) 36(7):537–48. doi: 10.1089/cbr.2019.3492
124. Wang JY, Lu AQ, Chen LJ. LncRNAs in Ovarian Cancer. *Clin Chim Acta* (2019) 490:17–27. doi: 10.1016/j.cca.2018.12.013
125. Luo Y, Gui R. Circulating Exosomal Circfoxp1 Confers Cisplatin Resistance in Epithelial Ovarian Cancer Cells. *J Gynecol Oncol* (2020) 31:e75. doi: 10.3802/jgo.2020.31.e75
126. Zhao Z, Ji M, Wang Q, He N, Li Y. Circular RNA Cdr1as Upregulates SCAI to Suppress Cisplatin Resistance in Ovarian Cancer *via* miR-1270 Suppression. *Mol Ther Nucleic Acids* (2019) 18:24–33. doi: 10.1016/j.omtn.2019.07.012
127. Chen YY, Tai YC. Hsa_circ_0006404 and Hsa_Circ_0000735 Regulated Ovarian Cancer Response to Docetaxel Treatment *via* Regulating P-GP Expression. *Biochem Genet* (2021). doi: 10.1007/s10528-021-10080-9
128. Wei S, Qi L, Wang L. Overexpression of Circ_CELSR1 Facilitates Paclitaxel Resistance of Ovarian Cancer by Regulating miR-149-5p/SIK2 Axis. *Anticancer Drugs* (2021) 32:496–507. doi: 10.1097/cad.0000000000001058
129. Zhang S, Cheng J, Quan C, Wen H, Feng Z, Hu Q, et al. Circcelsr1 (Hsa_Circ_0063809) Contributes to Paclitaxel Resistance of Ovarian Cancer Cells by Regulating FOXR2 Expression. *Via miR-1252 Mol Ther Nucleic Acids* (2020) 19:718–30. doi: 10.1016/j.omtn.2019.12.005
130. Xia B, Zhao Z, Wu Y, Wang Y, Zhao Y, Wang J. Circular RNA Circtnpo3 Regulates Paclitaxel Resistance of Ovarian Cancer Cells by miR-1299/NEK2 Signaling Pathway. *Mol Ther Nucleic Acids* (2020) 21:780–91. doi: 10.1016/j.omtn.2020.06.002
131. Zhao K, Cheng X, Ye Z, Li Y, Peng W, Wu Y, et al. Exosome-Mediated Transfer of Circ_0000338 Enhances 5-Fluorouracil Resistance in Colorectal Cancer Through Regulating MicroRNA 217 (miR-217) and miR-485-3p. *Mol Cell Biol* (2021) 41(5):e00517–20. doi: 10.1128/mcb.00517-20
132. Xu Y, Qiu A, Peng F, Tan X, Wang J, Gong X. Exosomal Transfer of Circular RNA FBXW7 Ameliorates the Chemoresistance to Oxaliplatin in Colorectal Cancer by Sponging miR-18b-5p. *Neoplasma* (2021) 68:108–18. doi: 10.4149/neo_2020_200417N414
133. Wang X, Zhang H, Yang H, Bai M, Ning T, Deng T, et al. Exosome-Delivered circRNA Promotes Glycolysis to Induce Chemoresistance Through the miR-122-PKM2 Axis in Colorectal Cancer. *Mol Oncol* (2020) 14:539–55. doi: 10.1002/1878-0261.12629
134. Sun Y, Cao Z, Shan J, Gao Y, Liu X, Ma D, et al. Hsa_circ_0020095 Promotes Oncogenesis and Cisplatin Resistance in Colon Cancer by Sponging miR-487a-3p and Modulating Sox9. *Front Cell Dev Biol* (2020) 8:604869. doi: 10.3389/fcell.2020.604869
135. Xi L, Liu Q, Zhang W, Luo L, Song J, Liu R, et al. Circular RNA Circcspp1 Knockdown Attenuates Doxorubicin Resistance and Suppresses Tumor Progression of Colorectal Cancer *via* miR-944/FZD7 Axis. *Cancer Cell Int* (2021) 21:153. doi: 10.1186/s12935-021-01855-6

136. Li Y, Zhang Y, Zhang S, Huang D, Li B, Liang G, et al. circRNA Circarnt2 Suppressed the Sensitivity of Hepatocellular Carcinoma Cells to Cisplatin by Targeting the miR-155-5p/PDK1 Axis. *Mol Ther Nucleic Acids* (2021) 23:244–54. doi: 10.1016/j.omtn.2020.08.037
137. Guan Y, Zhang Y, Hao L, Nie Z. CircRNA_102272 Promotes Cisplatin-Resistance in Hepatocellular Carcinoma by Decreasing MiR-326 Targeting of RUNX2. *Cancer Manag Res* (2020) 12:12527–34. doi: 10.2147/cmar.S258230
138. Xu J, Ji L, Liang Y, Wan Z, Zheng W, Song X, et al. CircRNA-SORE Mediates Sorafenib Resistance in Hepatocellular Carcinoma by Stabilizing YBX1. *Signal Transduct Target Ther* (2020) 5:298. doi: 10.1038/s41392-020-00375-5
139. Xu J, Wan Z, Tang M, Lin Z, Jiang S, Ji L, et al. N(6)-Methyladenosine-Modified CircRNA-SORE Sustains Sorafenib Resistance in Hepatocellular Carcinoma by Regulating Beta-Catenin Signaling. *Mol Cancer* (2020) 19:163. doi: 10.1186/s12943-020-01281-8
140. Shao F, Huang M, Meng F, Huang Q. Circular RNA Signature Predicts Gemcitabine Resistance of Pancreatic Ductal Adenocarcinoma. *Front Pharmacol* (2018) 9:584. doi: 10.3389/fphar.2018.00584
141. Zang R, Qiu X, Song Y, Wang Y. Exosomes Mediated Transfer of Circ_0000337 Contributes to Cisplatin (CDDP) Resistance of Esophageal Cancer by Regulating JAK2 *via* miR-377-3p. *Front Cell Dev Biol* (2021) 9:673237. doi: 10.3389/fcell.2021.673237
142. Qu F, Wang L, Wang C, Yu L, Zhao K, Zhong H. Circular RNA Circ_0006168 Enhances Taxol Resistance in Esophageal Squamous Cell Carcinoma by Regulating miR-194-5p/JMJD1C Axis. *Cancer Cell Int* (2021) 21:273. doi: 10.1186/s12935-021-01984-y
143. Chen J, Sun Y, Ou Z, Yeh S, Huang CP, You B, et al. Androgen Receptor-Regulated circFNTA Activates KRAS Signaling to Promote Bladder Cancer Invasion. *EMBO Rep* (2020) 21:e48467. doi: 10.15252/embr.201948467
144. Su Y, Yang W, Jiang N, Shi J, Chen L, Zhong G, et al. Hypoxia-Elevated Circelp3 Contributes to Bladder Cancer Progression and Cisplatin Resistance. *Int J Biol Sci* (2019) 15:441–52. doi: 10.7150/ijbs.26826
145. Wei W, Sun J, Zhang H, Xiao X, Huang C, Wang L, et al. Circ0008399 Interaction With WTAP Promotes Assembly and Activity of the M6a Methyltransferase Complex and Promotes Cisplatin Resistance in Bladder Cancer. *Cancer Res* (2021) 81(24):6142–56. doi: 10.1158/0008-5472.Can-21-1518
146. Chi BJ, Zhao DM, Liu L, Yin XZ, Wang FF, Bi S, et al. Downregulation of Hsa_Circ_0000285 Serves as a Prognostic Biomarker for Bladder Cancer and is Involved in Cisplatin Resistance. *Neoplasma* (2019) 66:197–202. doi: 10.4149/neo_2018_180318N185
147. Yan L, Liu G, Cao H, Zhang H, Shao F. Hsa_circ_0035483 Sponges hsa-miR-335 to Promote the Gemcitabine-Resistance of Human Renal Cancer Cells by Autophagy Regulation. *Biochem Biophys Res Commun* (2019) 519:172–8. doi: 10.1016/j.bbrc.2019.08.093
148. Huang XY, Zhang PF, Wei CY, Peng R, Lu JC, Gao C, et al. Circular RNA circMET Drives Immunosuppression and Anti-PD1 Therapy Resistance in Hepatocellular Carcinoma *via* the miR-30-5p/Snail/DPP4 Axis. *Mol Cancer* (2020) 19:92. doi: 10.1186/s12943-020-01213-6
149. Yao X, Mao Y, Wu D, Zhu Y, Lu J, Huang Y, et al. Exosomal Circ_0030167 Derived From BM-MSCs Inhibits the Invasion, Migration, Proliferation and Stemness of Pancreatic Cancer Cells by Sponging miR-338-5p and Targeting the Wif1/Wnt8/β-Catenin Axis. *Cancer Lett* (2021) 512:38–50. doi: 10.1016/j.canlet.2021.04.030
150. Su H, Lin F, Deng X, Shen L, Fang Y, Fei Z, et al. Profiling and Bioinformatics Analyses Reveal Differential Circular RNA Expression in Radioresistant Esophageal Cancer Cells. *J Transl Med* (2016) 14:225. doi: 10.1186/s12967-016-0977-7

**Conflict of Interest:** The authors declare that the research was conducted in the absence of any commercial or financial relationships that could be construed as a potential conflict of interest.

**Publisher's Note:** All claims expressed in this article are solely those of the authors and do not necessarily represent those of their affiliated organizations, or those of the publisher, the editors and the reviewers. Any product that may be evaluated in this article, or claim that may be made by its manufacturer, is not guaranteed or endorsed by the publisher.

frontiers in Pharmacology

ORIGINAL RESEARCH
published: 17 January 2022
doi: 10.3389/fphar.2021.798837

# Anlotinib Reverses Multidrug Resistance (MDR) in Osteosarcoma by Inhibiting P-Glycoprotein (PGP1) Function In Vitro and In Vivo

*Gangyang Wang[1,2†], Lingling Cao[3†], Yafei Jiang[1,2†], Tao Zhang[1,2], Hongsheng Wang[1,2], Zhuoying Wang[1,2], Jing Xu[1,2], Min Mao[1,2], Yingqi Hua[1,2], Zhengdong Cai[1,2], Xiaojun Ma[1,2*], Shuo Hu[1,2*] and Chenghao Zhou[1,2*]*

[1]Department of Orthopaedics, Shanghai General Hospital, Shanghai Jiao Tong University School of Medicine, Shanghai, China, [2]Shanghai Bone Tumor Institute, Shanghai, China, [3]Department of Rehabilitation, Shanghai Fifth Rehabilitation Hospital, Shanghai, China

OPEN ACCESS

**Edited by:**
Qingbin Cui,
University of Toledo, United States

**Reviewed by:**
Noor Ayad Hussein,
Stanford University, United States
Maitane Asensio,
University of Salamanca, Spain

***Correspondence:**
Xiaojun Ma
21827287@qq.com
Shuo Hu
hushuo10@163.com
Chenghao Zhou
fthree@yeah.net

[†]These authors have contributed equally to this work

**Specialty section:**
This article was submitted to Pharmacology of Anti-Cancer Drugs, a section of the journal Frontiers in Pharmacology

**Received:** 20 October 2021
**Accepted:** 28 December 2021
**Published:** 17 January 2022

**Citation:**
Wang G, Cao L, Jiang Y, Zhang T, Wang H, Wang Z, Xu J, Mao M, Hua Y, Cai Z, Ma X, Hu S and Zhou C (2022) Anlotinib Reverses Multidrug Resistance (MDR) in Osteosarcoma by Inhibiting P-Glycoprotein (PGP1) Function In Vitro and In Vivo. Front. Pharmacol. 12:798837. doi: 10.3389/fphar.2021.798837

Overexpression of the multidrug resistance (MDR)-related protein P-glycoprotein (PGP1), which actively extrudes chemotherapeutic agents from cells and significantly decreases the efficacy of chemotherapy, is viewed as a major obstacle in osteosarcoma chemotherapy. Anlotinib, a novel tyrosine kinase inhibitor (TKI), has good anti-tumor effects in a variety of solid tumors. However, there are few studies on the mechanism of anlotinib reversing chemotherapy resistance in osteosarcoma. In this study, cellular assays were performed *in vitro* and *in vivo* to evaluate the MDR reversal effects of anlotinib on multidrug-resistant osteosarcoma cell lines. Drug efflux and intracellular drug accumulation were measured by flow cytometry. The vanadate-sensitive ATPase activity of PGP1 was measured in the presence of a range of anlotinib concentrations. The protein expression level of ABCB1 was detected by Western blotting and immunofluorescence analysis. Our results showed that anlotinib significantly increased the sensitivity of KHOSR2 and U2OSR2 cells (which overexpress PGP1) to chemotherapeutic agents *in vitro* and in a KHOSR2 xenograft nude mouse model *in vivo*. Mechanistically, anlotinib increases the intracellular accumulation of PGP1 substrates by inhibiting the efflux function of PGP1 in multidrug-resistant cell lines. Furthermore, anlotinib stimulated the ATPase activity of PGP1 but affected neither the protein expression level nor the localization of PGP1. In animal studies, anlotinib in combination with doxorubicin (DOX) significantly decreased the tumor growth rate and the tumor size in the KHOSR2 xenograft nude mouse model. Overall, our findings suggest that anlotinib may be useful for circumventing MDR to other conventional antineoplastic drugs.

**Keywords: anlotinib, osteosarcoma, multidrug resistance, ATP-binding cassette (ABC) transporter, P-glycoprotein**

## INTRODUCTION

Osteosarcoma is one of the most common and most aggressive primary malignant bone tumors in children and adolescents, and the incidence of osteosarcoma has a second peak in adults over the age of 65 years (Mirabello et al., 2009). The standard treatment for osteosarcoma currently relies on conservative surgery and neoadjuvant chemotherapy, which has improved the survival rate from less

than 20% prior to the 1970s to 65–75% today (Jaffe, 2009; Chen et al., 2017). Unfortunately, the cure rate has not increased over the past 25–30 years. A three-drug combination regimen is routinely selected for systemic chemotherapy of osteosarcoma in clinical practice (Gill and Gorlick, 2021). Through nearly three decades of clinical trial testing, the multiple combinations of methotrexate, doxorubicin, epirubicin, ifosfamide and etoposide before and after definitive surgical resection of osteosarcoma has achieved consistent efficacy outcomes, with an overall event-free survival (EFS) rate of 12% at 4 months (Meyers et al., 2008; Ritter and Bielack, 2010; Gill and Gorlick, 2021). One of the fundamental obstacles to the successful treatment of osteosarcoma is the development of multidrug resistance (MDR), which causes tumor cells to become resistant to structurally and mechanistically distinct classes of chemotherapeutic agents (Vasiliou et al., 2009; Yang et al., 2017).

Several mechanisms have been shown to promote anticancer drug resistance in osteosarcoma. One important molecular basis for MDR is overexpression of plasma membrane P-glycoprotein (PGP1), which actively extrudes a variety of chemotherapeutic agents from cancer cells, thereby significantly decreasing the efficacy and increasing the side effects of chemotherapeutic drugs (Gillet et al., 2007). Previous studies have shown that PGP1 is overexpressed in various multidrug-resistant osteosarcoma cell lines and drug-resistant osteosarcoma tissues (Yang et al., 2014; Ye et al., 2016; Duan et al., 2017; Lu et al., 2017). Hence, developing new chemotherapeutic agents to inhibit the efflux function and/or downregulate the expression of PGP1 may make it possible to overcome MDR and chemotherapy resistance.

Most previous investigations have aimed to reverse and prevent MDR by targeting PGP1, but success has been limited due to unacceptable toxicity and problematic pharmacokinetic interactions (Liu, 2009; Xue et al., 2016). Tyrosine kinase inhibitors (TKIs) are a class of pharmaceutical drugs that inhibit tyrosine kinases (Boutayeb et al., 2012). The antitumor mechanism of TKIs is believed to inhibit functions of ATP for binding to the ATP site of the catalytic domain of several oncogenic tyrosine kinases (Azzariti et al., 2010). Several TKIs, including imatinib, nilotinib, gefitinib, apatinib, and afatinib, have been reported to significantly attenuate or reverse MDR mediated by ATP-binding cassette (ABC) transporters (Dai et al., 2008; Mi et al., 2010; Ma et al., 2014; Wang et al., 2014). Anlotinib, a novel antitumor drug, is a receptor TKI with multiple targets, notably vascular endothelial growth factor receptor type 2 (VEGFR2), VEGFR3, platelet-derived growth factor b (PDGFRβ), and stem cell factor receptor (c-Kit) (Zhong et al., 2018a; Lin et al., 2018). The antitumor effect of anlotinib has been reported in many preclinical and clinical trials (Sun et al., 2016; Han et al., 2018a; Han et al., 2018b; Li, 2021). Because it acts at the ATP-binding site of the tyrosine kinase domains of VEGFR, anlotinib may inhibit the functions of ABC transporters by binding to their ATP-binding sites; this mechanism is similar to the mechanism by which several of the TKIs mentioned above operate to reverse MDR. In the current study, we determined that anlotinib significantly reverses PGP1-mediated MDR in human

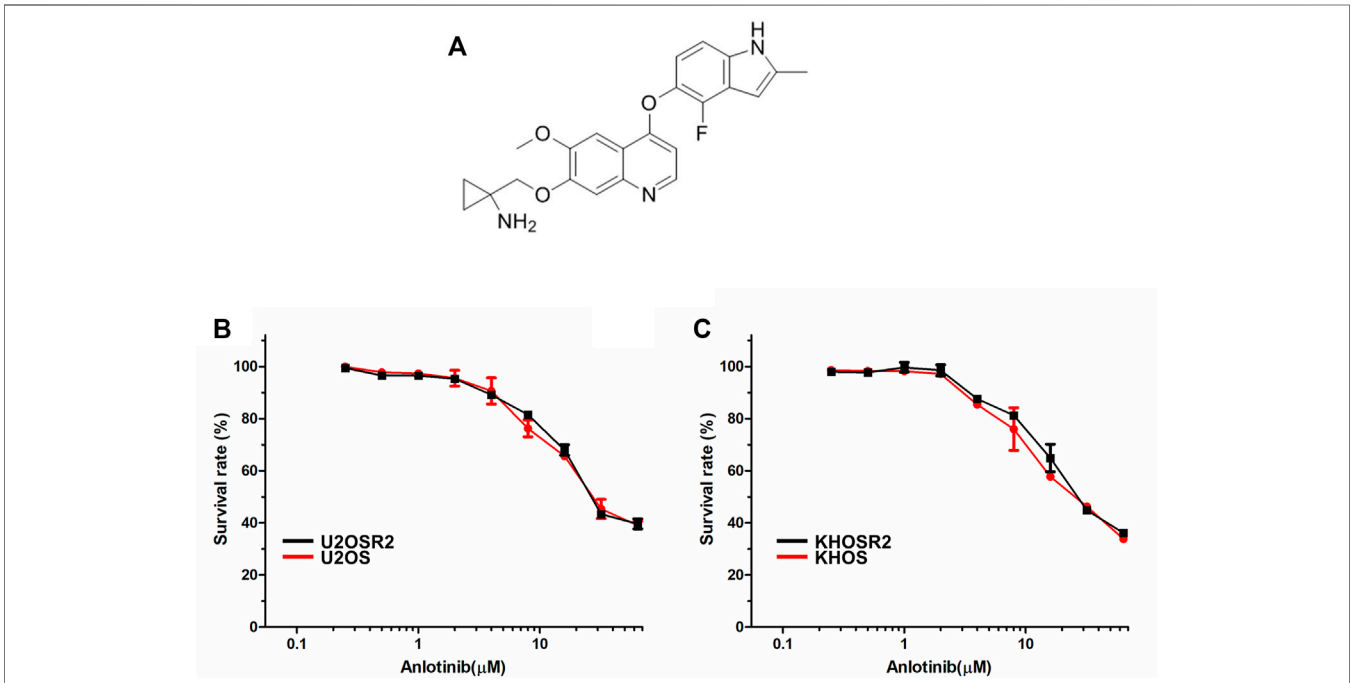


**FIGURE 1 |** The structure of anlotinib and the cytotoxicity of anlotinib in drug-resistant osteosarcoma cell lines and their drug-sensitive parental cell lines. **(A)**. The structure of anlotinib. Osteosarcoma drug-resistant and their drug-sensitive cell lines were treated with anlotinib at the indicated concentrations for 48 h. Cell viability was measured by CCK8 **(B)**. Cytotoxicity curves for the U2OSR2 and U2OS cell lines incubated with anlotinib alone. **(C)**. Cytotoxicity curves for the KHOSR2 and KHOS cell lines incubated with anlotinib alone. The data were shown as the mean ± SD from three independent experiments.

**TABLE 1 |** Ability of anlotinib to reverse drug resistance in multidrug-resistant osteosarcoma cell lines.

**Effect of anlotinib on reversing PGP1-mediated MDR in osteosarcoma cells**

| Compounds | IC50 ± SD (μM; fold-reversal) | | | |
|---|---|---|---|---|
| | U2OS | | U2OSR2 | |
| Doxorubicin | 0.1648 ± 0.0050 | (1.00) | 4.694 ± 0.1368 | (1.00) |
| plus anlotinib 0.1 μM | 0.1634 ± 0.0084 | (1.01) | 2.095 ± 0.0862 | (2.24) |
| plus anlotinib 0.2 μM | 0.1602 ± 0.0047 | (1.03) | 0.6648 ± 0.0519 | (7.06) |
| plus anlotinib 0.4 μM | 0.1683 ± 0.0088 | (0.98) | 0.2583 ± 0.0582 | (18.17) |
| plus verapamil 10 μM | 0.1509 ± 0.0067 | (1.09) | 0.1563 ± 0.0622 | (30.03) |
| Paclitaxel | 0.0140 ± 0.0019 | (1.00) | 0.1220 ± 0.0524 | (1.00) |
| plus anlotinib 0.1 μM | 0.0151 ± 0.0008 | (0.93) | 0.0646 ± 0.0188 | (1.89) |
| plus anlotinib 0.2 μM | 0.0128 ± 0.0016 | (1.09) | 0.0407 ± 0.0083 | (2.99) |
| plus anlotinib 0.4 μM | 0.0123 ± 0.0009 | (1.13) | 0.0298 ± 0.0052 | (4.09) |
| plus verapamil 10 μM | 0.0092 ± 0.0071 | (1.52) | 0.0139 ± 0.0051 | (8.78) |
| Vincristine | 0.0815 ± 0.0036 | (1.00) | 0.7484 ± 0.0501 | (1.00) |
| plus anlotinib 0.1 μM | 0.0782 ± 0.0088 | (1.04) | 0.3327 ± 0.0476 | (2.24) |
| plus anlotinib 0.2 μM | 0.0693 ± 0.0093 | (1.18) | 0.1716 ± 0.0499 | (4.36) |
| plus anlotinib 0.4 μM | 0.0639 ± 0.0087 | (1.28) | 0.1169 ± 0.0515 | (6.40) |
| plus verapamil 10 μM | 0.0686 ± 0.0063 | (1.18) | 0.0843 ± 0.0143 | (8.87) |
| | KHOS | | KHOSR2 | |
| Doxorubicin | 0.2496 ± 0.0690 | (1.00) | 4.795 ± 0.1891 | (1.00) |
| plus anlotinib 0.1 μM | 0.2170 ± 0.0751 | (1.15) | 2.185 ± 0.0828 | (2.19) |
| plus anlotinib 0.2 μM | 0.2372 ± 0.0604 | (1.05) | 0.7595 ± 0.0527 | (6.31) |
| plus anlotinib 0.4 μM | 0.2217 ± 0.012 | (1.13) | 0.3148 ± 0.0430 | (15.23) |
| plus verapamil 10 μM | 0.2322 ± 0.0431 | (1.07) | 0.2204 ± 0.0412 | (21.76) |
| Paclitaxel | 0.0213 ± 0.0067 | (1.00) | 0.6503 ± 0.0539 | (1.00) |
| plus anlotinib 0.1 μM | 0.0193 ± 0.0071 | (1.10) | 0.3071 ± 0.0693 | (2.12) |
| plus anlotinib 0.2 μM | 0.0175 ± 0.0045 | (1.21) | 0.1500 ± 0.0094 | (4.34) |
| plus anlotinib 0.4 μM | 0.0182 ± 0.0064 | (1.17) | 0.0583 ± 0.0082 | (11.15) |
| plus verapamil 10 μM | 0.01594 ± 0.0038 | (1.33) | 0.0174 ± 0.0035 | (37.37) |
| Vincristine | 0.0748 ± 0.0069 | (1.00) | 1.3440 ± 0.0498 | (1.00) |
| plus anlotinib 0.1 μM | 0.0683 ± 0.0084 | (1.09) | 0.6739 ± 0.0387 | (1.99) |
| plus anlotinib 0.2 μM | 0.0663 ± 0.0071 | (1.29) | 0.3608 ± 0.0483 | (3.72) |
| plus anlotinib 0.4 μM | 0.0680 ± 0.0085 | (1.10) | 0.1466 ± 0.0091 | (9.16) |
| plus verapamil 10 μM | 0.0675 ± 0.0038 | (1.11) | 0.0684 ± 0.0043 | (19.65) |

osteosarcoma cells *in vitro* and *in vivo*. Anlotinib, in combination with conventional antineoplastic drugs such as doxorubicin, could be a novel and effective therapy for the treatment of osteosarcoma patients.

# MATERIALS AND METHODS

## Reagents

Anlotinib was obtained from Chia Tai Tianqing Pharmaceutical Group Co., Ltd. (Nanjing, China). All cell culture reagents were purchased from Invitrogen Life Technologies (Carlsbad, CA, United States). Antibodies specific for P-gp/ABCB1 and GAPDH were purchased from Cell Signaling Technology, Inc. (Danvers, MA, United States). Dimethyl sulfoxide (DMSO), DOX, paclitaxel, vincristine, rhodamine 123 (Rho-123), and other chemicals were purchased from Sigma-Aldrich (St. Louis, MO, United States).

## Cell Lines and Cell Culture

The multidrug-resistant human osteosarcoma cell lines KHOSR2 and U2OSR2 (established by DOX selection) and their respective drug-sensitive parental cell lines, KHOS and U2OS, were kindly provided by Dr. Zhenfeng Duan (University of California, Los Angeles, UCLA, CA, United States). These multidrug-resistant osteosarcoma cell lines have been extensively characterized in previous studies as having a stable MDR phenotype (Ye et al., 2016; Duan et al., 2017). Compared to the drug-sensitive cells (KHOS and U2OS), the drug-resistant cells (KHOSR2 and U2OSR2) overexpressed PGP1 (also known as ABCB1); furthermore, the expression of MRP1 (also known as ABCC1) and BCRP (also known as ABCG2) was undetectable in the drug-resistant cell lines (Duan et al., 2009a; Duan et al., 2009b). All cell lines were cultured in DMEM containing 10% FBS and 1% penicillin/streptomycin at 37°C in 5% $CO_2$. All drug-resistant cell lines were periodically cultured with the affected drug to maintain their drug resistance characteristics. All cells were grown in drug-free culture medium for >2 weeks before being used for assays.

## Cell Cytotoxicity Assay

A cell counting kit-8 (CCK8, Dojindo, Kumamoto, Japan) assay was used to assess cell sensitivity to chemotherapeutic drugs, as described previously (Wang et al., 2017). Briefly, cell suspensions ($3\times10^4$/ml) were seeded into 96-well plates, incubated overnight and treated with increasing

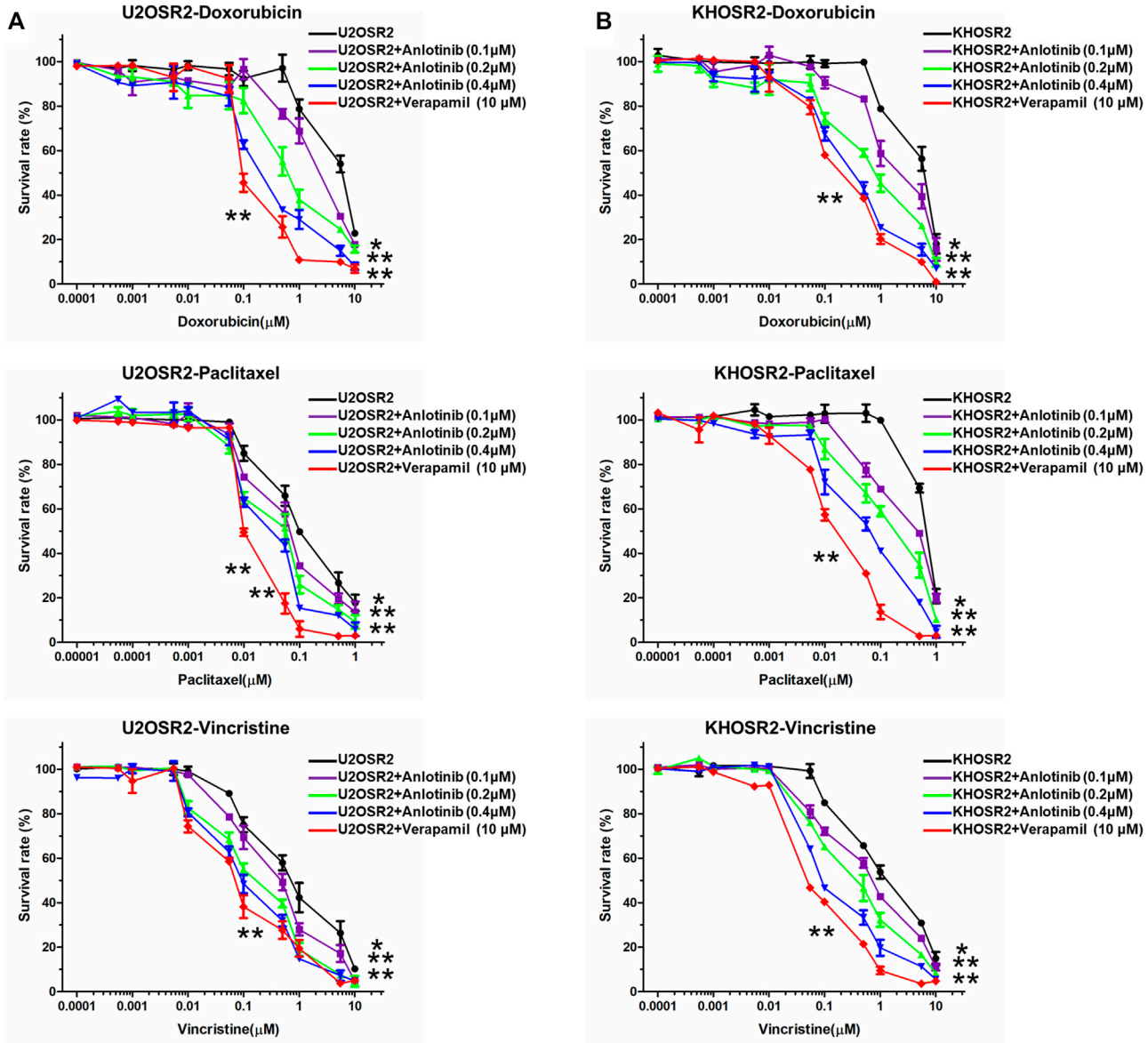


**FIGURE 2 |** Effect of anlotinib on the reversal of drug resistance in multidrug-resistant osteosarcoma cell lines. Cells were treated with chemotherapeutic drugs and anlotinib at the indicated concentrations. The relative sensitivity of each line to chemotherapeutic drugs was determined by a CCK8 assay 48 h after treatment. **(A)**. Reversal of drug resistance by anlotinib in U2OSR2 cells. **(B)**. Reversal of drug resistance by anlotinib in KHOSR2 cells. Data represent the mean ± SD of at least three independent experiments (*$p < 0.05$; **$p < 0.01$).

concentrations of anlotinib alone, chemotherapy drugs alone or a combination of both types of drugs. After incubation for 24 or 48 h, the cells were washed twice with PBS and incubated with CCK8 working solution for 2 h at 37°C according to the manufacturer's protocol. The absorption was measured at 490 nm by an iMark microplate reader (Molecular Devices, Sunnyvale, United States). The IC50 values were calculated using a probit model (Li et al., 2015). The degree of resistance was estimated by dividing the IC50 of the multidrug-resistant cells by that of the drug-sensitive parental cells. The fold reversal factor for MDR was calculated by dividing the IC50 of cells treated with antitumor drugs in the absence of anlotinib by that of cells treated in the presence of anlotinib.

## Drug Accumulation Assay

To determine the effect of anlotinib on the intracellular accumulation of antitumor drugs, a flow cytometric assay was performed. Cells were seeded in six-well plates at a density of $5\times10^5$/ml and treated with the indicated concentrations of anlotinib for 24 h. The cells were then incubated with 3 μM Rho-123 and 50 μM DOX for 2 h at 37°C. After incubation, the cells were harvested, washed 3 times with cold PBS, and

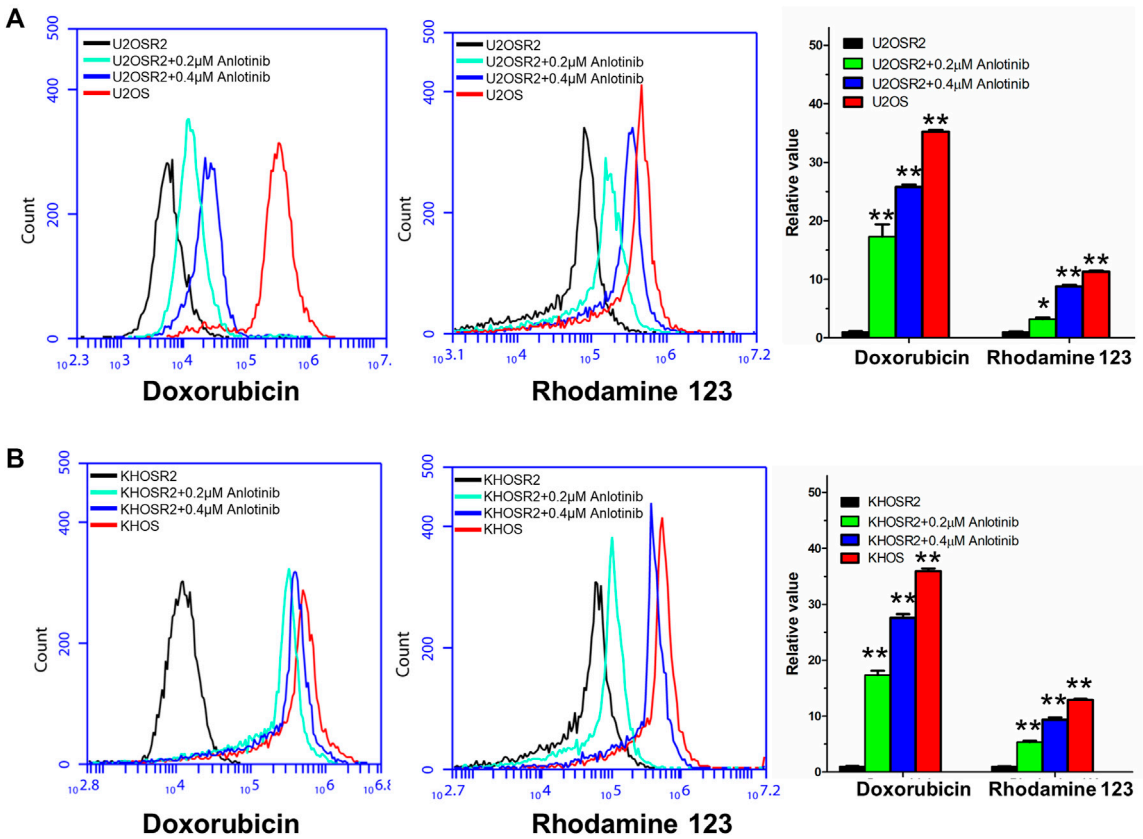


**FIGURE 3 |** Effect of anlotinib on the intracellular accumulation of DOX and Rho-123 in multidrug-resistant osteosarcoma cells and their respective drug-sensitive parental cells. **(A)**. The accumulation of DOX and Rho-123 in U2OSR2 and U2OS cells was measured by flow cytometric analysis. **(B)**. The accumulation of DOX and Rho-123 in KHOSR2 and KHOS cells was measured by flow cytometric analysis. The results were quantified as the fold change in fluorescence intensity between the drug-sensitive parental cells and the paired multidrug-resistant cells. In the presence of anlotinib, the intracellular accumulation of DOX and Rho-123 in the drug-resistant U2OSR2 and KHOSR2 cells significantly increased in a dose-dependent manner. Data represent the mean ± SD of at least three independent experiments (*$p$ < 0.05; **$p$ < 0.01).

analyzed by an Accuri C6 flow cytometer (BD Biosciences, Mountain View, CA, United States).

Fluorescence microscopy was used to visualize the effects of anlotinib on the intracellular accumulation of Rho-123 and DOX. Briefly, cells were seeded in six-well plates and exposed to Rho-123 and DOX with or without anlotinib pretreatment. The cells were washed twice with PBS, fixed with 4% paraformaldehyde for 20 min, permeabilized with 0.1% Triton X-100, and incubated with DAPI for 15 min. Fluorescence images were acquired by using a DMI3000B fluorescence microscope (Leica, Germany) and processed with LAS V4.3 software.

## Rho-123 Efflux Assay

A Rho-123 efflux assay was performed as described previously (Guo et al., 2018). Cells were seeded in six-well plates at a density of $5\times10^5$/ml and treated with 3 μM Rho-123 for 30 min. The cells were then collected, washed three times with cold PBS and subsequently incubated with or without 0.4 μM anlotinib for 0, 30, 60, 90 or 120 min. The cells were then harvested at the designed time points, washed 3 times with cold PBS, and analyzed by an Accuri C6 flow cytometer.

## PGP1 ATPase Assay

The vanadate-sensitive ATPase activity of PGP1 was measured as previously described (Ambudkar, 1998). Briefly, crude membranes isolated from High Five insect cells expressing PGP1 were incubated with various concentrations of anlotinib for 5 min. The ATPase reaction was then initiated by the addition of 5 mmol/l Mg-ATP to a 100 μl total reaction mixture. After 20 min of incubation at 37°C, 10% SDS solution was added to terminate the reaction. The amount of inorganic phosphate (IP) released was detected at 880 nm by a microplate spectrophotometer.

## Western Blot Analysis

Cells were seeded at a density of 500 cells/well in six-well plates evenly. After 24 h, cells were treated with various concentration of anlotinib (0, 0.1, 0.2, and 0.4 μM) for about 24 h. Cell samples were lysed for 30 min in ice-cold radioimmunoprecipitation assay (RIPA) buffer containing a protease inhibitor cocktail (Sigma-Aldrich). The cell lysates were centrifuged at 12,000 g for 15 min at 4°C, and the supernatant was collected. Then, the protein concentrations were quantified using a BCA Protein Assay (Thermo Scientific, Fremont, CA, United States). Equivalent

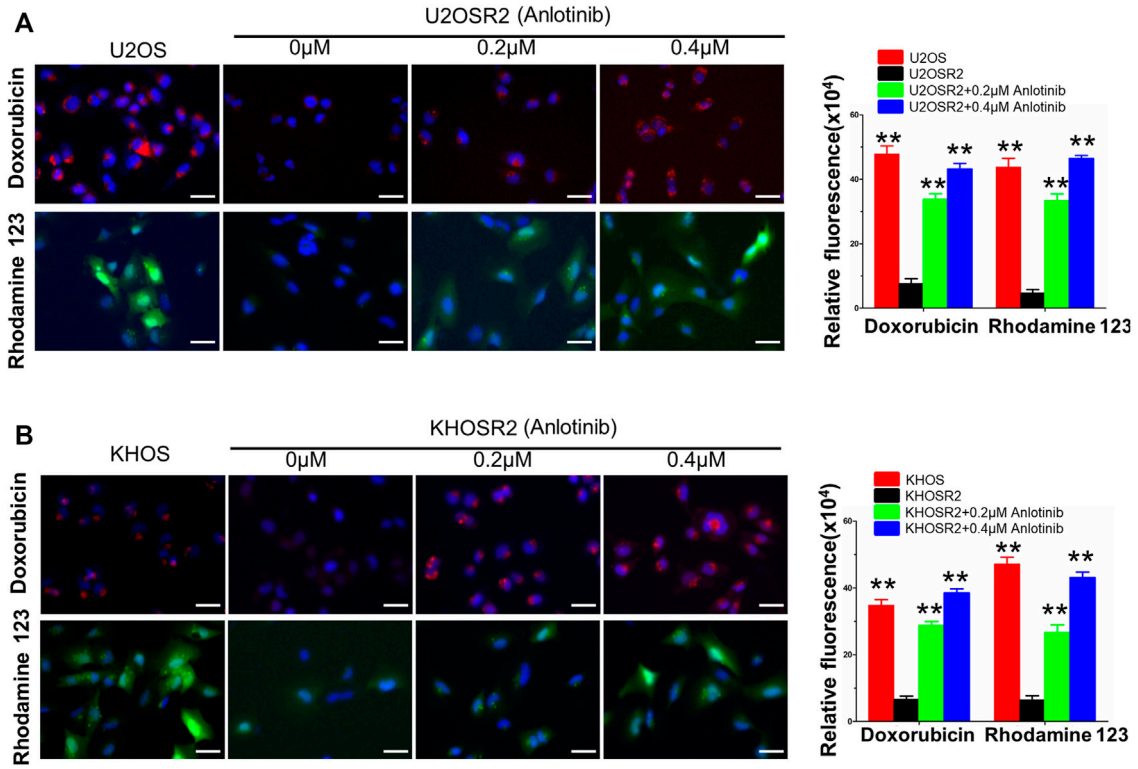


**FIGURE 4 |** Anlotinib increases the intracellular accumulation of DOX and Rho-123 in multidrug-resistant osteosarcoma cells. To visualize the effects of anlotinib on the intracellular retention of DOX and Rho-123, multidrug-resistant osteosarcoma cells and their respective drug-sensitive parental cells were seeded in six-well plates and exposed to Rho-123 and DOX with/without anlotinib pretreatment. The cells were fixed and stained with DAPI. Fluorescence images were acquired by using a DMI3000B fluorescence microscope. **(A)**. Anlotinib increases the intracellular accumulation of DOX and Rho-123 in U2OSR2 and U2OS cells. **(B)**. Anlotinib increases the intracellular accumulation of DOX and Rho-123 in KHOSR2 and KHOS cells. Scale bars = 50 μm. The fluorescence integrated density was quantified and is represented by the lower lane bar graph. Data represent the mean ± SD of at least three independent experiments (*$p < 0.05$; **$p < 0.01$).

amounts of protein were loaded and separated by SDS-PAGE, and the proteins were then transferred to polyvinylidene difluoride (PVDF) membranes (Millipore, Billerica, MA, United States). After blocking with 5% nonfat milk in PBST buffer for 1 h at room temperature, the membranes were incubated with primary antibodies at 4°C overnight. The membranes were washed with TBST and then incubated with secondary antibodies (Sigma-Aldrich, Inc.) for 1 h at room temperature. Bands were detected by an enhanced chemiluminescence kit (Millipore, Billerica, MA, United States).

## Immunofluorescence Analysis

Cells were seeded at a density of 500 cells/well on coverslips. After 24 h, cells were treated with various concentration of anlotinib (0, 0.1, 0.2, and 0.4 μM) for 24 h. After incubation, the cells were fixed with 4% paraformaldehyde, permeabilized with 0.1% Triton X-100 and blocked for 1 h with 6% BSA. Then, the cells were incubated with the indicated primary antibodies at 4°C overnight, followed by incubation with an Alexa Fluor 555-conjugated secondary antibody (1:1,000) for 1 h. Nuclei were stained with DAPI solution. Images were acquired with a confocal microscope (Leica, Wetzlar, Germany) and analyzed by image J software.

## Animal Experiments

All animal care and experimentation procedures were conducted according to the relevant guidelines with the approval of the Institutional Animal Care and Use Committee of the Shanghai Jiao Tong University School of Medicine. Four-week-old male BALB/c-nu mice (Shanghai SLAC Laboratory Animal Co., Ltd., Shanghai, China) weighing approximately 20 g were purchased from the Shanghai Laboratory Animal Center of the Chinese Academy of Sciences and provided with sterilized food and water in a standard animal laboratory.

A multidrug-resistant osteosarcoma orthotopic xenograft model was established as previously described, with minor modifications (Wang et al., 2017). Briefly, $1\times10^6$ KHOSR2 cells were suspended in 20 μl of sterile PBS and implanted into the tibial medullary cavity of each mouse. One week after cell inoculation, the mice were randomized into four groups (n = 5 per group) and received various treatments: 1) saline every other day (qod); 2) DOX (3 mg/kg, intraperitoneal (ip) injection, qod); 3) anlotinib (2 mg/kg, intragastric

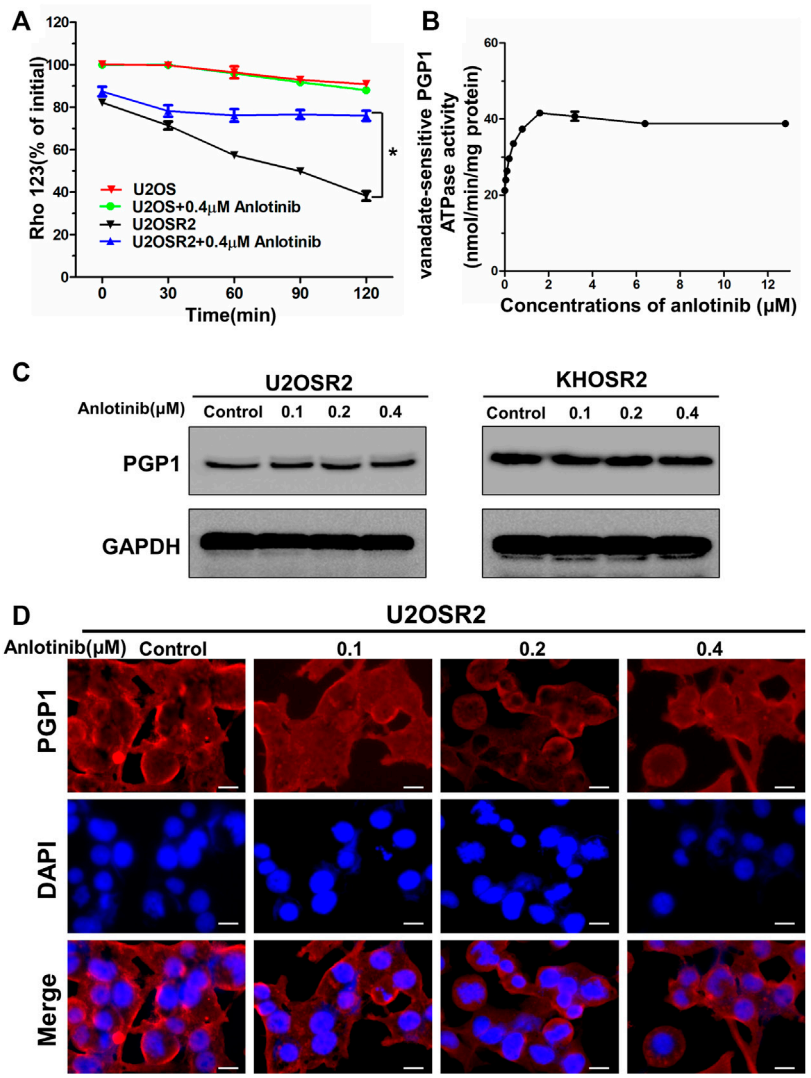


**FIGURE 5 |** Effect of anlotinib on the efflux of Rho-123 and on the ATPase activity and expression level of PGP1 in multidrug-resistant osteosarcoma cells. **(A)**. The time course of Rho-123 efflux from multidrug-resistant osteosarcoma cells was measured in the presence or absence of 0.4 μM anlotinib. Data represent the mean ± SD of at least three independent experiments. *$p < 0.05$; **$p < 0.01$. **(B)**. Vanadate-sensitive PGP1 ATPase activity was evaluated in the presence of the indicated concentrations of anlotinib. **(C)**. Effect of 24 h of treatment with the indicated concentrations of anlotinib on the expression level of PGP1 in multidrug-resistant osteosarcoma cells. **(D)**. Effect of 24 h of treatment with the indicated concentrations of anlotinib on the subcellular localization of PGP1 in U2OSR2 cells. Scale bars = 20 μm.

administration, qod); and 4) anlotinib (2 mg/kg, intragastric administration, qod, given 1 h before DOX administration) plus DOX (3 mg/kg, ip, qod). Mouse body weights and tumor sizes were measured every 2 days to observe dynamic changes in tumor growth. Tumor volumes were calculated by a standard formula: length × width$^2$/2. After 18 days of treatment, all mice were euthanized, and the tumors were harvested and weighed.

## Statistical Analysis

Data are presented as the mean ± SD. All experiments were performed at least three times, and differences were determined by using Student's t-test or One-way ANOVA. $p$-values < 0.05 (*) were considered statistically significant.

# RESULTS

## Anlotinib Reverses MDR in Osteosarcoma Cells

The structure of anlotinib is shown in **Figure 1A**. The cytotoxicity of anlotinib in different cell lines was analyzed by a CCK8 assay. The IC50 values were 32.07, 32.41, 27.17, and 30.64 μM for U2OS, U2OSR2, KHOS, and KHOSR2 cells, respectively (**Figure 1B**). Based on the cytotoxicity curves, we selected 0.4 μM as the maximum anlotinib concentration; at this concentration, the cell viability in all cell lines used in the MDR reversal study was greater than 90%.

To determine whether anlotinib can reverse MDR in osteosarcoma, cell survival assays were performed in the

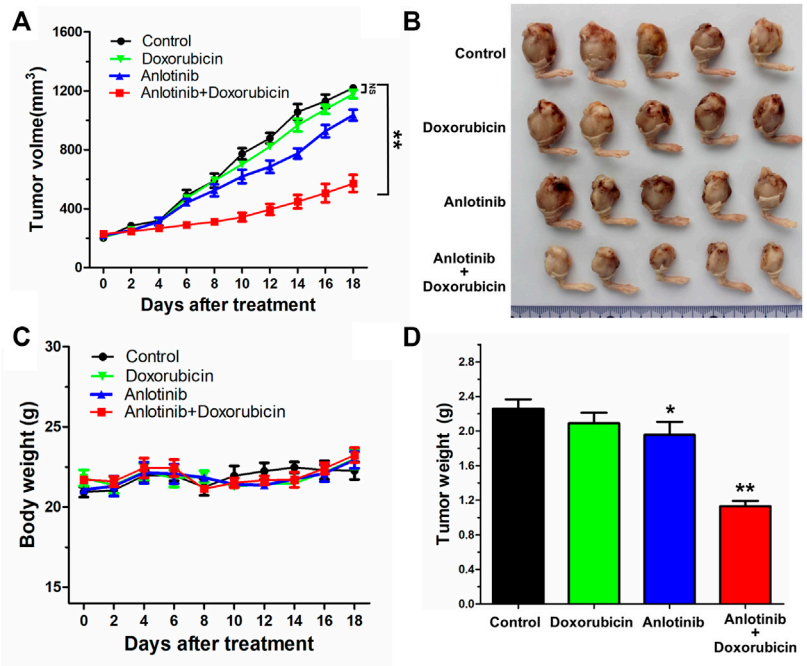


**FIGURE 6 |** Potentiation of the antitumor effects of DOX by anlotinib in a KHOSR2 xenograft model in athymic nude mice. **(A)**. Changes in tumor volume over time in the KHOSR2 xenograft model are shown (n = 5). The data shown are the mean ± SD of the tumor volumes for each group. **(B)**. A representative image of the sizes of KHOSR2 tumors excised from different mice on the 18th day after implantation is shown. **(C)**. The body weights of the mice were measured every 2 days, and the average percent change after treatment was calculated. **(D)**. Mean tumor weights for the groups after tumor excision on the 18th day after implantation. The results are presented as the mean ± SD. $^{*}p < 0.05$; $^{**}p < 0.01$.

presence or absence of anlotinib. The IC50 values of antineoplastic drugs in sensitive and resistant cells treated with different concentrations of anlotinib are shown in **Table 1**. As shown in **Table 1** and **Figure 2**, compared to its effect in the U2OS and KHOS cell lines, anlotinib significantly potentiated the cytotoxicity of DOX, paclitaxel and vincristine in the U2OSR2 and KHOSR2 cell lines in a concentration-dependent manner. However, in the parental cell lines KHOS and U2OS, which do not express PGP1, anlotinib did not modulate the activity of these cytotoxic agents (**Table 1**). Verapamil at a concentration of 10 μM was used as a positive control PGP1 inhibitor. The above results suggest that anlotinib significantly sensitizes multidrug-resistant osteosarcoma cells to antineoplastic drugs that are substrates of PGP1.

## Anlotinib Increased the Intracellular Accumulation of DOX and Rho-123 in Multidrug-Resistant Osteosarcoma Cells

The above results indicated that anlotinib could significantly enhance the sensitivity of multidrug-resistant osteosarcoma cells to antineoplastic drugs. The mechanism by which this effect occurs is unknown. Therefore, to gain insight into the mechanism of action of anlotinib, we determined the intracellular accumulation of DOX and Rho-123 in multidrug-resistant osteosarcoma cells in the presence or absence of anlotinib by flow cytometric analysis and fluorescence imaging. As shown in **Figures 3**, **4**, the intracellular accumulation of DOX and Rho-123 in the drug-resistant U2OSR2 and KHOSR2 cells was markedly lower than that in their respective drug-sensitive parental cells, U2OS and KHOS cells. In the presence of anlotinib, the intracellular accumulation of DOX and Rho-123 in the drug-resistant U2OSR2 and KHOSR2 cells significantly increased in a dose-dependent manner. This observation is consistent with the chemotherapy-sensitizing effect of anlotinib. These results suggested that anlotinib can increase the intracellular accumulation of chemotherapeutic agents in multidrug-resistant osteosarcoma cells.

## Anlotinib Decreased the Efflux of Rho-123 in Multidrug-Resistant Osteosarcoma Cells

To confirm whether the intracellular accumulation of DOX and Rho-123 was due to the inhibition of substrate drug efflux, we performed drug efflux assays in multidrug-resistant osteosarcoma cells in the presence or absence of anlotinib. We found that the efflux of Rho-123 from PGP1-overexpressing U2OSR2 cells was significantly higher than that from their drug-sensitive parental U2OS cells (**Figure 5A**). Treatment with anlotinib significantly decreased the efflux of Rho-123 from U2OSR2 cells, but it did not significantly alter the intracellular levels of Rho-123 in the parental cells. These results suggested that anlotinib increased

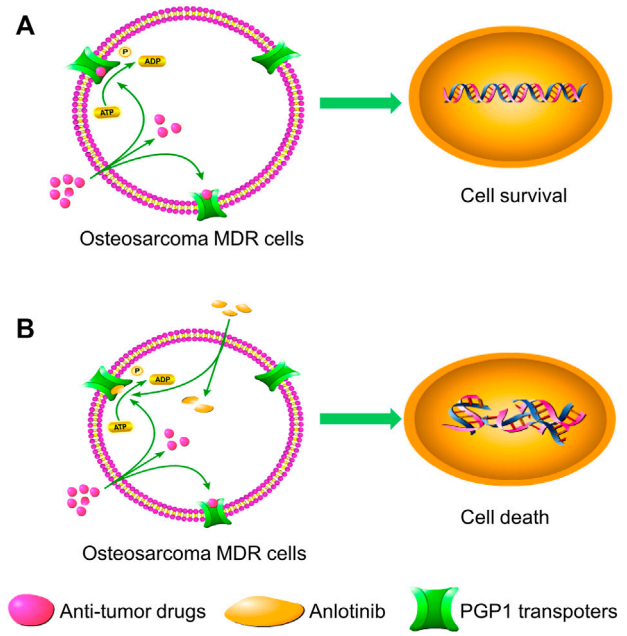


**FIGURE 7 |** Schematic diagram showing the MDR reversal effect of anlotinib. **(A)**. In the absence of anlotinib, PGP1 transporters utilize energy derived from ATP hydrolysis to extrude their substrate drugs across the membrane. **(B)**. However, when anlotinib is present, it may bind to the ATP-binding site of PGP1, thereby blocking the efflux of substrate drugs through the transporter and increasing the intracellular accumulation of substrate drugs. Therefore, anlotinib can increase the intracellular concentration of substrate drugs in multidrug-resistant cells.

the intracellular retention of Rho-123 by inhibiting PGP1-mediated efflux activity and that this effect was specific to PGP1-overexpressing U2OSR2 cells.

## Anlotinib Stimulated PGP1 ATPase Activity and did Not Affect PGP1 Expression

ABC transporters play a crucial role in the development of MDR by extruding drugs from cells. This process is coupled to the energy associated with ATP hydrolysis by the ATPase activity of ABC transporters, which is stimulated in the presence of transport substrates. To assess the effect of anlotinib on ATPase activity, we measured the vanadate-sensitive ATPase activity of PGP1 in the presence of a range of anlotinib concentrations. As shown in **Figure 5B**, anlotinib concentrations >2 μM stimulated the ATPase activity of PGP1 in a concentration-dependent manner, and this activity plateaued at approximately 42 nmol/min/mg protein and subsequently remained stable. Next, we further evaluated the effect of anlotinib on the expression level of PGP1 by Western blot and immunofluorescence analyses. Western blot analysis indicated that anlotinib did not directly interfere with the expression of PGP1 (**Figure 5C**), and the immunofluorescence assay indicated that anlotinib did not significantly alter the subcellular distribution of PGP1 in multidrug-resistant osteosarcoma cells. Therefore, the above data suggest that anlotinib may interact specifically with the PGP1 ATPase domain, which leads to inhibition of the efflux pump function of PGP1. In addition, treatment with anlotinib did not affect PGP1 expression.

## Anlotinib Potentiated the Anticancer Efficacy of DOX in a Multidrug-Resistant Osteosarcoma Cell Xenograft Model

To explore whether anlotinib could reverse PGP1-mediated MDR *in vivo,* a previously established KHOSR2 xenograft model in nude mice was used. As shown in **Figure 6A**, there was no significant difference in tumor size between animals treated with saline and animals treated with DOX alone. However, the KHOSR2 tumor growth rate recorded over a period of 18 days was significantly lower in the anlotinib-DOX combination group than in the groups treated with saline, anlotinib alone or DOX alone (**Figures 6A,B**). Notably, treatment with 2 mg/kg anlotinib also slightly decreased the growth rate of KHOSR2 xenografts. Furthermore, at the doses tested, no mortality or apparent decrease in body weight was observed in the anlotinib-DOX combination group (**Figure 6C**). Taken together, these results indicate that anlotinib improved the efficacy of DOX in the KHOSR2 osteosarcoma xenograft model and did not increase the incidence of toxic side effects.

# DISCUSSION

MDR is a major obstacle to the successful and effective chemotherapeutic treatment of cancer (Cancer multidrug resistan, 2000). In cancer cells, MDR produces resistance to numerous antineoplastic drugs that are structurally and mechanistically unrelated, and this resistance significantly decreases the efficacy of cancer chemotherapy (Krishna and Mayer, 2000). Numerous mechanisms, including the response to DNA damage, avoidance of apoptosis, induction of autophagy, overexpression of energy-dependent efflux proteins, activation of cancer stem cells, enhancement of drug efflux, and modification of cell cycle checkpoints, have been reported to mediate MDR (Gillet and Gottesman, 2010; Kartal-Yandim et al., 2016). One of the most important causes of MDR is the overexpression of ABC transporters, through which a wide range of structurally and functionally diverse antineoplastic drugs are extruded from tumor cells, thereby decreasing their intracellular accumulation and resulting in chemotherapeutic drug resistance (Pan et al., 2016). Previous studies have indicated that PGP1 is overexpressed in several multidrug-resistant osteosarcoma cell lines and drug-resistant osteosarcoma tissues (Rosier et al., 1995; Huang et al., 2012; Avnet et al., 2016). Therefore, inhibition of the drug transport function of PGP1 is a promising novel anticancer therapeutic strategy for reversing MDR in osteosarcoma. Most previous investigations have focused on reversing MDR by antagonizing the function or downregulating the expression of PGP1 in osteosarcoma, and several drugs to reverse MDR have been developed, including verapamil, cyclosporin A, biricodar and valspodar (Ferry et al., 1996; Mullin et al., 2004; Karthikeyan

and Hoti, 2015). However, none of these drugs have been approved for clinical use in the reversal of MDR due to their detrimental toxic effects at the concentrations required to inhibit PGP1. In recent years, studies have demonstrated that several TKIs, including imatinib, nilotinib, gefitinib, apatinib, and afatinib, can inhibit the function of ABC transporters; the discovery of these TKIs represents a new strategy for reversing MDR. Anlotinib, a novel TKI, exhibits potent anticancer activity in many cancers, including renal cancer, non-small cell lung cancer, and sarcoma (Zhong et al., 2018b; Chi et al., 2018; Lin et al., 2018). More importantly, anlotinib suppresses the activity of VEGFR-2, PDGFRα/β, c-Kit, Ret, Aurora-B, colony stimulating factor 1 receptor (c-FMS), and discoidin domain receptor 1 (DDR1) (Han et al., 2018a; Chi et al., 2018; Xie et al., 2018). Based on these observations, we hypothesized that anlotinib might interact with ABC transporters and effectively overcome MDR.

In the current study, we examined the effect of anlotinib on PGP1-mediated drug resistance *in vitro* and *in vivo*. In our cell viability assay, we used DOX-selected U2OSR2 and KHOSR2 osteosarcoma cells that have been extensively characterized as having both a stable MDR phenotype and PGP1 overexpression, consistent with previous reports (Ye et al., 2016). The cytotoxic effect of anlotinib in multidrug-resistant osteosarcoma cells and in the corresponding parental cells was not significantly different. Furthermore, treatment with 0.4 μM anlotinib (a concentration at which the cell viability was greater than 90%) significantly potentiated the efficacy of chemotherapeutic agents that are known PGP1 substrates in the multidrug-resistant U2OSR2 and KHOSR2 osteosarcoma cell lines. Moreover, anlotinib did not alter the sensitivity of the drug-sensitive parental U2OS and KHOS cells to chemotherapeutic agents. These results confirmed the chemotherapy-sensitizing effect of anlotinib in multidrug-resistant osteosarcoma cell lines. To further investigate whether anlotinib could enhance the efficacy of chemotherapeutic agents *in vivo*, we adopted a KHOSR2 xenograft nude mouse model. Anlotinib was found to significantly enhance the antitumor activity of the PGP1 substrate drug DOX in KHOSR2 cell xenografts without increasing its toxicity. Thus, our *in vitro* and *in vivo* results suggest that anlotinib may be a strong PGP1 inhibitor candidate, which supports further investigation of combination chemotherapy that includes anlotinib plus conventional anticancer drugs in cancer patients with PGP1 overexpression. The schematic diagram illustrating the reversal of MDR by anlotinib was showed in **Figure 7**.

To further investigate the mechanism underlying the reversal of PGP1-mediated MDR, we analyzed the effect of anlotinib on PGP1-mediated drug transport, PGP1 expression and PGP1 localization *in vitro*. Our data suggested that anlotinib inhibited the efflux of PGP1 substrates from the cells, thereby increasing the intracellular accumulation of Rho-123 and DOX. Since drug efflux depends on the energy released from ATP hydrolysis by the involved ATPase, we assessed the effect of anlotinib on PGP1 ATPase activity. Anlotinib stimulated the ATPase activity of PGP1 at a low concentration, supporting the idea that the structure of anlotinib may be similar to that of PGP1 substrates and that anlotinib could competitively inhibit PGP1 transporter activity. Furthermore, anlotinib did not affect either the expression or the localization of PGP1. These observations suggest that anlotinib activates the ATPase activity of PGP1, leading to inhibition of PGP1 efflux pump function by directly modulating the ATPase activity of the transporter, thereby reversing drug resistance. These findings are consistent with reports of other TKIs.

In conclusion, our results show that anlotinib reverses PGP1-mediated MDR by directly inhibiting PGP1 function, thus resulting in elevated intracellular concentrations of substrate chemotherapeutic drugs. Our analysis of the reversal effect of anlotinib *in vitro* and *in vivo* indicates that anlotinib may be adopted as a novel chemosensitizer to overcome MDR in patients with osteosarcoma or other types of tumors that overexpress PGP1.

## DATA AVAILABILITY STATEMENT

The original contributions presented in the study are included in the article/Supplementary Material, further inquiries can be directed to the corresponding authors.

## ETHICS STATEMENT

The animal study was reviewed and approved by the Shanghai General Hospital Animal Ethics Committee.

## AUTHOR CONTRIBUTIONS

GW, CZ, and SH contributed to the conception of the study. LC and GW contributed significantly to the analysis and manuscript preparation. YJ and GW revised the manuscript. GW, TZ, ZX, XM, and ZW performed the data analyses and wrote the manuscript. All authors contributed to the article and approved the submitted version.

## FUNDING

This project was supported by Shanghai Sailing Program (19YF1440200); Shanghai Jiaotong University Translation Medicine Cross Research Fund (ZH2018QNA17) and Doctoral Innovation Fund of Shanghai Jiaotong University School of Medicine (BXJ201732).

## ACKNOWLEDGMENTS

The content of this manuscript has been presented [IN PART] at The 4th Inaugural International Chinese Musculoskeletal Research Conference,ICMRC, 2019.

## REFERENCES


Ambudkar, S. V. (1998). Drug-stimulatable ATPase Activity in Crude Membranes of Human MDR1-Transfected Mammalian Cells. *Methods Enzymol.* 292, 504–514. doi:10.1016/s0076-6879(98)92039-0

Avnet, S., Lemma, S., Cortini, M., Pellegrini, P., Perut, F., Zini, N., et al. (2016). Altered pH Gradient at the Plasma Membrane of Osteosarcoma Cells Is a Key Mechanism of Drug Resistance. *Oncotarget* 7, 63408–63423. doi:10.18632/oncotarget.11503

Azzariti, A., Porcelli, L., Simone, G. M., Quatrale, A. E., Colabufo, N. A., Berardi, F., et al. (2010). Tyrosine Kinase Inhibitors and Multidrug Resistance Proteins: Interactions and Biological Consequences. *Cancer Chemother. Pharmacol.* 65, 335–346. doi:10.1007/s00280-009-1039-0

Boutayeb, S., Zakkouri, F. Z., Aitelhaj, M., Mesmoudi, M., Boutayeb, A., Boutayeb, W., et al. (2012). Protein Tyrosine Kinase Inhibitors in Cancer Therapy. *Pathol. Biol. (Paris)* 60, 229–233. doi:10.1016/j.patbio.2012.05.007

Cancer Multidrug Resistance, *Nat. Biotechnol.*, 18 Suppl Suppl. l (2000) IT18-20.

Chen, Y., Gokavarapu, S., Shen, Q., Liu, F., Cao, W., Ling, Y., et al. (2017). Chemotherapy in Head and Neck Osteosarcoma: Adjuvant Chemotherapy Improves Overall Survival. *Oral Oncol.* 73, 124–131. doi:10.1016/j.oraloncology.2017.08.017

Chi, Y., Fang, Z., Hong, X. N., Yao, Y., Sun, P., Wang, G., et al. (2018). Safety and Efficacy of Anlotinib, a Multikinase Angiogenesis Inhibitor, in Patients with Refractory Metastatic Soft Tissue Sarcoma. *Clin. Cancer Res.* 24 (21), 5233–5238. doi:10.1158/1078-0432.CCR-17-3766

Dai, C. L., Tiwari, A. K., Wu, C. P., Su, X. D., Wang, S. R., Liu, D. G., et al. (2008). Lapatinib (Tykerb, GW572016) Reverses Multidrug Resistance in Cancer Cells by Inhibiting the Activity of ATP-Binding Cassette Subfamily B Member 1 and G Member 2. *Cancer Res.* 68, 7905–7914. doi:10.1158/0008-5472.CAN-08-0499

Duan, Z., Choy, E., Harmon, D., Yang, C., Ryu, K., Schwab, J., et al. (2009). Insulin-like Growth Factor-I Receptor Tyrosine Kinase Inhibitor Cyclolignan Picropodophyllin Inhibits Proliferation and Induces Apoptosis in Multidrug Resistant Osteosarcoma Cell Lines. *Mol. Cancer Ther.* 8, 2122–2130. doi:10.1158/1535-7163.MCT-09-0115

Duan, Z., Choy, E., Jimeno, J. M., Cuevas, Cdel. M., Mankin, H. J., and Hornicek, F. J. (2009). Diverse Cross-Resistance Phenotype to ET-743 and PM00104 in Multi-Drug Resistant Cell Lines. *Cancer Chemother. Pharmacol.* 63, 1121–1129. doi:10.1007/s00280-008-0843-2

Duan, Z., Gao, Y., Shen, J., Choy, E., Cote, G., Harmon, D., et al. (2017). miR-15b Modulates Multidrug Resistance in Human Osteosarcoma *In Vitro* and *In Vivo*. *Mol. Oncol.* 11, 151–166. doi:10.1002/1878-0261.12015

Ferry, D. R., Traunecker, H., and Kerr, D. J. (1996). Clinical Trials of P-Glycoprotein Reversal in Solid Tumours. *Eur. J. Cancer* 32A, 1070–1081. doi:10.1016/0959-8049(96)00091-3

Gill, J., and Gorlick, R. (2021). Advancing Therapy for Osteosarcoma. *Nat. Rev. Clin. Oncol.* 18, 609–624. doi:10.1038/s41571-021-00519-8

Gillet, J. P., Efferth, T., and Remacle, J. (2007). Chemotherapy-induced Resistance by ATP-Binding Cassette Transporter Genes. *Biochim. Biophys. Acta* 1775, 237–262. doi:10.1016/j.bbcan.2007.05.002

Gillet, J. P., and Gottesman, M. M. (2010). Mechanisms of Multidrug Resistance in Cancer. *Methods Mol. Biol.* 596, 47–76. doi:10.1007/978-1-60761-416-6_4

Guo, X., To, K. K. W., Chen, Z., Wang, X., Zhang, J., Luo, M., et al. (2018). Dacomitinib Potentiates the Efficacy of Conventional Chemotherapeutic Agents via Inhibiting the Drug Efflux Function of ABCG2 *In Vitro* and *In Vivo*. *J. Exp. Clin. Cancer Res.* 37, 31. doi:10.1186/s13046-018-0690-x

Han, B., Li, K., Wang, Q., Zhang, L., Shi, J., Wang, Z., et al. (2018). Effect of Anlotinib as a Third-Line or Further Treatment on Overall Survival of Patients with Advanced Non-small Cell Lung Cancer: The ALTER 0303 Phase 3 Randomized Clinical Trial. *JAMA Oncol.* 4, 1569–1575. doi:10.1001/jamaoncol.2018.3039

Han, B., Li, K., Zhao, Y., Li, B., Cheng, Y., Zhou, J., et al. (2018). Anlotinib as a Third-Line Therapy in Patients with Refractory Advanced Non-small-cell Lung Cancer: a Multicentre, Randomised Phase II Trial (ALTER0302). *Br. J. Cancer* 118, 654–661. doi:10.1038/bjc.2017.478

Huang, J., Ni, J., Liu, K., Yu, Y., Xie, M., Kang, R., et al. (2012). HMGB1 Promotes Drug Resistance in Osteosarcoma. *Cancer Res.* 72, 230–238. doi:10.1158/0008-5472.CAN-11-2001

Jaffe, N. (2009). Osteosarcoma: Review of the Past, Impact on the Future. The American Experience. *Cancer Treat. Res.* 152, 239–262. doi:10.1007/978-1-4419-0284-9_12

Kartal-Yandim, M., Adan-Gokbulut, A., and Baran, Y. (2016). Molecular Mechanisms of Drug Resistance and its Reversal in Cancer. *Crit. Rev. Biotechnol.* 36, 716–726. doi:10.3109/07388551.2015.1015957

Karthikeyan, S., and Hoti, S. L. (2015). Development of Fourth Generation ABC Inhibitors from Natural Products: A Novel Approach to Overcome Cancer Multidrug Resistance. *Anticancer Agents Med. Chem.* 15, 605–615. doi:10.2174/1871520615666150113103439

Krishna, R., and Mayer, L. D. (2000). Multidrug Resistance (MDR) in Cancer. Mechanisms, Reversal Using Modulators of MDR and the Role of MDR Modulators in Influencing the Pharmacokinetics of Anticancer Drugs. *Eur. J. Pharm. Sci.* 11, 265–283. doi:10.1016/s0928-0987(00)00114-7

Li, H. Y., Zhang, J., Sun, L. L., Li, B. H., Gao, H. L., Xie, T., et al. (2015). Celastrol Induces Apoptosis and Autophagy via the ROS/JNK Signaling Pathway in Human Osteosarcoma Cells: an *In Vitro* and *In Vivo* Study. *Cell Death Dis* 6, e1604. doi:10.1038/cddis.2014.543

Li, S. (2021). Anlotinib: A Novel Targeted Drug for Bone and Soft Tissue Sarcoma. *Front. Oncol.* 11, 664853. doi:10.3389/fonc.2021.664853

Lin, B., Song, X., Yang, D., Bai, D., Yao, Y., and Lu, N. (2018). Anlotinib Inhibits Angiogenesis via Suppressing the Activation of VEGFR2, PDGFRβ and FGFR1. *Gene* 654, 77–86. doi:10.1016/j.gene.2018.02.026

Liu, F. S. (2009). Mechanisms of Chemotherapeutic Drug Resistance in Cancer Therapy-Aa Quick Review. *Taiwan J. Obstet. Gynecol.* 48, 239–244. doi:10.1016/S1028-4559(09)60296-5

Lu, Y., Li, F., Xu, T., and Sun, J. (2017). Tetrandrine Prevents Multidrug Resistance in the Osteosarcoma Cell Line, U-2OS, by Preventing Pgp Overexpression through the Inhibition of NF-Kb Signaling. *Int. J. Mol. Med.* 39, 993–1000. doi:10.3892/ijmm.2017.2895

Ma, S. L., Hu, Y. P., Wang, F., Huang, Z. C., Chen, Y. F., Wang, X. K., et al. (2014). Lapatinib Antagonizes Multidrug Resistance-Associated Protein 1-mediated Multidrug Resistance by Inhibiting its Transport Function. *Mol. Med.* 20, 390–399. doi:10.2119/molmed.2014.00059

Meyers, P. A., Schwartz, C. L., Krailo, M. D., Healey, J. H., Bernstein, M. L., Betcher, D., et al. (2008). Osteosarcoma: the Addition of Muramyl Tripeptide to Chemotherapy Improves Overall Survival-Aa Report from the Children's Oncology Group. *J. Clin. Oncol.* 26, 633–638. doi:10.1200/JCO.2008.14.0095

Mi, Y. J., Liang, Y. J., Huang, H. B., Zhao, H. Y., Wu, C. P., Wang, F., et al. (2010). Apatinib (YN968D1) Reverses Multidrug Resistance by Inhibiting the Efflux Function of Multiple ATP-Binding Cassette Transporters. *Cancer Res.* 70, 7981–7991. doi:10.1158/0008-5472.CAN-10-0111

Mirabello, L., Troisi, R. J., and Savage, S. A. (2009). International Osteosarcoma Incidence Patterns in Children and Adolescents, Middle Ages and Elderly Persons. *Int. J. Cancer* 125, 229–234. doi:10.1002/ijc.24320

Mullin, S., Mani, N., and Grossman, T. H. (2004). Inhibition of Antibiotic Efflux in Bacteria by the Novel Multidrug Resistance Inhibitors Biricodar (VX-710) and Timcodar (VX-853). *Antimicrob. Agents Chemother.* 48, 4171–4176. doi:10.1128/AAC.48.11.4171-4176.2004

Pan, S. T., Li, Z. L., He, Z. X., Qiu, J. X., and Zhou, S. F. (2016). Molecular Mechanisms for Tumour Resistance to Chemotherapy. *Clin. Exp. Pharmacol. Physiol.* 43, 723–737. doi:10.1111/1440-1681.12581

Ritter, J., and Bielack, S. S. (2010). Osteosarcoma. *Ann. Oncol.* 21 (Suppl. 7), vii320–vii325. doi:10.1093/annonc/mdq276

Rosier, R. N., Teot, L. A., Hicks, D. G., Schwartz, C., O'Keefe, R. J., and Puzas, J. E. (1995). Multiple Drug Resistance in Osteosarcoma. *Iowa Orthop. J.* 15, 66–73.

Sun, Y., Niu, W., Du, F., Du, C., Li, S., Wang, J., et al. (2016). Safety, Pharmacokinetics, and Antitumor Properties of Anlotinib, an Oral Multi-Target Tyrosine Kinase Inhibitor, in Patients with Advanced Refractory Solid Tumors. *J. Hematol. Oncol.* 9, 105. doi:10.1186/s13045-016-0332-8

Vasiliou, V., Vasiliou, K., and Nebert, D. W. (2009). Human ATP-Binding Cassette (ABC) Transporter Family. *Hum. Genomics* 3, 281–290. doi:10.1186/1479-7364-3-3-281

Wang, G., Zhang, T., Sun, W., Wang, H., Yin, F., Wang, Z., et al. (2017). Arsenic Sulfide Induces Apoptosis and Autophagy through the Activation of ROS/JNK and Suppression of Akt/mTOR Signaling Pathways in Osteosarcoma. *Free Radic. Biol. Med.* 106, 24–37. doi:10.1016/j.freeradbiomed.2017.02.015

Wang, X. K., To, K. K., Huang, L. Y., Xu, J. H., Yang, K., Wang, F., et al. (2014). Afatinib Circumvents Multidrug Resistance via Dually Inhibiting ATP Binding Cassette Subfamily G Member 2 *In Vitro* and *In Vivo*. *Oncotarget* 5, 11971–11985. doi:10.18632/oncotarget.2647

Xie, C., Wan, X., Quan, H., Zheng, M., Fu, L., Li, Y., et al. (2018). Preclinical Characterization of Anlotinib, a Highly Potent and Selective Vascular Endothelial Growth Factor Receptor-2 Inhibitor. *Cancer Sci.* 109, 1207–1219. doi:10.1111/cas.13536

Xue, C., Wang, C., Liu, Q., Meng, Q., Sun, H., Huo, X., et al. (2016). Targeting P-Glycoprotein Expression and Cancer Cell Energy Metabolism: Combination of Metformin and 2-deoxyglucose Reverses the Multidrug Resistance of K562/Dox Cells to Doxorubicin. *Tumour Biol.* 37, 8587–8597. doi:10.1007/s13277-015-4478-8

Yang, X., Yang, P., Shen, J., Osaka, E., Choy, E., Cote, G., et al. (2014). Prevention of Multidrug Resistance (MDR) in Osteosarcoma by NSC23925. *Br. J. Cancer* 110, 2896–2904. doi:10.1038/bjc.2014.254

Yang, X., Li, X., Duan, Z., and Wang, X. (2017). *An Update on Circumventing Multidrug Resistance in Cancer by Targeting P-Glycoprotein. Curr Cancer Drug Targets* 17, 1–20`. doi:10.2174/1568009617666170623114524

Ye, S., Zhang, J., Shen, J., Gao, Y., Li, Y., Choy, E., et al. (2016). NVP-TAE684 Reverses Multidrug Resistance (MDR) in Human Osteosarcoma by Inhibiting P-Glycoprotein (PGP1) Function. *Br. J. Pharmacol.* 173, 613–626. doi:10.1111/bph.13395

Zhong, C. C., Chen, F., Yang, J. L., Jia, W. W., Li, L., Cheng, C., et al. (2018). Pharmacokinetics and Disposition of Anlotinib, an Oral Tyrosine Kinase Inhibitor, in Experimental Animal Species. *Acta Pharmacol. Sin* 39, 1048–1063. doi:10.1038/aps.2017.199

Zhong, C. C., Chen, F., Yang, J. L., Jia, W. W., Li, L., Cheng, C., et al. (2018). "Pharmacokinetics and Disposition of Anlotinib, an Oral Tyrosine Kinase Inhibitor in Experimental Animal Species *Acta Pharmacol Sin* 39 (6), 1048–1063. doi:10.1038/aps.2017.199

**Conflict of Interest:** The authors declare that the research was conducted in the absence of any commercial or financial relationships that could be construed as a potential conflict of interest.

**Publisher's Note:** All claims expressed in this article are solely those of the authors and do not necessarily represent those of their affiliated organizations, or those of the publisher, the editors and the reviewers. Any product that may be evaluated in this article, or claim that may be made by its manufacturer, is not guaranteed or endorsed by the publisher.

frontiers in Oncology

REVIEW
published: 03 February 2022
doi: 10.3389/fonc.2022.836882

# Local Anesthetic Ropivacaine Exhibits Therapeutic Effects in Cancers

*Peng Xu[1†], Shaobo Zhang[1†], Lili Tan[2], Lei Wang[2], Zhongwei Yang[1] and Jinbao Li[1*]*

*[1] Department of Anesthesiology, Shanghai General Hospital, Shanghai Jiao Tong University School of Medicine, Shanghai, China, [2] Department of Anesthesiology, Gansu Provincial Maternity and Child Care Hospital, Lanzhou, China*

Despite the significant progress in cancer treatment, new anticancer therapeutics drugs with new structures and/or mechanisms are still in urgent need to tackle many key challenges. Drug repurposing is a feasible strategy in discovering new drugs among the approved drugs by defining new indications. Recently, ropivacaine, a local anesthetic that has been applied in clinical practice for several decades, has been found to possess inhibitory activity and sensitizing effects when combined with conventional chemotherapeutics toward cancer cells. While its full applications and the exact targets remain to be revealed, it has been indicated that its anticancer potency was mediated by multiple mechanisms, such as modulating sodium channel, inducing mitochondria-associated apoptosis, cell cycle arrest, inhibiting autophagy, and/or regulating other key players in cancer cells, which can be termed as multi-targets/functions that require more in-depth studies. In this review, we attempted to summarize the research past decade of using ropivacaine in suppressing cancer growth and sensitizing anticancer drugs both *in-vitro* and *in-vivo*, and tried to interpret the underlying action modes. The information gained in these findings may inspire multidisciplinary efforts to develop/discover more novel anticancer agents *via* drug repurposing.

**Keywords: drug repurposing, local anesthetics, ropivacaine, anticancer, mechanisms**

OPEN ACCESS

***Edited by:***
*Leli Zeng,*
*Sun Yat-sen University, China*

***Reviewed by:***
*Enming Du,*
*Henan Provincial People's Hospital, China*
*Kaiyan Liu,*
*University of Maryland, Baltimore, United States*

****Correspondence:***
*Jinbao Li*
*lijinbaoshanghai@163.com*

*[†]These authors have contributed equally to this work*

***Specialty section:***
*This article was submitted to Pharmacology of Anti-Cancer Drugs, a section of the journal Frontiers in Oncology*

***Received:*** *16 December 2021*
***Accepted:*** *10 January 2022*
***Published:*** *03 February 2022*

***Citation:***
*Xu P, Zhang S, Tan L, Wang L, Yang Z and Li J (2022) Local Anesthetic Ropivacaine Exhibits Therapeutic Effects in Cancers. Front. Oncol. 12:836882. doi: 10.3389/fonc.2022.836882*

## INTRODUCTION

Cancer has become a global health burden in both developing and developed countries. Despite the significant progress of chemotherapies and immunotherapies, unexpected low response rate, unfavorable adverse effects, multidrug resistance (MDR) and cancer recurrence are among the major challenges that undermine effective cancer treatment as summarized in **Figure 1** (1–4). New drugs with novel structures and/or mechanisms and novel therapeutic strategies remain unmet clinical needs to tackle these issues. The discovery and development of one new drug, especially *de novo* drug discovery, may approximately take at least ten years and one billion dollars, rendering it a highly challenging and risky task due to the fact of high attrition rates (5–7). Potential strategies that may serve as shortcuts in drug discovery are 1) old drugs repurposing, 2) co-crystallization between lead compound and its target protein, which may fasten the identification and optimization of drug candidates, 3) artificial intelligence (AI) and machine learning, and 4) others such as high throughput screening (HTS) in natural products or other commercial available compound libraries (8–12).


**FIGURE 1** | The effective cancer treatment can be undermined by many key challenges.

Recently, old drug repurposing has been proved to be a feasible strategy to develop new drugs from those approved drugs by defining new indications (13–18). More importantly, these approved drugs have already been evaluated in humans to possess favorable profiles of pharmacokinetic, pharmacodynamic profiles and safety, as well as controllable/acceptable adverse/toxic effects, which is a procedure of time-consuming (19). Drug repurposing may indeed shorten the overall time in developing and launching a new drug, and may substantially relief the financial burden as compared to *de novo* drug development (16, 17, 20, 21).

Retrospective clinical studies have suggested that the application of local anesthetics can improve the treatment outcomes of certain cancer patients in pain control and, more strikingly, in suppressing cancer growth (22, 23). In the past decade, researchers have studies intensively in discovering new agents with anticancer activities among local anesthetics, finding that several anesthetics possess broad-spectrum anticancer potencies (24), such as lidocaine (25–27), procaine (28–30), ropivacaine (31–35) and its stereoisomers bupivacaine (36, 37) and levobupivacaine (38, 39). Following our previous review of lidocaine in cancer treatment (11), in the current review, we aimed to summarize the anticancer studies of ropivacaine, another amide-linked local anesthetic (same as lidocaine) that has been widely used in perioperative period as a long acting local anesthetic (40, 41). Structurally, ropivacaine is the S-enantiomer of bupivacaine, while it has a weaker cardiotoxicity and other toxic effects than bupivacaine when used as an anesthetic (42, 43). Ropivacaine, when repurposed as anticancer agent that is administered by single or combination, inhibits cancer cells growth, proliferation, invasion and migration through multiple mechanisms, showing great potential in cancer treatment.

## ROPIVACAINE DEMONSTRATES ANTICANCER EFFICACIES

Growing evidence has suggested that at certain concentrations/doses, ropivacaine can work as an anticancer agent by monotherapy or combination. In this section, we summarized these studies categorized by the functions such as inhibiting proliferation or invasion, etc. Compared to lidocaine that has been evaluated in various cancer types *in-vitro* and *in-vivo* (11), relatively fewer studies were conducted using ropivacaine in cancer treatment. By far, it's still not clear about the direct interactions of local anesthetics on cancer cells. Further applications can be significantly expanded after deciphering the exact mechanism and the target of ropivacaine.

## ROPIVACAINE INHIBITS CANCER CELLS PROLIFERATION

### *Via* Regulating Ras and RhoA Signaling Pathway

There are studies that indicated the anticancer effects of ropivacaine are independent of its role in regulating sodium channel (44). RhoA and Ras are two important members of Ras superfamily that regulates many aspects of cancer cell biology including cell division, proliferation and migration, whose inhibitors hold promising activity against cancer (45, 46). Zheng et al. (44) found that ropivacaine (0.25, 0. 5, 1 and 2 mM) inhibited the proliferation and migration of human melanoma A375 and A431 cells in a concentration-dependent manner *via* inducing apoptosis (44). More importantly, it (0.5 mM) could also serve as chemosensitizer as it markedly enhanced the potencies of vemurafenib and dacarbazine, two widely used drugs in melanoma treatment, suggesting a broader screening of its potential in drug resistant cancers. Interestingly, its isomer bupivacaine didn't show such sensitizing effect as ropivacaine. These effects were independent of sodium channel but were mediated by the inhibition of RhoA and Ras, which can be reversed by pre-treatment with the activator of Ras and Rho, calpeptin (44). The Western blot analysis also showed that ropivacaine treatment (1 and 2 mM) not only caused the down-regulation but also inhibited the activities of several downstream signaling of Ras and RhoA, such as MAPK/ERK Kinase (MEK) and myosin phosphatase target subunit 1 (MYPT1) MLC, further verifying its mechanism (44).

### *Via* Regulating Integrin Alpha-2 (ITGα2) and ITGβ1

ITGα2 is a key protein that closely participates in cell adhesion. Serving as a therapeutic target, ITGA2 is found to be overexpressed in certain cancer cell lines and tumor tissues, which may cause the promotion of cancer aggression (47, 48). Ropivacaine (2.5-40 μM) inhibited the proliferation of gastric cancer AGS and BGC-823 cells as shown in a study by Qin et al. (49). Mechanistic study indicated that ropivacaine inhibited the expression of ITGA2 in a concentration-dependent manner,

resulting in significant apoptosis as supported by the down-regulated anti-apoptotic B-cell lymphoma 2 (Bcl-2), and up-regulated pro-apoptotic Bcl-2-associated X protein (Bax), cleaved caspase 3/9. Importantly, these effects could be reversed by the overexpression of ITGα2, indicating that ropivacaine's anticancer effects were mediated by inhibiting ITGα2 (49). In this study, ropivacaine was also found to suppress the invasion and metastasis of human papillary thyroid cancer (PTC) TPC-1 cells, suggesting it a multifunctional agent (49).

Another recent study by Wang and Li (50) showed that ropivacaine (200, 400, 800 μM) induced apoptosis and inhibited the proliferation and migration of colon cancer HCT116 and SW620 cells by targeting another subunit of integrin, ITGβ1 (50).

## *Via* Regulating Wnt/β-Catenin

Cancer stem cells (CSCs) are a subpopulation of cancer cells that have self-renewing and highly proliferative properties, which can often cause cancer recurrence and drug resistance (51–53). Wnt/β-catenin pathway plays critical role in regulating the pluripotency and renewal of CSCs. In addition, Wnt/β-catenin is found to be dys-regulated in cancer patients, indicating its potential therapeutic implication (54, 55). At clinical relevant concentrations, ropivacaine exhibits inhibitory effects towards CSCs. A study conducted by Li et al. (28) showed that ropivacaine (10, 50 and 100 μM) inhibited leukemia stem cell (LSC) stronger than normal hematopoietic stem cell (HSC), although ropivacaine was found to be less potent than lidocaine or bupivacaine (56). At the same concentrations, ropivacaine significantly repressed the colony numbers as well as the serial replating of LSC, likely *via* inhibiting Wnt/β-catenin as confirmed by Western blot analysis, suggesting its potential capabilities in inhibiting CSCs and warranting further studies (56).

## *Via* Regulating Autophagy Through Vascular Endothelial Growth Factor (VEGF)-A and Signal Transducer and Activator of Transcription 3 (STAT3)

Autophagy is a biological procedure that prompts cancer cells to respond nutrition changes by degrading and then recycling the intracellular biomacromolecules, serving as a promising therapeutic target in cancer (57–59). Combinational therapy of ropivacaine has also been attempted to inhibit pain relief and tumor growth simultaneously. Zhang et al. (20) developed a formulation of liposomes composed with ropivacaine (named as Rop-DPRL), and these liposomes, when combined with nutrition deprivation which may lead to activated autophagy, can suppress the tumor growth of melanoma B16 cells xenograft model and relieve the cancer pain (60). Further study indicated that these effects were mediated by reducing the expression of VEGF-A, and inhibiting the phosphorylation of STAT3 (60).

## *Via* Apoptosis-Associated Pathways and Cell Cycle Arrest

Most of cancer cells die due to apoptosis induced by different therapeutic strategies. Apoptosis, the programmed cell death, can be categorized into external and internal apoptosis which are initiated *via* distinct pathways. Both of them can serve as therapeutic targets that can be attacked by small-molecule drugs or macromolecule drugs *via* intervening the key components, e.g., either activating the pro-apoptotic proteins or suppressing the anti-apoptotic ones (61, 62).

One of the hallmarks of cancer cells is the uncontrollable cell division and proliferation. Key enzymes such as cyclin-dependent kinases (CDKs) and members of cyclins are dynamically stimulated to regulate the active cell cycle, rending them to be attracting and druggable targets (63, 64). Growing evidence has showed that ropivacaine can kill cancer cells *via* inducing apoptosis or cell cycle arrest.

Castelli et al. (65) evaluated the cytotoxicity of ropivacaine on drug-resistant human triple-negative breast cancer MDA-MB-231 cells, and melanoma A375 cells (65). Ropivacaine (5-1000 μM) was found to concentration-dependently inhibit the proliferation of both cell lines, and suppressed the migration as confirmed by the transwell assay. Ropivacaine induced significant apoptosis by up-regulating the cleaved caspase 3 and 9, and it also caused cell arrest *via* inhibiting the expression of cyclins B2, D1 and E. These effects suggested that ropivacaine suppressed cancer cells proliferation *via* cell cycle arrest and activating apoptosis pathway (65).

Another study showed that ropivacaine possessed similar activity in human non-small cell lung cancer (NSCLC) A549 and H520 cells (66). Ropivacaine (2-12 mM) inhibited the cell viability, suppressed the invasion and migration at 4.06 and 2.62 mM ($ED_{50}$ values) *via* inducing G0/G1 phase arrest and apoptosis by down-regulating anti-apoptotic but up-regulating pro-apoptotic proteins, provoking DNA damage and reactive oxygen species (ROS) production through activating mitogen-activated protein kinase (MAPK) pathways (66). It's worth noting that this study using much higher concentration of ropivacaine that that of in Castelli et al.'s study (65), which is a common issue using local anesthetic as anticancer agent, further pharmacokinetic studies are needed.

Li et al. (28) reported that at plasma concentrations (10, 35 μM, much lower than 1 mM) for 72 h, ropivacaine failed to decrease cell viability and migration of breast cancer MDA-MB-231 and MCF7 cells, while at higher concentrations (more than 1 mM), it significantly inhibited cell viability and showed cytotoxicity without affecting the viability of a non-cancerous breast cell line, MCF10A, suggesting its selective profile (67). At 10-fold plasma concentrations, ropivacaine suppressed the migration of MDA-MB-231 by inducing cell arrest at the S phase (64).

Another similar result was found that ropivacaine at 1 mM decreased the viability and proliferation of hepatocellular carcinoma (HCC) HuH7 cells while spared the well-differentiated HepaRG cells (68). The levels of mRNA of several key cell-cycle regulators, including cyclin A2, B1/2, and CDK1, as well as the marker of proliferation Ki-67 (MKI67) were significantly suppressed, indicating a cell arrest-mediated mechanism (68).

Mitochondria are pivotal organelles in cancer cells for their roles in ATP production (mitochondrial respiration) and endogenous apoptosis pathway initiating and regulating, rendering them to be attractive therapeutic targets (67, 69, 70).

Several studies have indicated that ropivacaine could exert its anticancer effects through inducing mitochondria-mediated apoptosis and/or impacting the respiration pathway (71, 72). In HCC Bel7402 and HLE cells, in the concentration- and time-dependent manners, ropivacaine markedly suppressed the cells proliferation and migration *via* damaging mitochondria by inducing endogenous apoptosis event as confirmed by the up-regulated caspase 3/9, apoptotic protease activating factor-1 (Apaf-1) and released cytochrome C from mitochondria and down-regulated anti-apoptotic Bcl-2 (73). Another study conducted by Yang et al. (32) showed that at clinically relevant concentrations, ropivacaine was able to suppress the angiogenesis of human lung tumor-associated endothelial cells (HLT-EC) *via* disturbing the complex II located in the mitochondrial respiration chain. The damaged mitochondrial respiration caused by ropivacaine further leads to ATP depletion, overproduced ROS and finally lethal damages to cells (74).

Another study by Gong et al. (33) showed that ropivacaine (0.5 and 1 mM) inhibited the activities of complex I and II in mitochondrial respiration chain in breast cancer MDA-MB-468 and SkBr cells, leading to the repressed growth, survival and colony formation through inducing oxidative stress (75). Further study indicated that ropivacaine could work as a chemo-sensitizing agent since it (0.5 mM) can enhance the sensitivity of 5-fluorouracil (5-FU) *via* inhibiting the phosphorylation of Akt, mammalian target of rapamycin (mTOR) and ErbB3 receptor-binding protein 1 (EBP1) (75).

Ropivacaine also exerts inhibitory effects towards mesenchymal stem cells (MSCs) which possess self-renewing property that may contribute in wounds healing and tumor growth (71, 72, 76). At 100 μM, ropivacaine induced proliferation inhibition, cell arrest at the G0/1-S phase, resulting in less colony formation and delayed wound healing *via* impacting mitochondrial respiration and reducing ATP production (77).

### *Via* Regulating Extracellular Signal-Regulated Kinases 1/2 (ERK1/2)

ERK1/2 signal pathway is one of the central players in regulating cell biology, such as proliferation, differentiation, autophagy, stress response apoptosis and survival (78). Several selective ERK1/2 inhibitors are undergoing clinical trials, showing their great potentials in certain cancers treatment (79). Yang et al. (80) found that ropivacaine (1 mM) significantly inhibited the proliferation and migration of gastric cancer AGS and HG-27 cells *via* down-regulating phosphorylated ERK1/2 (80). Further studies are necessary to elucidate the details of impacted signal pathway and associated cancer cell biology, e.g., the interaction of ERK1/2 down-regulation with autophagy (81), apoptosis (82), and cell cycle (83), etc.

### *Via* Micro RNAs/Long Non-Coding RNAs (lncRNAs) and Associated Signaling Pathways

Micro RNAs have drawn profound attentions for their roles in regulating cancer progression and migration, serving as therapeutic target (84). Zhang et al. (20) found that ropivacaine could up-regulate miR-520a-3p that can further suppressed the expression of WEE1 and phosphorylated PI3K, leading to concentration- and time-dependent inhibition of the proliferation of gastric cancer AGS and BGC-823 cells, suppression of the migration and invasion (85). More importantly, in the AGS cells xenograft mouse model, ropivacaine (20, 40, and 60 μM/kg) significantly reduced tumor growth, accompanied with up-regulated miR-520a-3p and decreased WEE1 and phosphorylated PI3K (85).

In breast cancer MDA-MB-231 and MCF-7 cells, ropivacaine (1 mM) induced apoptosis, leading to the time-dependent inhibition of the proliferation, and the reduction of the colony formation, as well as decreased cell invasion and migration (86). Ropivacaine was confirmed to up-regulate miR-27b-3p and its target gene *YAP* to exert its anticancer effects. Ropivacine (40 μM/Kg) inhibited the tumor growth of MDA-MB-231 cells xenograft model, which can be reversed by co-treatment of miR-27b-3p inhibitor (86).

Recently, lncRNAs have shown great potentials as key players in gene regulation and cancer progression. MEG2 lncRNA regulates epigenetic modifications through interacting with chromatin-modifying complexes, acting as a tumor suppressor that is down-regulated in various types of cancer (87). As a central player in cell biology and a therapeutic target, STAT3 is a transcription factor that regulates cell differentiation, proliferation and apoptosis, resulting in promoting cancer progression (88). Chen et al. (89) reported that ropivacaine (0.25, 0.5 and 1 mM) possessed inhibitory effects to cervical cancer SiHa, Caski cells *via* suppressing the expression of cyclin D1 and survivin, an anti-apoptotic protein (90, 91), by abrogating the phosphorylation and transcriptional activation of STAT3 whose overexpression could reverse the cytotoxicity of ropivacaine (89). These effects were mediated by up-regulating MEG2 and down-regulating microRNA96, suggesting ropivacaine as a potential therapeutic agent for cervical cancer (89).

## ROPIVACAINE INHIBITS CANCER CELLS INVASION AND MIGRATION

As discussed above, ropivacaine at certain concentrations/doses could not only suppress the proliferation, but also the invasion and migration *via* similar multiple mechanisms. While there are also studies indicated that ropivacaine can only inhibit the invasion and migration, but not be able to kill cancer cells, probably due to the applied different concentrations, e.g., lower concentrations.

### *Via* Regulating Sodium Channels

Proteins in regulating sodium channel such as NaV1.5 voltage-gated $Na^+$ channel (VGSC), can also prompt the tumorigenesis including the proliferation and metastasis of cancers (92, 93). Certain types of metastatic cancer cells, including breast and colon cancer cells, express high level of NaV1.5 VGSC, which may lead to poor prognosis of patients (93–96). Consequently, the block of NaV1.5 VGSC leads to the cease of cancer cell invasion (93, 97). As a local anesthesia, ropivacaine works by

inhibiting sodium channel that mediates the pain signal transduction (98). Accordingly, ropivacaine can also well exert its anticancer effects *via* the same mechanism of action through the inhibition of NaV1.5 VGSC. A study conducted by Baptista-Hon et al. (97) found that, ropivacaine blocked the NaV1.5 VGSC of both neonatal and adult splice variants in colon cancer SW620 cells, with $IC_{50}$ values of 2.5 and 3.9 μM, respectively. Consequently, ropivacaine inhibited the invasion of SW620 cells ($IC_{50}$ of 3.8 μM), suggesting its potential application in controlling colon cancer invasion (97).

In 2015, a systematic review by Koltai et al. was published, aiming in searching regulators of VGSCs (NaV1.1 to Nav1.9) and the potentials of their regulators in suppressing invasion and metastasis of cancers (99). In this review, they reported that a couple of local anesthetics, such as ropivacaine and lidocaine, as well as many other drugs, may serve as anticancer agents in suppressing metastasis and invasion of cancer cells (99). However, their further applications in clinic remain to be unveiled (99). This review also suggests a wider screening of this type of approved drugs for their potential in cancer treatment.

### *Via* Attenuating the Axis of Rac1/c-Jun N-Terminal Kinase (JNK)/Paxillin/Focal Adhesion Kinase (FAK)

A study in Zheng's group (2018) showed that at lower concentrations (less than 200 μM), ropivacaine didn't impact cancer cell growth and survival but suppress the cell migration (100). As shown in this research, at the clinically relevant concentration (50, 100 and 200 μM), ropivacaine inhibited the migration of esophageal cancer OE33, ESO26 and FLO-1 cells *via* decreasing the activities of GTPases of RhoA, Rac1 and Ras, and inhibiting the prenylation, which were independent of sodium channel. This work demonstrated that the potent anti-migratory effect of ropivacaine in esophageal cancer was mediated by attenuating the axis of Rac1/JNK/paxillin/FAK and prenylation-dependent migratory signaling pathways (100).

### *Via* Regulating Matrix Metalloproteinase 9 (MMP9)/Akt/FAK

MMP9 is a key protein that plays key role in cancer cells invasion, which serves as a prognostic biomarker in certain cancer patients, implying its potential role as a therapeutic target (101–103). In NCI-H838 lung adenocarcinoma cells, ropivacaine (1 nM-100 μM) significantly reduced TNFα-induced activation/phosphorylation of Akt, FAK, caveolin-1 as well as MMP9 *via* attenuating tyrosine protein kinase Src-dependent inflammatory pathway. Ropivacaine (1 μM) completely inhibited the invasion of NCI-H838 cells, suggesting its potential in suppressing the metastasis (104).

Similar results were also confirmed by Piegeler et al. (2012) that ropivacaine, through its anti-inflammatory effects, suppressed the Src and vascular intercellular adhesion molecule-1 (VCAM-1), two important key players in tumor growth and metastasis (104, 105). Ropivacaine (100 μM for 20 min) decreased the Src activity by 62% through decreasing Src-activation and intercellular adhesion molecule-1 phosphorylation (106).

### *Via* Nuclear Factor Kappa-Light-Chain-Enhancer of Activated B Cells (NF-κB) Pathway

NF-κB pathway regulates cancer cell proliferation, survival, and angiogenesis, playing pivotal role in cell biogenic activities and serving as an attracting target in cancer treatment (105). Su et al. (107) found that ropivacaine (10 μM), when combined with tumor necrosis factor α (TNFα), caused the inhibition of adhesion of three cancer cell lines, human hepatoma HepG2 cells, human colon cancer HT-29 cells and human leukemic monocyte THP-1 cells. These effects were mediated by down-regulating the expression of CD62E, a key protein in regulating adhesion (106, 108). Further mechanistic study showed that ropivacaine significantly suppressed the expression of several key components of NF-κB pathway, including the phosphorylation of p65, IκBα and IKKα/β, indicating that ropivacaine decreased the adhesion of cancer cells *via* modulating CD62E expression by inhibiting the NF-κB pathway (107).

### *Via* DNA Demethylation

DNA methylation is a procedure through which bases are modified by methyl group, which is found to be highly active in many cancers (109). The inhibitors of DNA methylation can produce anticancer potencies and several of these inhibitors have been approved by FDA (110). Ropivacaine showed epigenetic regulatory effects *via* modulating DNA methylation. As shown in Lirk et al.'s study (111), ropivacaine at clinically relevant concentrations (3 and 30 μM) didn't directly kill but decrease the DNA methylation in breast cancer BT-20 cells which lead to lower tumorigenesis properties (111).

## CLINICAL STUDIES

A recent retrospective cohort study of 215 pancreatic cancer patients by Chen et al. (112) showed that 0.375%-0.5% of intraoperative epidural ropivacaine significantly improve the overall survival (112). Several clinical trials have already been conducted by applying ropivacaine as an adjuvant therapy in shortening the recovery time and other beneficial effects in surgical cancer patients. A clinical study revealed recently (2020) that in liver cancer patients, ropivacaine, when combined with dezocine, could significantly shorten the recovery time of anesthesia and inhibit pain factors secretion, with markedly less adverse reaction, and this combination therapy could reduce stress response, promote patients' postoperative recovery after cancer surgery (113). Another study (NCT02256228) showed that *via* the anti-inflammatory and analgesic effects, intraperitoneal ropivacaine in ovarian cancer patients could prompt the postoperative recovery and shorten the time for chemotherapy, which may lead to better overall recovery (114). Similar results were also observed in breast cancer patients who underwent surgery. This study (NCT02691195) showed that in the treatment group, 25 ml of 0.5% ropivacaine could improve the quality of recovery as confirmed by analyzing the 40-item questionnaire, leading to higher patient satisfaction (115). Wang et al. (31) reported that

ropivacaine treatment might improve the postoperative cognitive dysfunction in patients following thoracotomy for esophageal cancer by down-regulating inflammatory cytokines such as IL-6 and TNFα (116).

Recently (2020), a study conducted in New Zealand to explore the long term of application of intraperitoneal ropivacaine in colonic cancer patients has been reported. This study had enrolled 60 patients of both benign and malignant colon cancer (stages I-III), and was analyzed by evaluating the overall survival, disease-free survival and recurrence. However, the revealed results showed that the treatment group by ropivacaine didn't exhibit better overall survival or reduced mortality than the placebo group treated by 0.9% saline solution. And even worse, higher incidence of cancer-specific mortality was found in the ropivacaine-treated group, indicating no beneficial effects by applying intraperitoneal ropivacaine in patients with colonic malignancy (117). While further studies are clearly needed to explore the indications, e.g., earlier stages of cancers, and certain combinational therapy with ropivacaine.

## DISCUSSION AND FUTURE PERSPECTIVES

The above studies indicate that local anesthetic ropivacaine may benefit cancer patients by two ways, 1) inhibit the proliferation or suppresses the migration of cancer cells as we summarized in **Table 1** and **Figure 2**, and 2) shortens the recovery times and improve the quality of life.

The studies performed *in-vitro* and *in-vivo* have proved that ropivacaine represses the cancer cells invasion and migration at lower concentrations (usually less than 200 μM) (100), while it suppresses cancer growth or kills cancer cells *via* various acting modes at higher concentrations/doses (mostly more than 1 mM) (118). However, the concentrations/doses vary when it comes to different cancer cells, requiring further in-depth studies for a clear therapeutic window in certain cancer type. In addition, ropivacaine appears to be an enhancer of the sensitivity of certain chemotherapy, suggesting its potential in the treatment of certain resistant cancers (44, 75). The information above may 1) suggest an appealing strategy in screening and identifying certain combinational therapy with ropivacaine, and 2) evoke a broad screening among local anesthetics and related drugs for cancer treatment. However, we cannot overstate the therapeutic implication until more results especially *in-vivo* and clinical studies are revealed.

In addition to its role in killing cancer cells, ropivacaine also improves the quality of life of cancer patients who have undergone surgical treatment. Many retrospective studies conducted among cancer patients upon treatment of local anesthetics including lidocaine and ropivacaine demonstrate a favorable trend of decrease in tumor metastasis and recurrence. While the clinical trials focusing on the anticancer effects of ropivacaine have yielded limited successes, there are still several ongoing trials for cancer-related diseases (see at http://6tt.co/tjEU on ClinicalTrials.gov), its potentials in cancer treatment remain to be fully revealed.

One interesting finding is the difference of anticancer efficacies of the analogs or isomers of ropivacaine. Ropivacaine and bupivacaine are optical isomers, while they possess different potentials and targets, e.g., GTPases (42), though they also exhibit similar effects in regulating certain targets such as hypoxia-inducible factor 2α (HIF-2α) signaling (115). More efforts are needed to decipher the underlying mechanisms, such as the binding targets, the network through which ropivacaine regulates certain signals transduction in cancers, etc. The application of ropivacaine in cancer treatment is still in its infant stage, more

**TABLE 1** | Summary of ropivacaine in cancer treatment.

| Targets/Mechanisms | Efficacies | Refs |
|---|---|---|
| **Ras superfamily** | Sensitizing vemurafenib and dacarbazine | (44) |
| **ITGα2 and ITGβ1** | Inhibiting the proliferation of AGS, and BGC-823 cells | (49, 50) |
| | Inhibiting proliferation and migration of HCT116 and SW620 cells | |
| **CSCs/Wnt/β-catenin** | Inhibiting the proliferation of LSC | (56) |
| **Autophagy/VEGF-A/STAT3** | Inhibiting B16 cells xenograft tumor growth | (60) |
| **Apoptosis-associated pathways** | Inhibiting the proliferation and migration of MDA-MB-231 and A375 cells | (65, 66, 73–75) |
| | Inhibiting the invasion and migration of A549 and H520 cells | |
| | Inhibiting the proliferation and migration of Bel7402 and HLE cells | |
| | Inhibiting the capillary formation and growth of HLT-EC | |
| | Inhibiting the proliferation of MDA-MB-468 and SkBr cells and sensitizing 5-FU | |
| **Cell arrest** | Inhibiting the proliferation and migration of MDA-MB-231 and MCF7 cells | (67, 68) |
| | Inhibiting the proliferation of HuH7 cells | |
| **ERK1/2** | Inhibiting the proliferation and migration of AGS and HG-27 cells | (80) |
| **miR-520a-3p** | Inhibiting the proliferation of gastric cancer AGS and BGC-823 cells | (84) |
| **miR-27b-3p** | Inhibiting MDA-MB-231 cells *in-vitro* and *in-vivo* | (85) |
| **miR96/MEG2/pSTAT3** | Inhibiting the proliferation of SiHa, Caski cells | (89) |
| **Sodium channel** | Inhibiting the invasion of SW620 cells | (97, 99) |
| **Rac1/JNK/paxillin/FAK** | Inhibiting the migration of OE33, ESO26 and FLO-1 cells | (95) |
| **NF-κB** | Inhibiting the adhesion of HUEVC | (107) |
| **MMP-9/Akt/FAK** | Inhibiting the invasion of NCI-H838 cells | (104) |
| **DNA demethylating** | Suppressing tumorigenesis properties | (111) |

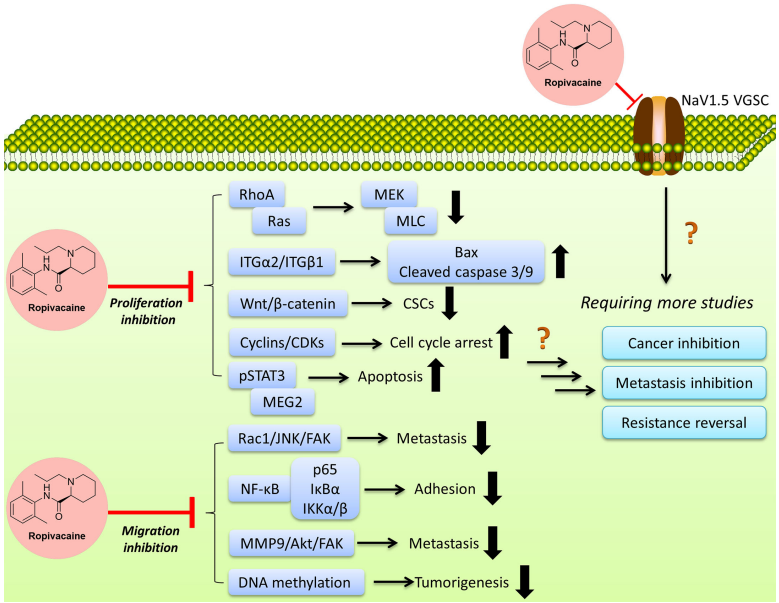


**FIGURE 2** | Ropivacaine suppresses cancer cells *via* multiple targets/functions by modulating multiple signal pathways. More efforts are needed to reveal the full map of the mechanisms.

effects are clearly needed to define its indications and administration strategies (either single use or combination). Meanwhile, there are still many questions to be answered, such as the exact targets, and the acting concentrations/doses, more efforts (such as more *in-vivo* models, combinations, and certain rescue experiments) are needed to fill the blanks to obtain a full view (**Figure 2**). As per the reported studies, ropivacaine appears to be a multi-target or multi-functional compound. Under clinical relevant (achievable) concentrations/doses, it exerts anti-metastatic, anti-CSCs *via* regulating sodium channel, anti-inflammatory function and signaling pathways that regulate these two and other associated pathways, leading to the inhibition of signaling transduction which may contribute in the metastasis and maintenance of CSCs (94). Under multiple-fold of clinical-achievable concentrations/doses, ropivacaine is able to kill cancer cells by suppressing key players (proteins or signal pathways) in prompting cancer cells growth, proliferation and migration, including those key proteins in regulating cell cycle, apoptosis, mRNA, epigenetics, autophagy, etc. (64, 116).

It's noteworthy that ropivacaine appears to exert its anticancer effects *via* the regulation of ITGα2 and/or members of Ras superfamily, because in the original studies, two pivotal experiments, such as the overexpression of ITGα2 (49) or the co-treatment of calpeptin, an activator of Ras and Rho (44), although other pathways can't be excluded. Another interesting thing is among all affected pathways, several of them are membrane-associated proteins, such as NaV1.5 VGSC, as well as ITG members, indicating that ropivacaine might preferably attack membrane proteins which require further investigations. Again, future studies of the direct interaction between associated proteins and ropivacaine are warranted, which may help finally explain and identify its exact targets/mechanisms.

## CONCLUSIONS

Ropivacaine exerts anticancer and chemotherapeutic re-sensitizing effects, showing potentials in benefiting certain cancer patients. Further studies are warranted to explore the mechanisms, combinations and indications.

## AUTHOR CONTRIBUTIONS

PX conceived the idea. PX, SZ, LT, and LW wrote the manuscript. PX, SZ, and JL revised the manuscript. All authors read and approved the final manuscript.

## REFERENCES

1. Assaraf YG, Brozovic A, Goncalves AC, Jurkovicova D, Line A, Machuqueiro M, et al. The Multi-Factorial Nature of Clinical Multidrug Resistance in Cancer. *Drug Resist Updat* (2019) 46:100645. doi: 10.1016/j.drup.2019.100645
2. Cui Q, Wang JQ, Assaraf YG, Ren L, Gupta P, Wei L, et al. Modulating ROS to Overcome Multidrug Resistance in Cancer. *Drug Resist Updat* (2018) 41:1–25. doi: 10.1016/j.drup.2018.11.001
3. Mahvi DA, Liu R, Grinstaff MW, Colson YL, Raut CP. Local Cancer Recurrence: The Realities, Challenges, and Opportunities for New Therapies. *CA Cancer J Clin* (2018) 68(6):488–505. doi: 10.3322/caac.21498

4. Zugazagoitia J, Guedes C, Ponce S, Ferrer I, Molina-Pinelo S, Paz-Ares L. Current Challenges in Cancer Treatment. *Clin Ther* (2016) 38(7):1551–66. doi: 10.1016/j.clinthera.2016.03.026
5. Takebe T, Imai R, Ono S. The Current Status of Drug Discovery and Development as Originated in United States Academia: The Influence of Industrial and Academic Collaboration on Drug Discovery and Development. *Clin Transl Sci* (2018) 11(6):597–606. doi: 10.1111/cts.12577
6. Munos B. Lessons From 60 Years of Pharmaceutical Innovation. *Nat Rev Drug Discov* (2009) 8(12):959–68. doi: 10.1038/nrd2961
7. Berdigaliyev N, Aljofan M. An Overview of Drug Discovery and Development. *Future Med Chem* (2020) 12(10):939–47. doi: 10.4155/fmc-2019-0307
8. Huang J. Can Drug Repositioning Work as a Systematical Business Model? *ACS Med Chem Lett* (2020) 11(6):1074–75. doi: 10.1021/acsmedchemlett.0c00122
9. Duggirala NK, Perry ML, Almarsson O, Zaworotko MJ. Pharmaceutical Cocrystals: Along the Path to Improved Medicines. *Chem Commun (Camb)* (2016) 52(4):640–55. doi: 10.1039/C5CC08216A
10. Cui Q, Yang DH, Chen ZS. Special Issue: Natural Products: Anticancer and Beyond. *Molecules* (2018) 23(6):1246–49. doi: 10.3390/molecules23061246
11. Zhou D, Wang L, Cui Q, Iftikhar R, Xia Y, Xu P. Repositioning Lidocaine as an Anticancer Drug: The Role Beyond Anesthesia. *Front Cell Dev Biol* (2020) 8:565/full. doi: 10.3389/fcell.2020.00565/full
12. Mak KK, Pichika MR. Artificial Intelligence in Drug Development: Present Status and Future Prospects. *Drug Discov Today* (2019) 24(3):773–80. doi: 10.1016/j.drudis.2018.11.014
13. Dinic J, Efferth T, Garcia-Sosa AT, Grahovac J, Padron JM, Pajeva I, et al. Repurposing Old Drugs to Fight Multidrug Resistant Cancers. *Drug Resist Updat* (2020) 52:100713. doi: 10.1016/j.drup.2020.100713
14. Krchniakova M, Skoda J, Neradil J, Chlapek P, Veselska R. Repurposing Tyrosine Kinase Inhibitors to Overcome Multidrug Resistance in Cancer: A Focus on Transporters and Lysosomal Sequestration. *Int J Mol Sci* (2020) 21(9):3157–75. doi: 10.3390/ijms21093157
15. Fan YF, Zhang W, Zeng L, Lei ZN, Cai CY, Gupta P, et al. Dacomitinib Antagonizes Multidrug Resistance (MDR) in Cancer Cells by Inhibiting The Efflux Activity of ABCB1 and ABCG2 Transporters. *Cancer Lett* (2018) 421:186–98. doi: 10.1016/j.canlet.2018.01.021
16. Parvathaneni V, Kulkarni NS, Muth A, Gupta V. Drug Repurposing: A Promising Tool to Accelerate the Drug Discovery Process. *Drug Discov Today* (2019) 24(10):2076–85. doi: 10.1016/j.drudis.2019.06.014
17. Polamreddy P, Gattu N. The Drug Repurposing Landscape From 2012 to 2017: Evolution, Challenges, and Possible Solutions. *Drug Discov Today* (2019) 24(3):789–95. doi: 10.1016/j.drudis.2018.11.022
18. Cui Q, Cai CY, Gao HL, Ren L, Ji N, Gupta P, et al. Glesatinib, a C-MET/SMO Dual Inhibitor, Antagonizes P-Glycoprotein Mediated Multidrug Resistance in Cancer Cells. *Front Oncol* (2019) 9:313. doi: 10.3389/fonc.2019.00313
19. Pushpakom S, Iorio F, Eyers PA, Escott KJ, Hopper S, Wells A, et al. Drug Repurposing: Progress, Challenges and Recommendations. *Nat Rev Drug Discov* (2018) 18(1):41–58. doi: 10.1038/nrd.2018.168
20. Zhang Z, Zhou L, Xie N, Nice EC, Zhang T, Cui Y, et al. Overcoming Cancer Therapeutic Bottleneck by Drug Repurposing. *Signal Transduct Target Ther* (2020) 5(1):113. doi: 10.1038/s41392-020-00213-8
21. Cui Q, Cai CY, Wang JQ, Zhang S, Gupta P, Ji N, et al. Chk1 Inhibitor MK-8776 Restores the Sensitivity of Chemotherapeutics in P-Glycoprotein Overexpressing Cancer Cells. *Int J Mol Sci* (2019) 20(17):4095–106. doi: 10.3390/ijms20174095
22. Siekmann W, Tina E, Von Sydow AK, Gupta A. Effect of Lidocaine and Ropivacaine on Primary (SW480) and Metastatic (SW620) Colon Cancer Cell Lines. *Oncol Lett* (2019) 18(1):395–401. doi: 10.3892/ol.2019.10332
23. Lynch CR. Local Anesthetics as...Cancer Therapy? *Anesth Analg* (2018) 127(3):601–02. doi: 10.1213/ANE.0000000000003659
24. Liu H, Dilger JP, Lin J. Effects of Local Anesthetics on Cancer Cells. *Pharmacol Ther* (2020) 212:107558. doi: 10.1016/j.pharmthera.2020.107558
25. Sun H, Sun Y. Lidocaine Inhibits Proliferation and Metastasis of Lung Cancer Cell. *via Regul miR-539/EGFR axis Artif Cells Nanomed Biotechnol* (2019) 47(1):2866–74. doi: 10.1080/21691401.2019.1636807
26. Chen J, Jiao Z, Wang A, Zhong W. Lidocaine Inhibits Melanoma Cell Proliferation by Regulating ERK Phosphorylation. *J Cell Biochem* (2019) 120(4):6402–08. doi: 10.1002/jcb.27927
27. Gao J, Hu H, Wang X. Clinically Relevant Concentrations of Lidocaine Inhibit Tumor Angiogenesis Through Suppressing VEGF/VEGFR2 Signaling. *Cancer Chemother Pharmacol* (2019) 83(6):1007–15. doi: 10.1007/s00280-019-03815-4
28. Li C, Gao S, Li X, Li C, Ma L. Procaine Inhibits the Proliferation and Migration of Colon Cancer Cells Through Inactivation of the ERK/MAPK/FAK Pathways by Regulation of RhoA. *Oncol Res* (2018) 26(2):209–17. doi: 10.3727/096504017X14944585873622
29. Li YC, Wang Y, Li DD, Zhang Y, Zhao TC, Li CF. Procaine Is a Specific DNA Methylation Inhibitor With Anti-Tumor Effect for Human Gastric Cancer. *J Cell Biochem* (2018) 119(2):2440–49. doi: 10.1002/jcb.26407
30. Ma XW, Li Y, Han XC, Xin QZ. The Effect of Low Dosage of Procaine on Lung Cancer Cell Proliferation. *Eur Rev Med Pharmacol Sci* (2016) 20(22):4791–95.
31. Wang W, Zhu M, Xu Z, Li W, Dong X, Chen Y, et al. Ropivacaine Promotes Apoptosis of Hepatocellular Carcinoma Cells Through Damaging Mitochondria and Activating Caspase-3 Activity. *Biol Res* (2019) 52(1):36. doi: 10.1186/s40659-019-0242-7
32. Yang J, Li G, Bao K, Liu W, Zhang Y, Ting W. Ropivacaine Inhibits Tumor Angiogenesis *via* Sodium-Channel-Independent Mitochondrial Dysfunction and Oxidative Stress. *J Bioenerg Biomembr* (2019) 51(3):231–38. doi: 10.1007/s10863-019-09793-9
33. Gong X, Dan J, Li F, Wang L. Suppression of Mitochondrial Respiration With Local Anesthetic Ropivacaine Targets Breast Cancer Cells. *J Thorac Dis* (2018) 10(5):2804–12. doi: 10.21037/jtd.2018.05.21
34. Piegeler T, Schlapfer M, Dull RO, Schwartz DE, Borgeat A, Minshall RD, et al. Clinically Relevant Concentrations of Lidocaine and Ropivacaine Inhibit TNFalpha-Induced Invasion of Lung Adenocarcinoma Cells *In Vitro* by Blocking the Activation of Akt and Focal Adhesion Kinase. *Br J Anaesth* (2015) 115(5):784–91. doi: 10.1093/bja/aev341
35. Zhu G, Zhang L, Dan J, Zhu Q. Differential Effects and Mechanisms of Local Anesthetics on Esophageal Carcinoma Cell Migration, Growth, Survival and Chemosensitivity. *BMC Anesthesiol* (2020) 20(1):126. doi: 10.1186/s12871-020-01039-1
36. Dan J, Gong X, Li D, Zhu G, Wang L, Li F. Inhibition of Gastric Cancer by Local Anesthetic Bupivacaine Through Multiple Mechanisms Independent of Sodium Channel Blockade. *Biomed Pharmacother* (2018) 103:823–28. doi: 10.1016/j.biopha.2018.04.106
37. Xuan W, Zhao H, Hankin J, Chen L, Yao S, Ma D. Local Anesthetic Bupivacaine Induced Ovarian and Prostate Cancer Apoptotic Cell Death and Underlying Mechanisms *In Vitro*. *Sci Rep* (2016) 6:26277. doi: 10.1038/srep26277
38. Li T, Chen L, Zhao H, Wu L, Masters J, Han C, et al. And Ma D.: Both Bupivacaine and Levobupivacaine Inhibit Colon Cancer Cell Growth But Not Melanoma Cells *In Vitro*. *J Anesth* (2019) 33(1):17–25. doi: 10.1007/s00540-018-2577-6
39. Jose C, Hebert-Chatelain E, Dias AN, Roche E, Obre E, Lacombe D, et al. And Rossignol R.: Redox Mechanism of Levobupivacaine Cytostatic Effect on Human Prostate Cancer Cells. *Redox Biol* (2018) 18:33–42. doi: 10.1016/j.redox.2018.05.014
40. Hansen TG. Ropivacaine: A Pharmacological Review. *Expert Rev Neurother* (2004) 4(5):781–91. doi: 10.1586/14737175.4.5.781
41. Casati A, Santorsola R, Cerchierini E, Moizo E. Ropivacaine. *Minerva Anestesiol* (2001) 67(9 Suppl 1):15–9.
42. Graf BM, Abraham I, Eberbach N, Kunst G, Stowe DF, Martin E. Differences in Cardiotoxicity of Bupivacaine and Ropivacaine Are the Result of Physicochemical and Stereoselective Properties. *Anesthesiol* (2002) 96(6):1427–34. doi: 10.1097/00000542-200206000-00023
43. Leone S, Di Cianni S, Casati A, Fanelli G. Pharmacology, Toxicology, and Clinical Use of New Long Acting Local Anesthetics, Ropivacaine and Levobupivacaine. *Acta Biomed* (2008) 79(2):92–105.
44. Zheng Q, Peng X, Zhang Y. Cytotoxicity of Amide-Linked Local Anesthetics on Melanoma Cells *via* Inhibition of Ras and RhoA Signaling Independent of Sodium Channel Blockade. *BMC Anesthesiol* (2020) 20(1):43. doi: 10.1186/s12871-020-00957-4

45. Phuyal S, Farhan H. Multifaceted Rho GTPase Signaling at the Endomembranes. *Front Cell Dev Biol* (2019) 7:127. doi: 10.3389/fcell.2019.00127
46. Qu L, Pan C, He SM, Lang B, Gao GD, Wang XL, et al. The Ras Superfamily of Small GTPases in Non-Neoplastic Cerebral Diseases. *Front Mol Neurosci* (2019) 12:121. doi: 10.3389/fnmol.2019.00121
47. Adorno-Cruz V, Liu H. Regulation and Functions of Integrin Alpha2 in Cell Adhesion and Disease. *Genes Dis* (2019) 6(1):16–24. doi: 10.1016/j.gendis.2018.12.003
48. Ren D, Zhao J, Sun Y, Li D, Meng Z, Wang B, et al. Overexpressed ITGA2 Promotes Malignant Tumor Aggression by Up-Regulating PD-L1 Expression Through the Activation of the STAT3 Signaling Pathway. *J Exp Clin Cancer Res* (2019) 38(1):485. doi: 10.1186/s13046-019-1496-1
49. Qin A, Liu Q, Wang J. Ropivacaine Inhibits Proliferation, Invasion, Migration and Promotes Apoptosis of Papillary Thyroid Cancer Cells *via* Regulating ITGA2 Expression. *Drug Dev Res* (2020) 81(6):700–7. doi: 10.1002/ddr.21671
50. Wang X, Li T. Ropivacaine Inhibits the Proliferation and Migration of Colorectal Cancer Cells Through ITGB1. *Bioengineered* (2021) 12(1):44–53. doi: 10.1080/21655979.2020.1857120
51. Yeldag G, Rice A, Del RHA. Chemoresistance and the Self-Maintaining Tumor Microenvironment. *Cancers (Basel)* (2018) 10(12):471–503. doi: 10.3390/cancers10120471
52. Prieto-Vila M, Takahashi RU, Usuba W, Kohama I, Ochiya T. Drug Resistance Driven by Cancer Stem Cells and Their Niche. *Int J Mol Sci* (2017) 18(12):2574–95. doi: 10.3390/ijms18122574
53. Suresh R, Ali S, Ahmad A, Philip PA, Sarkar FH. The Role of Cancer Stem Cells in Recurrent and Drug-Resistant Lung Cancer. *Adv Exp Med Biol* (2016) 890:57–74. doi: 10.1007/978-3-319-24932-2_4
54. Pai SG, Carneiro BA, Mota JM, Costa R, Leite CA, Barroso-Sousa R, et al. Wnt/beta-Catenin Pathway: Modulating Anticancer Immune Response. *J Hematol Oncol* (2017) 10(1):101. doi: 10.1186/s13045-017-0471-6
55. Li X, Xiang Y, Li F, Yin C, Li B, Ke X. WNT/beta-Catenin Signaling Pathway Regulating T Cell-Inflammation in the Tumor Microenvironment. *Front Immunol* (2019) 10:2293. doi: 10.3389/fimmu.2019.02293
56. Ni J, Xie T, Xiao M, Xiang W, Wang L. Amide-Linked Local Anesthetics Preferentially Target Leukemia Stem Cell Through Inhibition of Wnt/beta-Catenin. *Biochem Biophys Res Commun* (2018) 503(2):956–62. doi: 10.1016/j.bbrc.2018.06.102
57. Gao L, Jauregui CE, Teng Y. Targeting Autophagy as a Strategy for Drug Discovery and Therapeutic Modulation. *Future Med Chem* (2017) 9(3):335–45. doi: 10.4155/fmc-2016-0210
58. Mathiassen SG, De Zio D, Cecconi F. Autophagy and the Cell Cycle: A Complex Landscape. *Front Oncol* (2017) 7:51. doi: 10.3389/fonc.2017.00051
59. Yun CW, Lee SH. The Roles of Autophagy in Cancer. *Int J Mol Sci* (2018) 19(11):3466–83. doi: 10.3390/ijms19113466
60. Zhang J, Zhu S, Tan Q, Cheng D, Dai Q, Yang Z, et al. Combination Therapy With Ropivacaine-Loaded Liposomes and Nutrient Deprivation for Simultaneous Cancer Therapy and Cancer Pain Relief. *Theranostics* (2020) 10(11):4885–99. doi: 10.7150/thno.43932
61. Carneiro BA, El-Deiry WS. Targeting Apoptosis in Cancer Therapy. *Nat Rev Clin Oncol* (2020) 17(7):395–417. doi: 10.1038/s41571-020-0341-y
62. Shahar N, Larisch S. Inhibiting the Inhibitors: Targeting Anti-Apoptotic Proteins in Cancer and Therapy Resistance. *Drug Resist Updat* (2020) 52:100712. doi: 10.1016/j.drup.2020.100712
63. Otto T, Sicinski P. Cell Cycle Proteins as Promising Targets in Cancer Therapy. *Nat Rev Cancer* (2017) 17(2):93–115. doi: 10.1038/nrc.2016.138
64. Visconti R, Della MR, Grieco D. Cell Cycle Checkpoint in Cancer: A Therapeutically Targetable Double-Edged Sword. *J Exp Clin Cancer Res* (2016) 35(1):153. doi: 10.1186/s13046-016-0433-9
65. Castelli V, Piroli A, Marinangeli F, D'Angelo M, Benedetti E, Ippoliti R, et al. Local Anesthetics Counteract Cell Proliferation and Migration of Human Triple-Negative Breast Cancer and Melanoma Cells. *J Cell Physiol* (2020) 235(4):3474–84. doi: 10.1002/jcp.29236
66. Wang HW, Wang LY, Jiang L, Tian SM, Zhong TD, Fang XM. Amide-Linked Local Anesthetics Induce Apoptosis in Human Non-Small Cell Lung Cancer. *J Thorac Dis* (2016) 8(10):2748–57. doi: 10.21037/jtd.2016.09.66
67. Abate M, Festa A, Falco M, Lombardi A, Luce A, Grimaldi A, et al. Mitochondria as Playmakers of Apoptosis, Autophagy and Senescence. *Semin Cell Dev Biol* (2019) 98:139–53. doi: 10.1016/j.semcdb.2019.05.022
68. Le Gac G, Angenard G, Clement B, Laviolle B, Coulouarn C, Beloeil H. Local Anesthetics Inhibit the Growth of Human Hepatocellular Carcinoma Cells. *Anesth Analg* (2017) 125(5):1600–09. doi: 10.1213/ANE.0000000000002429
69. Cui Q, Wen S, Huang P. Targeting Cancer Cell Mitochondria as a Therapeutic Approach: Recent Updates. *Future Med Chem* (2017) 9(9):929–49. doi: 10.4155/fmc-2017-0011
70. Supinski GS, Schroder EA, Callahan LA. Mitochondria and Critical Illness. *Chest* (2019) 157(2):310–22. doi: 10.1016/j.chest.2019.08.2182
71. Pittenger MF, Discher DE, Peault BM, Phinney DG, Hare JM, Caplan AI. Mesenchymal Stem Cell Perspective: Cell Biology to Clinical Progress. *NPJ Regener Med* (2019) 4:22. doi: 10.1038/s41536-019-0083-6
72. Abdal DA, Lee SB, Kim K, Lim KM, Jeon TI, Seok J, et al. Production of Mesenchymal Stem Cells Through Stem Cell Reprogramming. *Int J Mol Sci* (2019) 20(8):1922–63. doi: 10.3390/ijms20081922
73. Wang W, Zhu M, Xu Z, Li W, Dong X, Chen Y, et al. Ropivacaine Promotes Apoptosis of Hepatocellular Carcinoma Cells Through Damaging Mitochondria and Activating Caspase-3 Activity. *Biol Res* (2019) 52(1):36. doi: 10.1186/s40659-019-0242-7
74. Yang J, Li G, Bao K, Liu W, Zhang Y, Ting W. Ropivacaine Inhibits Tumor Angiogenesis *via* Sodium-Channel-Independent Mitochondrial Dysfunction and Oxidative Stress. *J Bioenerg Biomembr* (2019) 51(3):231–38. doi: 10.1007/s10863-019-09793-9
75. Gong X, Dan J, Li F, Wang L. Suppression of Mitochondrial Respiration With Local Anesthetic Ropivacaine Targets Breast Cancer Cells. *J Thorac Dis* (2018) 10(5):2804–12. doi: 10.21037/jtd.2018.05.21
76. Chan TS, Shaked Y, Tsai KK. Targeting the Interplay Between Cancer Fibroblasts, Mesenchymal Stem Cells, and Cancer Stem Cells in Desmoplastic Cancers. *Front Oncol* (2019) 9:688. doi: 10.3389/fonc.2019.00688
77. Lucchinetti E, Awad AE, Rahman M, Feng J, Lou PH, Zhang L, et al. Antiproliferative Effects of Local Anesthetics on Mesenchymal Stem Cells: Potential Implications for Tumor Spreading and Wound Healing. *Anesthesiol* (2012) 116(4):841–56. doi: 10.1097/ALN.0b013e31824babfe
78. Wortzel I, Seger R. The ERK Cascade: Distinct Functions Within Various Subcellular Organelles. *Genes Cancer* (2011) 2(3):195–209. doi: 10.1177/1947601911407328
79. Kidger AM, Sipthorp J, Cook SJ. ERK1/2 Inhibitors: New Weapons to Inhibit the RAS-Regulated RAF-MEK1/2-ERK1/2 Pathway. *Pharmacol Ther* (2018) 187:45–60. doi: 10.1016/j.pharmthera.2018.02.007
80. Yang W, Cai J, Zhang H, Wang G, Jiang W. Effects of Lidocaine and Ropivacaine on Gastric Cancer Cells Through Down-Regulation of ERK1/2 Phosphorylation *In Vitro*. *Anticancer Res* (2018) 38(12):6729–35. doi: 10.21873/anticanres.13042
81. Xu C, Zhang W, Liu S, Wu W, Qin M, Huang J. Activation of the SphK1/ERK/p-ERK Pathway Promotes Autophagy in Colon Cancer Cells. *Oncol Lett* (2018) 15(6):9719–24. doi: 10.3892/ol.2018.8588
82. Melo-Lima S, Lopes MC, Mollinedo F. ERK1/2 Acts as a Switch Between Necrotic and Apoptotic Cell Death in Ether Phospholipid Edelfosine-Treated Glioblastoma Cells. *Pharmacol Res* (2015) 95-96:2–11. doi: 10.1016/j.phrs.2015.02.007
83. Lu Y, Liu B, Liu Y, Yu X, Cheng G. Dual Effects of Active ERK in Cancer: A Potential Target for Enhancing Radiosensitivity. *Oncol Lett* (2020) 20(2):993–1000. doi: 10.3892/ol.2020.11684
84. Ors-Kumoglu G, Gulce-Iz S, Biray-Avci C. Therapeutic microRNAs in Human Cancer. *Cytotechnol* (2019) 71(1):411–25. doi: 10.1007/s10616-018-0291-8
85. Zhang N, Xing X, Gu F, Zhou G, Liu X, Li B. Ropivacaine Inhibits the Growth, Migration and Invasion of Gastric Cancer Through Attenuation of WEE1 and PI3K/AKT Signaling *via* miR-520a-3p. *Onco Targets Ther* (2020) 13:5309–21. doi: 10.2147/OTT.S244550
86. Zhao L, Han S, Hou J, Shi W, Zhao Y, Chen Y. The Local Anesthetic Ropivacaine Suppresses Progression of Breast Cancer by Regulating miR-27b-3p/YAP Axis. *Aging (Albany NY)* (2021) 13(12):16341–52. doi: 10.18632/aging.203160

87. Sherpa C, Rausch JW, Le Grice SF. Structural Characterization of Maternally Expressed Gene 3 RNA Reveals Conserved Motifs and Potential Sites of Interaction With Polycomb Repressive Complex 2. *Nucleic Acids Res* (2018) 46(19):10432–47. doi: 10.1093/nar/gky722
88. Huynh J, Chand A, Gough D, Ernst M. Therapeutically Exploiting STAT3 Activity in Cancer - Using Tissue Repair as a Road Map. *Nat Rev Cancer* (2019) 19(2):82–96. doi: 10.1038/s41568-018-0090-8
89. Chen X, Liu W, Guo X, Huang S, Song X. Ropivacaine Inhibits Cervical Cancer Cell Growth *via* Suppression of the Mir96/MEG2/pSTAT3 Axis. *Oncol Rep* (2020) 43(5):1659–68. doi: 10.3892/or.2020.7521
90. Peery R, Kyei-Baffour K, Dong Z, Liu J, de Andrade HP, Dai M, et al. Synthesis and Identification of a Novel Lead Targeting Survivin Dimerization for Proteasome-Dependent Degradation. *J Med Chem* (2020) 63(1):7243–51. doi: 10.1021/acs.jmedchem.0c00475
91. Peery RC, Liu JY, Zhang JT. Targeting Survivin for Therapeutic Discovery: Past, Present, and Future Promises. *Drug Discov Today* (2017) 22(10):1466–77. doi: 10.1016/j.drudis.2017.05.009
92. Roger S, Gillet L, Le Guennec JY, Besson P. Voltage-Gated Sodium Channels and Cancer: Is Excitability Their Primary Role? *Front Pharmacol* (2015) 6:152. doi: 10.3389/fphar.2015.00152
93. Mao W, Zhang J, Korner H, Jiang Y, Ying S. The Emerging Role of Voltage-Gated Sodium Channels in Tumor Biology. *Front Oncol* (2019) 9:124. doi: 10.3389/fonc.2019.00124
94. Nelson M, Yang M, Millican-Slater R, Brackenbury WJ. Nav1.5 Regulates Breast Tumor Growth and Metastatic Dissemination *In Vivo*. *Oncotarget* (2015) 6(32):32914–29. doi: 10.18632/oncotarget.5441
95. Peng J, Ou Q, Wu X, Zhang R, Zhao Q, Jiang W, et al. Expression of Voltage-Gated Sodium Channel Nav1.5 in Non-Metastatic Colon Cancer and Its Associations With Estrogen Receptor (ER)-Beta Expression and Clinical Outcomes. *Chin J Cancer* (2017) 36(1):89. doi: 10.1186/s40880-017-0253-0
96. Djamgoz M, Fraser SP, Brackenbury WJ. *In Vivo* Evidence for Voltage-Gated Sodium Channel Expression in Carcinomas and Potentiation of Metastasis. *Cancers (Basel)* (2019) 11(11):1675–94. doi: 10.3390/cancers11111675
97. Baptista-Hon DT, Robertson FM, Robertson GB, Owen SJ, Rogers GW, Lydon EL, et al. Potent Inhibition by Ropivacaine of Metastatic Colon Cancer SW620 Cell Invasion and NaV1.5 Channel Function. *Br J Anaesth* (2014) 113(Suppl 1):i39–48. doi: 10.1093/bja/aeu104
98. Arlock P. Actions of Three Local Anaesthetics: Lidocaine, Bupivacaine and Ropivacaine on Guinea Pig Papillary Muscle Sodium Channels (Vmax). *Pharmacol Toxicol* (1988) 63(2):96–104. doi: 10.1111/j.1600-0773.1988.tb00918.x
99. Koltai T. Voltage-Gated Sodium Channel as a Target for Metastatic Risk Reduction With Re-Purposed Drugs. *F1000Res* (2015) 4:297. doi: 10.12688/f1000research.6789.1
100. Zhang Y, Peng X, Zheng Q. Ropivacaine Inhibits the Migration of Esophageal Cancer Cells *via* Sodium-Channel-Independent But Prenylation-Dependent Inhibition of Rac1/JNK/Paxillin/FAK. *Biochem Biophys Res Commun* (2018) 501(4):1074–79. doi: 10.1016/j.bbrc.2018.05.110
101. Huang H. Matrix Metalloproteinase-9 (MMP-9) as a Cancer Biomarker and MMP-9 Biosensors: Recent Advances. *Sensors (Basel)* (2018) 18(10):3249–67. doi: 10.3390/s18103249
102. Zarkesh M, Zadeh-Vakili A, Akbarzadeh M, Fanaei SA, Hedayati M, Azizi F. The Role of Matrix Metalloproteinase-9 as a Prognostic Biomarker in Papillary Thyroid Cancer. *BMC Cancer* (2018) 18(1):1199. doi: 10.1186/s12885-018-5112-0
103. Barillari G. The Impact of Matrix Metalloproteinase-9 on the Sequential Steps of the Metastatic Process. *Int J Mol Sci* (2020) 21(12):4526–53. doi: 10.3390/ijms21124526
104. Piegeler T, Schlapfer M, Dull RO, Schwartz DE, Borgeat A, Minshall RD, et al. Clinically Relevant Concentrations of Lidocaine and Ropivacaine Inhibit TNFalpha-Induced Invasion of Lung Adenocarcinoma Cells *In Vitro* by Blocking the Activation of Akt and Focal Adhesion Kinase. *Br J Anaesth* (2015) 115(5):784–91. doi: 10.1093/bja/aev341
105. Xia L, Tan S, Zhou Y, Lin J, Wang H, Oyang L, et al. Role of the NFkappaB-Signaling Pathway in Cancer. *Onco Targets Ther* (2018) 11:2063–73. doi: 10.2147/OTT.S161109
106. Dixon GL, Heyderman RS, van der Ley P, Klein NJ. High-Level Endothelial E-Selectin (CD62E) Cell Adhesion Molecule Expression by a Lipopolysaccharide-Deficient Strain of Neisseria Meningitidis Despite Poor Activation of NF-kappaB Transcription Factor. *Clin Exp Immunol* (2004) 135(1):85–93. doi: 10.1111/j.1365-2249.2004.02335.x
107. Su Z, Huang P, Ye X, Huang S, Li W, Yan Y, et al. Ropivacaine *via* Nuclear Factor Kappa B Signalling Modulates CD62E Expression and Diminishes Tumour Cell Arrest. *J Anesth* (2019) 33(6):685–93. doi: 10.1007/s00540-019-02699-1
108. Jassam SA, Maherally Z, Smith JR, Ashkan K, Roncaroli F, Fillmore HL, et al. CD15s/CD62E Interaction Mediates the Adhesion of Non-Small Cell Lung Cancer Cells on Brain Endothelial Cells: Implications for Cerebral Metastasis. *Int J Mol Sci* (2017) 18(7):1474–89. doi: 10.3390/ijms18071474
109. Kulis M, Esteller M. DNA Methylation and Cancer. *Adv Genet* (2010) 70:27–56. doi: 10.1016/B978-0-12-380866-0.60002-2
110. Giri AK, Aittokallio T. DNMT Inhibitors Increase Methylation in the Cancer Genome. *Front Pharmacol* (2019) 10:385. doi: 10.3389/fphar.2019.00385
111. Lirk P, Hollmann MW, Fleischer M, Weber NC. And Fiegl H.: Lidocaine and Ropivacaine, But Not Bupivacaine, Demethylate Deoxyribonucleic Acid in Breast Cancer Cells In Vitro. *Br J Anaesth* (2014) 113(Suppl 1):i32–38. doi: 10.1093/bja/aeu201
112. Chen W, Xu Y, Zhang Y, Lou W, Han X. Positive Impact of Intraoperative Epidural Ropivacaine Infusion on Oncologic Outcomes in Pancreatic Cancer Patients Undergoing Pancreatectomy: A Retrospective Cohort Study. *J Cancer* (2021) 12(15):4513–21. doi: 10.7150/jca.57661
113. Zhu R, Du T, Gao H. Effects of Dezocine and Ropivacaine Infiltration Anesthesia on Cellular Immune Function Indicators, Anesthesia Recovery Time and Pain Factors in Patients With Open Liver Resection. *Cell Mol Biol (Noisy-le-grand)* (2020) 66(3):149–54. doi: 10.14715/cmb/2020.66.3.23
114. Hayden JM, Oras J, Block L, Thorn SE, Palmqvist C, Salehi S, et al. Intraperitoneal Ropivacaine Reduces Time Interval to Initiation of Chemotherapy After Surgery for Advanced Ovarian Cancer: Randomised Controlled Double-Blind Pilot Study. *Br J Anaesth* (2020) 124(5):562–70. doi: 10.1016/j.bja.2020.01.026
115. Yao Y, Li J, Hu H, Xu T, Chen Y. Ultrasound-Guided Serratus Plane Block Enhances Pain Relief and Quality of Recovery After Breast Cancer Surgery: A Randomised Controlled Trial. *Eur J Anaesthesiol* (2019) 36(6):436–41. doi: 10.1097/EJA.0000000000001004
116. Wang Y, Cheng J, Yang L, Wang J, Liu H, Lv Z. Ropivacaine for Intercostal Nerve Block Improves Early Postoperative Cognitive Dysfunction in Patients Following Thoracotomy for Esophageal Cancer. *Med Sci Monit* (2019) 25:460–65. doi: 10.12659/MSM.912328
117. MacFater WS, Xia W, Barazanchi A, MacFater HS, Lightfoot N, Svirskis D, et al. Association Between Perioperative Intraperitoneal Local Anaesthetic Infusion and Long-Term Survival and Cancer Recurrence After Colectomy: Follow-Up Analysis of a Previous Randomized Controlled Trial. *ANZ J Surg* (2020) 90(5):802–06. doi: 10.1111/ans.15753
118. Li R, Xiao C, Liu H, Huang Y, Dilger JP, Lin J. Effects of Local Anesthetics on Breast Cancer Cell Viability and Migration. *BMC Cancer* (2018) 18(1):666. doi: 10.1186/s12885-018-4576-2


**Conflict of Interest:** The authors declare that the research was conducted in the absence of any commercial or financial relationships that could be construed as a potential conflict of interest.

**Publisher's Note:** All claims expressed in this article are solely those of the authors and do not necessarily represent those of their affiliated organizations, or those of the publisher, the editors and the reviewers. Any product that may be evaluated in this article, or claim that may be made by its manufacturer, is not guaranteed or endorsed by the publisher.

frontiers in Pharmacology

ORIGINAL RESEARCH
published: 23 February 2022
doi: 10.3389/fphar.2022.843829

# Overexpression of ABCB1 Associated With the Resistance to the KRAS-G12C Specific Inhibitor ARS-1620 in Cancer Cells

*Xing-Duo Dong[1†], Meng Zhang[2†], Chao-Yun Cai[1], Qiu-Xu Teng[1], Jing-Quan Wang[1], Yi-Ge Fu[1], Qingbin Cui[1,3], Ketankumar Patel[1], Dong-Tao Wang[2,4]* and Zhe-Sheng Chen[1]**

[1]Department of Pharmaceutical Sciences, College of Pharmacy and Health Sciences, St. John's University, Queens, NY, United States, [2]Department of Traditional Chinese Medicine, Shenzhen Hospital, Southern Medical University, Shenzhen, China, [3]School of Public Health, Guangzhou Medical University, Guangzhou, China, [4]Department of the Ministry of Science and Technology, Guangxi International Zhuang Medicine Hospital, Nanning, China

OPEN ACCESS

**Edited by:**
Daotai Nie,
Southern Illinois University Carbondale, United States

**Reviewed by:**
Zhi-hang Zhou,
Chongqing Medical University, China
Zhihui Song,
Fox Chase Cancer Center, United States
Shuang Fan,
University Medical Center Göttingen, Germany
Sihe Zhang,
Nankai University, China

***Correspondence:**
Dong-Tao Wang
95401864@qq.com
Zhe-Sheng Chen
chenz@stjohns.edu

†These authors have contributed equally to this work

**Specialty section:**
This article was submitted to Pharmacology of Anti-Cancer Drugs, a section of the journal Frontiers in Pharmacology

**Received:** 27 December 2021
**Accepted:** 08 February 2022
**Published:** 23 February 2022

**Citation:**
Dong X-D, Zhang M, Cai C-Y, Teng Q-X, Wang J-Q, Fu Y-G, Cui Q, Patel K, Wang D-T and Chen Z-S (2022) Overexpression of ABCB1 Associated With the Resistance to the KRAS-G12C Specific Inhibitor ARS-1620 in Cancer Cells. Front. Pharmacol. 13:843829. doi: 10.3389/fphar.2022.843829

The KRAS-G12C inhibitor ARS-1620, is a novel specific covalent inhibitor of KRAS-G12C, possessing a strong targeting inhibitory effect on KRAS-G12C mutant tumors. Overexpression of ATP-binding cassette super-family B member 1 (ABCB1/P-gp) is one of the pivotal factors contributing to multidrug resistance (MDR), and its association with KRAS mutations has been extensively studied. However, the investigations about the connection between the inhibitors of mutant KRAS and the level of ABC transporters are still missing. In this study, we investigated the potential drug resistance mechanism of ARS-1620 associated with ABCB1. The desensitization effect of ARS-1620 was remarkably intensified in both drug-induced ABCB1-overexpressing cancer cells and ABCB1-transfected cells as confirmed by cell viability assay results. This desensitization of ARS-1620 could be completely reversed when co-treated with an ABCB1 reversal agent. In mechanism-based studies, [$^3$H] -paclitaxel accumulation assay revealed that ARS-1620 could be competitively pumped out by ABCB1. Additionally, it was found that ARS-1620 remarkably stimulated ATPase activity of ABCB1, and the HPLC drug accumulation assay displayed that ARS-1620 was actively transported out of ABCB1-overexpressing cancer cells. ARS-1620 acquired a high docking score in computer molecular docking analysis, implying ARS-1620 could intensely interact with ABCB1 transporters. Taken all together, these data indicated that ARS-1620 is a substrate for ABCB1, and the potential influence of ARS-1620-related cancer therapy on ABCB1-overexpressing cancer cells should be considered in future clinical applications.

**Keywords: ARS-1620, KRAS-G12C inhibitor, multidrug resistance, ABC transporter, ABCB1**

## INTRODUCTION

Multidrug resistance (MDR) has long been considered a major barrier to the success of cancer chemotherapy since it enhanced the survival of cancer cells by attenuating the effectiveness of anticancer drugs (Shen et al., 2008; Paškevičiūtė and Petrikaitė, 2019). The ATP-binding cassette (ABC) transporters, which consist of seven classes of membrane proteins, are strongly associated with MDR, as the overexpression of ABC transporters is deemed to be the dominant contributor to

MDR. ABC transporters act as efflux pumps on the cell membrane and their primary function is to protect diverse organs such as the intestine or kidney by pumping out toxins and xenobiotics (Dassa and Bouige, 2001; Al-Ali et al., 2019). The overexpression of ABC transporters in cancer cells accelerates the efflux of chemotherapeutic drugs, resulting in cancer drug resistance, recurrence and ultimately death in cancer patients (Gillet and Gottesman, 2010; Wu et al., 2011). Several predominant and most well-characterized ABC transporters, such as ABCB1 (P-glycoprotein, P-gp; multidrug resistance 1, MDR1), ABCG2 (breast cancer resistance protein, BCRP; mitoxantrone resistance, MXR), and ABCC1 (multidrug resistance protein 1, MRP1) have been extensively studied on MDR (Dean, 2009; Li et al., 2016; Robey et al., 2018). ABCB1 was the first recognized and examined ABC transporter (Juliano and Ling, 1976). The wide use of chemotherapeutic drugs that are substrates of ABCB1 including paclitaxel and doxorubicin could lead to the activation/overexpression of ABCB1, at the same time, the overexpression of ABCB1 confers resistance to these drugs in cancer cells and cancer patients (Genovese et al., 2017). What more serious is that this acquired drug resistance may shift to other kinds of substrates of ABCB1 and a growing number of molecularly targeted chemotherapeutic drugs have been identified as substrates for ABCB1 at present, for example, mTOR inhibitor WYE-354 (Wang J. et al., 2020), histone deacetylase six inhibitor ricolinostat (Wu et al., 2018), or ALK tyrosine kinase inhibitor ceritinib (Katayama et al., 2016). In addition, ABCB1 is broadly present in the gastrointestinal tract, the blood-brain barrier, liver, and kidney, and the overexpression of it in these sites certainly has considerable clinical significance for the application of all ABCB1 substrates (Gottesman et al., 2002; Szakács et al., 2006). Therefore, determining whether existing anticancer drugs are ABCB1 substrates could predict the treatment outcome to develop improved cancer therapy regimens *via* combination.

Three RAS genes, HRAS, NRAS, and KRAS, are the most frequently mutated oncogenes in cancer, with the most paramount mutation being the KRAS mutation (Hobbs et al., 2016). KRAS plays a certainly critical role in multiple signaling pathways for cell proliferation, differentiation, and survival, being acknowledged as an eminent tumor driver (Downward, 2003; van Hattum and Waldmann, 2014). KRAS mutations trigger the activation of KRAS by intervening in the normal RAS cycles between the GDP-bound inactive state and GTP-active state, shifting the equilibrium in favor of the GTP-active state (Hunter et al., 2015; Ostrem and Shokat, 2016). Among KRAS mutations, KRAS-G12C mutation is a single point mutation with a glycine-to-cysteine substitution at codon 12, which can be observed in colorectal and pancreatic cancers, and is particularly prevalent in non-small cell lung cancer (NSCLC) (Shin et al., 2019). The attempts toward recognizing small-molecule inhibitors for KRAS failed over years, consequently, KRAS was considered as an undruggable target (Downward, 2003; Wang et al., 2012; Papke and Der, 2017). Recently, covalent inhibitors targeting specific KRAS-G12C mutation have been developed and shown satisfactory preclinical efficacy in KRAS-G12C mutated tumor models (Patricelli et al., 2016; Fell et al., 2018). ARS-1620, as a potent and covalent specific inhibitor of KRAS-G12C, has an encouraging effect on tumor regressions in the KRAS-G12C mutated cancer cell line (Janes et al., 2018) and its outstanding anti-tumor activity in the mouse xenograft model offered the first *in vivo* verification of a potential approach that directly covalent targeting of KRAS-G12C mutation (Janes et al., 2018). As a preclinic drug, ARS-1620 has been also reported to disrupt the association between KRAS and Argonaute two on the plasma membrane, which may bring the therapeutic feasibility for pancreatic cancer (Shankar et al., 2020).

There has been considerable research regarding the relationship of expression levels of ABC transporters with KRAS mutations in cancer cells (Mohelnikova-Duchonova et al., 2013; Wei et al., 2016), while the link between the level of ABC transporters and KRAS inhibitors is poorly understood. In this study, we investigated the connection between novel emerged KRAS-G12C inhibitor, ARS-1620, and ABCB1-overexpressing cancer cells. Stirringly, we found that the overexpression of ABCB1 confers resistance to ARS-1620. Furthermore, our study provides the possible scenario in which the cancer cells might develop resistance to ARS-1620 *via* ABCB1 overexpression, and the possible solution for this scenario is the combination therapy of ARS-1620 with an ABCB1 inhibitor.

# MATERIALS AND METHODS

## Chemicals

ARS-1620 was a free sample from ChemieTek (Indianapolis, IN). The monoclonal antibodies against ABCB1 (clone F4, Cat # SAB4200775) and other chemicals were purchased from Sigma Chemical Co (St. Louis, MO) except otherwise specified. Antibiotics (penicillin/streptomycin), trypsin-EDTA, and fetal bovine serum (FBS) were obtained from Hyclone (Waltham, MA, United States). The Horseradish peroxidase (HRP)-conjugated rabbit anti-mouse IgG secondary antibody (Cat # 7076S, lot #: 32) was the product of Cell Signaling Technology Inc. (Danvers, MA, United States). The GAPDH loading control monoclonal antibody (GA1R) (Cat # MA5-15738, lot #: SA247966), Alexa Fluor 488 conjugated goat anti-mouse IgG cross-adsorbed secondary antibody (Cat # A32723) were acquired from Thermo Fisher Scientific Inc. (Rockford, IL, United States). [$^3$H]-paclitaxel (15 Ci/mmol) was obtained from Moravek Biochemicals, Inc. (Brea, CA).

## Cell Lines and Cell Culture

All the cells were cultured as previously described (Zhang et al., 2020). In brief, the human epidermoid carcinoma cell line KB-3-1 and its colchicine-induced ABCB1-overexpressing KB-C2 cell line, human colon carcinoma cell line SW620, and its doxorubicin-induced ABCB1-overexpressing SW620/Ad300 cell line were used (Lyall et al., 1987; Lai et al., 1991). The KB-3-1 and KB-C2 were not KRAS-G12C mutation cell lines, the SW620 and SW620/Ad300 were KRAS-G12V mutation but not KRAS-G12C mutation cell lines. HEK293/pcDNA3.1, HEK293/ABCB1, HEK293/ABCG2, and HEK293/ABCC1 were

human embryonic kidney HEK293 cells transfected with empty vector pcDNA3.1, full-length *ABCB1*, full-length *ABCG2*, and full-length *ABCC1*, respectively (Fung et al., 2014). The moist incubator (37°C, 5% $CO_2$) was used to culture the above cell lines.

## Cell Viability Assay

Cell survival percentage after treatment with ARS-1620 and other substrates was determined by MTT assay as described earlier (Dong et al., 2020). In short, the cells were seeded into 96-well plates ($5\times10^3$/well). After cell attachment, the cells were treated with serial diluted ARS-1620 or other chemotherapeutic agents in the presence or absence of ABCB1 inhibitor verapamil for 68 h. Then, MTT solution was added for another 4 h incubation. Later, the supernatant was discarded and DMSO was added to dissolve the formazan. The optical density was obtained by reading the plate at 570 nm with a microplate analyzer.

## Immunoblotting Assay

We performed Western blotting as described earlier (Feng et al., 2020). Briefly, cells were treated with ARS-1620 (3 μM) at 37°C for 0, 24, 48, or 72 h, and then lysed. Protein concentration in each group was determined by BCA protein quantitative method. An equivalent amount (20 μg) of protein was subjected to SDS-PAGE followed by transfer to the PVDF membranes. Next, blocking of the membranes were processed in 5% skimmed milk at room temperature for 2 h. Primary antibodies (ABCB1 or GAPDH) (1:1000) were applied to membranes at 4°C overnight. After washing the membranes with TBST 3 times, the HRP-conjugated anti-mouse antibody (1:1000) was incubated with the membranes at room temperature for 2 h. ECL chemiluminescence kit was used and the signal was captured by X-ray film. The analysis of protein expression levels was performed by ImageJ (NIH, MD).

## Immunofluorescence Assay

Immunofluorescence was carried out as previously described (Wang JQ. et al., 2020). Cells ($1\times10^5$) were incubated in 24-well plates with ARS-1620 (3 μM) for 0, 24, 48, or 72 h. The cells were fixed and permeated, then blocked with 6% BSA and incubated overnight with ABCB1 antibody (1:1000). Later, Alexa Fluor 488 IgG secondary antibody (1:1000) was applied to the cells for 2 h, and nuclei were re-stained with DAPI. The image was captured by EvoS FL fluorescence microscope (Life Technologies, MD).

## HPLC Accumulation Assay

KB-3-1 and KB-C2 cells ($3\times10^5$) were seeded into 6-well plates with 2 ml complete DMEM. After 2 days incubation, the medium was replaced with plain DMEM with or without 3 μM verapamil and incubated for 2 h, followed by adding 30 μM ARS-1620 to the wells for another 2 h. Afterwards, the cells were washed with PBS twice then lysed with 0.5% sodium dodecyl sulfate and acetonitrile. Samples were harvested and centrifuged at 14,000 rpm for 10 min. The supernatant was collected for intracellular concentration analysis using HPLC.

## [$^3$H]-Paclitaxel Accumulation Assay

24-well plates were used for the culture of the cells ($1\times10^5$). On the second day, the cells were treated for 2 h with or without ARS-1620 or verapamil. Afterward, [$^3$H] -paclitaxel was added to the specified wells and incubated for 2 h. After washing with PBS, the cells were gathered and shifted to scintillation vials and the radioactivity of different treatments were measured using Packard Tricarb 1900CA liquid scintillation analyzer (Packard Instrument, Dners Grove, IL).

## ATPase Assay

As previously described, the vanadate-sensitive ATPase activity of ABCB1 was measured in terms of the amount of inorganic phosphate ($P_i$) generated by hydrolysis of ATP (Sarkadi et al., 1992). The quantity of $P_i$ was determined using the improved colorimetric method by Murphy and Riley (Ojida et al., 2004).

## Molecular Modeling

Docking analysis was conducted with software Maestro 11.5 (Schrödinger, LLC, New York, NY, 2018) (Cai et al., 2020). Ligand preparation was essentially performed with the default protocol. Human ABCB1 (PDB ID: 6QEX) (Alam et al., 2019) protein preparation was conducted to optimize the structure, remove waters, and minimize the energy. Subsequently, a grid of 20 Å at the binding pocket of ABCB1 protein was generated. Glide XP docking was performed, followed by induced-fit docking (IFD) was carried out using the default protocol.

## Statistical Analysis

All data are expressed as mean ± SD and were acquired from a minimum of three independently repetitions. Statistical analysis was based on one-way ANOVA followed by the Dunnett's test. *p*-value below 0.05 represents significant differences.

# RESULTS

## The Cytotoxicity of ARS-1620 Was Decreased in ABCB1-Overexpressing Cells but Not in ABCG2- or ABCC1-Overexpressing Cells

Firstly, we conducted the MTT assay to examine the cytotoxicity of ARS-1620 (the chemical structure is presented in **Figure 1A**) in KB-3-1, KB-C2, SW620, and SW620/Ad300 cell lines. As **Figures 1B,C** showed, the parental KB-3-1 and SW620 cells were significantly more sensitive to ARS-1620 than their drug-selected KB-C2 and SW620/Ad300 cells that overexpressing ABCB1. To further certify our observation, the cytotoxicity of ARS-1620 was also tested in gene-transfected cells HEK293/pcDNA3.1 and HEK293/ABCB1 (**Figure 1D**). Consistent with our previous results, HEK293/ABCB1 was more resistant and less sensitive to ARS-1620 compared with its parental cells HEK293/pcDNA3.1. Meanwhile, the cell survival curve of wild-type HEK293/ABCG2 and HEK293/ABCC1 cells displayed no significant increased sensitivity or reduced sensitivity. Additionally, the $IC_{50}$ values (concentrations for 50% inhibition) of ARS-1620 and resistance fold (RF) were

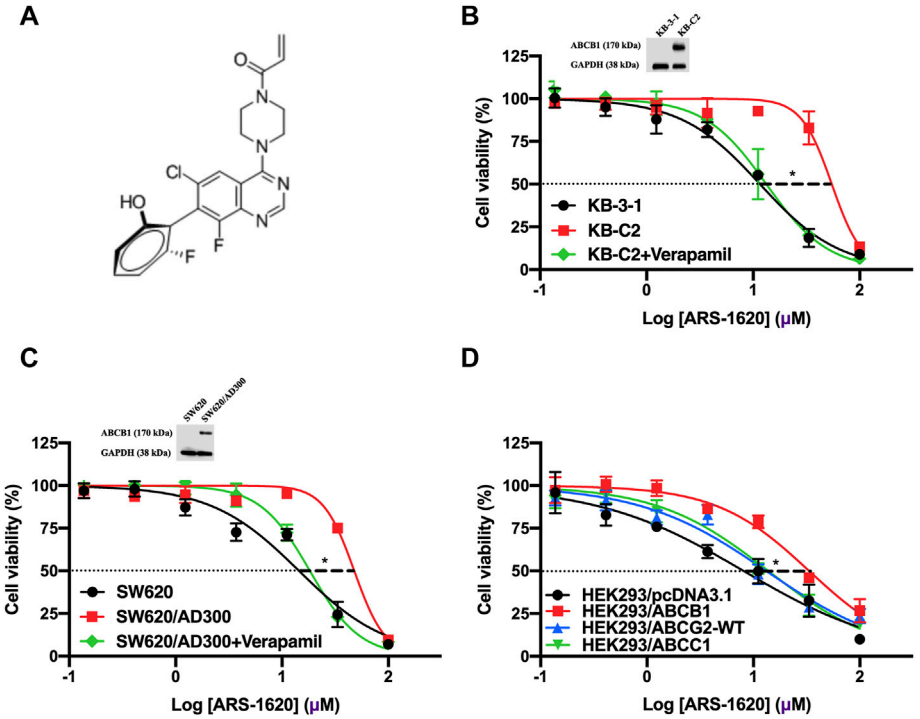


**FIGURE 1 |** Cytotoxicity curves of ARS-1620 in parental and ABCB1-overexpressing cancer cells. **(A)** Chemical structure of ARS-1620. **(B, C)** KB-3-1, KB-C2, SW620, and SW620/Ad300 cells. The corresponding ABCB1 expression level were also displayed. **(D)** HEK293/pcDNA3.1, HEK293/ABCB1, HEK293/ABCG2 and HEK293/ABCC1 cells. Verapamil of 3 μM was used as positive control. Data are displayed as mean ± SD with three independent assays. *$p < 0.05$.

**TABLE 1 |** The cytotoxicity of ARS-1620 on ABCB1-overexpressing cancer cells.

| Cell lines | $IC_{50}$ ± SD[a] (RF[b]) (μM) | | | | | |
|---|---|---|---|---|---|---|
| | Doxorubicin | Doxorubicin + verapamil 3 μM | Paclitaxel | Paclitaxel + verapamil 3 μM | ARS-1620 | ARS-1620 + verapamil 3 μM |
| KB-3-1 | 0.023 ± 0.010 (1.00) | 0.030 ± 0.007 (1.31) | 0.006 ± 0.001 (1.00) | 0.005 ± 0.002 (0.83) | 9.300 ± 3.605 (1.00) | 11.001 ± 1.082 (1.18) |
| KB-C2 | 1.546 ± 0.047 (66.48) | 0.021 ± 0.004 (0.91)* | 2.961 ± 0.350 (534.10) | 0.126 ± 0.020 (22.70)* | 58.566 ± 2.363 (6.30) | 25.020 ± 3.971 (2.69)* |
| SW620 | 0.090 ± 0.020 (1.00) | 0.094 ± 0.006 (1.05) | 0.051 ± 0.004 (1.00) | 0.060 ± 0.013 (1.18) | 14.916 ± 1.120 (1.00) | 12.923 ± 1.737 (0.87) |
| SW620/Ad300 | 5.329 ± 0.092 (59.18) | 0.795 ± 0.139 (8.83)* | 3.522 ± 0.122 (69.01) | 0.342 ± 0.106 (6.69)* | 44.063 ± 3.695 (2.95) | 14.751 ± 1.652 (0.99)* |
| HEK293/pcDNA3.1 | 0.078 ± 0.011 (1.00) | 0.107 ± 0.044 (1.37) | 0.045 ± 0.008 (1.00) | 0.059 ± 0.009 (1.37) | 10.991 ± 1.700 (1.00) | 11.380 ± 2.485 (1.04) |
| HEK293/ABCB1 | 2.382 ± 0.703 (30.58) | 0.062 ± 0.009 (0.80)* | 1.610 ± 0.222 (35.65) | 0.057 ± 0.019 (1.26)* | 33.739 ± 7.157 (3.07) | 12.027 ± 3.322 (1.09)* |

[a]*$IC_{50}$ values were represented as mean ± SD acquired from at least three independent experiments.*

[b]*Resistance fold (RF) was calculated from dividing the $IC_{50}$ values of parental or resistant cells in each treatment by the $IC_{50}$ values of corresponding parental cells with doxorubicin, paclitaxel or ARS-1620, and without verapamil.*

*p < *0.05 versus control treatment.*

summarized in **Table 1**. The KB-C2 and SW620/Ad300 cells, compared with their parental KB-3-1 and SW620 cells, possessed 6.30- and 2.95-fold resistance to ARS-1620, respectively. HEK293/ABCB1 cells showed 3.07-fold resistance to ARS-1620 compared with HEK293/pcDNA3.1. These results indicated the possibility that the overexpression of ABCB1 decreased the cytotoxicity of ARS-1620, which renders the ability of ABCB1-overexpressing cells to survive with high concentrations of ARS-1620.

## The Reinstated Sensitivity of ABCB1-Overexpressing Cells to ARS-1620 by the Introduction of Verapamil

Towards to get more supporting evidence that the overexpression of ABCB1 transporter leads to ARS-1620 resistance in ABCB1-overexpressing cells, verapamil, the pervasive used first-generation inhibitor of ABCB1, was used to co-treat with ARS-1620 in KB-C2, SW620/Ad300, and HEK293/ABCB1 cells. As shown in **Figures 1B,C** and **Table 1**, in the presence

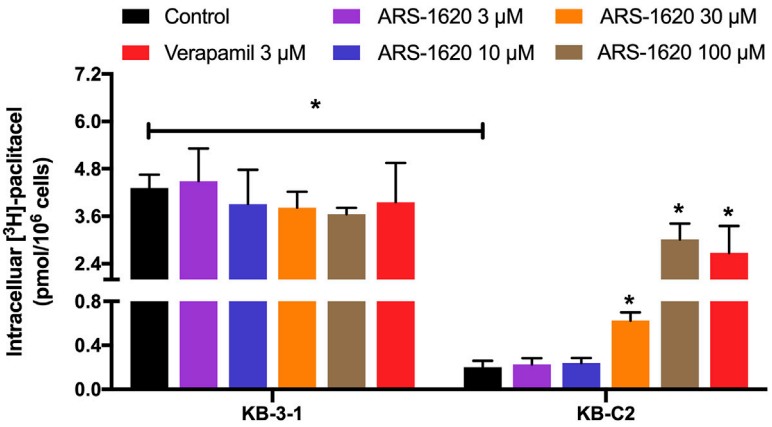


**FIGURE 2 |** ARS-1620 affected Intracellular [$^3$H]-paclitaxel accumulation in ABCB1-overexpressing cancer cells. Different concentrations (3, 10, 30, 100 μM) of ARS-1620 were used in ABCB1-overexpressing cell lines. Results are expressed as mean ± SD of three independent assays. * represents $p < 0.05$.

of 3 μM verapamil, the resistance to ARS-1620 was significantly reversed in KB-C2, SW620/Ad300, and HEK293/ABCB1 cells, the resistance fold dropped to 2.69-, 0.99-, and 1.09-fold, respectively. These results reinforced our assumption that the overexpression of ABCB1 exists as one predominant contributor to the resistance of ARS-1620.

## Higher Concentrations of ARS-1620 Boosted the Accumulation of [$^3$H]-Paclitaxel

Next, we tested the accumulation of intracellular [$^3$H]-paclitaxel when the cells were co-treated with distinct concentrations of ARS-1620 (3, 10, 30, 100 μM) over a short period. As observed in **Figure 2**, ARS-1620 at the concentration of 3 μM or even the toxic concentration of 10 μM did not influence the accumulation of [$^3$H]-paclitaxel in KB-C2 cells. However, when the concentrations of ARS-1620 reached 30 and 100 μM, the [$^3$H]-paclitaxel level was significantly increased in KB-C2 cells. In addition, the accumulation of [$^3$H]-paclitaxel in parental KB-3-1 cells was not perturbed by ARS-1620. Notably, the toxic concentrations chosen in this assay were unlikely to affect the viability and function of the parental and resistant cells in this short treatment period. The restored accumulation of [$^3$H]-paclitaxel in resistant cell treating with high concentrations of ARS-1620 implied that high concentrations of ARS-1620 might compete with paclitaxel for binding to substrate binding site, providing potential and indirect evidence that ARS-1620 is a substrate of ABCB1.

## ARS-1620 Dramatically Stimulated ATPase Activity of ABCB1

The ATPase activity was considered a non-negligible factor affecting the function of ABCB1, since the energy supplied to pump out the substrate drugs was generated through the hydrolysis of ATP. Thus, we measured the effect of ARS-1620 (0–160 μM) on the ATP hydrolysis in ABCB1 membrane vesicles. As displayed in **Figure 3A**, ARS-1620 showed a stimulatory effect on ABCB1-associated ATPase activity in a dose-depend manner. The stimulatory effect of ARS-1620 reached 50% maximal ($EC_{50}$) at 14.8 μM. Besides, a maximum of 4.23-fold of the basal activity was

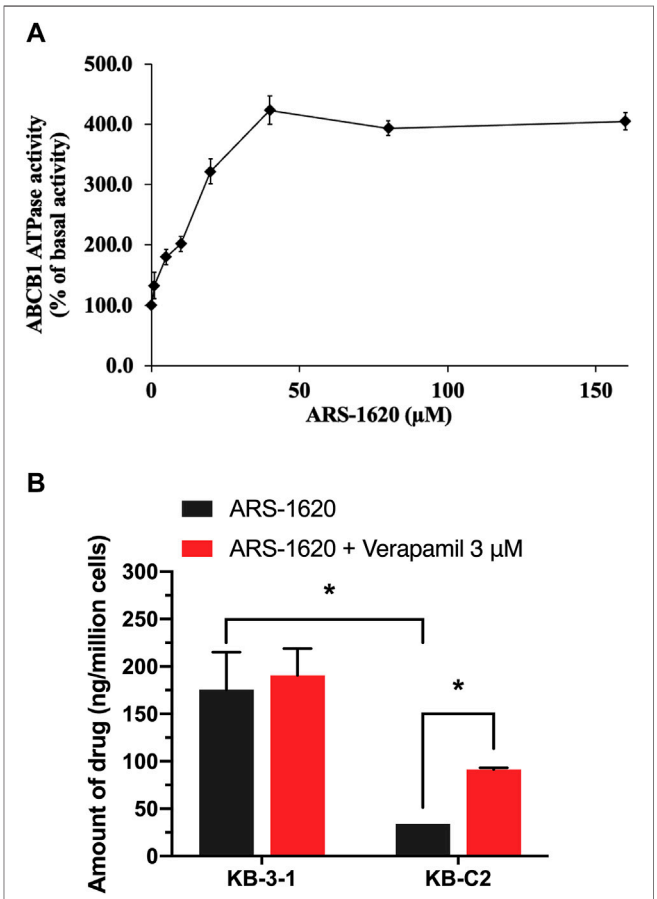


**FIGURE 3 |** The effect of ARS-1620 on the ATPase activity of ABCB1 and ARS-1620 got actively transported out by ABCB1-overexpressing cancer cells. **(A)** ARS-1620 (0–160 μM) stimulates ABCB1 ATPase activity. **(B)** The intracellular accumulation of ARS-1620 in KB-3-1 and KB-C2 cells. Data are displayed as mean ± SD of three independent assays. *$p < 0.05$.

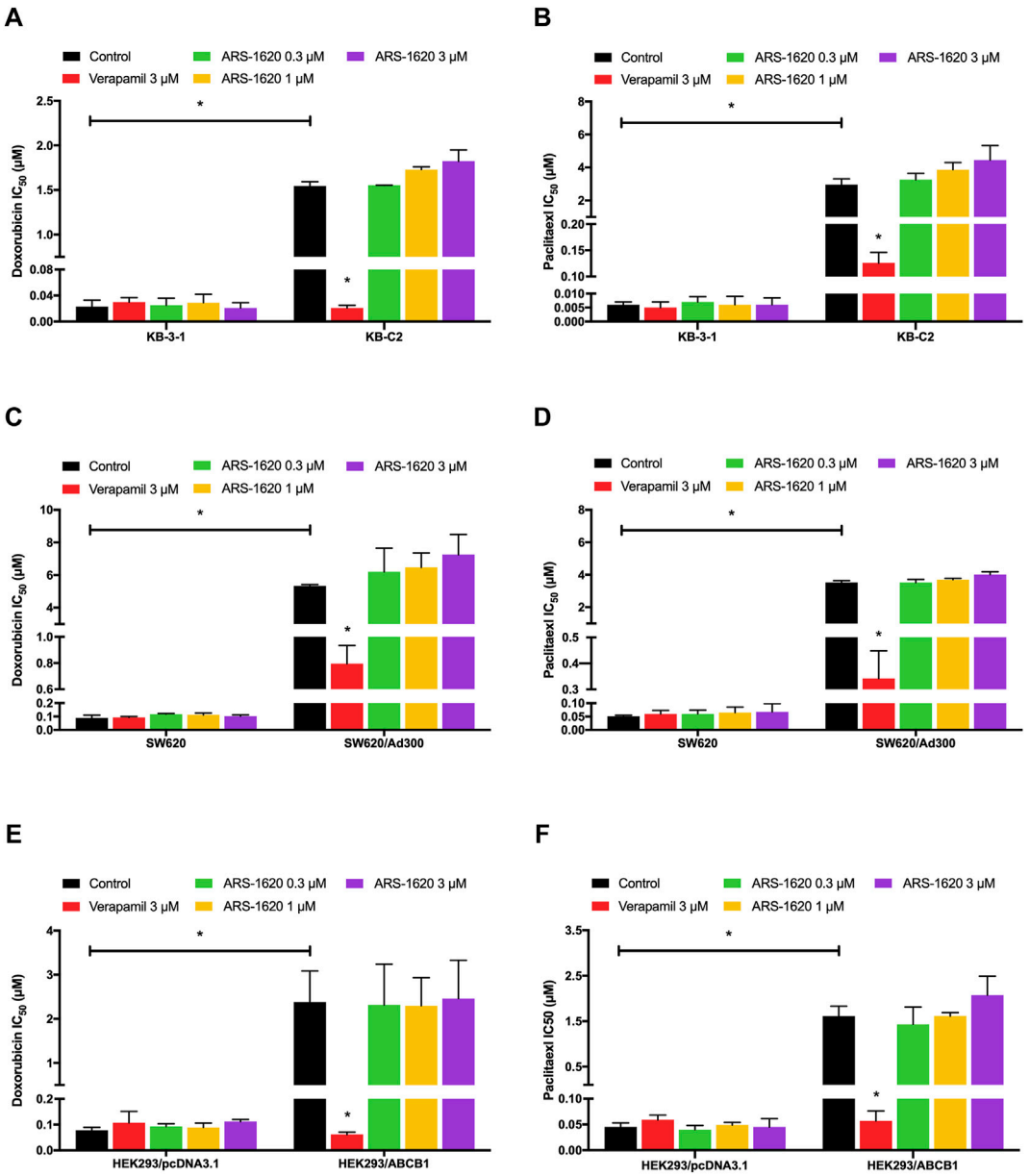


**FIGURE 4 |** Non-toxic concentrations of ARS-1620 were not able to reverse ABCB1-mediated MDR. In parental **(A, C, E)** and resistant **(B, D, F)** cell lines, ARS-1620 (0.3, 1, 3 μM) did not re-sensitize ABCB1-overexpressing cells to ABCB1 substrates (doxorubicin and paclitaxel) like verapamil, the positive control. *$p < 0.05$.

achieved by ARS-1620. Understanding that stimulation of ATPase activity is commonly relevant to ABC-mediated substrates transport, the above results illustrated that ARS-1620 may act as a substrate of ABCB1 transporter which was in accord with the cytotoxicity results.

## The Decreased Intracellular Accumulation of ARS-1620 in ABCB1-Overexpressing Cells

For further verification of ARS-1620 is a substrate of ABCB1 transporter, an HPLC assay was performed to examine the concentration of ARS-1620 with or without adding verapamil in KB-3-1 and KB-C2 cells. In **Figure 3B**, the amount of ARS-1620 was 5-times higher in KB-3-1 than KB-C2. After co-incubation with verapamil, the concentration of ARS-1620 was significantly increased in KB-C2 cells compared with KB-3-1 cells. These results provided direct and strong evidence that ARS-1620 resistance was conferred by overexpression of ABCB1 and efflux by ABCB1.

## ARS-1620 Could not Reverse ABCB1-Mediated MDR

It has been reported that some substrates could act as reversal reagents that competed with other conventional substrates like

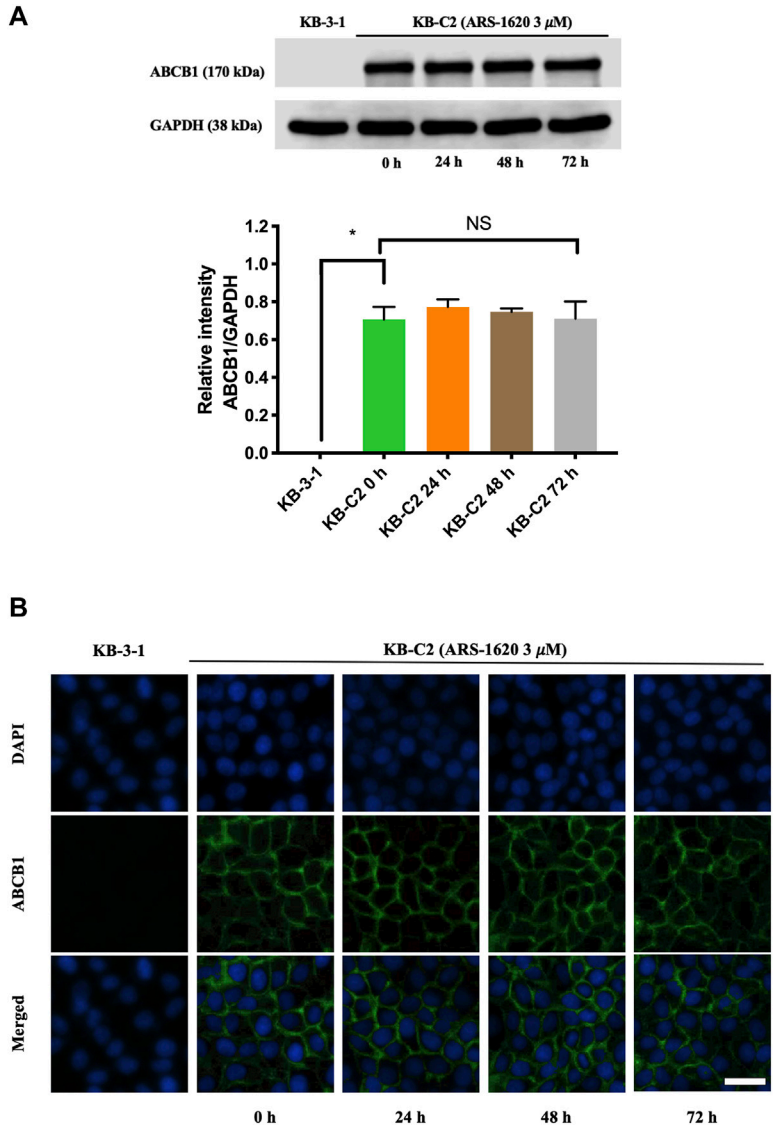


**FIGURE 5 |** ARS-1620 did not influence the protein expression level and localization of ABCB1. **(A)** The ABCB1 expression level in KB-C2 cells with ARS-1620 (3 μM) for 0, 24, 48, and 72 h. **(B)** The captured images displayed subcellular localization of ABCB1 transporter with ARS-1620 (3 μM) for 0, 24, 48 and 72 h. Green showed ABCB1; blue showed DAPI counterstains the nuclei; Scale bar: 200 μm. Results are showed as mean ± SD of three independent experiments. NS indicates no significance.

paclitaxel or doxorubicin at the substrate-binding site of ABCB1 transporter (Wang J. et al., 2020; Wu et al., 2020), resulting in a higher concentration of paclitaxel or doxorubicin remained in cells. Therefore, reversal experiments were carried out in three pairs of cell lines to examine this potentiality. Based on the results of the cytotoxicity assay (**Figure 1**), the non-toxic concentration of ARS-1620 (0.3, 1, 3 μM) was selected. As shown in **Figure 4**, the $IC_{50}$ values of doxorubicin and paclitaxel were slightly but not significantly increased in drug resistant cells by the addition of ARS-1620 in a concentration-dependent manner which signifies that ARS-1620 could not behave as an inhibitor of ABCB1 at non-toxic concentrations. The verapamil that significantly re-sensitized the resistant cells was used as a positive inhibitor of ABCB1.

## ARS-1620 has no Significant Effect on the Expression or Localization of ABCB1 Protein

Knowing that substrate drugs may interact with ABCB1 protein which brings about increasing the protein expression of ABCB1 or altering the localization of ABCB1 on the cell membrane (Wu et al., 2020), we conducted immunoblotting and immunofluorescence to investigate these potentialities. According to **Figure 5A**, the non-toxic concentration of ARS-1620 (3 μM) did not affect the expression level of ABCB1 in KB-C2 cells after comparing the relative intensity of groups with different treating periods (0, 24, 48, 72 h). Furthermore, the results from **Figure 5B** showed that ABCB1 protein still

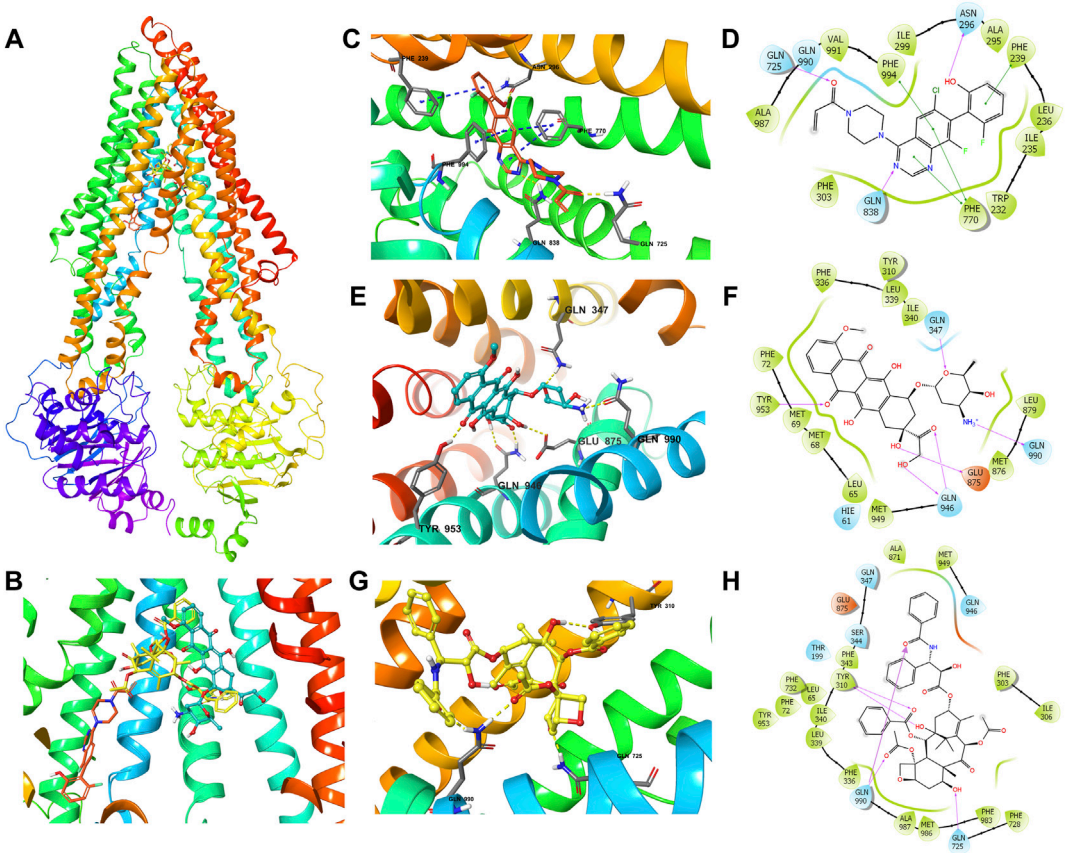


**FIGURE 6 |** The molecular modeling of ARS-1620, doxorubicin, and paclitaxel with human ABCB1. **(A)** The binding site of ARS-1620 (orange), doxorubicin (cyan), and paclitaxel (yellow) within human ABCB1. **(B)** The enlarged diagram of ARS-1620, paclitaxel, and doxorubicin within the binding site of human ABCB1. The interactions of ARS-1620 **(C)**, doxorubicin **(E)**, and paclitaxel **(G)** with the ABCB1 model in the three-dimension diagram. Ligands are shown as ball and stick mode: nitrogen—blue, oxygen—red, hydrogen—white, chloride—green, fluoride—light cyan. Interactions are indicated: hydrogen bonds—yellow dotted short line, π-π stacking—blue dotted short line. The interactions of ARS-1620 **(D)**, doxorubicin **(F)**, and paclitaxel **(H)** with the ABCB1 model in the two-dimension diagram: purple arrow hydrogen bond, green short line—π-π interaction.

located on the cell membrane without alterations during the 24–72 h treating periods with ARS-1620. The parental KB-3-1 cells in these experiments were set as the negative control.

## ARS-1620 Possessed a High-Affinity Score With the Human ABCB1 Model in the Docking Study

The results showed that ARS-1620, doxorubicin, and paclitaxel have high binding affinities with human ABCB1 (**Figure 6**) with docking scores -12.807, -12.241, and -15.527 kcal/mol, respectively. As exhibited in **Figures 6C,D**, the interactions between ARS-1620 and ABCB1 include hydrogen bonds and π-π interaction. The three aromatic rings of ARS-1620 are involved in the π-π interactions with the residues Phe239, Phe770, and Phe994. The carbonyl group and a nitrogen atom on quinazoline ring ARS-1620 formed hydrogen bonds with Gln725 and Gln838 as hydrogen-bond acceptors, while the hydroxyl group interacted with Asn296 as hydrogen bond donor. Distinct from ARS-1620, paclitaxel and doxorubicin with more oxygen atoms in their structures, tended to form hydrogen bonds rather than π-π interactions with ABCB1. Residues Gln347, Glu 875, Gln946, Tyr953, and Gln990 formed hydrogen bonds with doxorubicin. Gln946 interacted with a carbonyl group and a hydroxyl group as hydrogen bond donor and acceptor, respectively. Interestingly, the amino group became a cation and interacted with Gln990 with a hydrogen bond. Due to the acidic cancer microenvironment (Boedtkjer and Pedersen, 2020), the amino group can become protonated to a cation, and bind with the residues. Paclitaxel formed hydrogen bonds with residues Tyr310, Gln725, and Gln990, where Tyr310 interacted with both carbonyl and hydroxyl groups.

## DISCUSSION

RAS is the most common oncogene in cancer, and KRAS mutations are the predominant oncogene among the three RAS subtypes (HRAS, NRAS, and KRAS) (Hobbs et al., 2016), which was regarded as "untreatable" targets for a long time. To

devise treatment strategies, the downstream effector pathways have been extensively studied, for instance, the ERK MAPK cascade (Ryan and Corcoran, 2018; Ryan et al., 2020). However, recently, covalent inhibitors targeting specific KRAS mutations - glycine 12 to cysteine (G12C) have been developed, providing an unprecedented opportunity to directly target KRAS and showing encouraging preclinical efficacy in KRAS-G12C tumor models (Patricelli et al., 2016; Fell et al., 2018; Janes et al., 2018). Two KRAS-G12C inhibitors have completed preliminary safety assessments in phase 1 clinical trials: AMG510 (NCT03600883) and MRTX1257 (NCT03785249). As the first two drugs to directly inhibit mutated KRAS, they offer an unprecedented therapeutic opportunity to target this key oncogene. ARS-1620, another newly developed mutant-specific inhibitor of KRAS-G12C, has a strong inhibitory effect on KRAS-G12C mutant tumors (Molina-Arcas et al., 2019). At the same time, the overexpression of the ABC transporter is one of the causes of MDR in tumor cells leading to chemotherapy failure, and while the relationship between ABC expression level and KRAS mutation in cancer cells can be confirmed (Mohelnikova-Duchonova et al., 2013; Wei et al., 2016), the relationship between the expression level of ABC transporters and KRAS inhibitor is not clear, and the effect of ARS-1620 on ABCB1-mediated MDR has not been studied yet. Therefore, we investigated the potential interaction of ABCB1 with ARS-1620.

In this study, we surveyed the connection of ARS-1620 with ABCB1-overexpressing cancer cells and we found that the overexpression of ABCB1 confers resistance to ARS-1620, which may affect its effectiveness in clinical anticancer treatments. Cell viability was measured in both drug selected ABCB1-overexpressing cells and *ABCB1* gene transfected cells. The ABCB1-overexpressing KB-C2 and SW620/Ad300 were highly resistant to doxorubicin, paclitaxel, as well as ARS-1620. Considering drug-induced MDR has a variety of mechanisms, we also used ABCB1-transfected HEK293/ABCB1 cells which the overexpression of ABCB1 was a unique element resulting in MDR. Compared with the parental cells, the ABCB1-overexpressing cell lines were more resistant to ARS-1620, and the results suggested that the overexpression of ABCB1 could reduce the cytotoxicity of ARS-1620, which may eventually lead to its drug resistance. Furthermore, co-treatment with the ABCB1 inhibitor verapamil restored the sensitivity of ABCB1-overexpressing cells to ARS-1620, a result similar to other substrate drugs, such as ceritinib (Katayama et al., 2016). Additionally, the results of MTT assay in HEK293/ABCG2 and HEK293/ABCC1 revealed that ARS-1620 was not the substrate of these two transporters.

To better validate it, we further tested the accumulation of intracellular [$^3$H]-paclitaxel when the cells were co-treated with ARS-1620 (3, 10, 30, 100 μM) over a short period. Results showed that ARS-1620 at the concentration of 3 μM or even the toxic concentration of 10 μM did not influence the accumulation of [$^3$H]-paclitaxel in KB-C2 cells. However, when the concentrations of ARS-1620 reached 30 and 100 μM, the [$^3$H]-paclitaxel level was significantly increased in KB-C2 cells. Moreover, the accumulation of [$^3$H]-paclitaxel in parental KB-3-1 cells was not perturbed by ARS-1620, suggesting that ABCB1 was the main cause for the decrease of substrate accumulation in drug-resistant cells. Since ABC transporters utilize the energy generated by ATP catabolism to pump out exogenous substrate drugs, leading to decreased concentration of effective substrate drugs in cells, weakened efficacy, and the development of drug resistance (Bloise et al., 2016), the effect of ARS-1620 on ATPase activity of ABCB1 was measured by ATPase assay. The results showed that ARS-1620, like other substrates, significantly stimulated the activity of ABCB1-related ATPase in a concentration-dependent manner. Taken the previous results together, we concluded ARS-1620 is a substrate of the ABCB1 transporter. Later, the results of the HPLC assay confirmed our assumption that ARS-1620 was positively transported by KB-C2 cells compared with KB-3-1 cells and this outcome could be reversed by verapamil. This measurement of intracellular ARS-1620 accumulation directly offers compelling evidence that ARS-1620 is transported by ABCB1 as a substrate. After determining ARS-1620 is a substrate of ABCB1, it drew our attention that whether it can act as an inhibitor to reverse ABCB1 overexpression-associated MDR, as it has been investigated that certain substrates possess such ability (Levy et al., 2019). MTT assay was conducted with non-toxic ARS-1620, while no significant difference was found between various treatments. These results implied that high concentrations of ARS-1620 may serve as a competitive inhibitor to compete with paclitaxel for binding to substrate binding site, which also provided the indirect evidence that ARS-1620 is a substrate of ABCB1. In addition, usually substrate-drugs might affect the expression and location of corresponding ABC transporters to some extend (Yang et al., 2021). In our study, the ABCB1 expression level was not altered during 24–72 h of ARS-1620 treatment. This is probably because KB-C2 cells were already resistant to ARS-1620, rendering the induction effect of ARS-1620 ignorable. Then the immunofluorescence results showed that ARS-1620 did not affect the localization of ABCB1. However, we cannot rule out the possibility that longer incubation time may change the expression and cellular localization of the ABCB1 transporter protein. More in-depth studies such as whether ARS-1620 can induce ABCB1 expression in parental cells also should be further investigated.

Molecular docking is a theoretical simulation method that focuses on studying intermolecular interactions and predicting binding modes and affinities (Rosano et al., 2013; Lionta et al., 2014), aiming to find the optimal binding sites for substrate and receptor molecules and evaluate the binding strength between docked molecules. IFD analysis simulated the molecular interaction between ARS-1620 and the human ABCB1 drug-binding pocket and results suggested that ARS-1620 has a high binding affinity to ABCB1 with a docking score of −12.807 kcal/mol similar to the known ABCB1 substrates doxorubicin (-12.241 kcal/mol) and paclitaxel (−15.527 kcal/mol). Besides, the higher docking score of paclitaxel than ARS-1620 may indicate that paclitaxel is more potent to bind ABCB1 to be preferentially pumped out than ARS-1620, but ARS-1620 takes priority when the concentration of paclitaxel unchanged and ARS-1620 increased to a specific level. This could be the explanation of the results in our [$^3$H]-paclitaxel accumulation assay. However, more investigations regarding the relationship of docking score and reality interaction should be done as molecular docking cannot serve as an exact predictor.

In conclusion, our study strongly demonstrates that the overexpression of ABCB1 is associated with the resistance of ARS-1620 in cancer cells, which provides a valuable basis for future using of ARS-1620 in clinical studies. It also should be noted that KB-3-1 and SW620 cells are not KRAS-12C mutant cells, and more in-depth studies of KRAS-12C mutant ABCB1-overexpressing cells will allow us to further our comprehensive understanding and establish advanced clinical strategies.

## DATA AVAILABILITY STATEMENT

The original contributions presented in the study are included in the article/supplementary material, further inquiries can be directed to the corresponding authors.

## AUTHOR CONTRIBUTIONS

X-DD and MZ designed the experiments. X-DD, C-YC, Q-XT, J-QW, Y-GF, and KP performed the experiments. X-DD, MZ, and QC analyzed the data. X-DD and MZ wrote the manuscript. Z-SC, D-TW, Q-XT, and QC reviewed the paper. All authors read and approved the final manuscript.

## FUNDING

This work was funded by National Natural Science Foundation of China (81874394 and 81872901), Guangdong Basic and Applied Basic Research Foundation (2020A1515010058), Shenzhen Science and Technology Project (JCYJ20180306174037820), and Innovation and Practice Base for Postdoctoral Researchers of Guangxi International Zhuang Medicine Hospital.

## ACKNOWLEDGMENTS

Authors thank Chemietek for offering ARS-1620. We appreciate all the cells provided by Dr. Shin-ichi Akiyama (Kagoshima University, Kagoshima, Japan), Drs. Susan Bates and Robert Robey (NCI, NIH, MD).

## REFERENCES

Al-Ali, A. A. A., Nielsen, R. B., Steffansen, B., Holm, R., and Nielsen, C. U. (2019). Nonionic Surfactants Modulate the Transport Activity of ATP-Binding Cassette (ABC) Transporters and Solute Carriers (SLC): Relevance to Oral Drug Absorption. *Int. J. Pharm.* 566, 410–433. doi:10.1016/j.ijpharm.2019.05.033

Alam, A., Kowal, J., Broude, E., Roninson, I., and Locher, K. P. (2019). Structural Insight into Substrate and Inhibitor Discrimination by Human P-Glycoprotein. *Science* 363, 753–756. doi:10.1126/science.aav7102

Bloise, E., Ortiga-Carvalho, T. M., Reis, F. M., Lye, S. J., Gibb, W., and Matthews, S. G. (2016). ATP-binding Cassette Transporters in Reproduction: a New Frontier. *Hum. Reprod. Update* 22, 164–181. doi:10.1093/humupd/dmv049

Boedtkjer, E., and Pedersen, S. F. (2020). The Acidic Tumor Microenvironment as a Driver of Cancer. *Annu. Rev. Physiol.* 82, 103–126. doi:10.1146/annurev-physiol-021119-034627

Cai, C. Y., Zhang, W., Wang, J. Q., Lei, Z. N., Zhang, Y. K., Wang, Y. J., et al. (2020). Biological Evaluation of Non-basic Chalcone CYB-2 as a Dual ABCG2/ABCB1 Inhibitor. *Biochem. Pharmacol.* 175, 113848. doi:10.1016/j.bcp.2020.113848

Dassa, E., and Bouige, P. (2001). The ABC of ABCS: a Phylogenetic and Functional Classification of ABC Systems in Living Organisms. *Res. Microbiol.* 152, 211–229. doi:10.1016/s0923-2508(01)01194-9

Dean, M. (2009). ABC Transporters, Drug Resistance, and Cancer Stem Cells. *J. Mammary Gland Biol. Neoplasia* 14, 3–9. doi:10.1007/s10911-009-9109-9

Dong, X. D., Zhang, M., Ma, X., Wang, J. Q., Lei, Z. N., Teng, Q. X., et al. (2020). Bruton's Tyrosine Kinase (BTK) Inhibitor RN486 Overcomes ABCB1-Mediated Multidrug Resistance in Cancer Cells. *Front Cell Dev Biol* 8, 865. doi:10.3389/fcell.2020.00865

Downward, J. (2003). Targeting RAS Signalling Pathways in Cancer Therapy. *Nat. Rev. Cancer* 3, 11–22. doi:10.1038/nrc969

Fell, J. B., Fischer, J. P., Baer, B. R., Ballard, J., Blake, J. F., Bouhana, K., et al. (2018). Discovery of Tetrahydropyridopyrimidines as Irreversible Covalent Inhibitors of KRAS-G12c with *In Vivo* Activity. *ACS Med. Chem. Lett.* 9, 1230–1234. doi:10.1021/acsmedchemlett.8b00382

Feng, W., Zhang, M., Wu, Z. X., Wang, J. Q., Dong, X. D., Yang, Y., et al. (2020). Erdafitinib Antagonizes ABCB1-Mediated Multidrug Resistance in Cancer Cells. *Front. Oncol.* 10, 955. doi:10.3389/fonc.2020.00955

Fung, K. L., Pan, J., Ohnuma, S., Lund, P. E., Pixley, J. N., Kimchi-Sarfaty, C., et al. (2014). MDR1 Synonymous Polymorphisms Alter Transporter Specificity and Protein Stability in a Stable Epithelial Monolayer. *Cancer Res.* 74, 598–608. doi:10.1158/0008-5472.CAN-13-2064

Genovese, I., Ilari, A., Assaraf, Y. G., Fazi, F., and Colotti, G. (2017). Not only P-Glycoprotein: Amplification of the ABCB1-Containing Chromosome Region 7q21 Confers Multidrug Resistance upon Cancer Cells by Coordinated Overexpression of an Assortment of Resistance-Related Proteins. *Drug Resist. Updat* 32, 23–46. doi:10.1016/j.drup.2017.10.003

Gillet, J. P., and Gottesman, M. M. (2010). Mechanisms of Multidrug Resistance in Cancer. *Methods Mol. Biol.* 596, 47–76. doi:10.1007/978-1-60761-416-6_4

Gottesman, M. M., Fojo, T., and Bates, S. E. (2002). Multidrug Resistance in Cancer: Role of ATP-dependent Transporters. *Nat. Rev. Cancer* 2, 48–58. doi:10.1038/nrc706

Hobbs, G. A., Der, C. J., and Rossman, K. L. (2016). RAS Isoforms and Mutations in Cancer at a Glance. *J. Cell Sci* 129, 1287–1292. doi:10.1242/jcs.182873

Hunter, J. C., Manandhar, A., Carrasco, M. A., Gurbani, D., Gondi, S., and Westover, K. D. (2015). Biochemical and Structural Analysis of Common Cancer-Associated KRAS Mutations. *Mol. Cancer Res.* 13, 1325–1335. doi:10.1158/1541-7786.MCR-15-0203

Janes, M. R., Zhang, J., Li, L. S., Hansen, R., Peters, U., Guo, X., et al. (2018). Targeting KRAS Mutant Cancers with a Covalent G12C-specific Inhibitor. *Cell* 172, 578–e17. e517. doi:10.1016/j.cell.2018.01.006

Juliano, R. L., and Ling, V. (1976). A Surface Glycoprotein Modulating Drug Permeability in Chinese Hamster Ovary Cell Mutants. *Biochim. Biophys. Acta* 455, 152–162. doi:10.1016/0005-2736(76)90160-7

Katayama, R., Sakashita, T., Yanagitani, N., Ninomiya, H., Horiike, A., Friboulet, L., et al. (2016). P-glycoprotein Mediates Ceritinib Resistance in Anaplastic Lymphoma Kinase-Rearranged Non-small Cell Lung Cancer. *EBioMedicine* 3, 54–66. doi:10.1016/j.ebiom.2015.12.009

Lai, G. M., Chen, Y. N., Mickley, L. A., Fojo, A. T., and Bates, S. E. (1991). P-glycoprotein Expression and Schedule Dependence of Adriamycin Cytotoxicity in Human colon Carcinoma Cell Lines. *Int. J. Cancer* 49, 696–703. doi:10.1002/ijc.2910490512

Levy, E. S., Samy, K. E., Lamson, N. G., Whitehead, K. A., Kroetz, D. L., and Desai, T. A. (2019). Reversible Inhibition of Efflux Transporters by Hydrogel Microdevices. *Eur. J. Pharm. Biopharm.* 145, 76–84. doi:10.1016/j.ejpb.2019.10.007

Li, W., Zhang, H., Assaraf, Y. G., Zhao, K., Xu, X., Xie, J., et al. (2016). Overcoming ABC Transporter-Mediated Multidrug Resistance: Molecular Mechanisms and Novel Therapeutic Drug Strategies. *Drug Resist. Updat* 27, 14–29. doi:10.1016/j.drup.2016.05.001

Lionta, E., Spyrou, G., Vassilatis, D. K., and Cournia, Z. (2014). Structure-based Virtual Screening for Drug Discovery: Principles, Applications and Recent Advances. *Curr. Top. Med. Chem.* 14, 1923–1938. doi:10.2174/1568026614666140929124445

Lyall, R. M., Hwang, J. L., Cardarelli, C., Fitzgerald, D., Akiyama, S., Gottesman, M. M., et al. (1987). Isolation of Human KB Cell Lines Resistant to Epidermal Growth Factor-Pseudomonas Exotoxin Conjugates. *Cancer Res.* 47, 2961–2966.

Mohelnikova-Duchonova, B., Brynychova, V., Oliverius, M., Honsova, E., Kala, Z., Muckova, K., et al. (2013). Differences in Transcript Levels of ABC Transporters between Pancreatic Adenocarcinoma and Nonneoplastic Tissues. *Pancreas* 42, 707–716. doi:10.1097/MPA.0b013e318279b861

Molina-Arcas, M., Moore, C., Rana, S., Van Maldegem, F., Mugarza, E., Romero-Clavijo, P., et al. (2019). Development of Combination Therapies to Maximize the Impact of KRAS-G12c Inhibitors in Lung Cancer. *Sci. Transl Med.* 11, 1. doi:10.1126/scitranslmed.aaw7999

Ojida, A., Mito-Oka, Y., Sada, K., and Hamachi, I. (2004). Molecular Recognition and Fluorescence Sensing of Monophosphorylated Peptides in Aqueous Solution by bis(Zinc(II)-dipicolylamine)-based Artificial Receptors. *J. Am. Chem. Soc.* 126, 2454–2463. doi:10.1021/ja038277x

Ostrem, J. M., and Shokat, K. M. (2016). Direct Small-Molecule Inhibitors of KRAS: from Structural Insights to Mechanism-Based Design. *Nat. Rev. Drug Discov.* 15, 771–785. doi:10.1038/nrd.2016.139

Papke, B., and Der, C. J. (2017). Drugging RAS: Know the Enemy. *Science* 355, 1158–1163. doi:10.1126/science.aam7622

Paškevičiūtė, M., and Petrikaitė, V. (2019). Overcoming Transporter-Mediated Multidrug Resistance in Cancer: Failures and Achievements of the Last Decades. *Drug Deliv. Transl Res.* 9, 379–393. doi:10.1007/s13346-018-0584-7

Patricelli, M. P., Janes, M. R., Li, L. S., Hansen, R., Peters, U., Kessler, L. V., et al. (2016). Selective Inhibition of Oncogenic KRAS Output with Small Molecules Targeting the Inactive State. *Cancer Discov.* 6, 316–329. doi:10.1158/2159-8290.CD-15-1105

Robey, R. W., Pluchino, K. M., Hall, M. D., Fojo, A. T., Bates, S. E., and Gottesman, M. M. (2018). Revisiting the Role of ABC Transporters in Multidrug-Resistant Cancer. *Nat. Rev. Cancer* 18, 452–464. doi:10.1038/s41568-018-0005-8

Rosano, C., Viale, M., Cosimelli, B., Severi, E., Gangemi, R., Ciogli, A., et al. (2013). ABCB1 Structural Models, Molecular Docking, and Synthesis of New Oxadiazolothiazin-3-One Inhibitors. *ACS Med. Chem. Lett.* 4, 694–698. doi:10.1021/ml300436x

Ryan, M. B., and Corcoran, R. B. (2018). Therapeutic Strategies to Target RAS-Mutant Cancers. *Nat. Rev. Clin. Oncol.* 15, 709–720. doi:10.1038/s41571-018-0105-0

Ryan, M. B., Fece De La Cruz, F., Phat, S., Myers, D. T., Wong, E., Shahzade, H. A., et al. (2020). Vertical Pathway Inhibition Overcomes Adaptive Feedback Resistance to KRASG12C Inhibition. *Clin. Cancer Res.* 26, 1633–1643. doi:10.1158/1078-0432.CCR-19-3523

Sarkadi, B., Price, E. M., Boucher, R. C., Germann, U. A., and Scarborough, G. A. (1992). Expression of the Human Multidrug Resistance cDNA in Insect Cells Generates a High Activity Drug-Stimulated Membrane ATPase. *J. Biol. Chem.* 267, 4854–4858. doi:10.1016/s0021-9258(18)42909-2

Shankar, S., Tien, J. C., Siebenaler, R. F., Chugh, S., Dommeti, V. L., Zelenka-Wang, S., et al. (2020). An Essential Role for Argonaute 2 in EGFR-KRAS Signaling in Pancreatic Cancer Development. *Nat. Commun.* 11, 2817. doi:10.1038/s41467-020-16309-2

Shen, F., Chu, S., Bence, A. K., Bailey, B., Xue, X., Erickson, P. A., et al. (2008). Quantitation of Doxorubicin Uptake, Efflux, and Modulation of Multidrug Resistance (MDR) in MDR Human Cancer Cells. *J. Pharmacol. Exp. Ther.* 324, 95–102. doi:10.1124/jpet.107.127704

Shin, Y., Jeong, J. W., Wurz, R. P., Achanta, P., Arvedson, T., Bartberger, M. D., et al. (2019). Discovery of N-(1-Acryloylazetidin-3-yl)-2-(1H-indol-1-yl) acetamides as Covalent Inhibitors of KRASG12C. *ACS Med. Chem. Lett.* 10, 1302–1308. doi:10.1021/acsmedchemlett.9b00258

Szakács, G., Paterson, J. K., Ludwig, J. A., Booth-Genthe, C., and Gottesman, M. M. (2006). Targeting Multidrug Resistance in Cancer. *Nat. Rev. Drug Discov.* 5, 219–234. doi:10.1038/nrd1984

van Hattum, H., and Waldmann, H. (2014). Chemical Biology Tools for Regulating RAS Signaling Complexity in Space and Time. *Chem. Biol.* 21, 1185–1195. doi:10.1016/j.chembiol.2014.08.001

Wang, J., Yang, D. H., Yang, Y., Wang, J. Q., Cai, C. Y., Lei, Z. N., et al. (2020a). Overexpression of ABCB1 Transporter Confers Resistance to mTOR Inhibitor WYE-354 in Cancer Cells. *Int. J. Mol. Sci.* 21, 1. doi:10.3390/ijms21041387

Wang, J. Q., Teng, Q. X., Lei, Z. N., Ji, N., Cui, Q., Fu, H., et al. (2020b). Reversal of Cancer Multidrug Resistance (MDR) Mediated by ATP-Binding Cassette Transporter G2 (ABCG2) by AZ-628, a RAF Kinase Inhibitor. *Front. Cell Dev Biol* 8, 601400. doi:10.3389/fcell.2020.601400

Wang, W., Fang, G., and Rudolph, J. (2012). Ras Inhibition via Direct Ras Binding-Iis There a Path Forward? *Bioorg. Med. Chem. Lett.* 22, 5766–5776. doi:10.1016/j.bmcl.2012.07.082

Wei, H., Lu, W., Li, M., Zhang, Q., and Lu, S. (2016). Concomitance of P-Gp/LRP Expression with EGFR Mutations in Exons 19 and 21 in Non-small Cell Lung Cancers. *Yonsei Med. J.* 57, 50–57. doi:10.3349/ymj.2016.57.1.50

Wu, C. P., Hsieh, C. H., and Wu, Y. S. (2011). The Emergence of Drug Transporter-Mediated Multidrug Resistance to Cancer Chemotherapy. *Mol. Pharm.* 8, 1996–2011. doi:10.1021/mp200261n

Wu, C. P., Hsieh, Y. J., Murakami, M., Vahedi, S., Hsiao, S. H., Yeh, N., et al. (2018). Human ATP-Binding Cassette Transporters ABCB1 and ABCG2 Confer Resistance to Histone Deacetylase 6 Inhibitor Ricolinostat (ACY-1215) in Cancer Cell Lines. *Biochem. Pharmacol.* 155, 316–325. doi:10.1016/j.bcp.2018.07.018

Wu, Z. X., Yang, Y., Wang, J. Q., Zhou, W. M., Chen, J., Fu, Y. G., et al. (2020). Elevated ABCB1 Expression Confers Acquired Resistance to Aurora Kinase Inhibitor GSK-1070916 in Cancer Cells. *Front. Pharmacol.* 11, 615824. doi:10.3389/fphar.2020.615824

Yang, Y., Wu, Z. X., Wang, J. Q., Teng, Q. X., Lei, Z. N., Lusvarghi, S., et al. (2021). OTS964, a TOPK Inhibitor, Is Susceptible to ABCG2-Mediated Drug Resistance. *Front. Pharmacol.* 12, 620874. doi:10.3389/fphar.2021.620874

Zhang, M., Chen, X. Y., Dong, X. D., Wang, J. Q., Feng, W., Teng, Q. X., et al. (2020). NVP-CGM097, an HDM2 Inhibitor, Antagonizes ATP-Binding Cassette Subfamily B Member 1-Mediated Drug Resistance. *Front. Oncol.* 10, 1219. doi:10.3389/fonc.2020.01219

**Conflict of Interest:** The authors declare that the research was conducted in the absence of any commercial or financial relationships that could be construed as a potential conflict of interest.

**Publisher's Note:** All claims expressed in this article are solely those of the authors and do not necessarily represent those of their affiliated organizations, or those of the publisher, the editors, and the reviewers. Any product that may be evaluated in this article, or claim that may be made by its manufacturer, is not guaranteed or endorsed by the publisher.

frontiers in Oncology

ORIGINAL RESEARCH
published: 24 February 2022
doi: 10.3389/fonc.2022.847556

# Complex Crystal Structure Determination of Hsp90$^N$-NVP-AUY922 and *In Vitro* Anti-NSCLC Activity of NVP-AUY922

*Chun-Xia He[1†], You Lv[2†], Meng Guo[3†], Huan Zhou[4], Wei Qin[1], Dong Zhao[1], Hui-Jin Li[1], Lu Xing[1], Xin Zhou[1], Peng-Quan Li[1], Feng Yu[4*], Jian-Hua He[4,5*] and Hui-Ling Cao[1,3*]*

[1] Xi'an Key Laboratory of Basic and Translation of Cardiovascular Metabolic Disease, Shaanxi Key Laboratory of Ischemic Cardiovascular Disease, Institute of Basic & Translational Medicine, Xi'an Medical University, Xi'an, China, [2] College of Bioresources Chemical and Materials Engineering, Shaanxi University of Science & Technology, Xi'an, China, [3] College of Pharmacy, Shaanxi University of Chinese Medicine, Xianyang, China, [4] Shanghai Synchrotron Radiation Facility, Shanghai Advanced Research Institute, Chinese Academy of Sciences, Shanghai, China, [5] Institute for Advanced Studies, Wuhan University, Wuhan, China

New targeted chemotherapy agents greatly improved five-year survival in NSCLC patients, but which were susceptible to drug resistance. NVP-AUY922, terminated in phase II clinical trials, exhibited promising anti-NSCLC (non-small-cell lung cancer) activity targeting to Hsp90$^N$ (heat shock protein), which demonstrated advantages in overcoming drug resistance as a broad-spectrum anti-cancer target. It was expected to develop novel anti-NSCLC drugs to overcome drug resistance by the structural optimization of NVP-AUY922. However, the absence of high-resolution complex crystal structure of Hsp90$^N$-NVP-AUY922 blocked the way. Herein, 1.59 Å-resolution complex crystal structure of Hsp90$^N$-NVP-AUY922 (PDB ID 6LTI) was successfully determined by X-ray diffraction. Meanwhile, there was a strong binding capability between NVP-AUY922 and its target Hsp90$^N$ verified by TSA ($\Delta$Tm, −15.56 ± 1.78°C) and ITC ($K_d$, 5.10 ± 2.10 nM). Results by the complex crystal structure, TSA and ITC verified that NVP-AUY922 well accommodated in the ATP-binding pocket of Hsp90$^N$ to disable the molecular chaperone activity of Hsp90. Therefore, NVP-AUY922 exhibited approving inhibitory activity on NSCLC cell line H1299 ($IC_{50}$, 2.85 ± 0.06 μM) by inhibiting cell proliferation, inducing cell cycle arrest and promoting cell apoptosis. At the basis of the complex crystal structure and molecular interaction analysis, thirty-two new NVP-AUY922 derivatives were further designed, and among which twenty-eight new ones display enhanced binding force with Hsp90$^N$ by molecular docking evaluation. The results would promote anti-NSCLC new drug development to overcome drug resistance based on the lead compound NVP-AUY922.

**Keywords: NVP-AUY922, Hsp90$^N$, non-small-cell lung cancer (NSCLC), complex crystal structure, molecular interaction, drug design**

OPEN ACCESS

***Edited by:***
*Qingbin Cui,*
*University of Toledo, United States*

***Reviewed by:***
*Wen Zhao,*
*Zhengzhou University, China*
*Guangwen Lu,*
*Sichuan University, China*

****Correspondence:***
*Feng Yu*
*yufeng@sari.ac.cn*
*Jian-Hua He*
*hejianhua@whu.edu.cn*
*Hui-Ling Cao*
*caohuiling_jzs@xiyi.edu.cn*

*†These authors have contributed equally to this work*

***Specialty section:***
*This article was submitted to Pharmacology of Anti-Cancer Drugs, a section of the journal Frontiers in Oncology*

***Received:*** *02 January 2022*
***Accepted:*** *31 January 2022*
***Published:*** *24 February 2022*

***Citation:***
*He C-X, Lv Y, Guo M, Zhou H, Qin W, Zhao D, Li H-J, Xing L, Zhou X, Li P-Q, Yu F, He J-H and Cao H-L (2022) Complex Crystal Structure Determination of Hsp90$^N$-NVP-AUY922 and In Vitro Anti-NSCLC Activity of NVP-AUY922. Front. Oncol. 12:847556. doi: 10.3389/fonc.2022.847556*

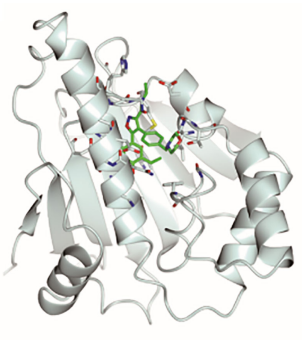

**GRAPHICAL ABSTRACT** | Stereoscopic images of complex crystal structure of Hsp90N-NVP-AUY922. A high-resolution complex crystal structure of Hsp90N-NVP-AUY922 was determined by X-ray diffraction (resolution limit 1.59 Å, PDB ID 6LTI), which suggested that NVP-AUY922 perfectly bound in the N-terminal ATP-binding pocket of Hsp90 to disable its molecular chaperone function, therefore suppressed or killed cancer cells.

## HIGHLIGHTS

1. A high-resolution complex crystal structure of Hsp90N-NVP-AUY922 was successfully determined by X-ray diffraction.
2. NVP-AUY922 well accommodated in the ATP-binding pocket to disable the molecular chaperone function of Hsp90N to inhibit cancer cells verified by the complex crystal structure, thermal shift assay (TSA) and isothermal titration calorimetry (ITC).
3. Thirty-two new NVP-AUY922 derivatives were designed and twenty-eight new ones exhibited increased binding force with the target Hsp90N, which was proven a feasible scheme by molecular docking evaluation.
4. NVP-AUY922 exhibited favourable *in vitro* anti-NSCLC activity.

## INTRODUCTION

Lung cancer remained the top mortality cancer causing 1.8 million deaths (18%) among 10.0 million deaths for cancers worldwide in 2020 (1). Lung cancer is therapeutically divided into non-small-cell lung carcinoma (NSCLC) and small cell lung cancer (SCLC), in which NSCLC covers 80% of patients (2). Recently, targeted therapies for lung cancer have been made remarkable progress based on the genomic studies on the subtypes of NSCLC, leading to the improvement of clinical outcomes for NSCLC, but there is still a low 5-year survival rate of less than 20% and susceptible to drug resistance (3). As is well known, cancer cells carry mutant genes and proteins to survive from therapeutic toxins (4). Thus, heat shock protein 90 (Hsp90) inhibitors with non-targeted therapies with broad-spectrum effects demonstrated advantages in overcoming drug resistance, which would be another choice for NSCLC patients with drug resistance.

Hsp90 inhibitors resulted in unfolded and unmatured multiple important client proteins to be captured and degraded by the proteasome by inhibiting molecular chaperone function of Hsp90, therefore suppressed cancer cells (5–7). Hsp90 inhibitors were designed targeting to three domains of Hsp90 monomer that consequently typed as $Hsp90^{N}$ inhibitors, $Hsp90^{M}$ inhibitors, and $Hsp90^{C}$ inhibitors. $Hsp90^{N}$ inhibitors have been a hot spot against tumor cells *in vitro* and *in vivo* (8–12) and many papers and patents focused on $Hsp90^{N}$ inhibitors (13–15). NVP-AUY922, a small molecule inhibitor for $Hsp90^{N}$, is a resorcinol derivative based on the structure of 4,5-diarylisoxazole scaffold, and displayed favorable anti-cancer activity *in vitro* and *in vivo* (16). NVP-AUY922 was evaluated in a phase I clinical trial concerning solid-organ malignancies (primarily breast, ovarian, and colon cancer), and a phase II clinical trial evaluation in NSCLC patients was also carried out by grouping to epidermal growth factor receptor (EGFR) mutations, KRAS proto-oncogene GTPase (KRAS) mutations, anaplastic lymphoma kinase (ALK) rearrangement, and wild-type NSCLC. In phase I clinical trial, major side effects were dose-limiting toxicities, namely, visual symptoms and diarrhea. In phase II clinical trial, NVP-AUY922 exhibited high efficacy in the ALK rearrangement and EGFR mutations. Unfortunately, further development of AUY922 was stopped by Novartis in December of 2014 on account of the failure in meeting its endpoint of complete and partial response of phase II clinical trial in NSCLC patients (7, 17–21).

In brief, NVP-AUY922 was a promising inhibitor for anti-NSCLC new drug development and it was expected to develop novel anti-NSCLC drugs by structural improvement of NVP-AUY922. The absence of high-resolution complex crystal structure of $Hsp90^{N}$-NVP-AUY922 blocked the way. Herein, we successfully determined a high-resolution complex crystal structure (1.59 Å) of $Hsp90^{N}$-NVP-AUY922 by X-ray diffraction (XRD). The molecular interaction mechanism of $Hsp90^{N}$-AUY922 was explored based on the complex crystal structure, thermal shift assay (TSA) and isothermal titration calorimetry (ITC). The findings would promote novel anti-NSCLC drug

development to overcome drug resistance based on the lead compound NVP-AUY922.

# MATERIALS AND METHODS

## Materials and Methods

Human NSCLC cell line H1299 was acquired from the AOLUKEJI (Shanghai, China). The medium RPMI 1640 and fetal bovine serum were purchased from Gibco-BRL (Gaithersburg, MD, USA).

Tris, Tris–HCl, sodium acetate (NaAc), magnesium chloride ($MgCl_2$), dimethylsulfoxide (DMSO) and PEG4000 were all from Sigma-Aldrich Corp. (St. Louis, MO, USA). Crystal loop was supplied by Hampton Research Corp. (Aliso Viejo, CA, USA). Sodium chloride (NaCl), glycerol, hydrochloric acid (HCl), sodium hydroxide (NaOH) and ethyl alcohol were obtained from the Xi'an Chemical Reagent Company (Xi'an, China). NVP-AUY922 was from Target Molecule Corp. (Boston, MA, USA). DMSO was used to dissolve NVP-AUY922 and double distilled water ($ddH_2O$) was used for other chemicals.

## Cell Viability Assay

First of all, quantitative $IC_{50}$ value was determined. RPMI 1640 with 10% (v/v) fetal bovine serum was used to cultured NSCLC cell line H1299 cells at 37°C in a humidified 5% $CO_2$ atmosphere incubator (Thermo Fisher Scientific Inc., Waltham, MA, USA). Briefly, cells were seeded in 96-well plates at $4 \times 10^3$ per well in triplicates and were treated with NVP-AUY922 (100, 10, 1, 0.1, 0.01 μM) for 72 h after incubating for 24 h. OD450 was then detected after 2.5 h adding CCK-8 (7Sea, Shanghai, China) by ELISA plate reader (BioTek Instruments, USA).

Cell viability assay was followed and performed. H1299 cells were placed in 96-well plates as described above. Afterwards, cells were treated with 4 × 2.85 μM NVP-AUY922 for 24, 48, and 72 h. After incubating with CCK-8 for 2.5 h, $OD_{450}$ was valued to analyze the cell viability.

## Cell Cycle Analysis

To monitor effects of NVP-AUY922 on cell cycle progression, cells were seeded in 6-well plates at $3 \times 10^5$ per well. After treating with 4 × 2.85 μM NVP-AUY922, or the same amount of DMSO for 72 h at 37°C, cells were harvested and resuspended with 3 ml PBS/ethanol mixture (v:v = 1:2) and then preserved at 4°C. The samples were resuspended with 400 μl buffer after 5 min-centrifugation at 1,000*g* and washing in 2 ml PBS once. Lastly, 50 μl propidium iodide (PI) and the same volume of RNase were then added into the cells to be incubated for 30 min in the dark at 37°C (22). Flow cytometry (Becton Dickinson, NJ, USA) was used to analyze the distribution of cell cycle phases.

## Apoptosis Assay

The apoptosis rate was detected by the Annexin V-FITC/PI Apoptosis Detection Kit (556547, Becton Dickinson, USA) according to the manufacturer's instructions. Briefly, cells were seeded and incubated with NVP-AUY922 as is mentioned in *Cell Cycle Analysis*. Subsequently, cells were resuspended in 100 μl binding buffer after washing with 2 ml PBS. Ultimately, 5 μl Annexin V-FITC and 10 μl PI were added and incubated at 4°C for 30 min in the dark. Also, flow cytometry was adopted for cell apoptosis analysis.

## Protein Purification and Crystallization

The recombination plasmid, pET28a with the synthesized $Hsp90^N$ gene (residues 9–236) was transferred into *E. coli* BL21 (DE3) (TIANGEN Biotech Corp., Beijing, China) for the target $Hsp90^N$ expression. The protein was purified by Nickel affinity chromatography and molecular sieve chromatography, as previously reported (23).

For crystallization, NVP-AUY922 was mixed with $Hsp90^N$ protein (20 mg/ml) with 5:1 molar ratio to incubate for 30 min at 4°C. The mixture was then centrifuged for 10 min at 3,000*g* to collect the supernate. Mixing with the same volume of precipitant (pH 8.5, 0.1 M Tris–HCl, 0.2 M $MgCl_2$, 25% PEG4000) (24) was conducted for 3–7 d at 4°C. Hanging drop vapor diffusion method was used. Co-crystallization was accomplished in a bath circulator controlled incubator (PolyScience 9712, PolyScience, USA).

## Data Collection, Structure Determination and Refinement

$Hsp90^N$-NVP-AUY922 complex crystal image of was obtained by a stereomicroscope (M165, Leica Microsystems, Germany). Mounted with cryo-loop (Hampton Research Corp., Aliso Viejo, CA, USA), the complex crystals were flash-frozen in liquid nitrogen for XRD after soaking briefly in the cryoprotectant solution (pH8.5, 0.1 M Tris–HCl, 0.2 M $MgCl_2$, 25% PEG4000, and 20–25% glycerol). All data sets were acquired at 100 K on Macromolecular Crystallography Beamline17U1 (BL17U1) using an ADSC Quantum 315r CCD detector at Shanghai Synchrotron Radiation Facility (SSRF, Shanghai, China) (25) and the diffraction data were auto-processed by aquarium pipeline (26). The complex crystal structure was analyzed by molecular replacement method using the PHENIX software (27) according to the reported $Hsp90^N$-FS23 (PDB ID, 5CF0) (28). The program Coot was used to rebuild the initial model (29). CCP4MG software was used for graphic reconstruction and molecular interaction analysis (30).

## Thermal Shift Assay (TSA)

The ligand NVP-AUY922, dissolved in DMSO, and the target $Hsp90^N$ were mixed at a molar ratio of 1:5 in a 20 μl TSA dye reaction buffer with 20 mM Tris–HCl, 150 mM NaCl and 10% glycerol (pH 7.5). The melting-curve (25 to 95°C with a ramp rate of 1°C/min) was determined on ABI 7500 system (7500, ABI Corp., USA). Fluorescence was stimulated by environmentally-sensitive TSA dye binding to the exposed hydrophobic regions during protein unfolding as it is heated. Binding capacity of protein–ligand can be closely evaluated by the melting temperature (Tm) and melting temperature shift (ΔTm) which was calculated based on the melt curves (31).

## Isothermal Titration Calorimetry (ITC)

ITC was performed to further illustrate molecular interaction mechanism of $Hsp90^N$-NVP-AUY922 using an ITC-200 calorimeter (Malvern Instrument Ltd., UK). All measurements were carried out in PBS (pH 7.5) at 25°C. Briefly, fresh-purified $Hsp90^N$ protein was concentrated to 50 μM. The ligand NVP-AUY922 was prepared in a concentration of 500 μM. Sample was degassed before use. For each titration in the cell, 2 μl aliquot of NVP-AUY922 was added into $Hsp90^N$ solution at a 200 s-interval and stirring speed of 750 rpm. The experimental data was fitted to a bimolecular binding model by adjusting three parameters, namely, stoichiometry (n), enthalpy ($\Delta H°$) and association constant ($K$a) using Microcal Origin software embedded in the equipment. The thermodynamic parameters $\Delta G°$ (free energy) and $\Delta S°$ (entropy) were obtained according to the formula, $-RT \ln K\text{a} = \Delta G° = \Delta H° - T\Delta S°$ (32).

## New NVP-AUY922 Derivatives Design and Molecular Docking Evaluation

Based on the analysis of the $Hsp90^N$-NVP-AUY922 crystal structure, TSA and ITC, we designed a series of novel NVP-AUY922 derivatives. Evaluation of the derivatives was performed through molecular docking on software SYBYL-X 2.0 (Tripos Associates Inc., St. Louis, MO, USA).

First, a library of novel NVP-AUY922 derivatives was built and a geometric and force field optimization was carried out over 10,000 times. Second, the protein optimization was performed, such as adding hydrogenation and charge. Lastly, the molecular docking evaluation was performed by Surflex-Dock module of SYBYL software. Further, complex 3D structure reconstruction was simulated by CCP4MG software and molecular interaction mechanism was also analyzed (30).

## Statistical Analysis

All data were exhibited as the mean ± standard deviation (SD). The difference significance between two variables was evaluated by Unpaired Student's t-test, and $P$ <0.05 was considered having statistical significance. Data analysis was performed using GraphPad Prism 5.01 (GraphPad Software, San Diego, USA) and SPSS 13.0 (International Business Machines Corporation, USA). Flow cytometry (Becton Dickinson, NJ, USA) was adopted for cell apoptosis analysis.

# RESULTS

## Anti-NSCLC Activity *In Vitro*

AUY-922, as a positive prodrug control, performed favorable anti-NSCLC activity on NSCLC cell lines H460, A549 and H1975 (33). Herein, the effects of NVP-AUY922 on cell viability, cell cycle progression and cell apoptosis of another NSCLC cell line H1299 were analyzed.

NVP-AUY922 exhibited favorable inhibitory activity against H1299 cells ($IC_{50}$, 2.85 ± 0.063 μM). As shown in **Figure 1A**, NVP-AUY922 significantly inhibited H1299 cell viability at 24 h ($P$ <0.01), 48 h ($P$ <0.001) and 72 h ($P$ <0.0001), and its inhibitory activity was increased with extended treat time.

As can be seen from **Figures 1B–D**, after treated with NVP-AUY922 for 72 h, the percentage of H1299 cells in G1, S and G2 phases was obviously changed (NVP-AUY922, G1,↓33.79%; S,↑0.56%; G2,↑33.24% *vs* Control), indicating that when treated with NVP-AUY922, H1299 cells were notably arrested at G2 phase.

Effects of NVP-AUY922 on H1299 cell apoptosis was also analyzed by the annexin V and PI double staining kit by flow cytometry. Briefly, during early apoptosis, Annexin V can bind to phosphatidylserine (PS) that exists on the external leaflet of the plasma membrane. While, early apoptotic cells exclude PI, late apoptotic cells and necrotic cells can be stained positively (34). Cell percentage at different apoptosis stages are shown in **Figures 1E–G**. Compared with the control, NVP-AUY922 elevated both the early apoptosis rate and later apoptosis rate of H1299 cells obviously (NVP-AUY922, normal cell rate,↓39.00%; early apoptosis rate,↑14.60%; late apoptosis rate,↑21.80% *vs* Control).

## Molecular Interaction Mechanism Analysis

The thermal stability of proteins with or without ligands was detected by TSA according to the Tm and ΔTm calculated by the protein melting curve, which closely reflect the protein–ligand binding force. The affinity between target $Hsp90^N$ and ligand can be indicated by the absolute value of ΔTm, while |ΔTm| >3 is usually considered as a favorable ligand. The results showed that after binding with NVP-AUY922, the thermal stability of $Hsp90^N$ was shifted by approximately 15.56°C (ΔTm, 15.56 ± 1.78°C), suggesting a strong binding force between the $Hsp90^N$ and NVP-AUY922 (**Figures 2A–C**).

The dissociation constant of $Hsp90^N$-NVP-AUY922 was further determined by ITC at 25°C in PBS. As can be seen in **Figure 2D**, a perfect S-shaped curve was established by nonlinear data fitting. The negative peaks in the raw ITC titration data revealed that the binding process of $Hsp90^N$-NVP-AUY922 was exothermic at 25°C. The stoichiometric ratio was 0.78 ± 0.04, suggesting a 1:1 binding mode between $Hsp90^N$ and NVP-AUY922. The $K$d values derived here was 5.10 ± 2.10 nM, further indicating a strong binding force of $Hsp90^N$-NVP-AUY922, as shown in **Table 1**. The thermodynamic signature was dominated by a large enthalpy change, indicating favorable thermodynamic interactions established in the $Hsp90^N$-NVP-AUY922 binding process.

As is shown in **Figure 3**, the empty ATP-binding site of $Hsp90^N$ showed continuous and strong electron density, which was well matched with NVP-AUY922 molecule structure (**Figures 3A, C, D**). A major part of NVP-AUY922 was buried in the ATP-binding pocket of $Hsp90^N$, while the morpholine ring was extending out of the pocket. As shown in **Figure 3B**, the complex hydrogen bond networks were responsible for strong binding force of $Hsp90^N$-NVP-AUY922. Three direct hydrogen bonds were formed between NVP-AUY922 and residue D93 (2.7 Å), residue K58 (3.0 Å) and residue G97 (3.0 Å) of $Hsp90^N$, respectively. Furthermore, one hydroxy group of the isoxazole ring of NVP-AUY922 formed four water-mediated hydrogen bonds with residues D93, T184, and G97. The other hydroxy group of phenyl ring formed three water-mediated hydrogen bonds with residues L48 and S52. The carbanyl group of carboxamide moiety formed three water-mediated hydrogen bonds with residues K58 and D54. In addition to hydrogen

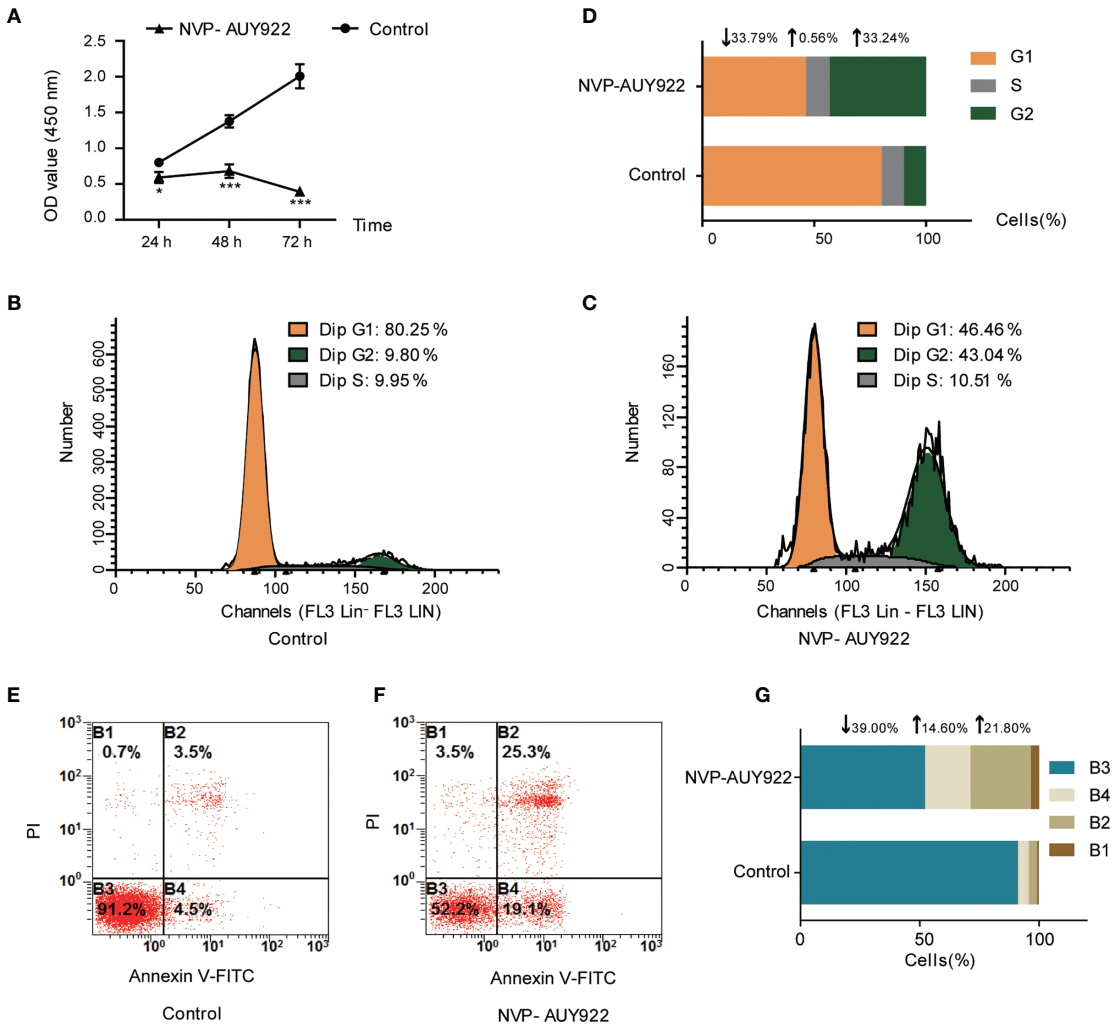


**FIGURE 1** | Cell inhibition activity of NVP-AUY922 on NSCLC cell line H1299. **(A)** NVP-AUY922 inhibited H1299 cell viability. NVP-AUY922 significantly suppressed cell viability against H1299 and its inhibition activity increased with elongated treat time. The data was presented as Mean ± SD, *$P$ <0.05, ***$P$ <0.001 (*vs* Control, n = 3) indicated a significant difference versus the control. **(B)** Cell cycle distribution for H1299 treated with DMSO for 72 h. **(C)** Cell cycle distribution for H1299 treated with NVP-AUY922 for 72 h. **(D)** Bar graph for cell percentage in G1, S and G2 phase of H1299 treated with NVP-AUY922 or DMSO for 72 h NVP-AUY922 induced H1299 cell cycle arrest in G2 phase. **(E)** Cell distribution in four quadrants of H1299 treated with DMSO. **(F)** Cell distribution in four quadrants of H1299 treated with NVP-AUY922. **(G)** Bar graph for cell percentage in four quadrants of H1299 treated with NVP-AUY922 or DMSO. Control, H1299 treated with DMSO; NVP-AUY922, H1299 treated with NVP-AUY922. The four quadrants represented as: B1, necrotic cell rate; B2, late apoptotic rate; B3, Normal cell rate; B4, early apoptotic rate. NVP-AUY922 promoted H1299 cell apoptosis. The results indicated that NVP-AUY922 exhibited favorable inhibition activity against H1299 cells by suppressing cell viability, inducing cell cycle arrest and promoting cell apoptosis.

bonds, hydrophobic effects, derived from isopropyl group of the benzene ring in NVP-AUY922 with surrounding residues of $Hsp90^N$, also played an important role for their powerful binding force. The results suggested a competitive ATP-binding inhibition of NVP-AUY922 against $Hsp90^N$, which inactivated the molecular chaperone function of $Hsp90^N$, resulting in inhibiting or killing cancer cells.

## Complex Crystal Structure Determination

$Hsp90^N$ protein, expressed in *E. coli* BL21 DE3, was purified by immobilized Ni+ affinity chromatography, and followed by gel filtration chromatography. $Hsp90^N$ was co-crystallized with NVP-AUY922 by hanging-drop vapor diffusion method. The complex crystals of $Hsp90^N$-NVP-AUY922 were obtained at 4 °C after growing for 3–5 d. Crystals were rhombus, with the average dimension of approximately 120 μm × 70 μm × 50 μm (**Supplementary 1, Figure S1**).

Meanwhile, the complex crystal structure of $Hsp90^N$-NVP-AUY922 was determined by molecular replacement method, and $Hsp90^N$-FS23 (PDB ID 5CF0) (25) was taken as the analytic model. The coordinates and structure factors have been deposited in PDB (PDB ID 6LTI). Data for collection and

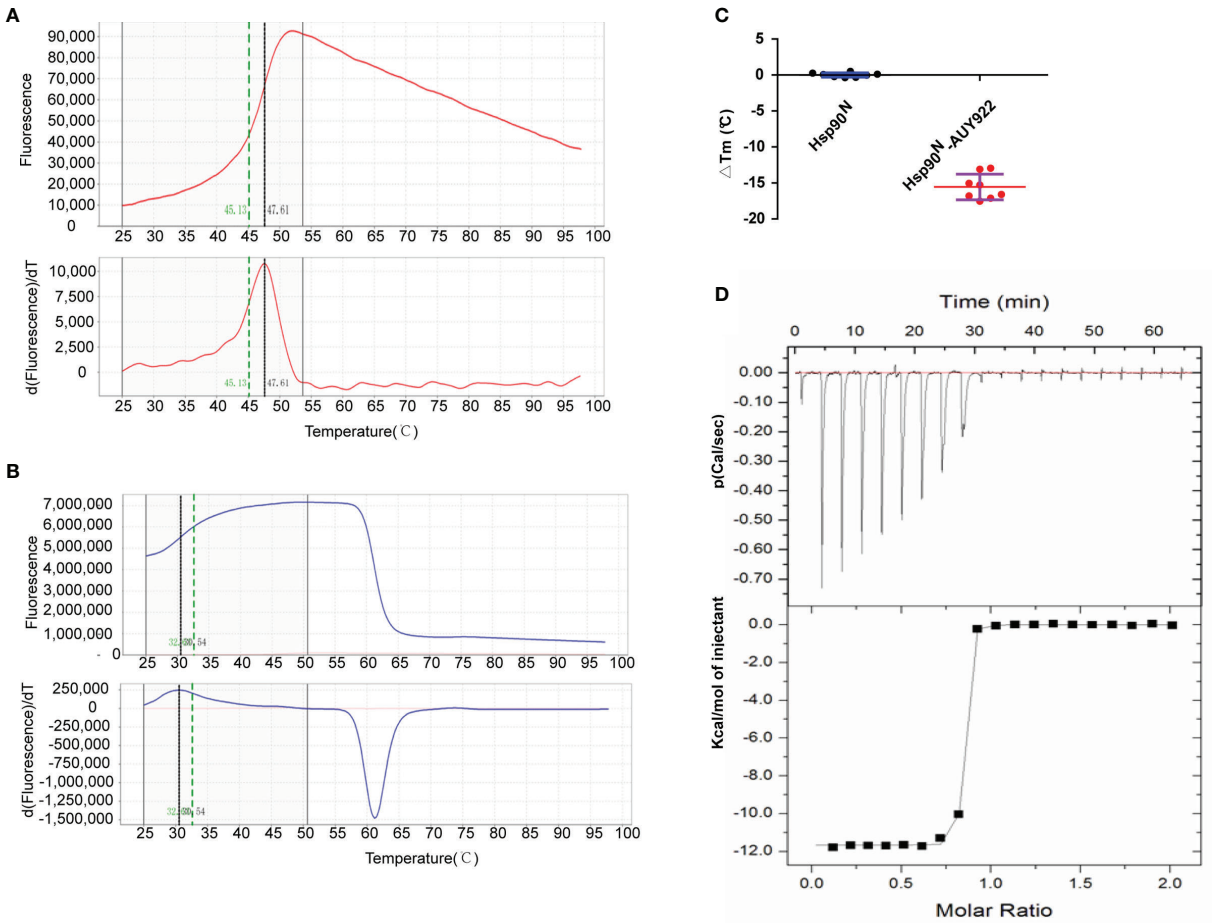


**FIGURE 2** | New NVP-AUY922 derivatives design according to complex crystal structure and molecular docking evaluation. **(A)** Design scheme for new NVP-AUY922 derivatives. **(B)** Top ten new derivatives with the highest Total scores evaluated by molecular docking using SYBYL-X 2.0 software. **(C)** Simulated overall 3D structure of $Hsp90^N$-A15. Cartoon for $Hsp90^N$ and stick for A15. **(D)** Simulated intermolecular force between $Hsp90^N$ and A15. For A15, the carbon, nitrogen, oxygen and sulfur atoms of were marked in green, blue, red and yellow, respectively. For $Hsp90^N$, the carbon, nitrogen, oxygen and sulfur atoms were marked in cyan, blue, red and yellow, respectively. The red dashed line represents the hydrogen bond. **(E)** Connolly surface of simulated complex 3D structure of $Hsp90^N$-A15. **(F)** Molecular structure of A15.

**TABLE 1** | Dissociation constant and thermodynamic data for the target $Hsp90^N$ binding with its ligand NVP-AUY922 at 25°C.

| Items | Thermodynamic data (Mean ± SD, n = 4) |
|---|---|
| N | 0.78 ± 0.04 |
| $K_d$ (nM) | 5.10 ± 2.10 |
| $\Delta G_a$ (kcal/mol) | −11.50 |
| $\Delta H_a$ (kcal/mol) | −11.40 ± 0.30 |
| $T\Delta S_a$ (kcal/mol) | 0.10 |

refinement statistics are described in **Table 2**. A 1.59 Å resolution limit diffraction data was collected with a final $R_{free}$ of 0.20 and $R_{work}$ of 0.18, co-crystal space group of $I$ 222, and unit cell parameters of $a$ = 66.18 Å, $b$ = 89.29 Å, $c$ = 99.56 Å; $\alpha = \beta = \gamma =$ 90.00°. Residues Glu16–Lys224 were observed in the refined model structure with no electron density for N-terminal residues Asp9–Glu15 and C-terminal residues Glu225–Glu236. The missing residues were conceivable for the N- and C-termini disordered electron density.

## New NVP-AUY922 Derivatives Design and Molecular Docking Evaluation

A series of novel NVP-AUY922 derivatives was designed according to the complex crystal structure and molecular interaction analysis, as is shown in **Figure 4A**. For the new derivative design, it was crucial to maintain the special molecular conformation of NVP-AUY922. First, hydrogen bonds played a key role and introduction of hydrophilic groups could be a favorable strategy. For instance, the 2,4-Dihydroxy-5-isopropyl-phenyl ring moiety was varied to an amino group or sulfydryl group, the isoxazole ring was modified to a 1*H*-pyrazole ring and the carbanyl group of formamide group was changed by a sulfonyl group. Second, hydrophobic effects were another specific

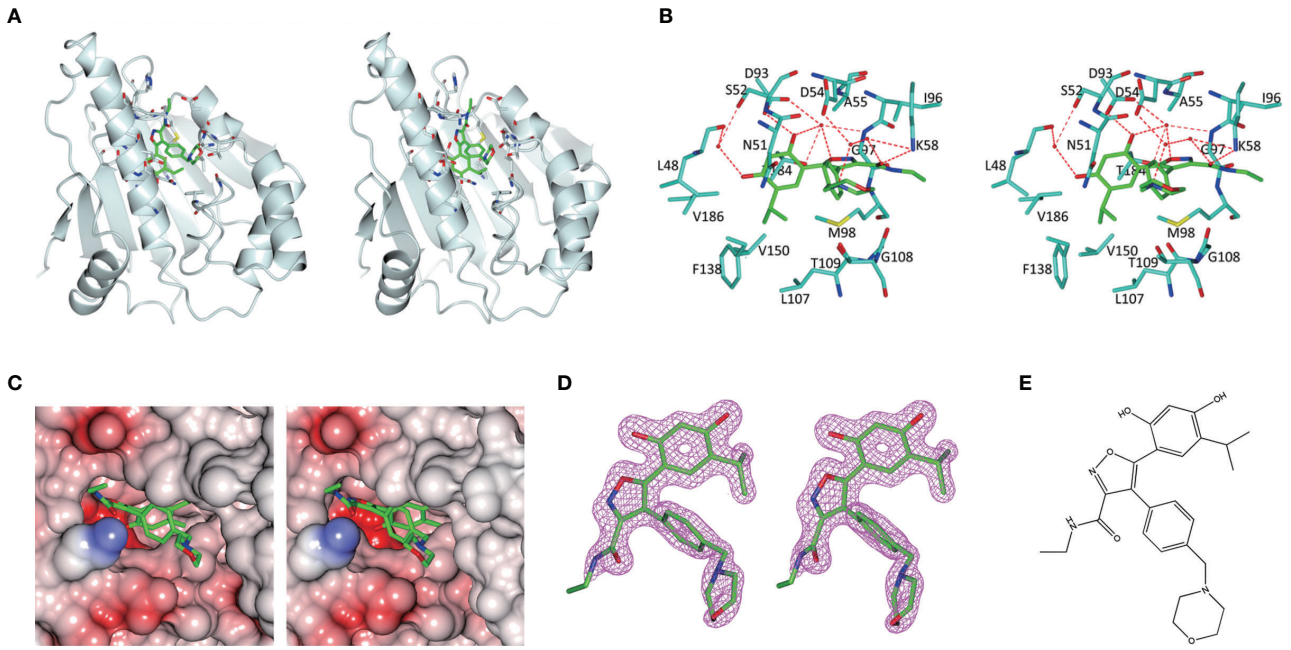


**FIGURE 3** | Molecular interaction analysis for NVP-AUY922 and Hsp90$^N$ by thermal shift assay (TSA) and isothermal titration calorimetry (ITC). **(A)** Melting curve of protein Hsp90$^N$. **(B)** Melting curve of Hsp90$^N$ binding with NVP-AUY922. **(C)** ΔTm. (°C) The melting temperature differences of Hsp90$^N$ binding with or without NVP-AUY922 (−15.56 ± 1.78°C). Values were presented as Mean ± SD, ***$P < 0.001$, n = 8. **(D)** ITC plots for Hsp90$^N$ binding with its ligand NVP-AUY922. Upper panel: the raw titration data. A constant temperature against time was maintained, interaction heat for injection was given by the area of each peak. Lower panel: the bimolecular data fitting of normalized heats against the molar concentration during Hsp90$^N$-NVP-AUY922 binding process. Titrations were performed in PBS (pH 7.5) at 25°C.

factor contributed to their affinity. Therefore, transformation of hydrophobic functional groups was considered as appropriate structural modification scheme, followed by isopropyl group on the 2,4-Dihydroxy-5-isopropyl-phenyl ring moiety was replaced by a dimethylamino, trifluoromethyl, ethane or tert-butyl group, respectively. Last, considering the further drug metabolism, a thiomorpholine, piperazine or 1-methyl-piperazine was used to substitute the morpholine ring.

Based on the scheme, thirty-two novel NVP-AUY922 derivatives were successfully designed and evaluated by molecular docking with Total score and Cscore. The molecular structures, Total scores and Total score increments compared with NVP-AUY922 for new derivatives are presented in **Supplementary 2 Table S1**. Total score, evaluates the binding force between target and ligand, is the negative logarithmic value (−log) of the dissociation constant ($K_d$) of target-ligand, with effects of hydrophobic interaction, polarity, repulsion, entropy change, hydrogen bonds, collision, and so on, to be considered. Higher values indicate stronger binding force of target-ligand. Cscore is a comprehensive score of D-score, PMF-score, G-score, Chem-score, and Total score. The max score is five points. Usually, derivatives with high scores (Total score ≥6, Csore ≥4) were recognized as favorable ligands. Twenty-eight novel NVP-AUY922 derivatives showed increased binding force with the target Hsp90$^N$ shown as high Total scores, which manifested a feasible design scheme by molecular docking evaluation. The molecular structures and the Total score increment of top ten new derivatives are shown in **Figure 4B**.

A15 perfomed the top optimal representative (Total score, 11.9). Thereby, simulated complex 3D structure of Hsp90$^N$-A15 was built, and analyzed their molecular interaction mechanism in detail. A15 was accommodated appropriately in the ATP-binding pocket of Hsp90$^N$ (**Figure 4C**). Compared with NVP-AUY922, the 5-amino-2-tert-butyl-phenol group of A15 was obviously shifted from the interior of cavity to the exterior. Meanwhile, the branched chain of pyrazole ring was moved oppositely from the external space into the internal pocket. Besides, the piperazine ring of A15 was shrunk gently into the pocket (**Figures 4C–E**), while the morpholine ring of NVP-AUY922 was extended out of the cavity (**Figure 4A**).

Three hydrogen bonds between A15 and residues D93 (2.9 Å), L107 (2.7 Å) and G135 (3.0 Å) of Hsp90$^N$ were formed, respectively. Meanwhile, the piperazine ring together with adjacent aromatic ring formed hydrophobic interactions with residue G135, the pyrazole ring with branched chain arranged hydrophobic contacts with residues S52, M98, and V186, the 5-amino-2-tert-butyl-phenol group formed hydrophobic contacts with residues D54 and A55 (**Figure 4D**). Therefore, the hydrogen bonds and hydrophobic interactions played an important role for the intense binding of Hsp90$^N$-A15. The results would provide promising lead compounds for anti-NSCLC new drug development based on NVP-AUY922.

**TABLE 2 |** Data processing and refinement for complex crystal of $Hsp90^N$-NVP-AUY922.

| Diffraction source | BL17U1, SSRF[a] |
|---|---|
| ***Diffraction data*** | |
| Resolution (Å) | 50.00–1.59 (1.62–1.59)[a] |
| Space group | *I* 222 |
| Unit cell parameters | |
| *a*, *b*, *c* (Å) | 66.18, 89.29, 99.56 |
| $\alpha$, $\beta$, $\gamma$ (°) | 90.00, 90.00, 90.00 |
| Wavelength (Å) | 0.97890 |
| Total reflections | 521,803 |
| Unique reflections | 40,044 |
| Redundancy | 13.00 (12.10)[a] |
| Mean I/$\sigma$ (I) | 134.80/2.90 (1.90/1.10) |
| Completeness (%) | 99.70 (100.0)[a] |
| $R_{sym}$ *or* $R_{merge}$[a] | 0.074 (1.013)[a] |
| ***Refinement data*** | |
| Resolution range (Å) | 44.64–1.59 |
| Reflections in working set | 38,034 |
| Reflections in test set | 2,000 |
| $R_{work}$[b]/$R_{free}$[c] (%) | 0.18/0.20 |
| Mean temperature factor (Å$^2$) | 32.23 |
| Bond lengths (Å) | 0.007 |
| Bond angles (°) | 0.844 |

[a]*Data in parentheses are values for the highest-resolution shells.*

[b]$R_{work}= \Sigma_{hkl} ||F_{obs}| - |F_{calc}||/\Sigma_{hkl}|F_{obs}|$, $F_{obs}$ *are observed structure factors,* $F_{calc}$ *are calculated structure factors.*

[c]$R_{free}$, *calculated similar as* $R_{work}$, *with 5% of data from a test set excluded from the refinement calculation.*

## DISCUSSION

Lung cancer is the top one mortality cancer and NSCLC covers 80% of patients (2). Recently, targeted therapies for lung cancer have been made remarkable progress based on the genomic studies on the subtypes of NSCLC, leading to the improvement of clinical outcomes for NSCLC, but there is still a low 5-year survival rate of less than 20% and susceptible to drug resistance (3). As is well known, cancer cells carry mutant genes and proteins to survive from therapeutic toxins (4). Hsp90, a well-known molecular chaperone, played a crucial role in tumorigenesis and progression. Hsp90 can assist over 280 client proteins in correct folding and conformational maturation, which are widely involved in signal transduction, cell cycle and apoptosis regulation in cancer cells. Therefore, Hsp90 demonstrated advantages in overcoming drug resistance as a broad-spectrum anti-cancer target, which would be another choice for NSCLC patients with drug resistance. Because the activity of chaperone molecule must obtain energy from ATP hydrolysis, $Hsp90^N$ inhibitors disabled molecular chaperone function of Hsp90 by competitively suppressing ATP-binding to result in multiple misfolded or immature client proteins that were captured and degraded by the proteasome, cancer cells were thereby suppressed or killed. Therefore, the development of Hsp90 inhibitors has always been a significant tactic for anti-NSCLC drug development (5–9).

NVP-AUY922, a promising second generation $Hsp90^N$ inhibitor, exhibited high objective response rate in NSCLC patients with the ALK rearrangement and EGFR mutations. Though NVP-AUY922 was terminated in a phase II clinical trial by Novartis for unsatisfied endpoint of complete and partial response (7, 17–20), NVP-AUY922 was still a promising lead compound for anti-NSCLC new drug development by the structural optimization of NVP-AUY922.

Herein, a 1.59 Å-high-resolution complex crystal structure of $Hsp90^N$-NVP-AUY922 was successfully determined by XRD, which made it possible to clearly exhibit the binding mode and molecular interaction in detail between NVP-AUY922 and its target $Hsp90^N$. The continuous and clear electron density was presented in the empty ATP-binding pocket of $Hsp90^N$ and well matched with NVP-AUY922 molecule structure. Except for hydrophobic interactions, NVP-AUY922 exhibited strong affinity to $Hsp90^N$ for complex hydrogen bond networks, namely, direct hydrogen bonds and water-mediated hydrogen bonds. There was still a vast room around NVP-AUY922 in the ATP-binding pocket for further structural optimization.

Crystal structure analysis, TSA and ITC were comprehensively assessed to study the molecular interaction mechanism of $Hsp90^N$-NVP-AUY922. Melting temperature (Tm) is a definite parameter for protein under certain conditions which is changed while binding ligands (ΔTm). TSA was applied to detect the protein thermal stability with or without ligands according to the Tm and ΔTm calculated by protein melting curve. Greater affinity was indicated by Greater ΔTm and $|\Delta Tm| > 3$ is usually deemed as a favorable ligand. There was a strong affinity between the $Hsp90^N$ and its ligand NVP-AUY922 (ΔTm, −15.56 ± 1.78°C), suggesting that NVP-AUY922 binding to $Hsp90^N$ enhanced the protein thermostability. This was further verified by ITC ($K_d$, 5.10 ± 2.10 nM). ITC evaluated target-ligand binding force by examining the endothermic and exothermic amount when ligand binding to its target. Smaller the $K_d$ is, stronger the binding force is. The large enthalpy change indicated favorable thermodynamic interactions established in the $Hsp90^N$-NVP-AUY922 binding process. The molecular interaction analysis suggested that NVP-AUY922 can inactivate the molecular chaperone function of Hsp90 by accommodating in the ATP-binding pocket, which took the responsibility for the favorable anti-NSCLC activity of NVP-AUY922. In practice, NVP-AUY922 suppressed cell proliferation ($IC_{50}$, 2.85 ± 0.06 μM), induced cell cycle arresting at G2 phase and accelerated cell apoptosis of the NSCLC cell line H1299.

For further structural optimization, it was crucial to keep the special molecular conformation of NVP-AUY922, which was kept by hydrogen bonds and hydrophobic interactions. The design scheme devoted to promote these beneficial interactions by functional group replacements. Under the precise reference of molecular interaction analysis by complex crystal structure, TSA and ITC of $Hsp90^N$-NVP-AUY922, thirty-two new NVP-AUY922 derivatives were designed and molecular docking evaluation showed twenty-eight of them displayed enhanced binding force to the target $Hsp90^N$. This also verified a practicable design scheme. A15 as the optimal representative, simulated $Hsp90^N$-A15 3D structure was built and detailed molecular interaction mechanism was analyzed. Compared with NVP-AUY922, A15 exhibited increased binding force with $Hsp90^N$ and hydrophobic interactions contributed more than hydrogen bonds for $Hsp90^N$-A15 binding. The results would promote novel anti-NSCLC drug development to

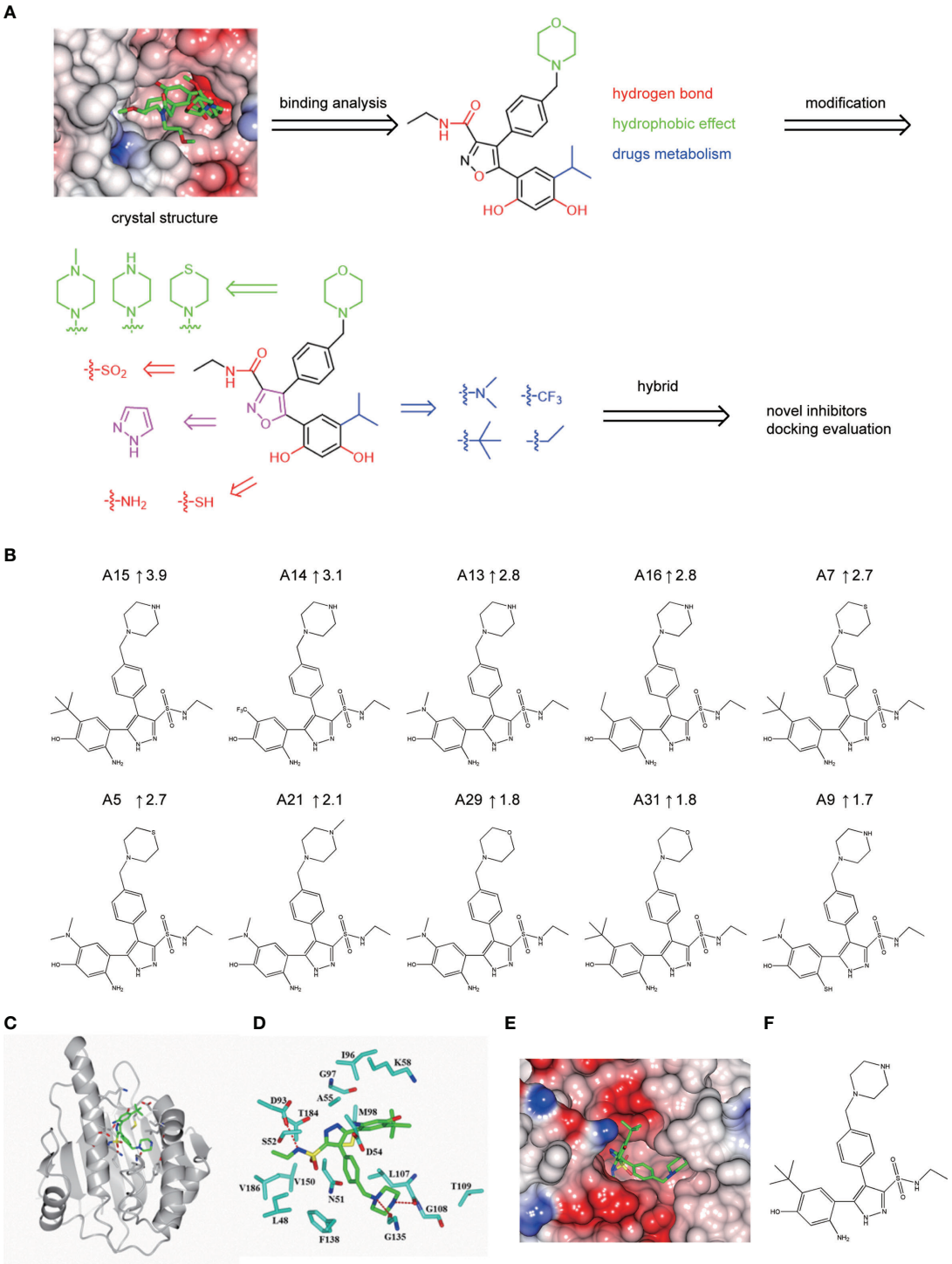


**FIGURE 4** | Hsp90$^{N}$-NVP-AUY922 complex crystal structure. **(A)** Overall structural view of Hsp90$^{N}$-NVP-AUY922. Hsp90$^{N}$ and NVP-AUY922 were indicated by cartoon and stick, respectively. **(B)** Intermolecular forces between Hsp90$^{N}$ and NVP-AUY922. For NVP-AUY922, the carbon, nitrogen and oxygen atoms were colored in green, blue and red, respectively. For Hsp90$^{N}$, the carbon, nitrogen, oxygen and sulfur atoms were shown in cyan, blue, red and yellow, respectively. The red dashed line represents the hydrogen bond. The red spheres showed water molecules. **(C)** Distribution of electrostatic potential on Hsp90$^{N}$-NVP-AUY922 crystal structure surface. Red colored surface reflects the negative charge of electrostatic potential, and blue for positive charge. **(D)** Electron density map (*2Fo-Fc*) of NVP-AUY922. The map was calculated in the vicinity of NVP-AUY922. **(E)** Molecular structure of NVP-AUY922.

overcome drug resistance based on the lead compound NVP-AUY922.

## DATA AVAILABILITY STATEMENT

The original contributions presented in the study are included in the article/**Supplementary Material**. Further inquiries can be directed to the corresponding authors.

## AUTHOR CONTRIBUTIONS

H-LC designed the research study. C-XH, YL, MG, H-JL, LX, XZ, and P-QL performed the research. FY, HZ and J-HH provided help and advice on study design. C-XH, WQ, DZ, and P-QL analyzed the data. C-XH, YL, and MG wrote the manuscript. H-LC, FY, and J-HH revised the paper. All authors listed have made a substantial, direct, and intellectual contribution to the work and approved it for publication.

## FUNDING

This work was funded by the National Natural Science Foundation of China (U1932130), the Program of Shaanxi Provincial Science and Technology Department (2021JQ-786), the Key Program of Shaanxi Provincial Education Department (17JS117), the Program of Shaanxi Administration of Traditional Chinese Medicine (2019-ZZ-ZY009), the Key Program of Weiyang District Bureau of Science, Technology and Industry Information Technology (201928), the Program of Shaanxi Provincial Research Center for the Project of Prevention and Treatment of Respiratory Diseases (2016HXKF05), and the Talent Program of Xi'an Medical University (2016DOC13, 2017GJFY03).

## SUPPLEMENTARY MATERIAL

The Supplementary Material for this article can be found online at: https://www.frontiersin.org/articles/10.3389/fonc.2022.847556/full#supplementary-material

## REFERENCES

1. Sung H, Ferlay J, Siegel RL, Laversanne M, Soerjomataram I, Jemal A, et al. Global Cancer Statistics 2020: Globocan Estimates of Incidence and Mortality Worldwide for 36 Cancers in 185 Countries. *CA Cancer J Clin* (2021) 0:1–41. doi: 10.3322/caac.21660
2. Molina JR, Yang P, Cassivi SD, Schild SE, Adjei AA. Non-Small Cell Lung Cancer: Epidemiology, Risk Factors, Treatment, and Survivorship. *Mayo Clin Proc* (2008) 83(5):584–94. doi: 10.1016/S0025-6196(11)60735-0
3. O smani L, Askin F, Gabrielson E, Li QK. Current WHO Guidelines and the Critical Role of Immunohistochemical Markers in the Subclassification of Non-Small Cell Lung Carcinoma (NSCLC): Moving From Targeted Therapy to Immunotherapy. *Semin Cancer Biol* (2018) 52(Pt 1):103–9. doi: 10.1016/j.semcancer
4. Siegel RL, Miller KD, Jemal A. Cancer Statistics, 2015. *CA Cancer J Clin* (2015) 65(1):5–29. doi: 10.3322/caac.21254
5. Vahid S, Thaper D, Zoubeidi A. Chaperoning the Cancer: The Proteostatic Functions of the Heat Shock Proteins in Cancer. *Recent Pat Anticancer Drug Discov* (2017) 12(1):35–47. doi: 10.2174/1574892811666161102125252
6. Taldone T, Ochiana SO, Patel PD, Chiosis G. Selective Targeting of the Stress Chaperome as a Therapeutic Strategy. *Trends Pharmacol Sci* (2014) 35 (11):592–603. doi: 10.1016/j.tips.2014.09.001
7. Chatterjee S, Bhattacharya S, Socinski MA, Burns TF. HSP90 Inhibitors in Lung Cancer: Promise Still Unfulfilled. *Clin Adv Hematol Oncol* (2016) 14 (5):346–56.
8. Jiang F, Guo AP, Xu JC, Wang HJ, Mo XF, You QD, et al. Identification and Optimization of Novel 6-Acylamino-2-Aminoquinolines as Potent Hsp90 C-Terminal Inhibitors. *Eur J Med Chem* (2017) 141:1–14. doi: 10.1016/j.ejmech.2017.07.080
9. Akram A, Khalil S, Halim SA, Younas H, Iqbal S, Mehar S. Therapeutic Uses of HSP90 Inhibitors in Non-Small Cell Lung Carcinoma (NSCLC). *Curr Drug Metab* (2018) 19(4):335–41. doi: 10.2174/1389200219666180307122441
10. Eccles SA, Massey A, Raynaud FI, Sharp SY, Box G, Valenti M, et al. NVP-AUY922: A Novel Heat Shock Protein 90 Inhibitor Active Against Xenograft Tumor Growth, Angiogenesis, and Metastasis. *Cancer Res* (2008) 68(8):2850–60. doi: 10.1158/0008-5472.CAN-07-5256
11. Moser C, Lang SA, Hackl C, Wagner C, Scheiffert E, Schlitt HJ, et al. Targeting HSP90 by the Novel Inhibitor NVP-AUY922 Reduces Growth and Angiogenesis of Pancreatic Cancer. *Anticancer Res* (2012) 32(7):2551–61.
12. Best OG, Mulligan SP. Heat Shock Protein-90 Inhibitor, NVP-AUY922, Is Effective in Combination With Fludarabine Against Chronic Lymphocytic Leukemia Cells Cultured on CD40L-Stromal Layer and Inhibits Their Activated/Proliferative Phenotype. *Leuk Lymphoma* (2012) 53(11):2314–20. doi: 10.3109/10428194.2012.698278
13. Fernandes JC, Alves P. Recent Patents on Heat Shock Proteins Targeting Antibodies. *Recent Pat Anticancer Drug Discov* (2017) 12(1):48–54. doi: 10.2174/1574892812666161123141516
14. Carlos GE, Michael J. Combination of Hsp90 and Herceptin Inhibitors. (2017). JP2017-141278.
15. David P. Combination Therapy of Hsp90 Inhibitors With Platinum-Containing Agents. (2018). US20180221345.
16. Sidera K, Patsavoudi E. HSP90 Inhibitors: Current Development and Potential in Cancer Therapy. *Recent Pat Anticancer Drug Discov* (2014) 9(1):1–20. doi: 10.2174/15748928113089990031
17. Sessa C, Shapiro GI, Bhalla KN, Britten C, Jacks KS, Mita M, et al. First-In-Human Phase I Dose-Escalation Study of the HSP90 Inhibitor AUY922 in Patients With Advanced Solid Tumors. *Clin Cancer Res* (2013) 19:3671–80. doi: 10.1158/1078-0432.CCR-12-3404
18. Felip E, Barlesi F, Besse B, Chu Q, Gandhi L, Kim SW, et al. Phase 2 Study of the HSP-90 Inhibitor AUY922 in Previously Treated and Molecularly Defined Patients With Advanced Non-Small Cell Lung Cancer. *J Thorac Oncol* (2018) 13(4):576–84. doi: 10.1016/j.jtho.2017.11.131
19. Johnson ML, Yu HA, Hart EM, Weitner BB, Rademaker AW, Patel JD, et al. Phase I/II Study of HSP90 Inhibitor AUY922 and Erlotinib for EGFR-Mutant Lung Cancer With Acquired Resistance to Epidermal Growth Factor Receptor Tyrosine Kinase Inhibitors. *J Clin Oncol* (2015) 33(15):1666–73. doi: 10.1200/JCO.2014.59.7328
20. Vermes K. *Vernalis PLC Stumbles As Novartis AG Abandons Work On Auy922*. Available at: http://www.biospace.com/News/vernalisplc-stumbles-as-novartis-ag-abandons-/358835.
21. Brough PA, Aherne W, Barril X, Borgognoni J, Boxall K, Cansfield JE, et al. 4,5-Diarylisoxazole Hsp90 Chaperone Inhibitors: Potential Therapeutic Agents for the Treatment of Cancer. *J Med Chem* (2008) 51(2):196–218. doi: 10.1021/jm701018h
22. Stebbins CE, Russo AA, Schneider C, Rosen N, Hartl FU, Pavletich NP. Crystal Structure of an Hsp90–geldanamycin Complex: Targeting of a Protein Chaperone by an Antitumor Agent. *Cell* (1997) 89:239–50. doi: 10.1016/S0092-8674(00)80203-2
23. Wang Q, Zhang K, Cui Y, Wang ZJ, Pan QY, Liu K, et al. Upgrade of Macromolecular Crystallography Beamline BL17U1 at SSRF. *Nucl Sci Tech* (2018) 29(5):68. doi: 10.1007/s41365-018-0398-9
24. Yu F, Wang Q, Li M, Zhou H, Liu K, Zhang KH, et al. Aquarium: An Automatic Data-Processing and Experiment Information Management System for Biological Macromolecular Crystallography Beamlines. *J Appl Crystallogr* (2019) 52:472–7. doi: 10.1107/S1600576719001183

25. Li J, Shi F, Chen DQ, Cao HL, Xiong B, Shen JK, et al. FS23 Binds to the N-Terminal Domain of Human Hsp90: A Novel Small Inhibitor for Hsp90. *Nucl Sci Tech* (2015) 26:060503. doi: 10.13538/j.1001-8042/nst.26.060503
26. Liebschner D, Afonine PV, Baker ML, Bunkóczi G, Chen VB, Croll TI, et al. Macromolecular Structure Determination Using X-Rays, Neutrons and Electrons: Recent Developments in Phenix. *Acta Crystallogr D Struct Biol* (2019) 75(Pt 10):861–77. doi: 10.1107/S2059798319011471
27. Cao H, Lyu KK, Liu B, Li J, He JH. Discovery of a Novel Small Inhibitor RJ19 Targeting to Human Hsp90. *Nucl Sci Tech* (2017) 28:148. doi: 10.1007/s41365-017-0300-1
28. Emsley P, Cowtan K. Coot: Model-Building Tools for Molecular Graphics. *Acta Crystallogr D* (2004) 60:2126–32. doi: 10.1107/S0907444904019158
29. Winn MD, Ballard CC, Cowtan KD, Dodson EJ, Emsley P, Evans PR, et al. Overview of the CCP4 Suite and Current Developments. *Acta Crystallogr D* (2011) 67:235–42. doi: 10.1107/S0907444910045749
30. Andreotti G, Monticelli M, Cubellis MV. Looking for Protein Stabilizing Drugs With Thermal Shift Assay. *Drug Test Anal* (2015) 7:831–4. doi: 10.1002/dta.1798
31. He Y, Roth C, Turkenburg JP, Davies GJ. Three-Dimensional Structure of a Streptomyces Sviceus GNAT Acetyltransferase With Similarity to the C-Terminal Domain of the Human GH84 O-GlcNAcase. *Acta Crystallogr D* (2014) 70:186–95. doi: 10.1107/S1399004713029155
32. Olszewska P, Cal D, Zagórski P, Mikiciuk-Olasik E. A Novel Trifluoromethyl 2-Phosphonopyrr- Ole Analogue Inhibits Human Cancer Cell Migration and Growth by Cell Cycle Arrest at G1 Phase and Apoptosis. *Eur J Pharmacol* (2020) 871:172943. doi: 10.1016/j.ejphar.2020.172943
33. Wu WC, Liu YM, Liao YH, Hsu KC, Lien ST, Chen IC, et al. Fluoropyrimidin-2,4-Dihydroxy-5-Isopropylbenzamides as Antitumor Agents Against CRC and NSCLC Cancer Cells. *Eur J Med Chem* (2020) 203(1):12540. doi: 10.1016/j.ejmech.2020.112540
34. Ye K, Wei Q, Gong Z, Huang Y, Liu H, Li Y, et al. Effect of Norcantharidin on the Proliferation, Apoptosis, and Cell Cycle of Human Mesangial Cells. *Ren Fail* (2017) 39(1):458–64. doi: 10.1080/0886022X.2017.1308257

**Conflict of Interest:** The authors declare that the research was conducted in the absence of any commercial or financial relationships that could be construed as a potential conflict of interest.

**Publisher's Note:** All claims expressed in this article are solely those of the authors and do not necessarily represent those of their affiliated organizations, or those of the publisher, the editors and the reviewers. Any product that may be evaluated in this article, or claim that may be made by its manufacturer, is not guaranteed or endorsed by the publisher.

frontiers in Pharmacology

ORIGINAL RESEARCH
published: 08 March 2022
doi: 10.3389/fphar.2022.861642

# The Resistance of Cancer Cells to Palbociclib, a Cyclin-Dependent Kinase 4/6 Inhibitor, is Mediated by the ABCB1 Transporter

*Han Fu[1†], Zhuo-Xun Wu[2†], Zi-Ning Lei[2,3], Qiu-Xu Teng[2], Yuqi Yang[2], Charles R. Ashby[2], Yixiong Lei[1], Yuyin Lian[1]* and Zhe-Sheng Chen[2]**

[1]School of Public Health, Guangzhou Medical University, Guangzhou, China, [2]Department of Pharmaceutical Sciences, College of Pharmacy and Health Sciences, St. John's University, Queens, NY, United States, [3]Guangdong Provincial Key Laboratory of Digestive Cancer Research, Precision Medicine Center, The Seventh Affiliated Hospital, Sun Yat-Sen University, Shenzhen, China

OPEN ACCESS

**Edited by:**
Cong Wang,
Zhengzhou University, China

**Reviewed by:**
Haotian Cao,
Sun Yat-sen Memorial Hospital, China
Hui-Ling Cao,
Xi'an Medical University, China

***Correspondence:**
Yuyin Lian
lianyuyin@126.com
Zhe-Sheng Chen
chenz@stjohns.edu

[†]These authors have contributed equally to this work and share first authorship

**Specialty section:**
This article was submitted to Pharmacology of Anti-Cancer Drugs, a section of the journal Frontiers in Pharmacology

**Received:** 24 January 2022
**Accepted:** 18 February 2022
**Published:** 08 March 2022

**Citation:**
Fu H, Wu Z-X, Lei Z-N, Teng Q-X, Yang Y, Ashby CR, Lei Y, Lian Y and Chen Z-S (2022) The Resistance of Cancer Cells to Palbociclib, a Cyclin-Dependent Kinase 4/6 Inhibitor, is Mediated by the ABCB1 Transporter. Front. Pharmacol. 13:861642. doi: 10.3389/fphar.2022.861642

Palbociclib was approved by the United States Food and Drug Administration for use, in combination with letrozole, as a first-line treatment for estrogen receptor-positive/human epidermal growth factor receptor 2-negative (ER+/HER2-) postmenopausal metastatic breast cancer. However, recent studies show that palbociclib may be an inhibitor of the ABCB1 transporter, although this remains to be elucidated. Therefore, we conducted experiments to determine the interaction of palbociclib with the ABCB1 transporter. Our *in vitro* results indicated that the efficacy of palbociclib was significantly decreased in the ABCB1-overexpressing cell lines. Furthermore, the resistance of ABCB1-overexpressing cells to palbociclib was reversed by 3 μM of the ABCB1 inhibitor, verapamil. Moreover, the incubation of ABCB1-overexpressing KB-C2 and SW620/Ad300 cells with up to 5 μM of palbociclib for 72 h, significantly upregulated the protein expression of ABCB1. The incubation with 3 μM of palbociclib for 2h significantly increased the intracellular accumulation of [$^3$H]-paclitaxel, a substrate of ABCB1, in ABCB1 overexpressing KB-C2 cells but not in the corresponding non-resistant parental KB-3-1 cell line. However, the incubation of KB-C2 cells with 3 μM of palbociclib for 72 h decreased the intracellular accumulation of [$^3$H]-paclitaxel due to an increase in the expression of the ABCB1 protein. Palbociclib produced a concentration-dependent increase in the basal ATPase activity of the ABCB1 transporter ($EC_{50}$ = 4.73 μM). Molecular docking data indicated that palbociclib had a high binding affinity for the ABCB1 transporter at the substrate binding site, suggesting that palbociclib may compete with other ABCB1 substrates for the substrate binding site of the ABCB1. Overall, our results indicate that palbociclib is a substrate for the ABCB1 transporter and that its *in vitro* anticancer efficacy is significantly decreased in cancer cells overexpressing the ABCB1.

**Keywords: ATP-binding cassette transporter, ABCB1, palbociclib, multidrug resistance, CDK4/6 inhibitor**

## INTRODUCTION

Multidrug resistance (MDR) in tumors is defined as the development of resistance to structurally and mechanistically unrelated classes of anticancer drugs (Szakács et al., 2006). MDR is a major cause of cancer chemotherapy failure, which can lead to tumor recurrence and the death of cancer patients (Lage and Dietel, 2000). MDR can occur due to 1) the overexpression of certain adenosine triphosphate (ATP)-binding cassette (ABC) transporter proteins (Robey et al., 2018); 2) an increase in the repair of damaged DNA (Helleday et al., 2008); 3) mutations in the target of the anticancer drugs which decrease or abrogate the efficacy of these drugs (Chandrasekhar et al., 2019); 4) an increased tolerance to the stressful tumor microenvironment (TME) (Erin et al., 2020; Seebacher et al., 2021); 5) evasion of programmed cell death (Shahar and Larisch, 2020; Neophytou et al., 2021); 6) higher levels of reactive oxidative species (Cui et al., 2018); 7) an increase in the biotransformation of the anticancer drugs to less active or inactive metabolites (Zaal and Berkers, 2018); 8) sequestration of drugs by organelles or intracellular molecules that decrease their interaction with their cellular target(s), and 9) specific long noncoding RNAs (lncRNAs) (Liu et al., 2020). Numerous studies have shown that one of the primary mechanisms that mediates MDR in cancer cells is the overexpression of ABCB1 (i.e., P-gp or MDR1), ABCG2 (i.e., BCRP or MXR), and ABCC1 (i.e., MRP1) transporters (Fletcher et al., 2016), which significantly decrease the intracellular levels of certain anticancer drugs by extrusion from cancer cells, thereby decreasing or even abolishing their efficacy (Wu and Fu, 2018). The ABCB1 transporter was discovered in 1976 and is the most studied ABC transporter. It is constitutively expressed in the blood-brain barrier, kidneys and liver, to protect normal cells from xenobiotic compounds. When overexpressed in cancer cells, ABCB1 produces an MDR phenotype to various chemotherapeutic drugs, including paclitaxel, doxorubicin, and tyrosine kinase inhibitors (TKIs) such as GSK-1070916 and TAK243 (Wu et al., 2020c; Wu et al., 2022). Over the past 4 decades, researchers have developed three generations of ABCB1 inhibitors, but their reversal effect was limited by their toxicity and/or low efficacy *in vivo*. Recently, it was reported that some TKIs, such as GS-9973, and sitravatinib, inhibit the efflux function of ABCB1, thereby reversing, reversing drug resistance (Yang et al., 2020; Narayanan et al., 2021). Similarly, ABCG2 is also a major mediator of MDR in cancer cells. ABCG2 mediates the efflux of the chemotherapeutic drugs, mitoxantrone, topotecan, irinotecan, and various tyrosine kinase inhibitors (TKIs), such as tivantinib and pevonedistat (Wu et al., 2020a; Wei et al., 2020). In contrast to ABCB1, the development of ABCG2 inhibitors has been significantly slower. In addition to the commonly used ABCG2 inhibitors, Ko143 and fumitremorgin C, recent studies showed that the TKIs, poziotinib, and CC-671, inhibit the efflux function of ABCG2 (Wu et al., 2020b; Zhang et al., 2020b). However, none of these inhibitors have been evaluated in clinical trials.

It is well known that unregulated cell division can lead to the development and progression of cancer (Sherr, 1996). Cyclin-dependent kinases (CDKs) are a family of serine/threonine protein kinases that regulate cell cycle and gene transcription (Manning et al., 2002). The CDK family can be divided into two major groups: 1) those that regulate cell cycle progression and interact with multiple cyclins, i.e., CDK1, CDK2, CDK4 and CDK6 and 2) those that regulate transcription and interact only with a single cyclin, i.e., CDK7, CDK8, CDK9, CDK11, CDK12, and CDK13 (Schmitz and Kracht, 2016; Wood and Endicott, 2018; Liang et al., 2020). The cell cycle can be divided into four successive phases: G1 (pre-DNA synthesis), S (DNA synthesis phase), G2 (late DNA synthesis), and M (mitotic phase) (Xu et al., 2018). The cyclin D-CDK4/6-RB-p16$^{INK4A}$ pathway is a key regulatory pathway in the transition from G1 to S phase (Basso and Doll, 2006; Asghar et al., 2015). The dysregulation of this pathway facilitates cancer cell cycle progression and proliferation (Shapiro, 2006; Burkhart and Sage, 2008; Knudsen and Knudsen, 2008). CDK4/6 is a key regulator of the transition from G1 to S phase (Yuan et al., 2021) and the inhibition of CDK4/6 blocks progression of the cell cycle from the G1 to S phase in cancer cells (Anders et al., 2011; O'Leary et al., 2016; Kato et al., 2021). The CDK 4/6 inhibitor, palbociclib, in combination with other drugs, has been approved by the FDA to treat metastasized breast cancer that is estrogen receptor (ER) positive and human epidermal growth factor receptor 2 (HER2) negative (Ciruelos et al., 2020). The inhibition of CDK4/6 by palbociclib inhibits the phosphorylation of the retinoblastoma protein (RB), thereby blocking the progression of the cell cycle from the G1 to S phase, which inhibits cancer cell proliferation (Weinberg, 1995; Spring et al., 2020). A recent clinical trial reported that in patients with previously untreated ER-positive, HER2-negative advanced breast cancer, the combination of palbociclib with letrozole produced a longer progression-free survival than letrozole alone (Finn et al., 2016). Another trial reported that palbociclib, in combination with fulvestrant, improved the overall survival compared to fulvestrant alone, in ER-positive, HER2-negative advanced breast cancer patients (Turner et al., 2018). Although palbociclib and endocrine therapy is an effective treatment for ER-positive and HER2-negative metastatic breast cancer, the addition of palbociclib to standard endocrine therapy did not significantly improve treatment outcomes, compared to endocrine therapy alone (Finn et al., 2015; Cristofanilli et al., 2016; Harbeck et al., 2016; Malorni et al., 2018; Rugo et al., 2018; Johnston et al., 2019; Gnant et al., 2021; Mayer et al., 2021).

Previously it has been reported that in *ABCB1* and *ABCG2*-transfected Madin-Darby canine kidney II (MDCKII) cell lines, palbociclib was a substrate for the ABCB1 and ABCG2 transporters (Parrish et al., 2015). Similarly, the penetration of palbociclib across the blood-brain barrier of *ABCB1* and *ABCG2* gene knockout mice was significantly decreased by ABCB1 and ABCG2 transporters, suggesting that palbociclib was a substrate for ABCB1 and ABCG2 transporters (De Gooijer et al., 2015). In contrast, studies by Gao et al. (2017) and Sorf et al. (2020) suggested that palbociclib may be an inhibitor of the ABCB1 transporter. Therefore, it is crucial to determine if palbociclib is a substrate or an inhibitor because if it is a substrate of the ABCB1 transporter, cancer cells that overexpress ABCB1 transporter will

have lower intracellular levels of palbociclib, which could decrease or abrogate its efficacy. Therefore, in this study, we conducted *in vitro* experiments and to determine if palbociclib is an inhibitor or a substrate of the ABCB1 or ABCG2 transporter.

# MATERIALS AND METHODS

## Reagents

Colchicine, doxorubicin (adriamycin), mitoxantrone, and verapamil were purchased from Sigma Aldrich Trading Co. (Shanghai, China). All of the drugs were dissolved in 100% DMSO to produce a 10 mM stock solution.

## Cell Lines and Cell Culture

The human epidermoid carcinoma cell line, KB-3-1, was used as the parental cell line, and its colchicine–selected subline KB-C2, which overexpresses the ABCB1 transporter (Fojo et al., 1985), was used as a drug-resistant cell line. The human colon cancer cell line, SW620, was used as the parental cell line, and the doxorubicin-selected subline, SW620/Ad300, which overexpresses the ABCB1 transporter (Lai et al., 1991a; Lai et al., 1991b), was used as another drug-resistant cell line. We also used SW620 parental and SW620/Ad300 drug-resistant cell sublines, where the gene for the *ABCB1* transporter was knocked out using the CRISPR/Cas9 system (Lei et al., 2021). The human large cell lung cancer cell line, NCI-H460, was used as the parental cell line and its mitoxantrone-selected subline, NCI-H460/MX20, which overexpresses the ABCG2 transporter (Henrich et al., 2007), was used as another drug-resistant cell line. The drug resistance of the KB-C2, SW620/Ad300 and NCI-H460/MX20 cells was maintained in media containing 2 μg/ml of colchicine, 300 ng/ml of doxorubicin and 20 nM of mitoxantrone, respectively. The HEK293/pcDNA3.1, HEK293/ABCB1, and HEK293/ABCG2-WT cell lines were transfected with the empty vector pcDNA3.1, the pcDNA3.1 vector containing a full-length gene coding for the ABCB1 transporter and the pcDNA3.1 vector containing a full-length gene coding for the wild-type (WT) ABCG2, respectively (Robey et al., 2008; Mi et al., 2010). All gene transfected cell lines were maintained in a medium containing 2 mg/ml of G418, an aminoglycoside derivative used for the selection of eukaryotic expression vectors containing the related resistance genes (Robey et al., 2003). All the MDR cell lines were cultured in complete medium, containing 10% fetal bovine serum and 1% of penicillin/streptomycin and incubated at 37°C in an incubator with 5% $CO_2$. Prior to the experiment, all the cells were cultured in drug-free complete medium for at least 2 weeks.

## Cytotoxicity Assay

The efficacy of palbociclib was determined using the MTT assay, which assesses cytotoxicity, as previously described (Zhang et al., 2016). Briefly, the cells were seeded in 96-well plates and incubated with different concentrations of palbociclib (0.03–100 μM) in the presence or absence of 3 μM of verapamil. The 96-well plates were incubated for 72 h. On the last day, MTT solution (5 mg/ml) was added to each well and the cells were incubated for 4 h at 37°C. At the end of the incubation, the supernatant was discarded and 100 μL of DMSO was added to each well to dissolve the purple formazan crystals. Subsequently, the absorbance at 570 nm was read using a AccuSkan™ GO UV/Vis Microplate Spectrophotometer (Thermo Fisher Scientific Inc., Waltham, MA, United States).

## ABCB1 ATPase Assay

An ATPase assay of kit (TEBU-BIO nv, Boechout, Belgium) was used to determine the effect of palbociclib on basal ABCB1 ATPase activity, as previously described (De Bruijn et al., 1986). Briefly, High Five insect cell membrane vesicles, containing the ABCB1 transporter, were incubated in microcentrifuge tubes at 37°C for 5 min in the supplied assay buffer, in the presence or absence of the phosphorotyrosol phosphatase inhibitor, $Na_3VO_4$. Subsequently, the cells were incubated with vehicle (DMSO) or 0.1–20 μM of palbociclib for 3 min at 37°C. Subsequently, 5 mM of $Mg^{2+}$ATP was added to activate ATP hydrolysis, and 20 min later, the reaction was terminated by adding 0.1 ml of a 5% sodium dodecyl sulfate solution. The inorganic phosphate produced by the activation of the ATPase was measured as previously described (Ambudkar, 1998; Shi et al., 2007; Shi et al., 2011). In a separate experiment, High Five insect cell membrane vesicles were incubated with palbociclib (0.1–20 μM) and 3 μM of tepotinib, an inhibitor of the ABCB1 transporter, and ATPase activity was determined as above mentioned.

## [$^3$H]-Paclitaxel Accumulation Assay

The intracellular accumulation of [$^3$H]-paclitaxel in the KB-3-1 parental and KB-C2 resistant cell lines was used to determine the effect of palbociclib on ABCB1-mediated drug efflux activity, following the same protocol as previously described (Wu et al., 2020c). The samples were assayed for radioactivity using a Packard TRI-CARB 1900 CA liquid scintillation analyzer (Packard Instrument, Downers Grove, IL).

## Western Blot Analysis

Drug-resistant KB-C2 and SW620/Ad300 cells were incubated with 0.3–5 μM of palbociclib for up to 72 h at 37°C and the corresponding parental cells KB-3-1 and SW620 were used as negative control. The cell lysates were prepared by adding RIPA lysis buffer to the cells, then centrifuged at 12,000 g, 4°C for 20 min to collect the supernatant. The protein concentration in the lysates was determined using the bicinchoninic acid assay, as previously described (Wang et al., 2020a). Protein samples were subjected to SDS-PAGE, transferred to PVDF membrane and incubated with the primary antibodies (anti-ABCB1 antibody and anti-GAPDH antibody) overnight at 4°C after being blocked with 5% skim milk powder for 2 h at room temperature. The next day, after washing the PVDF membranes with TBST buffer, the PVDF membranes were incubated with horseradish peroxidase-labeled secondary antibodies (anti-mouse antibody, 1:1,000 dilution) for 2 h at room temperature and the immunoreactive bands were visualized by chemiluminescence by using an enhanced chemiluminescence detection system (Amersham, NJ, United States). Finally, the results were quantified using

ImageJ software, which was used to determine the relative density of the immunoreactive bands.

## Molecular Docking of Palbociclib With Human ABCB1 Models

The 3-D structure of palbociclib was established for docking simulations, using a human ABCB1 model, as previously described (Ji et al., 2018; Zhang et al., 2020a; Zhang et al., 2020b). The human ABCB1 protein model 6QEX (paclitaxel bound) was acquired from Protein Data Bank. The model was an inward-facing human ABCB1 with a resolution of 3.6 Å (6QEX). Docking grid (length: 30 Å) center coordinates were defined by setting the centroid with the amino acid residues that are suggested to interact with paclitaxel, an ABCB1 substrate. The receptor and ligand preparations and docking simulations were done using the default settings in Maestro v11.1 (Schrodinger, LLC, Cambridge, MA). The top-scoring pose, expressed as kcal/mol, was selected for further analysis and visualization.

## Statistical Analysis

All experiments were repeated at least three times and $IC_{50}$ values were expressed as the mean ± standard deviation (SD) of at least three independent experiments. All data were expressed as mean ± SD and statistically analyzed using a one-way analysis of variance (ANOVA), followed by Tukey's *post hoc* test. GraphPad Prism 8.1 software was used in to plot the graphs and analyze the data. The *a priori* significance levels were $p < 0.05$.

# RESULTS

## The *in Vitro* Efficacy of Palbociclib was Significantly Decreased in Cells Overexpressing the ABCB1 Transporter

In order to ascertain if palbociclib is a substrate for the ABCB1 transporter, we determined the efficacy of palbociclib in the ABCB1 overexpressing cell lines, KB-C2, SW620/Ad300, and HEK293/ABCB1, using the MTT assay.

As shown in **Figure 1**, we determined the cytotoxicity of palbociclib in ABCB1-overexpressing KB-C2 ($IC_{50}$ = 22.573 μM), SW620/Ad300 ($IC_{50}$ = 9.045 μM), and HEK293/ABCB1 ($IC_{50}$ = 13.855 μM) cells and their parental cell lines, KB-3-1 ($IC_{50}$ = 5.014 μM), SW620 ($IC_{50}$ = 3.921 μM), and HEK293/pcDNA3.1 ($IC_{50}$ = 4.071 μM), respectively.

As shown in **Table 1** and **Figures 1 A, C, D**, compared to the corresponding parental KB-3-1 and SW620 cells, there was a significant difference in the resistance of KB-C2 and SW620/Ad300 cells to palbociclib and the resistance-fold (RF) values were 4.50- and 2.31-fold, respectively. Similarly, compared to HEK293/pcDNA3.1 cells, there was a significant difference in the resistance of HEK293/ABCB1 cells to palbociclib and the RF value was 3.40-fold. These results indicated that overexpression of the ABCB1 transporter decreased the efficacy of palbociclib in drug-resistant cells. SW620 cells express a low endogenous level of the ABCB1 transporter and thus to eliminate the effect of the ABCB1 transporters on palbociclib level, we used the cells that did not contain the gene for the ABCB1 transporter, SW620-ABCB1ko and SW620/Ad300-ABCB1ko cells. There was no significant difference in the RF value for palbociclib between the non-modified (RF = 1) and *ABCB1* knockout SW620 cells (RF = 1.16). In contrast, the efficacy of palbociclib was increased in SW620/Ad300 cells that did not have the gene for the ABCB1 transporter (RF = 1.23), compared to the non-modified SW620/Ad300 cells (RF = 2.31). These results indicated that knocking out the *ABCB1* transporter gene increased the efficacy of palbociclib in the drug-resistant SW620/Ad300 cells to a magnitude similar to that of the parental SW620 cells. Overall, the above results indicated that the efficacy of palbociclib was significantly decreased in drug-resistant cells overexpressing the ABCB1 transporter.

## The Efficacy of Palbociclib is Not Significantly Altered in Cells Overexpressing the ABCG2 Transporter

In order to ascertain if palbociclib was a substrate for the ABCG2 transporter, we determined the efficacy of palbociclib in the ABCG2 overexpressing cell lines, NCI-H460/MX20 and HEK293/ABCG2-WT. Palbociclib was cytotoxic in NCI-H460/MX20 ($IC_{50}$ = 5.258 μM) and HEK293/ABCG2-WT ($IC_{50}$ = 4.644 μM) cells overexpressing the ABCG2 transporter and their parental cell lines, NCI-H460 ($IC_{50}$ = 5.598 μM), and HEK293/pcDNA3.1 ($IC_{50}$ = 4.071 μM), respectively.

As shown in **Table 1** and **Figures 1 B, D**, compared to the corresponding parental NCI-H460 cells, there was no significant difference in the resistance of NCI-H460/MX20 cells to palbociclib (RF = 0.94). Similarly, compared to the corresponding empty vector control HEK293/pcDNA3.1 cells, there was no significant difference in the resistance of HEK293/ABCG2-WT cells to palbociclib (RF = 1.14). These results suggest that the overexpression of the ABCG2 transporter does not decrease the efficacy of palbociclib in drug-resistant cells.

## The ABCB1 Inhibitor, Verapamil, Restores the Efficacy of Palbociclib in Cells Overexpressing the ABCB1 Transporter

As shown in **Table 1**, in the presence of 3 μM of verapamil, an inhibitor of the ABCB1 transporter (Muller et al., 1994), the resistance–fold (RF) value of palbociclib in KB-C2 and SW620/Ad300 cancer cells was significantly decreased the from 4.50- to 1.21-fold and 2.31- to 1.16-fold, respectively. Similarly, in HEK293 cells that overexpress the ABCB1 gene (HEK293/*ABCB1*), palbociclib resistance was significantly decreased by 3 μM of verapamil (from 3.40- to 1.32-fold; **Table 1**). These results indicated that verapamil increased the efficacy of palbociclib in the resistant cancer cells to a magnitude similar to that of the parental cancer cells. In contrast, verapamil did not significantly alter the efficacy of palbociclib in the parental cell lines, KB-3-1, SW620, and HEK293/pcDNA3.1 cells, which do not overexpress the ABCB1 transporter. Thus, the resistance of KB-C2, SW620/Ad300 and HEK293/ABCB1 cells to palbociclib

**TABLE 1 |** The cytotoxicity of palbociclib in parental and MDR cells.

| Treatment | Overexpressed transporter | $IC_{50}$ value ± SD[a] (μM, resistance fold[b]) | |
|---|---|---|---|
| | | Palbociclib | Palbociclib + verapamil 3 μM |
| KB-3-1 | - | 5.014 ± 1.407 (1.00) | 5.745 ± 1.039 (1.15) |
| KB-C2 | ABCB1 | 22.573 ± 4.424 (4.50)* | 6.071 ± 0.293 (1.21) |
| SW620 | - | 3.921 ± 0.412 (1.00) | 5.470 ± 0.739 (1.40) |
| SW620/Ad300 | ABCB1 | 9.045 ± 0.297 (2.31)* | 4.563 ± 0.766 (1.16) |
| SW620 ABCB1 ko | - | 4.559 ± 0.836 (1.16) | 6.812 ± 1.446 (1.74) |
| SW620/Ad300 ABCB1 ko | - | 4.826 ± 0.23 (1.23) | 5.952 ± 1.221 (1.52) |
| NCI-H460 | - | 5.598 ± 0.258 (1.00) | - |
| NCI-H460/MX20 | ABCG2 | 5.258 ± 0.712 (0.94) | - |
| HEK293/pcDNA3.1 | - | 4.071 ± 0.738 (1.00) | 4.948 ± 0.512 (1.22) |
| HEK293/ABCB1 | ABCB1 | 13.855 ± 6.964 (3.40)* | 5.371 ± 1.054 (1.32) |
| HEK293/ABCG2-WT | ABCG2 | 4.644 ± 0.306 (1.14) | - |

[a]*$IC_{50}$ values represent the mean ± SD of at least three independent experiments.*

[b]*RF: Resistance-fold was calculated by dividing the $IC_{50}$ values of the ABCB1 or ABCG2 substrate in the presence or absence of verapamil by the $IC_{50}$ value for the parental cells in the absence of the verapamil.*

*p < *0.05 versus the control group in the absence of the inhibitor.*

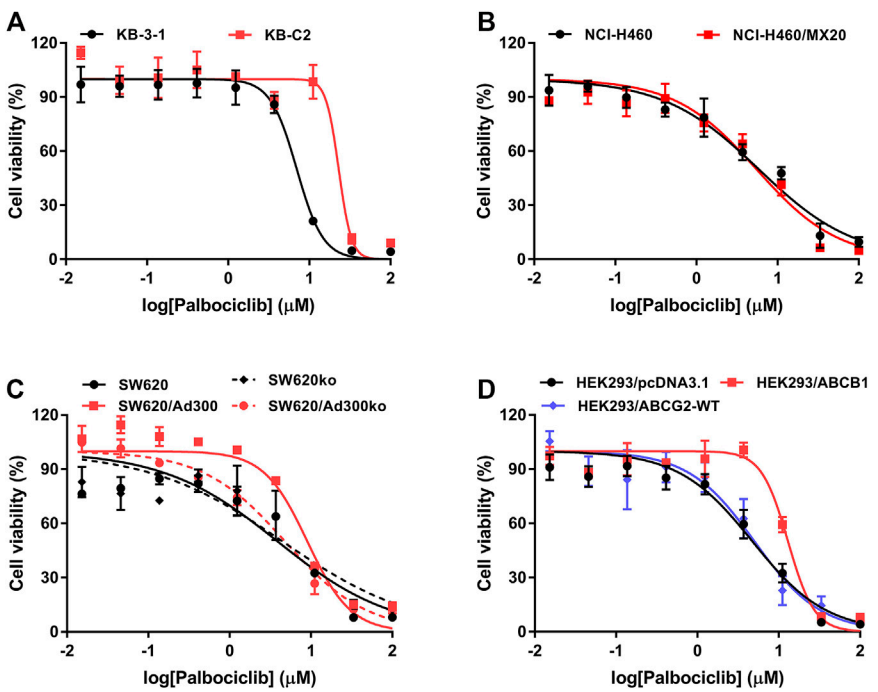


**FIGURE 1 |** Cytotoxicity of palbociclib in parental and MDR cell lines. The efficacy of palbociclib in **(A)** KB-3-1 and KB-C2 cells, **(B)** NCI-H460 and NCI-H460/MX20 cells, **(C)** SW620, SW620/Ad300, SW620-ABCB1ko, and SW620/Ad300-ABCB1ko cells, and **(D)** HEK293/pcDNA3.1, HEK293/ABCB1, and HEK293/ABCG2-WT. All data are expressed as the mean ± SD of three independent experiments.

was due to the overexpression of the ABCB1 transporter. Finally, the $IC_{50}$ values of palbociclib in the presence of verapamil for the knockout cell lines, SW620 *ABCB1* knockout and SW620/Ad300 *ABCB1* knockout, were not significantly different from the $IC_{50}$ values of palbociclib alone, further indicating that SW620/Ad300 cells to palbociclib was due to the overexpression of the ABCB1 transporter.

## Palbociclib Stimulates the Basal Activity of the ABCB1 Transporter ATPase

Previously, it has been reported that ABCB1 substrates increase the hydrolysis of ATP, which is coupled to the efflux function of the ABCB1 transporter (Dastvan et al., 2019; Szöllősi et al., 2020). Therefore, we determined the effect of palbociclib on the basal activity of the ABCB1 ATPase in Insect High Five cell

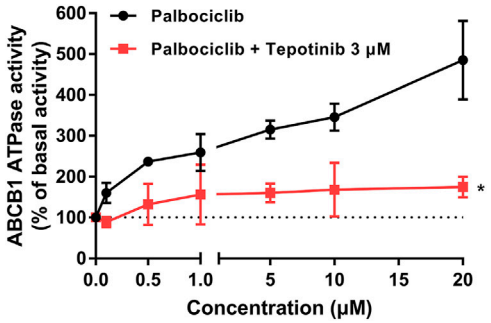


**FIGURE 2 |** The effect of palbociclib on ABCB1 ATPase activity in the absence or presence of the ABCB1 ATPase inhibitor, tepotinib. The black line represents the basal ABCB1 ATPase activity after incubation with vehicle (0 μM) or palbociclib (0.1–20 μM). The red line represents the basal ABCB1 ATPase activity after incubation with vehicle (0 μM), palbociclib (0.1–20 μM) and tepotinib (3 μM). All data are expressed as mean ± SD from three independent experiments. *$p < 0.05$ versus the palbociclib single treatment.

membranes. As shown in **Figure 2**, palbociclib produced a concentration-dependent (0.1–20 μM) increase in the basal activity of ABCB1 ATPase. Palbociclib produced a maximal increase of 4.85-fold in the basal level of ATPase activity, compared to cells incubated with the vehicle (**Figure 2**). At 4.73 μM, palbociclib produced a 50% increase in the basal ATPase activity.

To further support our hypothesis that palbociclib is a substrate of ABCB1, we determined the effect of tepotinib, an inhibitor of ABCB1 ATPase (Wu et al., 2019), on the palbociclib-induced increase in Insect High Five ABCB1 ATPase activity. The results indicated that tepotinib significantly inhibited the palbociclib-induced increase in ABCB1 ATPase activity. Overall, these results suggest that palbociclib is a substrate for the ABCB1 transporter.

## Palbociclib Increases the Accumulation of the ABCB1 Transporter Substrate, [$^3$H]-paclitaxel

To further validate our hypothesis that palbociclib is a substrate for the ABCB1 transporter, we determined the effect of palbociclib on the intracellular levels of further assess the interaction between palbociclib and [$^3$H]-paclitaxel, a substrate of ABCB1 transporter (Gao et al., 2001; Taub et al., 2005). As previously reported (Cui et al., 2019a; Cui et al., 2019b; Li et al., 2020), our results indicated that the accumulation of [$^3$H]-paclitaxel in the parental cancer cell line, KB-3-1, which does not overexpresses the ABCB1 transporter, was significantly greater than that of KB-C2 drug-resistant cancer cell line, due to an increase in the extrusion of [$^3$H]-paclitaxel from the cancer cells (**Figure 3A**). The incubation of KB-3-1 cells for 2 h with either palbociclib (1, 3, or 10 μM) or verapamil (3 μM) did not significantly alter the intracellular accumulation of [$^3$H]-paclitaxel (**Figure 3A**), as these cells do not overexpress the ABCB1 transporter. In contrast, in KB-C2 cells, 3 and 10 μM

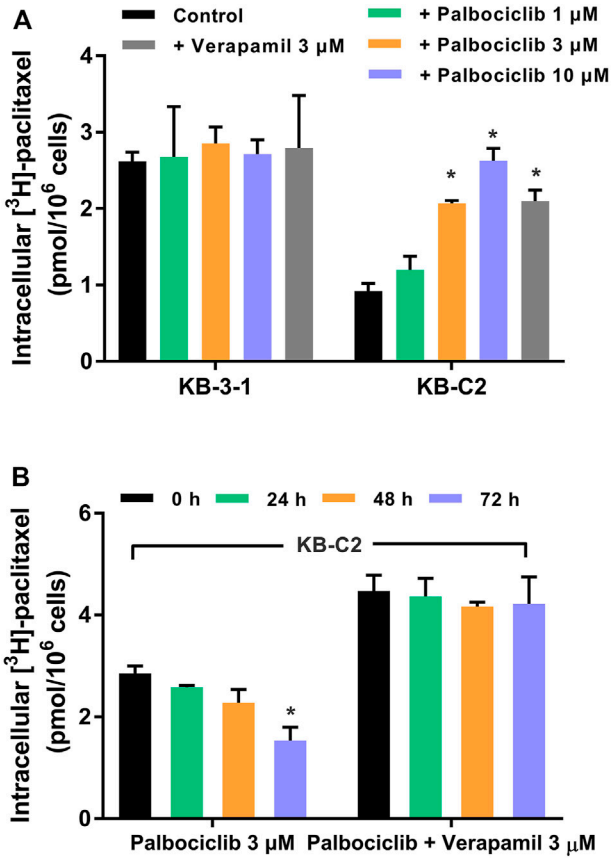


**FIGURE 3 |** The effect of palbociclib on the intracellular accumulation of [$^3$H]-paclitaxel in KB-3-1 and KB-C2 cells. **(A)** KB-3-1 and KB-C2 cells were incubated with either vehicle (control group), 3 μM of verapamil or 1, 3, or 10 μM of palbociclib for 2 h, followed by incubation with [$^3$H]-paclitaxel for 2 h. **(B)** Left side bar graphs: KB-C2 cells were incubated with 3 μM of palbociclib and [$^3$H]-paclitaxel for 0, 24, 48, or 72 h and the intracellular accumulation of [$^3$H]-paclitaxel was determined using liquid scintography. Right side bar graphs: KB-C2 cells were incubated with 3 μM of palbociclib, 3 μM of verapamil (an inhibitor of the ABCB1 transporter), and [$^3$H]-paclitaxel for 24, 48, 72 h) and the intracellular accumulation of [$^3$H]-paclitaxel was determined using liquid scintography. All data are expressed as mean ± SD based on three independent experiments. *$p < 0.05$ compared to the corresponding control group.

of palbociclib, compared to vehicle, significantly increased the accumulation of [$^3$H]-paclitaxel (**Figure 3A**) Similarly, the incubation of KB-C2 cells with 3 μM of verapamil significantly increased the intracellular accumulation of paclitaxel compared to cells incubated with vehicle (**Figure 3A**). Palbociclib, at 1 μM, produced a lower inhibition of the ABCB1 transporter, compared to 3 μM of verapamil (**Figure 3A**). However, 3 and 10 μM of palbociclib increased the accumulation of [$^3$H]-paclitaxel in KB-C2 cells to a level similar to that of the parental KB-3-1 cells (**Figure 3A**).

As shown in **Figure 3B**, the incubation of KB-C2 cells with 3 μM of palbociclib for 24 or 48 h did not significantly alter the accumulation of intracellular [$^3$H]-paclitaxel compared to 0 h. However, the incubation of KB-C2 cells with 3 μM of palbociclib

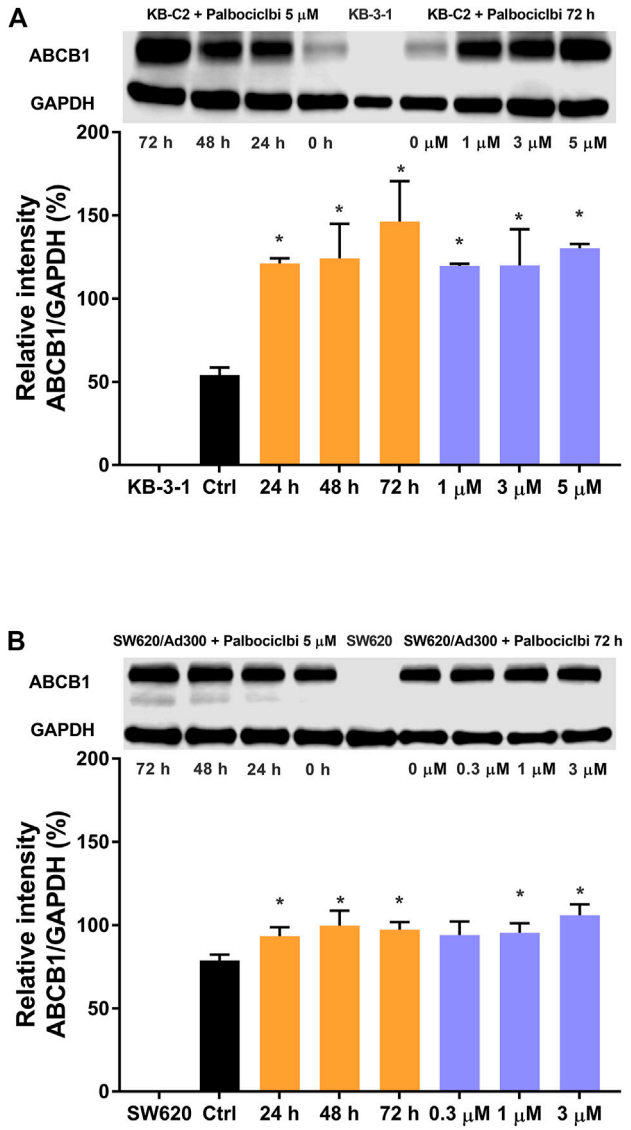


**FIGURE 4 |** The effect of palbociclib on the expression level of the ABCB1 protein in cancer cell lines. **(A)** Left panel: The effect of the incubation of vehicle (0 μM) or 5 μM of palbociclib for 24, 48, or 72 h on the expression level of the ABCB1 protein in KB-C2 cells. **(A)** Right panel: The effect of the incubation of vehicle (0 μM) or 1, 3, or 5 μM of palbociclib for 72 h on the expression level of the ABCG2 protein in KB-C2 cells **(B)** Left panel: The effect of the incubation of vehicle (0 μM) or 3 μM of palbociclib for 24, 48, or 72 h on the expression level of the ABCB1 protein in SW620/Ad300 cells. **(B)** Right panel: The effect of the incubation of vehicle (0 μM) or 0.3, 1, or 3 μM of palbociclib for 72 h on the expression level of the ABCG2 protein in SW620/Ad300 cells. All data are expressed as the mean ± SD based on three independent experiments. *$p < 0.05$ compared to the corresponding control group.

for 72 h significantly decreased the accumulation of [$^3$H]-paclitaxel compared to 0 h (**Figure 3B**). This effect could have been due to a palbociclib-induced increase in the expression level of the ABCB1 transporter (see *Palbociclib Upregulates the Expression of the ABCB1 Transporter Protein* below).

The incubation of KB-C2 cells with 3 μM of palbociclib and 3 μM of verapamil for 24, 48, or 72 h significantly increased the accumulation of [$^3$H]-paclitaxel, compared to KB-C2 cells incubated with only palbociclib (**Figure 3B**). These results suggest that the overexpression of the ABCB1 transporter was the primary cause for the decreased accumulation of [$^3$H]-paclitaxel in the KB-C2 cells.

## Palbociclib Upregulates the Expression of the ABCB1 Transporter Protein

In the above experiments, one of the results indicated that 3 μM of palbociclib significantly decreased the intracellular levels of [$^3$H]-paclitaxel in the drug resistant KB-C2 cancer cells. It is possible that this could have been due to a palbociclib-induced increase in the expression level of the ABCB1 transporter. Therefore, we determined the *in vitro* effect of palbociclib on the expression of the ABCB1 protein in KB-C2 cells using the western blotting assay. The incubation of KB-C2 cells with 5 μM of palbociclib for 24, 48, or 72 h, significantly increased the levels of the ABCB1 protein, compared to KB-C2 cells incubated with vehicle (control, 0 μM; **Figure 4A**, left panel). In contrast, there was no band in the western blot assay for the parental KB-3-1 cells, a finding consistent with the fact that these cells do not overexpress the ABCB1 transporter. The incubation of KB-C2 cells with 1, 3, or 5 μM of palbociclib also significantly increased the expression of the ABCB1 protein compared to KB-C2 cells incubated with vehicle (control, 0 μM; **Figure 4B**, right panel).

We also determined the effect of palbociclib on the expression of the ABCB1 protein in SW620/Ad300 cancer cells, which also overexpress the ABCB1 transporter. Similar to the results for KB-C2 cells, the incubation of SW620/Ad300 cells with 3 μM of palbociclib significantly increased the expression of the ABCB1 protein compared to cells incubated with vehicle (control, 0 μM; **Figure 4B** left panel). However, no band for the ABCB1 protein was obtained for the SW620 parental cancer cells, as they did not overexpress the ABCB1 transporter. The incubation of SW620/Ad300 cells with 1 or 3 μM of palbociclib for 72 h also significantly increased the expression of the ABCB1 protein (**Figure 4B**, right panel).

## Docking Simulation of Palbociclib in the Drug-Binding Area of Human ABCB1

A docking simulation of the paclitaxel binding site (6QEX) of ABCB1 protein was performed. A docking simulation of palbociclib with paclitaxel-bound ABCB1 protein model (6QEX) was performed. The results showed that palbociclib has multiple interactions with the substrate binding site for the ABCB1 protein and an affinity score of -9.616 kcal/mol (**Figure 5**). Palbociclib was positioned and stabilized in the hydrophobic cavity formed by Met68, Met69, Phe303, Ile306, Tyr307, Tyr310, Phe336, Leu339, Ile340, Asn721, Leu724, Gln725, Phe728, Ser766, Met949, Tyr953, Phe983, and Met986. Therefore, hydrophobic interactions played an important role in the binding of palbociclib with ABCB1 protein. Furthermore, the formation of hydrogen bonds

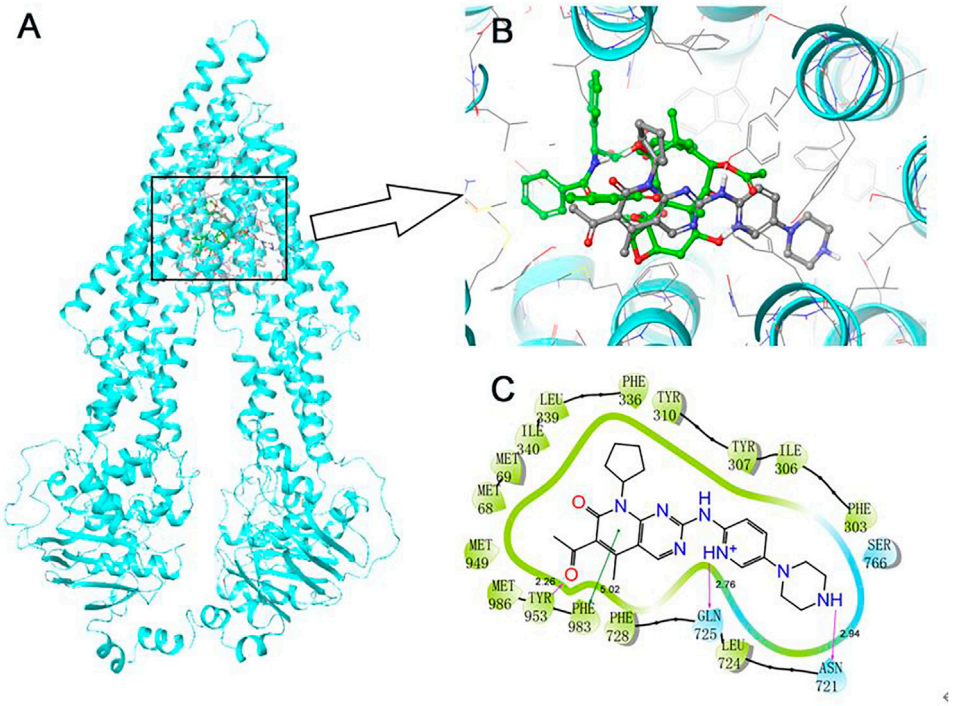


**FIGURE 5 |** Induce-fitted docking predicted binding poses for palbociclib in the human ABCB1 model. **(A)** A ribbon diagram (cyan) of homology model of human ABCB1 and the location of palbociclib and paclitaxel are shown within the ABCB1 internal cavity. **(B)** The detailed interactions of palbociclib (green) and paclitaxel (grey) are depicted as a ball and stick model with the ABCB1 residues. **(C)** A 2D schematic diagram of ligand–receptor interaction between palbociclib and the human ABCB1 model. Amino acids within 3 Å are depicted in colored bubbles, polar residues are depicted in light blue and hydrophobic residues are depicted in green. Purple arrows denote H-bonds, and the green lines indicate π-π interactions. The relevant distances are in Å.

with Asn721, Gln725, and Tyr953 contributed to the stability of the carbonyl group and the amide group of palbociclib and the pyridine group of palbociclib was stabilized by the formation of a π-π bond with the phenol ring of Phe983 of ABCB1.

## DISCUSSION

Numerous studies have shown that the overexpression of the ABC transporters, ABCB1 and ABCG2, in certain types of solid tumors and leukemia, produce acquired drug resistance and attenuate, as well as abrogate, the efficacy of anticancer drugs with different chemical structures and mechanisms of action (Mohammad et al., 2018; Boyer et al., 2019; Wu et al., 2020c; Yang et al., 2021). It has been reported that palbociclib, a CDK4/6 inhibitor, may be a substrate of the ABCB1 and ABCG2 transporters (De Gooijer et al., 2015; Parrish et al., 2015) and an ABCB1 chemosensitizer (Fojo et al., 1985; Gao et al., 2017; Sorf et al., 2020). However, the exact interaction palbociclib with the ABCB1 and ABCG2 transporters remained to be determined, as this depends on the concentration range of the drug, the methodology and the activity of the transporters in the various cell types (Yang et al., 2021). Thus, given that the overexpression of MDR-associated ABC transporters is still an issue in cancer treatment, identifying drugs that can be pumped out from cancer cells could help to produce the maximal efficacy of cancer therapy, thereby potentially improving the patients' quality of life. Therefore, in this study, we conducted experiments to determine the interaction of palbociclib with ABCB1 and ABCG2 transporters.

One of the main findings of this study was that the efficacy of palbociclib was significantly lower, as indicated by the higher $IC_{50}$ values, in the drug-selected cancer cell lines, KB-C2 and SW620/Ad300, which overexpress the ABCB1 transporter, compared to the drug-sensitive parental cancer cell lines, KB-3-1 and SW620, which do not overexpress the ABCB1 transporter. Furthermore, the incubation of the ABCB1 overexpressing cell lines with 3 μM of verapamil, an inhibitor of the ABCB1 transporter, increased the efficacy of palbociclib similar to that of their respective parental cell lines. Similarly, the efficacy of palbociclib was decreased in HEK293 cells transfected with the *ABCB1* gene, where drug resistance was mediated only by the overexpression of the ABCB1 transporter. This finding was further confirmed by the fact that the knockout of the *ABCB1* gene reversed the resistance to palbociclib (i.e., its efficacy was restored) produced by the overexpression of the ABCB1 transporter. However, the efficacy of palbociclib was not significantly altered in either the drug-selected or the gene-transfected cells overexpressing the ABCG2 transporter, as indicated by the similar $IC_{50}$ values

for palbociclib in the drug-resistant and drug-sensitive cells. Overall, these results indicated that the overexpression of ABCB1, not the ABCG2 transporter, significantly decreased the efficacy of palbociclib. Subsequently, we conducted experiments to determine the mechanism of resistance to palbociclib in cells overexpressing the ABCB1 transporter.

Cancer cell resistance to anticancer drugs can occur due to an increase in the expression of the certain ABC transporters (Chen et al., 2021). Therefore, we used western blot assays to determine if palbociclib upregulates the expression level of the ABCB1 transporter. Our results indicated that the incubation of the drug resistant KB-C2 and SW620/Ad300 cells, which overexpress the ABCB1 transporter, with 5 μM of palbociclib for 24, 48, or 72 h, significantly increased the expression of the ABCB1 protein compared to the control group. Furthermore, the incubation of KB-C2 and SW620/Ad300 cells with 1, 3, or 5 μM of palbociclib for 72 h, significantly increased the expression of the ABCB1 protein, compared to SW620/Ad300 cells without treatment. Overall, these results suggest that palbociclib resistance may be due to an increase in the level of the ABCB1 protein.

It has been reported that the hydrolysis of ATP is coupled to the drug efflux function of the ABCB1 transporter (Yang et al., 2020). Consequently, we conducted an ATPase assay to determine if palbociclib increases the vanadate-sensitive ATPase activity of the ABCB1 transporter. Our results indicated that palbociclib can increase the ABCB1 ATPase activity in a concentration-dependent manner. The maximum stimulation was 4.85-fold greater than the basal level of ABCB1 ATPase activity. This increase is congruent with other studies reporting that drugs that are ABCB1 substrates, such as GSK-1070916 (2.6-fold) (Wu et al., 2020c) and volasertib (3.0-fold) (Wu et al., 2015). Furthermore, the incubation of High Five Insect cell membrane expressing ABCB1 ATPase with 3 μM of tepotinib, an inhibitor of ABCB1 ATPase activity (Wu et al., 2019), decreased the palbociclib-induced increase in ATPase activity to that of membranes incubated with palbociclib, i.e., the basal activity. These results suggest that palbociclib is a substrate of the ABCB1 transporter.

To further characterize the interaction between palbociclib and ABCB1 transporter, the [$^3$H]-paclitaxel accumulation assay was performed to evaluate the effect of palbociclib on ABCB1 efflux activity. Previously, it has been reported that [$^3$H]-paclitaxel is a substrate for the ABCB1 transporter (Zhou, 2008). The incubation of KB-C2 cells, which overexpress the ABCB1 transporter, with 3 or 10 μM of palbociclib, for 2 h, significantly increased the intracellular level of [$^3$H]-paclitaxel. Similarly, the intracellular accumulation of [$^3$H]-paclitaxel was increased by 3 μM of verapamil, a known inhibitor of the ABCB1 transporter. In contrast, palbociclib did not significantly alter the intracellular accumulation of [$^3$H]-paclitaxel in the corresponding parental KB-3-1 cells, which do not overexpress the ABCB1 transporter. Based on these results, we hypothesized that palbociclib may compete with [$^3$H]-paclitaxel and thus, decrease the efflux of [$^3$H]-paclitaxel for the KB-C2 cells that overexpress the ABCB1 transporter. However, this hypothesis remains to be further validated. Since the western blot results indicated that palbociclib upregulated the protein expression of ABCB1 transporter, it was necessary to determine if the drug resistant cells had a higher resistance phenotype towards ABCB1 substrate drugs after incubation with palbociclib. Therefore, we incubated KB-C2 cells for 72 h with 3 μM of palbociclib and measured the intracellular levels of [$^3$H]-paclitaxel. Our results showed that the KB-C2 cells accumulated a significantly lower level of [$^3$H]-paclitaxel, suggesting that palbociclib increased the efflux activity of the ABCB1 transporter. This finding is validated by our results indicating that the ABCB1 inhibitor, verapamil, which inhibits the efflux function of the ABCB1 transporter, increased the intracellular accumulation of [$^3$H]-paclitaxel to that of cells incubated with vehicle. It should be noted that, while palbociclib upregulates ABCB1 expression, the accumulation assay was conducted by incubating the cells with palbociclib for 2 h. Therefore, palbociclib is unlikely to modulate the expression of the ABCB1 protein within the short period of time, thereby allowing us to determine the binding of the substrate to the ABCB1 transporter.

Computational molecular docking analysis is widely used to predict ligand-protein interactions, even though it does not depict the actual binding interaction of the ligand (i.e., drug) with the protein (Salmaso and Moro, 2018). Recently, docking simulation has become a reliable method in screening for drugs that may be modulators or substrates of the ABC transporters (Wu et al., 2020c; Yang et al., 2020). We used an *in silico* molecular docking analysis to simulate the interaction of palbociclib and the ABCB1 protein. We postulated that palbociclib significantly increased ABCB1 ATPase activity due to its interaction at the drug-substrate binding domain of ABCB1 and therefore, we used the ABCB1 protein (6QEX) in this study. The docking analysis indicated that the docking score of palbociclib for the ABCB1 protein was −9.616 kcal/mol, which is comparable to that of other known ABCB1 substrates, such as GSK-1070916 (−8.0 kcal/mol) (Wu et al., 2020c) and WYE-354 (−12.241 kcal/mol) (Wang et al., 2020b). Also, our results showed that palbociclib is positioned in the hydrophobic cavity of the transmembrane domain formed by the amino acid residues and stabilized by hydrogen bonding interactions with Asn721, Gln725, Tyr953, and π- π interaction formed by the phenol ring with Phe983 of ABCB1 protein.

## CONCLUSION

Overall, our *in vitro* results indicate that the anticancer efficacy of palbociclib is significantly decreased by the overexpression of the ABCB1 transporter. In addition, it is likely that palbociclib is a substrate for the ABCB1 transporter, as palbociclib increased the ATPase activity of the ABCB1 transporter and upregulated the expression of the ABCB1 protein. Furthermore, the cytotoxic efficacy of palbociclib in drug resistant cells was restored by an ABCB1 inhibitor or the deletion of the *ABCB1* gene.

## DATA AVAILABILITY STATEMENT

The original contributions presented in the study are included in the article/Supplementary Material, further inquiries can be directed to the corresponding authors.

## AUTHOR CONTRIBUTIONS

Conceptualization, HF, Z-XW, YYL, and Z-SC; methodology, HF, Z-XW, Z-NL, Q-XT, YY, and YL; writing–original draft preparation, HF and Z-XW; writing–review and editing, Z-XW, YY, and CA; supervision, YYL and Z-SC.

## FUNDING

This work is supported by the National Natural Science Foundation of China (81872901).

## ACKNOWLEDGMENTS

The authors would like to thank Drs. Robert W. Robey and Susan E. Bates (NCI, NIH, Bethesda, MD) for providing the NCI-H460, NCI-H460/MX20, and HEK293 gene-transfectant cell lines. We thank Dr. Shin-Ichi Akiyama (Kagoshima University, Kagoshima, Japan) for the gift of KB-3-1 and KB-C2 cell lines.

## REFERENCES

Ambudkar, S. V. (1998). Drug-stimulatable ATPase Activity in Crude Membranes of Human MDR1-Transfected Mammalian Cells. *Methods Enzymol.* 292, 504–514. doi:10.1016/s0076-6879(98)92039-0

Anders, L., Ke, N., Hydbring, P., Choi, Y. J., Widlund, H. R., Chick, J. M., et al. (2011). A Systematic Screen for CDK4/6 Substrates Links FOXM1 Phosphorylation to Senescence Suppression in Cancer Cells. *Cancer Cell* 20, 620–634. doi:10.1016/j.ccr.2011.10.001

Asghar, U., Witkiewicz, A. K., Turner, N. C., and Knudsen, E. S. (2015). The History and Future of Targeting Cyclin-dependent Kinases in Cancer Therapy. *Nat. Rev. Drug Discov.* 14, 130–146. doi:10.1038/nrd4504

Basso, A. D., and Doll, R. J. (2006). Inhibition of Cyclin-dependent Kinases - a Review of the Recent Patent Literature. *Recent Pat Anticancer Drug Discov.* 1, 357–367. doi:10.2174/157489206778776916

Boyer, T., Gonzales, F., Barthélémy, A., Marceau-Renaut, A., Peyrouze, P., Guihard, S., et al. (2019). Clinical Significance of ABCB1 in Acute Myeloid Leukemia: A Comprehensive Study. *Cancers (Basel* 11. doi:10.3390/cancers11091323

Burkhart, D. L., and Sage, J. (2008). Cellular Mechanisms of Tumour Suppression by the Retinoblastoma Gene. *Nat. Rev. Cancer* 8, 671–682. doi:10.1038/nrc2399

Chandrasekhar, C., Kumar, P. S., and Sarma, P. V. G. K. (2019). Novel Mutations in the Kinase Domain of BCR-ABL Gene Causing Imatinib Resistance in Chronic Myeloid Leukemia Patients. *Sci. Rep.* 9, 2412. doi:10.1038/s41598-019-38672-x

Chen, X. Y., Yang, Y., Wang, J. Q., Wu, Z. X., Li, J., and Chen, Z. S. (2021). Overexpression of ABCC1 Confers Drug Resistance to Betulin. *Front. Oncol.* 11, 640656. doi:10.3389/fonc.2021.640656

Ciruelos, E., Villagrasa, P., Pascual, T., Oliveira, M., Pernas, S., Paré, L., et al. (2020). Palbociclib and Trastuzumab in HER2-Positive Advanced Breast Cancer: Results from the Phase II SOLTI-1303 PATRICIA Trial. *Clin. Cancer Res.* 26, 5820–5829. doi:10.1158/1078-0432.ccr-20-0844

Cristofanilli, M., Turner, N. C., Bondarenko, I., Ro, J., Im, S. A., Masuda, N., et al. (2016). Fulvestrant Plus Palbociclib versus Fulvestrant Plus Placebo for Treatment of Hormone-Receptor-Positive, HER2-Negative Metastatic Breast Cancer that Progressed on Previous Endocrine Therapy (PALOMA-3): Final Analysis of the Multicentre, Double-Blind, Phase 3 Randomised Controlled Trial. *Lancet Oncol.* 17, 425–439. doi:10.1016/S1470-2045(15)00613-0

Cui, Q., Cai, C. Y., Gao, H. L., Ren, L., Ji, N., Gupta, P., et al. (2019a). Glesatinib, a C-MET/SMO Dual Inhibitor, Antagonizes P-Glycoprotein Mediated Multidrug Resistance in Cancer Cells. *Front. Oncol.* 9, 313. doi:10.3389/fonc.2019.00313

Cui, Q., Wang, J. Q., Assaraf, Y. G., Ren, L., Gupta, P., Wei, L., et al. (2018). Modulating ROS to Overcome Multidrug Resistance in Cancer. *Drug Resist. Updat* 41, 1–25. doi:10.1016/j.drup.2018.11.001

Cui, Q., Cai, C. Y., Wang, J. Q., Zhang, S., Gupta, P., Ji, N., et al. (2019b). Chk1 Inhibitor MK-8776 Restores the Sensitivity of Chemotherapeutics in P-Glycoprotein Overexpressing Cancer Cells. *Int. J. Mol. Sci.* 20.

Dastvan, R., Mishra, S., Peskova, Y. B., Nakamoto, R. K., and Mchaourab, H. S. (2019). Mechanism of Allosteric Modulation of P-Glycoprotein by Transport Substrates and Inhibitors. *Science* 364, 689–692. doi:10.1126/science.aav9406

De Bruijn, M. H., Van Der Bliek, A. M., Biedler, J. L., and Borst, P. (1986). Differential Amplification and Disproportionate Expression of Five Genes in Three Multidrug-Resistant Chinese Hamster Lung Cell Lines. *Mol. Cel Biol* 6, 4717–4722. doi:10.1128/mcb.6.12.4717

De Gooijer, M. C., Zhang, P., Thota, N., Mayayo-Peralta, I., Buil, L. C., Beijnen, J. H., et al. (2015). P-glycoprotein and Breast Cancer Resistance Protein Restrict the Brain Penetration of the CDK4/6 Inhibitor Palbociclib. *Invest. New Drugs* 33, 1012–1019. doi:10.1007/s10637-015-0266-y

Erin, N., Grahovac, J., Brozovic, A., and Efferth, T. (2020). Tumor Microenvironment and Epithelial Mesenchymal Transition as Targets to Overcome Tumor Multidrug Resistance. *Drug Resist. Updat* 53, 100715. doi:10.1016/j.drup.2020.100715

Finn, R. S., Crown, J. P., Lang, I., Boer, K., Bondarenko, I. M., Kulyk, S. O., et al. (2015). The Cyclin-dependent Kinase 4/6 Inhibitor Palbociclib in Combination with Letrozole versus Letrozole Alone as First-Line Treatment of Oestrogen Receptor-Positive, HER2-Negative, Advanced Breast Cancer (PALOMA-1/TRIO-18): a Randomised Phase 2 Study. *Lancet Oncol.* 16, 25–35. doi:10.1016/S1470-2045(14)71159-3

Finn, R. S., Martin, M., Rugo, H. S., Jones, S., Im, S. A., Gelmon, K., et al. (2016). Palbociclib and Letrozole in Advanced Breast Cancer. *N. Engl. J. Med.* 375, 1925–1936. doi:10.1056/NEJMoa1607303

Fletcher, J. I., Williams, R. T., Henderson, M. J., Norris, M. D., and Haber, M. (2016). ABC Transporters as Mediators of Drug Resistance and Contributors to Cancer Cell Biology. *Drug Resist. Updat* 26, 1–9. doi:10.1016/j.drup.2016.03.001

Fojo, A., Akiyama, S., Gottesman, M. M., and Pastan, I. (1985). Reduced Drug Accumulation in Multiply Drug-Resistant Human KB Carcinoma Cell Lines. *Cancer Res.* 45, 3002–3007.

Gao, J., Murase, O., Schowen, R. L., Aubé, J., and Borchardt, R. T. (2001). A Functional Assay for Quantitation of the Apparent Affinities of Ligands of P-Glycoprotein in Caco-2 Cells. *Pharm. Res.* 18, 171–176. doi:10.1023/a:1011076217118

Gao, Y., Shen, J., Choy, E., Mankin, H., Hornicek, F., and Duan, Z. (2017). Inhibition of CDK4 Sensitizes Multidrug Resistant Ovarian Cancer Cells to Paclitaxel by Increasing Apoptosiss. *Cel Oncol (Dordr)* 40, 209–218. doi:10.1007/s13402-017-0316-x

Gnant, M., Dueck, A. C., Frantal, S., Martin, M., Burstein, H. J., Greil, R., et al. (2021). Adjuvant Palbociclib for Early Breast Cancer: The PALLAS Trial Results (ABCSG-42/AFT-05/BIG-14–03. *J. Clin. Oncol.* Jco2102554.

Harbeck, N., Iyer, S., Turner, N., Cristofanilli, M., Ro, J., André, F., et al. (2016). Quality of Life with Palbociclib Plus Fulvestrant in Previously Treated Hormone Receptor-Positive, HER2-Negative Metastatic Breast Cancer: Patient-Reported Outcomes from the PALOMA-3 Trial. *Ann. Oncol.* 27, 1047–1054. doi:10.1093/annonc/mdw139

Helleday, T., Petermann, E., Lundin, C., Hodgson, B., and Sharma, R. A. (2008). DNA Repair Pathways as Targets for Cancer Therapy. *Nat. Rev. Cancer* 8, 193–204. doi:10.1038/nrc2342

Henrich, C. J., Robey, R. W., Bokesch, H. R., Bates, S. E., Shukla, S., Ambudkar, S. V., et al. (2007). New Inhibitors of ABCG2 Identified by High-Throughput Screening. *Mol. Cancer Ther.* 6, 3271–3278. doi:10.1158/1535-7163.MCT-07-0352

Ji, N., Yang, Y., Lei, Z. N., Cai, C. Y., Wang, J. Q., Gupta, P., et al. (2018). Ulixertinib (BVD-523) Antagonizes ABCB1- and ABCG2-Mediated Chemotherapeutic Drug Resistance. *Biochem. Pharmacol.* 158, 274–285. doi:10.1016/j.bcp.2018.10.028

Johnston, S., Puhalla, S., Wheatley, D., Ring, A., Barry, P., Holcombe, C., et al. (2019). Randomized Phase II Study Evaluating Palbociclib in Addition to Letrozole as Neoadjuvant Therapy in Estrogen Receptor-Positive Early Breast Cancer: PALLET Trial. *J. Clin. Oncol.* 37, 178–189. doi:10.1200/JCO.18.01624

Kato, S., Okamura, R., Adashek, J. J., Khalid, N., Lee, S., Nguyen, V., et al. (2021). Targeting G1/S Phase Cell-Cycle Genomic Alterations and Accompanying Co-alterations with Individualized CDK4/6 Inhibitor-Based Regimens. *JCI Insight* 6. doi:10.1172/jci.insight.142547

Knudsen, E. S., and Knudsen, K. E. (2008). Tailoring to RB: Tumour Suppressor Status and Therapeutic Response. *Nat. Rev. Cancer* 8, 714–724. doi:10.1038/nrc2401

Lage, H., and Dietel, M. (2000). Effect of the Breast-Cancer Resistance Protein on Atypical Multidrug Resistance. *Lancet Oncol.* 1, 169–175. doi:10.1016/s1470-2045(00)00032-2

Lai, G. M., Chen, Y. N., Mickley, L. A., Fojo, A. T., and Bates, S. E. (1991a). P-glycoprotein Expression and Schedule Dependence of Adriamycin Cytotoxicity in Human colon Carcinoma Cell Lines. *Int. J. Cancer* 49, 696–703. doi:10.1002/ijc.2910490512

Lai, G. M., Moscow, J. A., Alvarez, M. G., Fojo, A. T., and Bates, S. E. (1991b). Contribution of Glutathione and Glutathione-dependent Enzymes in the Reversal of Adriamycin Resistance in colon Carcinoma Cell Lines. *Int. J. Cancer* 49, 688–695. doi:10.1002/ijc.2910490511

Lei, Z. N., Teng, Q. X., Wu, Z. X., Ping, F. F., Song, P., Wurpel, J. N. D., et al. (2021). Overcoming Multidrug Resistance by Knockout of ABCB1 Gene Using CRISPR/Cas9 System in SW620/Ad300 Colorectal Cancer Cells. *MedComm* 2, 765–777. doi:10.1002/mco2.106

Li, Y. D., Mao, Y., Dong, X. D., Lei, Z. N., Yang, Y., Lin, L., et al. (2020). Methyl-Cantharidimide (MCA) Has Anticancer Efficacy in ABCB1- and ABCG2-Overexpressing and Cisplatin Resistant Cancer Cells. *Front. Oncol.* 10, 932. doi:10.3389/fonc.2020.00932

Liang, S., Hu, L., Wu, Z., Chen, Z., Liu, S., Xu, X., et al. (2020). CDK12: A Potent Target and Biomarker for Human Cancer Therapy. *Cells* 9.

Liu, K., Gao, L., Ma, X., Huang, J. J., Chen, J., Zeng, L., et al. (2020). Long Non-coding RNAs Regulate Drug Resistance in Cancer. *Mol. Cancer* 19, 54. doi:10.1186/s12943-020-01162-0

Malorni, L., Curigliano, G., Minisini, A. M., Cinieri, S., Tondini, C. A., D'hollander, K., et al. (2018). Palbociclib as Single Agent or in Combination with the Endocrine Therapy Received before Disease Progression for Estrogen Receptor-Positive, HER2-Negative Metastatic Breast Cancer: TREnd Trial. *Ann. Oncol.* 29, 1748–1754. doi:10.1093/annonc/mdy214

Manning, G., Whyte, D. B., Martinez, R., Hunter, T., and Sudarsanam, S. (2002). The Protein Kinase Complement of the Human Genome. *Science* 298, 1912–1934. doi:10.1126/science.1075762

Mayer, E. L., Dueck, A. C., Martin, M., Rubovszky, G., Burstein, H. J., Bellet-Ezquerra, M., et al. (2021). Palbociclib with Adjuvant Endocrine Therapy in Early Breast Cancer (PALLAS): Interim Analysis of a Multicentre, Open-Label, Randomised, Phase 3 Study. *Lancet Oncol.* 22, 212–222. doi:10.1016/S1470-2045(20)30642-2

Mi, Y. J., Liang, Y. J., Huang, H. B., Zhao, H. Y., Wu, C. P., Wang, F., et al. (2010). Apatinib (YN968D1) Reverses Multidrug Resistance by Inhibiting the Efflux Function of Multiple ATP-Binding Cassette Transporters. *Cancer Res.* 70, 7981–7991. doi:10.1158/0008-5472.CAN-10-0111

Mohammad, I. S., He, W., and Yin, L. (2018). Understanding of Human ATP Binding Cassette Superfamily and Novel Multidrug Resistance Modulators to Overcome MDR. *Biomed. Pharmacother.* 100, 335–348. doi:10.1016/j.biopha.2018.02.038

Muller, C., Bailly, J. D., Goubin, F., Laredo, J., Jaffrézou, J. P., Bordier, C., et al. (1994). Verapamil Decreases P-Glycoprotein Expression in Multidrug-Resistant Human Leukemic Cell Lines. *Int. J. Cancer* 56, 749–754. doi:10.1002/ijc.2910560523

Narayanan, S., Wu, Z. X., Wang, J. Q., Ma, H., Acharekar, N., Koya, J., et al. (2021). The Spleen Tyrosine Kinase Inhibitor, Entospletinib (GS-9973) Restores Chemosensitivity in Lung Cancer Cells by Modulating ABCG2-Mediated Multidrug Resistance. *Int. J. Biol. Sci.* 17, 2652–2665. doi:10.7150/ijbs.61229

Neophytou, C. M., Trougakos, I. P., Erin, N., and Papageorgis, P. (2021). Apoptosis Deregulation and the Development of Cancer Multi-Drug Resistance. *Cancers (Basel)* 13. doi:10.3390/cancers13174363

O'leary, B., Finn, R. S., and Turner, N. C. (2016). Treating Cancer with Selective CDK4/6 Inhibitors. *Nat. Rev. Clin. Oncol.* 13, 417–430. doi:10.1038/nrclinonc.2016.26

Parrish, K. E., Pokorny, J., Mittapalli, R. K., Bakken, K., Sarkaria, J. N., and Elmquist, W. F. (2015). Efflux Transporters at the Blood-Brain Barrier Limit Delivery and Efficacy of Cyclin-dependent Kinase 4/6 Inhibitor Palbociclib (PD-0332991) in an Orthotopic Brain Tumor Model. *J. Pharmacol. Exp. Ther.* 355, 264–271. doi:10.1124/jpet.115.228213

Robey, R. W., Honjo, Y., Morisaki, K., Nadjem, T. A., Runge, S., Risbood, M., et al. (2003). Mutations at Amino-Acid 482 in the ABCG2 Gene Affect Substrate and Antagonist Specificity. *Br. J. Cancer* 89, 1971–1978. doi:10.1038/sj.bjc.6601370

Robey, R. W., Pluchino, K. M., Hall, M. D., Fojo, A. T., Bates, S. E., and Gottesman, M. M. (2018). Revisiting the Role of ABC Transporters in Multidrug-Resistant Cancer. *Nat. Rev. Cancer* 18, 452–464. doi:10.1038/s41568-018-0005-8

Robey, R. W., Shukla, S., Finley, E. M., Oldham, R. K., Barnett, D., Ambudkar, S. V., et al. (2008). Inhibition of P-Glycoprotein (ABCB1)- and Multidrug Resistance-Associated Protein 1 (ABCC1)-Mediated Transport by the Orally Administered Inhibitor, CBT-1((R)). *Biochem. Pharmacol.* 75, 1302–1312. doi:10.1016/j.bcp.2007.12.001

Rugo, H. S., Diéras, V., Gelmon, K. A., Finn, R. S., Slamon, D. J., Martin, M., et al. (2018). Impact of Palbociclib Plus Letrozole on Patient-Reported Health-Related Quality of Life: Results from the PALOMA-2 Trial. *Ann. Oncol.* 29, 888–894. doi:10.1093/annonc/mdy012

Salmaso, V., and Moro, S. (2018). Bridging Molecular Docking to Molecular Dynamics in Exploring Ligand-Protein Recognition Process. *Front. Pharmacol.* 9, 923. doi:10.3389/fphar.2018.00923

Schmitz, M. L., and Kracht, M. (2016). Cyclin-Dependent Kinases as Coregulators of Inflammatory Gene Expression. *Trends Pharmacol. Sci.* 37, 101–113. doi:10.1016/j.tips.2015.10.004

Seebacher, N. A., Krchniakova, M., Stacy, A. E., Skoda, J., and Jansson, P. J. (2021). Tumour Microenvironment Stress Promotes the Development of Drug Resistance. *Antioxidants (Basel)* 12. doi:10.3390/antiox10111801

Shahar, N., and Larisch, S. (2020). Inhibiting the Inhibitors: Targeting Anti-apoptotic Proteins in Cancer and Therapy Resistance. *Drug Resist. Updat* 52, 100712. doi:10.1016/j.drup.2020.100712

Shapiro, G. I. (2006). Cyclin-dependent Kinase Pathways as Targets for Cancer Treatment. *J. Clin. Oncol.* 24, 1770–1783. doi:10.1200/JCO.2005.03.7689

Sherr, C. J. (1996). Cancer Cell Cycles. *Science* 274, 1672–1677. doi:10.1126/science.274.5293.1672

Shi, Z., Peng, X. X., Kim, I. W., Shukla, S., Si, Q. S., Robey, R. W., et al. (2007). Erlotinib (Tarceva, OSI-774) Antagonizes ATP-Binding Cassette Subfamily B Member 1 and ATP-Binding Cassette Subfamily G Member 2-mediated Drug Resistance. *Cancer Res.* 67, 11012–11020. doi:10.1158/0008-5472.CAN-07-2686

Shi, Z., Tiwari, A. K., Shukla, S., Robey, R. W., Singh, S., Kim, I. W., et al. (2011). Sildenafil Reverses ABCB1- and ABCG2-Mediated Chemotherapeutic Drug Resistance. *Cancer Res.* 71, 3029–3041. doi:10.1158/0008-5472.CAN-10-3820

Sorf, A., Sucha, S., Morell, A., Novotna, E., Staud, F., Zavrelova, A., et al. (2020). Targeting Pharmacokinetic Drug Resistance in Acute Myeloid Leukemia Cells with CDK4/6 Inhibitors. *Cancers (Basel)* 12. doi:10.3390/cancers12061596

Spring, L. M., Wander, S. A., Andre, F., Moy, B., Turner, N. C., and Bardia, A. (2020). Cyclin-dependent Kinase 4 and 6 Inhibitors for Hormone Receptor-Positive Breast Cancer: Past, Present, and Future. *Lancet* 395, 817–827. doi:10.1016/S0140-6736(20)30165-3

Szakács, G., Paterson, J. K., Ludwig, J. A., Booth-Genthe, C., and Gottesman, M. M. (2006). Targeting Multidrug Resistance in Cancer. *Nat. Rev. Drug Discov.* 5, 219–234. doi:10.1038/nrd1984

Szöllősi, D., Chiba, P., Szakacs, G., and Stockner, T. (2020). Conversion of Chemical to Mechanical Energy by the Nucleotide Binding Domains of ABCB1. *Sci. Rep.* 10, 2589. doi:10.1038/s41598-020-59403-7

Taub, M. E., Podila, L., Ely, D., and Almeida, I. (2005). Functional Assessment of Multiple P-Glycoprotein (P-Gp) Probe Substrates: Influence of Cell Line and

Modulator Concentration on P-Gp Activity. *Drug Metab. Dispos* 33, 1679–1687. doi:10.1124/dmd.105.005421

Turner, N. C., Slamon, D. J., Ro, J., Bondarenko, I., Im, S. A., Masuda, N., et al. (2018). Overall Survival with Palbociclib and Fulvestrant in Advanced Breast Cancer. *N. Engl. J. Med.* 379, 1926–1936. doi:10.1056/NEJMoa1810527

Wang, J., Wang, J. Q., Cai, C. Y., Cui, Q., Yang, Y., Wu, Z. X., et al. (2020a). Reversal Effect of ALK Inhibitor NVP-Tae684 on ABCG2-Overexpressing Cancer Cells. *Front. Oncol.* 10, 228. doi:10.3389/fonc.2020.00228

Wang, J., Yang, D. H., Yang, Y., Wang, J. Q., Cai, C. Y., Lei, Z. N., et al. (2020b). Overexpression of ABCB1 Transporter Confers Resistance to mTOR Inhibitor WYE-354 in Cancer Cells. *Int. J. Mol. Sci.* 21.

Wei, L. Y., Wu, Z. X., Yang, Y., Zhao, M., Ma, X. Y., Li, J. S., et al. (2020). Overexpression of ABCG2 Confers Resistance to Pevonedistat, an NAE Inhibitor. *Exp. Cel Res* 388, 111858. doi:10.1016/j.yexcr.2020.111858

Weinberg, R. A. (1995). The Retinoblastoma Protein and Cell Cycle Control. *Cell* 81, 323–330. doi:10.1016/0092-8674(95)90385-2

Wood, D. J., and Endicott, J. A. (2018). Structural Insights into the Functional Diversity of the CDK-Cyclin Family. *Open Biol.* 8. doi:10.1098/rsob.180112

Wu, C. P., Hsieh, C. H., Hsiao, S. H., Luo, S. Y., Su, C. Y., Li, Y. Q., et al. (2015). Human ATP-Binding Cassette Transporter ABCB1 Confers Resistance to Volasertib (BI 6727), a Selective Inhibitor of Polo-like Kinase 1. *Mol. Pharm.* 12, 3885–3895. doi:10.1021/acs.molpharmaceut.5b00312

Wu, S., and Fu, L. (2018). Tyrosine Kinase Inhibitors Enhanced the Efficacy of Conventional Chemotherapeutic Agent in Multidrug Resistant Cancer Cells. *Mol. Cancer* 17, 25. doi:10.1186/s12943-018-0775-3

Wu, Z., Yang, Y., Lei, Z., Narayanan, S., Wang, J., Teng, Q., et al. (2022). ABCB1 Limits the Cytotoxic Activity of TAK-243, an Inhibitor of the Ubiquitin-Activating Enzyme UBA1. *Front. Biosci. (Landmark Ed.* 27, 5. doi:10.31083/j.fbl2701005

Wu, Z. X., Teng, Q. X., Cai, C. Y., Wang, J. Q., Lei, Z. N., Yang, Y., et al. (2019). Tepotinib Reverses ABCB1-Mediated Multidrug Resistance in Cancer Cells. *Biochem. Pharmacol.* 166, 120–127. doi:10.1016/j.bcp.2019.05.015

Wu, Z. X., Yang, Y., Wang, G., Wang, J. Q., Teng, Q. X., Sun, L., et al. (2020b). Dual TTK/CLK2 Inhibitor, CC-671, Selectively Antagonizes ABCG2-Mediated Multidrug Resistance in Lung Cancer Cells. *Cancer Sci.* 111, 2872–2882. doi:10.1111/cas.14505

Wu, Z. X., Yang, Y., Wang, J. Q., Zhou, W. M., Chen, J., Fu, Y. G., et al. (2020c). Elevated ABCB1 Expression Confers Acquired Resistance to Aurora Kinase Inhibitor GSK-1070916 in Cancer Cells. *Front. Pharmacol.* 11, 615824. doi:10.3389/fphar.2020.615824

Wu, Z. X., Yang, Y., Teng, Q. X., Wang, J. Q., Lei, Z. N., Wang, J. Q., et al. (2020a). Tivantinib, A C-Met Inhibitor in Clinical Trials, Is Susceptible to ABCG2-Mediated Drug Resistance. *Cancers (Basel)* 12. doi:10.3390/cancers12010186

Xu, F., Cui, W.-Q., Wei, Y., Cui, J., Qiu, J., Hu, L.-L., et al. (2018). Astragaloside IV Inhibits Lung Cancer Progression and Metastasis by Modulating Macrophage Polarization through AMPK Signaling. *J. Exp. Clin. Cancer Res.* 37, 207. Availableat: https://jeccr.biomedcentral.com/articles/210.1186/s13046-13018-10878-13040.

Yang, Y., Ji, N., Cai, C. Y., Wang, J. Q., Lei, Z. N., Teng, Q. X., et al. (2020). Modulating the Function of ABCB1: *In Vitro* and *In Vivo* Characterization of Sitravatinib, a Tyrosine Kinase Inhibitor. *Cancer Commun. (Lond)* 40, 285–300. doi:10.1002/cac2.12040

Yang, Y., Wu, Z. X., Wang, J. Q., Teng, Q. X., Lei, Z. N., Lusvarghi, S., et al. (2021). OTS964, a TOPK Inhibitor, Is Susceptible to ABCG2-Mediated Drug Resistance. *Front. Pharmacol.* 12, 620874. doi:10.3389/fphar.2021.620874

Yuan, K., Wang, X., Dong, H., Min, W., Hao, H., and Yang, P. (2021). Selective Inhibition of CDK4/6: A Safe and Effective Strategy for Developing Anticancer Drugs. *Acta Pharm. Sin B* 11, 30–54. doi:10.1016/j.apsb.2020.05.001

Zaal, E. A., and Berkers, C. R. (2018). The Influence of Metabolism on Drug Response in. *Cancer* 8.

Zhang, L., Li, Y., Wang, Q., Chen, Z., Li, X., Wu, Z., et al. (2020a). The PI3K Subunits, P110α and P110β Are Potential Targets for Overcoming P-Gp and BCRP-Mediated MDR in Cancer. *Mol. Cancer* 19, 10. doi:10.1186/s12943-019-1112-1

Zhang, X. Y., Zhang, Y. K., Wang, Y. J., Gupta, P., Zeng, L., Xu, M., et al. (2016). Osimertinib (AZD9291), a Mutant-Selective EGFR Inhibitor, Reverses ABCB1-Mediated Drug Resistance in Cancer Cells. *Molecules* 21.

Zhang, Y., Wu, Z. X., Yang, Y., Wang, J. Q., Li, J., Sun, Z., et al. (2020b). Poziotinib Inhibits the Efflux Activity of the ABCB1 and ABCG2 Transporters and the Expression of the ABCG2 Transporter Protein in Multidrug Resistant Colon Cancer Cells. *Cancers (Basel)* 12. doi:10.3390/cancers12113249

Zhou, S. F. (2008). Structure, Function and Regulation of P-Glycoprotein and its Clinical Relevance in Drug Disposition. *Xenobiotica* 38, 802–832. doi:10.1080/00498250701867889

**Conflict of Interest:** The authors declare that the research was conducted in the absence of any commercial or financial relationships that could be construed as a potential conflict of interest.

**Publisher's Note:** All claims expressed in this article are solely those of the authors and do not necessarily represent those of their affiliated organizations, or those of the publisher, the editors and the reviewers. Any product that may be evaluated in this article, or claim that may be made by its manufacturer, is not guaranteed or endorsed by the publisher.

frontiers in Pharmacology

MINI REVIEW
published: 11 March 2022
doi: 10.3389/fphar.2022.851589

# A Mini-Review of Flavone Isomers Apigenin and Genistein in Prostate Cancer Treatment

*Xiaozhen Ji[1†], Kai Liu[1†], Qingyue Li[1], Qun Shen[1], Fangxuan Han[1], Qingmei Ye[1,2,3*] and Caijuan Zheng[2,3*]*

[1]Hainan General Hospital and Hainan Affiliated Hospital of Hainan Medical University, Haikou, China, [2]Key Laboratory of Tropical Medicinal Plant Chemistry of Ministry of Education, College of Chemistry and Chemical Engineering, Hainan Normal University, Haikou, China, [3]Key Laboratory of Tropical Medicinal Plant Chemistry of Hainan Province, College of Chemistry and Chemical Engineering, Hainan Normal University, Haikou, China

The initial responses to standard chemotherapies among prostate cancer (PCa) patients are usually significant, while most of them will finally develop drug resistance, rendering them with limited therapies. To discover new regimens for the treatment of PCa including resistant PCa, natural products, the richest source of bioactive compounds, can serve as a library for screening and identifying promising candidates, and flavones such as apigenin and genistein have been used in lab and clinical trials for treating PCa over decades. In this mini-review, we take a look into the progress of apigenin and genistein, which are isomers, in treating PCa in the past decade. While possessing very similar structure, these two isomers can both target the same signaling pathways; they also are found to work differently in PCa cells. Given that more combinations are being developed and tested, genistein appears to be the more promising option to be approved. The anticancer efficacies of these two flavones can be confirmed by *in-vitro* and *in-vivo* studies, and their applications remain to be validated in clinical trials. Information gained in this work may provide important information for new drug development and the potential application of apigenin and genistein in treating PCa.

**Keywords: prostate cancer, resistance, flavone, apigenin, genistein**

OPEN ACCESS

***Edited by:***
*Qingbin Cui,*
*University of Toledo, United States*

***Reviewed by:***
*Fangfang Xu,*
*Guangzhou University of Chinese Medicine, China*

****Correspondence:***
*Qingmei Ye*
*qingmei-ye@hainmc.edu.cn*
*Caijuan Zheng*
*caijuan2002@163.com*

*†These authors have contributed equally to this work*

***Specialty section:***
*This article was submitted to Pharmacology of Anti-Cancer Drugs, a section of the journal Frontiers in Pharmacology*

***Received:*** *10 January 2022*
***Accepted:*** *20 January 2022*
***Published:*** *11 March 2022*

***Citation:***
*Ji X, Liu K, Li Q, Shen Q, Han F, Ye Q and Zheng C (2022) A Mini-Review of Flavone Isomers Apigenin and Genistein in Prostate Cancer Treatment. Front. Pharmacol. 13:851589. doi: 10.3389/fphar.2022.851589*

## INTRODUCTION

Prostate cancer (PCa) is the most commonly diagnosed cancer and the second leading cause of cancer death in men (do Pazo and Webster, 2021; Whitaker et al., 2020; Komura et al., 2018; Dunn, 2017). There will be an estimate of 248,530 cases and 34,130 deaths in the United States in 2021, posing a serious burden on health care in the United States and worldwide. The initial response rate of androgen deprivation therapy is usually high, while a significant proportion (around 90%) of PCa patients develops cartration-resistant PCa (CRPC) (Thoma, 2016; Huang et al., 2018; Makino et al., 2021; Welti et al., 2021). And even worse, the vast majority of CRPC patients will eventually become resistant to the first-line treatment docetaxel and enzalutamide (Scott, 2018; Lin et al., 2020; Moussa et al., 2020; Peery et al., 2020). In addition, death is usually not caused by the primary tumor but by the formation of distinct metastatic tumors that show resistant properties to varied therapies (Shore, 2020; Sayegh et al., 2021). There are unmet clinical needs to tackle drug resistance in PCa through discovering novel chemical entities or certain combinations.

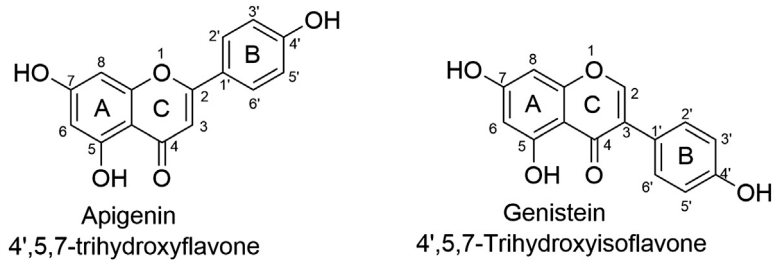


**FIGURE 1 |** The chemical structures of isomers apigenin and genistein. Apigenin and genistein share the same formulate but structurally differ at the linking position of ring B and C. Such minor difference has led to significant different pharmacological profiles.

Natural active products serve as a rich resource for the identification of hit compounds that can be used for the consequent structural modification and optimization, accounting for approximately 40% of FDA-approved drugs (Cui et al., 2018; Newman and Cragg, 2020). Among all those various active components found in traditional herbals, flavone is one of the most studied both in lab and in clinical trials (Amawi et al., 2017; Bondonno et al., 2019; Bisol et al., 2020). In addition, of roughly 3,000 flavonoids (Ye et al., 2019), apigenin and genistein, two isomers as shown in **Figure 1**, are particularly interesting to us.

Apigenin, 4′, 5, 7-trihydroxyflavone, is abundant in vegetables and certain foods that have been used as medicinal plants worldwide for centuries (Salehi et al., 2019; Su et al., 2020; Xu et al., 2021). Genistein, 4′, 5, 7-trihydroxyisoflavone, was first reported in 1899, and its structure was identified in 1926 (Jung et al., 2020). Apigenin and genistein both target dozens of pharmacological targets, such as estrogen receptors, ABC transporters, membrane proteins, mitochondria-associated proteins, cell cycle-associated proteins, epigenetic regulators, cytokines, and many signaling pathways including NF-κB, MAPK/ERK, JAK/STAT, PI3K/Akt and Wnt/β-catenin pathways, exhibiting therapeutic applications in cardiovascular diseases, neurodegenerative diseases, cancers, etc. (Mukund et al., 2017; Jaiswal et al., 2019; Kim and Park, 2020; Javed et al., 2021). Apigenin and genistein have been launched into market as dietary supplements for decades; meanwhile, they are also actively tested in clinical trials, especial for genistein as more clinical trials use it as a candidate for the treatment of various diseases including malignant cancers (Yu et al., 2021). Thus, in the current mini-review, we attempted to have an overview of the progress made in the past decade of the studies (2012–2021) of apigenin and genistein in the treatment of PCa, including resistant forms of PCa, as flavonoids have also shown promising therapeutic application in resistant cancers (Ye et al., 2019). We would like to have a brief discussion of the differences except their structures, including acting modes, targets, and the signaling pathways network.

## APIGENIN AND GENISTEIN SHOW GREAT POTENTIALS IN TREATING PCA

One thing we need to bear in mind is that these two flavones are multi-targeted or multi-functional compounds, meaning they exert their anticancer activities via multiple mechanisms. We attempted to interpret the pharmacological effects including inhibiting cancer cells proliferation and metastasis, enhancing the sensitivity of certain chemotherapeutics.

## APIGENIN

### Inhibiting IκB Kinase α (IKKα)

IKKα functions to activate NF-κB that works as a critical mediator to regulate the crosstalk of inflammation and cancer initiation and progression, serving as a druggable target (Lv et al., 2020; Mo et al., 2021).

Shukla et al. (2015) confirmed that apigenin could directly bind IKKα. Apigenin (2.5–20 μM) attenuated IKKα kinase activity and suppresses the activation of NF-κB/p65 in human PCa PC-3 and 22Rv1 cells. Apigenin caused cell cycle arrest similar to the effects induced by the knockdown of IKKα. *In-vivo* studies of xenograft mouse model indicate that apigenin (20 and 50 μg/day, gavage) suppressed tumor growth, lowered cancer cells proliferation, and enhanced apoptosis, mediated with the inhibition of p-IKKα, NF-κB/p65 (Shukla et al., 2015). This study suggested that apigenin inhibited cancer growth via suppressing IKKα and its downstream targets NF-κB (Shukla et al., 2015).

In the same group, Shukla et al. (2014a) identified another mechanism related to IKKα/β in apigenin-induced cytotoxicity in PCa (Shukla et al., 2014a). Forkhead box O (FoxO) transcription factors play an important role as tumor suppressors in human malignancies (Yadav et al., 2018). Disruption of FoxO activity due to loss of phosphatase and tensin homolog and the activation of phosphatidylinositol-3 kinase (PI3K)/Akt are frequently observed in PCa. In a model of TRAMP (transgenic adenocarcinoma of the mouse prostate) mice, Apigenin (20 and 50 μg/day, 6 days/week for 20 weeks) treatment suppressed the tumor growth and metastasis (Shukla et al., 2014a). Apigenin, via increasing nuclear retention and decreasing the binding of FoxO3a with 14-3-3, reduced the p-Akt (Ser473) and FoxO3a (Ser253) as confirmed by histologic analyses. Similar results were also observed in human PCa LNCaP and PC-3 cells, as apigenin (10 and 20 μM) increased the binding of FoxO3a with p27/Kip1, leading to cell arrest at G1 phase. *In-silico* molecular modeling

study confirmed a strong affinity of apigenin to either IKKα or IKKβ, which was then validated by *in-vitro* ELISA assay (Shukla et al., 2014a). Further study showed that apigenin can preferably bind IKKα over IKKβ, leading to the inactivation of NF-κB in PC-3 and 22Rv1 cells, providing convincing evidence that apigenin suppressed PCa progression by targeting the IKK/NF-κB pathway (Shukla et al., 2014a).

## Inhibiting Inhibitor of Apoptosis Proteins

IAP family members, including XIAP, c-IAP1/2 and survivin, are historically regarded as the major regulators of the apoptosis pathway due to their ability to inhibit pro-apoptotic caspases, highlighting that IAPs can serve as potential therapeutic targets in cancers (Peery et al., 2017; Dizdar et al., 2018; Lalaoui and Vaux, 2018; Rada et al., 2018; Hrdinka and Yabal, 2019).

Shukla et al. (2014b) found that in human PCa PC-3 and DU145 cells that are androgen-refractory, apigenin (5–40 μM) treatment decreased cell viability and induced significant apoptosis mediated by the up-regulation of cleaved caspase 3/9 and PARP (poly [ADP-ribose] polymerase), accompanied with down-regulated levels of IAP members including XIAP, c-IAP1/2, and survivin, as well as the decreased levels of Bcl-xL and Bcl-2 and the increased cytochrome C, a key player in executing apoptosis. Importantly, pretreatment of the inhibitors of caspase 9 (z-LEHD-fmk) and caspase 3 (z-DEVD-fmk) was able to alleviate apigenin-induced apoptosis. Further study indicated that the increased Bax was mediated by the inhibition of histone deacetylases (HDACs) induced by apigenin, which then caused the Ku70 acetylation that lead to the dissociation of Bax from Ku70. In addition, apigenin (20, 50 μg/day, gavage) also showed dose-dependent tumor growth inhibition in PC-3 cells xenograft mouse model, strengthening its role as an anticancer agent (Shukla et al., 2014b).

## Targeting Adenine Nucleotide Translocase-2

ANT2 is a mitochondria-associated protein that functions to exchange ADP and ATP (Jang et al., 2008; Lee et al., 2019), serving as a therapeutic target that can be regulated by apigenin but not genistein as confirmed by Oishi et al. (2013). Apigenin was able to bind and inhibit ANT2, leading to the increased death receptor 5 (DR5) and improved apoptosis induced by Apo2L/TRAIL. Meanwhile, these effects induced by apigenin could be attenuated by the ANT2 knockdown, verifying that its mechanism involved ANT2 (Oishi et al., 2013).

## Suppressing Epithelial-to-Mesenchymal Transition

Apeginin at a wide range of concentrations/doses has been found to repress cancer cells migration. EMT is a process that cancer cells initiate the migration and invasion, playing critical roles in cancer migration and drug resistance (Brabletz et al., 2018; Georgakopoulos-Soares et al., 2020).

Zhu et al. (2015) found that apigenin (10–80 μM) suppressed the proliferation of the DU145 cells via inducing G2/M phase cell cycle arrest. Aigenin (5–20 μM) inhibited the migration and invasive potentials as shown in the wound healing assay. Western blot analysis showed that upon apigenin (5, 10, 20 μM) treatment, E-cadherin, an essential component to reverse EMT, was significantly up-regulated (Zhu et al., 2015).

Later, Chien et al. (2019) found that Apigenin (0–80 μM) inhibited cell viabilities of four human PCa cell lines including metastatic hormone-sensitive cell line (LNCap) and metastatic CRPC cell lines (DU145, PC-3, and PC-3 M) in both time- and dose-dependent manners, and it reduced colony formation numbers of all 4 cell lines, suggesting it is a broad-spectrum anticancer agent. Apigenin (20 and 40 μM) significantly suppressed the characteristics of migration and invasion of PC-3 M cells. More importantly, apigenin (3 mg/kg/day, IP) significantly reduced tumor metastasis to the lung, liver, pancreas, spine, bone, and brain in an intracardiac injection model constructed by PC-3 M cells, leading to a prolonged survival rate. SPOCK1 (Sparc/osteonectin, cwcv, and kazal-like domains proteoglycan 1) is a crucial modulator in prompting EMT, which is overexpressed in PC-3 M cells. Apigenin (10, 20, 40 μM *in-vitro* and 3 mg/kg/day *in-vivo*) induced apoptosis and inhibited metastasis through down-regulating SPOCK1, as well as Snail1/2, which can be reversed by exotic overexpression of SPOCK1, suggesting a pharmacological targeting effect of apigenin (Chien et al., 2019).

## Suppressing Cancer Stem Cells

CSCs, a subset of cancer cells that show self-renewing and differentiation properties, are regarded as key players that are responsible for chemoresistance, tumor relapse, and metastasis (Sancho et al., 2016; Cui et al., 2017; Luo et al., 2018; Carvalho et al., 2021). Apigenin has been shown to negatively regulate CSCs, resulting in the re-sensitization of certain chemotherapeutics.

Erdogan et al. (2017) tested apgenin's effect towards $CD44^+$ PCa stem cells that were isolated from human androgen-independent PC-3 PCa cells. Apigenin (15 μM) significantly enhanced cisplatin's (7.5 μM) cytotoxic and apoptosis-inducing and migration-suppressing effects through the down-regulation of anti-apoptotic Bcl-2, sharpin and survivin, and the up-regulation of pro-apoptotic members such as caspase-8, Apaf-1 (apoptotic protease activating factor-1), and p53 mRNA expression. The combined therapy down-regulated p-PI3K, p-Akt, NF-κB, and arrested cell cycle at G2/M and S phases (Erdogan et al., 2017).

A similar study by the same group (2016) showed that apigenin (0–100 μM) inhibited CSCs ($CD44^+$ PCa stem cells) and PC-3 cell survival, with a significant increase of p21 and p27, both of which are anti-apoptotic proteins. It appeared that apigenin induced apoptosis via an extrinsic caspase-dependent pathway mediated by up-regulating the mRNA expressions of caspases-8, -3, and TNF-α, but failed to trigger the intrinsic pathway as determined by the levels of pro-apoptotic Bax, cytochrome C, and Apaf-1 in CSCs. While in contrast in PC-3 cells, apigenin exerted cytotoxic effects via intrinsic apoptosis pathway. Apigenin (25 μM) suppressed the migration of CSCs via down-regulating matrix metallopeptidases-2, -9, (MMP2/9), and Snail1/2. Similarly, the expressions of NF-κB p105/p50, p-PI3K, and p-Akt were all decreased after apigenin treatment. Moreover, apigenin treatment significantly reduced the

**TABLE 1 |** Summary (2012–2021) of apigenin and genistein in the treatment of PCa.

| Flavone | Mechanisms | *In-vitro* | *In-vivo* | References |
|---|---|---|---|---|
| Apigenin | Inhibiting IKKα | Inhibiting the proliferation of PC-3 and 22Rv1 cells | Reducing tumor growth of PC-3 and 22Rv1 cells xenografts | Shukla et al. (2015) |
| | Targeting PI3K/Akt/FoxO | Inducing cell arrest of PC-3 and 22Rv1 cells | Reducing tumor growth and metastasis of TRAMP mice | Shukla et al. (2014a) |
| | Inhibiting IAP | Inducing apoptosis of PC-3 and DU145 cells | Reducing tumor growth of PC-3 cells xenograft | Shukla et al. (2014b) |
| | Inhibiting ANT2 | Sensitizing TRAIL in DU145 cells | ND[a] | Oishi et al. (2013) |
| | Suppressing EMT | Inhibiting DU145 and PC-3 M cells proliferation and migration | Reducing tumor growth and metastasis of PC-3 M cells xenograft | Zhu et al., 2015; Chien et al., 2019 |
| | Suppressing CSCs | Sensitizing cisplatin in $CD44^+$ PCa stem cells | ND | Erdogan et al. (2016); Erdogan et al. (2017) |
| Genistein | | | | |
| | Suppressing CSCs | Inhibiting the tumorigenicity of PCa CSCs | Reducing tumor growth of PCa CSCs cells xenograft | Zhang et al. (2012) |
| | Targeting PI3K/Akt | Inhibiting PC-3 cells proliferation and migration | Reducing tumor growth of PC-3 cells xenograft | Song et al. (2020) |
| | Targeting MMP2 and apoptosis | Inhibiting PC-3 cells proliferation and migration | ND | Shafiee et al. (2020) |
| | Targeting DNA repair | Sensitizing AG1024 and radiotherapy in PC-3 and DU145 cells | Reducing tumor growth of DU145 cells xenograft | Tang et al. (2018) |
| | | Sensitizing DOX | Reducing tumor growth | Wang et al. (2018) |
| | Inhibiting Glu-1 | Synergizing with celecoxib in PC-3 and LNCap cells | ND | Tian et al. (2019) |
| | Demethylating | Inhibiting LNCap and LAPC cells proliferation | ND | Mahmoud et al. (2015) |
| | Inhibiting IGF-1 | Inhibiting PC-3 cells growth | ND | Lee et al. (2012) |
| | Regulating miRNA and lncRNA | Inhibiting PC-3 and DU145 cells | ND | Chiyomaru et al. (2012); Chiyomaru et al. (2013b) |
| | Inducing apoptosis | Sensitizing cabazitaxel, topotecan and radiotherapy in PC-3 or LNCaP cells | Reducing tumor growth of PC-3 cells xenograft | Hörmann et al., 2012; Zhang et al. (2013); Jackson et al. (2019) |

[a]*ND, not determined.*

protein expression of pluripotency marker Oct3/4, indicating apigenin's strong potential in suppressing CSCs, warranting further *in-vivo* study (Erdogan et al., 2016).

# GENISTEIN

Genistein in some cases shows similar or even the same mechanism as apigenin toward certain targets, such as CSCs (Zhang et al., 2012), PI3K/Akt signaling pathway (Song et al., 2020), MMP2 and apoptosis-related proteins including caspase 3 (Shafiee et al., 2020), while genistein appears to regulate more targets than apigenin.

## Inactivating DNA Repair Pathways

Homologous recombination (HR) and the nonhomologous end joining (NHEJ) pathways are two DNA repair pathways that are activated by PCa cells when treated by certain chemotherapeutics, resulting in drug resistance (Sharda et al., 2020; Xiang et al., 2020; Filsinger et al., 2021). Genistein can work as chemotherapy sensitizer via impacting HR and NHEJ. Tang et al. (2018) developed a triple combination therapy composed with genistein (30 μM), AG1024 (10 μM), and radiotherapy. As shown in PC-3 and DU145 cells, the pretreatment of genistein and AG1024 could markedly enhance the inhibition of cells proliferation and induction of apoptosis induced by radiotherapy, which was mediated by the up-regulated Bax and cleaved caspase 3, leading to reduced colony formation (Tang et al., 2018). The triple combination induced a cell arrest at the S phase and decreased the G2/M phases. Further study indicated that this combination could induce double-strand breaks mediated by the inactivation of HR and NHEJ pathways, evidenced by the down-regulation of DNA-PKcs (Thr2609), Rad51, and Ku70. The *in-vivo* study also confirmed that this triple combination (100 mg/kg/day of genistein and AG1024, plus X-irradiation) surpassed the efficacies of other dual therapies, without showing any obvious adverse effects (Tang et al., 2018).

Genistein was also shown to regulate another key player in DNA repair, which was the APE1 (apurinic/apyrimidinic endonuclease1) that served as an oxidative DNA repair enzyme (Maayah et al., 2015; Pekhale et al., 2017; Lebedeva et al., 2020). In order to reduce the severely toxic effects toward normal tissues of doxorubicin (DOX), a nanoparticles system named as DOX-NPs, loaded with DOX and genistein, was synthesized by Wang et al. (2018) and evaluated *in-vitro* and *in-vivo*. Not only could genistein, when worked as an APE1 inhibitor, enhance DOX-induced cell death mediated by overproduced ROS (reactive oxygen species), it can also alleviate DOX-induced toxic effects. DOX-NPs showed a strong activity in suppressing distant metastasis in the *in-vivo* model (Wang et al., 2018).

## Inhibiting Glucose Transporter 1

Glut-1 functions to the transportation of glucose across cell membrane, facilitating ATP production (Almahmoud et al., 2019;

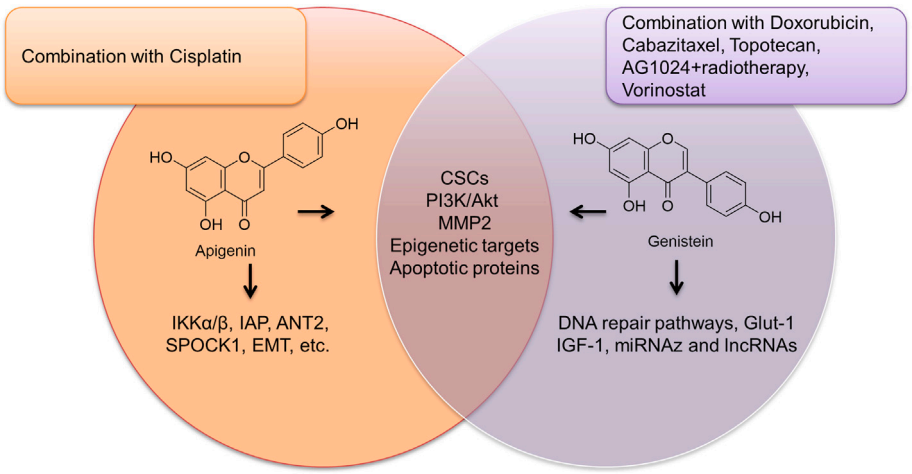


**FIGURE 2 |** The overview of apigenin and genistein in PCa treatment.

Pragallapati and Manyam, 2019; Qamar et al., 2019; Ahopelto et al., 2020). Enhanced Glut-1 protein as well as COX-2 (cyclooxygenase-2) is reported as one of the major driving factors, leading to the initiation and progress of PCa (Carreño et al., 2019; Gasinska et al., 2020; King et al., 2020; Joshi et al., 2021). Tian et al. (2019) synthesized a liposomal system composed with COX-2 inhibitor celecoxib and genistein (100 μM celecoxib and 10 μM genistein), and this liposomal system exhibited selective cytotoxic effects towards PC-3 and LNCaP cells over non-cancer cells via inducing apoptosis as confirmed by up-regulated cleaved caspase 3, and it suppressed PC-3 cells migration. This liposomal system could induce ROS production, decrease GSH level, and inhibit COX-2 and Glut-1 receptors simultaneously, leading to decreased glucose uptake in PC-3 and LNCaP cells, indicating a dual targeting (Tian et al., 2019). Further models are clearly needed to elucidate its safety and efficacy.

## Demethylating Effect

Similar as apigenin, genistein can also regulate epigenetic proteins. Methylation of certain genes can be hijacked by cancer cells to promote its tumorigenesis (Wu et al., 2020; Zhao et al., 2020; Tolkach et al., 2021), while genistein was shown to down-regulate methylation.

ER-β (Estrogen receptor β) promoter hyper-methylation has a tumor inducing effect in PCa. Mahmoud et al. (2015) found that genistein (0.5–10 μM) significantly reduced the methylation of ER-β promoter accompanied with corresponding dose-dependent increased of ER-β expression in LNCaP and LAPC-4 but not in PC-3 cells with lower basal levels of ER-β promoter methylation. Genistein (0.5–10 μM) could down-regulate DNA methyl transferases (DNMTs) and increase the phosphorylation, nuclear translocation, and transcriptional activity of ER-β (working as a cancer suppressor) in all three PCa cell lines. Inhibitory effects of genistein on LAPC-4 and PC-3 cell proliferation were diminished using a specific ER-β antagonist, suggesting an ER-β-mediated mechanism (Mahmoud et al., 2015).

## Inhibiting Insulin-like Growth Factor-1 Receptor

IGF-1, an essential player in anabolism, is found to be elevated in several different cancers, including PCa (Uzunlulu et al., 2016; Mancarella et al., 2017; Larsson et al., 2020; Ohishi et al., 2020). The inhibition of IGF-1 and its downstream signaling pathways may have therapeutic implications (Nordstrand et al., 2013; Nordstrand et al., 2017).

Lee at al. (2012) found that genistein treatment caused a significant inhibition of IGF-1-stimulated PC-3 cells growth through decreasing the proliferation of IGF-1-stimulated cells and inducing cell arrest at G0/G1 phase (Lee et al., 2012). Genistein effectively inhibited the phosphorylation of IGF-1R and the phosphorylation of its downstream targets, such as Src, Akt, and GSK-3β (glycogen synthase kinase-3β), and it greatly attenuated IGF-1-induced β-catenin signaling and cyclin D1 levels in PC-3 cells (Phillip et al., 2012).

## Modulating miRNAs and Long Non-coding RNAs

Different with apigenin, genistein could regulate miRNAz and lncRNAs to achieve its treatment efficacies in PCa.

Hirata et al. (2014) found that miRNA-1260b expression was significantly decreased by genistein (25 μM for 4 days) in PC-3 and DU-145 cells; meanwhile, the knockdown of miR-1260b suppressed cell proliferation, invasion, migration, and TCF reporter activity in PC cells, similar phenomenon as genistein treatment (Hirata et al., 2014).

Chiyomaru et al. (2013a) found that genistein may impact the axis of lncRNAs and miRNAs as confirmed by microarray assay which showed that lncRNA HOTAIR and miR-34a were regulated by genistein (25 μM) in PC-3 and DU145 cells (Chiyomaru et al., 2013a). By this same group (2013), they reported another finding that genistein (25 and 50 μM) might up-regulate tumor suppressor miR-574-3p in PC-3 cells and in PCa tissues (Chiyomaru et al., 2013b). In addition, Chiyomaru

et al. (2012) also identified another key player, oncogenic miR-151, which can be down-regulated by genistein (25 μM) in PC-3 and DU145 cells (Chiyomaru et al., 2012).

### Certain Combinations That Induced Apoptosis

Genistein could work as a chemosensitizer.

Zhang et al. (2013) found that genistein (5 and 10 μg/ml) when combined with cabazitaxel (5–100 nM) could enhance the sensitivity of cabazitaxel to metastatic CRPC cells *in-vitro* and *in-vivo* via increasing the expression of pro-apoptotic Bax and cleaved caspase 3 (Zhang et al., 2013). In a PC-3-luciferase xenograft model, the combined treatment with genistein (100 mg/kg) and cabazitaxel (5 mg/kg) significantly retarded the growth of mCRPC when compared to vehicle control, cabazitaxel, or genistein (Zhang et al., 2013).

Another study showed that the combination of topotecan and genistein exhibited better efficacy in LNCaP and PCa cells than either monotherapy, which was mediated by inducing apoptosis activated by caspase-3 and -9 and by ROS generation (Hörmann et al., 2012).

Another genistein nano-suspension (named as BIO 300) was synthesized by Jackson et al. (2019). BIO 300 positively synergized with radiation, resulting in tumor growth delay and prolonged survival as confirmed in hormone-sensitive and insensitive prostate tumor-bearing mice (Jackson et al., 2019). Their data also strongly support the clinical translation of BIO 300 for mitigation of ED (erectile dysfunction) among PCa patients (Jackson et al., 2019).

## CLINICAL EVIDENCE

Many ongoing clinical studies of different stages have also revealed that genistein may benefit PCa patients via either inhibiting metastasis or suppressing tumor growth (Pavese et al., 2014). Retrospective clinical studies have shown that high consumption of soybean products (genistein as its major active component) has been associated with a low incidence of PCa (Hwang et al., 2009). Wu et al. (2015) reported a preliminarily evaluation of the associations among plasma genistein and PCa in a Chinese population composed with 100 men aged over 40 and diagnosed with PCa (Zhu et al., 2015) or PCa-free (Zhang et al., 2012), and analyzed the physiological data before and after certain doses of genistein dietary intake. Their data showed that cancer-free patients possessed higher plasma genistein concentration than PCa patients, and the plasma genistein concentration negatively correlated to PCa (Wu et al., 2015). Bilir et al. (2017) invested the effects of genistein on Norwegian patients who received 30 mg genistein or placebo capsules daily for 3–6 weeks before prostatectomy. Microarrays and qPCR data showed that several differentially methylated sites and expressed genes between placebo and genistein groups. Importantly, the MYC activity reduced and PTEN activity increased in patients receiving genistein, highlighting the Pca-preventive of genistein (Bilir et al., 2017).

While some clinical studies showed unfavorable results towards the remission of PCa (Jarrard et al., 2016), or the plasma genistein concentration was not associated with PCa risk in large cohort of European men (Travis et al., 2012), more clinical trials with well-filtered qualified PCa patients are warranted.

## SUMMARY AND BRIEF DISCUSSION

The above information strongly supports the potential application of apigenin and genistein in treating PCa including resistant forms of PCa as shown in **Table 1**.

While apigenin and genistein are isomers, they appear to treat PCa via a slight different mechanism. Both of them can regulate CSCs (Zhang et al., 2012; Erdogan et al., 2016), PI3K/Akt (Shukla et al., 2014a; Song et al., 2020), MMP2, and apoptosis-related proteins including caspase 3 (Shafiee et al., 2020) and DNA damage-associated repair pathway (Phillip et al., 2012; Sharma et al., 2014; Tang et al., 2018). While apigenin was able to inhibit IAP members, genistein seems to impact membrane-associated proteins, such as certain receptors including Glut-1 and IGF-1 (Lee et al., 2012; Tian et al., 2019) as summarized in **Figure 2**.

Genistein appears to be more useful in combination than apigenin that only was shown to sensitize cisplatin. Several combinations regimens, such as genistein + celecoxib (Tian et al., 2019), genistein + cabazitaxel (Zhang et al., 2013), genistein + topotecan (Hörmann et al., 2012), genistein + vorinostat, as well as triple combination of genistein + AG1024 + radiotherapy (Jackson et al., 2019), were optimized and tested in cell-based assay and in animal models, strongly supporting its potential as chemotherapy in PCa.

Furthermore, these two flavones can serve as leading compound that undergo structural modifications to achieve higher activities but lower toxic effects (Chen et al., 2015; Xiong et al., 2015; George et al., 2018).

## CONCLUSION

Flavones isomers apigenin and genistein, by mono-therapy or combinational therapy, exhibited great potentials in the treatment of PCa including resistant PCa.

## AUTHOR CONTRIBUTIONS

XJ, KL, and QY designed this review; XJ, KL, QL, QS, and FH wrote the manuscript; QY and CZ revised the manuscript. All authors read and approved the final manuscript. All authors contributed to the article and approved the submitted version. XJ and KL have contributed equally to this work.

## FUNDING

We are grateful to the support from the National Natural Science Foundation of China (Grant number: 82160735) and Hainan Normal University 2021 Annual Graduate Innovation and Scientific Research Project (Grant number: hsyx 2021-4).

## REFERENCES


Ahopelto, K., Laitinen, A., Hagström, J., Böckelman, C., and Haglund, C. (2020). Transketolase-Like Protein 1 and Glucose Transporter 1 in Gastric Cancer. *Oncology* 98 (9), 643–652. doi:10.1159/000507350

Almahmoud, S., Wang, X., Vennerstrom, J. L., and Zhong, H. A. (2019). Conformational Studies of Glucose Transporter 1 (GLUT1) as an Anticancer Drug Target. *Molecules* 24 (11), 2159. doi:10.3390/molecules24112159

Amawi, H., Ashby, C. R., and Tiwari, A. K. (2017). Erratum to: Cancer Chemoprevention through Dietary Flavonoids: What's Limiting. *Chin. J. Cancer* 36 (1), 70. doi:10.1186/s40880-017-0237-0

Bilir, B., Sharma, N. V., Lee, J., Hammarstrom, B., Svindland, A., Kucuk, O., et al. (2017). Effects of Genistein Supplementation on Genomewide DNA Methylation and Gene Expression in Patients with Localized Prostate Cancer. *Int. J. Oncol.* 51 (1), 223–234. doi:10.3892/ijo.2017.4017

Bisol, Â., de Campos, P. S., and Lamers, M. L. (2020). Flavonoids as Anticancer Therapies: A Systematic Review of Clinical Trials. *Phytother. Res.* 34 (3), 568–582. doi:10.1002/ptr.6551

Bondonno, N. P., Dalgaard, F., Kyrø, C., Murray, K., Bondonno, C. P., Lewis, J. R., et al. (2019). Flavonoid Intake Is Associated with Lower Mortality in the Danish Diet Cancer and Health Cohort. *Nat. Commun.* 10 (1), 3651. doi:10.1038/s41467-019-11622-x

Brabletz, T., Kalluri, R., Nieto, M. A., and Weinberg, R. A. (2018). EMT in Cancer. *Nat. Rev. Cancer* 18 (2), 128–134. doi:10.1038/nrc.2017.118

Carreño, D., Corro, N., Torres-Estay, V., Véliz, L. P., Jaimovich, R., Cisternas, P., et al. (2019). Fructose and Prostate Cancer: toward an Integrated View of Cancer Cell Metabolism. *Prostate Cancer Prostatic Dis.* 22 (1), 49–58. doi:10.1038/s41391-018-0072-7

Carvalho, L. S., Gonçalves, N., Fonseca, N. A., and Moreira, J. N. (2021). Cancer Stem Cells and Nucleolin as Drivers of Carcinogenesis. *Pharmaceuticals (Basel)* 14 (1), 60. doi:10.3390/ph14010060

Chen, Q. H., Yu, K., Zhang, X., Chen, G., Hoover, A., Leon, F., et al. (2015). A New Class of Hybrid Anticancer Agents Inspired by the Synergistic Effects of Curcumin and Genistein: Design, Synthesis, and Anti-proliferative Evaluation. *Bioorg. Med. Chem. Lett.* 25 (20), 4553–4556. doi:10.1016/j.bmcl.2015.08.064

Chien, M. H., Lin, Y. W., Wen, Y. C., Yang, Y. C., Hsiao, M., Chang, J. L., et al. (2019). Targeting the SPOCK1-Snail/slug axis-mediated Epithelial-To-Mesenchymal Transition by Apigenin Contributes to Repression of Prostate Cancer Metastasis. *J. Exp. Clin. Cancer Res.* 38 (1), 246. doi:10.1186/s13046-019-1247-3

Chiyomaru, T., Yamamura, S., Fukuhara, S., Hidaka, H., Majid, S., Saini, S., et al. (2013). Genistein Up-Regulates Tumor Suppressor microRNA-574-3p in Prostate Cancer. *PLoS One* 8 (3), e58929. doi:10.1371/journal.pone.0058929

Chiyomaru, T., Yamamura, S., Fukuhara, S., Yoshino, H., Kinoshita, T., Majid, S., et al. (2013). Genistein Inhibits Prostate Cancer Cell Growth by Targeting miR-34a and Oncogenic HOTAIR. *PLoS One* 8 (8), e70372. doi:10.1371/journal.pone.0070372

Chiyomaru, T., Yamamura, S., Zaman, M. S., Majid, S., Deng, G., Shahryari, V., et al. (2012). Genistein Suppresses Prostate Cancer Growth through Inhibition of Oncogenic microRNA-151. *PLoS One* 7 (8), e43812. doi:10.1371/journal.pone.0043812

Cui, Q., Wen, S., and Huang, P. (2017). Targeting Cancer Cell Mitochondria as a Therapeutic Approach: Recent Updates. *Future Med. Chem.* 9 (9), 929–949. doi:10.4155/fmc-2017-0011

Cui, Q., Yang, D. H., and Chen, Z. S. (2018). Special Issue: Natural Products: Anticancer and beyond. *Molecules* 23 (6), 1246–1249. doi:10.3390/molecules23061246

Dizdar, L., Jünemann, L. M., Werner, T. A., Verde, P. E., Baldus, S. E., Stoecklein, N. H., et al. (2018). Clinicopathological and Functional Implications of the Inhibitor of Apoptosis Proteins Survivin and XIAP in Esophageal Cancer. *Oncol. Lett.* 15 (3), 3779–3789. doi:10.3892/ol.2018.7755

do Pazo, C., and Webster, R. M. (2021). The Prostate Cancer Drug Market. *Nat. Rev. Drug Discov.* 20 (9), 663–664. doi:10.1038/d41573-021-00111-w

Dunn, M. W. (2017). Prostate Cancer Screening. *Semin. Oncol. Nurs.* 33 (2), 156–164. doi:10.1016/j.soncn.2017.02.003

Erdogan, S., Doganlar, O., Doganlar, Z. B., Serttas, R., Turkekul, K., Dibirdik, I., et al. (2016). The Flavonoid Apigenin Reduces Prostate Cancer CD44(+) Stem Cell Survival and Migration through PI3K/Akt/NF-Kb Signaling. *Life Sci.* 162, 77–86. doi:10.1016/j.lfs.2016.08.019

Erdogan, S., Turkekul, K., Serttas, R., and Erdogan, Z. (2017). The Natural Flavonoid Apigenin Sensitizes Human CD44+ Prostate Cancer Stem Cells to Cisplatin Therapy. *Biomed. Pharmacother.* 88, 210–217. doi:10.1016/j.biopha.2017.01.056

Filsinger, G. T., Wannier, T. M., Pedersen, F. B., Lutz, I. D., Zhang, J., Stork, D. A., et al. (2021). Characterizing the Portability of Phage-Encoded Homologous Recombination Proteins. *Nat. Chem. Biol.* 17 (4), 394–402. doi:10.1038/s41589-020-00710-5

Gasinska, A., Jaszczynski, J., Rychlik, U., Łuczynska, E., Pogodzinski, M., and Palaczynski, M. (2020). Prognostic Significance of Serum PSA Level and Telomerase, VEGF and GLUT-1 Protein Expression for the Biochemical Recurrence in Prostate Cancer Patients after Radical Prostatectomy. *Pathol. Oncol. Res.* 26 (2), 1049–1056. doi:10.1007/s12253-019-00659-4

Georgakopoulos-Soares, I., Chartoumpekis, D. V., Kyriazopoulou, V., and Zaravinos, A. (2020). EMT Factors and Metabolic Pathways in Cancer. *Front. Oncol.* 10, 499. doi:10.3389/fonc.2020.00499

George, A., Raji, I., Cinar, B., Kucuk, O., and Oyelere, A. K. (2018). Design, Synthesis, and Evaluation of the Antiproliferative Activity of Hydantoin-Derived Antiandrogen-Genistein Conjugates. *Bioorg. Med. Chem.* 26 (8), 1481–1487. doi:10.1016/j.bmc.2018.01.009

Hirata, H., Hinoda, Y., Shahryari, V., Deng, G., Tanaka, Y., Tabatabai, Z. L., et al. (2014). Genistein Downregulates Onco-miR-1260b and Upregulates sFRP1 and Smad4 via Demethylation and Histone Modification in Prostate Cancer Cells. *Br. J. Cancer* 110 (6), 1645–1654. doi:10.1038/bjc.2014.48

Hörmann, V., Kumi-Diaka, J., Durity, M., and Rathinavelu, A. (2012). Anticancer Activities of Genistein-Topotecan Combination in Prostate Cancer Cells. *J. Cel. Mol. Med.* 16 (11), 2631–2636. doi:10.1111/j.1582-4934.2012.01576.x

Hrdinka, M., and Yabal, M. (2019). Inhibitor of Apoptosis Proteins in Human Health and Disease. *Genes Immun.* 20 (8), 641–650. doi:10.1038/s41435-019-0078-8

Huang, Y., Jiang, X., Liang, X., and Jiang, G. (2018). Molecular and Cellular Mechanisms of Castration Resistant Prostate Cancer. *Oncol. Lett.* 15 (5), 6063–6076. doi:10.3892/ol.2018.8123

Hwang, Y. W., Kim, S. Y., Jee, S. H., Kim, Y. N., and Nam, C. M. (2009). Soy Food Consumption and Risk of Prostate Cancer: a Meta-Analysis of Observational Studies. *Nutr. Cancer* 61 (5), 598–606. doi:10.1080/01635580902825639

Jackson, I. L., Pavlovic, R., Alexander, A. A., Connors, C. Q., Newman, D., Mahmood, J., et al. (2019). BIO 300, a Nanosuspension of Genistein, Mitigates Radiation-Induced Erectile Dysfunction and Sensitizes Human Prostate Cancer Xenografts to Radiation Therapy. *Int. J. Radiat. Oncol. Biol. Phys.* 105 (2), 400–409. doi:10.1016/j.ijrobp.2019.05.062

Jaiswal, N., Akhtar, J., Singh, S. P., Ahsan, F., and Ahsan, F. (2019). An Overview on Genistein and its Various Formulations. *Drug Res. (Stuttg)* 69 (6), 305–313. doi:10.1055/a-0797-3657

Jang, J. Y., Choi, Y., Jeon, Y. K., and Kim, C. W. (2008). Suppression of Adenine Nucleotide Translocase-2 by Vector-Based siRNA in Human Breast Cancer Cells Induces Apoptosis and Inhibits Tumor Growth *In Vitro* and *In Vivo*. *Breast Cancer Res.* 10 (1), R11. doi:10.1186/bcr1857

Jarrard, D., Konety, B., Huang, W., Downs, T., Kolesar, J., Kim, K. M., et al. (2016). Phase IIa, Randomized Placebo-Controlled Trial of Single High Dose Cholecalciferol (Vitamin D3) and Daily Genistein (G-2535) versus Double Placebo in Men with Early Stage Prostate Cancer Undergoing Prostatectomy. *Am. J. Clin. Exp. Urol.* 4 (2), 17–27.

Javed, Z., Sadia, H., Iqbal, M. J., Shamas, S., Malik, K., Ahmed, R., et al. (2021). Apigenin Role as Cell-Signaling Pathways Modulator: Implications in Cancer Prevention and Treatment. *Cancer Cel Int* 21 (1), 189. doi:10.1186/s12935-021-01888-x

Joshi, S. N., Murphy, E. A., Olaniyi, P., and Bryant, R. J. (2021). The Multiple Effects of Aspirin in Prostate Cancer Patients. *Cancer Treat. Res. Commun.* 26, 100267. doi:10.1016/j.ctarc.2020.100267

Jung, Y. S., Rha, C. S., Baik, M. Y., Baek, N. I., and Kim, D. O. (2020). A Brief History and Spectroscopic Analysis of Soy Isoflavones. *Food Sci. Biotechnol.* 29 (12), 1605–1617. doi:10.1007/s10068-020-00815-6

Kim, J. K., and Park, S. U. (2020). Recent Insights into the Biological Functions of Apigenin. *EXCLI J.* 19, 984–991. doi:10.17179/excli2020-2579

King, L., Christie, D., Arora, D., and Anoopkumar-Dukie, S. (2020). Cyclooxygenase-2 Inhibitors Delay Relapse and Reduce Prostate Specific Antigen (PSA) Velocity in Patients Treated with Radiotherapy for Nonmetastatic Prostate Cancer: a Pilot Study. *Prostate Int.* 8 (1), 34–40. doi:10.1016/j.prnil.2019.10.004

Komura, K., Sweeney, C. J., Inamoto, T., Ibuki, N., Azuma, H., and Kantoff, P. W. (2018). Current Treatment Strategies for Advanced Prostate Cancer. *Int. J. Urol.* 25 (3), 220–231. doi:10.1111/iju.13512

Lalaoui, N., and Vaux, D. L. (2018). Recent Advances in Understanding Inhibitor of Apoptosis Proteins. *F1000Res* 7, F1000. doi:10.12688/f1000research.16439.1

Larsson, S. C., Carter, P., Vithayathil, M., Kar, S., Mason, A. M., and Burgess, S. (2020). Insulin-like Growth Factor-1 and Site-specific Cancers: A Mendelian Randomization Study. *Cancer Med.* 9 (18), 6836–6842. doi:10.1002/cam4.3345

Lebedeva, N. A., Rechkunova, N. I., Endutkin, A. V., and Lavrik, O. I. (2020). Apurinic/Apyrimidinic Endonuclease 1 and Tyrosyl-DNA Phosphodiesterase 1 Prevent Suicidal Covalent DNA-Protein Crosslink at Apurinic/Apyrimidinic Site. *Front Cel Dev Biol* 8, 617301. doi:10.3389/fcell.2020.617301

Lee, C. H., Kim, M. J., Lee, H. H., Paeng, J. C., Park, Y. J., Oh, S. W., et al. (2019). Adenine Nucleotide Translocase 2 as an Enzyme Related to [18F] FDG Accumulation in Various Cancers. *Mol. Imaging Biol.* 21 (4), 722–730. doi:10.1007/s11307-018-1268-x

Lee, J., Ju, J., Park, S., Hong, S. J., and Yoon, S. (2012). Inhibition of IGF-1 Signaling by Genistein: Modulation of E-Cadherin Expression and Downregulation of β-catenin Signaling in Hormone Refractory PC-3 Prostate Cancer Cells. *Nutr. Cancer* 64 (1), 153–162. doi:10.1080/01635581.2012.630161

Lin, J. Z., Wang, W. W., Hu, T. T., Zhu, G. Y., Li, L. N., Zhang, C. Y., et al. (2020). FOXM1 Contributes to Docetaxel Resistance in Castration-Resistant Prostate Cancer by Inducing AMPK/mTOR-mediated Autophagy. *Cancer Lett.* 469, 481–489. doi:10.1016/j.canlet.2019.11.014

Luo, M., Shang, L., Brooks, M. D., Jiagge, E., Zhu, Y., Buschhaus, J. M., et al. (2018). Targeting Breast Cancer Stem Cell State Equilibrium through Modulation of Redox Signaling. *Cell Metab* 28 (1), 69–e6. doi:10.1016/j.cmet.2018.06.006

Lv, S., Wang, F., Wang, K., Fan, Y., Xu, J., Zheng, J., et al. (2020). IκB Kinase α: an Independent Prognostic Factor that Promotes the Migration and Invasion of Oral Squamous Cell Carcinoma. *Br. J. Oral Maxillofac. Surg.* 58 (3), 296–303. doi:10.1016/j.bjoms.2019.11.025

Maayah, Z. H., Ghebeh, H., Alhaider, A. A., El-Kadi, A. O., Soshilov, A. A., Denison, M. S., et al. (2015). Metformin Inhibits 7,12-Dimethylbenz[a] anthracene-Induced Breast Carcinogenesis and Adduct Formation in Human Breast Cells by Inhibiting the Cytochrome P4501A1/aryl Hydrocarbon Receptor Signaling Pathway. *Toxicol. Appl. Pharmacol.* 284 (2), 217–226. doi:10.1016/j.taap.2015.02.007

Mahmoud, A. M., Al-Alem, U., Ali, M. M., and Bosland, M. C. (2015). Genistein Increases Estrogen Receptor Beta Expression in Prostate Cancer via Reducing its Promoter Methylation. *J. Steroid Biochem. Mol. Biol.* 152, 62–75. doi:10.1016/j.jsbmb.2015.04.018

Makino, T., Izumi, K., and Mizokami, A. (2021). Undesirable Status of Prostate Cancer Cells after Intensive Inhibition of AR Signaling: Post-AR Era of CRPC Treatment. *Biomedicines* 9 (4), 414. doi:10.3390/biomedicines9040414

Mancarella, C., Casanova-Salas, I., Calatrava, A., García-Flores, M., Garofalo, C., Grilli, A., et al. (2017). Insulin-like Growth Factor 1 Receptor Affects the Survival of Primary Prostate Cancer Patients Depending on TMPRSS2-ERG Status. *BMC Cancer* 17 (1), 367. doi:10.1186/s12885-017-3356-8

Mo, D., Zhu, H., Wang, J., Hao, H., Guo, Y., Wang, J., et al. (2021). Icaritin Inhibits PD-L1 Expression by Targeting Protein IκB Kinase α. *Eur. J. Immunol.* 51 (4), 978–988. doi:10.1002/eji.202048905

Moussa, M., Papatsoris, A., Abou Chakra, M., Sryropoulou, D., and Dellis, A. (2020). Pharmacotherapeutic Strategies for Castrate-Resistant Prostate Cancer. *Expert Opin. Pharmacother.* 21 (12), 1431–1448. doi:10.1080/14656566.2020.1767069

Mukund, V., Mukund, D., Sharma, V., Mannarapu, M., and Alam, A. (2017). Genistein: Its Role in Metabolic Diseases and Cancer. *Crit. Rev. Oncol. Hematol.* 119, 13–22. doi:10.1016/j.critrevonc.2017.09.004

Newman, D. J., and Cragg, G. M. (2020). Natural Products as Sources of New Drugs over the Nearly Four Decades from 01/1981 to 09/2019. *J. Nat. Prod.* 83 (3), 770–803. doi:10.1021/acs.jnatprod.9b01285

Nordstrand, A., Bergström, S. H., Thysell, E., Bovinder-Ylitalo, E., Lerner, U. H., Widmark, A., et al. (2017). Inhibition of the Insulin-like Growth Factor-1 Receptor Potentiates Acute Effects of Castration in a Rat Model for Prostate Cancer Growth in Bone. *Clin. Exp. Metastasis* 34 (3-4), 261–271. doi:10.1007/s10585-017-9848-8

Nordstrand, A., Lundholm, M., Larsson, A., Lerner, U. H., Widmark, A., and Wikström, P. (2013). Inhibition of the Insulin-like Growth Factor-1 Receptor Enhances Effects of Simvastatin on Prostate Cancer Cells in Co-culture with Bone. *Cancer Microenviron* 6 (3), 231–240. doi:10.1007/s12307-013-0129-z

Ohishi, T., Abe, H., Sakashita, C., Saqib, U., Baig, M. S., Ohba, S. I., et al. (2020). Inhibition of Mitochondria ATP Synthase Suppresses Prostate Cancer Growth through Reduced Insulin-like Growth Factor-1 Secretion by Prostate Stromal Cells. *Int. J. Cancer* 146 (12), 3474–3484. doi:10.1002/ijc.32959

Oishi, M., Iizumi, Y., Taniguchi, T., Goi, W., Miki, T., and Sakai, T. (2013). Apigenin Sensitizes Prostate Cancer Cells to Apo2L/TRAIL by Targeting Adenine Nucleotide Translocase-2. *PLoS One* 8 (2), e55922. doi:10.1371/journal.pone.0055922

Pavese, J. M., Krishna, S. N., and Bergan, R. C. (2014). Genistein Inhibits Human Prostate Cancer Cell Detachment, Invasion, and Metastasis. *Am. J. Clin. Nutr.* 100 (Suppl. 1), 431S–6S. doi:10.3945/ajcn.113.071290

Peery, R., Kyei-Baffour, K., Dong, Z., Liu, J., de Andrade Horn, P., Dai, M., et al. (2020). Synthesis and Identification of a Novel Lead Targeting Survivin Dimerization for Proteasome-dependent Degradation. *J. Med. Chem.* 63 (13), 7243–7251. doi:10.1021/acs.jmedchem.0c00475

Peery, R. C., Liu, J. Y., and Zhang, J. T. (2017). Targeting Survivin for Therapeutic Discovery: Past, Present, and Future Promises. *Drug Discov. Today* 22 (10), 1466–1477. doi:10.1016/j.drudis.2017.05.009

Pekhale, K., Haval, G., Perween, N., Antoniali, G., Tell, G., Ghaskadbi, S., et al. (2017). DNA Repair Enzyme APE1 from Evolutionarily Ancient Hydra Reveals Redox Activity Exclusively Found in Mammalian APE1. *DNA Repair (Amst)* 59, 44–56. doi:10.1016/j.dnarep.2017.09.005

Phillip, C. J., Giardina, C. K., Bilir, B., Cutler, D. J., Lai, Y. H., Kucuk, O., et al. (2012). Genistein Cooperates with the Histone Deacetylase Inhibitor Vorinostat to Induce Cell Death in Prostate Cancer Cells. *BMC Cancer* 12, 145. doi:10.1186/1471-2407-12-145

Pragallapati, S., and Manyam, R. (2019). Glucose Transporter 1 in Health and Disease. *J. Oral Maxillofac. Pathol.* 23 (3), 443–449. doi:10.4103/jomfp.JOMFP_22_18

Qamar, S., Fatima, S., Rehman, A., Khokhar, M. A., Mustafa, Z., and Awan, N. (2019). Glucose Transporter 1 Overexpression in Oral Squamous Cell Carcinoma. *J. Coll. Physicians Surg. Pak* 29 (8), 724–727. doi:10.29271/jcpsp.2019.08.724

Rada, M., Nallanthighal, S., Cha, J., Ryan, K., Sage, J., Eldred, C., et al. (2018). Inhibitor of Apoptosis Proteins (IAPs) Mediate Collagen Type XI Alpha 1-driven Cisplatin Resistance in Ovarian Cancer. *Oncogene* 37 (35), 4809–4820. doi:10.1038/s41388-018-0297-x

Salehi, B., Venditti, A., Sharifi-Rad, M., Kręgiel, D., Sharifi-Rad, J., Durazzo, A., et al. (2019). The Therapeutic Potential of Apigenin. *Int. J. Mol. Sci.* 20 (6), 1305. doi:10.3390/ijms20061305

Sancho, P., Barneda, D., and Heeschen, C. (2016). Hallmarks of Cancer Stem Cell Metabolism. *Br. J. Cancer* 114 (12), 1305–1312. doi:10.1038/bjc.2016.152

Sayegh, N., Swami, U., and Agarwal, N. (2021). Recent Advances in the Management of Metastatic Prostate Cancer. *JCO Oncol. Pract.* 18, 45–55. doi:10.1200/OP.21.00206

Scott, L. J. (2018). Enzalutamide: A Review in Castration-Resistant Prostate Cancer. *Drugs* 78 (18), 1913–1924. doi:10.1007/s40265-018-1029-9

Shafiee, G., Saidijam, M., Tayebinia, H., and Khodadadi, I. (2020). Beneficial Effects of Genistein in Suppression of Proliferation, Inhibition of Metastasis, and Induction of Apoptosis in PC3 Prostate Cancer Cells. *Arch. Physiol. Biochem.*. 1–9. doi:10.1080/13813455.2020.1717541

Sharda, M., Badrinarayanan, A., and Seshasayee, A. S. N. (2020). Evolutionary and Comparative Analysis of Bacterial Nonhomologous End Joining Repair. *Genome Biol. Evol.* 12 (12), 2450–2466. doi:10.1093/gbe/evaa223

Sharma, H., Kanwal, R., Bhaskaran, N., and Gupta, S. (2014). Plant Flavone Apigenin Binds to Nucleic Acid Bases and Reduces Oxidative DNA Damage in Prostate Epithelial Cells. *PLoS One* 9 (3), e91588. doi:10.1371/journal.pone.0091588

Shore, N. D. (2020). Current and Future Management of Locally Advanced and Metastatic Prostate Cancer. *Rev. Urol.* 22 (3), 110–123.

Shukla, S., Bhaskaran, N., Babcook, M. A., Fu, P., Maclennan, G. T., and Gupta, S. (2014). Apigenin Inhibits Prostate Cancer Progression in TRAMP Mice via Targeting PI3K/Akt/FoxO Pathway. *Carcinogenesis* 35 (2), 452–460. doi:10.1093/carcin/bgt316

Shukla, S., Fu, P., and Gupta, S. (2014). Apigenin Induces Apoptosis by Targeting Inhibitor of Apoptosis Proteins and Ku70-Bax Interaction in Prostate Cancer. *Apoptosis* 19 (5), 883–894. doi:10.1007/s10495-014-0971-6

Shukla, S., Kanwal, R., Shankar, E., Datt, M., Chance, M. R., Fu, P., et al. (2015). Apigenin Blocks IKKα Activation and Suppresses Prostate Cancer Progression. *Oncotarget* 6 (31), 31216–31232. doi:10.18632/oncotarget.5157

Song, Y. Y., Yuan, Y., Shi, X., and Che, Y. Y. (2020). Improved Drug Delivery and Anti-tumor Efficacy of Combinatorial Liposomal Formulation of Genistein and Plumbagin by Targeting Glut1 and Akt3 Proteins in Mice Bearing Prostate Tumor. *Colloids Surf. B Biointerfaces* 190, 110966. doi:10.1016/j.colsurfb.2020.110966

Su, T., Huang, C., Yang, C., Jiang, T., Su, J., Chen, M., et al. (2020). Apigenin Inhibits STAT3/CD36 Signaling axis and Reduces Visceral Obesity. *Pharmacol. Res.* 152, 104586. doi:10.1016/j.phrs.2019.104586

Tang, Q., Ma, J., Sun, J., Yang, L., Yang, F., Zhang, W., et al. (2018). Genistein and AG1024 Synergistically Increase the Radiosensitivity of Prostate Cancer Cells. *Oncol. Rep.* 40 (2), 579–588. doi:10.3892/or.2018.6468

Thoma, C. (2016). Prostate Cancer: Targeting Apoptosis Resistance in CRPC. *Nat. Rev. Urol.* 13 (11), 631. doi:10.1038/nrurol.2016.200

Tian, J., Guo, F., Chen, Y., Li, Y., Yu, B., and Li, Y. (2019). Nanoliposomal Formulation Encapsulating Celecoxib and Genistein Inhibiting COX-2 Pathway and Glut-1 Receptors to Prevent Prostate Cancer Cell Proliferation. *Cancer Lett.* 448, 1–10. doi:10.1016/j.canlet.2019.01.002

Tolkach, Y., Zarbl, R., Bauer, S., Ritter, M., Ellinger, J., Hauser, S., et al. (2021). DNA Promoter Methylation and ERG Regulate the Expression of CD24 in Prostate Cancer. *Am. J. Pathol.* 191 (4), 618–630. doi:10.1016/j.ajpath.2020.12.014

Travis, R. C., Allen, N. E., Appleby, P. N., Price, A., Kaaks, R., Chang-Claude, J., et al. (2012). Prediagnostic Concentrations of Plasma Genistein and Prostate Cancer Risk in 1,605 Men with Prostate Cancer and 1,697 Matched Control Participants in EPIC. *Cancer Causes Control* 23 (7), 1163–1171. doi:10.1007/s10552-012-9985-y

Uzunlulu, M., Telci Caklili, O., and Oguz, A. (2016). Association between Metabolic Syndrome and Cancer. *Ann. Nutr. Metab.* 68 (3), 173–179. doi:10.1159/000443743

Wang, G., Zhang, D., Yang, S., Wang, Y., Tang, Z., and Fu, X. (2018). Co-administration of Genistein with Doxorubicin-Loaded Polypeptide Nanoparticles Weakens the Metastasis of Malignant Prostate Cancer by Amplifying Oxidative Damage. *Biomater. Sci.* 6 (4), 827–835. doi:10.1039/c7bm01201b

Welti, J., Sharp, A., Brooks, N., Yuan, W., McNair, C., Chand, S. N., et al. (2021). Targeting the P300/CBP Axis in Lethal Prostate Cancer. *Cancer Discov.* 11 (5), 1118–1137. doi:10.1158/2159-8290.CD-20-0751

Whitaker, H., Tam, J. O., Connor, M. J., and Grey, A. (2020). Prostate Cancer Biology & Genomics. *Transl Androl. Urol.* 9 (3), 1481–1491. doi:10.21037/tau.2019.07.17

Wu, A., Cremaschi, P., Wetterskog, D., Conteduca, V., Franceschini, G. M., Kleftogiannis, D., et al. (2020). Genome-wide Plasma DNA Methylation Features of Metastatic Prostate Cancer. *J. Clin. Invest.* 130 (4), 1991–2000. doi:10.1172/JCI130887

Wu, Y., Zhang, L., Na, R., Xu, J., Xiong, Z., Zhang, N., et al. (2015). Plasma Genistein and Risk of Prostate Cancer in Chinese Population. *Int. Urol. Nephrol.* 47 (6), 965–970. doi:10.1007/s11255-015-0981-5

Xiang, C., Wu, X., Zhao, Z., Feng, X., Bai, X., Liu, X., et al. (2020). Nonhomologous End Joining and Homologous Recombination Involved in Luteolin-Induced DNA Damage in DT40 Cells. *Toxicol. Vitro* 65, 104825. doi:10.1016/j.tiv.2020.104825

Xiong, P., Wang, R., Zhang, X., DeLa Torre, E., Leon, F., Zhang, Q., et al. (2015). Design, Synthesis, and Evaluation of Genistein Analogues as Anti-cancer Agents. *Anticancer Agents Med. Chem.* 15 (9), 1197–1203. doi:10.2174/1871520615666150520142437

Xu, L., Zaky, M. Y., Yousuf, W., Ullah, A., Abdelbaset, G. R., Zhang, Y., et al. (2021). The Anticancer Potential of Apigenin via Immunoregulation. *Curr. Pharm. Des.* 27 (4), 479–489. doi:10.2174/1381612826666200713171137

Yadav, R. K., Chauhan, A. S., Zhuang, L., and Gan, B. (2018). FoxO Transcription Factors in Cancer Metabolism. *Semin. Cancer Biol.* 50, 65–76. doi:10.1016/j.semcancer.2018.01.004

Ye, Q., Liu, K., Shen, Q., Li, Q., Hao, J., Han, F., et al. (2019). Reversal of Multidrug Resistance in Cancer by Multi-Functional Flavonoids. *Front. Oncol.* 9, 487. doi:10.3389/fonc.2019.00487

Yu, T., Huang, D., Wu, H., Chen, H., Chen, S., and Cui, Q. (2021). Navigating Calcium and Reactive Oxygen Species by Natural Flavones for the Treatment of Heart Failure. *Front. Pharmacol.* 12, 718496. doi:10.3389/fphar.2021.718496

Zhang, L., Li, L., Jiao, M., Wu, D., Wu, K., Li, X., et al. (2012). Genistein Inhibits the Stemness Properties of Prostate Cancer Cells through Targeting Hedgehog-Gli1 Pathway. *Cancer Lett.* 323 (1), 48–57. doi:10.1016/j.canlet.2012.03.037

Zhang, S., Wang, Y., Chen, Z., Kim, S., Iqbal, S., Chi, A., et al. (2013). Genistein Enhances the Efficacy of Cabazitaxel Chemotherapy in Metastatic Castration-Resistant Prostate Cancer Cells. *Prostate* 73 (15), 1681–1689. doi:10.1002/pros.22705

Zhao, S. G., Chen, W. S., Li, H., Foye, A., Zhang, M., Sjöström, M., et al. (2020). The DNA Methylation Landscape of Advanced Prostate Cancer. *Nat. Genet.* 52 (8), 778–789. doi:10.1038/s41588-020-0648-8

Zhu, Y., Wu, J., Li, S., Wang, X., Liang, Z., Xu, X., et al. (2015). Apigenin Inhibits Migration and Invasion via Modulation of Epithelial Mesenchymal Transition in Prostate Cancer. *Mol. Med. Rep.* 11 (2), 1004–1008. doi:10.3892/mmr.2014.2801

**Conflict of Interest:** The authors declare that the research was conducted in the absence of any commercial or financial relationships that could be construed as a potential conflict of interest.

**Publisher's Note:** All claims expressed in this article are solely those of the authors and do not necessarily represent those of their affiliated organizations, or those of the publisher, the editors, and the reviewers. Any product that may be evaluated in this article, or claim that may be made by its manufacturer, is not guaranteed or endorsed by the publisher.

frontiers in Chemistry

ORIGINAL RESEARCH
published: 25 March 2022
doi: 10.3389/fchem.2022.837987

# Combining EGFR-TKI With SAHA Overcomes EGFR-TKI-Acquired Resistance by Reducing the Protective Autophagy in Non-Small Cell Lung Cancer

*Peijun Cao[1†], Yongwen Li[2†], Ruifeng Shi[1†], Yin Yuan[1], Hao Gong[1], Guangsheng Zhu[1], Zihe Zhang[1], Chen Chen[2], Hongbing Zhang[1], Minghui Liu[1], Zhenhua Pan[2], Hongyu Liu[2]* and Jun Chen[1,2]**

[1]Department of Lung Cancer Surgery, Tianjin Medical University General Hospital, Tianjin, China, [2]Tianjin Key Laboratory of Lung Cancer Metastasis and Tumor Microenvironment, Tianjin Lung Cancer Institute, Tianjin Medical University General Hospital, Tianjin, China

OPEN ACCESS

**Edited by:**
Cong Wang,
Zhengzhou University, China

**Reviewed by:**
Sun-Young Han,
Gyeongsang National University, South Korea
Naoyuki Nishiya,
Iwate Medical University, Japan

***Correspondence:**
Jun Chen
huntercj2004@qq.com
Hongyu Liu
liuhongyu123@hotmail.com

[†]These authors have contributed equally to this work

**Specialty section:**
This article was submitted to Medicinal and Pharmaceutical Chemistry, a section of the journal Frontiers in Chemistry

**Received:** 17 December 2021
**Accepted:** 31 January 2022
**Published:** 25 March 2022

**Citation:**
Cao P, Li Y, Shi R, Yuan Y, Gong H, Zhu G, Zhang Z, Chen C, Zhang H, Liu M, Pan Z, Liu H and Chen J (2022) Combining EGFR-TKI With SAHA Overcomes EGFR-TKI-Acquired Resistance by Reducing the Protective Autophagy in Non-Small Cell Lung Cancer. Front. Chem. 10:837987. doi: 10.3389/fchem.2022.837987

Nowadays, lung cancer has the highest mortality worldwide. The emergence of epidermal growth factor receptor (EGFR) tyrosine kinase inhibitors (TKIs) has greatly improved the survival of patients with non-small cell lung cancer (NSCLC) having EGFR-TKI-sensitive mutations. Unfortunately, acquired resistance happens for most patients. In the present research, we found that EGFR-TKIs (such as gefitinib and osimertinib) can induce autophagy in NSCLC cell lines. Compared with parental sensitive cells, drug-resistant cells have higher autophagy activity. The use of an autophagy inhibitor could enhance the toxicity of gefitinib and osimertinib, which indicates that the enhancement of protective autophagy might be one of the mechanisms of EGFR-TKI resistance in NSCLC. In addition, increased autophagy activity is associated with decreased enhancer of zeste homolog 2 (EZH2) expression. Knockdown of EZH2 or EZH2 inhibitor treatment could lead to increased autophagy in NSCLC cells, indicating that EZH2 is a negative regulator of autophagy. We revealed that the increase in autophagy caused by the reduction of EZH2 was reversed *in vitro* and *in vivo* when combining gefitinib or osimertinib with suberoylanilide hydroxamic acid (SAHA), a broad-spectrum histone deacetylase inhibitor (HDACi). In conclusion, our results indicated that the combination of EGFR-TKIs and SAHA may be a new strategy to overcome EGFR-TKIs acquired resistance.

**Keywords: EGFR-TKI, SAHA, autophagy, EZH2, EGFR-TKI acquired resistance**

## INTRODUCTION

Lung cancer as the leading cause of cancer-related death worldwide (Sung et al., 2021), and the most common type is non-small cell lung cancer (NSCLC) (Thai et al., 2021). The five-year survival rate for lung cancer patients is only approximately 15% due to the limited effectiveness of current conventional treatments, including surgery, radiotherapy, and chemotherapy, for patients with advanced lung cancer (Zhou et al., 2011; Miller and Hanna, 2021). In recent years, lung cancer treatment has entered the era of precise individualized treatment owing to the popularization of next-generation sequencing technology and the discovery of various oncogenic driver mutations (Zhou

et al., 2011; Miller and Hanna, 2021). Among them, epidermal growth factor receptor (EGFR) tyrosine kinase inhibitors (TKIs) have become the first-line therapy for patients with advanced NSCLC harboring EGFR-TKI-sensitive mutations, considering their higher response rate and lower toxicity compared with conventional chemotherapy (Maemondo et al., 2010; Lee et al., 2017; Ramalingam et al., 2020). Unfortunately, despite the development of third-generation EGFR-TKIs, acquired drug resistance remains a difficult dilemma for EGFR-TKIs treatment (Remon et al., 2018). Studies have shown that there are various resistance mechanisms to different EGFR-TKIs, and approximately 20% of the resistance mechanisms are still not elucidated (Westover et al., 2018). Therefore, it is important to explore the possible resistance mechanisms to EGFR-TKIs and identify therapeutic options to reverse the acquired drug resistance.

Autophagy is a physiological mechanism that is commonly found in cells in normal and pathological states (Miller and Thorburn, 2021). In particular, under the conditions of intracellular and/or extracellular stress, such as hypoxia, nutrient deprivation, and pathogen infection, cells maintain cellular metabolic homeostasis by acquiring recyclable macromolecules such as nucleic acids and amino acids *via* autophagy; on the other hand, they can selectively remove certain cellular components, particularly damaged organelles, to maintain the stability of the intracellular environment. Therefore, autophagy may be considered as a potential mechanism to counteract cell killing (White et al., 2021). Autophagy has been described as a "double-edged sword" in the treatment of NSCLC with EGFR-TKIs. Wang et al. found that reduced autophagy was associated with resistance to erlotinib treatment (Wang et al., 2016a). Moreover, Li et al. showed that inhibition of osimertinib-induced autophagy enhanced the antitumor activity of osimertinib in lung adenocarcinoma (Li et al., 2019).

Enhancer of zeste homolog 2 (EZH2) belongs to the Polycomb group (PcG) family and plays an important role in epigenetic regulation as the main catalytically active subunit of Polycomb repressive complex 2 (PRC2) (Kim and Roberts, 2016). It has been shown that EZH2 exerts an essential role in the regulation of autophagy in tumor cells (Liu et al., 2020). Despite serving as a core member of the PRC2 complex, EZH2 expression is also regulated by protein translation modifications, and acetylation is one of the important modifications of EZH2 (Wan et al., 2015). A common finding in cancer cells is the high expression level of histone deacetylase (HDAC) isozymes and the corresponding hypoacetylation of histones, whereby HDAC is emerging as a prominent therapeutic target for cancer treatment (Libý et al., 2006; Nakagawa et al., 2007; Jenke et al., 2021). Suberoylanilide hydroxamic acid (SAHA), a broad-spectrum histone deacetylase inhibitor (HDACi), has also been shown to promote apoptosis induced by afatinib or third-generation TKI, including WZ4002 (Lee et al., 2015). However, the relationship between EZH2 acetylation modifications and autophagy is currently unknown.

In this study, we used gefitinib and osimertinib in combination with SAHA, respectively, and validated the inhibitory effect of this combination on tumor growth *in vitro* and *in vivo*. Moreover, SAHA was found to reduce gefitinib- and osimertinib-induced protective autophagy, and overcame acquired resistance to EGFR-TKIs.

## Cells Culture

NSCLC cell lines PC-9 and H1975 were obtained from the American Type Culture Collection. The PC-9/AB2 cell line was provided by Prof. Cai-Cun Zhou from Shanghai Pulmonary Hospital and the H1975OR cell line was provided by Prof. Jin-Jian Lu from the University of Macau (Ju et al., 2010; Tang et al., 2016). PC-9/AB2 and H1975OR were exposed to 1 μM gefitinib and 1 μM osimertinib, respectively, for a long period of time to maintain resistance. All cells were cultured in RPMI 1640 medium mixed with 10% fetal bovine serum, and were placed in a humid environment containing 5% $CO_2$ at 37°C.

## Reagents and Antibodies

Gefitinib (ZD1839), osimertinib (AZD9291), SAHA, DZNep, and HCQ were purchased from Selleck Chemicals LCC. Antibodies against LC3A, p62, EZH2, mTOR, p-mTOR, TSC2, PCAF, and GAPDH were obtained from Cell Signaling Technology.

## Transfection and Drug Treatment

When the cells are in the logarithmic growth phase and cell fusion has reached approximately 80%, drug treatment and gene transfection can be performed. After discarding the old medium, DMSO (NC group) or drugs mixed with the medium were used to incubate the cells at working concentrations. Cells were transfected with siEZH2 (Ribobio, Guangzhou, China) and siNC using Invitrogen Lipofactamine 3000 according to the instructions. Treated cells were collected to obtain protein and RNA for further experiments 48 h later.

## Cell Counting Kit-8 Assay

Cell Counting Kit-8 (CCK-8) assay was performed as described in our previous publications (Gong et al., 2020). Briefly, $1 \times 10^4$ cells were seeded in 96-well plates and incubated for 24 h. Cells were then treated with different concentrations of the drug for 48 h. Next, the CCK-8 reagent and medium were added to each well at a ratio of 1:10, followed by incubation at 37°C for 1 h. After incubation, absorbance was measured at 450 nm using a microplate reader (SpectraMax M5, Molecular Devices, Sunnyvale, CA, United States). The experiment was repeated at least three times.

## Colony Formation Assay

Approximately 500 cells in the logarithmic growth phase were inoculated in each well of a 6-well plate and incubated at 37°C for 24 h. The cells were then treated with the working concentrations of the drugs. After roughly 14 days, the colonies were fixed with methanol and stained with 0.5% crystal violet for 30 min at room temperature. The number of colonies (defined as >50 cells) was counted and photographed.

## Flow Cytometry Analysis of Apoptosis

Apoptotic cells were detected using membrane-linked protein V-FITC and PI staining according to BD's Apoptosis Detection

Kit instructions. The drug-treated cells for the assay were washed, collected, and transferred to flow cytometry tubes after warming with 500 ml of binding buffer. Then, 5 μl of Annexin V-FITC and 5 μl of PI were added, followed by incubation for 15 min at room temperature in dark condition. The stained cells were analyzed by NovoCyte flow cytometry (Agilent, United States).

## Western Blotting

The experiments were performed according to the method described in our published article (Zhang et al., 2021). A summary of the procedure is described as follows: After extraction of the cellular proteins, the protein concentration was measured by BCA assay (Thermo Fisher Scientific, Inc., Waltham, MA, United States), ensuring that the total amount of protein in each group of samples was 30 μg. After 2 h at a constant current of 250 mA (time can be adjusted appropriately according to the molecular weight of the target protein) the proteins in the gel were transferred to a PVDF membrane (Millipore, Billerica, MA, United States). The membranes were then blocked with 5% skim milk at room temperature for 2 h. The primary antibody and membranes were incubated overnight at 4°C. Subsequently, the membranes and secondary antibody (1: 5000 dilution; Thermo Fisher Scientific, Inc.) were incubated for 1 h at room temperature. The bands were visualized using the Pierce ECL substrate (Thermo Fisher Scientific, Inc.).

## Coimmunoprecipitation

To determine the cell concentration of each sample, trypsin-digested cells were precipitated, washed with PBS, resuspended, and counted using a cell counter (Bio-Rad TC20, CA, United States). Different volumes of RIPA lysis buffer were added to ensure the same total cell count for each sample according to the cell concentration of each sample. The samples were then incubated with rabbit anti-acetylated-lysine antibody (Cell Signaling Technology, Inc., MA, United States) or normal rabbit IgG antibody (Beyotime, Shanghai, China) at 4°C 24 h. The next day, protein A/G agarose beads (Beyotime, Shanghai, China) were added to the samples and slowly mixed for 3 h at 4°C in a refrigerator, then samples were centrifuged to remove the supernatant and the beads were washed five times with lysis buffer. After centrifugation, the precipitate was dissolved in SDS loading buffer and boiled at 100°C for 10 min. Protein blotting was performed with rabbit anti-EZH2 antibody.

## Autophagic Flux Measurement

Cells were cultured on slides, transfected with GFP-RFP-LC3 adenovirus (HanBio, Shanghai, China), and then treated with different small molecule compounds for 48 h. The cells were fixed in 4% paraformaldehyde after washing with PBS buffer. The slides were then blocked with DAPI-containing anti-quenching agent, and the localization of LC3 spots was observed by confocal fluorescence microscopy. The cell nuclei were stained with DAPI. Fluorescence images were captured using a confocal microscope (ZEISS, Germany) to detect autophagosomes (yellow dots in fusion images) and autolysosomes (red dots in fusion images).

## RNA Extraction and Quantitative PCR Assays

Total cellular RNA was extracted by Trizol (Invitrogen, CA, United States), quantified by a UV spectrophotometer (Beckman Coulter, CA, United States), and 1 μg of total RNA was reverse-transcribed by a PrimeScript RT kit (TaKaRa, Dalian, China). The obtained cDNA was mixed with ABI (ABI, CA, United States) SYBR Green Master Mix and the corresponding gene primers and subsequently amplified on an ABI 7900 real-time quantitative PCR instrument. The expression level of EZH2 was normalized to the expression level of the glyceraldehyde-3-phosphate dehydrogenase (GAPDH) –ΔΔCT method. All gene primers were obtained from BGI (Guangdong, China).

## Immunohistochemistry

Mouse xenograft tumor tissue was fixed overnight with 4% formalin, dehydrated using ethanol, and embedded in paraffin. Next, the paraffin blocks were cut into 5-μm-thick slices. The prepared tissue slices were first deparaffinized in xylene and then rehydrated with a gradient alcohol solution. After blocking with normal goat serum for 10 min, the sections were incubated with EZH2-specific antibody (1:50 dilution) and LC3A-specific antibody (1:1000 dilution) for 1 h at room temperature, washed with PBS, and incubated with secondary antibody (ZSJQ, Beijing, China) for 60 min. Finally, the cells were incubated with 3,3′-diaminobenzidine for 3 min at room temperature and counterstained with hematoxylin.

## *In vivo* Study

The source of nude mice and the feeding environment were consistent with those described in our previous publication (Gong et al., 2020). PC-9/AB2 cells ($2 \times 10^6$) were injected subcutaneously into the left groin of nude mice. When the tumor volume reached approximately 200 $mm^3$, mice were randomly divided into four groups (five mice/group). Drugs were prepared with sodium carboxymethylcellulose (CMC-Na). Tumor size was measured every other day in the NC group (CMC-Na), Gef group (50 mg/kg/day), SAHA group (50 mg/kg/day), and Gef + SAHA group (50 mg/kg/day of gefitinib plus 50 mg/kg/day of SAHA). Tumor volume (V) was calculated by the following formula: volume ($mm^3$) = [length × width$^2$ (Thai et al., 2021)] × 0.5. After 4 weeks, tumors were isolated from mice and stored in paraformaldehyde at 4°C. The experiments on the animals were approved by the ethics committee of Tianjin Medical University General Hospital.

## Statistical Analysis

Statistical analysis was performed by GraphPad Prism8 (GraphPad Software Inc., CA, United States). Differences between groups were analyzed by one-way ANOVA followed by Dunnett's *t*-test for individual comparisons. When the comparison involved only two groups, the Student's *t*-test was used. Tumor sizes in the nude mice and results of the CCK-8 assay were analyzed for differences using two-way ANOVA. $p < 0.05$ was determined to represent a significant difference.

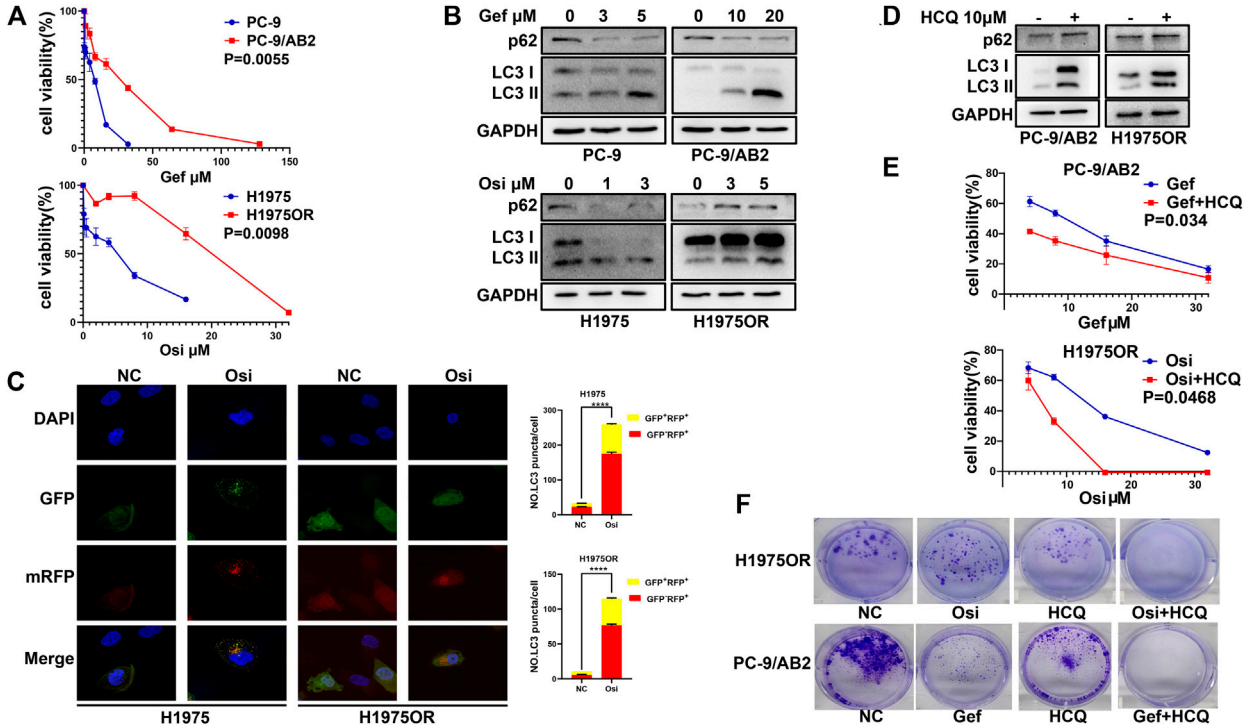


**FIGURE 1 |** EGFR-TKIs induced protective autophagy in NSCLC cells. **(A)** The CCK-8 method was used to detect parental PC-9 and H1975 cells and their corresponding drug-resistant cells, and the concentration of gefitinib or osimertinib was increased and treated for 48 h. Three replicates were used for the experiments, and data are presented as mean ± SEM. **(B)** EGFR-TKIs treatment decreased p62 protein levels and increased LC3-II accumulation in PC-9/H1975 and corresponding drug-resistant cells. **(C)** Fluorescence assay showing representative images of cells transfected with GFP-RFP-LC3 double-labeled adenovirus. Autophagic flux was significantly increased in H1975 and H1975OR after 1 μM osimertinib treatment for 48 h. Quantitative analysis of the number of yellow autophagosomes and red autolysosomes. $^{****}p < 0.0001$. **(D)** 10 μM HCQ can inhibit the autophagy level of drug-resistant cells. **(E)** CCK-8 assay suggested that the inhibitory effect on drug-resistant cells was significantly enhanced after EGFR-TKIs combined with 10 μM HCQ compared with single EGFR-TKI treatment. Three replicates were used for the experiments, and the data are presented as mean ± SEM. **(F)** The colony formation assay suggested that the number of colonies in the two-drug combination group was significantly lower than that in the single-drug group. NC: DMSO, Gef: 1 μM gefitinib, Osi: 1 μM osimertinib, HCQ: 10 μM HCQ, Gef + HCQ: 1 μM gefitinib + 10 μM HCQ, Osi + HCQ: 1 μM osimertinib + 10 μM HCQ.

# RESULTS

## EGFR-TKIs Induced Protective Autophagy in NSCLC Cells

Firstly, the IC50 of the gefitinib-sensitive cell line PC-9 with its corresponding drug-resistant cell line PC-9/AB2, and the osimertinib-sensitive cell line H1975 with its corresponding drug-resistant cell line H1975OR were investigated by CCK-8 assay (**Figure 1A**). To explore the effects of EGFR-TKIs on autophagy in NSCLC cells, the expression of p62 and LC3 were observed by western blotting (**Figure 1B**) or based on $GFP^+RFP^+$ and $GFP^-RFP^+$ puncta in cells using confocal microscopy (**Figure 1C**). The results displayed that both sensitive and drug-resistant cells treated with EGFR-TKIs showed increased LC3-II accumulation and decreased p62 expression. A significant increase of $GFP^+RFP^+$ yellow puncta representing the autophagosome and $GFP^-RFP^+$ red puncta representing the autolysosome could be seen in the cytoplasm under confocal microscopy (Yu et al., 2017). Which suggests that autophagy is prevalent in NSCLC cells treated with EGFR-TKIs. The completion of autophagy ultimately relies on the autolysosome to perform degradation functions. Hydroxychloroquine (HCQ) can inhibit autophagy by elevating the pH of the lysosome, inhibiting the function of the lysosome, and preventing the degradation of LC3-II (Wang et al., 2016b). After treating drug-resistant cells with 10 μM HCQ, we found that HCQ inhibited the degradation of p62 and increased the accumulation of LC3-II (**Figure 1D**). When combining treatment of EGFR-TKIs and HCQ in drug-resistant cells, both the CCK-8 and colony formation assays showed that HCQ enhanced the antitumor activity of EGFR-TKIs in drug-resistant cells (**Figures 1E,F**). These results suggested that the autophagy induced by EGFR-TKIs was protective in NSCLC cells.

## EZH2 is a Negative Regulator of Autophagy

When treated with different concentration gradients of EGFR-TKIs, expression of EZH2 was found to be declining in NSCLC cells (**Figure 2A**). The expression of EZH2 was lower in drug-resistant cells compared to sensitive cells, and the decreasing of p62 expression and the increasing of LC3-II accumulation in drug-resistant cells implied a higher degree of autophagy

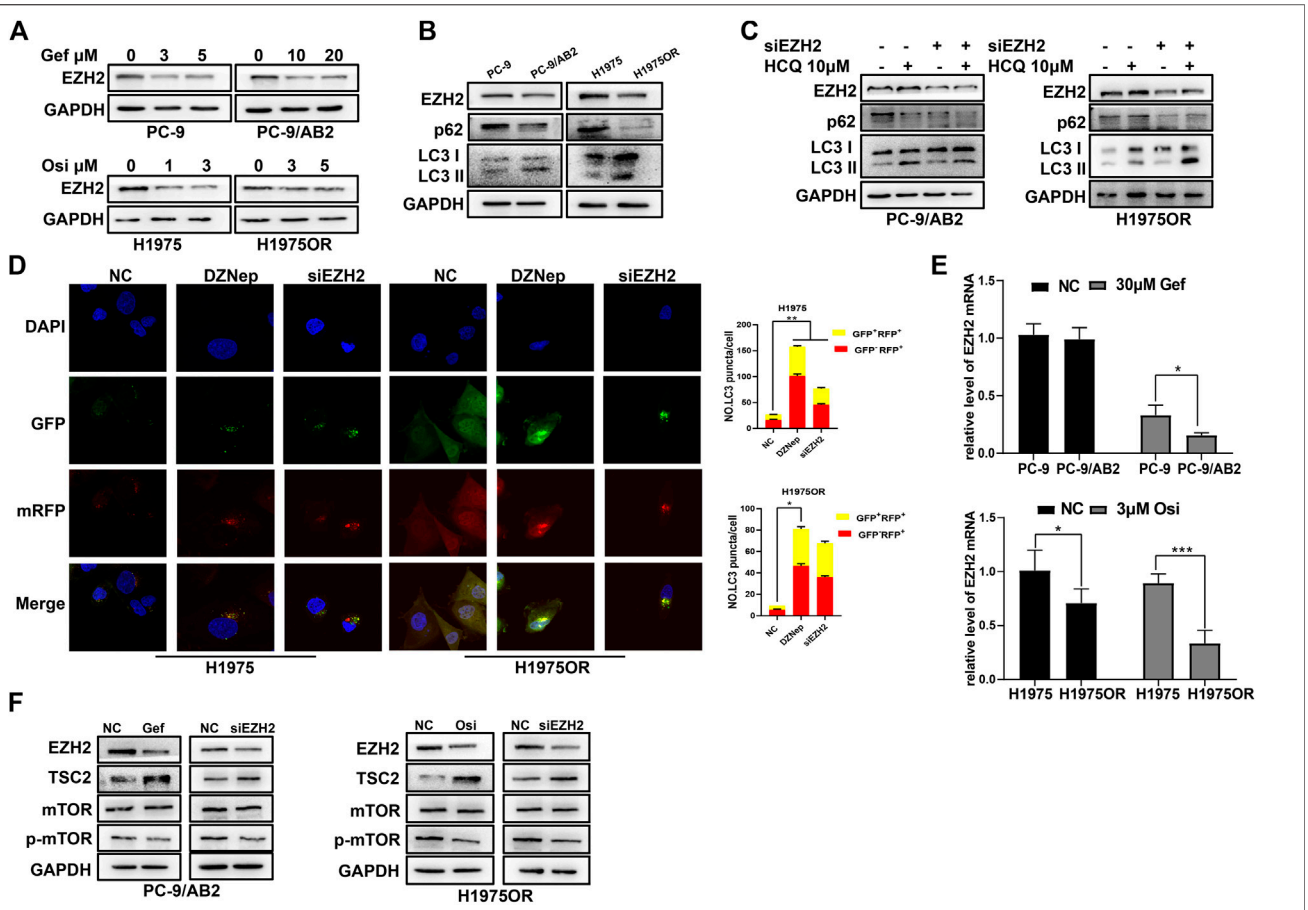


**FIGURE 2 |** EZH2 is a negative regulator of autophagy. **(A)** EGFR-TKIs can cause decreased expression of EZH2 protein in PC-9/H1975 and corresponding drug-resistant cells. **(B)** Western blotting revealed lower levels of EZH2 protein and higher autophagic activation in drug-resistant cells. **(C)** Western blotting showed enhanced autophagic activity of drug-resistant cells following transfection with siEZH2. **(D)** Fluorescence assay showing representative images of cells transfected with GFP-RFP-LC3 double-labeled adenovirus. Autophagic flux was increased after knockdown of EZH2 in H1975 and H1975OR. Quantitative analysis of the number of yellow autophagosomes and red autolysosomes. $^{*}p < 0.05$, $^{**}p < 0.01$. **(E)** RT-qPCR assays revealed lower levels of EZH2 mRNA in drug-resistant cells. **(F)** Western blotting showed that downregulation of EZH2 induced by EGFR-TKIs affects the mTOR signaling pathway and its suppressor TSC2.

(**Figures 2B,E**). To explore the relationship between EZH2 and autophagy, EZH2 inhibitor DZNep and siRNA were employed to knock down EZH2 expression. Only the decreasing of p62 was observed when treated with DZNep or siRNA alone in drug-resistant cells (**Supplementary Figures S1A,B**). Considering that cellular autophagy is a dynamic process, the degradation of LC3-II also increases when the degree of autophagy is enhanced. When DZNep/siEZH2 and HCQ were combined in drug-resistant cells, the degradation of LC3-II was found to be repressed, and p62 expression was decreased (**Figure 2C**, **Supplementary Figure S1C**). Similarly based on the findings of confocal microscopy, an increase in autophagosomes and autolysosomes was observed in the cells in which EZH2 expression was inhibited (**Figure 2D**). These results suggest that drug-resistant cell autophagy is significantly increased after EZH2 inhibition, and that EZH2 is a negative regulator of cellular autophagy activation.

It was recently shown that EGFR activation induces the activation of the mammalian target of rapamycin complex 1 (mTORC1) pathway, which in turn inhibits the formation of autophagosomes (Wei et al., 2015; Kwon et al., 2019). In our study, the mTOR signaling pathway was downregulated when treated with EGFR-TKIs or transfected with siEZH2 in drug-resistant cells, which was accompanied by an increase of TSC2, an mTOR signaling pathway inhibitor (**Figure 2F**). It indicates that downregulation of EZH2 plays a large role in autophagy induced by EGFR-TKIs in NSCLC cells.

## SAHA Reversed the Effects of Increased Autophagy and Decreased EZH2 Expression Induced by EGFR-TKIs

Existing studies have shown the presence of EZH2 acetylation modifications in NSCLC cells (Wan et al., 2015), but acetylated EZH2 is difficult to detect *via* western blotting after

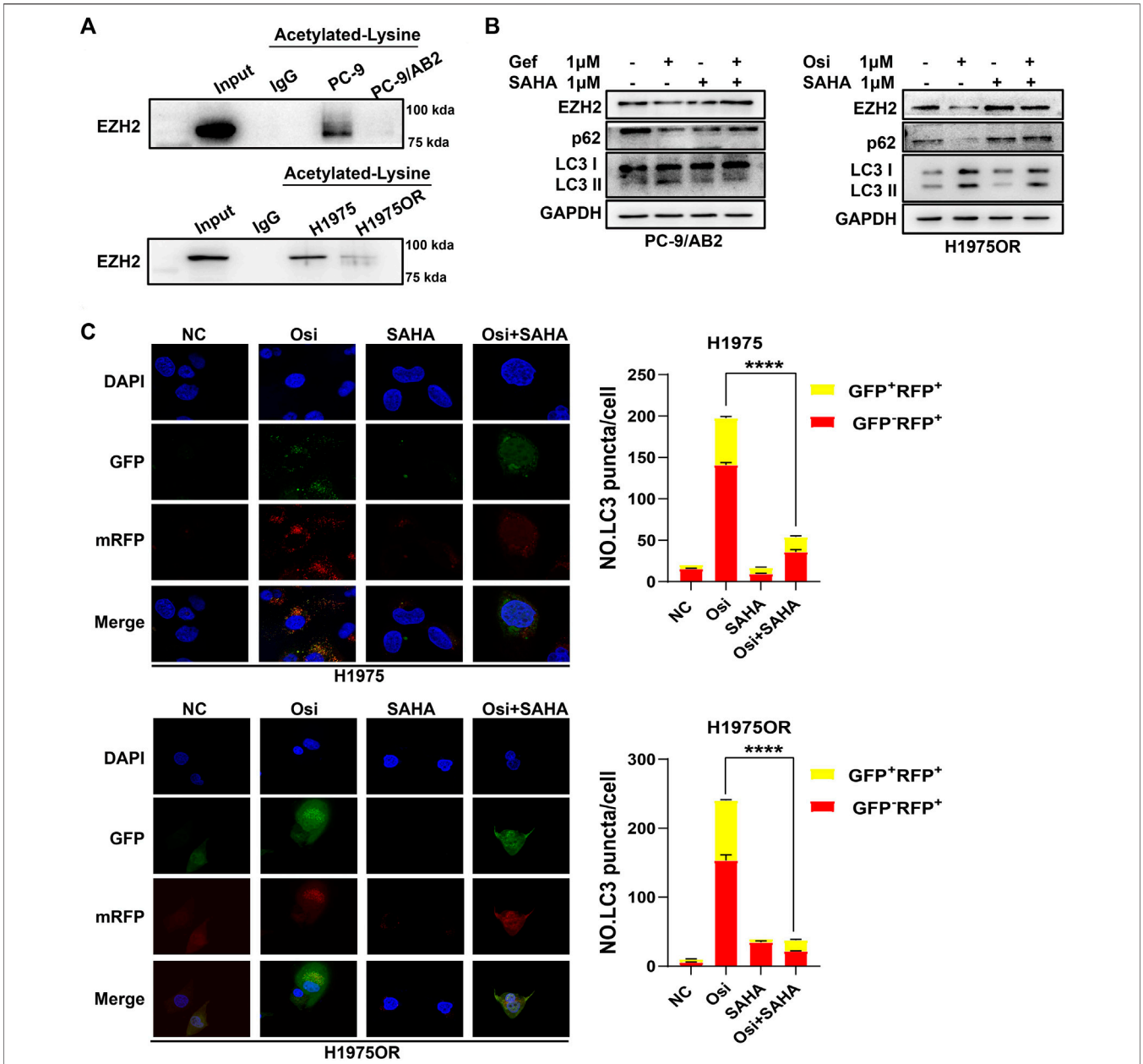


**FIGURE 3 |** SAHA reversed the effects of increased autophagy and decreased EZH2 expression induced by EGFR-TKIs. **(A)** The acetylation level of drug-resistant cells was lower than the corresponding sensitive cells. After treatment of cells with 1 μM SAHA for 48 h, cell lysates were immunoprecipitated with rabbit anti-acetylated-lysine antibody or normal rabbit IgG antibody, followed by anti-EZH2 antibody for immunoblotting. **(B)** Western blotting showed that SAHA reversed the effects of EGFR-TKIs on EZH2 protein expression and autophagy in drug-resistant cells. **(C)** Fluorescence assay showing representative images of cells transfected with GFP-RFP-LC3 double-labeled adenovirus. SAHA reversed the increased autophagic flux induced by EGFR-TKIs. ****$p < 0.0001$.

immunoprecipitation with rabbit anti-acetylated-lysine antibody, if cells are not treated with any deacetylase inhibitors. We treated the cells with SAHA a broad-spectrum deacetylase inhibitor and then detected the acetylated modification of EZH2 in the cells by co-immunoprecipitation. The results of the coimmunoprecipitation assay showed that the level of EZH2 acetylation was lower in drug-resistant cells compared to parental cells (**Figure 3A**). To further explore the effect of SAHA on EZH2 expression and autophagy, we treated the drug-resistant cells with EGFR-TKI in the presence and absence of SAHA. It showed that no changes of EZH2 and autophagy were found in drug-resistant cells when treated with SAHA alone (**Supplementary Figure S1D**). The downregulation of EZH2 and increased autophagy activation was found to be induced by EGFR-TKIs, while SAHA reversed these effects when combined with EGFR-

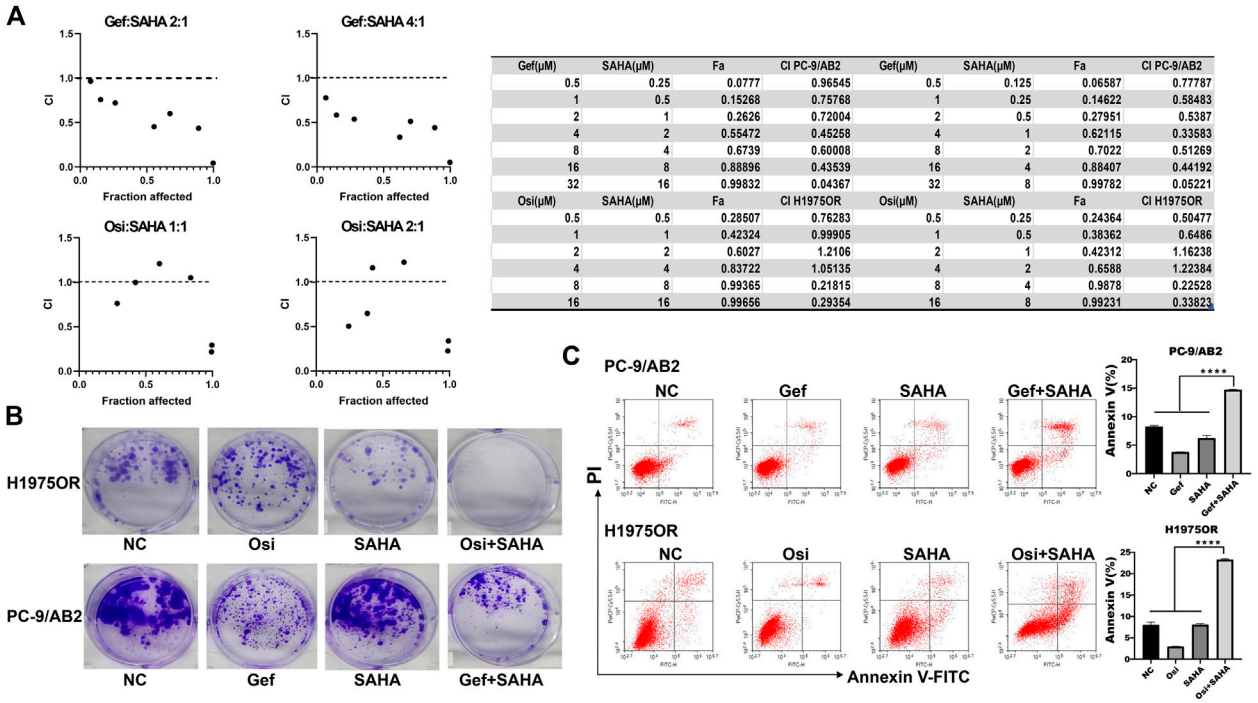


| Gef(μM) | SAHA(μM) | Fa | CI PC-9/AB2 | Gef(μM) | SAHA(μM) | Fa | CI PC-9/AB2 |
|---|---|---|---|---|---|---|---|
| 0.5 | 0.25 | 0.0777 | 0.96545 | 0.5 | 0.125 | 0.06587 | 0.77787 |
| 1 | 0.5 | 0.15268 | 0.75768 | 1 | 0.25 | 0.14622 | 0.58483 |
| 2 | 1 | 0.2626 | 0.72004 | 2 | 0.5 | 0.27951 | 0.5387 |
| 4 | 2 | 0.55472 | 0.45258 | 4 | 1 | 0.62115 | 0.33583 |
| 8 | 4 | 0.6739 | 0.60008 | 8 | 2 | 0.7022 | 0.51269 |
| 16 | 8 | 0.88896 | 0.43539 | 16 | 4 | 0.88407 | 0.44192 |
| 32 | 16 | 0.99832 | 0.04367 | 32 | 8 | 0.99782 | 0.05221 |
| Osi(μM) | SAHA(μM) | Fa | CI H1975OR | Osi(μM) | SAHA(μM) | Fa | CI H1975OR |
| 0.5 | 0.5 | 0.28507 | 0.76283 | 0.5 | 0.25 | 0.24364 | 0.50477 |
| 1 | 1 | 0.42324 | 0.99905 | 1 | 0.5 | 0.38362 | 0.6486 |
| 2 | 2 | 0.6027 | 1.2106 | 2 | 1 | 0.42312 | 1.16238 |
| 4 | 4 | 0.83722 | 1.05135 | 4 | 2 | 0.6588 | 1.22384 |
| 8 | 8 | 0.99365 | 0.21815 | 8 | 4 | 0.9878 | 0.22528 |
| 16 | 16 | 0.99656 | 0.29354 | 16 | 8 | 0.99231 | 0.33823 |

**FIGURE 4 |** SAHA enhanced the antitumor effect of EGFR-TKIs *in vitro*. **(A)** PC-9/AB2 and H1975OR cells were incubated with different concentrations of gefitinib or osimertinib combined with SAHA for 48 h. Cell viability was determined using the CCK-8 method. The combination effect of the two drugs was then evaluated according to the combination index (CI). **(B–C)** NC: DMSO, Gef: 1 μM gefitinib, Osi: 1 μM osimertinib, SAHA: 1 μM SAHA, Gef + SAHA: 1 μM gefitinib + 1 μM SAHA, Osi + SAHA: 1 μM osimertinib + 1 μM SAHA. The colony formation assay suggested that the number of colonies in the two-drug combination group was significantly lower than that in the single-drug group. Detection of apoptosis by flow cytometry revealed that the proportion of apoptotic cells in the two-drug combination group was much higher than that in the single-drug and NC groups. The bar graph shows the percentage of apoptotic cells in different groups ($n$ = 3, ****$p$ < 0.0001).

TKIs (**Figures 3B,C**). These data confirm that SAHA can reverse the reduced EZH2 expression and increased autophagy caused by EGFR-TKIs.

## SAHA Enhanced the Antitumor Effect of EGFR-TKIs *in vitro*

In light of the anti-autophagic effects of SAHA *in vitro*, to further determine whether SAHA enhanced the antitumor effects of EGFR-TKI in drug-resistant cells of NSCLC, we investigated the effects of the combination of EGFR-TKIs and SAHA on the viability of PC-9/AB2 and H1975OR using the CCK-8 assay. For PC-9/AB2, we used a combination of gefitinib and SAHA at fixed concentration ratios of 2:1 and 4:1, and for H1975OR, we used a combination of osimertinib and SAHA at fixed concentration ratios of 2:1 and 1:1. The combination index was calculated by the CompuSyn software (Hsu et al., 2020). A combination index (CI) less than 1 means that the combined drugs have a synergistic effect. Generally, when considering the therapeutic effects of antitumor drugs, CI values, which correspond to high inhibition rates, are given more importance. In our study, the CIs of Gef + SAHA (2:1/4:1) and Osi + SAHA (1:1/2:1) were 0.19228/0.19353 and 0.45807/0.44211, respectively, at a 97% inhibition rate, as calculated by the mathematical model proposed by Chou-Talalay, which suggested that the co-administration of SAHA with EGFR-TKIs had a stronger antitumor effect than administration of EGFR-TKI alone (**Figure 4A**). Similar results were obtained by the colony formation assay (**Figure 4B**). In addition, the proportion of apoptotic cells was significantly increased in EGFR-TKIs-resistant cells when administered SAHA and EGFR-TKIs (**Figure 4C**). These results showed that SAHA can enhance the antitumor effects of EGFR-TKIs on drug-resistant cells *in vitro*.

## SAHA Enhanced the Antitumor Effect of EGFR-TKIs *in vivo*

To validate the antitumor effects of the co-administration of SAHA with EGFR-TKI *in vitro*, we established *in vivo* xenografts in BALB/c nude mice using PC-9/AB2 cells. When tumors were palpable, mice were intragastrically administered gefitinib (50 mg/kg), SAHA (50 mg/kg), or the combination of both drugs for 3 weeks, respectively. As shown in **Figures 5A,B**, gefitinib and SAHA monotherapy led to only a slight reduction in tumor volume, while co-administration of SAHA with EGFR-TKI resulted in

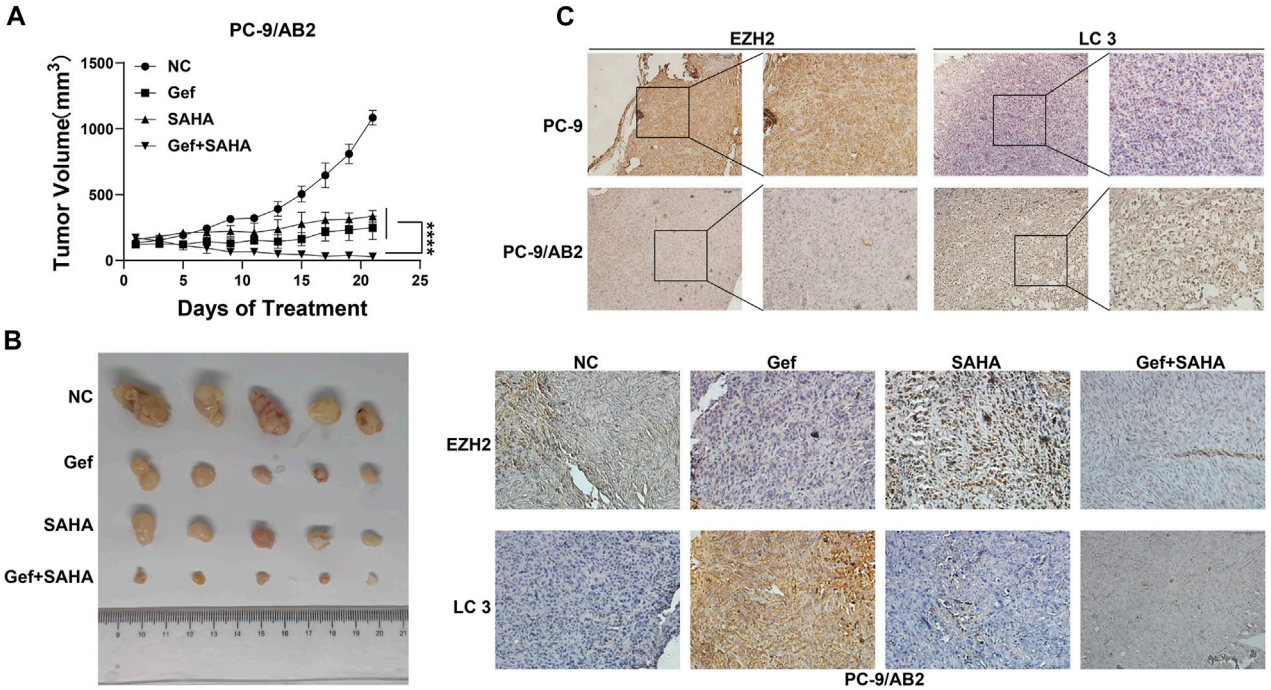


**FIGURE 5 |** SAHA enhanced the antitumor effect of EGFR-TKIs *in vivo*. **(A–B)** Nude mice with tumors of PC-9/AB2 cells received gefitinib (50 mg/kg orally), SAHA (50 mg/kg orally), and a Gef + SAHA combination after 3 weeks of treatment every other day. Results are presented as mean ± standard deviation. ****$p < 0.0001$. **(C)** Immunohistochemistry was performed to detect EZH2 and LC3 in tumor sections of nude mice.

significant tumor shrinkage (**Figures 5A,B**). To further investigate the mechanism underlying the antitumor effect, we analyzed xenograft tumor sections using immunohistochemistry to verify EZH2 and LC3 expression. Immunohistochemical analysis showed that lower EZH2 expression and higher LC3 expression were found in the resistant tumor tissues compared to parental sensitive cells, and the combined treatment of SAHA with gefitinib could reverse the decrease in EZH2 and increase in LC3 caused by gefitinib, which was consistent with the *in vitro* results (**Figure 5C**, **Supplementary Figure S2B**). To conclude, our results confirmed that SAHA enhances the antitumor effect of EGFR-TKIs in EGFR-TKI-resistant *in vivo* xenografts.

## DISCUSSION

In clinical practice, treatment targeting specific oncogenic driver mutations can inhibit tumor progression and prolong patient survival (Yang et al., 2020). Epidermal growth factor receptor (EGFR) mutations activated in non-small cell lung cancer (NSCLC) are effective targets for EGFR tyrosine kinase inhibitors (TKIs) (Zhou et al., 2011). Patients with EGFR mutation-positive lung adenocarcinoma have approximately an 80% response rate to EGFR-TKIs, achieving progression-free survival of 10–14 months (Wu and Shih, 2018). Unfortunately, the emergence of acquired resistance to EGFR-TKIs has limited the long-term use of this therapy (Wu and Shih, 2018; Terlizzi et al., 2019). Current studies have found that the most common mechanism of resistance with first- or second-generation EGFR-TKIs is the development of acquired EGFR T790M mutations, accounting for approximately 50% of cases (Tan et al., 2018). For this reason, third-generation EGFR-TKIs, represented by osimertinib, have emerged to treat patients with acquired resistance mutations in T790M. However, third-generation EGFR-TKIs still cannot prevent the development of acquired resistance due to persistent mutations in the gene (Lee, 2017; Remon et al., 2018). An increasing number of studies have shown that combining existing small molecule anticancer drugs with EGFR-TKIs can circumvent acquired drug resistance and enhance the antitumor effects of EGFR-TKIs through a bypass signaling mechanism (Rosell et al., 2021). In the present study, we found that the combination of EGFR-TKIs and SAHA is a potential treatment option to reverse the acquired resistance of EGFR-TKIs in NSCLC.

In NSCLC-targeted therapies, autophagy is referred to as a "double-edged sword" because it promotes both cell death and survival (Li et al., 2019; Wang et al., 2021). In our experiments, we found stronger activation of autophagy in drug-resistant models both *in vivo* and *in vitro*. The antitumor effects of EGFR-TKIs were significantly enhanced when we inhibited autophagy with an autophagy inhibitor. All these results suggested that protective autophagy is one of the mechanisms of acquired EGFR-TKI resistance in NSCLC.

Further, we explored the mechanism of protective autophagy occurrence in NSCLC. Fu et al. found that when EZH2 expression

was suppressed, the expression of TSC2, an mTOR signaling pathway suppressor, was upregulated, causing inhibition of the mTOR signaling pathway (Wei et al., 2015). mTOR is a major regulator of cell growth and metabolism, promoting anabolic processes and inhibiting catabolic processes, such as autophagy (Johnson and Tee, 2017). In our study, we showed that EGFR-TKIs caused significant downregulation of EZH2 and increased autophagy in NSCLC cells and tissues. siEZH2 was applied to inhibit EZH2 expression in drug-resistant cells, and we found that the changes of TSC2, p-mTOR, and autophagy were the same as those observed in drug-resistant cells treated with EGFR-TKIs alone. Altogether, we conclude that EGFR-TKIs can mediate autophagy through the EZH2/TSC2/p-mTOR signaling pathway to develop acquired drug resistance.

EZH2, with histone methyltransferase (HMTase) activity, is an important epigenetic regulator. It catalyzes the trimethylation of histone H3 lysine 27 (H3K27me3), leading to transcriptional silencing (Zhang et al., 2020). Similarly, the amino acid sequence of EZH2 protein makes it suitable for covalent modifications including phosphorylation, acetylation, O-GlcNAcylation, methylation, ubiquitination, and SUMOylation modifications (Cha et al., 2005; Riising et al., 2008; Lo et al., 2018; Li et al., 2020). In this study, we found that the acetylation level of EZH2 in drug-resistant cells was significantly lower than parental sensitive cells, suggesting that deacetylase inhibitors may be a new strategy to reverse EGFR-TKI acquired resistance in NSCLC. Studies have reported that EZH2 can be acetylated by the acetyltransferase PCAF and deacetylated by the deacetylase SIRT1, which alter the state of the PRC2 complex (Wan et al., 2015). However, no significantly change of SIRT1 was found between drug-resistant cell lines and parental sensitive cell lines when treated with EGFR-TKIs (**Supplementary Figure S1E**), which suggested that EZH2 deacetylation caused by EGFR-TKIs is an SIRT1-independent process. SAHA can inhibit a wide range of histone deacetylases and has been identified to have antitumor effects in lymphoma, breast cancer, and lung cancer (Alqosaibi et al., 2022). Interestingly, when drug-resistant cells were treated with SAHA alone, there were no significant changes in EZH2 expression. However, the decreasing of EZH2 and increasing of autophagy induced by EGFR-TKIs were reversed when treatment was combined with EGFR-TKIs and SAHA. These results suggests that SAHA has a potential role in overcoming acquired resistance of EGFR-TKIs in NSCLC. Furthermore, we confirmed that the combination of SAHA and EGFR-TKIs had a stronger antitumor effect than EGFR-TKIs alone in both *in vivo* and *in vitro* drug-resistant models. Nevertheless, the correlation of EZH2 deacetylation, EZH2 expression, and acquired resistance of EGFR-TKIs is still unclear and needs to be further explored.

In conclusion, our study suggests that combined treatment with SAHA and EGFR-TKIs is a potential treatment to overcome acquired resistance to EGFR-TKIs in NSCLC.

## DATA AVAILABILITY STATEMENT

The original contributions presented in the study are included in the article/**Supplementary Material**, further inquiries can be directed to the corresponding authors.

## ETHICS STATEMENT

The animal study was reviewed and approved by the ethics committee of Tianjin Medical University General Hospital.

## AUTHOR CONTRIBUTIONS

JC and HL designed and supervised the study. PC, YL, HL, and JC wrote the manuscript. PC, RS, YY, HG, GZ, and ZZ performed the experiments. HZ, ZP, ML, and CC assisted with the performance of some experiments. All authors analyzed the data together, discussed the manuscript and approved the final manuscript.

## FUNDING

This work was supported by the National Natural Science Foundation of China (82072595, 82172569, 81773207 and 61973232), Natural Science Foundation of Tianjin (19YFZCSY00040, and 19JCYBJC27000), Shihezi University Oasis Scholars Research Startup Project (LX202002), Project of Tianjin Lung Cancer Institute (TJLCZD2021-04, TJLCZD2021-01, TJLCMS2021-01, TJLCZJ2021-03), and Tianjin Key Medical Discipline (Specialty) Construction Project.

## SUPPLEMENTARY MATERIAL

The Supplementary Material for this article can be found online at: https://www.frontiersin.org/articles/10.3389/fchem.2022.837987/full#supplementary-material

## REFERENCES

Alqosaibi, A. I., Abdel-Ghany, S., Al-Mulhim, F., and Sabit, H. (2022). Vorinostat Enhances the Therapeutic Potential of Erlotinib via MAPK in Lung Cancer Cells. *Cancer Treat. Res. Commun.* 30, 100509. doi:10.1016/j.ctarc.2022.100509

Cha, T.-L., Zhou, B. P., Xia, W., Wu, Y., Yang, C.-C., Chen, C.-T., et al. (2005). Akt-mediated Phosphorylation of EZH2 Suppresses Methylation of Lysine 27 in Histone H3. *Science* 310 (5746), 306–310. doi:10.1126/science.1118947

Gong, H., Li, Y., Yuan, Y., Li, W., Zhang, H., Zhang, Z., et al. (2020). EZH2 Inhibitors Reverse Resistance to Gefitinib in Primary EGFR Wild-type Lung Cancer Cells. *BMC cancer* 20 (1), 1189. doi:10.1186/s12885-020-07667-7

Hsu, C.-C., Liao, B.-C., Liao, W.-Y., Markovets, A., Stetson, D., Thress, K., et al. (2020). Exon 16-Skipping HER2 as a Novel Mechanism of Osimertinib

Resistance in EGFR L858R/T790M-Positive Non-small Cell Lung Cancer. *J. Thorac. Oncol.* 15 (1), 50–61. doi:10.1016/j.jtho.2019.09.006

Jenke, R., Reßing, N., Hansen, F. K., Aigner, A., and Büch, T. (2021). Anticancer Therapy with HDAC Inhibitors: Mechanism-Based Combination Strategies and Future Perspectives. *Cancers* 13 (4), 634. doi:10.3390/cancers13040634

Johnson, C. E., and Tee, A. R. (2017). Exploiting Cancer Vulnerabilities: mTOR, Autophagy, and Homeostatic Imbalance. *Essays Biochem.* 61 (6), 699–710. doi:10.1042/ebc20170056

Ju, L. X., Zhou, C. C., Tang, L., Zhao, Y. M., Yang, X. J., Su, B., et al. (2010). Drug Resistance Mechanism of Non Small Cell Lung Cancer PC9/AB2 Cell Line with Acquired Drug Resistance to Gefitinib. *Zhonghua Jie He He Hu Xi Za Zhi* 33 (5), 354–358.

Kim, K. H., and Roberts, C. W. M. (2016). Targeting EZH2 in Cancer. *Nat. Med.* 22 (2), 128–134. doi:10.1038/nm.4036

Kwon, Y., Kim, M., Jung, H. S., Kim, Y., and Jeoung, D. (2019). Targeting Autophagy for Overcoming Resistance to Anti-EGFR Treatments. *Cancers* 11 (9), 1374. doi:10.3390/cancers11091374

Lee, C. K., Davies, L., Wu, Y.-L., Mitsudomi, T., Inoue, A., Rosell, R., et al. (2017). Gefitinib or Erlotinib vs Chemotherapy for EGFR Mutation-Positive Lung Cancer: Individual Patient Data Meta-Analysis of Overall Survival. *J. Natl. Cancer Inst.* 109 (6), djw279. doi:10.1093/jnci/djw279

Lee, D. H. (2017). Treatments for EGFR-Mutant Non-small Cell Lung Cancer (NSCLC): The Road to a success, Paved with Failures. *Pharmacol. Ther.* 174, 1–21. doi:10.1016/j.pharmthera.2017.02.001

Lee, T.-G., Jeong, E.-H., Kim, S. Y., Kim, H.-R., and Kim, C. H. (2015). The Combination of Irreversible EGFR TKIs and SAHA Induces Apoptosis and Autophagy-Mediated Cell Death to Overcome Acquired Resistance in EGFRT790M-Mutated Lung Cancer. *Int. J. Cancer* 136 (11), 2717–2729. doi:10.1002/ijc.29320

Li, L., Wang, Y., Jiao, L., Lin, C., Lu, C., Zhang, K., et al. (2019). Protective Autophagy Decreases Osimertinib Cytotoxicity through Regulation of Stem Cell-like Properties in Lung Cancer. *Cancer Lett.* 452, 191–202. doi:10.1016/j.canlet.2019.03.027

Li, Z., Li, M., Wang, D., Hou, P., Chen, X., Chu, S., et al. (2020). Post-translational Modifications of EZH2 in Cancer. *Cell Biosci* 10 (1), 143. doi:10.1186/s13578-020-00505-0

Libý, P., Kostrouchová, M., Pohludka, M., Yilma, P., Hrabal, P., Sikora, J., et al. (2006). Elevated and Deregulated Expression of HDAC3 in Human Astrocytic Glial Tumours. *Folia biologica* 52, 21–33.

Liu, Z., Yang, L., Zhong, C., and Zhou, L. (2020). Retracted : EZH2 Regulates H2B Phosphorylation and Elevates colon Cancer Cell Autophagy. *J. Cel Physiol* 235 (2), 1494–1503. doi:10.1002/jcp.29069

Lo, P.-W., Shie, J.-J., Chen, C.-H., Wu, C.-Y., Hsu, T.-L., and Wong, C.-H. (2018). O-GlcNAcylation Regulates the Stability and Enzymatic Activity of the Histone Methyltransferase EZH2. *Proc. Natl. Acad. Sci. USA* 115 (28), 7302–7307. doi:10.1073/pnas.1801850115

Maemondo, M., Inoue, A., Kobayashi, K., Sugawara, S., Oizumi, S., Isobe, H., et al. (2010). Gefitinib or Chemotherapy for Non-small-cell Lung Cancer with Mutated EGFR. *N. Engl. J. Med.* 362 (25), 2380–2388. doi:10.1056/NEJMoa0909530

Miller, D. R., and Thorburn, A. (2021). Autophagy and Organelle Homeostasis in Cancer. *Dev. Cel.* 56 (7), 906–918. doi:10.1016/j.devcel.2021.02.010

Miller, M., and Hanna, N. (2021). Advances in Systemic Therapy for Non-small Cell Lung Cancer. *Bmj* 375, n2363. doi:10.1136/bmj.n2363

Nakagawa, M., Oda, Y., Eguchi, T., Aishima, S.-I., Yao, T., Hosoi, F., et al. (2007). Expression Profile of Class I Histone Deacetylases in Human Cancer Tissues. *Oncol. Rep.* 18 (4), 769–774. doi:10.3892/or.18.4.769

Ramalingam, S. S., Vansteenkiste, J., Planchard, D., Cho, B. C., Gray, J. E., Ohe, Y., et al. (2020). Overall Survival with Osimertinib in Untreated, EGFR-Mutated Advanced NSCLC. *N. Engl. J. Med.* 382 (1), 41–50. doi:10.1056/NEJMoa1913662

Remon, J., Steuer, C. E., Ramalingam, S. S., and Felip, E. (2018). Osimertinib and Other Third-Generation EGFR TKI in EGFR-Mutant NSCLC Patients. *Ann. Oncol.* 29, i20–i27. doi:10.1093/annonc/mdx704

Riising, E. M., Boggio, R., Chiocca, S., Helin, K., and Pasini, D. (2008). The Polycomb Repressive Complex 2 Is a Potential Target of SUMO Modifications. *PloS one* 3 (7), e2704. doi:10.1371/journal.pone.0002704

Rosell, R., Cardona, A. F., Arrieta, O., Aguilar, A., Ito, M., Pedraz, C., et al. (2021). Coregulation of Pathways in Lung Cancer Patients with EGFR Mutation: Therapeutic Opportunities. *Br. J. Cancer* 125, 1602–1611. doi:10.1038/s41416-021-01519-2

Sung, H., Ferlay, J., Siegel, R. L., Laversanne, M., Soerjomataram, I., Jemal, A., et al. (2021). Global Cancer Statistics 2020: GLOBOCAN Estimates of Incidence and Mortality Worldwide for 36 Cancers in 185 Countries. *CA A. Cancer J. Clin.* 71 (3), 209–249. doi:10.3322/caac.21660

Tan, C.-S., Kumarakulasinghe, N. B., Huang, Y.-Q., Ang, Y. L. E., Choo, J. R.-E., Goh, B.-C., et al. (2018). Third Generation EGFR TKIs: Current Data and Future Directions. *Mol. Cancer* 17 (1), 29. doi:10.1186/s12943-018-0778-0

Tang, Z.-H., Jiang, X.-M., Guo, X., Fong, C. M. V., Chen, X., and Lu, J.-J. (2016). Characterization of Osimertinib (AZD9291)-Resistant Non-small Cell Lung Cancer NCI-H1975/OSIR Cell Line. *Oncotarget* 7 (49), 81598–81610. doi:10.18632/oncotarget.13150

Terlizzi, M., Colarusso, C., Pinto, A., and Sorrentino, R. (2019). Drug Resistance in Non-small Cell Lung Cancer (NSCLC): Impact of Genetic and Non-genetic Alterations on Therapeutic Regimen and Responsiveness. *Pharmacol. Ther.* 202, 140–148. doi:10.1016/j.pharmthera.2019.06.005

Thai, A., Solomon, B., Sequist, L., Gainor, J., and Heist, R. (2021). Lung Cancer. *Lancet*. doi:10.1016/s0140-6736(21)00312-3

Wan, J., Zhan, J., Li, S., Ma, J., Xu, W., Liu, C., et al. (2015). PCAF-primed EZH2 Acetylation Regulates its Stability and Promotes Lung Adenocarcinoma Progression. *Nucleic Acids Res.* 43 (7), 3591–3604. doi:10.1093/nar/gkv238

Wang, Y., Qin, C., Yang, G., Zhao, B., and Wang, W. (2021). The Role of Autophagy in Pancreatic Cancer Progression. *Biochim. Biophys. Acta (Bba) - Rev. Cancer* 1876 (2), 188592. doi:10.1016/j.bbcan.2021.188592

Wang, Y., Shi, K., Zhang, L., Hu, G., Wan, J., Tang, J., et al. (2016). Significantly Enhanced Tumor Cellular and Lysosomal Hydroxychloroquine Delivery by Smart Liposomes for Optimal Autophagy Inhibition and Improved Antitumor Efficiency with Liposomal Doxorubicin. *Autophagy* 12 (6), 949–962. doi:10.1080/15548627.2016.1162930

Wang, Z., Du, T., Dong, X., Li, Z., Wu, G., and Zhang, R. (2016). Autophagy Inhibition Facilitates Erlotinib Cytotoxicity in Lung Cancer Cells through Modulation of Endoplasmic Reticulum Stress. *Int. J. Oncol.* 48 (6), 2558–2566. doi:10.3892/ijo.2016.3468

Wei, F.-Z., Cao, Z., Wang, X., Wang, H., Cai, M.-Y., Li, T., et al. (2015). Epigenetic Regulation of Autophagy by the Methyltransferase EZH2 through an MTOR-dependent Pathway. *Autophagy* 11 (12), 2309–2322. doi:10.1080/15548627.2015.1117734

Westover, D., Zugazagoitia, J., Cho, B. C., Lovly, C. M., and Paz-Ares, L. (2018). Mechanisms of Acquired Resistance to First- and Second-Generation EGFR Tyrosine Kinase Inhibitors. *Ann. Oncol.* 29, i10–i19. doi:10.1093/annonc/mdx703

White, E., Lattime, E. C., and Guo, J. Y. (2021). Autophagy Regulates Stress Responses, Metabolism, and Anticancer Immunity. *Trends Cancer* 7 (8), 778–789. doi:10.1016/j.trecan.2021.05.003

Wu, S.-G., and Shih, J.-Y. (2018). Management of Acquired Resistance to EGFR TKI-Targeted Therapy in Advanced Non-small Cell Lung Cancer. *Mol. Cancer* 17 (1), 38. doi:10.1186/s12943-018-0777-1

Yang, C.-Y., Yang, J. C.-H., and Yang, P.-C. (2020). Precision Management of Advanced Non-small Cell Lung Cancer. *Annu. Rev. Med.* 71, 117–136. doi:10.1146/annurev-med-051718-013524

Yu, T., Guo, F., Yu, Y., Sun, T., Ma, D., Han, J., et al. (2017). Fusobacterium Nucleatum Promotes Chemoresistance to Colorectal Cancer by Modulating Autophagy. *Cell* 170 (3), 548–563. e16. doi:10.1016/j.cell.2017.07.008

Zhang, T., Gong, Y., Meng, H., Li, C., and Xue, L. (2020). Symphony of Epigenetic and Metabolic Regulation-Interaction between the Histone Methyltransferase EZH2 and Metabolism of Tumor. *Clin. Epigenet* 12 (1), 72. doi:10.1186/s13148-020-00862-0

Zhang, Z., Shi, R., Xu, S., Li, Y., Zhang, H., Liu, M., et al. (2021). Identification of Small Proline-rich Protein 1B ( SPRR1B ) as a Prognostically Predictive Biomarker for Lung Adenocarcinoma by Integrative Bioinformatic Analysis. *Thorac. Cancer* 12 (6), 796–806. doi:10.1111/1759-7714.13836

Zhou, Q., Zhang, X.-C., Chen, Z.-H., Yin, X.-L., Yang, J.-J., Xu, C.-R., et al. (2011). Relative Abundance of EGFR Mutations Predicts Benefit from Gefitinib Treatment for Advanced Non-small-cell Lung Cancer. *Jco* 29 (24), 3316–3321. doi:10.1200/jco.2010.33.3757

**Conflict of Interest:** The authors declare that the research was conducted in the absence of any commercial or financial relationships that could be construed as a potential conflict of interest.

**Publisher's Note:** All claims expressed in this article are solely those of the authors and do not necessarily represent those of their affiliated organizations, or those of the publisher, the editors and the reviewers. Any product that may be evaluated in this article, or claim that may be made by its manufacturer, is not guaranteed or endorsed by the publisher.

frontiers in Pharmacology

REVIEW
published: 28 March 2022
doi: 10.3389/fphar.2022.815603

# Research Progress on Natural Diterpenoids in Reversing Multidrug Resistance

*Zhuo-fen Deng[1†], Irina Bakunina[2†], Hua Yu[3†], Jaehong Han[4], Alexander Dömling[5]*, Maria-José U Ferreira[6]* and Jian-ye Zhang[1]**

[1]Key Laboratory of Molecular Target & Clinical Pharmacology, The State & NMPA Key Laboratory of Respiratory Disease, School of Pharmaceutical Sciences and the Fifth Affiliated Hospital, Guangzhou Medical University, Guangzhou, China, [2]G.B. Elyakov Pacific Institute of Bioorganic Chemistry, Far Eastern Branch, Russian Academy of Sciences, Vladivostok, Russia, [3]Institute of Chinese Medical Sciences, State Key Laboratory of Quality Research in Chinese Medicine, University of Macau, Macao SAR, China, [4]Metalloenzyme Research Group and Department of Plant Science and Technology, Chung-Ang University, Anseong, Korea, [5]Department of Pharmacy, University of Groningen, Groningen, Netherlands, [6]Research Institute for Medicines (iMed.ULisboa), Faculty of Pharmacy, Universidade de Lisboa, Lisboa, Portugal*

OPEN ACCESS

**Edited by:**
*Qingbin Cui,*
*University of Toledo, United States*

**Reviewed by:**
*Hui Zhang,*
*Shandong University, China*
*Mariana A Reis,*
*University of Porto, Portugal*

***Correspondence:**
*Jian-ye Zhang*
*jianyez@163.com*
*Maria-José U Ferreira*
*mjuferreira@ff.ulisboa.pt*
*Alexander Dömling*
*a.s.s.domling@rug.nl*

*†These authors have contributed equally to this work*

**Specialty section:**
*This article was submitted to Pharmacology of Anti-Cancer Drugs, a section of the journal Frontiers in Pharmacology*

**Received:** *15 November 2021*
**Accepted:** *27 January 2022*
**Published:** *28 March 2022*

**Citation:**
*Deng Z-f, Bakunina I, Yu H, Han J, Dömling A, Ferreira MJU and Zhang J-y (2022) Research Progress on Natural Diterpenoids in Reversing Multidrug Resistance. Front. Pharmacol. 13:815603. doi: 10.3389/fphar.2022.815603*

Multidrug resistance (MDR) is one of the main impediments in successful chemotherapy in cancer treatment. Overexpression of ATP-binding cassette (ABC) transporter proteins is one of the most important mechanisms of MDR. Natural products have their unique advantages in reversing MDR, among which diterpenoids have attracted great attention of the researchers around the world. This review article summarizes and discusses the research progress on diterpenoids in reversing MDR.

**Keywords: cancer, chemotherapy, multidrug resistance, natural products, diterpenoids**

## INTRODUCTION

Cancer, one of major public health problems, imposes a serious challenge to the survival of human beings worldwide (Wu et al., 2019). Although there are several different cancer treatment modalities, chemotherapy is still one of the main approaches of cancer therapy (Bukowski et al., 2020). However, the development of chemoresistance especially multidrug resistance (MDR) has greatly restricted the effectiveness of drugs for cancer management, which can result in treatment failure (Holohan et al., 2013). MDR refers to the resistance of cancer cells to various chemotherapy drugs with different structures and mechanisms. Therefore, there is a need to clarify the mechanisms of MDR and seek some effective reversal strategies.

At present, many MDR reversal agents have been developed to overcome MDR. Natural products, characterized for having high binding ability to various biological targets, and frequently low toxicity, might be crucial for overcoming MDR (Guo et al., 2017). A significant number of studies have shown that natural products possessed the potential to reverse MDR (Kumar and Jaitak, 2019). Diterpenoids, an important group of bioactive compounds in natural products, have been playing an important role in drug discovery. In recent years, it was found that some

**Abbreviations:** ABCB1, ATP-binding cassette subfamily B member 1; ABCC1, multidrug resistance-associated protein 1; ABCC2, multidrug resistance-associated protein 2; ABCG2, breast cancer resistance protein; FAR, fluorescence activity ratio; RF, reversal fold; MDR, multidrug resistance; SAR, structure activity relationship; Rh123, Rhodamine 123; ADR, adriamycin; VCR, vincristine; TAX, paclitaxel; NF-κB; nuclear factor κB; MAPK, mitogen-activated protein kinases; PI3K-PKB, phosphoinositide-3-kinase-protein kinase B; $IC_{50}$, half maximal inhibitory concentration; $EC_{50}$, half maximal effective concentration; MTT, 3-(4, 5-dimethylthiazol-2-yl)-2, 5-diphenyltetrazolium bromide.

diterpenoids, mostly macrocyclic diterpenes, were able to reverse MDR in cancer cells (Molnar et al., 2006; Kumar and Jaitak, 2019). This review discusses the research progress on diterpenoids in reversing MDR.

# MULTIDRUG RESISTANCE

## ATP-Binding Cassette Transporter-Mediated Multidrug Resistance

MDR of cancer cells is associated with various mechanisms (Bukowski et al., 2020). Of all mechanisms, increased drug-efflux of structurally different anticancer drugs, mediated by ABC-transporter proteins is a common one (Borst and Elferink, 2002). In the 1970s, ABCB1, a member of ABC transporters, was first discovered (Juliano and Ling, 1976). To date, other ABC transporters have been found, such as ABCC1, ABCC2 and ABCG2, which are associated with MDR (Takano et al., 2006; Lu et al., 2015). Besides the involvement in MDR, transmembrane transport of endogenous or exogenous molecules is one of the main physiological functions of ABC transporters (Wang JQ et al., 2021). They possess the function of energy dependent "drug-pump".

## ATP-Binding Cassette Subfamily B Member 1

ABCB1 is one of the research hotspots in ABC transporter family because its expression is up-regulated in many drug-resistant and refractory tumors (Kadioglu et al., 2016). Studies have shown that the expression of ABCB1 is regulated by various signaling pathways, such as nuclear factor κB (NF-κB) (Sun et al., 2012), mitogen-activated protein kinases (MAPK) (Luo et al., 2016) and phosphoinositide-3-kinase–protein kinase B (PI3K-PKB) (Dong et al., 2017). Therefore, by clarifying these signaling pathways, it may help exploring targets for reversing MDR.

At present, four generations of ABCB1 inhibitors have been developed. The first-generation reversal inhibitors include calcium channel blockers, immunosuppressants, protein kinase C inhibitors and so on. These inhibitors have low affinity and high toxicity (Shen et al., 2008). The second-generation inhibitors were obtained by improving the first-generation inhibitors, including dexverapamil, biricodar. Compared with the first-generation inhibitors, they have stronger affinity for ABCB1, less toxicity and better effect (Thomas and Coley, 2003). The third-generation of ABCB1 inhibitors, such as tariquidar and zosuquidar, were much more effective than the first-generation and second-generation inhibitors (Martin et al., 1999). However, further development of the third-generation ABCB1 inhibitors was limited by some unexpected side effects in clinical trials (Chen et al., 2017). The fourth-generation ABCB1 inhibitors include 1) peptidomimetics, 2) compounds isolated from natural sources and their derivatives, and 3) dual ligands (compounds capable of inhibiting ABCB1 and another mediator of MDR) (Dong et al., 2020). Many of them possess both antitumoral and MDR reversing activities. Nevertheless, most of fourth-generation ABCB1 inhibitors have been evaluated in cancer cells *in vitro*, and their efficacy and safety *in vivo* have not been determined.

## Diterpenoids as Multidrug Resistance Reversal Agents

Diterpenoids (C20), one of the largest groups of natural products, are derived from four C5 isoprene units. The main skeleton types of diterpenoids include, among others, kaurenes, clerodanes, abietanes and labdanes. Lathyranes and jatrophanes are macrocyclic diterpenes characteristic of *Euphorbia* genus (Euphorbiaceae family), from which many compounds showed significant MDR reversing activity. Some other diterpenoids from *Euphorbia* species were also reported as MDR reversers, such as ingenanes, segetanes, and jatropholanes. Some diterpenes from other plants, such as *Pseudolarix*, *Taxus*, *Briareum*, *Sindora* species and so on, also possess certain reversal activity.

## Jatrophanes

Six new jatrophane-type diterpenoids and three known diterpenes were isolated from the whole undried plants of *Euphorbia esula* (**Table 1**), most of which were able to enhance the Rhodamine 123 (Rh123) accumulation in human *ABCB1*-transfected L5178Y mouse T-lymphoma cells, overexpressing ABCB1 (Vasas et al., 2011). Rh123 accumulation assay is commonly used to characterize potential ABCB1 inhibitors (Jouan et al., 2016). According to the experimental results, compounds **1** and **2** were the most powerful inhibitors of ABCB1 efflux-pump activity, whose efficacy was 2–5 times higher than that of the standard modulator verapamil [Fluorescence activity ratio (FAR) = 52.5 at 40 μg/ml and 119.9 at 40 μg/ml]. The FAR was calculated on the basis of the measured fluorescence values via the following equation: FAR = $\frac{MDR\,treated/MDR\,control}{parental\,treated/parental\,control}$ (Vasas et al., 2011).

Compounds **2**-**6** were isolated from *Euphorbia welwitschii* (**Table 1**). The property of interaction of compound **6** with ABCB1 was studied by ATPase assay (Reis et al., 2016). Two complementary assays compose the ATPase experiment (activation assay to test the effect on the basal ATPase activity, inhibition assay to test the effect on drug-stimulated ATPase activity). Maintaining the efflux function of ABCB1 requires energy generated by ATP hydrolysis, which requires ATPase (Szollosi et al., 2018). The ATPase activity of ABCB1 is one of the most attractive targets for the design of inhibitors (Mollazadeh et al., 2018). The measurement of catalytic activity is a means of investigating candidate regulators as substrates or inhibitors, and inhibited the verapamil-stimulated ATPase activity, being a complete inhibition attained at 50 and 100 μM. The effects of compound **6** on the ATPase activity of ABCB1 showed it to interact with the transporter and to be able to reduce the transport of a second substrate. The Rh123 efflux assay results also showed that all these compounds were able to inhibit the efflux activity of ABCB1 at 20 μM. Their efficacy was 2–3 times higher than that of the positive control verapamil in a mouse T-lymphoma *ABCB1*-transfected cell model (FAR = 12.5 at 20 μM) (Reis et al., 2016).

**TABLE 1 |** Jatrophanes.

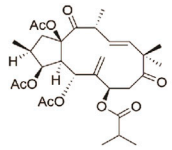

1

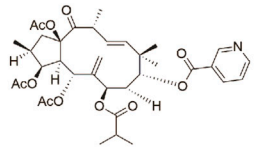

2

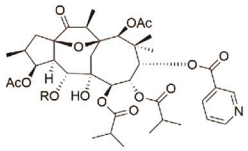

R
3 Ac
4 H

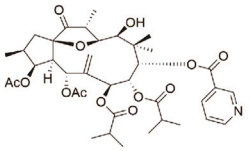

5

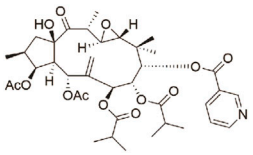

6

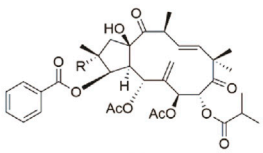

R
7 OH
8 OAc

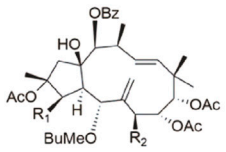

| | $R_1$ | $R_2$ |
|---|---|---|
| 9 | OAc | OiBu |
| 10 | H | OAc |

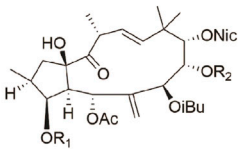

| | $R_1$ | $R_2$ | $R_1$ | $R_2$ |
|---|---|---|---|---|
| 11 | Pr | / | 14 Pr | iBu |
| 12 | iBu | / | 15 iBu | Bz |
| 13 | Pr | Bz | 16 iBu | Nic |

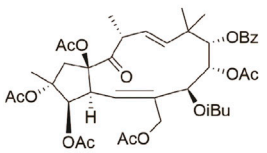

17

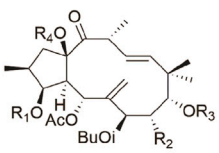

| | $R_1$ | $R_2$ | $R_3$ | $R_4$ |
|---|---|---|---|---|
| 18 | Ac | OAc | Nic | Ac |
| 19 | Pr | ONic | Ac | H |

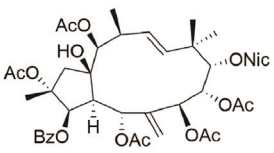

20

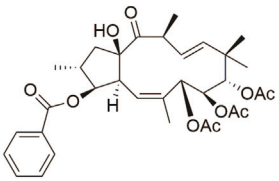

21

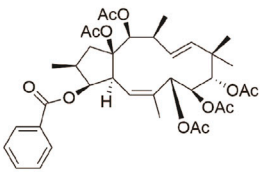

22

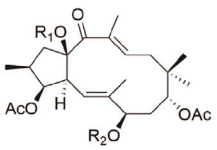

| | $R_1$ | $R_2$ |
|---|---|---|
| 23 | Ac | Bz |
| 24 | Ac | Bu |
| 25 | H | Bz |

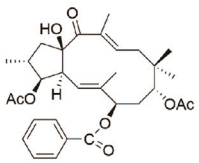

26

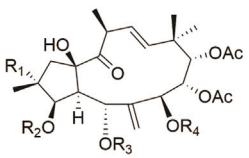

| | $R_1$ | $R_2$ | $R_3$ | $R_4$ |
|---|---|---|---|---|
| 27 | OAc | H | iBu | Bz |
| 28 | OAc | H | MeBu | Bz |
| 29 | OAc | H | Nic | Bz |
| 30 | H | H | iBu | Bz |
| 31 | H | Ac | iBu | Bz |
| 32 | OH | Ac | iBu | Bz |
| 33 | OAc | PhOAc | Ac | iBu |
| 34 | OAc | Nic | Ac | iBu |
| 35 | H | Bz | Ac | iBu |

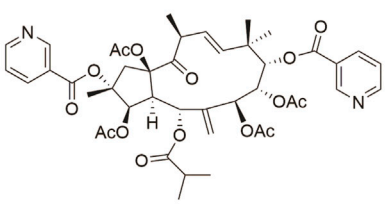

36

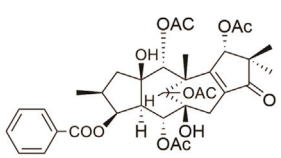

37

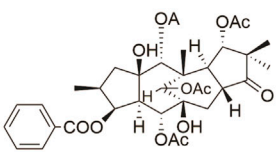

38

| Compound | Name | Plant | Ref |
|---|---|---|---|
| **1** | esulatin J | *E. esula* | Vasas et al. (2011) |
| **2** | esulatin M | *E. esula* | Vasas et al. (2011) |
| | | *E. welwitschii* | Reis et al. (2016) |

(Continued on following page)

**TABLE 1 |** (*Continued*) Jatrophanes.

| Compound | Name | Plant | Ref |
|---|---|---|---|
| **3** | euphowelwitschine A | *E. welwitschii* | Reis et al. (2016) |
| **4** | euphowelwitschine B | *E. welwitschii* | Reis et al. (2016) |
| **5** | welwitschene | *E. welwitschii* | Reis et al. (2016) |
| **6** | epoxywelwitschene | *E. welwitschii* | Reis et al. (2016) |
| **7** | euphoglomeruphane K | *E.glomerulans* | Hasan et al. (2019) |
| **8** | euphoglomeruphane L | *E.glomerulans* | Hasan et al. (2019) |
| **9** | euphosorophane A | *E.sororia* | Hu et al. (2018) |
| **10** | euphosorophane I | *E.sororia* | Yang et al. (2021) |
| **11** | euphodendrophane A | *E. dendroides* | Aljancic et al. (2011) |
| | | *E. nicaeensis* | Krstic et al. (2018) |
| **12** | euphodendrophane B | *E. dendroides* | Aljancic et al. (2011) |
| | | *E. nicaeensis* | Krstic et al. (2018) |
| **13** | euphodendrophane H | *E. dendroides* | Jadranin et al. (2013) |
| **14** | euphodendrophane J | *E. dendroides* | Jadranin et al. (2013) |
| **15** | euphodendrophane K | *E. dendroides* | Jadranin et al. (2013) |
| **16** | euphodendrophane L | *E. dendroides* | Jadranin et al. (2013) |
| **17** | euphodendrophane S | *E. dendroides* | Jadranin et al. (2013) |
| **18** | nicaeenin F | *E. nicaeensis* | Krstic et al. (2018) |
| **19** | nicaeenin G | *E. nicaeensis* | Krstic et al. (2018) |
| **20** | pepluanin A | *E. peplus* | Corea et al. (2004) |
| **21** | euphomelliferine | *E. mellifera* | Valente et al. (2012) |
| **22** | euphomelliferene A | *E. mellifera* | Valente et al. (2012) |
| **23** | pubescene A | *E. pubescens* | Valente et al. (2004) |
| | | | Ferreira et al. (2005) |
| **24** | pubescene B | *E. pubescens* | Valente et al. (2004) |
| | | | Ferreira et al. (2005) |
| **25** | pubescene C | *E. pubescens* | Valente et al. (2004) |
| | | | Ferreira et al. (2005) |
| **26** | pubescene D | *E. pubescens* | Valente et al. (2004) |
| | | | Ferreira et al. (2005) |
| **27** | euphodendroidin A | *E. dendroides* | Corea et al. (2003) |
| **28** | euphodendroidin B | *E. dendroides* | Corea et al. (2003) |
| **29** | euphodendroidin C | *E. dendroides* | Corea et al. (2003) |
| **30** | euphodendroidin D | *E. dendroides* | Corea et al. (2003) |
| **31** | euphodendroidin E | *E. dendroides* | Corea et al. (2003) |
| **32** | euphodendroidin F | *E. dendroides* | Corea et al. (2003) |
| **33** | Jatrophane diterpene | *E. dendroides* | Corea et al. (2003) |
| **34** | euphodendroidin G | *E. dendroides* | Corea et al. (2003) |
| **35** | euphodendroidin H | *E. dendroides* | Corea et al. (2003) |
| **36** | euphodendroidin I | *E. dendroides* | Corea et al. (2003) |
| **37** | euphoportlandol A | *E. portlandica* | Madureira et al. (2006) |
| **38** | euphoportlandol B | *E. portlandica* | Madureira et al. (2006) |

Seventeen new jatrophane diterpenoids and five known were isolated from the whole plant of *Euphorbia esula* (**Table 1**). Their reversal fold (RF) values on MCF-7/ADR cells overexpressing ABCB1 (MCF-7 cell line with adriamycin resistance) ranged from 2.3 to 12.9 at 10 μM. The methods used to assay MDR-reversal activity mainly include RF and FAR values. RF value can be calculated by the MTT method, which can reveal reversal activities and cytotoxicity of compounds. The Rh123 efflux assay is to determine whether compounds have an effect on the function of ABCB1 transport substrate, from which FAR value is calculated. Compared to RF value, FAR value can give a direct quantitative assessment whether compounds modulate the efflux mediated by ABCB1. Their reversal fold values on MCF-7/ADR cells overexpressing ABCB1 ranged from 2.3 to 12.9 at 10 μM. Among them, the MDR reversal activities of compounds **7** and **8** were as good as that of verapamil (RF = 13.7), with RF values of 12.9 and 12.3 at 10 μM, respectively (Hasan et al., 2019).

Five new jatrophane diterpenoids were isolated from the fructus of *Euphorbia sororia* (**Table 1**). Among them, the most effective compound was compound **9**. Compound **9** showed reversal potency with RF values of 36.82, 20.59 at a concentration of 10.0 mM in the MCF-7/ADR cells. The advantages of compound **9** included high potency ($EC_{50}$ = 92.68 ± 18.28 nM) in overcoming ABCB1-mediated MDR to adriamycin (ADR), stimulating ABCB1-ATPase activity in a concentration-dependent manner, and potency in reversing resistance to other cross-resistant chemotherapeutic agents, such as ADR and vincristine (VCR), and inhibition of ABCB1-mediated Rh123 efflux function in MCF-7/ADR cells. In addition, it did not downregulate the expression of ABCB1 in the MCF-7/ADR cells. The Dixon plot analysis indicated that compound **9** was competitive inhibitor of ABCB1-mediated ADR transport, which was in agreement with the Lineweaver-Burk analysis (Hu et al., 2018).

Also, eight new and fourteen known were isolated from the fructus of *Euphorbia sororia*. Among them, fourteen compounds showed lower cytotoxicity and promising ability to reverse MDR, compared to verapamil, which was used as positive control. Within these jatrophanes, compound **10** appeared to be the most powerful ABCB1 inhibitor ($EC_{50}$ = 1.82 μM). Fluorescence microscopy showed that compound **10** was able to enhance the Rh123 accumulation of multidrug-resistant cells in a dose-dependent manner. Further studies showed that compound **10** stimulated ABCB1-ATPase activity in a concentration-dependent manner instead of down regulating ABCB1 expression and mRNA levels (Yang et al., 2021).

Seven new diterpenoids were isolated from *Euphorbia dendroides* and were investigated for the biological activities on the MDR cell line NCI-H460/R. These compounds included six new jatrophanes, among which two compounds (**11** and **12**, **Table 1**) exerted high potency in overcoming ABCB1-mediated MDR (FAR = 3.0 to 3.2 at 20 μM). The results suggested that they had the potential to reverse the drug resistance of ADR and paclitaxel (TAX) in the MDR cancer cell line. Notablely, it was showed for the first time that a synergistic effect existed between the TAX and jatrophanes (Aljancic et al., 2011).

Some jatrophane diterpenoids, including compounds **11** and **12**, were isolated from the latex of *Euphorbia nicaeensis*, together with seven previously undescribed jatrophanes (**Table 1**), among which compounds **18** and **19** were the most active compounds (FAR = 4.52 and 5.02 at 5 μM on non-small cell lung carcinoma NCI-H460/R, FAR = 5.89 and 4.39 on colorectal carcinoma DLD1-TxR) (Krstic et al., 2018).

Some new diterpenes were isolated from the whole plant of *Euphorbia peplus* and their inhibitory activity to ABCB1 was investigated in ABCB1-overexpressing K562/R7 human leukemic cells (**Table 1**). The results showed that compound **20** was the most active inhibitor, whose efficiency was at least two-fold higher than the conventional modulator, which was taken here as reference (100%) (cyclosporin A, 5 μM). The study on structure activity relationship (SAR) showed the importance of substitution on medium-size rings (carbons 8, 9, 14 and 15) (Corea et al., 2004).

Five jatrophane diterpenes, including three new compouds, were isolated from *Euphorbia mellifera* (**Table 1**). Compounds **21** and **22** exhibited significant activity on multidrug-resistant mouse lymphoma cells and on human colon adenocarcinoma cells in a dose-dependent manner. (FAR = 12.1, 23.1 at 20 μM, and FAR = 72.9, 82.2 at 60 μM respectively, on MDR mouse lymphoma cells; FAR = 5.1 and 5.5 at 20 μM on human colon adenocarcinoma cells) (Valente et al., 2012).

Four jatrophane diterpenes were isolated from *Euphorbia pubescens* (compounds **23–26, Table 1**) (Valente et al., 2004). The anti-MDR activities of these compounds were investigated on mouse lymphoma cells. All the compounds displayed a significant effect on inhibiting ABCB1 efflux-pump activity compared with that of the positive control verapamil (FAR = 21.28 at 20 μM) (Ferreira et al., 2005).

Ten jatrophane diterpenes were isolated from *Euphorbia dendroides* (**Table 1**). A SAR study showed the general effect of lipophilicity on activity, and also emphasized the correlation of substitution patterns at positions 2, 3 and 5, indicating that the fragment was involved in binding. Among all these compounds, compound **30** was the most active inhibitor in ABCB1-overexpressing human K562/R7 leukemic cells, which was almost two-fold more efficient (183 ± 17% at 5 μM) than cyclosporin A, which was taken here as reference (100%) (Corea et al., 2003).

Compounds **37** and **38** are rearranged jatrophane diterpenoids of the segetane group that were isolated from *Euphorbia portlandica* (**Table 1**). Their biological activity was investigated against MDR in human *ABCB1*-gene transfected mouse lymphoma cells. The result showed that both compounds were effective (FAR = 40.3 and 30.7 at 40 μg/ml, respectively). When comparing the results with those found for macrocyclic jatrophanes, the authors concluded that these rearranged derivatives were less active. Thus, according to the authors, the macrocycle scaffold of these diterpenes and its substitution pattern seem to play an important role in reversing ABCB1-mediated MDR (Madureira et al., 2006).

Some studies on a structurally heterogeneous set of jatrophane polyesters revealed the positive effect of overall lipophilicity on ABCB1 binding and suggested the importance of the oxygen substituent at C-9 (Hohmann et al., 2002). A study showed that the saturated five membered ring had an important effect on the activity (Zhu et al., 2016).

## Lathyranes

Two highly modified lathyrane diterpenoids were isolated from the leaves and twigs of *Jatropha gossypiifolia* (**Table 2**). The ability of both compounds as MDR modulators was assessed on ADR-resistant HepG2/ADR and HCT-15/5-FU cell lines. The results suggested that only compound **40** showed decent activity, with RF values of 3.3 and 5.8 at 10 μM, respectively on the two cell lines, compared to verapamil (RF = 6.2). In addition, compound **40** had no intrinsic cytotoxicity to both of the MDR cell lines (Li et al., 2020).

Four new lathyrol-type diterpenoids and some known diterpenoids were isolated from *Euphorbia Lathyris* (**Table 2**). All the compounds were evaluated for MDR reversing activity against HepG2/ADR cells. Most of them were able to reverse MDR, with RF values of 10.05–448.39 at 20 μM. Among them, compound **41** showed the best activity. To investigate the mechanism of reversing MDR of lathyrane diterpenes, Yang et al. examined the effect of compound **41** on the cell viability of HepG2/ADR cells and the ADR accumulation of HepG2/ADR in the presence of the compound at 20 μM. The results showed that this compound with the best MDR reversing activity had low cytotoxicity and was able to promote ADR accumulation in HepG2/ADR cells in time-dependent model (Yang et al., 2020).

Twenty diterpenoids were isolated from *Euphorbia macrorrhiza*, including two lathyranes, namely compounds **42** and **43** (**Table 2**). Among them, compound **43** showed significant inhibitory activity on ABCB1-mediated drug efflux in KBv200 cell line (RF = 43.63) The inhibitory effect of compound **43** on ABCB1-mediated drug efflux was further tested at several concentrations by Rh123 accumulation assay. Compound **43** exhibited significant effect in increasing the intracellular accumulation of Rh123 (FAR = 2.12 at 30 μM) when compared with the postive control verapamil (FAR = 1.63 at 10 μM) (Gao et al., 2016).

**TABLE 2 |** Lathyranes.

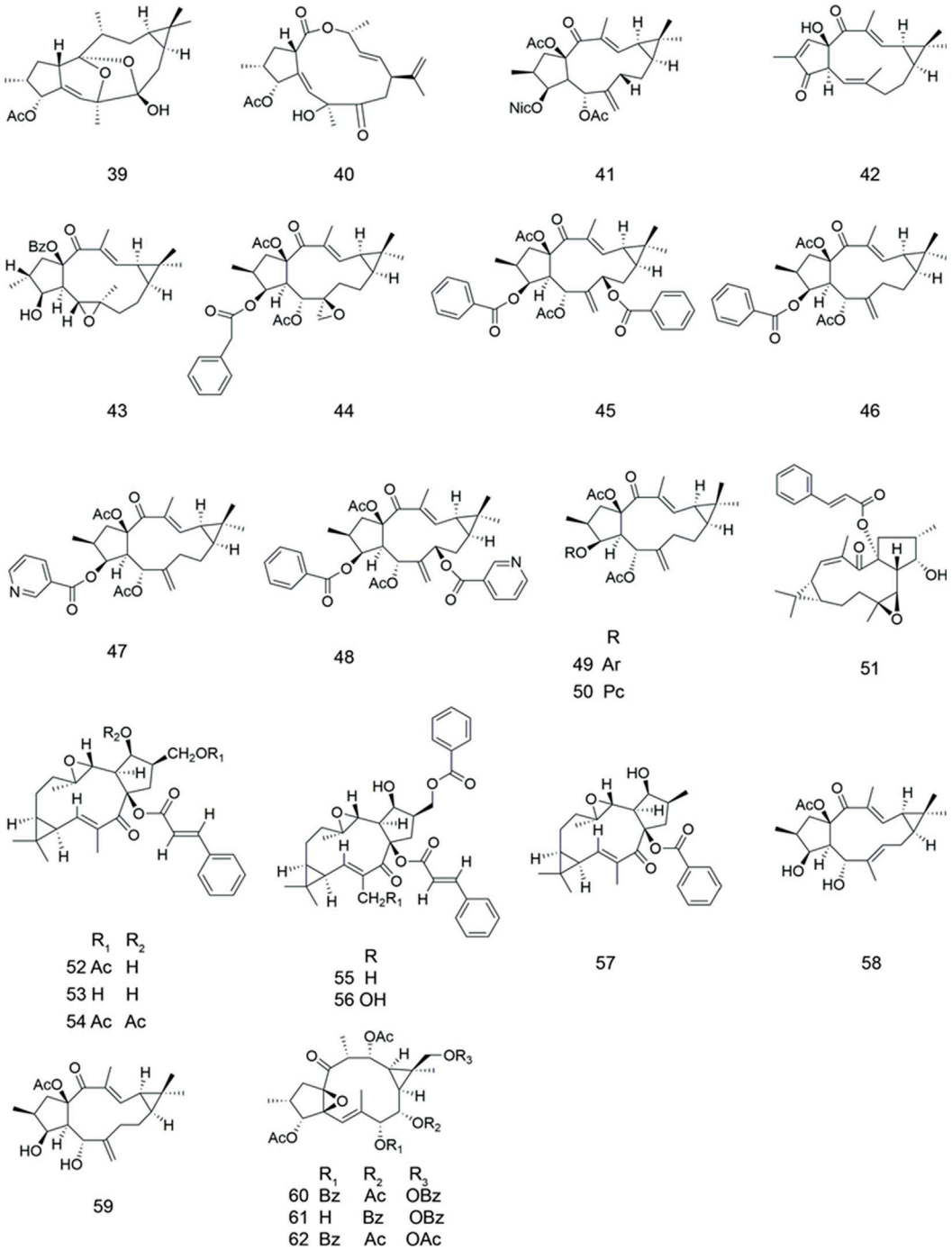


| Compound | Name | Plant | Ref |
|---|---|---|---|
| **39** | jatrofoliane A | *J. gossypiifolia* | Li et al. (2020) |
| **40** | jatrofoliane B | *J. gossypiifolia* | Li et al. (2020) |
| **41** | 5, 15-di-O-acetoxy-3-nicotinoyllathyol-6,12-diene-14-one | *E. lathyris* | Yang et al. (2020) |
| **42** | macrorilathyrone A | *E. macrorrhiza* | Gao et al. (2016) |
| **43** | macrorilathyrone B | *E. macrorrhiza* | Gao et al. (2016) |
| **44** | euphorbia factor L1 | *E. lathyris* | Zhang et al. (2011)<br>Zhang et al. (2013) |

(Continued on following page)

**TABLE 2 |** (*Continued*) Lathyranes.

| Compound | Name | Plant | Ref |
|---|---|---|---|
| **45** | euphorbia factor L2 | *E. lathyris* | Teng et al. (2018) |
| **46** | euphorbia factor L3 | *E. lathyris* | Teng et al. (2018) |
| **47** | euphorbia factor L8 | *E. lathyris* | Teng et al. (2018) |
| **48** | euphorbia factor L9 | *E. lathyris* | Teng et al. (2018) |
| **49** | euphoboetirane A | *E. boetica* | Neto et al. (2019) |
| **50** | euphoboetirane B | *E. boetica* | Neto et al. (2019) |
| **51** | EM-E-11–4 | *E. micractina* | Liu et al. (2015)<br>Liu et al. (2020) |
| **52** | latilagascene A | *E. lagascae* | Duarte et al. (2006)<br>Duarte et al. (2007) |
| **53** | latilagascene B | *E. lagascae* | Duarte et al. (2006)<br>Duarte et al. (2007) |
| **54** | latilagascene C | *E. lagascae* | Duarte et al. (2006)<br>Duarte et al. (2007) |
| **55** | latilagascene D | *E. lagascae* | Duarte et al. (2006)<br>Duarte et al. (2007) |
| **56** | latilagascene E | *E. lagascae* | Duarte et al. (2007) |
| **57** | latilagascene F | *E. lagascae* | Duarte et al. (2007) |
| **58** | piscatoriol A | *E. piscatoria* | Reis et al. (2014) |
| **59** | piscatoriol B | *E. piscatoria* | Reis et al. (2014) |
| **60** | euphornan K | *E. marginata* | Zhang et al. (2020) |
| **61** | euphornan N | *E. marginata* | Zhang et al. (2020) |
| **62** | euphornan R | *E. marginata* | Zhang et al. (2020) |

Compound **44** was isolated from Caper *Euphorbia* seed (seeds of *Euphorbia lathyris*) (**Table 2**). For the first time, researchers showed that compound **44** enhanced the sensitivity of established ABCB1 substrates and increased accumulation of ADR and Rh123 in ABCB1-mediated MDR KBv200 and MCF-7/ADR cells. In the meantime, compound **44** did not downregulate the expression of ABCB1 either in protein or mRNA level (Zhang et al., 2011). A further study was conducted on reversal activities of compound **44** against ABCB1-mediated MDR and apoptosis sensitization in K562/ADR cells. The results showed that the combination of compound **44** and ABCB1 substrate chemotherapeutic drugs may help to overcome MDR. The mitochondrial pathway was involved in the apoptosis sensitization by compound **44** (Zhang et al., 2013). The cytotoxicity of compounds **44**–**48** was evaluated against A549, MDA-MB-231, KB, and MCF-7 cancer cell lines and the KB-VIN MDR cancer cell line. Compound **45** exhibited selectivity against KB-VIN and compound **48** showed the strongest cytotoxicity (Teng et al., 2018).

Compounds **49** and **50** were isolated from *Euphorbia boetica* (**Table 2**). The activity of reversing MDR was evaluated using a combination of transport and chemosensitivity assays in L5178Y-MDR and Colo320 cell models. The results confirmed the importance of macrocyclic lathyrane diterpenes as effective lead compounds for reversing MDR (Neto et al., 2019).

Compound **51**, isolated from *Euphorbia micractina*, was found to remarkably increase TAX uptake in Caco-2 cells overexpressing ABCB1 (**Table 2**). The results showed that compound **51** was an effective potential drug to reverse ABCB1-mediated MDR by inhibiting ABCB1 transport function and increasing the intracellular concentration of TAX (Liu et al., 2015). Further study has showed that compound **51** could reverse βIII-tubulin and ABCB1-mediated TAX resistance in tumor cells. Most notably, it was showed for the first time that a small molecule natural product could specifically inhibit the expression of βIII-tubulin (Liu et al., 2020). Some research showed that overexpression of βIII-tubulin might contribute to chemotherapy resistance (Katsetos et al., 2003; Katsetos and Draber, 2012).

Some lathyrane-type diterpenoids, including compounds **52**–**54**, were isolated from *Euphorbia lagascae* (**Table 2**). Their effects on the reversal of MDR were examined on mouse lymphoma cells. Among them compound **53** displayed the highest inhibition of Rh123 efflux of human *ABCB1* gene transfected mouse lymphoma cells (FAR = 102.1 at 40 μg/ml) (Duarte et al., 2006). Duarte et al. also isolated compounds **55**–**57** from *Euphorbia lagascae* (**Table 1**) and evaluated their biological activity against MDR on mouse lymphoma cells. Compounds **55** and **57** showed very strong activity compared with the positive control verapamil (FAR = 110.4 and 216.8 at 4 μg/ml, respectively) (Duarte et al., 2007).

Compounds **58** and **59** were isolated from *Euphorbia piscatoria* (**Table 2**). Their biological activity against MDR was evaluated through a drug combination assay in the L5178Y mouse T lymphoma cell line transfected with the human *ABCB1* gene. They were able to synergistically enhance the antiproliferative activity of ADR. Most notably, they were further investigated if this synergistic effect could be relevant to the inhibition of ABCB1, using the Rh123 efflux assay, which was negative. These results indicated that these compounds had the reversal effect of MDR independent from ABCB1 by targeting other cellular pathways that are responsible for MDR (Reis et al., 2014).

**TABLE 3 |** Clerodanes.

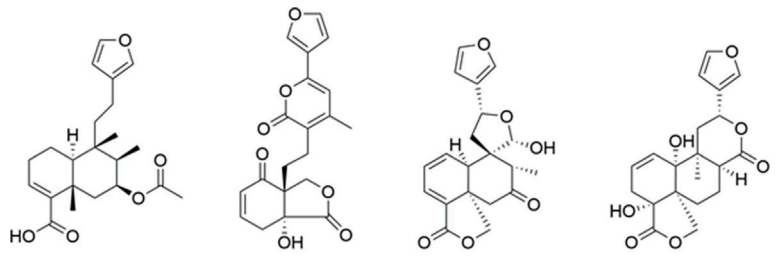

63 64 65 66

| Compound | Name | Plant | Ref |
|---|---|---|---|
| **63** | (+)-7β-acetoxy-15,16-epoxycleroda-3,13 (16),14-trien-18-oic acid | *S. sumatrana* | Jung et al. (2010) |
| **64** | amarissinin A | *S. amarissima* | Bautista et al. (2016) |
| **65** | amarissinin B | *S. amarissima* | Bautista et al. (2016) |
| **66** | amarissinin C | *S. amarissima* | Bautista et al. (2016) |

Twenty new ingol diterpenoids, which are a subgroup of lathyrane diterpenoids, were isolated from *Euphorbia marginata*. All compounds were tested for their biological activity against MDR on ABCB1-dependent MDR cancer cell line HepG2/ADR, and compounds **60**–**62** were identified as potent MDR modulators (Table 19). They enhanced the efficacy of antitumor drug ADR to about 20 folds at 5 μM (Zhang et al., 2020).

By SAR studies, it was concluded that the presence of an aromatic component on the lathyrane scaffold significantly improved the inhibition of Rh123 efflux (Reis et al., 2020).

## Clerodanes

Some diterpenoids were extracted from *Sindora sumatrana* (Fabaceae) and their effects on ABCB1 in a ADR-resistant human breast cancer cell line were investigated (Table 20). Among them, compound **63** inhibited the function of ABCB1, which increased the accumulation of ADR by more than four times. Research on SAR indicated that the furan ring had an important effect on its inhibitory activity (Jung et al., 2010).

The ability to modulate the MDR by compounds **64**–**66** was assayed in the MCF-7 cancer cell line (**Table 3**). The results showed that compounds **64**–**66** were less active as MDR modulators than teotihuacanin, a rearranged clerodane diterpene with potent modulatory activity of MDR in the MCF-7 cancer cell line resistant to vinblastine (Bautista et al., 2016).

## Pimaranes

Compounds **67** and **68** were isolated from *Ephemerantha lonchophylla* (Orchidaceae) (**Table 4**). Both of them showed the capability to sensitize B16/hMDR-1 cells with MDR phenotype to the toxicity of the anticancer drug ADR However, both compounds were very weak inhibitors of ABCB1, with $ED_{50}$ values of 193 and 195 μM for compounds **67** and **68**, respectively. In contrast, the $ED_{50}$ of verapamil, an effective ABCB1 inhibitor, was approximately 3 μM (Ma et al., 1998).

**TABLE 4 |** Pimaranes.

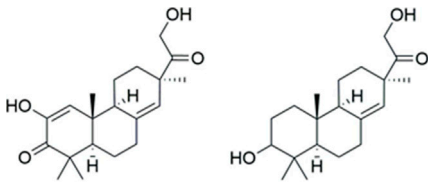

67 68

| Compound | Name | Plant | Ref |
|---|---|---|---|
| **67** | lonchophylloid A | *E.lonchophylla* | Ma et al. (1998) |
| **68** | lonchophylloid B | *E.lonchophylla* | Ma et al. (1998) |

## Ingenanes

Compound **69** and compound **70** were isolated from *Euphorbia kansui* (**Table 5**). Compound **70** showed significant MDR reversal activity and compound **69** exhibited moderate MDR reversal activity in HepG-2/ADR cells (RF = 186.4 at 3.87 μM and 57.4 at 12.6 μM, respectively) (Wang S et al., 2021).

Two undescribed compounds (**71** and **72**) were isolated from *Euphorbia kansui* (**Table 5**). The results showed that compounds **71** and **72** were potent low-cytotoxic MDR modulators with greater ability to reverse MDR than verapamil on ADR resistant human breast adenocarcinoma cell line MCF-7/ADR (RF = 21.5 and 18.8 at 5 μM, respectively) (Chen et al., 2021).

## Segetane

Compound **73** was isolated from *Euphorbia taurinensis* (**Table 6**). It showed significant MDR modulating effect (FAR = 44.44 at 20 μM) in the L5178 mouse lymphoma cell line (Redei et al., 2018).

**TABLE 5 |** Ingenanes.

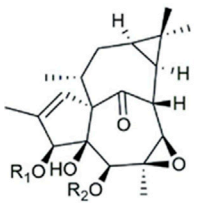

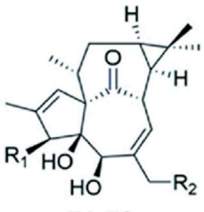

| | $R_1$ | $R_2$ |
|---|---|---|
| 69 | Ac | Bz |
| 70 | Bz | H |

| | $R_1$ | $R_2$ |
|---|---|---|
| 71 | -O-CO-CH($CH_3$)-CH($CH_3$)$_2$ | OH |
| 72 | OH | -O-CO-CH($CH_3$)-CH($CH_3$)$_2$ |

| Compound | Name | Plant | Ref |
|---|---|---|---|
| **69** | euphorksol A | *E. kansui* | Wang S et al. (2021) |
| **70** | 6β,7β-epoxy- 3β,4β,5β-trihydroxyl-20-deoxyingenol | *E. kansui* | Wang S et al. (2021) |
| **71** | kansuininol A | *E. kansui* | Chen et al. (2021) |
| **72** | kansuininol B | *E. kansui* | Chen et al. (2021) |

**TABLE 6 |** Segetanes.

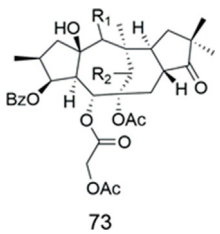

73

| Compound | Name | Plant | Ref |
|---|---|---|---|
| **73** | 6,14-Diacetoxy-5-(2-acetoxyacetoxy)-3-benzoyloxy-15-hydroxy-9-oxo-segetane | *E. taurinensis* | Redei et al. (2018) |

**TABLE 7 |** Briaranes.

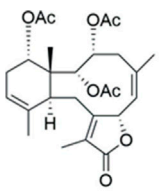

74

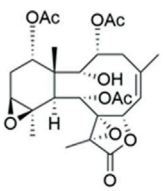

75

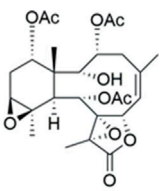

76

| Compound | Name | Source | Ref |
|---|---|---|---|
| **74** | brianthein A | *B. excavatum* | Aoki et al. (2001) |
| **75** | brianthein B | *B. excavatum* | Aoki et al. (2001) |
| **76** | brianthein C | *B. excavatum* | Aoki et al. (2001) |

**TABLE 8 |** Jatropholane.

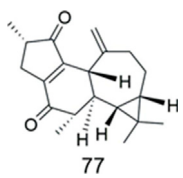

77

| Compound | Name | Plant | Ref |
|---|---|---|---|
| **77** | sikkimenoid A | *E. macrorrhiza* | Gao et al. (2016) |

## Briaranes

Compounds **74**–**76** were isolated from the gorgonian *Briareum excavatum* (Briareidae) (**Table 7**). Compound **74** completely reversed the resistance to colchicine in KB-C2 cells and showed weak cytotoxicity at 10 μg/ml. From the SAR study, each of the double bond at C-11 and 2,3 and 14-acetoxyl groups in compound **74** were found to be essential to the MDR reversing activity (Aoki et al., 2001).

**TABLE 9 |** Pseudolaric acid.

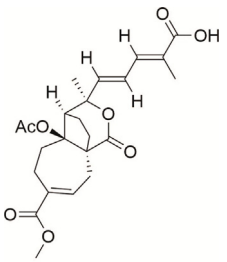

78

| Compound | Name | Plant | Ref |
|---|---|---|---|
| **78** | pseudolaric acid B | *P. kaempferi* | Wong et al. (2005)<br>Sun and Li, (2014)<br>Yu et al. (2015) |

## Jatropholane

Compound **77** was isolated from *Euphorbia macrorrhiza* (**Table 8**). It was tested for cytotoxicity by MTT assay in the human oral epidermoid carcinoma (KB) cell line, using its navelbine-selected ABCB1 overexpressing (KBv200) cell line as experimental model. It was found to exhibit weak cytotoxicity against both KB and resistant KBv200 sublines. Compound **77** was tested along with the classic chemotherapeutic drug navelbine for modulability of MDR against a KBv200 cell line that overexpresses ABCB1 in which verapamil, a well-known chemosensitizer, was used as the positive control. The $IC_{50}$ values for navelbine in combination with compound **77** decreased (from 2.14 to 0.48 μM), suggesting that compound **77** had MDR reversal potential. However, compound **77** was much less active in the MDR reversal assay (RF = 4.47 at 10 μM), compared to that of the positive control (RF = 43.63 at 10 μM) (Gao et al., 2016).

**TABLE 10 |** Taxanes.

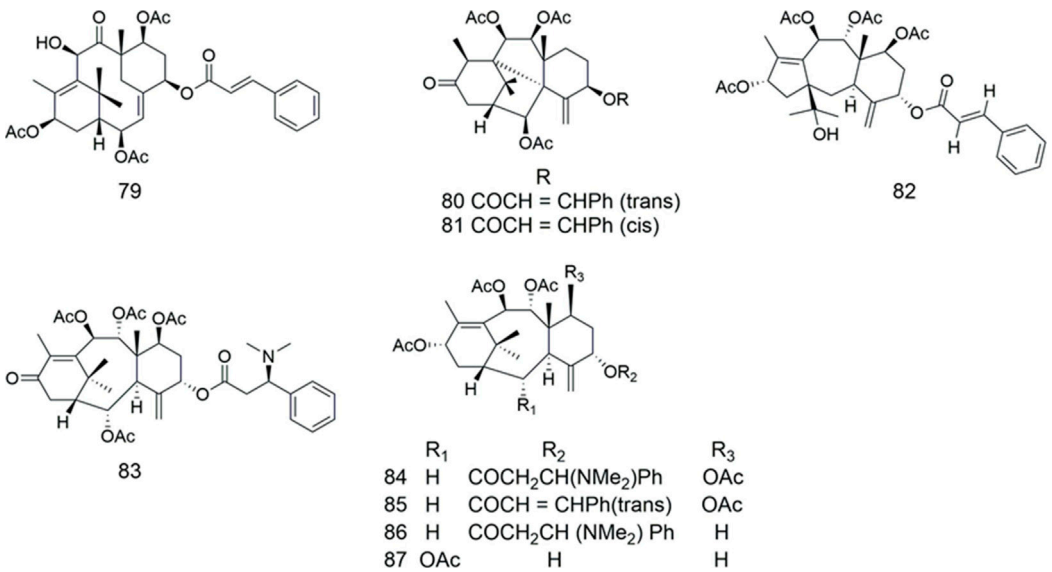

79

R
80 COCH = CHPh (trans)
81 COCH = CHPh (cis)

82

83

| | $R_1$ | $R_2$ | $R_3$ |
|---|---|---|---|
| 84 | H | $COCH_2CH(NMe_2)Ph$ | OAc |
| 85 | H | COCH = CHPh(trans) | OAc |
| 86 | H | $COCH_2CH(NMe_2)Ph$ | H |
| 87 | OAc | H | H |

| Compound | Name | Plant | Ref |
|---|---|---|---|
| **79** | taxuspine B | *T. cuspidata* | Kobayashi et al. (1994)<br>Kobayashi et al. (1997) |
| **80** | taxuspine C | *T. cuspidata* | Kobayashi et al. (1994)<br>Kobayashi et al. (1997)<br>Kobayashi et al. (1998) |
| **81** | 7H-6a,10-Methano-1H-benz [c]azulene, 2-propenoic acid deriv | *T. cuspidata* | Kobayashi et al. (1994) |
| **82** | taxuspine J | *T. cuspidata* | Kobayashi et al. (1997) |
| **83** | taxine II | *T. cuspidata* | Kobayashi et al. (1997) |
| **84** | 2-desacetoxyaustrospicatine | *T. cuspidata* ;<br>*T. mairei* | Kobayashi et al. (1994)<br>Kobayashi et al. (1997) |
| **85** | 2-desacetoxytaxinine J | *T. cuspidata* | Kobayashi et al. (1997) |
| **86** | 7,2′-didesacetoxyaustrospicatine | *T. cuspidata* | Kobayashi et al. (1997) |
| **87** | 2-decinnamoyltaxinine J | *T. cuspidata* | Kobayashi et al. (1997) |

**TABLE 11 |** Euphoractine.

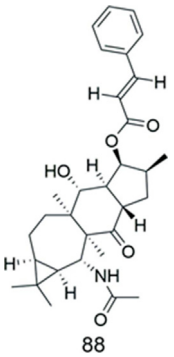

88

| Compound | Name | Plant | Ref |
|---|---|---|---|
| **88** | sooneuphoramine | *E.soongarica* | Gao and Asia, (2017) |

## Pseudolaric Acid

Compound **78** was isolated from *Pseudolarix amabilis* (Pinaceae) (**Table 9**). A study was conducted on the efficacy of compound **78** toward MDR phenotypes in a ABCB1-overexpressing cell line. The results showed that compound **78** circumvented MDR induced by ABCB1 overexpression (Wong et al., 2005). Sun et al. carried a study on the underlying molecular mechanisms involved in the MDR reversing activity of compound **78**. It was demonstrated that compound **78** (5, 10, and 20 μmol/L) alone or in combination with ADR could inhibit protein expression levels of ABCB1, and reversed MDR of gastric neoplasm to anticancer drugs by downregulating the Cox-2/PKC-α/ABCB1/mdr1 signaling pathway in human gastric cancer SGC7901/ADR Cells (Sun and Li, 2014). Other studies have reached similar conclusions (Yu et al., 2015).

## Taxanes

Compounds **79–81** (**Table 10**) were isolated from Japanese yew *Taxus cuspidata* (Taxaceae). In all compounds but one, these taxoids (10 μg/ml) increased cellular accumulation of vincristine in multidrug-resistant 2780AD cells (Kobayashi et al., 1994). Some taxoids were isolated from Japanese yew *Taxus cuspidata*, among which compounds **79–80, 82–86** increased cellular accumulation of vincristine in multidrug-resistant human ovarian cancer 2780AD cells as potent as verapamil (Kobayashi et al., 1997). Regardless natural or designed, some taxoids may be good regulators of MDR in cancer chemotherapy (Kobayashi et al., 1998). The research also showed that compound **80** interacted directly with ABCB1 and overcome MDR *in vivo*, like verapamil (Kobayashi et al., 2010). The 6/8/6-membered ring system of some taxanes took commonly "cage"-like backbone structures, which might be important for their effective affinity to ABCB1 (Kobayashi and Shigemori, 2002).

## Euphoractine

Compound **88** was isolated from *Euphorbia soongarica* (**Table 11**). It was tested for MDR reversal activity using the Rh123 accumulation assay in KBv200 cell lines. The results showed that its activity against MDR was lower than that of verapamil (FAR = 0.63 at 10 μM), which was inactive (Gao and Aisa, 2017).

# CONCLUSIONS

In summary, many diterpenic structures showed MDR-reversal potential. Most of the diterpenoids with significant activity against MDR were jatrophane and lathyrane macrocyclic diterpenes isolated from *Euphorbia* species. Aiming at optimizing the structures of diterpenes for reversing MDR, some researchers have prepared hemi-synthetic derivatives, allowing SAR studies.

Inhibiting of ABCB1 function or expression can reverse ABCB1-mediated MDR in cancer cells, which can increase the efficacy of chemotherapy. For the compounds mentioned in this review, inhibiting ABCB1 function was the most common mechanism. For example, compound **10** exhibited superior MDR reversal effect in MCF-7/ADR cells due to the enhancement of ATPase. In addition, compound **10** did not downregulate expression of ABCB1 and mRNA levels in MCF-7/ADR cells (Yang et al., 2021). The most common drug-resistant cell lines involved in this review are HepG2/ADR and MCF-7/ADR cell lines. Most of the active diterpenes were lipophilic compounds, thus corroborating previous studies that defined effective ABCB1 modulator candidates should have a log *p* value of 2.92 or higher (Wang et al., 2003). SAR studies on macrocyclic diterpenes emphasized the importance of an aromatic moiety for ABCB1 binding, through electronic and steric interactions (Reis et al., 2013).

However, most of the works reported focused on cell experiments *in vitro*, and only few studies moved forward to the experiment *in vivo* and showed a certain effect (Zhu et al., 2016; Fang et al., 2018). Thus, further in-depth *in vivo* studies of these compounds are urgently needed (Dong et al., 2020). Moreover, pharmacokinetics studies and the evaluation of the potential toxicity of compounds should also be carried out. Some researchers synthesized a series of derivatives and studied their SAR on the basis of retaining the pharmacodynamic groups of diterpenes (Wang et al., 2020).

Also, the mechanisms of their action were studied by cell biology and molecular biotechnology, which showed that they were being further developed. It is expected to obtain compounds with strong activity and good water solubility, and further confirm their pharmacological activity in *in vivo* experiments. It would also important to assess the ability of these compounds to modulate other ABC transporters involved in MDR, namely ABCC1 and ABCG2.

According to the different structures, the MDR activities of some diterpenoids were described based on their structures. Most of the diterpenoids with good activity against MDR, such as jatrophanes, ingenanes and lathyranes, were isolated from *Euphorbia* species. Some compounds from other species, such as *Pseudolarix*, *Taxus*, *Briareum*, *Sindora* species and so on, also have shown certain reversal activity. Therefore, there is great hope to find more lead compounds from those species, which can reverse MDR and enhance the sensitivity of cancer cells to chemotherapeutic drugs. Overall, diterpenoids with

good activity against MDR and low toxicity from natural sources could be developed into lead compounds of new drugs. The structures of diterpenes have important guiding significance for further searching for new drugs to reverse tumor MDR.

## AUTHOR CONTRIBUTIONS

J-yZ, MJUF and AD designed and revised this review article. Z-fD, IB and HY wrote the manuscript. Z-fD drawed the chemical structures. IB, JH and HY collected important background information and amended the text. All authors agreed with the final version of this manuscript.

## FUNDING

This work was supported by National Key R&D Program of China (2021YFE0202000), National Natural Science Foundation of China (U1903126), Fund of Guangdong Education Department (2021ZDZX2006), the Natural Science Foundation of Guangdong Province (2020A1515010605) and Fundação para a Ciência e a Tecnologia (FCT), Portugal (PTDC/MED-QUI/30591/2017).

## REFERENCES

Aljančić, I. S., Pešić, M., Milosavljević, S. M., Todorović, N. M., Jadranin, M., Milosavljević, G., et al. (2011). Isolation and Biological Evaluation of Jatrophane Diterpenoids from Euphorbia Dendroides. *J. Nat. Prod.* 74, 1613–1620. doi:10.1021/np200241c

Aoki, S., Okano, M., Matsui, K., Itoh, T., Satari, R., Akiyama, S.-i., et al. (2001). Brianthein A, a Novel Briarane-type Diterpene Reversing Multidrug Resistance in Human Carcinoma Cell Line, from the Gorgonian Briareum Excavatum. *Tetrahedron* 57, 8951–8957. doi:10.1016/S0040-4020(01)00894-8

Bautista, E., Fragoso-Serrano, M., Ortiz-Pastrana, N., Toscano, R. A., and Ortega, A. (2016). Structural Elucidation and Evaluation of Multidrug-Resistance Modulatory Capability of Amarissinins A-C, Diterpenes Derived from Salvia Amarissima. *Fitoterapia* 114, 1–6. doi:10.1016/j.fitote.2016.08.007

Borst, P., and Elferink, R. O. (2002). Mammalian ABC Transporters in Health and Disease. *Annu. Rev. Biochem.* 71, 537–592. doi:10.1146/annurev.biochem.71.102301.093055

Bukowski, K., Kciuk, M., and Kontek, R. (2020). Mechanisms of Multidrug Resistance in Cancer Chemotherapy. *Int. J. Mol. Sci.* 21. doi:10.3390/ijms21093233

Chen, C. Y., Lin, C. M., Lin, H. C., Huang, C. F., Lee, C. Y., Si Tou, T. C., et al. (2017). Structure-activity Relationship Study of Novel 2-aminobenzofuran Derivatives as P-Glycoprotein Inhibitors. *Eur. J. Med. Chem.* 125, 1023–1035. doi:10.1016/j.ejmech.2016.08.044

Chen, Y., Luo, D., Chen, N.-Y., Zhang, Y., Liang, D.-E., Zhan, Z.-J., et al. (2021). New Ingenane Diterpenoids from Euphorbia Kansui Reverse Multi-Drug Resistance. *Phytochemistry Lett.* 43, 169–172. doi:10.1016/j.phytol.2021.03.023

Corea, G., Fattorusso, E., Lanzotti, V., Motti, R., Simon, P. N., Dumontet, C., et al. (2004). Jatrophane Diterpenes as Modulators of Multidrug Resistance. Advances of Structure-Activity Relationships and Discovery of the Potent lead Pepluanin A. *J. Med. Chem.* 47, 988–992. doi:10.1021/jm030951y

Corea, G., Fattorusso, E., Lanzotti, V., Taglialatela-Scafati, O., Appendino, G., Ballero, M., et al. (2003). Jatrophane Diterpenes as P-Glycoprotein Inhibitors. First Insights of Structure-Activity Relationships and Discovery of a New, Powerful lead. *J. Med. Chem.* 46, 3395–3402. doi:10.1021/jm030787e

Dong, J., Qin, Z., Zhang, W. D., Cheng, G., Yehuda, A. G., Ashby, C. R., Jr., et al. (2020). Medicinal Chemistry Strategies to Discover P-Glycoprotein Inhibitors: An Update. *Drug Resist. Updat.* 49, 100681. doi:10.1016/j.drup.2020.100681

Dong, J., Zhai, B., Sun, W., Hu, F., Cheng, H., and Xu, J. (2017). Activation of Phosphatidylinositol 3-kinase/AKT/snail Signaling Pathway Contributes to Epithelial-Mesenchymal Transition-Induced Multi-Drug Resistance to Sorafenib in Hepatocellular Carcinoma Cells. *PLoS One* 12, e0185088. doi:10.1371/journal.pone.0185088

Duarte, N., Gyémánt, N., Abreu, P. M., Molnár, J., and Ferreira, M. J. U. (2006). New Macrocyclic Lathyrane Diterpenes, from Euphorbia Lagascae, as Inhibitors of Multidrug Resistance of Tumour Cells. *Planta Med.* 72, 162–168. doi:10.1055/s-2005-873196

Duarte, N., Varga, A., Cherepnev, G., Radics, R., Molnár, J., and Ferreira, M. J. U. (2007). Apoptosis Induction and Modulation of P-Glycoprotein Mediated Multidrug Resistance by New Macrocyclic Lathyrane-type Diterpenoids. *Bioorg. Med. Chem.* 15, 546–554. doi:10.1016/j.bmc.2006.09.028

Fang, Y., Sun, J., Zhong, X., Hu, R., Gao, J., Duan, G., et al. (2018). ES2 Enhances the Efficacy of Chemotherapeutic Agents in ABCB1-Overexpressing Cancer Cells *In Vitro* and *In Vivo*. *Pharmacol. Res.* 129, 388–399. doi:10.1016/j.phrs.2017.11.001

Ferreira, M. J. U., Gyémánt, N., Madureira, A. M., Tanaka, M., Koós, K., Didziapetris, R., et al. (2005). The Effects of Jatrophane Derivatives on the Reversion of MDR1- and MRP-Mediated Multidrug Resistance in the MDA-MB-231 (HTB-26) Cell Line. *Anticancer Res.* 25, 4173–4178. doi:10.1016/j.cej.2007.11.042

Ferreira, R. J., dos Santos, D. J., Ferreira, M. J. U., and Guedes, R. C. (2011). Toward a Better Pharmacophore Description of P-Glycoprotein Modulators, Based on Macrocyclic Diterpenes from Euphorbia Species. *J. Chem. Inf. Model.* 51, 1315–1324. doi:10.1021/ci200145p

Gao, J., and Aisa, H. A. (2017). Terpenoids from Euphorbia Soongarica and Their Multidrug Resistance Reversal Activity. *J. Nat. Prod.* 80, 1767–1775. doi:10.1021/acs.jnatprod.6b01099

Gao, J., Chen, Q. B., Liu, Y. Q., Xin, X. L., Yili, A., and Aisa, H. A. (2016). Diterpenoid Constituents of Euphorbia Macrorrhiza. *Phytochemistry* 122, 246–253. doi:10.1016/j.phytochem.2015.12.003

Guo, Q., Cao, H., Qi, X., Li, H., Ye, P., Wang, Z., et al. (2017). Research Progress in Reversal of Tumor Multi-Drug Resistance via Natural Products. *Anticancer Agents Med. Chem.* 17, 1466–1476. doi:10.2174/1871520617666171016105704

Hasan, A., Liu, G. Y., Hu, R., and Aisa, H. A. (2019). Jatrophane Diterpenoids from Euphorbia Glomerulans. *J. Nat. Prod.* 82, 724–734. doi:10.1021/acs.jnatprod.8b00507

Hohmann, J., Molnár, J., Rédei, D., Evanics, F., Forgo, P., Kálmán, A., et al. (2002). Discovery and Biological Evaluation of a New Family of Potent Modulators of Multidrug Resistance: Reversal of Multidrug Resistance of Mouse Lymphoma Cells by New Natural Jatrophane Diterpenoids Isolated from Euphorbia Species. *J. Med. Chem.* 45, 2425–2431. doi:10.1021/jm0111301

Holohan, C., Van Schaeybroeck, S., Longley, D. B., and Johnston, P. G. (2013). Cancer Drug Resistance: an Evolving Paradigm. *Nat. Rev. Cancer* 13, 714–726. doi:10.1038/nrc3599

Hu, R., Gao, J., Rozimamat, R., and Aisa, H. A. (2018). Jatrophane Diterpenoids from Euphorbia Sororia as Potent Modulators against P-Glycoprotein-Based Multidrug Resistance. *Eur. J. Med. Chem.* 146, 157–170. doi:10.1016/j.ejmech.2018.01.027

Jadranin, M., Pešić, M., Aljančić, I. S., Milosavljević, S. M., Todorović, N. M., Podolski-Renić, A., et al. (2013). Jatrophane Diterpenoids from the Latex of Euphorbia Dendroides and Their Anti-P-glycoprotein Activity in Human Multi-Drug Resistant Cancer Cell Lines. *Phytochemistry* 86, 208–217. doi:10.1016/j.phytochem.2012.09.003

Jouan, E., Le Vée, M., Mayati, A., Denizot, C., Parmentier, Y., and Fardel, O. (2016). Evaluation of P-Glycoprotein Inhibitory Potential Using a Rhodamine 123 Accumulation Assay. *Pharmaceutics* 8, 12. doi:10.3390/pharmaceutics8020012

Juliano, R. L., and Ling, V. (1976). A Surface Glycoprotein Modulating Drug Permeability in Chinese Hamster Ovary Cell Mutants. *Biochim. Biophys. Acta* 455, 152–162. doi:10.1016/0005-2736(76)90160-7

Jung, H. J., Chung, S. Y., Nam, J. W., Chae, S. W., Lee, Y. J., Seo, E. K., et al. (2010). Inhibition of P-Glycoprotein-Induced Multidrug Resistance by a Clerodane-type Diterpenoid from Sindora Sumatrana. *Chem. Biodivers.* 7, 2095–2101. doi:10.1002/cbdv.201000010

Kadioglu, O., Saeed, M. E., Valoti, M., Frosini, M., Sgaragli, G., and Efferth, T. (2016). Interactions of Human P-Glycoprotein Transport Substrates and Inhibitors at the Drug Binding Domain: Functional and Molecular Docking Analyses. *Biochem. Pharmacol.* 104, 42–51. doi:10.1016/j.bcp.2016.01.014

Katsetos, C. D., and Dráber, P. (2012). Tubulins as Therapeutic Targets in Cancer: from Bench to Bedside. *Curr. Pharm. Des.* 18, 2778–2792. doi:10.2174/138161212800626193

Katsetos, C. D., Herman, M. M., and Mörk, S. J. (2003). Class III Beta-Tubulin in Human Development and Cancer. *Cell Motil. Cytoskeleton* 55, 77–96. doi:10.1002/cm.10116

Kobayashi, J., Hosoyama, H., Wang, X. X., Shigemori, H., Sudo, Y., and Tsuruo, T. (1998). Modulation of Multidrug Resistance by Taxuspine C and Other Taxoids from Japanese Yew. *Bioorg. Med. Chem. Lett.* 8, 1555–1558. doi:10.1016/s0960-894x(98)00262-5

Kobayashi, J., and Shigemori, H. (2002). Bioactive Taxoids from the Japanese Yew Taxus Cuspidata. *Med. Res. Rev.* 22, 305–328. doi:10.1002/med.10005

Kobayashi, J., Shigemori, H., Hosoyama, H., Chen, Z., Akiyama, S., Naito, M., et al. (2010). Multidrug Resistance Reversal Activity of Taxoids from Taxus Cuspidata in KB-C2 and 2780AD Cells. *Jpn. J. Cancer Res.* 91, 638–642. doi:10.1111/j.1349-7006.2000.tb00993.x

Kobayashi, J. i., Hosoyama, H., Wang, X.-x., Shigemori, H., Koiso, Y., Iwasaki, S., et al. (1997). Effects of Taxoids from Taxus Cuspidata on Microtubule Depolymerization and Vincristine Accumulation in MDR Cells. *Bioorg. Med. Chem. Lett.* 7, 393–398. doi:10.1016/S0960-894X(97)00029-2

Kobayashi, J., Ogiwara, A., Hosoyama, H., Shigemori, H., Yoshida, N., Sasaki, T., et al. (1994). Taxuspines A ~ C, New Taxoids from Japanese Yew Taxus Cuspidata Inhibiting Drug Transport Activity of P-Glycoprotein in Multidrug-Resistant Cells. *Tetrahedron* 50, 7401–7416. doi:10.1016/s0040-4020(01)90470-3

Krstić, G., Jadranin, M., Todorović, N. M., Pešić, M., Stanković, T., Aljančić, I. S., et al. (2018). Jatrophane Diterpenoids with Multidrug-Resistance Modulating Activity from the Latex of Euphorbia Nicaeensis. *Phytochemistry* 148, 104–112. doi:10.1016/j.phytochem.2018.01.016

Kumar, A., and Jaitak, V. (2019). Natural Products as Multidrug Resistance Modulators in Cancer. *Eur. J. Med. Chem.* 176, 268–291. doi:10.1016/j.ejmech.2019.05.027

Li, W., Tang, Y. Q., Sang, J., Fan, R. Z., Tang, G. H., and Yin, S. (2020). Jatrofolianes A and B: Two Highly Modified Lathyrane Diterpenoids from Jatropha Gossypiifolia. *Org. Lett.* 22, 106–109. doi:10.1021/acs.orglett.9b04029

Liu, Q., Cai, P., Guo, S., Shi, J., and Sun, H. (2020). Identification of a Lathyrane-type Diterpenoid EM-E-11-4 as a Novel Paclitaxel Resistance Reversing Agent with Multiple Mechanisms of Action. *Aging (Albany NY)* 12, 3713–3729. doi:10.18632/aging.102842

Liu, Q., Sun, H., Chen, X. G., Li, Y., Chen, H., You, F., et al. (2015). EM-E-11-4 Increases Paclitaxel Uptake by Inhibiting P-Glycoprotein-Mediated Transport in Caco-2 Cells. *J. Asian Nat. Prod. Res.* 17, 649–655. doi:10.1080/10286020.2015.1049535

Lu, J. F., Pokharel, D., and Bebawy, M. (2015). MRP1 and its Role in Anticancer Drug Resistance. *Drug Metab. Rev.* 47, 406–419. doi:10.3109/03602532.2015.1105253

Luo, W., Song, L., Chen, X. L., Zeng, X. F., Wu, J. Z., Zhu, C. R., et al. (2016). Identification of Galectin-1 as a Novel Mediator for Chemoresistance in Chronic Myeloid Leukemia Cells. *Oncotarget* 7, 26709–26723. doi:10.18632/oncotarget.8489

Madureira, A. M., Gyémant, N., Ascenso, J. R., Abreu, P. M., Molnar, J., and Ferreira, M. J. U. (2006). Euphoportlandols A and B, Tetracylic Diterpene Polyesters from Euphorbia Portlandica and Their Anti-MDR Effects in Cancer Cells. *J. Nat. Prod.* 69, 950–953. doi:10.1021/np060046r

Martin, C., Berridge, G., Mistry, P., Higgins, C., Charlton, P., and Callaghan, R. (1999). The Molecular Interaction of the High Affinity Reversal Agent XR9576 with P-Glycoprotein. *Br. J. Pharmacol.* 128, 403–411. doi:10.1038/sj.bjp.0702807

Mollazadeh, S., Sahebkar, A., Hadizadeh, F., Behravan, J., and Arabzadeh, S. (2018). Structural and Functional Aspects of P-Glycoprotein and its Inhibitors. *Life Sci.* 214, 118–123. doi:10.1016/j.lfs.2018.10.048

Molnár, J., Gyémánt, N., Tanaka, M., Hohmann, J., Bergmann-Leitner, E., Molnár, P., et al. (2006). Inhibition of Multidrug Resistance of Cancer Cells by Natural Diterpenes, Triterpenes and Carotenoids. *Curr. Pharm. Des.* 12, 287–311. doi:10.2174/138161206775201893

Na, G. X., Wang, T. S., Yin, L., Pan, Y., Guo, Y. L., LeBlanc, G. A., et al. (1998). Two Pimarane Diterpenoids from Ephemerantha Lonchophylla and Their Evaluation as Modulators of the Multidrug Resistance Phenotype. *J. Nat. Prod.* 61, 112–115. doi:10.1021/np970065o

Neto, S., Duarte, N., Pedro, C., Spengler, G., Molnár, J., and Ferreira, M. J. U. (2019). Effective MDR Reversers through Phytochemical Study of Euphorbia Boetica. *Phytochem. Anal.* 30, 498–511. doi:10.1002/pca.2841

Rédei, D., Kúsz, N., Sátori, G., Kincses, A., Spengler, G., Burián, K., et al. (2018). Bioactive Segetane, Ingenane, and Jatrophane Diterpenes from Euphorbia Taurinensis. *Planta Med.* 84, 729–735. doi:10.1055/a-0589-0525

Reis, M., Ferreira, R. J., Santos, M. M., dos Santos, D. J., Molnár, J., and Ferreira, M. J. U. (2013). Enhancing Macrocyclic Diterpenes as Multidrug-Resistance Reversers: Structure-Activity Studies on Jolkinol D Derivatives. *J. Med. Chem.* 56, 748–760. doi:10.1021/jm301441w

Reis, M. A., Ahmed, O. B., Spengler, G., Molnár, J., Lage, H., and Ferreira, M. J. U. (2016). Jatrophane Diterpenes and Cancer Multidrug Resistance - ABCB1 Efflux Modulation and Selective Cell Death Induction. *Phytomedicine* 23, 968–978. doi:10.1016/j.phymed.2016.05.007

Reis, M. A., Matos, A. M., Duarte, N., Ahmed, O. B., Ferreira, R. J., Lage, H., et al. (2020). Epoxylathyrane Derivatives as MDR-Selective Compounds for Disabling Multidrug Resistance in Cancer. *Front. Pharmacol.* 11, 599. doi:10.3389/fphar.2020.00599

Reis, M. A., Paterna, A., Mónico, A., Molnar, J., Lage, H., and Ferreira, M. J. U. (2014). Diterpenes from Euphorbia Piscatoria: Synergistic Interaction of Lathyranes with Doxorubicin on Resistant Cancer Cells. *Planta Med.* 80, 1739–1745. doi:10.1055/s-0034-1383244

Shen, F., Chu, S., Bence, A. K., Bailey, B., Xue, X., Erickson, P. A., et al. (2008). Quantitation of Doxorubicin Uptake, Efflux, and Modulation of Multidrug Resistance (MDR) in MDR Human Cancer Cells. *J. Pharmacol. Exp. Ther.* 324, 95–102. doi:10.1124/jpet.107.127704

Sun, J., Yeung, C. A., Co, N. N., Tsang, T. Y., Yau, E., Luo, K., et al. (2012). Clitocine Reversal of P-Glycoprotein Associated Multi-Drug Resistance through Down-Regulation of Transcription Factor NF-Kb in R-HepG2 Cell Line. *PLoS One* 7, e40720. doi:10.1371/journal.pone.0040720

Sun, Q., and Li, Y. (2014). The Inhibitory Effect of Pseudolaric Acid B on Gastric Cancer and Multidrug Resistance via Cox-2/pkc-A/p-Gp Pathway. *PLoS One* 9, e107830. doi:10.1371/journal.pone.0107830

Szöllősi, D., Rose-Sperling, D., Hellmich, U. A., and Stockner, T. (2018). Comparison of Mechanistic Transport Cycle Models of ABC Exporters. *Biochim. Biophys. Acta Biomembr.* 1860, 818–832. doi:10.1016/j.bbamem.2017.10.028

Takano, M., Yumoto, R., and Murakami, T. (2006). Expression and Function of Efflux Drug Transporters in the Intestine. *Pharmacol. Ther.* 109, 137–161. doi:10.1016/j.pharmthera.2005.06.005

Teng, Y. N., Wang, Y., Hsu, P. L., Xin, G., Zhang, Y., Morris-Natschke, S. L., et al. (2018). Mechanism of Action of Cytotoxic Compounds from the Seeds of Euphorbia Lathyris. *Phytomedicine* 41, 62–66. doi:10.1016/j.phymed.2018.02.001

Thomas, H., and Coley, H. M. (2003). Overcoming Multidrug Resistance in Cancer: an Update on the Clinical Strategy of Inhibiting P-Glycoprotein. *Cancer Control* 10, 159–165. doi:10.1177/107327480301000207

Valente, C., Ferreira, M. J. U., Abreu, P. M., Gyémánt, N., Ugocsai, K., Hohmann, J., et al. (2004). Pubescenes, Jatrophane Diterpenes, from Euphorbia Pubescens, with Multidrug Resistance Reversing Activity on Mouse Lymphoma Cells. *Planta Med.* 70, 81–84. doi:10.1055/s-2004-815464

Valente, I., Reis, M., Duarte, N., Serly, J., Molnár, J., and Ferreira, M. J. U. (2012). Jatrophane Diterpenes from Euphorbia Mellifera and Their Activity as P-Glycoprotein Modulators on Multidrug-Resistant Mouse Lymphoma and Human colon Adenocarcinoma Cells. *J. Nat. Prod.* 75, 1915–1921. doi:10.1021/np3004003

Vasas, A., Sulyok, E., Rédei, D., Forgo, P., Szabó, P., Zupkó, I., et al. (2011). Jatrophane Diterpenes from Euphorbia esula as Antiproliferative Agents and Potent Chemosensitizers to Overcome Multidrug Resistance. *J. Nat. Prod.* 74, 1453–1461. doi:10.1021/np200202h

Wang, C., Wang, X., Sun, Y., Taouil, A. K., Yan, S., Botchkina, G. I., et al. (2020). Design, Synthesis and SAR Study of 3rd-Generation Taxoids Bearing 3-CH3, 3-CF3O and 3-CHF2O Groups at the C2-Benzoate Position. *Bioorg. Chem.* 95, 103523. doi:10.1016/j.bioorg.2019.103523

Wang, J. Q., Yang, Y., Cai, C. Y., Teng, Q. X., Cui, Q., Lin, J., et al. (2021). Multidrug Resistance Proteins (MRPs): Structure, Function and the Overcoming of Cancer Multidrug Resistance. *Drug Resist. Updat.* 54, 100743. doi:10.1016/j.drup.2021.100743

Wang, R. B., Kuo, C. L., Lien, L. L., and Lien, E. J. (2003). Structure-activity Relationship: Analyses of P-Glycoprotein Substrates and Inhibitors. *J. Clin. Pharm. Ther.* 28, 203–228. doi:10.1046/j.1365-2710.2003.00487.x

Wang, S., Li, J., Liu, D., Yang, T., Chen, X., and Li, R. (2021). Ingenane and Jatrophane-type Diterpenoids from Euphorbia Kansui with Multidrug Resistance Reversal Activity. *Phytochemistry* 188, 112775. doi:10.1016/j.phytochem.2021.112775

Wong, V. K., Chiu, P., Chung, S. S., Chow, L. M., Zhao, Y. Z., Yang, B. B., et al. (2005). Pseudolaric Acid B, a Novel Microtubule-Destabilizing Agent that Circumvents Multidrug Resistance Phenotype and Exhibits Antitumor Activity *In Vivo*. *Clin. Cancer Res.* 11, 6002–6011. doi:10.1158/1078-0432.CCR-05-0209

Wu, C., Li, M., Meng, H., Liu, Y., Niu, W., Zhou, Y., et al. (2019). Analysis of Status and Countermeasures of Cancer Incidence and Mortality in China. *Sci. China Life Sci.* 62, 640–647. doi:10.1007/s11427-018-9461-5

Yang, H., Mamatjan, A., Tang, D., and Aisa, H. A. (2021). Jatrophane Diterpenoids as Multidrug Resistance Modulators from Euphorbia Sororia. *Bioorg. Chem.* 112, 104989. doi:10.1016/j.bioorg.2021.104989

Yang, T., Wang, S., Li, H., Zhao, Q., Yan, S., Dong, M., et al. (2020). Lathyrane Diterpenes from Euphorbia Lathyris and the Potential Mechanism to Reverse the Multi-Drug Resistance in HepG2/ADR Cells. *Biomed. Pharmacotherpharmacother* 121, 109663. doi:10.1016/j.biopha.2019.109663

Yu, F., Li, K., Chen, S., Liu, Y., and Li, Y. (2015). Pseudolaric Acid B Circumvents Multidrug Resistance Phenotype in Human Gastric Cancer SGC7901/ADR Cells by Downregulating Cox-2 and P-Gp Expression. *Cell Biochem. Biophys.* 71, 119–126. doi:10.1007/s12013-014-0170-7

Zhang, J. Y., Lin, M. T., Yi, T., Tang, Y. N., Fan, L. L., He, X. C., et al. (2013). Apoptosis Sensitization by Euphorbia Factor L1 in ABCB1-Mediated Multidrug Resistant K562/ADR Cells. *Molecules* 18, 12793–12808. doi:10.3390/molecules181012793

Zhang, J. Y., Mi, Y. J., Chen, S. P., Wang, F., Liang, Y. J., Zheng, L. S., et al. (2011). Euphorbia Factor L1 Reverses ABCB1-Mediated Multidrug Resistance Involving Interaction with ABCB1 Independent of ABCB1 Downregualtion. *J. Cel. Biochem.* 112, 1076–1083. doi:10.1002/jcb.23021

Zhang, Y., Fan, R. Z., Sang, J., Tian, Y. J., Chen, J. Q., Tang, G. H., et al. (2020). Ingol Diterpenoids as P-glycoprotein-dependent Multidrug Resistance (MDR) Reversal Agents from Euphorbia Marginata. *Bioorg. Chem.* 95, 103546. doi:10.1016/j.bioorg.2019.103546

Zhu, J., Wang, R., Lou, L., Li, W., Tang, G., Bu, X., et al. (2016). Jatrophane Diterpenoids as Modulators of P-glycoprotein-dependent Multidrug Resistance (MDR): Advances of Structure-Activity Relationships and Discovery of Promising MDR Reversal Agents. *J. Med. Chem.* 59, 6353–6369. doi:10.1021/acs.jmedchem.6b00605

**Conflict of Interest:** The authors declare that the research was conducted in the absence of any commercial or financial relationships that could be construed as a potential conflict of interest.

**Publisher's Note:** All claims expressed in this article are solely those of the authors and do not necessarily represent those of their affiliated organizations, or those of the publisher, the editors, and the reviewers. Any product that may be evaluated in this article, or claim that may be made by its manufacturer, is not guaranteed or endorsed by the publisher.

frontiers | Frontiers in Pharmacology

ORIGINAL RESEARCH
published: 01 April 2022
doi: 10.3389/fphar.2022.867128

# Ribociclib Inhibits P-gp-Mediated Multidrug Resistance in Human Epidermoid Carcinoma Cells

*Lei Zhang[1,2,3], Biwei Ye[2,4], Yunfeng Lin[2,4], Yi-Dong Li[1], Jing-Quan Wang[1], Zhuo Chen[2,3], Feng-Feng Ping[5]* and Zhe-Sheng Chen[1]**

[1]Department of Pharmaceutical Sciences, College of Pharmacy and Health Sciences, St. John's University, Queens, NY, United States, [2]State Key Laboratory of Structural Chemistry, Fujian Institute of Research on the Structure of Matter, Chinese Academy of Sciences, Fuzhou, China, [3]University of Chinese Academy of Sciences, Beijing, China, [4]Fujian Agriculture and Forestry University, Fuzhou, China, [5]Department of Reproductive Medicine, Wuxi People's Hospital Affiliated to Nanjing Medical University, Wuxi, China

The efficacy of cancer chemotherapy can be attenuated or abrogated by multidrug resistance (MDR) in cancer cells. In this study, we determined the effect of the CDK4/6 inhibitor, ribociclib (or LEE011), on P-glycoprotein (P-gp)-mediated MDR in the human epidermoid carcinoma MDR cell line, KB-C2, which is widely used for studying P-gp-mediated MDR in cancers. The incubation of KB-C2 cells with ribociclib (3–9 μM) increased the efficacy of colchicine, a substrate for P-gp. The cell expression of P-gp was down-regulated at both translation and transcription levels. Furthermore, ribociclib produced a 3.5-fold increase in the basal activity of P-gp ATPase, and the concentration required to increase basal activity by 50% ($EC_{50}$) was 0.04 μM. Docking studies indicated that ribociclib interacted with the drug-substrate binding site of P-gp. The short-term and long-term intracellular accumulation of doxorubicin greatly increased in the KB-C2 cells co-cultured with ribociclib, indicating ribociclib inhibited the drug efflux activity of P-gp. The results of our study indicate that LEE011 may be a potential agent for combined therapy of the cancers with P-gp mediated MDR.

**Keywords: cancer, ribociclib-LEE011, multidrug resistance (MDR), cyclin dependent kinases, CDKs 4 and 6, P-glycoprotein (ABCB1 protein)**

OPEN ACCESS

***Edited by:***
*Qianxiong Zhou,*
*Technical Institute of Physics and Chemistry (CAS), China*

***Reviewed by:***
*Zhangfeng Zhong,*
*University of Macau, China*
*Yang Chen,*
*Dalian Institute of Chemical Physics (CAS), China*

****Correspondence:***
*Feng-Feng Ping*
*pingfengfeng2017@njmu.edu.cn*
*Zhe-Sheng Chen*
*chenz@stjohns.edu*

***Specialty section:***
*This article was submitted to Pharmacology of Anti-Cancer Drugs, a section of the journal Frontiers in Pharmacology*

***Received:*** *31 January 2022*
***Accepted:*** *08 March 2022*
***Published:*** *01 April 2022*

***Citation:***
*Zhang L, Ye B, Lin Y, Li Y-D, Wang J-Q, Chen Z, Ping F-F and Chen Z-S (2022) Ribociclib Inhibits P-gp-Mediated Multidrug Resistance in Human Epidermoid Carcinoma Cells. Front. Pharmacol. 13:867128. doi: 10.3389/fphar.2022.867128*

## INTRODUCTION

The cyclin-dependent kinases (CDKs) are members of serine-threonine kinases that regulate the cell cycle and affect cell proliferation and apoptosis (Braun et al., 1998; Diani et al., 2009; Szwarcwort-Cohen et al., 2009; Chung and Bunz, 2010; Hirai et al., 2010; Li et al., 2010; Duan et al., 2015; Rainey et al., 2017; Czudor et al., 2018; Menzl et al., 2019; Liang et al., 2020; Loyer and Trembley, 2020; Robert et al., 2020). They bind to their corresponding cyclin, forming a cyclin-CDK complex, where CDKs catalyze the phosphorylation of certain serine and threonine residues in target proteins, leading to regulation of gene transcription and cell division (Rank et al., 2000). The downregulation of CDK4/6 promotes cellular apoptosis, suppresses tumor proliferation, migration, and invasion (Liu et al., 2014; Guo et al., 2020; Hu et al., 2020). Currently, the CDK4/6 inhibitors, ribociclib, palbociclib and abemaciclib, have been approved by the U.S. Food and Drug Administration (FDA) for the treatment of breast cancer that is hormone receptor-positive and human epidermal growth factor receptor 2-negative, advanced or metastatic (Kwapisz, 2017; Tripathy et al., 2017) In cell-free assays, all three compounds are potent inhibitors of CDK4 and CDK6 ($IC_{50}$ values from 2 to 39 nM) and

ribociclib and abemaciclib inhibit CDK9 ($IC_{50}$ of 1.51 μM and 57 nM, respectively) (Tripathy et al., 2017). Ribociclib induces the dephosphorylation of cyclin Rb, producing $G_1$ phase cell cycle arrest (Aristizabal Prada et al., 2018; Tai et al., 2019). In addition, ribociclib can 1) overcome the resistance of OML1-R cancer cells to radiation (Tai et al., 2019) and 2) increase the anti-tumor efficacy of 5-fluorouracil or everolimus by downregulating the activity of the PI3K-Akt-mTOR and Ras-Raf-MEK-ERK pathways (Aristizabal Prada et al., 2018). Currently, the mechanisms involved in the reversal of MDR cancer by CDK4/6 inhibitors remains to be elucidated (Aristizabal Prada et al., 2018).

P-glycoprotein (P-gp/ABCB1) is an ATP-binding cassette (ABC) transporter that extrudes various anticancer drugs (e.g., paclitaxel, etoposide, vincristine, and doxorubicin) from cancer cells, as well as various endogenous molecules (Kathawala et al., 2015). The structure of P-gp consists of two symmetrical transmembrane domains (TMDs) formed by a group of helixes and two cytoplasmic nucleotide-binding domains (NBDs) in the form of a dimer occluding two ATPs, where the hydrolysis of ATP catalyzes the transport of P-gp substrates out of the cell (Kim and Chen, 2018). The overexpression of P-gp by various cancers can produce multidrug resistance (MDR), defined as the resistance to anticancer drugs that have distinct structures and differing mechanisms of action (Kathawala et al., 2015).

It has been reported that P-gp can significantly decrease the levels of ribociclib in the brain, suggesting that its efficacy may be limited by cancer cells that overexpress P-gp (Martinez-Chavez et al., 2019). Recently, it has been reported that ribociclib reverses the resistance to daunorubicin mediated by P-gp in acute myeloid leukemia cells by interacting with P-gp and inhibiting its efflux activity (Sorf et al., 2020). However, it remains to be ascertained if ribociclib reverses P-gp mediated MDR in solid tumor cells. Therefore, in this study, we determined the effect of ribociclib on P-gp-mediated MDR in cancer, by inhibiting the expression and the drug efflux activity of P-gp in the human epidermoid carcinoma MDR cell line, KB-C2. Our results indicated that ribociclib has effects on the ATPase activity of P-gp and, through direct interaction with P-gp, attenuates the activity of P-gp to extrude its substrate drugs, like colchicine and doxorubicin, further enhances the anticancer therapy efficacy of these drugs.

# MATERIALS AND METHODS

## Cells, Plasmids, and Chemicals

The human epidermoid carcinoma cell line, KB-3-1, was used as the parental cell line. KB-C2, an MDR cell line that is resistant to colchicine due to the overexpression of P-gp, was created by exposing KB-3-1 cells to increasing concentrations of colchicine over a period of at least 2 months (Akiyama et al., 1985; Yoshimura et al., 1989). Both cell lines were kindly provided by Dr Shinichi Akiyama (Kagoshima University, Kagoshima, Japan). KB-3-1 and KB-C2 cells and their CDK4- and CDK6-deleted sublines were cultivated with DMEM supplemented with 10% FBS and 1% penicillin/streptomycin in a humidified incubator containing 5% $CO_2$ at 37°C. CRISPR/Cas9 all-in-one plasmids, encoding single guide RNA (SgRNA) and Cas9, were purchased from GeneCopoeia Inc (Rockville, MD). Because KB-C2 cells are widely used for studying P-gp-mediated MDR in cancers, KB-C2 cells were used to determine the reversal of P-gp-mediated MDR.

Ribociclib was kindly provided by ChemieTek (Indianapolis, IN). Paclitaxel, colchicine, and doxorubicin were purchased form Sigma Chemical Co. (St. Louis, MO). Mouse anti-P-gp, HRP ligated or fluorescent secondary rabbit or goat-anti mouse antibodies, were purchased from Invitrogen, Thermo Fisher (Carlsbad, CA). Mouse-anti-CDK4 and CDK6 antibodies were purchased from R&D Systems (Minneapolis, MN). All other reagents were purchased from VWR International (West Chester, PA).

## Determination of Cell Viability: MTT Assay

Exponentially growing cells were seeded into 96 well plates at $5 \times 10^3$ cells/well. These experiments were conducted in triplicate. After 72 h of incubation, 20 μl of MTT (5 mg/ml) was added to each well. After incubation for an additional 4 h, the medium containing MTT was discarded and replaced with 150 μl of DMSO. The plates were gently shaken until the dark blue-purple crystal were completely dissolved in DMSO. The absorbance was measured at a wavelength of 490 nm, using an ELx 800 Universal Microplate Reader (Bio-Tek, Inc. Winooski, VT). The relative survival rate (%) for the cells was analyzed using the SPSS 20 program (SPSS Inc., Chicago, IL) and the survival rate - drug concentration curves were generated using Origin 9.0 software (OriginLab corporation, Northampton, MA). The concentration of drug required to inhibit cell viability by 50% ($IC_{50}$ value) was determined using Origin 9.0 software.

## Determination of the Efficacy of Ribociclib to Reverse MDR in Human Epidermoid Carcinoma KB-C2 Cancer Cells

Cells were seeded into 96-well plates ($5 \times 10^3$ cells per well) and cultured overnight. The cells were incubated with ribociclib (0, 0.3, 1 and 3 μM) for 1 or 2 h, followed by incubation with gradient concentrations of colchicine and paclitaxel, which are substrates for the P-gp transporter. The $IC_{50}$ values of the anti-cancer drugs were determined using the MTT assay as described above.

## Western Blot Assay

Parental KB-3-1 cells and MDR KB-C2 cells were incubated with 9 μM of ribociclib for 2 h and co-cultured with paclitaxel or colchicine for 24–72 h. Western blot and immune-fluorescence (IF) assays were conducted to determine the effect of ribociclib on the expression of the P-gp protein. For the Western blot assay, the cells were lysed with SDS lysate reagent and separated on a gradient polyacrylamide gel (4%–20%, containing 0.1% SDS). The proteins on the SDS-PAGE gel were transferred to a PVDF membrane. After blocking with 5% milk, the membrane was washed with TBST buffer (150 mM NaCl, 10 mM Tris pH 8.0, 0.1% v/v Tween20) three times, incubated with mouse anti-P-gp

antibody at 4°C for 2 h, adequately washed with TBST, and incubated with goat anti-mouse IgG-HRP (horseradish peroxidase) at RT for 2 h. The membrane was then washed with TBST four times and exposed to the SignalFire™ ECL Reagent developing reagent (Cell Singling Technology, Danvers, MA), and the results were quantified using an AI600 RGB GEL Imaging System (GE, Fairfield, CT) set for the chemiluminescence mode.

## RT-Quantitative-PCR Analysis of *ABCB1* Transcription

RT-PCR of *ABCB1* mRNA level was performed to investigate the influence of ribociclib on the ABCB1 expression on the transcription level. Ribociclib (9 μM) showing the effect of reversing ABCB1 mediated MDR in cancer cells was added to the cell culture medium. The cells cultured without ribociclib were set as control. After 48 h of cell culture, the cells were sampled for mRNA extraction and RT-q-PCR (QuantStudio™ 5 Real-Time PCR System, ThermoFisher Scientific, CA). *ABCB1* and *GAPDH* were the objective and internal reference genes, respectively. Primers for amplification of *ABCB1* gene were: GAAAGTGAAAAGGTTG (Forward), and CTGGCGCTTTGTTCCA (Reverse). Primers for amplification of *GAPDH* gene were ATTGACCTCAACTACA (Forward), and AGAGATGATGACCCTT (Reverse). Expression deviation was calculated according to the formular: Ratio $_{Sample/Control} = 2^{-\Delta\Delta CT}$, where $C_T$ value was automatically calculated by QuantStudio™ Design and Analysis Software v1.3.1 according to the ΔRn-Cycle curve.

## ATPase Activity Assay

The ATPase activity of P-gp was determined using the PREDEASY ATPase Kits (SOLVO Biotechnology, Szeged, Hungary), according to the manufacturer's protocol (Ambudkar, 1998). Briefly, the membranes (20 μg) were incubated in assay buffer (50 mM of MES at pH 6.8, 50 mM of KCl, 5 mM of sodium azide, 2 mM of EGTA, 2 mM of DTT, 1 mM of ouabain and 10 mM of $MgCl_2$). The membrane vesicles from Sf9 cells were provided by the manufacturer, expressing high levels of human ABCB1, were incubated with ribociclib (0.05, 0.1, 0.2, 0.4, 0.6, 0.8, 1, 5, 10 and 20 μM) for 3 min. ATP hydrolysis was initiated by adding 5 mM of Mg-ATP and the reaction was terminated using a 5% SDS solution. Subsequently, the light absorption was measured at 800 nm using a Bio-Rad SmartSpec 30,000 UV/Vis spectrophotometer (Bio-Rad Laboratories, Hercules, CA).

## Efflux of Doxorubicin by Accumulation Assay

Because doxorubicin is a fluorescent substrate that can be extruded from cancer cells by the P-gp transporter (Mi et al., 2010), its intracellular accumulation was used to determine if ribociclib can directly inhibit the efflux function of the P-gp transporter, thereby increasing the accumulation of doxorubicin. The parental and MDR cells were incubated with 9 μM of ribociclib for 1 h. Doxorubicin (0.2 μM) was added and co-incubated with the cells for 2 h. This incubation period and the relatively low concentration of doxorubicin were used to maintain cell viability. The cells were gently washed with PBS buffer three times and lysed using SDS lysate reagent (50 mM, pH 8.0 Tris, 1% SDS, 2 mM of sodium pyrophosphate, 25 mM of β-glycerophosphate, 1 mM of EDTA, 1 mM of $Na_3VO_4$ and 0.5 μg/ml of leupeptin). The fluorescence intensity, an indicator of doxorubicin accumulation, was determined using a SynergyTM 4 Multi-Mode Microplate Reader (Bio Tek Instruments, Inc. VT, Excitation/Emission: 450/550 nm).

For the long-term evaluation of the efflux of doxorubicin, cells were seeded at $3 \times 10^3$ cells per well, cultured for 8 h, and incubated with 9 μM of ribociclib and doxorubicin (1 μM for the MDR KB-C2 cells and 0.1 μM for drug-sensitive KB-3-1 cells to maintain MDR and cell viability above 60%) for 72 h. Because the membrane of the dead or severely apoptotic cells was damaged, which could lead to the inaccurate quantification of the intercellular doxorubicin levels, the distribution of doxorubicin was determined in triplicate, using fluorescent microscopy.

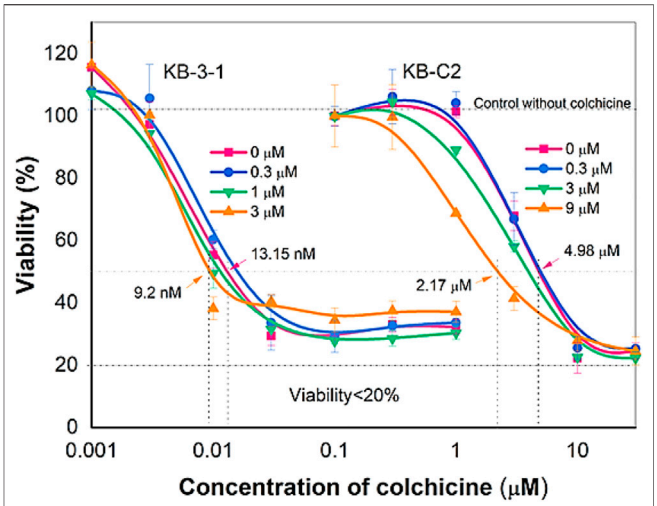


**FIGURE 1 |** Reversal effect of ribociclib on MDR in KB-C2 cell line. Ribociclib reverses MDR in KB-C2 cells but does not significantly affect the efficacy of colchicine in the parental KB-3-1 cells. Ribociclib at 9 μM significantly decreased the $IC_{50}$ of colchicine in KB-C2 cancer cells ($p < 0.05$).

## Docking Analysis of the Interaction of Ribociclib With CDK4, CDK6 and the P-gp Transporter

We first determined the transcripts for the P-gp and CDK4/6 proteins in the KB-C2 cell line. According to the open reading frame (ORF) sequences detected in the major transcripts of P-gp in KB-C2 cell line, the structure was achieved by structure modelling using a Swiss model platform (https://swissmodel.expasy.org/). The interactions between ribociclib and P-gp, CDK4 or CDK6 were calculated using HEX 8.0 software (LORIA/Inria Nancy Research Centre in Nancy, France),

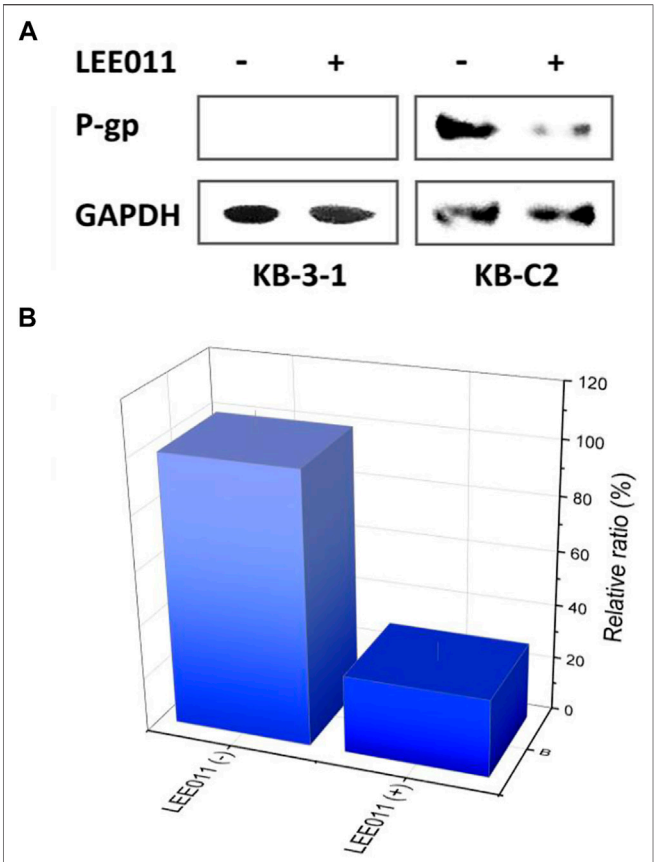


**FIGURE 2 |** ABCB1 expression deviation between the robociclib/LEE011 treated KB-C2 cells and the robociclib non-treated KB-C2 cells. **(A)** Western blot indicated that P-gp expression was significantly downregulated by incubating the cells with 9 μM of ribociclib for 48 h **(B)** *ABCB1* mRNA level was analyzed by RT-q-PCR, using *GAPDH* mRNA as the inner reference. The cells without robociclib treatment were set as control.

based on the most stable calculated structures of the complexes by molecular docking (Kaczor et al., 2013). PyMOL (version 1.8. x) was used to analyze the data and determine the most stable complex structures, binding positions (such as residues or chemical groups) and interactions.

# RESULTS

## Ribociclib Significantly Increases the Efficacy of Colchicine in KB-C2 Cancer Cells Overexpressing the P-gp Transporter

We conducted experiments to determine if ribociclib could increase the efficacy of colchicine (i.e., reversing resistance to colchicine) in MDR KB-C2 cancer cells. As previously reported, colchicine potently decreased ($IC_{50}$ = 13.15 nM) the viability of the colchicine-sensitive KB-3-1 cancer cells (**Figure 1**). In contrast, the $IC_{50}$ value for colchicine was 4.98 μM in the colchicine-resistant KB-C2 cancer cells, indicating these cells were almost three orders of magnitude more resistant to colchicine compared to the parental KB-3-1 cancer cells (**Figure 1**).

Ribociclib non-significantly decreased the $IC_{50}$ value of colchicine in the KB-3-1 cancer cells, whereas in the colchicine-resistant KB-C2 cancer cells, 9 μM of ribociclib significantly decreased the $IC_{50}$ of colchicine in KB-C2 cancer cells (**Figure 1**). These results suggested that the resistance of KB-C2 cancer cells to colchicine, which was mediated by the overexpression of the P-gp transporter[36], could be partially attenuated by ribociclib (**Figure 1**).

## Ribociclib Significantly Down-Regulates the Expression of the P-gp Transporter

It is possible that ribociclib increases the efficacy of colchicine in KB-C2 cancer cells by affecting the expression of the P-gp protein. Therefore, we used Western blotting to determine the effect of ribociclib on P-gp expression. Our results indicated the incubation of KB-C2 cancer cells with 9 μM (a non-toxic concentration) of ribociclib for 72 h produced a significant decrease in the expression of P-gp protein levels compared to cells incubated with vehicle (**Figure 2A**). The remaining P-gp transporters expressed by the KB-C2 cells most likely mediated the lowered drug resistance produced by P-gp (**Figure 2A**). In contrast, P-gp protein expression was not significantly altered in KB-3-1 cancer cells incubated with 9 μM of ribociclib compared to cells incubated with vehicle (**Figure 2A**).

Treatment with ribociclib remarkably downregulated *ABCB1* transcription in the KB-C2 cells (**Figure 2B**). Approximately 5.6% of the *ABCB1* mRNA amounts was detected in the cells treated with ribociclib (9 μM), as compared with that detected in the cells without ribociclib treatment. This conclusion was coherent with the that supported by Western blot (**Figure 2B**). This phenomenom implied that the ribociclib down regulated P-gp at both the translational and transcriptional levels.

## Ribociclib's Interaction With a Human Homology Model of the P-gp Transporter

Although ribociclib showed decent inhibition activity when it binds CDK4 or CDK6 (**Supplementary Figures S1–S4**), we also performed docking analysis experiments to determine if ribociclib interacted with the P-gp transporter and if so, what chemical interactions were involved. Our results indicated that a strong interaction between P-gp and ribociclib existed. Docking studies indicated that ribociclib interacted with the drug-substrate binding site of P-gp, and had a Docking Score/Etotal (Eforce + Eshape, Kalaiselvi et al., 2015) of - 271.06. The molecular modeling indicated electrostatic interactions between N,N-dimethylamide cluster (positively charged with a proton at physiological conditions) in ribociclib and E273 and E1129 (with negative charges), in a trough-like structure between TMDs and NBDs in P-gp, which is adjacent to the interphase of the inner membrane (**Figure 3**, **Figure 4**). Since ribociclib was estimated to bind in a non-representative, drug-substrate pocket of P-gp, it was unknown as to whether this interaction results in a

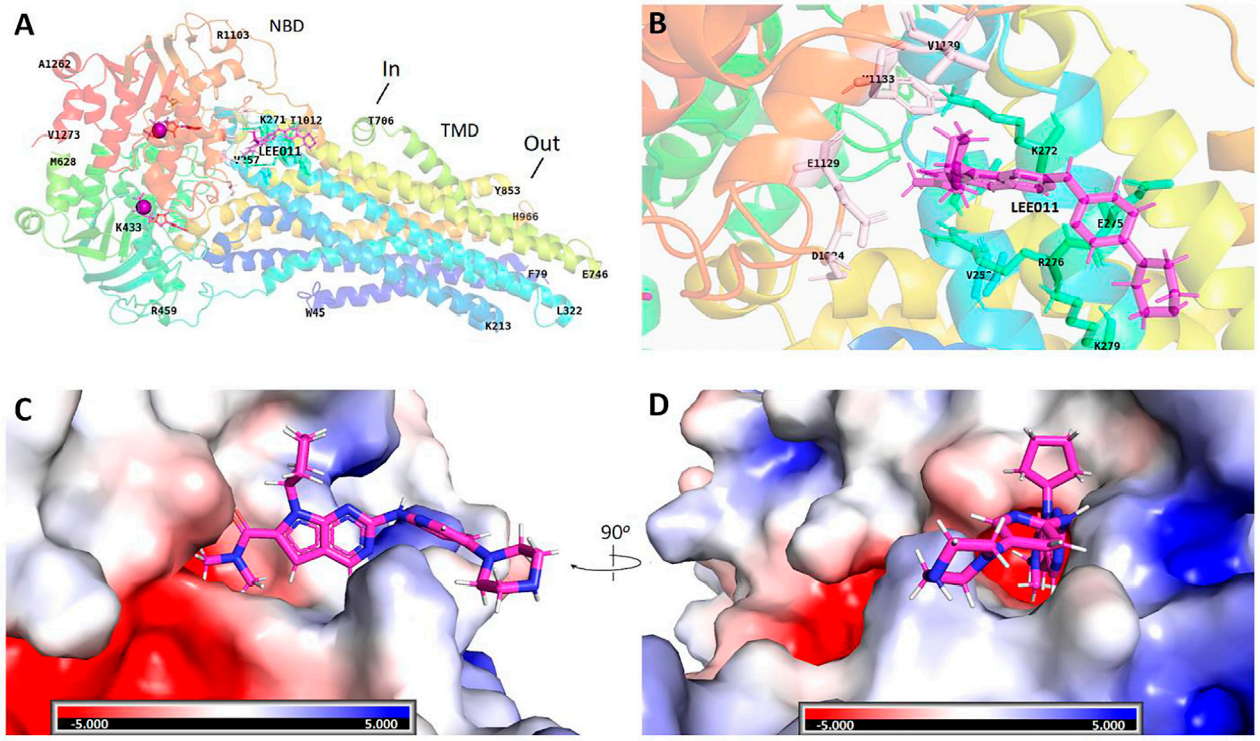


**FIGURE 3 |** Structural basis for the interaction of ribociclib with P-gp. Docking analysis of the 3-dimentional structure of the ribociclib-P-gp complex were performed using HEX 8.0 software. **(A)** Ribociclib interacted with the NBD domain near the interface at the inner side. **(B)** The magnified region showing the amino groups that interact with ribociclib **(C, D)** Spatial structure and charge distributions of the site that binds ribociclib.

change in the efflux function of P-gp, which is frequently associated with a change in the ATPase activity of P-gp and the intracellular accumulation of antitumor drugs (Zhang et al., 2020). Therefore, we conducted experiments to determine if ribociclib affected ATPase activity.

## Ribociclib Increases the ATPase Activity of the P-gp Transporter

Although ribociclib has been reported to be highly efficacious in inhibiting CDK4/6 (Kwapisz, 2017; Tripathy et al., 2017), it remains to be elucidated whether ribociclib interacts with P-gp. Therefore, we conducted experiments to determine if ribociclib 1) interacts directly with P-gp and alters the efflux activity and 2) alters ATPase activity of human P-gp in the membrane vehicles.

Studies have shown that P-gp transporter hydrolyzes ATP, which is involved in drug efflux (Kim and Chen, 2018) and ATPase activity can be stimulated or inhibited by various P-gp substrates (Feng et al., 2020; Wu et al., 2020). It has been postulated that the stimulation of the P-gp ATPase activity by an experimental compound suggests that it is interacting with the transporter at the drug-substrate binding site (Zhang et al., 2020). Therefore, we determined the effect of various concentrations of ribociclib on P-gp ATPase activity. The incubation of membrane vesicles from sf9 insect cells (which express high levels of P-gp) with ribociclib (0.05–20 μM) produced a maximal increase of 3.5-fold in the basal activity of the P-gp transporter ATPase and the $EC_{50}$ value was 0.04 μM (**Figure 5A**). The stimulation of P-gp transporter ATPase activity by ribociclib suggests that it may interact with the transporter at the drug-substrate binding site, although this remains to be definitively proven.

## The Effect of Ribociclib on the Intracellular Accumulation of Doxorubicin in KB-3-1 and KB-C2 Cancer Cells

It is possible that ribociclib reverses the drug resistance of KB-C2 cancer cells by inhibiting the efflux function of P-gp. Therefore, we determined the effect of ribociclib (using a 2 h incubation period) on the intracellular accumulation on doxorubicin, a substrate for the P-gp transporter, in KB-C2 cancer cells. As previously reported (Zhang et al., 2020), the accumulation of doxorubicin was significantly greater in the parental cell line, KB-3-1, compared to MDR KB-C2 cells, which overexpress the P-gp transporter (**Figure 5B**) (Akiyama et al., 1985; Yoshimura et al., 1989). Doxorubicin accumulation was significantly increased in KB-C2 cancer cells incubated with 9 μM of ribociclib compared to cells incubated with vehicle (**Figure 5B**). In contrast, doxorubicin accumulation in the parental KB-3-1 cells, which do not overexpress the P-gp transporter, was not significantly altered by 9 μM of ribociclib. The relationship between the interaction of

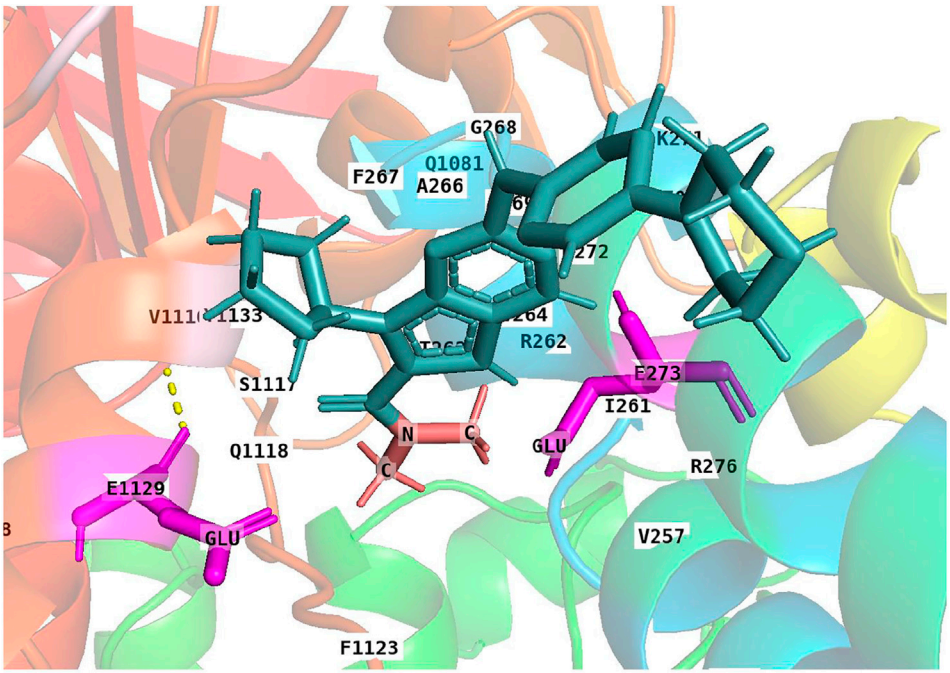


**FIGURE 4 |** A 3-D structural model showing the electrostatic interaction between ribociclib and P-gp. Under physiological conditions, the N,N-dimethylamide cluster is positively charged and may bind to a cavity containing E273 and E1129 with negative charges due to the dissociation of hydrogen protons from the carboxyl group at neutral or higher pH values.

ribociclib with the P-gp transporter and its inhibition of drug efflux and increase in ATPase activity is summarized in **Figure 5C**.

These results indicated that ribociclib increases the ATPase activity of P-gp and inhibits the drug-efflux function of P-gp, suggesting that ribociclib can interact with P-gp directly, which may contribute to the reversal of P-gp-mediated MDR in KB-C-2 cells.

### The Effect of the Incubation of KB-3-1 and KB-C2 Cancer Cells With Ribociclib for 72 h on the Intracellular Accumulation of the P-gp Transporter Substrate, Doxorubicin

These studies were conducted to ascertain if the prolonged incubation (72 h) of KB-3-1 and KB-C2 cancer cells with ribociclib would inhibit the efflux of doxorubicin. The incubation of the parental KB-3-1 cells with 9 μM of ribociclib for 72 h did not significantly alter the intracellular accumulation of doxorubicin compared to cells incubated with vehicle (**Figure 6**). We concluded that the presence of ribociclib had no effect on the accumulation of DOX within KB-3-1 cells, which did not express P-gp and could not extrude DOX efficiently (Zhang et al., 2022). In contrast, doxorubicin accumulation was significantly increased in the KB-C2 cells incubated with 9 μM of ribociclib compared to cells incubated with vehicle (**Figure 6**). Thus, the accumulation of doxorubicin in the KB-C2 cells that overexpress the P-gp transporter is significantly increased after 2 or 72 h of incubation with 9 μM of ribociclib, suggesting that ribociclib increases the intracellular accumulation of doxorubicin by inhibiting the efflux function of P-gp in KB-C2 cells.

## DISCUSSION

Cancers with multidrug resistance caused by overexpression of P-gp are one of the major causes for failure of chemotherapy. Seeking for inhibitors of P-gp is an applicable approach for improving the efficiency of MDR treatment. As previously reported, KB-C2 cancer cells, which overexpress P-gp, were highly resistant to colchicine, a substrate for P-gp (Yang et al., 2014). Ribociclib, at 9 μM, a concentration that did not affect cell viability, significantly decreased the $IC_{50}$ value of colchicine (i.e., decreased drug resistance) in the KB-C2 cells, whereas it had no significant effect on the efficacy of colchicine in the parental KB-3-1 cells (**Figure 1**). To our knowledge, this is the first study to show that ribociclib decreases resistance of KB-C2 cancer cells to colchicine. Subsequently, we conducted studies to determine the mechanism(s) by which ribociclib reverses resistance to the P-gp substrates, colchicine and doxorubicin, in human epidermoid carcinoma KB-C2 cells, which have been frequently used to study P-gp-mediated MDR in cancers (Akiyama et al., 1985; Yoshimura et al., 1989). It is possible that ribociclib could reverse resistance by inhibiting the efflux function and/or the expression of the P-gp transporter,

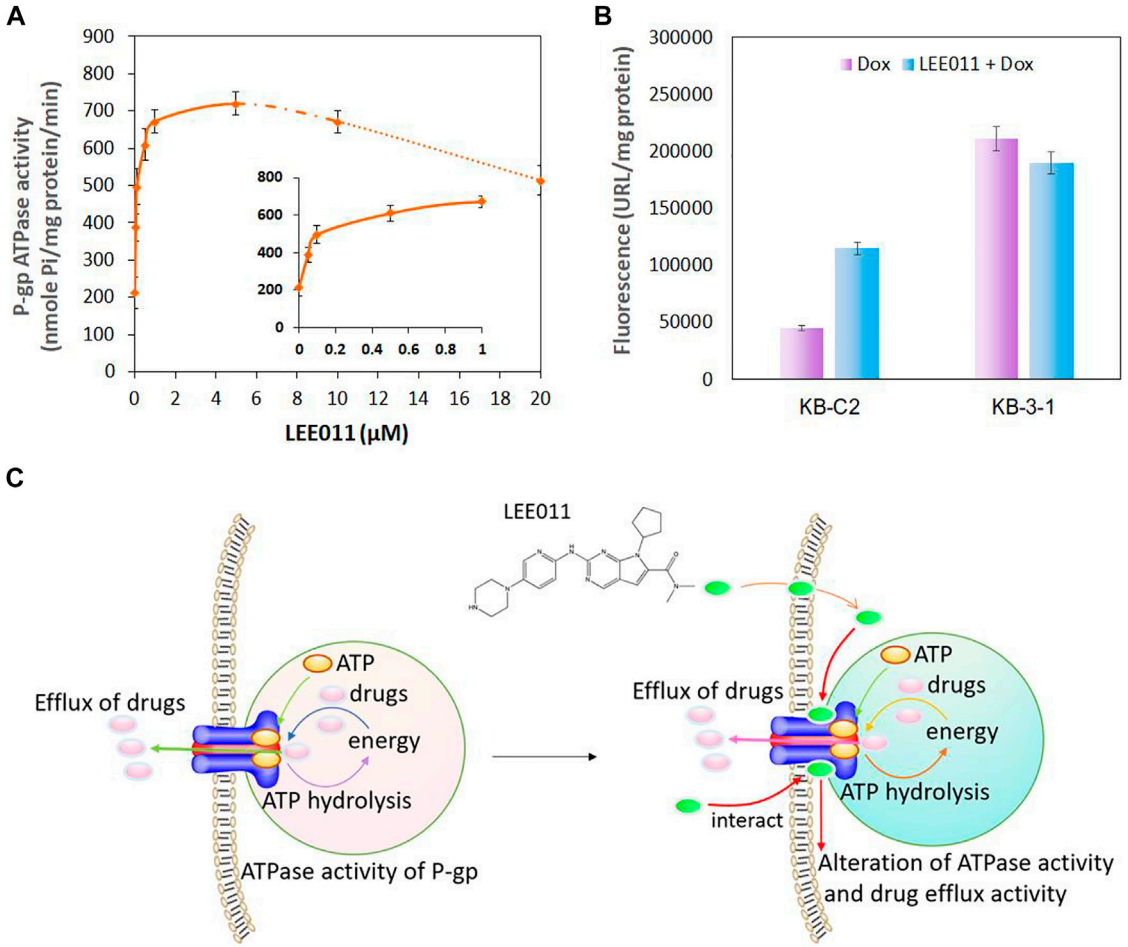


**FIGURE 5 |** The interaction between ribociclib and the P-gp transporter alters the ATPase activity of P-gp and drug efflux activity in KB-C2 cells. **(A)** ATPase activity of P-gp following incubation with ribociclib. **(B)** A comparison of the drug accumulation in MDR KB-C2 cells over-expressing P-gp and the drug sensitive KB-3-1 cells in the presence or absence of ribociclib. The cells were co-cultured with ribociclib (9 μM) and Dox (0.2 μM) for 2 h. The level of Dox fluorescence was measured at 550 nm. **(C)** A Scheme showing that ribociclib alters ATPase activity and drug efflux by interacting with the P-gp transporter.

thereby increasing the intracellular concentration of substrate drugs. Our results indicated that, the intracellular accumulation of doxorubicin, a substrate of P-gp transporter, was significantly decreased in the drug resistant KB-C2 cancer cells compared to the KB-3-1 cancer cells. The incubation of KB-C2 cancer cells with 9 μM of ribociclib, for 2 or 72 h, produced a 2-fold increase in the accumulation of doxorubicin in KB-C2 cells compared to vehicle (**Figure 5**). However, ribociclib did not significantly alter the concentration of doxorubicin in KB-3-1 cancer cells, which do not overexpress the P-gp transporter. Previously, it has been reported that abemaciclib, a CDK4/6 inhibitor (Iriyama et al., 2018), increased the intracellular accumulation of doxorubicin by competitively inhibiting P-gp - or ABCG2-mediated drug efflux in cells overexpressing these transporters (Wu et al., 2017).

These data tentatively suggested that ribociclib can reverse resistance to P-gp substrates in KB-C2 cancer cells by suppressing the expression of P-gp. To further delineate the mechanism of action of ribociclib, we conducted docking study to determine the magnitude of the interaction of ribociclib with a human homology model of the P-gp transporter (**Figure 3**, **Figure 4**). The result showed that ribociclib significantly interacts with the P-gp transporter. In addition to the surface matching and van der Waals interactions, there is a strong electrostatic interaction between the N,N-dimethylamide cluster in ribociclib and the amino acids E273 and E1129 in P-gp protein. These results, in addition to the intracellular drug accumulation data, suggest that ribociclib interacts with the drug-substrate binding pocket of P-gp, further suggesting that it could be a substrate of P-gp that inhibits the binding of other P-gp substrates, such as colchicine and doxorubicin.

Ribociclib could reverse P-gp-mediated MDR by decreasing the expression of the P-gp transporter. Western blot and IF data indicated that the incubation of KB-C2 cells with 9 μM of ribociclib for 72 h significantly decreased the expression level of the P-gp protein compared to cells incubated with vehicle (**Figure 1**). In contrast to our results with ribociclib, it has been

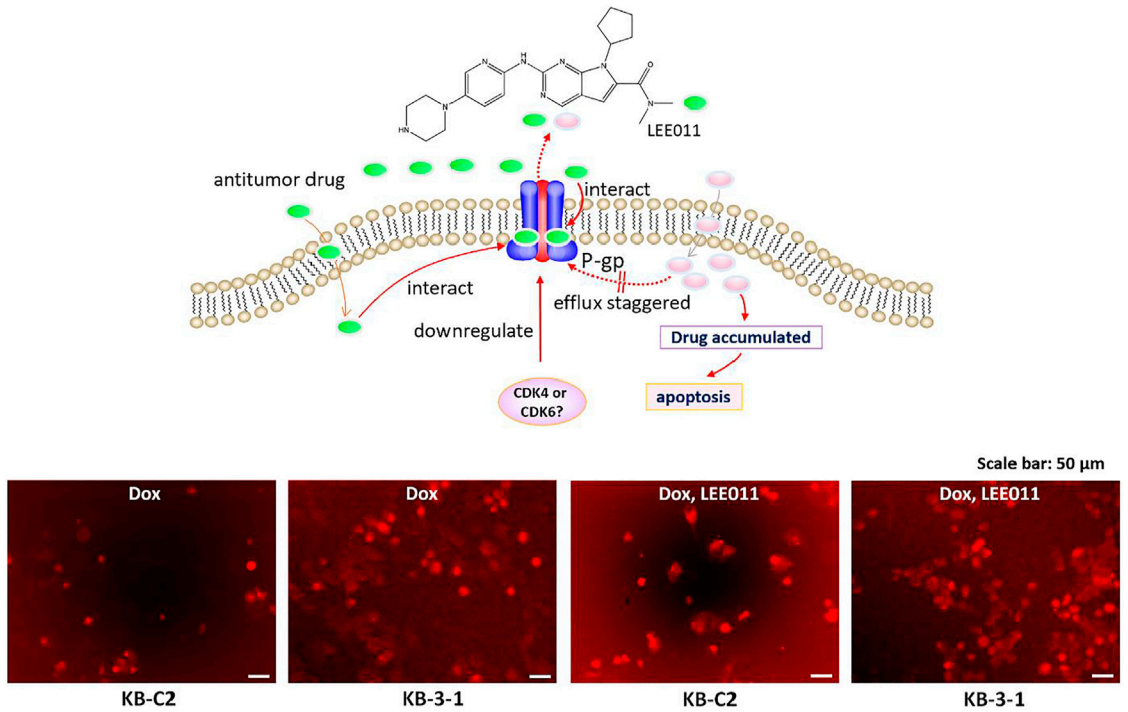


**FIGURE 6 |** Ribociclib significantly increases the accumulation of doxorubicin (Dox) in KB-C2 cells after 72 h of incubation, producing apoptosis or necrosis. KB-C2 and parental KB-3-1 cells were co-cultured with doxorubicin (1 μM for KB-C2 and 0.1 μM for KB-3-1) and ribociclib 1 (9 μM) for 72 h. The cells incubated with vehicle were used as controls. The fluorescence of Dox was imaged using fluorescent microscopy (set to the red fluorescent channel). The schematic figure shows that ribociclib increases the accumulation of Dox by 1) decreasing its efflux, which increases apoptosis and 2) downregulating the levels of P-gp protein expression which also increases the intracellular levels of Dox.

reported that abemaciclib, a CDK4/6 inhibitor, did not significantly alter the expression of the P-gp transporter in cancer cells overexpressing the P-gp transporter (Wu et al., 2017). The exact explanation for the differential effect of abemaciclib and ribociclib on the expression level of the P-gp remains to be determined. However, this could be due to differences in their intracellular accumulation and interaction with their targets. Overall, ribociclib decreases the resistance to colchicine and doxorubicin in KB-C2 cancer cells by 1) interacting with the P-gp protein and inhibiting the efflux function, thereby increasing the intracellular accumulation of these anticancer drugs and 2) decreasing the expression of the P-gp transporter, which decreases the number of transporters and thus, drug efflux.

Studies have reported that certain compounds or drugs can stimulate the ATPase activity of ABC transporters by binding to the substrate-drug binding site (Lee et al., 2019; Li et al., 2020). In this study, ribociclib produced a significant increase (3.5-fold) in the ATPase activity of the P-gp transporter (**Figure 5A**). This result suggests that ribociclib interacts with the substrate-drug binding site which could inhibit the binding of other P-gp transporter substrates, further inhibiting their efflux, thus increasing their intracellular levels. Similarly, voruciclib, a CDK4/6 inhibitor (Gupta et al., 2018; Gupta et al., 2018), significantly increased the ATPase activity of P-gp and inhibited the efflux of paclitaxel or mitoxantrone from human colorectal adenocarcinoma SW620/AD300 cells overexpressing P-gp and non-small cell lung cancer NCI-H460/MX20 cells overexpressing BCRP, respectively, thus reversing the MDR mediated by P-gp and BCRP, respectively (Gupta et al., 2018). However, the expression level of P-gp and BCRP was not significantly altered by the incubation of cells with 5 μM of voruciclib (Gupta et al., 2018). The difference between ribociclib and voruciclib on the expression level of P-gp could be due to their differential interaction with proteins that control the transcription of the P-gp protein, although this remains to be elucidated.

When the KB-C2 cells were cocultured with ribociclib at higher concentrations (exceeding 9 μM), reversal effects on MDR in KB-C2 cells increased. But the cell proliferation was also inhibited when using only ribiciclib (instead of colchicine) higher concentrations. This could be caused by the enhanced inhibition effect on CDK4/6 by a greater number of ribociclib molecules that had entered the cells in addition to their interaction with the membrane P-gp transporters. Thus, the functions of inhibiting cancer cell proliferation and reversing P-gp mediated MDR could synergize each other during combined chemotherapy based on ribociclib and P-gp substrate drugs.

By single gene knockout using CRISPR/Cas9 technique in human epidermoid carcinoma MDR cell line KB-C2, we recently revealed that CDK6-PI3K signaling axis is an efficient target for attenuating ABCB1/P-gp mediated MDR in cancer cells (Zhang et al., 2022). CDK6 knockout downregulated PI3K 110$\alpha$ and 110$\beta$,

and PI3K 110$\alpha$/110$\beta$ deficiency in-return downregulated CDK6. CDK6-PI3K axis synergizes in regulating ABCB1 expression, which further strengthened the regulation of ABCB1 over single regulation by either CDK6 or PI3K 110$\alpha$/110$\beta$.

It will be instructive if we know the mechanisms of the interaction between ribociclib and P-gp, which will benefit modification of the structure of ribociclib and improving its affinity to P-gp. Till now, no study about this aspect has been reported, however, we are still making efforts on its exploration, which is an undergoing project in our laboratories.

In our laboratories, we are currently performing modification and optimization of a serial of combined drug-systems that can reverse MDR in cancers and inhibit cancer cell growth as well. Based on these studies, our tasks in the next stage will contain animal study to testify the biocompatibility and tumor killing efficacy of these drug systems.

In conclusion, the results of this study indicated that in KB-C2 cells, ribociclib inhibited the efflux of the P-gp transporter substrates, doxorubicin and colchicine and decreased the expression of the P-gp transporter, resulting in the reversal of MDR. P-gp expression was downregulated by ribociclib. Furthermore, protein docking data reveals that ribociclib binds near the P-gp transporter drug-substrate binding site and it stimulates the basal activity of the P-gp ATPase. ATPase analysis and drug accumulation experiments further demonstrated that the activity of P-gp was inhibited by ribociclib. Thus, ribiciclib may be a promising inhibiter for the application in combination of anticancer therapies against solid tumor cells with P-gp mediated MDR.

## DATA AVAILABILITY STATEMENT

The original contributions presented in the study are included in the article/**Supplementary Material**, further inquiries can be directed to the corresponding authors.

## AUTHOR CONTRIBUTIONS

LZ and Z-SC conceived this study and designed the experiments; LZ, Z-SC, F-FP, and ZC sponsored the project; LZ performed MTT assay, immunofluorescence analysis, docking, drug accumulation experiments; LZ, BY, and YL performed RT-PCR; LZ and YL performed Western blot; J-QW performed ATPase assay; LZ, YL, and Z-SC analyzed the data and wrote the paper; LZ, Z-SC, YL, and F-FP revised the paper. All authors read and approved the final manuscript.

## FUNDING

We thank the National Nature Science Foundation of China (21877113, 81971983, and 81874330), the Natural Science Foundation of Fujian Province (2020I0036), Six Talent Peaks of Jiangsu Province (YY-128), Wuxi Taihu Lake Talent Plan Top Talents Projects (BJ 2020001) for support on this work. This study was partially supported by Department of Pharmaceutical Sciences, College of Pharmacy and Health Sciences, St. John's University (New York, United States).

## ACKNOWLEDGMENTS

We thank Dr. Shin-Ich Akiyama (Kagoshima University, Japan) for providing us the KB-3-1 and KB-C2 cell lines. We thank Dr. Charles R. Ashby Jr (St. John's University) for editing the article.

## SUPPLEMENTARY MATERIAL

The Supplementary Material for this article can be found online at: https://www.frontiersin.org/articles/10.3389/fphar.2022.867128/full#supplementary-material

## REFERENCES

Akiyama, S., Fojo, A., Hanover, J. A., Pastan, I., and Gottesman, M. M. (1985). Isolation and Genetic Characterization of Human KB Cell Lines Resistant to Multiple Drugs. *Somat Cel Mol Genet* 11, 117–126. doi:10.1007/BF01534700

Ambudkar, S. V. (1998). Drug-stimulatable ATPase Activity in Crude Membranes of Human MDR1-Transfected Mammalian Cells. *Methods Enzymol.* 292, 504–514. doi:10.1016/s0076-6879(98)92039-0

Aristizabal Prada, E. T., Nölting, S., Spoettl, G., Maurer, J., and Auernhammer, C. J. (2018). The Novel Cyclin-dependent Kinase 4/6 Inhibitor Ribociclib (LEE011) Alone and in Dual-Targeting Approaches Demonstrates Antitumoral Efficacy in Neuroendocrine Tumors *In Vitro*. *Neuroendocrinology* 106, 58–73. doi:10.1159/000463386

Braun, K., Hölzl, G., Pusch, O., and Hengstschläger, M. (1998). Deregulated Expression of CDK2- or CDK3-Associated Kinase Activities Enhances C-Myc-Induced Apoptosis. *DNA Cel Biol* 17, 789–798. doi:10.1089/dna.1998.17.789

Chung, J. H., and Bunz, F. (2010). Cdk2 Is Required for P53-independent G2/M Checkpoint Control. *Plos Genet.* 6, e1000863. doi:10.1371/journal.pgen.1000863

Czudor, Z., Balogh, M., Bánhegyi, P., Boros, S., Breza, N., Dobos, J., et al. (2018). Novel Compounds with Potent CDK9 Inhibitory Activity for the Treatment of Myeloma. *Bioorg. Med. Chem. Lett.* 28, 769–773. doi:10.1016/j.bmcl.2018.01.002

Diani, L., Colombelli, C., Nachimuthu, B. T., Donnianni, R., Plevani, P., Muzi-Falconi, M., et al. (2009). Saccharomyces CDK1 Phosphorylates Rad53 Kinase in Metaphase, Influencing Cellular Morphogenesis. *J. Biol. Chem.* 284, 32627–32634. doi:10.1074/jbc.M109.048157

Duan, C., Liu, Y., Lu, L., Cai, R., Xue, H., Mao, X., et al. (2015). CDK14 Contributes to Reactive Gliosis via Interaction with Cyclin Y in Rat Model of Spinal Cord Injury. *J. Mol. Neurosci.* 57, 571–579. doi:10.1007/s12031-015-0639-x

Feng, W., Zhang, M., Wu, Z. X., Wang, J. Q., Dong, X. D., Yang, Y., et al. (2020). Erdafitinib Antagonizes ABCB1-Mediated Multidrug Resistance in Cancer Cells. *Front. Oncol.* 10, 955. doi:10.3389/fonc.2020.00955

Guo, Z., Lv, X., and Jia, H. (2020). MiR-186 Represses Progression of Renal Cell Cancer by Directly Targeting CDK6. *Hum. Cel* 33, 759–767. doi:10.1007/s13577-020-00357-3

Gupta, P., Zhang, Y. K., Zhang, X. Y., Wang, Y. J., Lu, K. W., Hall, T., et al. (2018). Voruciclib, a Potent CDK4/6 Inhibitor, Antagonizes ABCB1 and ABCG2-Mediated Multi-Drug Resistance in Cancer Cells. *Cell Physiol. Biochem.* 45, 1515–1528. doi:10.1159/000487578

Hirai, H., Shimomura, T., Kobayashi, M., Eguchi, T., Taniguchi, E., Fukasawa, K., et al. (2010). Biological Characterization of 2-Aminothiazole-Derived Cdk4/6 Selective Inhibitor *In Vitro* and *In Vivo*. *Cell Cycle* 9, 1590–1600. doi:10.4161/cc.9.8.11306

Hu, Q. L., Xu, Z. P., Lan, Y. F., and Li, B. (2020). MiR-636 Represses Cell Survival by Targeting CDK6/Bcl-2 in Cervical Cancer. *Kaohsiung J. Med. Sci.* 36, 328–335. doi:10.1002/kjm2.12181

Iriyama, N., Hino, H., Moriya, S., Hiramoto, M., Hatta, Y., Takei, M., et al. (2018). The Cyclin-dependent Kinase 4/6 Inhibitor, Abemaciclib, Exerts Dose-dependent Cytostatic and Cytocidal Effects and Induces Autophagy in Multiple Myeloma Cells. *Leuk. Lymphoma* 59, 1439–1450. doi:10.1080/10428194.2017.1376741

Kaczor, A. A., Selent, J., Sanz, F., and Pastor, M. (2013). Modeling Complexes of Transmembrane Proteins: Systematic Analysis of Protein; Protein Docking Tools. *Mol. Inform.* 32, 717–733. doi:10.1002/minf.201200150

Kalaiselvi, M., Amsaveni, R., and Bhuvaneshwari, V. (2015). Molecular Docking of Compounds Elucidated from Ixora Coccinea Linn. Flowers with Insulin Receptors. *Scholars Researdh Libr.* 7, 344–348.

Kathawala, R. J., Gupta, P., Ashby, C. R., and Chen, Z. S. (2015). The Modulation of ABC Transporter-Mediated Multidrug Resistance in Cancer: A Review of the Past Decade. *Drug Resist. Updat* 18, 1–17. doi:10.1016/j.drup.2014.11.002

Kim, Y., and Chen, J. (2018). Molecular Structure of Human P-Glycoprotein in the ATP-Bound, Outward-Facing Conformation. *Science* 359, 915–919. doi:10.1126/science.aar7389

Kwapisz, D. (2017). Cyclin-dependent Kinase 4/6 Inhibitors in Breast Cancer: Palbociclib, Ribociclib, and Abemaciclib. *Breast Cancer Res. Treat.* 166, 41–54. doi:10.1007/s10549-017-4385-3

Lee, T. D., Lee, O. W., Brimacombe, K. R., Chen, L., Guha, R., Lusvarghi, S., et al. (2019). A High-Throughput Screen of a Library of Therapeutics Identifies Cytotoxic Substrates of P-Glycoprotein. *Mol. Pharmacol.* 96, 629–640. doi:10.1124/mol.119.115964

Li, Q., Liu, X., Zhang, M., Ye, G., Qiao, Q., Ling, Y., et al. (2010). Characterization of A Novel Human CDK5 Splicing Variant that Inhibits Wnt/Beta-Catenin Signaling. *Mol. Biol. Rep.* 37, 2415–2421. doi:10.1007/s11033-009-9752-7

Li, M., Yin, D., Li, J., Shao, F., Zhang, Q., Jiang, Q., et al. (2020). Rosmarinic Acid, the Active Component of Salvia Miltiorrhizae, Improves Gliquidone Transport by Regulating the Expression and Function of P-Gp and BCRP in Caco-2 Cells. *Pharmazie* 75, 18–22. doi:10.1691/ph.2020.9754

Liang, S., Hu, L., Wu, Z., Chen, Z., Liu, S., Xu, X., et al. (2020). CDK12: A Potent Target and Biomarker for Human Cancer Therapy. *Cells* 9, 1483. doi:10.3390/cells9061483

Liu, Z., Long, X., Chao, C., Yan, C., Wu, Q., Hua, S., et al. (2014). Knocking Down CDK4 Mediates the Elevation of Let-7c Suppressing Cell Growth in Nasopharyngeal Carcinoma. *BMC Cancer* 14, 274. doi:10.1186/1471-2407-14-274

Loyer, P., and Trembley, J. H. (2020). Roles of CDK/Cyclin Complexes in Transcription and Pre-mrna Splicing: Cyclins L and CDK11 at the Cross-Roads of Cell Cycle and Regulation of Gene Expression. *Semin. Cel Dev Biol* 107, 36–45. doi:10.1016/j.semcdb.2020.04.016

Martínez-Chávez, A., van Hoppe, S., Rosing, H., Lebre, M. C., Tibben, M., Beijnen, J. H., et al. (2019). P-glycoprotein Limits Ribociclib Brain Exposure and CYP3A4 Restricts its Oral Bioavailability. *Mol. Pharm.* 16, 3842–3852. doi:10.1021/acs.molpharmaceut.9b00475

Menzl, I., Zhang, T., Berger-Becvar, A., Grausenburger, R., Heller, G., Prchal-Murphy, M., et al. (2019). A Kinase-independent Role for CDK8 in BCR-Abl1+ Leukemia. *Nat. Commun.* 10, 4741. doi:10.1038/s41467-019-12656-x

Mi, Y. J., Liang, Y. J., Huang, H. B., Zhao, H. Y., Wu, C. P., Wang, F., et al. (2010). Apatinib (YN968D1) Reverses Multidrug Resistance by Inhibiting the Efflux Function of Multiple ATP-Binding Cassette Transporters. *Cancer Res.* 70, 7981–7991. doi:10.1158/0008-5472.CAN-10-0111

Rainey, M. D., Quachthithu, H., Gaboriau, D., and Santocanale, C. (2017). DNA Replication Dynamics and Cellular Responses to ATP Competitive CDC7 Kinase Inhibitors. *ACS Chem. Biol.* 12, 1893–1902. doi:10.1021/acschembio.7b00117

Rank, K. B., Evans, D. B., and Sharma, S. K. (2000). The N-Terminal Domains of Cyclin-dependent Kinase Inhibitory Proteins Block the Phosphorylation of Cdk2/Cyclin E by the CDK-Activating Kinase. *Biochem. Biophys. Res. Commun.* 271, 469–473. doi:10.1006/bbrc.2000.2648

Robert, T., Johnson, J. L., Guichaoua, R., Yaron, T. M., Bach, S., Cantley, L. C., et al. (2020). Development of A CDK10/CycM *In Vitro* Kinase Screening Assay and Identification of First Small-Molecule Inhibitors. *Front. Chem.* 8, 147. doi:10.3389/fchem.2020.00147

Sorf, A., Sucha, S., Morell, A., Novotna, E., Staud, F., Zavrelova, A., et al. (2020). Targeting Pharmacokinetic Drug Resistance in Acute Myeloid Leukemia Cells with CDK4/6 Inhibitors. *Cancers (Basel)* 12, 1596. doi:10.3390/cancers12061596

Szwarcwort-Cohen, M., Kasulin-Boneh, Z., Sagee, S., and Kassir, Y. (2009). Human Cdk2 Is A Functional Homolog of Budding Yeast Ime2, the Meiosis-specific Cdk-like Kinase. *Cell Cycle* 8, 647–654. doi:10.4161/cc.8.4.7843

Tai, T. S., Lin, P. M., Wu, C. F., Hung, S. K., Huang, C. I., Wang, C. C., et al. (2019). CDK4/6 Inhibitor LEE011 Is a Potential Radiation-Sensitizer in Head and Neck Squamous Cell Carcinoma: An *In Vitro* Study. *Anticancer Res.* 39, 713–720. doi:10.21873/anticanres.13167

Tripathy, D., Bardia, A., and Sellers, W. R. (2017). Ribociclib (LEE011): Mechanism of Action and Clinical Impact of This Selective Cyclin-dependent Kinase 4/6 Inhibitor in Various Solid Tumors. *Clin. Cancer Res.* 23, 3251–3262. doi:10.1158/1078-0432.CCR-16-3157

Wu, T., Chen, Z., To, K. K. W., Fang, X., Wang, F., Cheng, B., et al. (2017). Effect of Abemaciclib (LY2835219) on Enhancement of Chemotherapeutic Agents in ABCB1 and ABCG2 Overexpressing Cells *In Vitro* and *In Vivo*. *Biochem. Pharmacol.* 124, 29–42. doi:10.1016/j.bcp.2016.10.015

Wu, C. P., Hung, T. H., Hsiao, S. H., Huang, Y. H., Hung, L. C., Yu, Y. J., et al. (2020). Erdafitinib Resensitizes ABCB1-Overexpressing Multidrug-Resistant Cancer Cells to Cytotoxic Anticancer Drugs. *Cancers (Basel)* 12, 1366. doi:10.3390/cancers12061366

Yang, D., Kathawala, R. J., Chufan, E. E., Patel, A., Ambudkar, S. V., Chen, Z. S., et al. (2014). Tivozanib Reverses Multidrug Resistance Mediated by ABCB1 (P-Glycoprotein) and ABCG2 (BCRP). *Future Oncol.* 10, 1827–1841. doi:10.2217/Fon.13.253

Yoshimura, A., Kuwazuru, Y., Sumizawa, T., Ikeda, S., Ichikawa, M., Usagawa, T., et al. (1989). Biosynthesis, Processing and Half-Life of P-Glycoprotein in A Human Multidrug-Resistant KB Cell. *Biochim. Biophys. Acta* 992, 307–314. doi:10.1016/0304-4165(89)90089-5

Zhang, L., Li, Y., Wang, Q., Chen, Z., Li, X., Wu, Z., et al. (2020). The PI3K Subunits, P110α and P110β Are Potential Targets for Overcoming P-Gp and BCRP-Mediated MDR in Cancer. *Mol. Cancer* 19, 10. doi:10.1186/s12943-019-1112-1

Zhang, L., Li, Y., Hu, C., Chen, Y., Chen, Z., Chen, Z.-S., et al. (2022). CDK6-PI3K Signaling axis Is an Efficient Target for Attenuating ABCB1/P-Gp Mediated Multi-Drug Resistance (MDR) in Cancer Cells. *Mol. Cancer*. In press. doi:10.1186/s12943-022-01524-w

**Conflict of Interest:** The authors declare that the research was conducted in the absence of any commercial or financial relationships that could be construed as a potential conflict of interest.

**Publisher's Note:** All claims expressed in this article are solely those of the authors and do not necessarily represent those of their affiliated organizations, or those of the publisher, the editors and the reviewers. Any product that may be evaluated in this article, or claim that may be made by its manufacturer, is not guaranteed or endorsed by the publisher.

frontiers | Frontiers in Chemistry

REVIEW
published: 01 April 2022
doi: 10.3389/fchem.2022.867318

# Research Advances on Matrine

*Xiao-Ying Sun[1†], Li-Yi Jia[1†], Zheng Rong[1†], Xin Zhou[2], Lu-Qi Cao[2], Ai-Hong Li[3], Meng Guo[1], Jie Jin[1], Yin-Di Wang[1], Ling Huang[1], Yi-Heng Li[4], Zhong-Jing He[4], Long Li[2], Rui-Kang Ma[2], Yi-Fan Lv[2], Ke-Ke Shao[2], Juan Zhang[1]* and Hui-Ling Cao[1,2,3,4]**

[1]College of Pharmacy, Shaanxi University of Chinese Medicine, Xianyang, China, [2]Xi'an Key Laboratory of Basic and Translation of Cardiovascular Metabolic Disease, Shaanxi Key Laboratory of Ischemic Cardiovascular Disease, Institute of Basic and Translational Medicine, Xi'an Medical University, Xi'an, China, [3]Shaanxi Key Laboratory of Chinese Herb and Natural Drug Development, Medicine Research Institute, Shaanxi Pharmaceutical Holding Group Co., LTD, Xi'an, China, [4]College of Life Sciences, Northwest University, Xi'an, China

Matrine is an alkaloid extracted from traditional Chinese herbs including *Sophora flavescentis*, *Sophora alopecuroides*, *Sophora* root, etc. It has the dual advantages of traditional Chinese herbs and chemotherapy drugs. It exhibits distinct benefits in preventing and improving chronic diseases such as cardiovascular disease and tumors. The review introduced recent research progresses on extraction, synthesis and derivatization of Matrine. The summary focused on the latest research advances of Matrine on anti-atherosclerosis, anti-hypertension, anti-ischemia reperfusion injury, anti-arrhythmia, anti-diabetic cardiovascular complications, anti-tumor, anti-inflammatory, anti-bacterium, anti-virus, which would provide new core structures and new insights for new drug development in related fields.

**Keywords: matrine, extraction, synthesis, derivatization, molecular mechanism, pharmacological effects**

OPEN ACCESS

***Edited by:***
*Cong Wang,*
*Zhengzhou University, China*

***Reviewed by:***
*Yi-Chao Zheng,*
*Zhengzhou University, China*
*Linxi Chen,*
*University of South China, China*

****Correspondence:***
*Juan Zhang*
*rouerou@sina.com*
*Hui-Ling Cao*
*caohuiling_jzs@xiyi.edu.cn*

*†These authors have contributed equally to this work*

***Specialty section:***
*This article was submitted to Medicinal and Pharmaceutical Chemistry, a section of the journal Frontiers in Chemistry*

***Received:*** *31 January 2022*
***Accepted:*** *22 February 2022*
***Published:*** *01 April 2022*

***Citation:***
*Sun X-Y, Jia L-Y, Rong Z, Zhou X, Cao L-Q, Li A-H, Guo M, Jin J, Wang Y-D, Huang L, Li Y-H, He Z-J, Li L, Ma R-K, Lv Y-F, Shao K-K, Zhang J and Cao H-L (2022) Research Advances on Matrine. Front. Chem. 10:867318. doi: 10.3389/fchem.2022.867318*

## INTRODUCTION

Matrine is an alkaloid extracted and isolated from the root bark of *Sophora flavescens* by Japanese researcher Nagai (Bohlmann et al., 2010). Later, Matrine was also found in *Sophora flavescens, Sophora alopecuroides*, mountain bean root, and other leguminous *Sophora* plants (Zhang and Shen, 2018a). Matrine is a tetracyclic quinolizidine alkaloid with the chemical formula $C_{15}H_{24}N_2O$ and a molecular weight of 248.36. Matrine exists in two states of matter: solid and liquid (Zhao et al., 2015a). α-Matrine is an acicular or columnar crystal with a melting point of 76°C, β-Matrine is an orthorhombic crystal with a melting point of 87°C, δ-Matrine is a columnar crystal with a melting point of 84°C, γ-Matrine is a liquid with a boiling point of 223°C (Feng, 2005). The most common is α-Matrine, which is soluble in water, methanol, ethyl alcohol, trichloromethane, methylbenzene and is slightly soluble in petroleum ether. Two quinazine rings bind Matrine together. The molecule contains four six-membered rings. The six-membered rings are isomers of the chair and boat conformations. The chair conformation of Matrine is determined to be the least energetic and most stable of the eight conformational isomers (Fu, 2017). Matrine contains four chiral centers in the 5S, 6S, 7R, and 11R configurations (Zhang et al., 2019). Its molecular structure consists of two saturated tertiary amines and 2 N atoms, each of which includes a pair of unpaired electrons. It is alkaline due to its attraction to protons. It has an n-1 molecular structure. Oxymatrine is generated after oxidation, which can be reduced to Matrine using a reducing agent. Lactam's system can be saponified to yield Matric Acid or its derivatives, and Matric Acid can be dehydrated and condensed to yield Matrine.

Matrine has the dual advantages of both traditional Chinese herbs and chemotherapeutic agents. On the one hand, Matrine comes from traditional Chinese herbs such as *Sophora flavescens, Sophora*

**TABLE 1 |** The extraction methods, conditions and yield of Matrine.

| Solvent extraction | Liquid to material ratio (g/ml) | Solvent | Extraction times | Extraction speed (ml/min) | Extraction time (min) | Extraction temperature (°C) | Extraction frequency (kHz)or power (W) | Matrine yield (mg/ 100 g) | Refrences |
|---|---|---|---|---|---|---|---|---|---|
| Percolation | 1:6 | 65% Ethanol | | 4 | - | | - | 0.145 | Li et al. (2015) |
| Decoction | 1:8 | Pure water | 3 | - | 120 | - | - | 0.21 | Guo et al. (2014) |
| acid reflux method | 1:12 | 0.3%Acetic acid | 3 | - | - | | - | 0.31 | Cui et al. (2007) |
| Ultrasonic extraction | 1:10 | Pure water | - | - | 45 | 80 | - | 0.46 | Chen et al. (2017) |
| Optimizing Ultrasound | 1:40 | 60% ethanol | - | - | 30 | 50 | 35 kHz | 0.34 | Fu et al. (2015) |
| Microwave extraction | 1:40 | 80% ethanol | - | - | 20 | 75 | 500 W | 0.48 | Wang et al. (2011) |

*alopecuroides*, and mountain bean root. After thousands of years of clinical practices, it has the advantages of definite pharmacological effects, mild efficacy, and high safety of traditional Chinese herbs. On the other hand, Matrine, as a monomer, has the advantage of known definite chemical structure to facilitate to new drug development. Matrine has a wide range of pharmacological effects, such as cardiovascular protection (Liu and Guo, 2011), anti-tumor (Chen et al., 2022), anti-inflammatory (Huang et al., 2014), immunosuppression (Kan et al., 2013), etc. Matrine has unique advantages in the treatment of various chronic diseases and widely used to treat viral hepatitis, liver fibrosis, arrhythmia, and autoimmune diseases. Due to the large dosage and low pharmacological activity of Matrine, its clinical application is limited. The researchers modified and optimized the structure of Matrine to obtain new derivatives with high efficiency and low toxicity (Huang and Wang, 2016). The review introduced recent research progresses of Matrine on extraction, synthesis, and derivatization. It focused on the latest research advances of Matrine on anti-atherosclerosis, anti-hypertension, anti-ischemia-reperfusion injury, anti-arrhythmic, anti-diabetic cardiovascular complications, anti-tumor, anti-inflammatory, anti-bacterial, anti-viral, which would provide new core structures and new insights for new drug development in related fields.

# EXTRACTION AND SYNTHESIS OF MATRINE

## Extraction of Matrine

The primary source of Matrine is extraced from natural plants. The common procedures are solvent extraction, ultrasonic aided extraction, and microwave-assisted extraction. Solvent extraction is appropriate for industrial manufacturing, while ultrasonic-assisted and microwave-assisted extraction are suitable for laboratory preparation. The solvent extraction method adopts the principle of similarity and compatibility (Han et al., 2018). Guo et al. (Guo et al., 2014) used the water decocting method to screen the optimum extraction conditions of Matrine: the ratio of material to liquid (g/ml) 1:8, water extraction 3 times, 2 h each time, the concentration of 1.0 g/ml, after alcohol precipitation, adjust to pH 9–11, trichloromethane extraction 3 times, matrine yielded 0.21 mg per 100 g raw materials, as shown in **Table 1**. Zhang et al. (Cui et al., 2007) adopted the acid water reflux method, took crude extract recovery rate as the index, and adopted the orthogonal experimental design to optimize extraction conditions. The optimal condition was as follows: 60 mesh *Sophora flavescens* powder, 0.3% HCl as solvent, 1: 12 solid-liquid ratio (g/ml), reflux for 3 times, matrine yielded 0.31 mg per 100 g raw materials, as shown in **Table 1**. Li et al. (Li et al., 2015) optimized the best percolation extraction process of Matrine by using four-factor and three-level orthogonal experimental design. The optimal condition was as follows: coarse powder, 65% ethanol as solvent, 1:6 solid-liquid ratio (g/ml), 24 h soaking, 4 ml/min percolation speed, matrine yielded 0.15 mg per 100 g raw materials, as shown in **Table 1**. Solvent extraction has the characteristics of simple operation, low cost, and high extraction efficiency, which is a traditional extraction method in industrial production.

The ultrasonic extraction method is to utilize the cavitation effects, mechanical effects, and thermal effects of ultrasonic wave to disintegrate the plant cell wall, promote the outward diffusion and dissolution of intracellular active ingredients under the high-frequency vibration of ultrasonic wave, to enhance extraction efficiency (Wan et al., 2008). Chen et al. (Chen et al., 2017) found the optimal condition for ultrasonic extraction method was as follows: pure water as solvent, 1:10 solid-liquid ratio (g/ml), 45 min ultrasonic treatment, 80°C extraction temperature, matrine yielded 0.46 mg per 100 g raw materials, as shown in **Table 1**. Fu et al. (Fu et al., 2015) optimized the ultrasonic extraction conditions by orthogonal test to obtain low extraction temperature as follows: 1500 W ultrasonic power, 35 kHz ultrasonic frequency, 60% ethanol as solvent, 1: 40 solid-liquid ratio (g/ml), 20 min soaking, 50°C extraction temperature, 32 min extraction time, matrine yielded 0.34 mg per 100 g raw materials, as shown in **Table 1**. The ultrasonic extraction method has a high extraction efficiency. Still, it requires more control conditions, a more complex operation, a higher cost, and fewer single extractions, making it suited for laboratory preparation.

The microwave-assisted extraction method is to use the intense penetration and high heat energy of microwave to

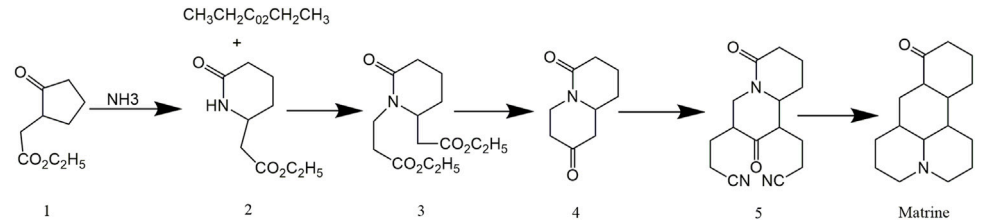


**FIGURE 1 |** Synthetic route of Matrine by Mandell et al. (1965).

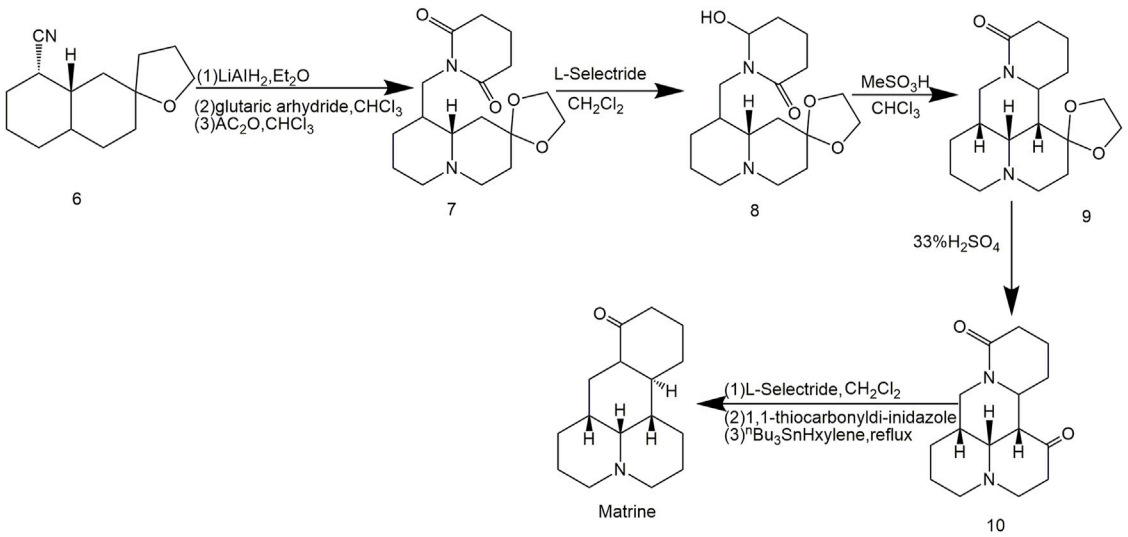


**FIGURE 2 |** Synthetic route of Matrine by Chen et al. (1986).

rupture the plant cell wall and accelerate the dissolution of active ingredients. Wang et al. (Wang et al., 2011) obtained the best microwave extraction conditions by single factor orthogonal test as follows: 500 W microwave power, 80% ethanol as solvent, 1:40 liquid-material ratio (g/ml), 75°C extraction temperature, 20 min extraction time, matrine yielded 0.48 mg per 100 g raw materials, as shown in **Table 1**. Microwave-assisted extraction has high efficiency, but the operation is complex and suitable for laboratory preparation.

## Complete Synthesis of Matrine

Many researchers focused on the synthesis pathway of Matrine since its discovery. There were three classical total synthesis methods of Matrine with high yield. For the first time, Leon et al. (Mandell et al., 1965) described a method for the complete synthesis of Matrine. The Dickmann and the stork enamine were used to yield Matrine from cyclopentanone 2-ethyl acetate (**Figure 1-1**). The overall yield of Matrine was approximately 12% with high yield, short synthetic process and convenient perform, as shown in **Figure 1**.

Chen et al. (Chen et al., 1986) obtained Matrine from 4-cyanoquinolisidine acetal (**Figures 2-6**) by selective reduction and deacetal reaction. The synthesis technique reached a new milestone for Matrine synthesis and total yield rate of Matrine jumped to 23%, as shown in **Figure 2**.

By intramolecular addition cyclization, Fleming et al. (Fleming et al., 1997) synthesized Matrine from unsaturated nitrile, which provided an ideal synthetic route of Matrine with fewer reaction steps, simple operations and easy-handling products, as shown in **Figure 3**.

# PHARMACOLOGICAL EFFECTS OF MATRINE

## Cardiovascular and Cerebrovascular Protection Activity

Cardiovascular and cerebrovascular diseases as global people's leading cause, its new drug development is indispensable. Matrine, as a Chinese herb monomer with multiple activities, has unique advantages in preventing and improving atherosclerosis, hypertension, ischemia-reperfusion injury, arrhythmia, and diabetic cardiovascular complications (Liu and Guo, 2011).

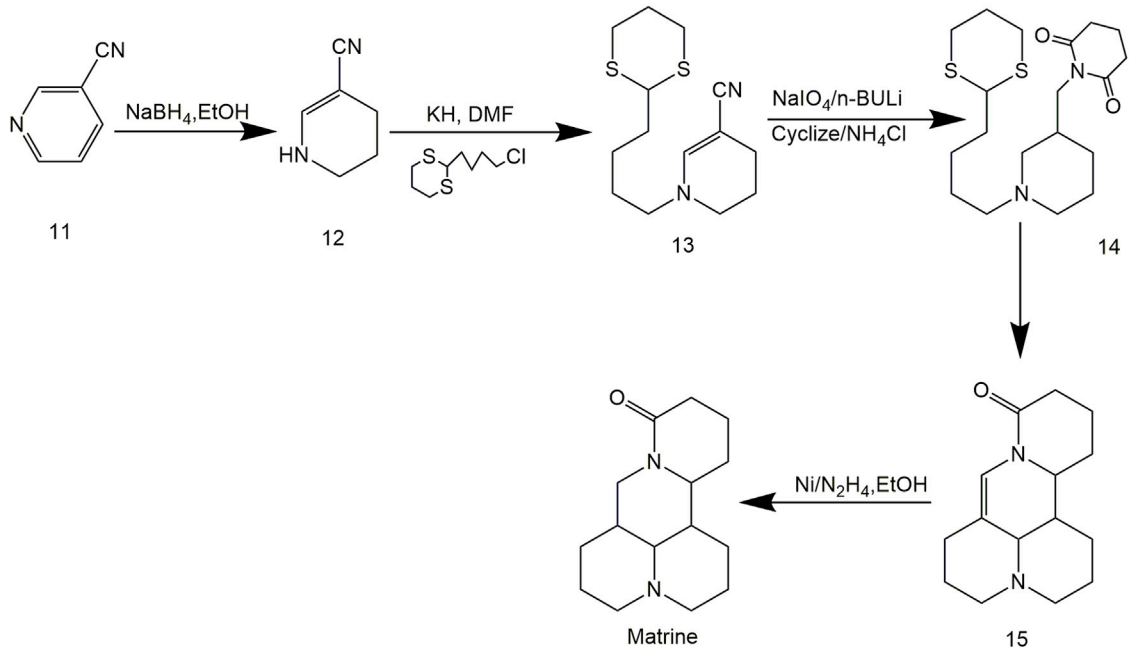


**FIGURE 3 |** Synthetic route of Matrine by Fleming et al. (1997).

1) Anti-atherosclerosis activity

AS (Atherosclerosis) is the primary pathological basis of cardiovascular and cerebrovascular diseases such as hypertension, coronary heart disease, stroke, cerebral infarction and diabetic cardiovascular complications. Its molecular pathogenesis involves in inflammation, endothelial injury, immune dysfunction, lipid metabolism disorders and foam cell formation (Xu et al., 2007). The foam cells were formed by the excessive lipid phagocytosis and cholesterol accumulation by macrophages (Tsai et al., 2010). Matrine could reduce the level of LDL-C (low-density lipoprotein cholesterol) and TG (triglyceride) in the blood of hypercholesterolemic mice, hyperlipidemic rats, and pigeon models to prevent AS (Lu and Zhu, 2003). ABCA1(ATP-binding cassette transporterA1) can regulate the RCT (reverse cholesterol transport). Its dysfunction can lead to the excessive cholesterol accumulation in macrophages to form foam cells, then infiltrate blood vessel walls, and promote the occurrence and development of AS (Li et al., 2013). Matrine could upregulate the ABCA1 expression to promote RCT, reduce the cholesterol accumulation in foam cells, and improve AS (Jiang et al., 2007).

Excessive accumulation of cytotoxic free cholesterol in foam cells induces cell apoptosis, and then, lipids and cell debris can infiltrate the inner membrane of vascular walls to form AS plaques. Subsequently, macrophages release inflammatory factors, such as TNF-α (tumor necrosis factor-α), IL-6 (interleukin-6), etc, which promotes the proliferation and migration of macrophages and VSMCs (vascular smooth muscle cells) to accelerate the AS progression (Moriya, 2018). Matrine could suppress the cell inflammatory response, inhibit the proliferation and apoptosis of VSMCs to improve AS by inhibiting JAK/STAT3 (Janus kinase1/activation of signal transduction and activator of transcription3) signaling pathway (Lu et al., 2018). Additionally, Matrine could also downregulate the overexpression of VCAM-1 (vascular cell adhesion molecule-1) and ICAM-1 (intercellular adhesion molecule-1) induced by TNF-α to decrease cell adhesion to improve AS by downregulating NF-κB (nuclear factor kappa-B) and MAPK (mitogen-activated protein kinase) signaling pathways (Liu et al., 2016).

2) Anti-hypertension activity

Hypertension is an independent risk factor for cardiovascular disease. Systolic blood pressure increases every 20 mmHg, diastolic blood pressure increases by 10 mmHg, and cardiovascular risk doubles (China National Center for Cardiocascular Disease, 2020). Therefore, controlling blood pressure can significantly reduce morbidity and mortality of cardiovascular diseases. Hypertension pathogenesis involves in sympathetic nerve excitation, renin-angiotensin-aldosterone system, $Ca^{2+}$ release, vascular remodeling and so on (He et al., 1999; Zheng et al., 2009; Wei, 2016; Li et al., 2020a; Ge and Xu, 2020; Sun et al., 2021).

Matrine could inhibit α-Adrenoceptor activation to interfere with intracellular $Ca^{2+}$ release and extracellular $Ca^{2+}$ influx, thereby reducing blood pressure induced by phenylephrine (Zheng et al., 2009). Abnormal proliferation of pulmonary artery smooth muscle cells is the key cause to induce pulmonary hypertension. Matrine could inhibit the proliferation of human pulmonary artery smooth muscle cells, block cell cycle from G0/G1 to S phase, promote cell apoptosis, therefore, improving pulmonary hypertension (Ge and Xu, 2020).

Inflammatory cytokines such as IL-6 and TGF-β1 (transforming growth factor-β1) play an essential role in the occurrence and development of pulmonary hypertension. Inflammatory cytokines could infiltrate pulmonary artery vessels, make pulmonary artery smooth muscle cells proliferate abnormally, and induce pulmonary vascular remodeling. Matrine could downregulate TNF-α and IL-1β expression by NF-κB signaling pathway to prevent vascular injury and protect pulmonary vessels, thereby, improving pulmonary hypertension in rats. In addition, Matrine could improve pathological changes of the lung in pulmonary hypertension model mice by inhibiting oxidative stress (Li et al., 2020a). Cardiovascular remodeling and target organ injury are closely related to the occurrence and development of hypertension. Hypertension treatment can effectively reduce blood pressure, reverse cardiovascular remodeling, prevent myocardial fibrosis, and protect target organ injury. Matrine could improve vascular remodeling by inhibiting the abnormal proliferation of VSMCs induced by AngII (angiotensinII) (He et al., 1999). RhoA (Ras homologous gene family proteinA)/Rock1(Rho related coiled-coil forming protein kinase1) signaling pathway is closely related to myocardial fibrosis. Matrine could inhibit the activation of RhoA/Rock1 signaling pathway, reduce myocardial fibrosis, prevent ventricular remodeling, and improve cardiac function in rats with heart failure (Sun et al., 2021). Left ventricular hypertrophy is a complication of hypertension. Matrine could up-regulate the expression of ciliary ganglion neurotrophic factor, downregulate the expression of IGF-1 (insulin-like growth factor1), TGF-β1, ICAM-1 and macrophage inflammatory protein 2 by inhibiting NF-κB signaling pathway to improve isoproterenol-induced left ventricular hypertrophy (Wei, 2016).

3) Anti-ischemia reperfusion injury activity

I/R (ischemia reperfusion injury) refers to that the ischemic injury of tissues and organs aggravates by blood reperfusion after ischemia, which involves in oxidative stress and inflammatory response. Matrine could significantly downregulate MDA (malondialdehyde), upregulate SOD (superoxide dismutase) and GSH (glutathione peroxidase) to inhibit oxidative stress in rats after cerebral I/R, significantly downregulate caspase-3 and the ratio of Bax/Bcl-2 to inhibit apoptosis, and therefore protect nerves cells (Zhao et al., 2015b). Matrine could also inhibit oxidative stress to alleviate acute liver injury after hepatic I/R by inhibiting NF-κB pathway (Zhang et al., 2011a).

Hsp70 (heat shock protein 70) is a cardiac protective molecule that can inhibit cardiomyocyte apoptosis after myocardial I/R or hypoxia/reperfusion injury. Matrine could up-regulate Hsp70 expression by activating JAK2/STAT3 pathway to protect cardiomyocyte after hypoxia/reperfusion injury (Guo et al., 2018). AMPK (AMP-dependent protein kinase) and SIRT3 (sirtuin3) are classical anti-apoptotic pathways involved in the occurrence and development of many diseases. Matrine could activate the AMPK/SIRT3 signaling pathway, inhibit cardiomyocyte apoptosis induced by I/R to protect cardiomyocyte (Lu et al., 2020). Matrine could down-regulate the level of Akt phosphorylation at Thr495 and up-regulate the expression of eNOS (endogenous nitric oxide synthase), downregulate the expression of DDAH2 (dimethylarginine dimethylaminohydrolase2) and up-regulate phosphorylation level of GSK-3β (glycogen synthase kinase3β), reduce subendocardial necrosis, relieve inflammatory cell infiltration and interstitial edema, and improve the acute myocardial I/R injury induced by super dose isoproterenol in rats (Li et al., 2012a).

4) Anti-arrhythmia activity

Arrhythmia is a heart disease characterized by abnormal heartbeat frequency and rhythm. Electrophysiology is characterized by changes in the origin, conduction velocity, or activation order of electrical activities in the myocardium. The arrhythmia pathogenesis includes spontaneous depolarization, abnormal electrical triggering and reentry, abnormal action potential and so on (Zhang et al., 2020a), which involves in ion channels on cardiomyocytes, such as sodium channel, calcium channel, potassium channel, etc (Bers et al., 2003; Antzelevitch and Belardinelli, 2006; Jost et al., 2009; Sun and Wang, 2010; Varró et al., 2010; Passini et al., 2014; Wu et al., 2020). Matrine could block the increase of L-type $Ca^{2+}$ current and $Ca^{2+}$ transient, up-regulate L-type calcium channel current, activate M3 receptor, up-regulate the expression of IkM3 (delayed rectifier potassium current), prolong the time course of the action potential, restore the transient outward potassium current and inward rectifier potassium current of rat ventricular myocytes after myocardial infarction, and reduce $Ca^{2+}$ in cardiomyocytes, therefore, improve ouabain induced action potential prolongation and arrhythmia in rats, and improve arrhythmia caused by coronary artery ligation or myocardial infarction in rats (Zhou et al., 2014a). Matrine could inhibit cardiomyocyte apoptosis to prevent heart failure in rats by inhibiting the β3-Ar pathway, (Yu et al., 2014).

Cardiac fibrosis promotes atrial fibrillation by disrupting the continuity of fiber bundles and causing abnormal local electrical conduction (Research, 2009; Yue et al., 2010). Matrine could improve myocardial fibrosis in mice induced by aortic ligation or injection of isoproterenol by up-regulating ribosomal protein S5 and inhibiting p38 activation, therefore, reduce the susceptibility to atrial fibrillation after myocardial infarction, and shorten the onset time of atrial fibrillation (Antzelevitch and Belardinelli, 2006).

5) Anti-diabetic cardiovascular complications activity

DM (diabetes mellitus), a complex and multifactorial metabolic disease, is characterized by with elevated blood glucose levels induced insulin resistance and β-Cell failure. T2DM (type 2 diabetes mellitus) accounts for majority of DM patients. The cardiovascular risk in DM is 2–4 times higher than that in normal subjects. A high glucose environment in DM patients will produce AGEs (advanced glycation end products) by glycosylated modification of macromolecules such as protein, lipid, and nucleic acid. It is the main

pathogenic pathway and the primary source of glucotoxicity in DM patients to induce intracellular pathological changes induced by AGEs binding with its receptor RAGE (receptor for advanced glycation end products). AGEs could transform HCSMCs (human coronary artery smooth muscle cells) from contractile to the synthetic phenotype to lose their contractility and up-regulate ECM (extra cellular matrix) expression to induce AS to induce diabetic cardiovascular complications. Matrine could down-regulate RyR2 expression, inhibit calcium overload caused by endoplasmic reticulum leakage to protect mitochondrial function, reduce age-induced heart injury and inhibit cardiomyocyte apoptosis (Wang et al., 2019a). Matrine could up-regulate poldip2 (polymerase δ Interacting protein2) expression, down-regulate Akt and mTOR phosphorylation, down-regulate phosphorylation level of downstream effector translation regulator P70S6K (70 kDa ribosomal S6 kinase), inhibit ECM protein expression, therefore, inhibit age-induced phenotypic transformation and fibrosis of HCMC (Ma et al., 2019).

Hyperglycemia can promote myocardial fibrosis and scar formation, and lead to changes in myocardial structure. Matrine could downregulate expression of TNF-α, IL-6 in serum and cardiomyocytes of rats to alleviate metabolic disturbance syndrome and vascular injury in streptozotocin-induced diabetic cardiomyopathy rats. Matrine could downregulate TGF-β1 expression and phosphorylation level of cardiomyocyte PERK (protein kinase RNA like endoplasmic reticulum kinase) to reduce cardiomyocyte apoptosis (Hou et al., 2019). Matrine could down-regulate TGF-β1 and Smad expression to improve the heart compliance and left ventricular function of diabetic myocardial fibrosis mice (Zhang et al., 2018a). Matrine could downregulate NFAT (nuclear factor of activated T-cell) signaling pathway and ECM gene expression to improve diabetic myocardial fibrosis and to protect cardiac function (Liu et al., 2017).

Oxidative stress is closely related to cardiovascular complications in DM. Under high glucose stimulation, ROS (reactive oxygen species) will release significantly, triggering apoptosis cascade reactions and inducing cardiomyocyte apoptosis in diabetic cardiomyopathy. Matrine could inhibit the activation of the ROS/TLR-4 signaling pathway, reduce the ROS in cells, inhibit the cardiomyocyte apoptosis, and improve heart function in diabetic cardiomyopathy mice (Liu et al., 2015). Matrine could dose-dependently reduce cellular ROS, down-regulate the expression of NLRP3 (NLR family protein3) inflammatory bodies, inhibit the secretion of inflammatory factors, reduce cell apoptosis and inhibit age-induced arterial cell injury (Zhang et al., 2018b).

Matrine could inhibit the release of inflammatory factors, regulate VEGF (vascular endothelial growth factor) and angiopoietin-1, inhibit the proliferation of retinal microvascular endothelial cells, and reduce diabetic retinopathy (Zhang, 2019). Matrine could downregulate TNF-α and IL-6 expression in serum, reduce the excretion rate of urinary microprotein caused by an inflammatory reaction, increase insulin sensitivity and assist treatment of T2DM nephropathy (Lu et al., 2015).

## Anti-Cancer Activity

The malignant tumor is the second leading death cause worldwide and chemotherapy is the major treatment way. The toxic side effects from chemotherapy seriously threaten cancer patients' health and life quality. Matrine, a Chinese herb monomer, has the dual advantages of traditional Chinese herbs and chemotherapy drugs, which could provide a new core structure and new insights for anti-cancer new drug development. Matrine injection has been clinically used as an anti-tumor adjuvant therapy in China. Matrine could inhibit the proliferation of a variety of tumor cells, induce cell cycle arrest, promote apoptosis, inhibit metastasis and invasion, reverse multidrug resistance, reduce the toxicity of radiotherapy and chemotherapy, and show favorable anti-tumor activity (Warburg, 1956; Zhang et al., 2009a; Li et al., 2012b; Zhou et al., 2012; Shao et al., 2013; Zhou et al., 2014b; Liu, 2014; Raimondi et al., 2014; Hu et al., 2015a; Wang et al., 2015; Zhang et al., 2015; An et al., 2016; Chan et al., 2017; Wu et al., 2017; Xiao et al., 2017; Zhou, 2017; Zhuo and Ji, 2017; Pu et al., 2018; Xiao et al., 2018; Xie et al., 2018; Zhou et al., 2018; Dai et al., 2019a; Wang et al., 2019b; Chen et al., 2019; Wang et al., 2019c; Dong, 2019; Guo et al., 2019; Hao et al., 2019; Kang et al., 2019; Lin et al., 2019; Liu et al., 2019; Li et al., 2020b; Ren et al., 2020; Dai et al., 2021a).

1) Anti-lung cancer activity

The occurrence and development of lung cancer are related to the imbalance of multiple signal pathways, such as the activation of PI3K/Akt/mTOR signaling pathway (Hao et al., 2019), CCR7(chemokine receptor7) (Pu et al., 2018), EGFR (Zhuo and Ji, 2017), and the high expression of TMEM16A (transmembrane protein 16A) (Guo et al., 2019). Matrine could inhibit PI3K/Akt/mTOR signaling pathway (Hao et al., 2019), down-regulate the expression of CCR7, EGFR, TMEM16A, down-regulate the ratio of apoptosis-related protein Bcl-2/Bax, inhibit cancer cell proliferation (Xie et al., 2018), migration and invasion (Zhang et al., 2009a), inhibit angiogenesis (Zhou et al., 2012), induce apoptosis (An et al., 2016), and inhibit the xenograft growth in tumor-bearing mice model (Hao et al., 2019).

The activation of cancer-promoting factor EGFR can up-regulate the expression of IL-6, JAK1/STAT3 signaling pathway and deteriorate NSCLC (non-small cell lung cancer), which was the reason for drug resistance. Additionally, drug resistance of lung cancer cells is also related to β-catenin/survivin, Nrf2/annexina4, etc. Matrine could inhibit the growth of NSCLC cell line H1975 by inhibiting EGFR and inhibiting the activation of the IL-6/JAK1/STAT3 signaling pathway. Matrine combined with afatinib could reverse the drug resistance of afatinib resistant strain H1975 cells by inhibiting the activation of the IL-6/JAK1/STAT3 signaling pathway (Chan et al., 2017). Matrine combined with cisplatin, 5-fluorouracil, and paclitaxel could enhance its anti-proliferation effects on A549 cells (Wang et al., 2015). β-catenin pathway is a potential target pathway to improve the

sensitivity to cisplatin of tumor cells. Matrine could reverse the drug resistance of cisplatin-resistant strains of A549 and H460 cells and to induce cell apoptosis of mitochondrial pathway by inhibiting β-catenin/survivin signaling pathway (Pu et al., 2018). The combination of low-dose Matrine and cisplatin could reverse the drug resistance of NSCLC cell lines A549 and DDP to cisplatin and promote cell apoptosis, which was related to the regulation of Nrf2/annexina4 (Liu et al., 2019).

2) Anti-hepatoma activity

Tumor stem cells are the basis of unlimited tumor proliferation. CD90, CD133 and EpCAM are the stem markers of liver cancer cells. Matrine could significantly inhibit the activation of Akt in hepatoma cell lines HepG2 and Huh7, inhibit the expression of stem cell genes such as CD90, CD133 and EpCAM, and then inhibit the proliferation and metastasis of hepatoma cells (Dai et al., 2019a). Matrine could inhibit cell proliferation (Zhou, 2017), metastasis (Kang et al., 2019), promote apoptosis (Zhou, 2017), and inhibit the xenograft growth of human hepatoma cell line HepG2 in tumor-bearing mice model, which was related to inhibiting ERK signaling pathway (Liu et al., 2017), inhibiting the expression of miRNA-122, livin and survivin genes (Zhou, 2017), activating cysteine protease independent pathway and promoting programmed cell death (Zhou et al., 2014b). Matrine combined with cisplatin could enhance inhibitory of cisplatin on xenograft growth of HepG2 in tumor-bearing mice model, which was related to down-regulating the expression of survivin, up-regulating the expression of caspase-3, and promoting the apoptosis of liver cancer cells (Hu et al., 2015a).

Tumor cell metastasis is the primary cause of cancer death and recurrence, closely related to the activation of EMT to loss cell adhesion. Hypoxic conditions are the microenvironment required for tumor migration and mir-199a-5p, and HIF-1 α are the critical factor of tumor metastasis (Raimondi et al., 2014). Under hypoxia, Matrine could inhibit the cell migration of human hepatoma cell lines BEL7402 and SMMC-7721, inhibit the xenograft growth of in hepatoma tumor-bearing mice model, which was attributed to up-regulating the expression of mir-199a-5p to induce HIF-1α downregulation, followed to activate EMT (Dai et al., 2021a). Matrine could significantly inhibit the migration and invasion of human hepatoma cell lines PLC/PRF/5 and MHCC97l, which was related to downregulating the expression of MMP-9 to inhibit degradation of extracellular matrix. Wang et al. (Wang et al., 2019b) found that Matrine could inhibit the cell proliferation, migration, and invasion of human hepatoma cell line SMMC-7721, which was related to the expression of Myc proto-oncogene protein, intercellular adhesion factor-1, EGFR, cysteine protease3, and MMP-2.

3) Anti-breast cancer activity

Matrine could inhibit the proliferation, migration and invasion, promote apoptosis of human breast cancer cell lines 4T1 (Dong, 2019), MCF-7 (Li et al., 2012b), BT-474 and MDA-MB-231 (Shao et al., 2013), inhibit xenograft growth in tumor-bearing mice model (Dong, 2019), which was attributed to inhibiting Wnt/β-Catenin pathway (Xiao et al., 2018), inhibiting the expression of miR-21, activating downstream phosphatase and tensin homologues, downregulating Akt phosphorylation level, activating JNK1/AP-1 signaling pathway, downregulating p53 expression (Shao et al., 2013), down-regulating VEGF expression (Xiao et al., 2018), up-regulating the ratio of apoptosis-related protein Bax/Bcl-2 (Dong, 2019).

LIN28A is a common biomarker and therapeutic target for breast cancer, while LET-7b is a tumor suppressor. LIN28A can inhibit the expression of LET-7b, which plays a key role in regulating breast cancer stem cell renewal and tumorigenesis. Matrine could inhibit the proliferation and differentiation of human breast cancer cell lines McF-7 and T47-D by down-regulating LIN28A expression and up-regulating LET-7b expression, inhibiting Wnt/β-catenin pathway, down-regulating CCND1 (cyclin-D1) expression, and inhibiting the proliferation and differentiation of human breast cancer cell lines McF-7 and T47-D (Li et al., 2020b). Endoplasmic reticulum stress leads to mitochondrial dysfunction and promotes cell apoptosis. Matrine could activate endoplasmic reticulum stress, down-regulate the expression of hexokinase2 to promote apoptosis of MCF-7 cells (Xiao et al., 2017). ITGB1 (integrin β1) is highly expressed in invasive breast cancer cells and plays a crucial role in breast cancer cell migration. Matrine could down-regulate ITGB1 and ETM and inhibit the proliferation and migration of human breast cancer cell lines MDA-MB-231 and MCF-7 (Ren et al., 2020).

ABCB1 (ATP binding cassette transporter B1) transporter is activated to promote the efflux of intracellular chemotherapeutic drugs to produce multidrug resistance. The combination of Matrine and doxorubicin could downregulate ABCB1 expression, reduce doxorubicin efflux and reverse the drug resistance of breast cancer resistant K562/ADR cells. Matrine could activate NF-κB signaling pathway to promote resistant K562/ADR cell apoptosis (Chen et al., 2019). Matrine could inhibit PI3K/Akt signaling pathway to down-regulate the expression of MDR1 (multidrug resistance1) and MRP1 (multidrug resistance-associated protein1), thereby reverse the drug resistance of MCF-7/ADR (Zhou et al., 2018).

4) Anti-leukemia activity

Tumor cells also use glycolysis to produce energy when oxygen is sufficient, that is, the Warburg effects (Warburg, 1956). Matrine could down-regulate the expression of hexokinase 2, inhibit glycolysis level, inhibit cell energy metabolism, inhibit the proliferation of human chronic myeloid leukemia cell line K562 and promote cell apoptosis (Lin et al., 2019). Matrine could induce K562 cell cycle arrest in the S phase, delay the G2/M phase, inhibit mitosis, inhibit K562 cell proliferation and induce apoptosis, which is related to the up-regulation of p27kipl protein expression (Wang et al., 2019c). The combination of NK (natural killer cells) and its receptor NKG2D helps lyse leukemia cells. NKG2D in leukemia cells is downregulated to avoid immune cell killing. Matrine could up-regulate NKG2D

expression in K562 cells, activate NK cells, release pro-inflammatory factors, increase NK cytotoxicity to K562 cells and inhibit the proliferation of K562 cells (Zhang et al., 2015).

Matrine could inhibit the growth and proliferation of human acute myeloid leukemia cell lines HL-60, THP-1, and C1498, which was related to inhibiting the Akt/mTOR signaling pathway (Wu et al., 2017).

PML/RARA (promyelocytic leukemia/retinoic acid receptor A) fusion protein can block the differentiation and maturation of granulocytes, which is the main cause of APL (acute promyelocytic leukemia). ATRA (all trans-retinoic acid) is widely used to treat APL, but it is susceptible to drug resistance. Matrine could cooperate with ATRA to inhibit telomerase activity and PML/RARA fusion protein expression, promote the degradation of PML/RARA fusion protein, up-regulate the expression of phospholipid reptilase1, and thereby reverse the drug resistance of ATRA (Liu, 2014).

## Anti-Inflammatory, Anti-Bacterium and Anti-Virus Effects

1) Anti-inflammatory activity

NF-κB signaling pathway is closely related to the secretion of inflammatory factors TNF and IL. Matrine could inhibit the NF-κB pathway, down-regulating pro-inflammatory factor TNF-α and IL-1β expression, down-regulating the expression of MMP2 and MMP3, and reducing the inflammatory response synovial tissue loss of type II CIA (collagen-induced arthritis) model mice. Matrine could inhibit the NF-κB pathway, down-regulate COX-2 (cyclooxygenase2) and iNOS expression to alleviate the pain caused by inflammatory response (Pu et al., 2016). Lu et al. (Lu et al., 2019) found that Matrine could clinically improve telangiectasia and edema caused by acute inflammation, which presented similar curative effects with aspirin.

Inflammatory mediator HMGB1 (high mobility group box1) is closely related to autoimmune encephalomyelitis. HMGB1 binding with Toll2 (Toll receptor2) can activate NF-κB pathway, promoting the release of pro-inflammatory factors and aggravating the inflammatory response. Matrine could inhibit HMGB1/Toll2/NF-κB pathway, downregulating TNF-α, IL-6, and IL-1β expression, inhibit inflammatory infiltration, reduce inflammatory injury in encephalomyelitis model mice (Chu et al., 2021). Matrine could up-regulate the expression of mirRNA-9 and inhibit JNK and NF-κB pathway to improve the inflammatory injury of PC12 cells induced by lipopolysaccharide and reduce the secondary damage of spinal cord injury in mice (Jiang and Jiang, 2020).

Matrine could inhibit the NF-κB pathway, down-regulate the expression of SOCS3 (suppressor of cytokine signaling proteins 3), inhibit the release of pro-inflammatory cytokines, inhibit inflammatory factors to stimulate airway epithelial cells to improve the symptoms of allergic airway inflammation in mice (Sun et al., 2016). Matrine could promote neutrophil apoptosis and reduce lung inflammation and injury caused by cigarette smoke (Yu et al., 2019).

In clinical trials, Matrine suppositories was used to treat chronic pelvic inflammatory disease, and the relieving effects of Matrine treatment group was better than that of the control group. Serum TNF-α, IL-1β, and IL-6 in Matrine group were significantly lower than that of the control group (Liu et al., 2020). 2, 4, 6-trinitrobenzene sulfonic acid can induce colitis in mice and cause intestinal flora imbalance. Matrine could reduce the secretion of inflammatory factors, regulate intestinal flora, and alleviate colon injury in mice (Li et al., 2019). Retinal neuritis is the leading cause of visual impairment in adolescents. Matrine could down-regulate NF expression, inhibit the release of pro-inflammatory cytokines, up-regulate Bcl-2/Bax ratio, reduce inflammatory infiltration and demyelination, and reduce retinal optic nerve ganglion cell apoptosis in retinal neuritis model mice (Kang et al., 2021).

2) Anti-bacterium activity

Matrine has broad-spectrum anti-bacterial effects. It has inhibitory effects on cocci and bacilli, such as *Staphylococcus aureus* and *Escherichia coli*, and has certain inhibitory effects on fungi. The formation of bacterial biofilm can protect bacteria from drug and environmental stimuli to produce drug resistance. Matrine could increase the membrane permeability of *Staphylococcus epidermidis* to induce its death in a dose-dependent manner, the efficacy was better than ciprofloxacin and erythromycin (Ren et al., 2020). Matrine had favorable inhibitory effects on *Staphylococcus aureus* (MIC, 25 μg/ml) (Chen et al., 2019), *E. coli* (MIC, 12.5 μg/ml) (Zhu, 2014), *Bacillus subtilis* (MIC, 12.5 μg/ml) (Liu et al., 2011), *Pseudomonas aeruginosa* (MIC, 25 μg/ml) (Zhang et al., 2011b), *Candida albicans* (MIC, 25 μg/ml) (Zhang et al., 2011b). Jing et al. (Jing et al., 2019) showed that Matrine could reduce endometritis caused by phosphoteichoic acid of *Staphylococcus aureus*, which was attributed to inhibiting TLR2/NF-κB signaling pathway.

Zhang et al. (Zhang et al., 2020b) showed that Matrine had favorable inactivation effects on *Aspergillus fumigatus*, *Trichophyton mentagrophyte*, and *Cryptococcus neoformans*. Fluconazole is a commonly used drug for fungal infections. With the increase of drug use times, fungi can develop drug resistance. Matrine could inhibit the transformation of *Candida albicans* from yeast to mycelium and reverse the drug resistance of fluconazole-resistant *Candida albicans* (Shao et al., 2014). 90% of pecan trees will be infected with pecan dry rot fungi, causing substantial economic losses to farmers. Pan (Pan, 2018) found that Matrine could act on pecan dry rot fungi, which could change the permeability of fungal cell membrane, inhibit the spore germination, inhibit the mycelial growth, inhibit the fungal glycolysis pathway, enhance aerobic respiration and produce a large number of ROS to injury pecan dry rot fungi.

3) Anti-virus activity

Yang et al. (Yang et al., 2012) found that Matrine could inhibit the RNA replication of human enterovirus 71 (EV71) in rhabdomyosarcoma cells and reduce the mortality of mice

**TABLE 2 |** 1-position modification of Matrine.

| Name of matrine derivative | Basic structure of derivatives | R Substituent structure | Structure of matrine derivatives | Pharmacological activity | Refrences |
|---|---|---|---|---|---|
| Matrine acetylsalicylate | 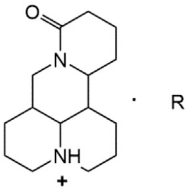 | 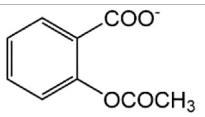 | 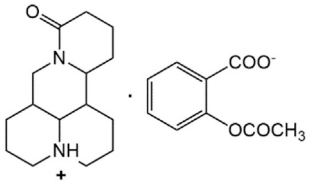 | Anti-inflammation and pain relief | Fu et al. (2011) |
| Matrine 3-nitrooxymethyl benzoate | 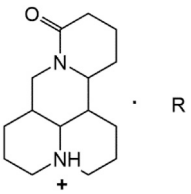 | 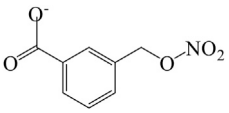 | 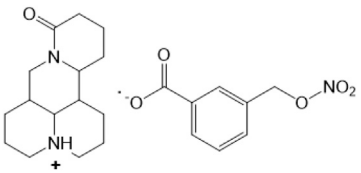 | Anti-myocardial ischemia | Li et al. (2015) |
| Matrine [$GaCl_4$] complex | 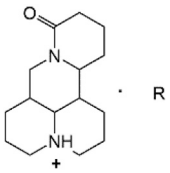 | 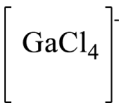 | 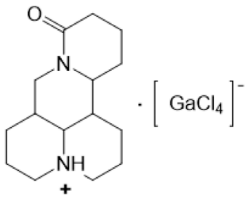 | Anti tumor | Chen et al. (2011) |
| Matrine [$AuCl_4$] complex | 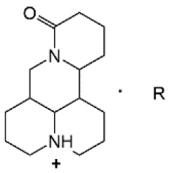 | 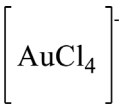 | 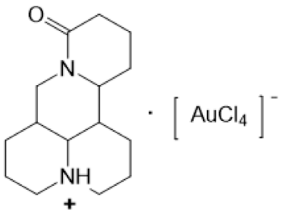 | Anti tumor | Chen et al. (2011) |

under the lethal dose of the virus. Clinical trials found that the positive serum HBV DNA in patients with chronic hepatitis B was significantly turned into negative by intramuscular injection of Matrine, which greatly improved liver function without noticeable side effects (Long et al., 2004). Animal experiments confirmed that Matrine could block the adsorption of hepatitis virus, inhibit the expression and secretion of HBsAg, HBeAg, and HBV-DNA by hepatocytes to produce anti-hepatitis virus effects (Zhang and Shen, 2018b). Yang found that Matrine sodium chloride injection had an excellent clinical impact in treating new Coronavirus pneumonia (Yang et al., 2020). Peng et al. (Peng et al., 2020) explored the mechanism of Matrine in treating COVID-19 by molecular docking technology. It was indicated that Matrine could inhibit viral replication and promote apoptosis of infected cells by downregulating TNF-α and IL-6 and up-regulating the expression of caspase-3. The mixed infection of PRRSV (porcine reproductive and respiratory syndrome virus) and PCV2 (porcine circovirus type2) could result in pig death. Nasun et al. (Sun et al., 2020) found that Matrine decreased the replication of the two viruses in the mouse liver and enhanced the immune function of mice in a dose-dependent manner. Matrine could inhibit PRRSV infection in Marc-145 cells, which was related to directly inactivate PRRSV, down-regulate PRRSV protein expression (Sun et al., 2014). Matrine had favorable inhibitory effects on tobacco mosaic virus, which was superior to commercial drug ribavirin (Ni et al., 2017).

## Other Effects

1) Analgesic activity

The N atom at position one of Matrine is an influential group for its analgesic effects, and it has noticeable analgesic effects. Haiyan et al. (Haiyan et al., 2013a) found that Matrine (7.5–30 mg/kg) could obviously reduce neuropathic pain by ligating the sciatic nerve of mice. Yang et al. (Yang et al., 2016) found that Matrine could reduce visceral inflammation and pain caused by acetic acid, physical pain caused by thermal stimulation, and neuropathic pain caused by sciatic nerve ligation, which was not attributed to central analgesia induced by activating opioid receptors. Gong (Gong, 2017) found that Matrine could reduce the neuropathic pain caused by vincristine and improve the

**TABLE 3 |** Hydrolysis modification of D-ring lactam of Matrine.

| Name of matrine derivative | Basic structure of derivatives | R1 substituent structure | R2 substituent structure | Structure of matrine derivatives | Pharmacol-ogical activity | Refrence |
|---|---|---|---|---|---|---|
| Butyl 12-benzyl matrine | 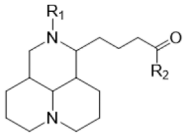 | 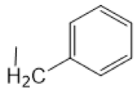 | 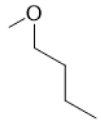 | 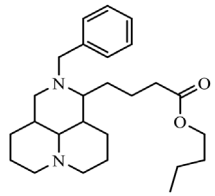 | Anti tumor | Chao et al. (2013) |
| 12-matrine thiomorphamide | 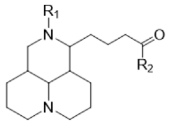 | 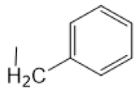 | 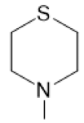 | 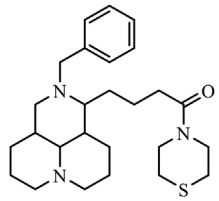 | Anti tumor | Chao et al. (2013) |
| 12-N-Benzenesulfonyl Matrine Butane | 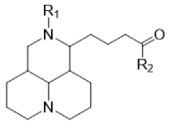 | 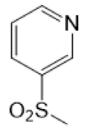 | 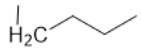 | 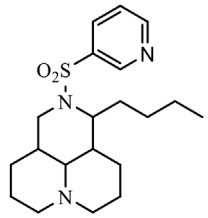 | Antivirus | Li et al. (2017a) |
| 12-N-4-Methoxybenzyl Sophora Ethanol | 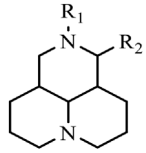 | 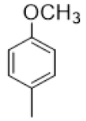 | 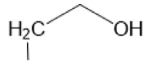 | 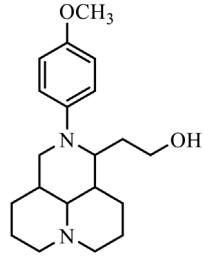 | Antivirus | Li et al. (2020) |
| 12-N-dodecyl matrine butyl ester | 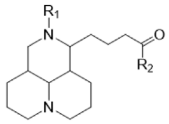 | $-C_{12}H_{25}$ | $-CH_3$ | 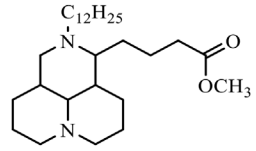 | Antivirus | Fu and TangSLi (2014) |

neuropathic changes of the sciatic nerve, dorsal root ganglion, and dorsal horn of the dorsal spinal cord, which was related to inhibiting the expression of the inflammatory factor TNF-α, IL-10 and IL-6 to disable RAS (renin-angiotensin system), affecting the phosphorylation of downstream key molecule RAF (rheumatoid arthritis factor), failing activation of downstream factor ERK1/2 (extracellular regulated protein kinase1/2) and blocking the transmission of pain signals. Matrine could reduce mechanical hyperalgesia and thermal hyperalgesia in a dose-dependent manner to reduce the neuropathic pain caused by chronic constriction injury (Haiyan et al., 2013b). Acetaminophen is commonly used anti-pyretic and analgesic drug with favorable analgesic effects, but it has specific liver toxicity. The combination of Matrine and acetaminophen had better analgesic effects than acetaminophen alone and could alleviate the hepatotoxic injury caused by acetaminophen (Dai et al., 2021b). ATP combined with its receptor P2X can increase the sensitivity of neurons to induce neuropathic pain (Yin et al., 2019). When the nerve is damaged, the expression of P2X2 and P2X3 is up-regulated, and the threshold of neuropathic pain is reduced. Matrine could reduce neuropathic pain in rats by downregulating the expression of P2X2 and P2X3 in neurons (Li et al., 2020c).

2) Immunosuppressive activity

Matrine has immunosuppressive effects and Matrine suppresses autoimmune response by inhibiting the immune activity of T cells, B cells and macrophages (Ji and Zhang, 2014). Wang et al. (Wang, 2018) showed that intraperitoneal injection of 5 mg/kg Matrine could inhibit the immune rejection after corneal transplantation, which was attributed to increasing the secretion of IL-10 and TGF-β1 in rats. Kan et al. (Kan et al., 2013) showed that Matrine could treat experimental autoimmune encephalomyelitis by inhibiting the migration and infiltration of inflammatory cells into the central nervous system, which was related to significantly downregulate the expression of CVAM-1 and ICAM-1, chemokine CCL3, CCL5, and Toll receptor4 in a dose-dependent manner. Matrine could reduce neurological injury in the mouse model of mild encephalomyelitis, which was related to inhibit the migration of immune cells, prevent the destruction of the blood-brain barrier and prevent the central nervous system from inflammatory infiltration (Jiang et al., 2021).

## ADVANCES ON DERIVATIZATION OF MATRINE

Matrine has analgesic effects and the tertiary amino group at the N-1 position is critical for analgesic effects (Wu, 2014; Li, 2015). With modification around N-1 position, Matrine derivatives with lipophilic N-1 structure modification were obtained, and their analgesic activity was enhanced (He et al., 2011). The amide bond may be one of the groups with anti-cancer activity when the lactam of Matrine D-ring was hydrolyzed into Matric acid, the anti-cancer activity disappeared, and after the carboxyl group of Matrine was converted into amide group, the anti-cancer activity recovered. Additionally, the anti-cancer activity was higher than that of Matrine after the conversion of carboxylic acid to esters with longer alkane chain (Hu et al., 2015b). The oxidation or dehydrogenation of Matrine could reduce the toxicity of Matrine, and it was concluded that the toxicity of Sophoramine > Sophocarpine > Matrine (Han, 2012). The molecular conformation of Matrine also affected the anti-tumor activity and Matrine with 5S conformation had better anti-tumor activity than 5R conformation.

Although Matrine has a wide range of pharmacological effects, its low bioavailability and high dosage limit its clinical application. Matrine derivatives were obtained by structural optimization to improve its efficacy and main modification sites were as follows: (1) Tertiary amine at N-1 position. (2) D-ring lactam hydrolysis. (3) C-15 position carbonyl group. (4) C-13 position and C-14 position double bond. (5) C-14 position α-H. The main modification stratigies of Matrine include introducing liposoluble groups and nitrogen-containing heterocyclic structures (N-substituted pyrrole, N-substituted indole, benzenesulfonyl and organic nitrates), combining with active compounds (cisplatin and salicylic acid), and forming complexes with metal ions ($[GaCl_4]^-$ $[FCl_4]^-$ and $[AuCl_4]$).

### N-1 Modification

The A and B rings of Matrine were relatively stable with inactive reactivity. However, the tertiary amine at the N-1 position with strong basicity can react with acidic substances to form salts (He et al., 2011). Acetylsalicylic acid, with anti-pyretic and analgesic effects, can react with Matrine to form acetylsalicylic acid Matrine salt (**Table 2**). It can increase anti-pyretic and analgesic effects and reduce the side effects of acetylsalicylic acid on the intestinal tract and the toxicity of Matrine (Fu et al., 2011). Cinnamic acid has anti-tumor activity. It was combined with Matrine to obtain Matrine cinnamic acid salt to improve its anti-cancer activity (**Table 2**) (Zhang et al., 2009b). Li et al. (Li, 2015) synthesized a series of derivatives by the reaction of organic nitrates with Matrine, among which 3-nitroxymethylbenzoic acid Matrine (**Table 2**) had better protective effects on myocardial morphology and structure of isoproterenol-induced myocardial ischemia rats than Matrine. Matrine metal ion complexes (**Table 2**) exhibited comparable anti-cancer efficacy with combination of Matrine and cisplatin by reaction with $[GaCl_4]^-$ and $[AuCl_4]^-$ (Chen et al., 2011).

### Hydrolytic Modification of D-Ring Lactam

The D-ring lactam of Matrine was hydrolyzed in an alkaline solution to give stable matric acid with two modified secondary amino and carboxylic groups. The introduction of nitrogen-containing heterocycles is a common strategy for structural modification of natural products, which improves their bioactivity. The bioactivity of Matrine with high soluble in water would be improved by introducing hydrophobic groups (He et al., 2011). Chao et al.

**TABLE 4 |** C-15 position modification of Matrine.

| Name of matrine derivative | Name of matrine derivative | Pharmacological activity | Refrence |
|---|---|---|---|
| Deoxymatrine | 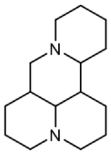 | Resistance to tobacco mosaic virus | Ni et al. (2017) |
| Compound 1 | 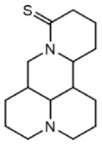 | No change in activity | Li et al. (2020) |
| (E)-15-(N-4-biphenyl) matrine | 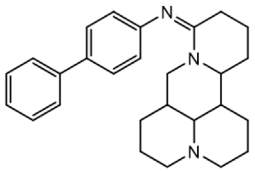 | Anti tumor | Hassan et al. (2015) |
| (E) -15- (N-4-phenoxyphenyl) matrine | 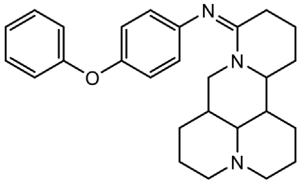 | Anti tumor | Hassan et al. (2015) |

(Chao et al., 2013) introduced the benzyl group at the 12-position of Marine and introduced ester, aminoalkyl, and nitrogen-containing heterocycles with different alkyl chain length at the 11-position of Matrine. The new Matrine derivatives exhibited better anti-proliferation activity than Matrine (**Table 3**). The inhibitory effects of 12-matric acid thiomorphinamide (**Table 3**) on HepG2 cell proliferation was better than paclitaxel and was 20 times higher than matrine. Amide bond plays a vital role in anti-tumor. Li et al. (Li et al., 2017a) introduced a butanyl side chain at the C-11 position of Matrine and conducted a systematic study on substituting the 12-position atom. It was found that introducing a benzenesulfonyl group at the 12-position gave the derivative 12-N-Benzenesulfonyl kushenbutane (**Table 3**), which increased the activity against the Coxsackie virus ($EC_{50}$, 2.02 μM for Coxsackie B3, 7.41 μM for Coxsackie A16), which was expected to become a drug candidate for treating Coxsackie virus infection. Matrine was hydrolyzed, matric acid as an intermediate, ethanol was introduced at the C-11 position, and 4-methoxybenzyl was presented at the N-12 position to obtain 12-N-4-methoxybenzyl matrine ethanol (**Table 3**). It exhibited favorable anti-hepatitis B virus activity ($EC_{50}$, 3.2 μmol) (LI et al., 2020). Fu and TangSLi (Fu and TangSLi, 2014) used 12-benzylmatric acid as the lead compound and replaced the N-12 group with different hydrophobic groups such as n-butyl, n-octyl, n-dodecyl and aromatic groups. The anti-tuberculosis activity and structure-activity relationship of Matrine derivatives were investigated and 12-N-dodecyl *Sophora* flavescens butyl methyl ester (**Table 3**) showed 16 times high anti-tuberculosis activity than the lead compound. The modification with 11-position ester group, acid group, alcohol group and 12 position hydrophobic group increased anti-tuberculosis effects of Matrine.

## C-15 Modification

There are three main modification strategies at C-15 position of Matrine. (1) Reducing the carbonyl group to an alkyl group by a reducing agent. The lactam of Matrine was reduced to a secondary amine to obtain Deoxymatrine (**Table 4**), which lost its anti-cancer activity. However, it presented better anti-tobacco mosaic virus activity than Matrine. It was speculated that lone pair electrons enhanced the bioactivity of two nitrogen atoms (Ni et al., 2017). (2) O-atom arrangement of the carbonyl group. The carbonyl oxygen atom at C-15 position of Matrine was replaced with sulfur atom to obtain compound 1 (**Table 4**), which exhibited comparable bioactivity with Matrine (LI et al., 2020). (3) N-15 position modification. 15-N-substituted Matrine imine derivatives were obtained by synthesizing amidines with aromatic amines and lactams. It was found that (E)-15-(N-4-Biphenyl) Matrine and (E)-15-(N-4-phenoxy phenyl) (**Table 4**) exhibited favorable *in vitro* anti-tumor activity against human liver cancer cell line HepG2 ($IC_{50}$, <50 μM) and human cervical cancer cell line HeLa ($IC_{50}$, <50 μM) (Hassan et al., 2015).

## C-14 Modification

The αH at 14-position of Matrine was affected by the electron-withdrawing effects of the carbonyl group. The introduction of double bonds and aromatic rings could significantly improve

**TABLE 5 |** C-14 position modification of Matrine.

| Name of matrine derivative | Basic structure of derivatives | R Substituent structure | Structure of matrine derivatives | Pharmacological activity | Refrence |
|---|---|---|---|---|---|
| N-benzyl-2-pyrromethene matrine | 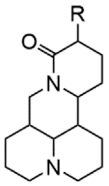 | 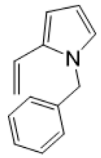 | 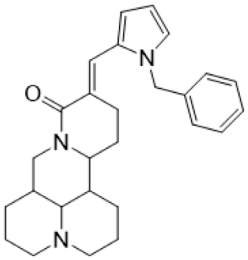 | Anti tumor | Zhang et al. (2018a) |
| N-3,5 dimethoxybenzyl-2-pyrromethene matrine | 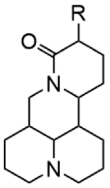 | 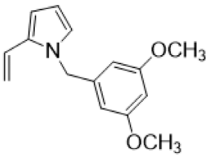 | 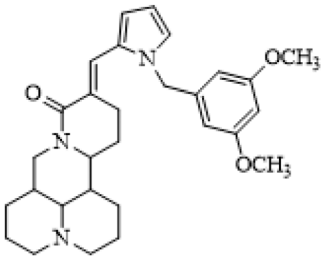 | Anti tumor | Zhang et al. (2018a) |
| N- 3-chlorobenzyl-3-6-methoxyindole methylene matrine | 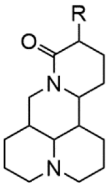 | 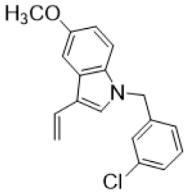 | 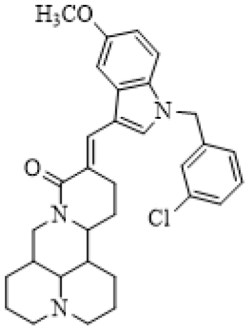 | Anti tumor | Zhang et al. (2018a) |
| 14–3,4,5-trimethoxybenzylidene matrine | 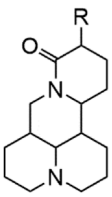 | 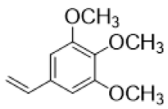 | 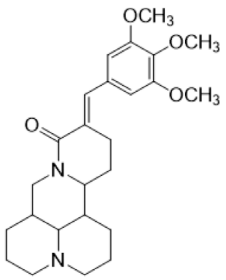 | Anti tumor | Wei et al. (2013) |
| Compound 2 | 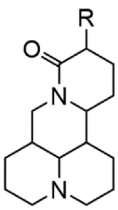 | 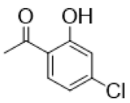 | 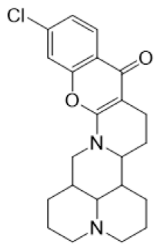 | Anti tumor | Wu et al. (2016) |

(Continued on following page)

**TABLE 5 |** (*Continued*) C-14 position modification of Matrine.

| Name of matrine derivative | Basic structure of derivatives | R Substituent structure | Structure of matrine derivatives | Pharmacological activity | Refrence |
|---|---|---|---|---|---|
| 14-[2-(6-bromo) naphthalene hydroxymethenyl] matrine | 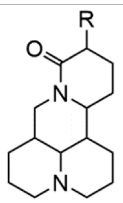 | 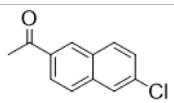 | 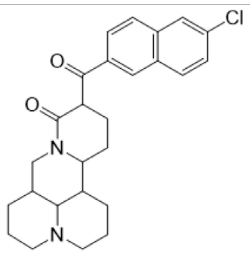 | Anti tumor | Yang (2015) |

anti-tumor activity. N-substituted pyrrole scaffolds were key groups to increase anti-cancer activity. Zhang et al. (Zhang et al., 2018a) introduced N-(substituted-2-pyrrolylene) and N-(substituted-2-polymethylene) skeletons at C14-position and found that the introduction of benzyl group at nitrogen atom to obtained N-benzyl-2-pyrrolomethyl Matrine (**Table 5**), which exhibited 115–172 times higher *in vitro* anti-cancer activity against SMMC-7721, A549, and CNE2 cells than Matrine. N-3,5 dimethoxybenzyl-2-pyrromethene Matrine and N-3-chlorobenzyl-3-6 methoxyindole methylene Matrine could significantly promote SMMC-7721 and CNE2 cell apoptosis in a dose-dependent manner. The Matrine derivatives were obtained by aldol condensation reaction with Matrine and 3-methoxy benzaldehyde, 2,3-dimethoxybenzaldehyde, 3, 4, 5-trimethoxybenzaldehyde or 2, 3, 4-trimethoxybenzaldehyde, which exhibited better anti-proliferation activity against cancer cells HT-29 and PANC-1 than Matrine (Wei et al., 2013). The anti-cancer activity of 14-3,4,5-trimethoxybenzylidene Matrine (**Table 5**) was 3 times higher than Matrine. The number and position of substituted methoxy groups on benzaldehyde affected its anti-cancer activity, and decreasing the steric hindrance could increase the anti-cancer activity. Wu et al. (Wu et al., 2016) introduced an enol group at 14-position of Matrine and replaced the hydroxyl group with the carbonyl group at 15-position to obtain six 6-member ring Matrine derivatives. The optimal compound 2 (**Table 5**) exhibited 48–109 times higher anti-cancer activity than Matrine. Compound 2 could inhibit cell migration and induce cell arrest at G1 phase of human hepatoma cell lines BEL-7402 and HepG2 by upregulating p21 and p27 and downregulating N-cadherin. Matrine derivatives exhibited favorable anti-proliferative activity against A549, BT-20, MCF-7, and U20S tumor cells by introducing nitrogen heterocycle, oxygen heterocycle, and naphthalene ring into Matrine (Yang, 2015). The optimal derivative 14-[2-(6-Bromo) naphthalene hydroxymethenyl] Matrine (**Table 5**) exhibited 1000 times higher anti-proliferation activity than Matrine. It could induce A549 cell cycle arrest at G1 phase and promote cell apoptosis by producing ROS in a dose-dependent manner.

## C-13 Modification

Guo et al. (Guo et al., 2011) replaced the carbonyl group at 15-position with the sulfur atom and introduced different amino side chains at 13-position of Matrine by a classic Michael addition reaction to obtain Matrine derivatives with Sophocarpine as the raw material. The derivative 13-(N-methylene) amino-18-thiomatrine (**Table 6**) exhibited the optimal anti-cancer activity. The introduction of polyamines can improve anti-inflammation activity of Matrine. Matrine derivative MASM (**Table 6**), 13-(N-methyl)-amino-18-thiomatrine, exhibited anti-rheumatoid arthritis activity *in vivo* and *in vitro* (Zou, 2018). Han et al. (Han et al., 2012) introduced methoxyl at 13-position to produce 13-α-methoxymatrine with Sophocarpine as raw material, which exhibited better anti-bacterial propagules activity than Matrine. Alkylating agent has always been used as effective chemotherapeutic drug. Cui et al. (Cui et al., 2015) used Sophocarpine as raw material to introduce anti-cancer drugs into Mareine, such as mustard anti-neoplastic drugs melphalan {L3 [p-[bis(2-chloroethyl)amino]phenyl] alanine}, bendamustine (4-[5-[bis(2-chloroethyl)amino]-1-methylbenzimidazol-2-yl] butyric acid) and phosphoryl nitrogen mustard dichloride, the active metabolite of cyclophosphamide compounds 3, 4 and 5 (**Table 6**). Compound 1 and compound 2 exhibited better anti-tumor activitie than melphalan and bendamustine. Dai et al. (Dai et al., 2019b) synthesized 10 novel 13-hydroxyethyl amine Matrine derivatives. The derivative 13-(N-butyl benzyl) hydroxyethyl amine Matrine (**Table 6**) exhibited 30 times higher anti-proliferation activity against HepG-2 cells and HeLa cells than Matrine and Sophorine.

## CONCLUDING REMARKS

Matrine is an alkaloid extracted from traditional Chinese herbs including *Sophora* flavescentis, *Sophora* alopecuroides, *Sophora* root, etc, which was the main resource of Matrine. The common procedures are solvent extraction, ultrasonic aided extraction, and microwave-assisted extraction. Solvent extraction is appropriate for industrial manufacturing, while ultrasonic-assisted and microwave-assisted extraction are suitable for laboratory preparation. But, the yield of Matrine was low by extraction from natural plants. Researchers developed three main total synthesis strategies to increase the yield of Matrine. However, most of the synthesis routes were long, the synthesis conditions were not easy to control, and the yield was low (He

**TABLE 6 |** C-13 position modification of Matrine.

| Name of matrine derivative | R Substituent structure | Structure of matrine derivatives | Pharmacological activity | Refrence |
|---|---|---|---|---|
| 13 - (N-methylene) amino-18 thiomatrine | 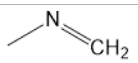 | 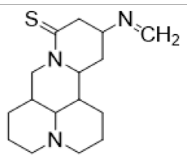 | Anti-inflammatory | Guo et al. (2011) |
| 13-(N-methyl)-amino-18-thiomatrine | 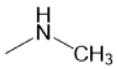 | 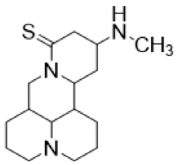 | Anti-inflammatory | Zou (2018) |
| 13-α-methoxy matrine | 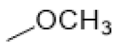 | 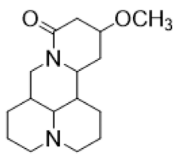 | Sterilization | Han et al. (2012) |
| Compound 3 | 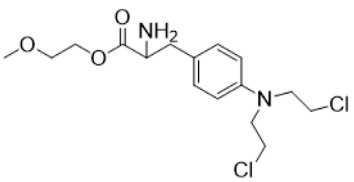 | 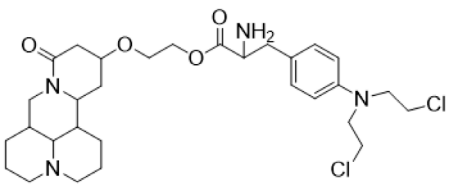 | Anti tumor | Cui et al. (2015) |
| Compound 4 | 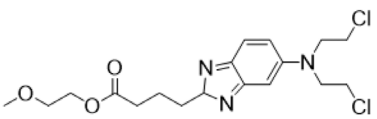 | 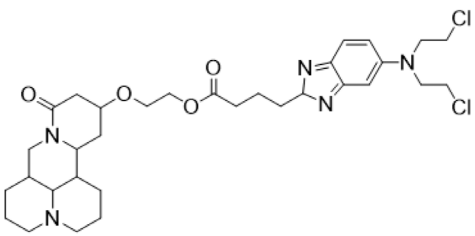 | Anti tumor | Cui et al. (2015) |
| Compound 5 | 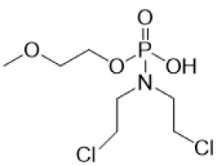 | 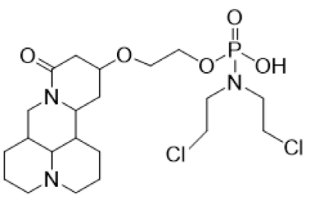 | Anti tumor | Cui et al. (2015) |
| 13- (N-4-tert-butylbenzyl) hydroxyethylamin-e matrine | 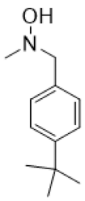 | 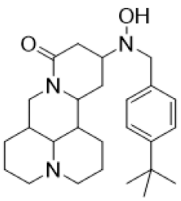 | Anti tumor | Dai et al. (2019b) |

et al., 2011), which needed further study to develop optimal synthesis strategies.

Matrine has the dual advantages of traditional Chinese herbs and chemotherapy drugs and exhibits distinct benefits in preventing and improving chronic diseases such as cardiovascular disease and tumors. Matrine exhibited favorable activity on anti-atherosclerosis, anti-hypertension, anti-ischemia reperfusion injury, anti-arrhythmia, anti-diabetic cardiovascular

complications, anti-tumor, anti-inflammatory, anti-bacterium, anti-virus. But the molecular function mechanism of Matrine is in the air, which needs further research works to explore.

Although Matrine exhibited multiple bioactivities, its low bioavailability and high dosage limit its clinical application. Matrine derivatives were obtained by structural optimization to improve its efficacy and main modification sites were as follows: (1) Tertiary amine at N-1 position. (2) D-ring lactam hydrolysis. (3) C-15 position carbonyl group. (4) C-13 position and C-14 position double bond. (5) C-14 position α-H. The main modification stratigies of Matrine include introducing liposoluble groups and nitrogen-containing heterocyclic structures (N-substituted pyrrole, N-substituted indole, benzenesulfonyl and organic nitrates), combining with active compounds (cisplatin and salicylic acid), and forming complexes with metal ions ($[GaCl_4]^-$ $[FCl_4]^-$ and $[AuCl_4]$). Various Matrine derivatives exhibited better bioactivity than Matrine, which would provide new core structures and new insights for new drug development in related fields. There are still further research works needed to be done to obtained optimal derivatives with high bioactivity and low side effects. With the further research in derivatization and molecular mechanism, Matrine would have wider application prospects in the future.

## AUTHOR CONTRIBUTIONS

H-LC designed the research study. X-YS, L-YJ, ZR, wrote the manuscript. L-QC, MG, JJ, Y-DW, LH, Y-HL, collected the references. Z-JH, LL, R-KM, Y-FL, K-KS analyzed the data. JZ, XZ, A-HL and H-LC revised the paper. All authors contributed to editorial changes in the manuscript. All authors read and approved the final manuscript.

## FUNDING

This work was supported by the National Natural Science Foundation of China (U1932130); the Key Program of Shaanxi Provincial Science and Technology Department (2021SF-303); the Key Program of Shaanxi Provincial Education Department (20JS138); the Program of Shaanxi Administration of Traditional Chinese Medicine (2019-ZZ-ZY009); the Key Program of Weiyang District Bureau of Science, Technology and Industry Information Technology (201928).

## REFERENCES

An, Q., Han, C., Zhou, Y., Li, F., Li, D., Zhang, X., et al. (2016). Matrine Induces Cell Cycle Arrest and Apoptosis with Recovery of the Expression of miR-126 in the A549 Non-small Cell Lung Cancer Cell Line. *Mol. Med. Rep.* 14 (5), 4042–4048. doi:10.3892/mmr.2016.5753

Antzelevitch, C., and Belardinelli, L. (2006). The Role of Sodium Channel Current in Modulating Transmural Dispersion of Repolarization and Arrhythmogenesis. *J. Cardiovasc. Electrophysiol.* 17, S79–S85. doi:10.1111/j.1540-8167.2006.00388.x

Bers, D. M., Eisner, D. A., and Valdivia, H. H. (2003). Sarcoplasmic Reticulum Ca 2+ and Heart Failure. *Circ. Res.* 93 (6), 487–490. doi:10.1161/01.res.0000091871.54907.6b

Bohlmann, F., Rahtz, D., and Arndt, C. (2010). Lupinen-Alkaloide, XI. Die Alkaloide aus Sophora flavescens. *Berichte der deutschen chemischen Gesellschaft* 91 (10), 2189–2193. doi:10.1002/cber.19580911026

Chan, S., Zhang, Z., and Zhang, J. (2017). Matrine Increases the Inhibitory Effects of Afatinib on H1975 Cells via the IL-6/JAK1/STAT3 Signaling Pathway. *Mol. Med. Rep.* 16 (3), 2733–2739. doi:10.3892/mmr.2017.6865

Chao, F., Wang, D.-E., Liu, R., Tu, Q., Liu, J.-J., and Wang, J. (2013). Synthesis, Characterization and Activity Evaluation of Matrinic Acid Derivatives as Potential Antiproliferative Agents. *Molecules* 18 (5), 5420–5433. doi:10.3390/molecules18055420

Chen, F., Pan, Y., Xu, J., Liu, B., and Song, H. (2022). Research Progress of Matrine's Anticancer Activity and its Molecular Mechanism. *J. Ethnopharmacol* 286, 114914. doi:10.1016/j.jep.2021.114914

Chen, J., Browne, L. J., and Gonnela, N. C. (1986). Tatal Synthesis of (±)-matrine. *J. Chem. Soc. Chem. Commun.* (12), 905–907. doi:10.1039/C39860000905

Chen, J., Yang, X. Q., and Tang, F. Y. (2017). Ultrasonic Extraction of Matrine and Oxymatrine in Sophora Flavescens. *J. Guangdong Chem. Industry* 44 (05), 62–63. doi:10.3969/j.issn.1007-1865.2017.05.028

Chen, Z., Nishimura, N., Okamoto, T., Wada, K., and Naora, K. (2019). Molecular Mechanism of Matrine from Sophora Alopecuroides in the Reversing Effect of Multi-Anticancer Drug Resistance in K562/ADR Cells. *Biomed. Res. Int.* 2019, 1269532. doi:10.1155/2019/1269532

Chen, Z.-F., Mao, L., Liu, L.-M., Liu, Y.-C., Peng, Y., Hong, X., et al. (2011). Potential New Inorganic Antitumour Agents from Combining the Anticancer Traditional Chinese Medicine (TCM) Matrine with Ga(III), Au(III), Sn(IV) Ions, and DNA Binding Studies. *J. Inorg. Biochem.* 105 (2), 171–180. doi:10.1016/j.jinorgbio.2010.10.007

China National Center for Cardiocascular Disease (2020). Practice Guidelines for Comprehensive Management of Cardiovascular Diseases at Primary Levels 2020. *Chin. J. Med. Front. (Chinese)* 12 (08), 1–73.

Chu, Y., Jing, Y., Zhao, X., Wang, M., Zhang, M., Ma, R., et al. (2021). Modulation of the HMGB1/TLR4/NF-Kb Signaling Pathway in the CNS by Matrine in Experimental Autoimmune Encephalomyelitis. *J. neuroimmunology* 352, 577480. doi:10.1016/j.jneuroim.2021.577480

Cui, X. Y., Zhang, N., and Tao, Z. W. (2015). Synthesis and Antitumor Activity of Matrine-Nitrogen Mustard Complex. *Chem. Reagents (Chinese)* 37309-312+370 (04), 309–312+70. doi:10.13822/j.cnki.hxsj.2015.04.006

Cui, Y., Zhang, Y., and Hu, C. M. (2007). Extraction and Isolation of Alkaloids from Sophora Flavescens. *J. Chongqing Inst. Tech. (Chinese)* 03, 113–116. doi:10.3969/j.issn.1674-8425-B.2007.03.033

Dai, G., Li, B., Xu, Y., Li, Z., Mo, F., and Wei, C. (2021). Synergistic Interaction between Matrine and Paracetamol in the Acetic Acid Writhing Test in Mice. *Eur. J. Pharmacol.* 895, 173869. doi:10.1016/j.ejphar.2021.173869

Dai, H., Sun, P., and Du, T. T. (2019). Synthesis and Antitumor Pharmacological Activity of 13-hydroxyethylamine Matrine Derivatives. *J. Chem. Res. Appl. (Chinese)* 31 (06), 1006–1012. doi:10.3969/j.issn.1004-1656.2019.06.002

Dai, M., Cai, Z., Chen, N., Li, J., Wen, J., Tan, L., et al. (2019). Matrine Suppresses Stemness of Hepatocellular Carcinoma Cells by Regulating β-catenin Signaling Pathway. *Nan Fang Yi Ke Da Xue Xue Bao* 39 (10), 1239–1245. doi:10.12122/j.issn.1673-4254.2019.10.17

Dai, M., Chen, N., Li, J., Tan, L., Li, X., Wen, J., et al. (2021). *In Vitro* and *In Vivo* Anti-metastatic Effect of the Alkaliod Matrine from Sophora Flavecens on Hepatocellular Carcinoma and its Mechanisms. *Phytomedicine* 87, 153580. doi:10.1016/j.phymed.2021.153580

Dong, H. D. (2019). Effects of Matrine on JNK1/AP-1 Signaling Pathway in a Breast Cancer Tumor Model of 4T1 Mice. *J. Liaoning Univ. Traditional Chin. Med. (Chinese)* 21 (11), 64–68. (Chinese). doi:10.13194/j.issn.1673-842x.2019.11.017

Feng, Y. (2005). The Medicinal Value of Matrine. *J. Qinghai Univ. (Natural Sci. Edition) (Chinese)* 06, 50–51. doi:10.13901/j.cnki.qhwxxbzk.2005.06.016

Fleming, F. F., Hussain, Z., Weaver, D., and Norman, R. E. (1997). α,β-Unsaturated Nitriles: Stereoselective Conjugate Addition Reactions. *J. Org. Chem.* 62 (5), 1305–1309. doi:10.1021/jo9619894

Fu, B. (2017). *Design, Synthesis and Antitumor Activity of Novel Matrine Derivatives [D]*. Shanghai, China: Second Military Medical University (Chinese). doi:10.7666/d.Y3247398

Fu, H. G., TangSand Li, Y. H. (2014). Synthesis of Novel 12-N-Substituted Matrine Derivatives and Their Antituberculosis Activity. *Chinese J. Syn. Chem.* 6 (22), 739–743.(Chinese). doi:10.15952/j.cnki.cjsc.2014.06.005

Fu, L., Liu, J., and He, L. Q. (2011). Synthesis of Acetylsalicylic Acid Matrine. *Anhui Chem. Industry* 37 (01), 46–47+69. (Chinese). doi:10.3969/j.issn.1008-553X.2011.01.011

Fu, Q. F., Cao, Q., and Lv, S. W. (2015). Optimization of Ultrasonic Extraction Process of Sophora Flavescens Alkaloids from Sophora Flavescens. *Chin. Med. Inf. (Chinese)* 32 (01), 11–13.

Ge, G. T. Y., and Xu, L. (2020). The Therapeutic Mechanism of Aloperine, a Monomer of Traditional Chinese Medicine, on Pulmonary Arterial Hypertension. *Electron. J. Cardiovasc. Dis. Integr. Chin. West. Med. (Chinese)* 8 (36), 35+45. doi:10.16282/j.cnki.cn11-9336/r.2020.36.025

Gong, S. S. (2017). *Analgesic Effect of Matrine on Vincristine-Induced Neuropathic Pain in Mice and its Effect on Ras/Raf/ERK1/2 Signaling Pathway [D]*. Yinchuan: Ningxia Medical University (Chinese).

Guo, D. X., Guo, Y. N., and Li, X. Y. (2014). Study on the Extraction and Purification Process of Matrine. *Chin. J. Vet. Med. (Chinese)* 48 (03), 24–26. doi:10.3969/j.issn.1004-5090.2013.03.004

Guo, J. X., Liang, M., and Zhang, C. M. (2011). Design, Synthesis and *In Vitro* Anti-inflammatory Activity of Novel Matrine Derivatives. *J. Second Mil. Med. Univ. (Chinese)* 32 (11), 1223–1226. doi:10.3724/SP.J.1008.2011.01223

Guo, S., Chen, Y., Pang, C., Wang, X., Shi, S., Zhang, H., et al. (2019). Matrine Is a Novel Inhibitor of the TMEM16A Chloride Channel with Antilung Adenocarcinoma Effects. *J. Cel Physiol* 234, 8698–8708. doi:10.1002/jcp.27529

Guo, S., Gao, C., Xiao, W., Zhang, J., Qu, Y., Li, J., et al. (2018). Matrine Protects Cardiomyocytes from Ischemia/Reperfusion Injury by Regulating HSP70 Expression via Activation of the JAK2/STAT3 Pathway. *Shock* 50 (6), 664–670. doi:10.1097/shk.0000000000001108

Haiyan, W., Yuxiang, L., Linglu, D., Tingting, X., Yinju, H., Hongyan, L., et al. (2013). Antinociceptive Effects of Matrine on Neuropathic Pain Induced by Chronic Constriction Injury. *Pharm. Biol.* 51 (7), 844–850. doi:10.3109/13880209.2013.767363

Haiyan, W., Yuxiang, L., Linglu, D., Tingting, X., Yinju, H., Hongyan, L., et al. (2013). Antinociceptive Effects of Matrine on Neuropathic Pain Induced by Chronic Constriction Injury. *Pharm. Biol.* 51 (7), 844–850. doi:10.3109/13880209.2013.767363

Han, G. W., Gao, Z. Y., and Zhao, E. L. (2018). Research Progress on Extraction and Purification of Alkaloids from Sophora Flavescens. *Mod. Foods* 15, 163–166. doi:10.16736/j.cnki.cn41-1434/ts.2018.15.050

Han, X. L., Ci, Y., and Chen, C. T. (2012). Synthesis and Bactericidal Effect of 13α-Methoxymatrine. *Chin. J. Disinfection* 29 (05), 376–378+81. (Chinese).

Han, X. L. (2012). *Synthesis, Characterization and Biological Properties of Matrine Compounds [D]*. Beijing, China: Beijing University of Chemical Technology (Chinese). doi:10.7666/d.y2138646

Hao, Y., Yin, H., Zhu, C., Li, F., Zhang, Y., Li, Y., et al. (2019). Matrine Inhibits Proliferation and Promotes Autophagy and Apoptosis in Non-small Cell Lung Cancer Cells by Deactivating PI3K/AKT/mTOR Pathway. *Nan Fang Yi Ke Da Xue Xue Bao* 39 (7), 760–765. doi:10.12122/j.issn.1673-4254.2019.07.02

Hassan, H., Mohammed, S., Robert, F., and Landais, Y. (2015). Total Synthesis of (±)-Eucophylline. A Free-Radical Approach to the Synthesis of the Azabicyclo [3.3.1]nonane Skeleton. *Org. Lett.* 17 (18), 4518–4521. doi:10.1021/acs.orglett.5b02218

He, L. R., Li, Y., and Yang, L. Z. (1999). Effects of Matrine on AngⅡ-Induced Vascular Smooth Muscle Cell Proliferation and Ultrastructural Changes. *J. Shanghai Univ. Traditional Chin. Med. (Chinese)* 04, 47–50.

He, X., Wei, X. C., and Tian, Y. C. (2011). Research Progress on the Synthesis and Biological Activity of Matrine and its Derivatives. *China Mod. Appl. Pharm. (Chinese)* 28 (09), 816–823. doi:10.13748/j.cnki.issn1007-7693.2011.09.010

Hou, H., Zhang, Q., Dong, H., and Ge, Z. (2019). Matrine Improves Diabetic Cardiomyopathy through TGF-β-induced Protein Kinase RNA-like Endoplasmic Reticulum Kinase Signaling Pathway. *J. Cel Biochem* 120 (8), 13573–13582. doi:10.1002/jcb.28632

Hu, G., Huang, Z., Zhou, X., Hu, J., and Huang, B. (2015). Matrine Enhances the Effect of Cisplatin against Human Hepatocellular Carcinoma Xenografts in Nude Mice and its Effect on the Expression of Survivin/caspase-3. *Chin. J. Hepatol. (Chinese)* 23 (09), 669–674. doi:10.3760/cma.j.issn.1007-3418.2015.09.007

Hu, H. P., Liu, J. H., and Sun, X. (2015). Research Progress on Biological Activity and Synthesis of Matrine and its Derivatives. *J. Ludong Univ. (Chinese)* 31 (04), 339–345.

Huang, Q., and Wang, Z. Z. (2016). Extraction Method of Natural Product Matrine. *Guangzhou Chem. Industry (Chinese)* 44 (19), 6–7.

Huang, W.-C., Chan, C.-C., Wu, S.-J., Chen, L.-C., Shen, J.-J., Kuo, M.-L., et al. (2014). Matrine Attenuates Allergic Airway Inflammation and Eosinophil Infiltration by Suppressing Eotaxin and Th2 Cytokine Production in Asthmatic Mice. *J. ethnopharmacology* 151 (1), 470–477. doi:10.1016/j.jep.2013.10.065

Ji, X. W., and Zhang, G. W. (2014). Pharmacological Effects and Clinical Application of Matrine Alkaloids. *J. Med. Res. Edu. (Chinese)* 31 (06), 85–88+99. doi:10.3969/j.issn.1674-490X.2014.06.021

Jiang, J., and Jiang, G. (2020). Matrine Protects PC12 Cells from Lipopolysaccharide-Evoked Inflammatory Injury via Upregulation of miR-9. *Pharm. Biol.* 58 (1), 314–320. doi:10.1080/13880209.2020.1719165

Jiang, Y., Ma, R., and Chu, Y. (2021). Matrine Treatment Induced an A2 Astrocyte Phenotype and Protected the Blood-Brain Barrier in CNS Autoimmunity. *J. Chem. Neuroanat.* 117, 102004. doi:10.1016/j.jchemneu.2021.102004

Jiang, Y. D., Zhang, H. P., Cao, J., Li, G. Z., and Wang, S. R. (2007). Effects of Matrine on ATP-Binding Cassette Transporter A1 and Cholesterol in Monocyte Cells. *Basic Clin. Med.* 09, 996–1000. doi:10.1007/s11767-005-0212-9

Jing, K., Guo, S., Yang, J., Liu, J., Shaukat, A., Zhao, G., et al. (2019). Matrine Alleviates *Staphylococcus aureus* Lipoteichoic Acid-Induced Endometritis via Suppression of TLR2-Mediated NF-kappaB Activation. *Int. immunopharmacology* 70, 201–207. doi:10.1016/j.intimp.2019.02.033

Jost, N., Acsai, K., Horváth, B., Bányász, T., Baczkó, I., Bitay, M., et al. (2009). Contribution of I Kr and I K1 to Ventricular Repolarization in Canine and Human Myocytes: Is There Any Influence of Action Potential Duration? *Basic Res. Cardiol.* 104 (1), 33–41. doi:10.1007/s00395-008-0730-3

Kan, Q.-C., Zhu, L., Liu, N., and Zhang, G.-X. (2013). Matrine Suppresses Expression of Adhesion Molecules and Chemokines as a Mechanism Underlying its Therapeutic Effect in CNS Autoimmunity. *Immunol. Res.* 56 (1), 189–196. doi:10.1007/s12026-013-8393-z

Kang, J., Liu, S., Song, Y., Chu, Y., Wang, M., Shi, Y., et al. (2021). Matrine Treatment Reduces Retinal Ganglion Cell Apoptosis in Experimental Optic Neuritis. *Sci. Rep.* 11 (1), 9520. doi:10.1038/s41598-021-89086-7

Kang, S. C., Yang, W., and Zheng, Y. (2019). Matrine Inhibits the Target of HepG2 Liver Cancer Cells-ERK Signaling Pathway. *Liver (Chinese)* 24 (02), 187–189.

Li, B. P. (2015). *Design and Synthesis of NO Donor Matrine Derivatives and Preliminary Study on Their Protective Effect against Myocardial Ischemia [D]*. Yinchuan: Ningxia Medical University (Chinese).

Li, L.-Q., Li, X.-L., Wang, L., Du, W.-J., Guo, R., Liang, H.-H., et al. (2012). Matrine Inhibits Breast Cancer Growth ViamiR-21/PTEN/AktPathway in MCF-7 Cells. *Cell Physiol Biochem* 30 (3), 631–641. doi:10.1159/000341444

Li, P., Lei, J., Hu, G., Chen, X., Liu, Z., and Yang, J. (2019). Matrine Mediates Inflammatory Response via Gut Microbiota in TNBS-Induced Murine Colitis. *Front. Physiol.* 10, 28. doi:10.3389/fphys.2019.00028

Li, R., Chen, R., and Li, C. X. (2015). Study on the Optimal Percolation Extraction Process of Sophora Flavescens Alkaloids by Orthogonal Experiment. *Heilongjiang Anim. Husbandry Vet. Med. (Chinese)* 21, 200–202.

Li, S., Liu, X., Chen, X., and Bi, L. (2020). Research Progress on Anti-inflammatory Effects and Mechanisms of Alkaloids from Chinese Medical Herbs. *Evidence-Based Complement. Altern. Med.* 2020 (4), 1–10. doi:10.1155/2020/1303524

Li, X., Liu, X. J., and Zhang, P. (2020). Effects of Matrine on P2X2 and P2X3 Receptors in Rats with Neuropathic Pain. *Chin. J. Clin. Pharmacol. (Chinese)* 36 (19), 3037–3040. doi:10.13699/j.cnki.1001-6821.2020.19.021

Li, X., Liang, T., Chen, S. S., Wang, M., Wang, R., Li, K., et al. (2020). Matrine Suppression of Self-renewal Was Dependent on Regulation of LIN28A/Let-7 Pathway in Breast Cancer Stem Cells. *J. Cel Biochem* 121 (3), 2139–2149. doi:10.1002/jcb.29396

Li, X., Wang, X., Guo, Y., Deng, N., Zheng, P., Xu, Q., et al. (2012). Regulation of Endothelial Nitric Oxide Synthase and Asymmetric Dimethylarginine by Matrine Attenuates Isoproterenol-Induced Acute Myocardial Injury in Rats. *J. Pharm. Pharmacol.* 64 (8), 1107–1118. doi:10.1111/j.2042-7158.2012.01502.x

Li, X. Y., Kong, L. X., Li, J., He, H-X., and Zhou, Y. D. (2013). Kaempferol Suppresses Lipid Accumulation in Macrophages through the Downregulation of Cluster of Differentiation36 and the Upregulation of Scavenger Receptor classB typeI and ATP-Binding Cassette transportersA1 andG1. *Int. J. Mol. Med. (Chinese)*. doi:10.3892/ijmm.2012.1204

Li, Y.-H., Wu, Z.-Y., Tang, S., Zhang, X., Wang, Y.-X., Jiang, J.-D., et al. (2017). Evolution of Matrinic Ethanol Derivatives as Anti-HCV Agents from Matrine Skeleton. *Bioorg. Med. Chem. Lett.* 27 (9), 1962–1966. doi:10.1016/j.bmcl.2017.03.025

Li, Y. H., Tang, S., Li, Y. H., Cheng, X. Y., Zhang, X., Wang, Y. X., et al. (2017). Novel 12N-Substituted Matrinanes as Potential Anti-coxsackievirus Agents. *Bioorg. Med. Chem. Lett.* 27 (4), 829–833. doi:10.1016/j.bmcl.2017.01.022

Li, Y., Wang, G., Liu, J., and Ouyang, L. (2020). Quinolizidine Alkaloids Derivatives from Sophora Alopecuroides Linn: Bioactivities, Structure-Activity Relationships and Preliminary Molecular Mechanisms. *Eur. J. Med. Chem.* 188, 111972. doi:10.1016/j.ejmech.2019.111972

Lin, G., Wu, Y., Cai, F., Li, Z., Su, S., Wang, J., et al. (2019). Matrine Promotes Human Myeloid Leukemia Cells Apoptosis through Warburg Effect Mediated by Hexokinase 2. *Front. Pharmacol.* 10, 1069. doi:10.3389/fphar.2019.01069

Liu, D., Zhou, W., Gao, X. B., Wang, X., Guo, S., Shi, L., et al. (2019). Matrine Inhibits Nrf2-Induced Annexin A4 Expression and Improves Cisplatin Resistance in Non-small Cell Lung Cancer. *J. Clin. Pathol. (Chinese)* 39 (03), 457–463. doi:10.3978/j.issn.2095-6959.2019.03.001

Liu, J. F., Ding, Z., and Ouyang, Y. (2011). Determination of Antibacterial Activity of Alkaloids from Sophora Japonica. *J. Beijing Univ. Chem. Tech. (Natural Sci. Edition (Chinese)* 38 (02), 84–88. doi:10.13543/j.cnki.bhxbzr.2011.02.003

Liu, J. Y., and Guo, S. R. (2011). Research Progress on the Effect of Matrine on Cardiovascular and its Mechanism. *J. Jishou Univ. (Chinese)* 32 (05), 103–106. doi:10.3969/j.issn.1007-2985.2011.05.025

Liu, J., Zhang, L., Ren, Y., Gao, Y., Kang, L., and Lu, S. (2016). Matrine Inhibits the Expression of Adhesion Molecules in Activated Vascular Smooth Muscle Cells. *Mol. Med. Rep.* 13, 2313–2319. doi:10.3892/mmr.2016.4767

Liu, T. T. (2014). *Study on the Mechanism of Matrine in Reversing Retinoic Acid Resistance in Acute Promyelocytic Leukemia [D]*. Hangzhou: Zhejiang University of Traditional Chinese Medicine (Chinese).

Liu, X. X., Hu, L. T., and Thu, S. P. (2020). Study on the Effect of Matrine Vaginal Expansion Suppository in the Treatment of Chronic Pelvic Inflammatory Disease. *J. Contemp. Med. (Chinese)* 18 (12), 100–102.

Liu, Z.-w., Wang, J.-k., Qiu, C., Guan, G.-c., Liu, X.-h., Li, S.-j., et al. (2015). Matrine Pretreatment Improves Cardiac Function in Rats with Diabetic Cardiomyopathy via Suppressing ROS/TLR-4 Signaling Pathway. *Acta Pharmacol. Sin* 36 (3), 323–333. doi:10.1038/aps.2014.127

Liu, Z., Zhang, Y., Tang, Z., Xu, J., Ma, M., Pan, S., et al. (2017). Matrine Attenuates Cardiac Fibrosis by Affecting ATF6 Signaling Pathway in Diabetic Cardiomyopathy. *Eur. J. Pharmacol.* 804, 21–30. doi:10.1016/j.ejphar.2017.03.061

Long, Y., Lin, X. T., Zeng, K. L., and Zhang, L. (2004). Efficacy of Intramuscular Matrine in the Treatment of Chronic Hepatitis B. *Hepatobiliary Pancreat. Dis. Int.* 3 (1), 69–72.

Lu, Q., Lin, X., Wu, J., and Wang, B. (2020). Matrine Attenuates Cardiomyocyte Ischemia-Reperfusion Injury through Activating AMPK/Sirt3 Signaling Pathway. *J. Recept Signal. Transduct Res.*, 1–6. doi:10.1080/10799893.2020.1828914

Lu, X. T., and Zhu, C. L. (2003). Experimental Study on the Hypolipidemic Effect of Matrine. *Today Pharm. (Chinese)* 013 (006), 32–34. doi:10.3969/j.issn.1674-229X.2003.06.016

Lu, Y. H., Wang, D., and Jing, H. Y. (2018). Effects of Matrine on oxLDL-Induced Inflammation, Proliferation and Apoptosis of Vascular Smooth Muscle Cells and its Molecular Mechanism. *Chin. J. Immunol. (Chinese)* 34 (04), 537–543. doi:10.3969/j.issn.1000-484X.2018.04.012

Lu, Y. H., Yi, Y., and Ji, Q. Q. (2015). Effects of Matrine on Serum IL-6, TNF-α Levels and Insulin Sensitivity in Patients with Diabetic Nephropathy. *Chin. J. Clinicians (Chinese)* 24 (9), 4585–4588. doi:10.3877/cma.j.issn.1674-0785.2015.24.020

Lu, Z. H., Peng, L., and Qian, J. (2019). Experimental Study on the Anti-inflammatory Effect of Jiangnan Peony Grass Matrine. *J. Hubei Univ. Traditional Chin. Med. (Chinese)* 21 (05), 36–38. doi:10.3969/j.issn.1008-987x.2019.05.09

Ma, W., Xu, J., Zhang, Y., Zhang, H., Zhang, Z., Zhou, L., et al. (2019). Matrine Pretreatment Suppresses AGEs- Induced HCSMCs Fibrotic Responses by Regulating Poldip2/mTOR Pathway. *Eur. J. Pharmacol.* 865, 172746. doi:10.1016/j.ejphar.2019.172746

Mandell, L., Singh, K. P., Gresham, J. T., and Freeman, W. J. (1965). The Total Syntheses of D,l-Matrine and D,l-Leontine1. *J. Am. Chem. Soc.* 87 (22), 5234–5236. doi:10.1021/ja00950a043

Moriya, J. (2018). Critical Roles of Inflammation in Atherosclerosis. *J. Cardiol.* 73 (1), 22–27. doi:10.1016/j.jjcc.2018.05.010

Ni, W., Li, C., Liu, Y., Song, H., Wang, L., Song, H., et al. (2017). Various Bioactivity and Relationship of Structure-Activity of Matrine Analogues. *J. Agric. Food Chem.* 65 (10), 2039–2047. doi:10.1021/acs.jafc.6b05474

Pan, J. L. (2018). *Antibacterial Mechanism of Matrine on Pecan Dry Rot Pathogenic Fungus Botryosphaeria Dothidea [D]*. Harbin: Northeast Forestry University (Chinese).

Passini, E., Rodriguez, B., Mincholé, A., Coppini, R., Cerbai, E., and Severi, S. (2014). "Late Sodium Current Inhibition Counteracts Pro-arrhythmic Mechanisms in Human Hypertrophic Cardiomyopathy," in proceedings of the Computing in Cardiology Conference (IEEE).

Peng, W., Xu, Y., Han, D., Feng, F., Wang, Z., Gu, C., et al. (2020). Potential Mechanism Underlying the Effect of Matrine on COVID-19 Patients Revealed through Network Pharmacological Approaches and Molecular Docking Analysis. *Arch. Physiol. Biochem.*, 1–8. doi:10.1080/13813455.2020.1817944

Pu, J., Fang, F.-F., Li, X.-Q., Shu, Z.-H., Jiang, Y.-P., Han, T., et al. (2016). Matrine Exerts a Strong Anti-arthritic Effect on Type II Collagen-Induced Arthritis in Rats by Inhibiting Inflammatory Responses. *Ijms* 17 (9), 1410. doi:10.3390/ijms17091410

Pu, J., Tang, X., Zhuang, X., Hu, Z., He, K., Wu, Y., et al. (2018). Matrine Induces Apoptosis via Targeting CCR7 and Enhances the Effect of Anticancer Drugs in Non-small Cell Lung Cancer *In Vitro*. *Innate Immun.* 24 (7), 394–399. doi:10.1177/1753425918800555

Raimondi, L., Amodio, N., Di Martino, M. T., Altomare, E., Leotta, M., Caracciolo, D., et al. (2014). Targeting of Multiple Myeloma-Related Angiogenesis by miR-199a-5p Mimics: *In Vitro* and *In Vivo* Anti-tumor Activity. *Oncotarget* 5 (10), 3039–3054. doi:10.18632/oncotarget.1747

Ren, L., Mo, W., Wang, L., and Wang, X. (2020). Matrine Suppresses Breast Cancer Metastasis by Targeting ITGB1 and Inhibiting Epithelial-To-Mesenchymal Transition. *Exp. Ther. Med.* 19 (1), 367–374. doi:10.3892/etm.2019.8207

Research, C. (2009). Changes in Connexin Expression and the Atrial Fibrillation Substrate in Congestive Heart Failure. *Circ. Res.* 105 (12), 1213–1222.

Shao, H., Yang, B., Hu, R., and Wang, Y. (2013). Matrine Effectively Inhibits the Proliferation of Breast Cancer Cells through a Mechanism Related to the NF-Kb Signaling Pathway. *Oncol. Lett.* 6 (2), 517–520. doi:10.3892/ol.2013.1399

Shao, J., Wang, T., Yan, Y., Shi, G., Cheng, H., Wu, D., et al. (2014). Matrine Reduces Yeast-To-Hypha Transition and Resistance of a Fluconazole-Resistant Strain of Candida Albicans. *J. Appl. Microbiol.* 117 (3), 618–626. doi:10.1111/jam.12555

Sun, D., Wang, J., Yang, N., and Ma, H. (2016). Matrine Suppresses Airway Inflammation by Downregulating SOCS3 Expression via Inhibition of NF-Kb Signaling in Airway Epithelial Cells and Asthmatic Mice. *Biochem. biophysical Res. Commun.* 477 (1), 83–90. doi:10.1016/j.bbrc.2016.06.024

Sun, N., Wang, Z.-W., Wu, C.-H., Li, E., He, J.-P., Wang, S.-Y., et al. (2014). Antiviral Activity and Underlying Molecular Mechanisms of Matrine against Porcine Reproductive and Respiratory Syndrome Virus *In Vitro*. *Res. Vet. Sci.* 96 (2), 323–327. doi:10.1016/j.rvsc.2013.12.009

Sun, N., Zhang, H., Sun, P., Khan, A., Guo, J., Zheng, X., et al. (2020). Matrine Exhibits Antiviral Activity in a PRRSV/PCV2 Co-infected Mouse Model. *Phytomedicine* 77, 153289. doi:10.1016/j.phymed.2020.153289

Sun, X., and Wang, H. S. (2010). Role of the Transient Outward Current (Ito) in Shaping Canine Ventricular Action Potential-Aa Dynamic Clamp Study. *J. Physiol.* 564 (Pt 2), 411–419. doi:10.1113/jphysiol.2004.077263

Sun, Z. R., Shen, Y. X., and Ren, Y. Y. (2021). Effects of Matrine on Cardiac Function in Rats with Heart Failure. *Chin. J. Clin. Pharmacol. (Chinese)* 37 (15), 2003–2006+14. doi:10.13699/j.cnki.1001-6821.2021.15.014

Tsai, J.-Y., Su, K.-H., Shyue, S.-K., Kou, Y. R., Yu, Y.-B., Hsiao, S.-H., et al. (2010). EGb761 Ameliorates the Formation of Foam Cells by Regulating the Expression

of SR-A and ABCA1: Role of Haem Oxygenase-1. *Cardiovasc. Res.* 88 (3), 415–423. doi:10.1093/cvr/cvq226

Varró, A., Nánási, P. P., and Lathrop, D. A. (2010). Potassium Currents in Isolated Human Atrial and Ventricular Cardiocytes. *Acta Physiol. Scand.* 149 (2), 133–142. doi:10.1111/j.1748-1716.1993.tb09605.x

Wan, S. C., Wang, Z. X., and Le, L. (2008). Application of Ultrasonic Extraction Technology in Extraction of Traditional Chinese Medicine and Natural Products. *Northwest J. Pharm. (Chinese)* 01, 60–62. doi:10.3969/j.issn.1004-2407.2008.01.039

Wang, F. (2018). *Effects of Matrine on CD4~+CD25~+ Regulatory T Cells during Rat Allogeneic Corneal Transplantation [D]*. Changchun: Jilin University (Chinese).

Wang, H.-Q., Jin, J.-J., and Wang, J. (2015). Matrine Induces Mitochondrial Apoptosis in Cisplatin-Resistant Non-small Cell Lung Cancer Cells via Suppression of β-catenin/survivin Signaling. *Oncol. Rep.* 33 (5), 2561–2566. doi:10.3892/or.2015.3844

Wang, J., Lin, G. B., and Cao, J. L. (2019). Matrine-induced K562 Cell Differentiation and STAT3 Gene Expression. *China Med. Innovation (Chinese)* 16 (07), 22–27. doi:10.3969/j.issn.1674-4985.2019.07.006

Wang, J., Tang, Z., Zhang, Y., Qiu, C., Zhu, L., Zhao, N., et al. (2019). Matrine Alleviates AGEs- Induced Cardiac Dysfunctions by Attenuating Calcium Overload via Reducing Ryanodine Receptor 2 Activity. *Eur. J. Pharmacol.* 842, 118–124. doi:10.1016/j.ejphar.2018.10.010

Wang, K. X., Gao, L., and Zhou, Y. Z. (2019). Study on the Anti-hepatocellular Carcinoma Effect and Mechanism of Matrine Based on Network Pharmacology. *Chin. J. Pharm. (Chinese)* 52 (06), 888–896. doi:10.16438/j.0513-4870.2017-0075

Wang, Y. H., Wang, Y. L., and Zhu, B. (2011). Microwave-assisted Extraction of Matrine from Radix Rhizome. *Pesticide (Chinese)* 50 (05), 338–340. doi:10.3969/j.issn.1006-0413.2011.05.008

Warburg, O. (1956). On Respiratory Impairment in Cancer Cells. *Science* 441 (3215), 424–430. doi:10.1126/science.124.3215.269

Wei, S. J. (2016). *Effects of Matrine on Cytokines in Myocardial Tissue of Rats with Isoproterenol-Induced Left Ventricular Hypertrophy [D]*. Yinchuan: Ningxia Medical University (Chinese).

Wei, X. C., Zheng, C., and He, X. (2013). Synthesis and Antitumor Activity of Aromatic Matrine Derivatives. *Fine Chem. Industry (Chinese)* 33 (8), 936–939.

Wu, J., Hu, G., Dong, Y., Ma, R., Yu, Z., Jiang, S., et al. (2017). Matrine Induces Akt/mTOR Signalling Inhibition-Mediated Autophagy and Apoptosis in Acute Myeloid Leukaemia Cells. *J. Cel. Mol. Med.* 21 (6), 1171–1181. doi:10.1111/jcmm.13049

Wu, L., Liu, S., Wei, J., Li, D., Liu, X., Wang, J., et al. (2016). Synthesis and Biological Evaluation of Matrine Derivatives as Anti-hepatocellular Cancer Agents. *Bioorg. Med. Chem. Lett.* 26 (17), 4267–4271. doi:10.1016/j.bmcl.2016.07.045

Wu, M. C. (2014). *Synthesis and Biological Activity of Novel Matrine and Triazole Derivatives [D]*. Shanghai: Second Military Medical University (Chinese).

Wu, M. F., Shen, R. C., and Wang, J. (2020). Antiarrhythmic Effects of Alkaloids and Their Molecular Mechanisms. *Subtropical Plant Science(chinese)* 49 (06), 490–499. doi:10.3969/j.issn.1009-7791.2020.06.015

Xiao, X., Ao, M., Xu, F., Li, X., Hu, J., Wang, Y., et al. (2018). Effect of Matrine against Breast Cancer by Downregulating the Vascular Endothelial Growth Factor via the Wnt/β-Catenin Pathway. *Oncol. Lett.* 15 (2), 1691–1697. doi:10.3892/ol.2017.7519

Xiao, Y., Ma, D., Wang, H., Wu, D., Chen, Y., Ji, K., et al. (2017). Matrine Suppresses the ER-Positive MCF Cells by Regulating Energy Metabolism and Endoplasmic Reticulum Stress Signaling Pathway. *Phytother. Res.* 31 (4), 671–679. doi:10.1002/ptr.5785

Xie, W., Lu, J., Lu, Q., Wang, X., Long, H., Huang, J., et al. (2018). Matrine Inhibits the Proliferation and Migration of Lung Cancer Cells through Regulation of the Protein Kinase B/glycogen Synthase Kinase-3β Signaling Pathways. *Exp. Ther. Med.* 16 (2), 723–729. doi:10.3892/etm.2018.6266

Xu, Y., Zhao, Y. K., and Bi, M. G. (2007). Anti-atherosclerosis Potential and Prospective Study of Heat-Clearing and Dampness-Drying Drugs. *China J. Traditional Chin. Medicine(Chinese)* 12, 93–95. doi:10.3969/j.issn.1005-5304.2007.12.057

Yang, F. F. (2015). *Synthesis and Antitumor Activity of Matrine 14-substituted Organisms [D]*. Nanning: Guangxi University (Chinese). doi:10.7666/d.Y2889265

Yang, L., Deng, Y. G., and Wu, S. X. (2016). Study on the Analgesic Effect of Matrine and its Non-correlation of Opioid Receptors. *Zhonghua J. Traditional Chin. Med. (Chinese)* 31 (03), 998–1001.

Yang, M. W., Chen, F., and Zhu, D. J. (2020), Analysis of Clinical Efficacy of Matrine and Sodium Chloride Injection in the Treatment of 40 Cases of Novel Coronavirus Pneumonia. *China J. Traditional Chin. Med. (Chinese)* 45 (10), 2221–2231. doi:10.19540/j.cnki.cjcmm.20200323.501

Yang, Y., Xiu, J., Zhang, X., Zhang, L., Yan, K., Qin, C., et al. (2012). Antiviral Effect of Matrine against Human Enterovirus 71. *Molecules* 17 (9), 10370–10376. doi:10.3390/molecules170910370

Yin, Y., Hong, J., Phạm, T., Shin, fnm., Gwon, fnm., Kwon, fnm., et al. (2019). Evans Blue Reduces Neuropathic Pain Behavior by Inhibiting Spinal ATP Release. *Ijms* 20 (18), 4443. doi:10.3390/ijms20184443

Yu, J., Yang, S., Wang, X., and Gan, R. (2014). Matrine Improved the Function of Heart Failure in Rats via Inhibiting Apoptosis and Blocking β3-adrenoreceptor/endothelial Nitric Oxide Synthase Pathway. *Mol. Med. Rep.* 10 (6), 3199–3204. doi:10.3892/mmr.2014.2642

Yu, X., Seow, H. J., Wang, H., Anthony, D., Bozinovski, S., Lin, L., et al. (2019). Matrine Reduces Cigarette Smoke-Induced Airway Neutrophilic Inflammation by Enhancing Neutrophil Apoptosis. *Clin. Sci.* 133 (4), 551–564. doi:10.1042/cs20180912

Yue, L., Xie, J., and Nattel, S. (2010). Molecular Determinants of Cardiac Fibroblast Electrical Function and Therapeutic Implications for Atrial Fibrillation. *Cardiovasc. Res.* 89 (4), 744–753. doi:10.1093/cvr/cvq329

Zhang, A. J., Zhang, C. F., and Wang, X. Q. (2011). Determination of Antibacterial Activity of Three Alkaloids *In Vitro*. *J. Changzhi Med. Coll. (Chinese)* 25 (05), 335–337. doi:10.3969/j.issn.1006-0588.2011.05.006

Zhang, F., Wang, X., Tong, L., Qiao, H., Li, X., You, L., et al. (2011). Matrine Attenuates Endotoxin-Induced Acute Liver Injury after Hepatic Ischemia/reperfusion in Rats. *Surg. Today* 41 (8), 1075–1084. doi:10.1007/s00595-010-4423-9

Zhang, J., Li, X. H., and Feng, X. L. (2020). Anti-Aspergillus fumigatus, Trichophyton Mentagrophytes and Cryptococcus Neoformans of Alkaloids from Sophora Japonica. *Chin. J. Mycol. (Chinese)* 15 (02), 72–77. doi:10.3969/j.issn.1673-3827.2020.02.003

Zhang, L., Zhang, H., Zhu, Z., Jiang, L., Lu, X., Zhou, M., et al. (2015). Matrine Regulates Immune Functions to Inhibit the Proliferation of Leukemic Cells. *Int. J. Clin. Exp. Med.* 8 (4), 5591–5600.

Zhang, M. F., and Shen, Ya. Q. (2018). Research Progress on Anti-inflammatory and Immunosuppressive Pharmacological Effects of Matrine. *Anti-infective Pharm. (Chinese)* 15 (05), 737–743. doi:10.13493/j.issn.1672-7878.2018.05-001

Zhang, M. F., and Shen, Y. Q. (2018). Research Progress on Clinical Pharmacological Effects of Matrine Alkaloids against Hepatitis B Virus. *Anti-infective Pharm. (Chinese)* 15 (01), 1–6. doi:10.13493/j.issn.1672-7878.2018.01-001

Zhang, Q. Y., Gu, H., and He, L. (2009). Synthesis of Cinnamon Acid Matrine. *Anhui Chem. Industry (Chines)* 35 (03), 21–22. doi:10.3969/j.issn.1008-553X.2009.03.009

Zhang, X., Hu, C., Zhang, N., Wei, W. Y., Li, L. L., Wu, H. M., et al. (2020). Matrine Attenuates Pathological Cardiac Fibrosis via RPS5/p38 in Mice. *Acta Pharmacol. Sin*, 1–12. doi:10.1038/s41401-020-0473-8

Zhang, X. W., Li, L. Y., and Shang, H. (2019). Research Progress on Structural Modification of Matrine and its Analogs. *Chin. Herbal Med. (Chinese)* 50 (23), 5892–5900. doi:10.7501/j.issn.0253-2670.2019.23.034

Zhang, Y., Cui, L., Guan, G., Wang, J., Qiu, C., Yang, T., et al. (2018). Matrine Suppresses Cardiac Fibrosis by Inhibiting the TGF-β/Smad P-athway in E-xperimental D-iabetic C-ardiomyopathy. *Mol. Med. Rep.* 17 (1), 1775–1781. doi:10.3892/mmr.2017.8054

Zhang, Y., Yang, X., Qiu, C., Liu, F., Liu, P., and Liu, Z. (2018). Matrine Suppresses AGE-Induced HAEC Injury by Inhibiting ROS-Mediated NRLP3 Inflammasome Activation. *Eur. J. Pharmacol.* 822, 207–211. doi:10.1016/j.ejphar.2018.01.029

Zhang, Y., Zhang, H., Yu, P., Liu, Q., Liu, K., Duan, H., et al. (2009). Effects of Matrine against the Growth of Human Lung Cancer and Hepatoma Cells as Well as Lung Cancer Cell Migration. *Cytotechnology* 59 (3), 191–200. doi:10.1007/s10616-009-9211-2

Zhang, Z. (2019). Effects of Matrine on Retinal Microvascular Endothelial Cell Proliferation and Vascular Endothelial Growth Factor Expression in Rats with

Diabetic Retinopathy. *Chin. J. Drug Eval. Anal. (Chinese)* 19 (04), 422–425+8. doi:10.14009/j.issn.1672-2124.2019.04.011

Zhao, L. H., Guo, J. H., and Cui, Y. L. (2015). Research Progress on Structural Modification of Matrine for Antitumor Effects. *Mod. Med. Clin. (Chinese)* 30 (05), 600–604. doi:10.7501/j.issn.1674-5515.2015.05.029

Zhao, P., Zhou, R., Zhu, X.-Y., Hao, Y.-J., Li, N., Wang, J., et al. (2015). Matrine Attenuates Focal Cerebral Ischemic Injury by Improving Antioxidant Activity and Inhibiting Apoptosis in Mice. *Int. J. Mol. Med.* 36 (3), 633–644. doi:10.3892/ijmm.2015.2260

Zheng, J., Zheng, P., Zhou, X., Yan, L., Zhou, R., Fu, X.-Y., et al. (2009). Relaxant Effects of Matrine on Aortic Smooth Muscles of guinea Pigs. *Biomed. Environ. Sci.* 22, 327–332. doi:10.1016/s0895-3988(09)60063-5

Zhou, B. G., Wei, C. S., Zhang, S., Zhang, Z., and Gao, H. m. (2018). Matrine Reversed Multidrug Resistance of Breast Cancer MCF-7/ADR Cells through PI3K/AKT Signaling Pathway. *J. Cel. Biochem.* 119 (5), 3885–3891. doi:10.1002/jcb.26502

Zhou, H., Xu, M., Gao, Y., Deng, Z., Cao, H., Zhang, W., et al. (2014). Matrine Induces Caspase-independent Program Cell Death in Hepatocellular Carcinoma through Bid-Mediated Nuclear Translocation of Apoptosis Inducing Factor. *Mol. Cancer* 13 (1), 59. doi:10.1186/1476-4598-13-59

Zhou, J., Ni, S. S., and Ben, S. Q. (2012). Effects of Matrine Combined with Cisplatin on the Expression of Lung Adenocarcinoma A549 Cells. *Traffic Med. (Chinese)* 26 (02), 112–115. doi:10.3969/j.issn.1006-2440.2012.02.003

Zhou, W. Y. (2017). *Inhibitory Effect of Matrine on Hepatocellular Carcinoma and its Mechanism of Action [D]*. Jinan: Shandong University (Chinese).

Zhou, Y., Wu, Y., Deng, L., Chen, L., Zhao, D., Lv, L., et al. (2014). The Alkaloid Matrine of the Root of Sophora Flavescens Prevents Arrhythmogenic Effect of Ouabain. *Phytomedicine* 21 (7), 931–935. doi:10.1016/j.phymed.2014.02.008

Zhu, J. L. (2014). *Effects of Matrine on the Formation of Staphylococcus Epidermidis Biofilm [D]*. Yinchuan: Ningxia University (Chinese).

Zhuo, X. F., and Ji, Y. H. (2017). Inhibitory Effect of Matrine on Proliferation, Invasion and Angiogenesis of Human Lung Cancer A549 Cells and its Mechanism. *Mod. Med. Clin. (Chinese)* 32 (05), 767–771. doi:10.7501/j.issn.1674-5515.2017.05.003

Zou, Y. M. (2018). *Therapeutic Effect and Mechanism of Matrine Derivative MASM on Rheumatoid Arthritis [D]*. Shanghai: Chinese People's Liberation Army Naval Medical University (Chinese).

**Conflict of Interest:** Authors A-HL and H-LC are employed by Shaanxi Pharmaceutical Holding Group Co., LTD, China.

The remaining authors declare that the research was conducted in the absence of any commercial or financial relationships that could be construed as a potential conflict of interest.

frontiers | Frontiers in Chemistry

ORIGINAL RESEARCH
published: 06 April 2022
doi: 10.3389/fchem.2022.815534

# Design, Synthesis, and Biological Evaluation of [1,2,4]triazolo[4,3-*a*] Pyrazine Derivatives as Novel Dual c-Met/VEGFR-2 Inhibitors

*Xiaobo Liu*[1,2†], *Yuzhen Li*[1†], *Qian Zhang*[1], *Qingshan Pan*[1], *Pengwu Zheng*[1], *Xinyang Dai*[1], *Zhaoshi Bai*[3*] *and Wufu Zhu*[1*]

[1]*Jiangxi Provincial Key Laboratory of Drug Design and Evaluation, School of Pharmacy, Jiangxi Science and Technology Normal University, Nanchang, China,* [2]*School of Chemical Engineering, Dalian University of Technology, Dalian, China,* [3]*Jiangsu Cancer Hospital and Jiangsu Institute of Cancer Research and the Affiliated Cancer Hospital of Nanjing Medical University, Nanjing, China*

OPEN ACCESS

**Edited by:**
*Qingbin Cui,*
*University of Toledo, United States*

**Reviewed by:**
*Ping Gong,*
*Shenyang Pharmaceutical University, China*
*Enming Du,*
*Henan Provincial People's Hospital, China*

***Correspondence:**
*Zhaoshi Bai*
*baizhaoshi23@126.com*
*Wufu Zhu*
*zhuwufu-1122@163.com*

*†These authors have contributed equally to this work and share first authorship*

***Specialty section:***
*This article was submitted to Medicinal and Pharmaceutical Chemistry, a section of the journal Frontiers in Chemistry*

***Received:*** *15 November 2021*
***Accepted:*** *15 February 2022*
***Published:*** *06 April 2022*

***Citation:***
*Liu X, Li Y, Zhang Q, Pan Q, Zheng P, Dai X, Bai Z and Zhu W (2022) Design, Synthesis, and Biological Evaluation of [1,2,4]triazolo[4,3-a] Pyrazine Derivatives as Novel Dual c-Met/VEGFR-2 Inhibitors. Front. Chem. 10:815534. doi: 10.3389/fchem.2022.815534*

In this study, we designed and synthesized a series of novel [1,2,4]triazolo [4,3-*a*]pyrazine derivatives, and evaluated them for their inhibitory activities toward c-Met/VEGFR-2 kinases and antiproliferative activities against tested three cell lines *in vitro*. Most of the compounds showed satisfactory activity compared with lead compound foretinib. Among them, the most promising compound **17l** exhibited excellent antiproliferative activities against A549, MCF-7, and Hela cancer cell lines with $IC_{50}$ values of 0.98 ± 0.08, 1.05 ± 0.17, and 1.28 ± 0.25 μM, respectively, as well as excellent kinase inhibitory activities (c-Met $IC_{50}$ = 26.00 nM and VEGFR-2 $IC_{50}$ = 2.6 μM). Moreover, compound **17l** inhibited the growth of A549 cells in G0/G1 phase in a dose-dependent manner, and induced the late apoptosis of A549 cells. Its intervention on intracellular c-Met signaling of A549 was verified by the result of Western blot. Fluorescence quantitative PCR showed that compound **17l** inhibited the growth of A549 cells by inhibiting the expression of c-Met and VEGFR-2, and its hemolytic toxicity was low. Molecular docking and molecular dynamics simulation indicated that compound **17l** could bind to c-Met and VEGFR-2 protein, which was similar to that of foretinib.

**Keywords: c-Met inhibitor, antiproliferative activity, antitumor, targeted drug, pyrazine derivatives**

## 1 INTRODUCTION

Cancer is one of the leading causes of death, which seriously endangers human health. Traditional antitumor drugs have great toxicity and side effects because of lack in specificity, which cause serious damage to human tissues and organs (Maeda and Khatami, 2018) (Schirrmacher, 2019). In recent years, small molecular targeted antitumor drugs have been widely studied, whose high selectivity and specificity make the drug less toxic and with less side effects (Tarver, 2012) (Jemal et al., 2003). However, single target agents are more likely to develop drug resistance. Studies showed that small-molecule drugs interfering at the same time with multiple drug targets might be more effective to overcome drug resistance (Korcsmáros et al., 2007) (Giordano and Petrelli, 2008).

Mesenchymal–epithelial transition factor (c-Met) is a receptor in the family of receptor tyrosine kinases (RTKs) whose greatest characteristic is high-affinity for hepatocyte growth factor (HGF) and is involved in epithelial tissue remodeling and cell migration (Furge et al., 2000) (Moustakas and Heldin, 2007) (Alsahafi et al., 2019). c-Met kinase is located at the intersection of numerous tumor

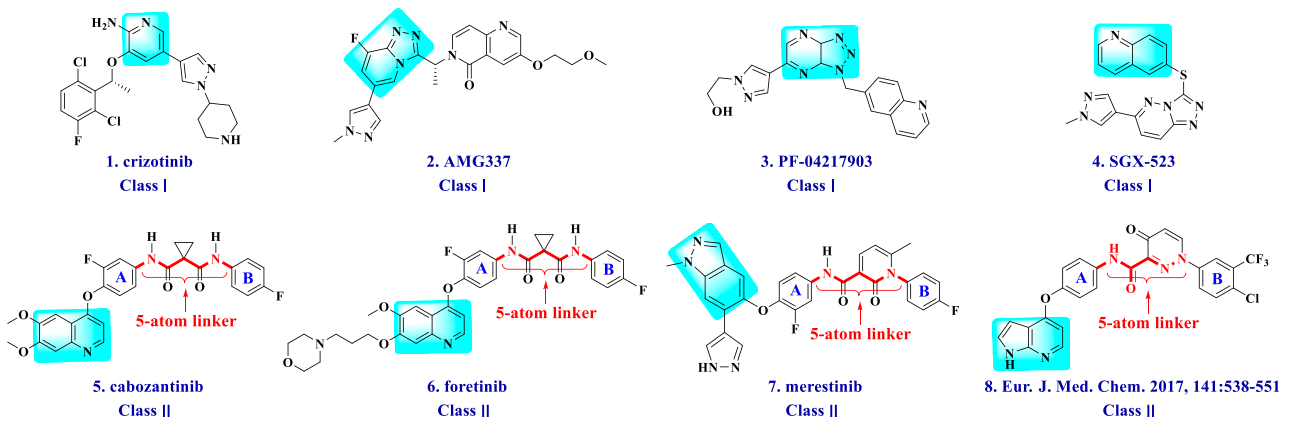


**FIGURE 1 |** Structures of small-molecule mesenchymal–epithelial transition factor (c-Met) inhibitors.

signaling pathways (Organ and Tsao, 2011), so dysregulation of the HGF/c-Met signaling pathway is a driving factor for many cancers, promoting tumor growth, invasion, spread, and/or angiogenesis (Parikh and Ghate, 2018), and is also associated with adverse clinical effects and drug resistance of some approved targeted therapies (Eder et al., 2009). Therefore, the development of novel and efficient small-molecule inhibitors targeting the HGF/c-Met signaling pathway has become a research hotspot (Liu et al., 2010). Vascular endothelial growth factor receptor (VEGFR) is a highly specific mitogen for vascular endothelial cells and is one of the most important regulators of angiogenesis activity (Ribatti, 2005). It can enhance vascular permeability, promote the growth, proliferation, migration, and differentiation of vascular endothelial cells, reduce cell apoptosis, induce vascular formation, change cytoskeleton function, and affect other cellular biological changes (Shibuya, 2001). Studies have shown that inhibition of VEGF signal cannot only block tumor angiogenesis but also change or destroy tumor blood vessels (Inai et al., 2004). Therefore, VEGFR is also an important target for tumor therapy. Several reports showed that dual c-Met/VEGFR inhibitors exhibited excellent antitumor activity and can also be able to compensate for the weakness of single-target inhibitors. Therefore, dual c-Met/VEGFR inhibitors may become a kind of potential antitumor agent, which can overcome drug resistance.

Currently, lots of c-Met kinase inhibitors, such as crizotinib (Cui et al., 2011) (1, Class I, **Figure 1**) and cabozantinib (Fujiwara et al., 2004) (5, Class II), have been approved, respectively, for the treatment of non-small cell lung cancer and medullary thyroid cancer by the FDA. Moreover, enormous small-molecule c-Met inhibitors have been reported and entered clinical studies (Pasquini and Giaccone, 2018). These inhibitors can be classified into three types on the basis of the structural characters and the binding model to c-Met kinase: Class I, Class II, and the others (Zhang et al., 2020c). Class I c-Met inhibitors bind to ATP-binding sites to form a "U" shape, such as crizotinib (1), AMG337 (2) (Boezio et al., 2016), PF-04217903 (3) (Cui et al., 2012), and SGX-523 (4) (Buchanan et al., 2009). Class II c-Met inhibitors, which can bind multiple targets, usually occupy deep hydrophobic back pockets of ATP, such as cabozantinib (5) (Yakes et al., 2011), foretinib (6) (Zillhardt et al., 2011), merestinib (7) (Prins et al., 2016), and compounds (8) (Li et al., 2017). Moreover, foretinib and cabozantinib are also typical VEGFR-2 inhibitors.

Multitarget kinase inhibitors have achieved good therapeutic results in clinical trials, and antitumor therapy based on dual-target c-Met/VEGFR. Tyrosine kinase inhibitors have become one of the most effective clinical treatment methods for cancer. Therefore, we selected typical II c-Met inhibitor foretinib as the lead compound, introducing the active pharmacophore of VEGFR-2 inhibitors and modifying the five-atom portion, aiming to obtain a range of c-Met/VEGFR-2 dual inhibitors with good antitumor activity. As shown in **Figure 2**, the structure of type II c-Met inhibitor foretinib is divided into four parts, represented by A, B, C, and D. Moiety A, as the parent nucleus, is mostly an aromatic heterocyclic ring containing pyridine, such as quinoline and pyridine; moiety B is mostly substituted or unsubstituted phenoxy and pyridyloxy; moiety C can be a cyclic or chain structure, moiety B has six chemical bonds between moiety D, which is referred to as "five-atom regulation"; moiety D is a hydrophobic segment, mostly substituted phenyl group.

In this paper, we modified the following four moieties and designed a series of compounds with completely novel structures. First, the 4-phenoxy quinoline scaffold has been reported as an important component of VEGFR-2 targets, and the quinoline structure is also present in many c-Met inhibitors. Based on the principle of bioelectronic isosteric principle, triazolopyrazine was selected and introduced into foretinib to replace the quinoline structure. Triazolopyrazine is also the active pharmacodynamic structure of Class I c-Met inhibitors, which have good antitumor activity and pharmacokinetic parameters (Albrecht et al., 2008), and we also kept the phenoxy structure of moiety B. Based on the "five-atom regulation," the five-membered heterocyclic rings with novel structure were introduced into part C by using the principle of fragmentation, such as pyrazole, iso-oxazole, and thiazole groups. The benzene ring in part D is used as a hydrophobic segment. In addition to introducing different types of substituents

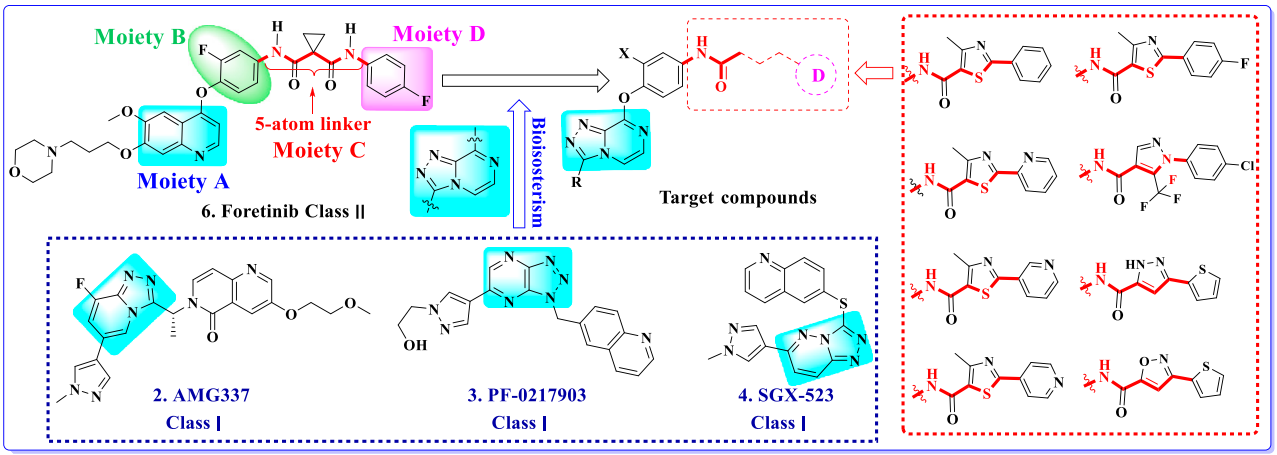


**FIGURE 2 |** Design strategy and structures of target compounds.

to adjust the electron distribution density on the benzene ring, it is also replaced with pyridine and thiophene structures to investigate these structures' influence on the potency of the compounds. What is more, some other substituents were also introduced. The structural fragment of urea is still retained because it is the active pharmacodynamic fragment of VEGFR-2 inhibitors. As a result, a series of novel target compounds with triazolopyrazine structure were designed as dual c-Met/VEGFR-2 inhibitors (16a-l and 17a-m). **Figure 2** illustrates the structures and the detailed design strategy of the target compounds.

The enzymatic inhibitory activity against c-Met kinase and the cellular effect on human lung adenocarcinoma (A549), human breast cancer (MCF-7), and human cervical carcinoma (Hela) cell lines of the synthesized compounds were assessed. The target compound **17l** showed good inhibitory effect on tumor cells and c-Met/VEGFR-2 kinase activity *in vitro*. Further studies on its apoptosis, cycle, and molecular docking were also conducted.

# 2 MATERIALS AND METHODS

## 2.1 Materials and Instruments

Reagents and materials used commonly were purchased commercially. We used the Büchi Melting Point B-540 instrument to measure melting points of target intermediates. The structure of compounds was confirmed by $^1$H NMR spectra, which were received by using a Bruker 400-MHz spectrometer and taking TMS as an internal standard, and mass spectra (MS) were recorded on electrospray ionization (ESI) mode on Agilent 1,100 liquid chromatography–mass spectrometry (LC-MS). Thin-layer chromatography (TLC) analysis, which was carried out on silica gel plates GF254 (Qingdao Haiyang Chemical, Qingdao, China), and the TLC plates were visualized by exposure to ultraviolet light (UV), was used to monitor the reaction process. All the reagents and materials were purchased commercially and utilized directly without purification except as otherwise noted.

## 2.2 Chemistry

The synthetic procedure of intermediates **12a–b** and **12c–d** is illuminated in **Scheme 1**. Taking 2,3-dichloropyrazine (9) as the starting material, which is commercially available, the hydrazine group of compound **10** was substituted *via* nucleophilic reaction using hydrazine hydrate in the presence of compound **9** in ethanol. Compound **10** was cyclized with triethoxy methane to synthesize the key intermediate **11**. Then compounds **12a–b** were synthesized by substituting compound **11** with 4-aminophenol or 2-fluoro-4-aminophenol, respectively. The synthetic method of intermediates **12c–d** was consistent with that of compounds **12a–b**.

**Scheme 2** shows the synthetic route of target compounds **16a–l** and **17a–m**. Compounds **14a–h** reacted with oxalyl chloride to form intermediates **15a–h**. Finally, anilines **12a–b** and acyl chloride **15a–h**, catalyzed by DIPEA in dichloromethane at room temperature, formed the target compounds **16a–l**. The synthetic method of target compounds **17a–m** was the same as that of compounds **16a–l**.

## 2.3 Biological Evaluation

### 2.3.1 Antitumor Assay

The standard MTT assay *in vitro* was used to evaluate the antitumor activities of target compounds (**16a-l** and **17a-m**) in A549, MCF-7, and Hela cell lines and foretinib was positive control. The cell lines used in the experiment were available from the Cell Culture Collection of Chinese Academy of Sciences (Shanghai Institutes for Biological Sciences, Chinese Academy of Sciences). Referring to the previous experimental methods of our research, all cells were cultured in suitable medium such as DMEM or RPMI-1640 containing 10% fetal bovine serum at 37°C in 5% $CO_2$ and propagated for 24 h. Then the compounds with different gradient concentrations were added into the medium and incubated for 72 h, and then MTT (thiazolyl blue tetrazolium bromide) with a concentration of 5 μg/ml was added to every well for 4 h at 37°C. The formazan crystals were dissolved in 100 μl of DMSO in each well. The absorbancy at 492 nm (for absorbance of

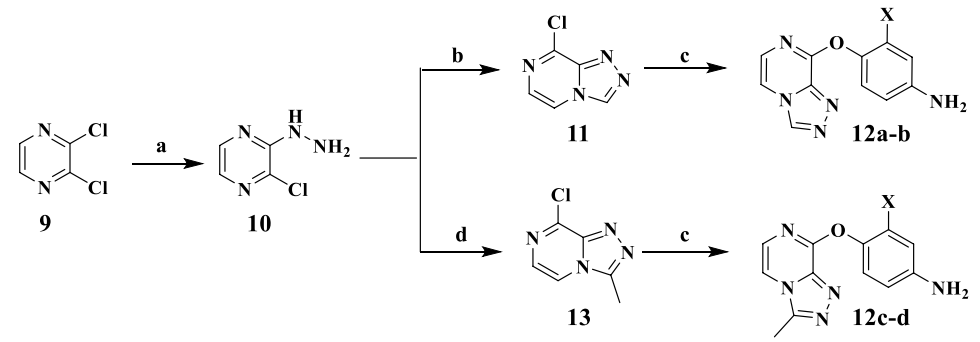


**SCHEME 1 |** Reagents and conditions: **(A)** $N_2H_4{\cdot}H_2O$, EtOH, 85°C, reflux. **(B)** Triethoxy methane, 80°C, reflux. **(C)** 4-Aminophenol, KTB, KI, THF. **(D)** Triethyl orthoacetate, 80°C, reflux.

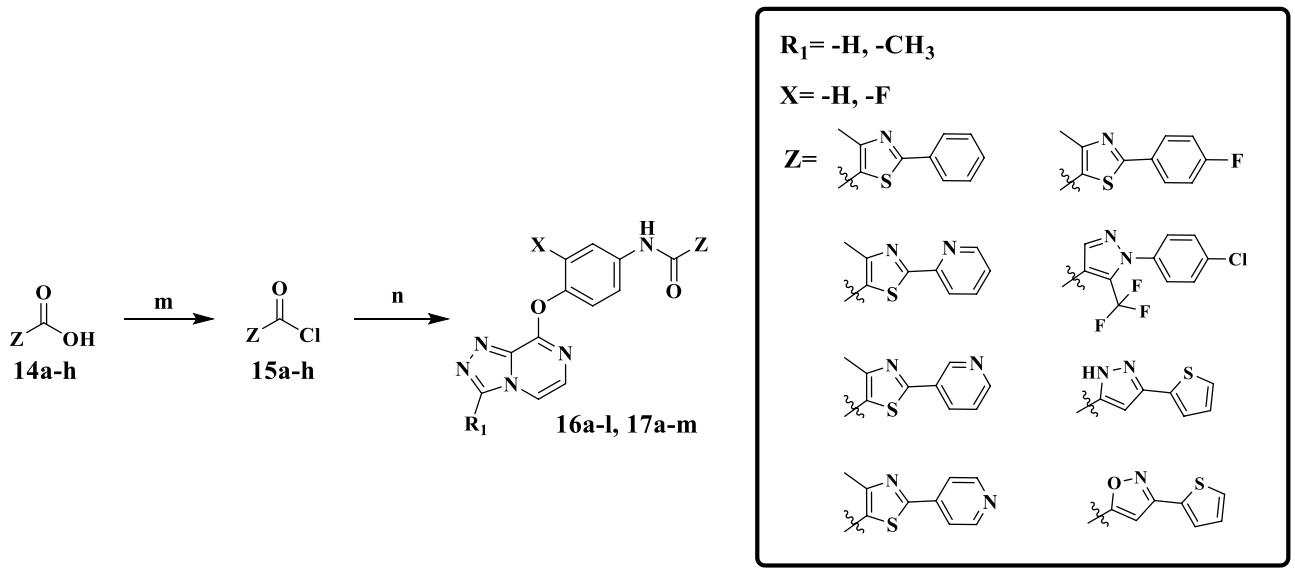


**SCHEME 2 |** Reagents and conditions: (m) oxalyl chloride, DMF, $CH_2Cl_2$, r.t., 5 min; (*n*) DIPEA, $CH_2Cl_2$, r.t., 0.5 h.

MTT formazan) and 630 nm (for the reference wavelength) was measured with an ELISA reader. All compounds were tested three times in each of the cell lines. The results, expressed as inhibition rates or $IC_{50}$ (half-maximal inhibitory concentration), were the averages of two determinations and calculated by using the Bacus Laboratories Incorporated Slide Scanner (Bliss) software.

### 2.3.2 Kinase Selectivity Assay

The target compounds were evaluated for their activity against c-Met kinase, taking foretinib as positive control. The kinase assay was performed by Pratzer Biotechnology Co. Ltd. (Changsha, China).

## 2.4 Cell Cycle Assay

The effect on cell cycle of the optimal compound **17l** was measured using foretinib as a control and performed by Pratzer Biotechnology Co. Ltd. (Changsha, China). A549 cells were placed in 12-well plates at a density of $10^6$/well with F-12 K containing 10% FBS as the medium, and the experiment was conducted on alternate days. Cells ($1–5\times10^6$) were collected, centrifuged at 1,500 rpm for 5 min to remove the supernatant, washed with PBS twice, and gently mixed with 200 μl of cell cycle rapid detection reagent to make a single-cell suspension, which was detected by flow cytometry within 1 h.

## 2.5 Cell Apoptosis Assay

We evaluated the effect of compound **17l** on cell apoptosis according to our previous methods (Zhao et al., 2020), using A549 cells, and taking foretinib as positive control. The cell apoptosis assay was performed by Pratzer Biotechnology Co. Ltd. (Changsha, China). After A549 cells were resuscitated, the cells were cultured in F-12 K medium containing 10% FBS and 1% pen/strep in incubator with 5% $CO_2$ at 37°C. A549 cells, being in the logarithmic growth phase, were digested with 25% trypsin and laid in six-well plates with a density of $2 \times 10^5$/well, and the cells were collected centrifugally after 72 h of treatment with each

**TABLE 1 |** Antiproliferative and mesenchymal–epithelial transition factor (c-Met) kinase inhibitory activities of the target compounds.

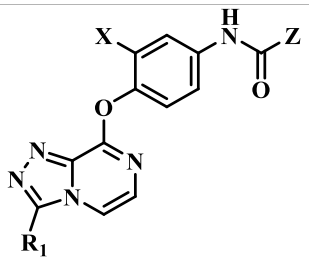

| Compounds | X | $R_1$ | Z | $IC_{50}$ (μM)[a] | | | |
|---|---|---|---|---|---|---|---|
| | | | | A549 | MCF-7 | Hela | c-Met |
| 16a | H | H |  | 12.36 ± 0.97 | 13.76 ± 1.23 | 21.54 ± 1.78 | 0.794 |
| 16b | H | H |  | 6.46 ± 0.33 | 7.87 ± 0.42 | 12.16 ± 1.08 | 0.379 |
| 16c | H | H |  | 5.58 ± 0.75 | 6.45 ± 0.81 | 14.31 ± 1.15 | 0.345 |
| 16d | H | H |  | 12.35 ± 0.98 | 11.52 ± 1.06 | 19.53 ± 1.94 | 0.722 |
| 16e | H | H |  | 5.44 ± 0.42 | 7.13 ± 0.63 | 11.19 ± 0.96 | 0.342 |
| 16f | H | H |  | 27.33 ± 0.86 | >50 | >50 | >1 |
| 16 g | F | H |  | 8.21 ± 0.65 | 9.17 ± 1.03 | 17.73 ± 1.29 | 0.658 |
| 16 h | F | H |  | 6.56 ± 0.42 | 8.18 ± 1.12 | 13.94 ± 1.59 | 0.437 |
| 16i | F | H |  | 17.35 ± 0.97 | 19.03 ± 1.32 | 24.96 ± 2.17 | ND[b] |
| 16j | F | H |  | 3.26 ± 0.67 | 3.68 ± 0.34 | 6.17 ± 0.58 | 0.110 |
| 16 k | F | H |  | 6.18 ± 0.34 | 6.51 ± 0.63 | 12.89 ± 1.06 | 0.380 |
| 16l | F | H |  | 11.44 ± 0.76 | 11.97 ± 1.24 | 23.32 ± 2.12 | 0.725 |
| 17a | H | $CH_3$ |  | **1.23 ± 0.13** | **1.43 ± 0.21** | **2.31 ± 0.29** | **0.055** |
| 17b | H | $CH_3$ |  | 4.31 ± 0.49 | 5.15 ± 0.72 | 9.46 ± 0.58 | 0.245 |
| 17c | H | $CH_3$ |  | 7.68 ± 0.71 | 8.79 ± 0.89 | 15.88 ± 1.10 | 0.532 |
| 17d | H | $CH_3$ | 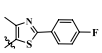 | 5.21 ± 0.37 | 6.95 ± 0.67 | 10.73 ± 1.42 | 0.289 |
| 17e | H | $CH_3$ |  | **2.05 ± 0.19** | **1.74 ± 0.22** | **4.78 ± 0.43** | **0.077** |
| 17f | H | $CH_3$ |  | 5.73 ± 0.54 | 6.38 ± 0.85 | 12.37 ± 1.53 | 0.300 |
| 17 g | F | $CH_3$ |  | 4.65 ± 0.66 | 4.83 ± 0.33 | 9.25 ± 0.45 | 0.232 |
| 17 h | F | $CH_3$ |  | 3.56 ± 0.32 | 4.25 ± 0.76 | 7.43 ± 0.38 | 0.156 |

(Continued on following page)

**TABLE 1 |** (*Continued*) Antiproliferative and mesenchymal–epithelial transition factor (c-Met) kinase inhibitory activities of the target compounds.

| Compounds | X | $R_1$ | Z | $IC_{50}$ (μM)[a] | | | |
|---|---|---|---|---|---|---|---|
| | | | | A549 | MCF-7 | Hela | c-Met |
| 17i | F | $CH_3$ |  | 188 | 25.44 ± 1.54 | >50 | ND |
| 17j | F | $CH_3$ |  | 7.16 ± 0.45 | 7.31 ± 0.77 | 14.18 ± 1.64 | 0.450 |
| 17 k | F | $CH_3$ | 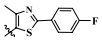 | 15.34 ± 0.51 | 18.17 ± 1.28 | 25.33 ± 2.40 | ND |
| 17l | F | $CH_3$ | 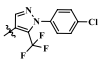 | **0.98 ± 0.08** | **1.05 ± 0.17** | **1.28 ± 0.25** | **0.026** |
| 17 m | F | $CH_3$ |  | 8.84 ± 0.97 | 9.34 ± 1.03 | 17.37 ± 1.56 | 0.653 |
| Foretinib[c] | - | - | - | 0.71 ± 0.05 | 0.93 ± 0.09 | 1.18 ± 0.25 | 0.019 |

*Note. A549, human lung adenocarcinoma; MCF-7, human breast cancer; Hela, human cervical carcinoma.*
*[a]The values are the average of two separate determinations.*
*[b]ND, not detected.*
*[c]Used as a positive control.*

**TABLE 2 |** Antiproliferative and some other kinase inhibitory activities of compound **17l.**

| Compound | $IC_{50}$ (μM) | | | | | |
|---|---|---|---|---|---|---|
| | c-Met | VEGFR-2 | $EGFR^{WT}$ | PC-9 | H460 | H1975 |
| 17l | 0.026 | 2.6 | >10 | 38.25 ± 1.58 | 5.86 ± 0.77 | 15.30 ± 1.18 |
| Staurosporine[a] | 0.125 | - | - | ND[c] | ND | ND |
| Sorafenib[b] | ND | ND | ND | 5.41 ± 0.73 | 5.27 ± 0.72 | 10.18 ± 1.00 |

*Note. VEGFR, vascular endothelial growth factor receptor; PC-9, exon 19 of EGFR; H1975, gefitinib cell line; H460, human non-small cell lung cancer cells.*
*[a]Used as a positive control.*
*[b]Used as a positive control.*
*[c]ND, not detected.*

compound. The cells were washed twice with PBS, which was precooled to 4°C. Then the cells were suspended with 500 μl of buffer, and the concentration was adjusted to $10^6$/ml. A 100-μl suspension was placed in a 5-ml flow tube, adding 5 μl of Annexin V-APC, adding 5 μl of propidiμm iodide, and the mixture was mixed and incubated at room temperature without light for 15 min detecting cell apoptosis by flow cytometry (FACS).

## 2.6 Western Blot

Western blot was utilized to further analyze the effect of compound **17l** on the downstream signal protein of c-Met and VEGFR-2. The detailed operations refer to the previous method of our research group (Zhao et al., 2020). A549 cells were treated with different concentrations of compound 17l and foretinib (positive control) for 24 h, and then RIPA lysis buffer was utilized to lysate cells for whole-cell protein extraction. The extracted protein was transferred to a PVDF membrane in ice bath conditions after 10% SDS polyacrylamide gel electrophoresis separating the protein by size. The PVDF membrane was rinsed with phosphate-buffered solution (PBST), shaken in a Petri dish three times for 3–5 min every time, and incubated with different target proteins (p-c-Met, *p*-VEGFR-2, *p*-ERK 1/2, *p*-AKT, and GADPH). Finally, the film was exposed and developed in a darkroom. Image Lab software (Molecular Dynamics, Sunnyvale, CA, USA) was utilized to analyze the shadow density of each band, which was then expressed as a percentage of GDPDH band density (Zhao et al., 2020).

## 2.7 Fluorescence Quantitative PCR

Fluorescence quantitative PCR was conducted to analyze the expression patterns of c-Met and VEGFR-2 in the signal pathway in the adherent cells cultured with compounds **17a** and **17l**. The detailed operations refer to our previous published paper (He et al., 2019), and the primers used in the experiments are listed in **Supplementary Table S1**.

## 2.8 Hemolytic Test

The hemolytic toxicity of **17l** was studied with 1% Triton and 0.9% normal saline, and the former was a positive control, and the latter was a negative control. Triolatone (1%), 0.9% normal saline, and compound **17l** of different concentrations prepared in 0.9% normal saline reacted with the prepared sheep red blood cells, respectively. Photos were taken, and the absorbance value was measured by ultraviolet spectrophotometer at a wavelength of 540 nm, and hemolysis ratio (hemolysis %) was calculated according to the following formula (Guo et al., 2017). The experiment was repeated twice in parallel.

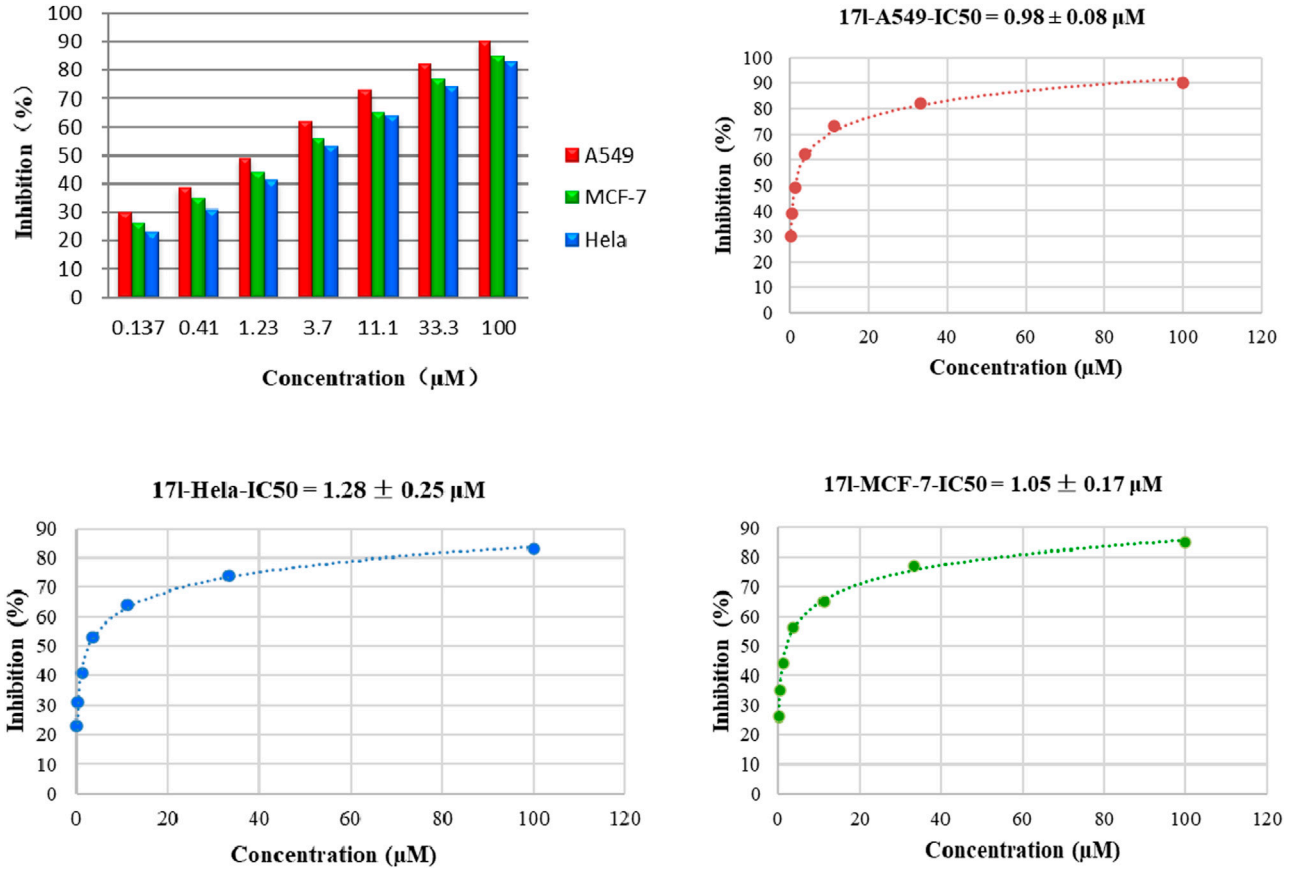


**FIGURE 3 |** Relationship between the inhibition rate and concentration of compound **17l** on three cancer cell lines.

$$\textbf{Hemolysis}\ \% = \frac{\mathrm{Abs}\left(\text{experimental group}\right) - \mathrm{Abs}\left(\text{negative control}\right)}{\mathrm{Abs}\left(\text{positive control}\right) - \mathrm{Abs}\left(\text{negative control}\right)}$$

## 2.9 Molecular Docking Study

The co-crystal structures of c-Met (PDB code 3LQ8) and VEGFR-2 (PDB code 4SAD) were selected as the template to generate docking models. The AutoDock 4.2 software (The Scripps Research Institute, United States ) was used to prepare the 3D structure of the docking ligands **17l** and perform energy minimization. c-Met protein as docking receptor went through the preparation process of flexible docking. Then compound **17l** was placed in the prepared system. After analyzing the interaction between **17l** and c-Met protein, the proper docking conformation was selected and preserved based on the calculated energy. PyMOL 1.8. x software (https://pymol.org) was utilized to perform and modify the docking results.

## 2.10 Molecular Dynamics Simulation

Gromacs 2019.3 (Lindahl et al., 2019) force field was used to deal with 3LQ8. For compound **17l**, restricted electrostatic potential (RESP) was calculated using Multiwfn (Wang et al., 2006) and eventually parameterized using Generation Amber Force Field (GAFF) (Wang et al., 2004). The long-range electrostatic interactions were calculated by the particle mesh Ewald (PME) (Darden et al., 1993). The prepared system had undergone double minimization. Compound **17l** was simulated for MD at 120 ns using the GROMACS-ver software. The 120-ns trajectory was analyzed after MD simulation, and the g-mmpbsa method was used to calculate the binding free energy and energy decomposition (Kumari et al., 2014).

# 3 RESULTS AND DISCUSSION

## 3.1 Chemistry

We synthesized all the compounds and intermediates by referring to our group's previous research methods (Zhang B. et al., 2020) (Zhang et al., 2020b). $^{1}$H NMR and ESI-MS were utilized to characterize all the synthesized compounds and intermediates. The detailed operating steps and spectrum information were obtained in the **Supplementary Material**.

## 3.2 Biological Evaluation

The antiproliferative effects of the target compounds **16a–l** and **17a–m** had been evaluated toward three cancer cell lines A549, MCF-7, and Hela by the method of MTT [3-(4,5-dimethylthiazolyl-2)-2,5- diphenyltetrazolium bromide] with

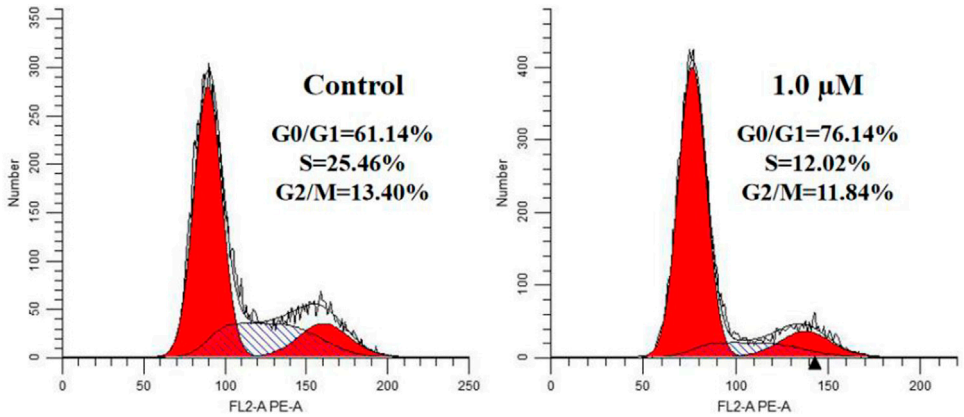


**FIGURE 4 |** Cell cycle progression analyses of human lung adenocarcinoma (A549) cells cultured with compound **17l** for 72 h.

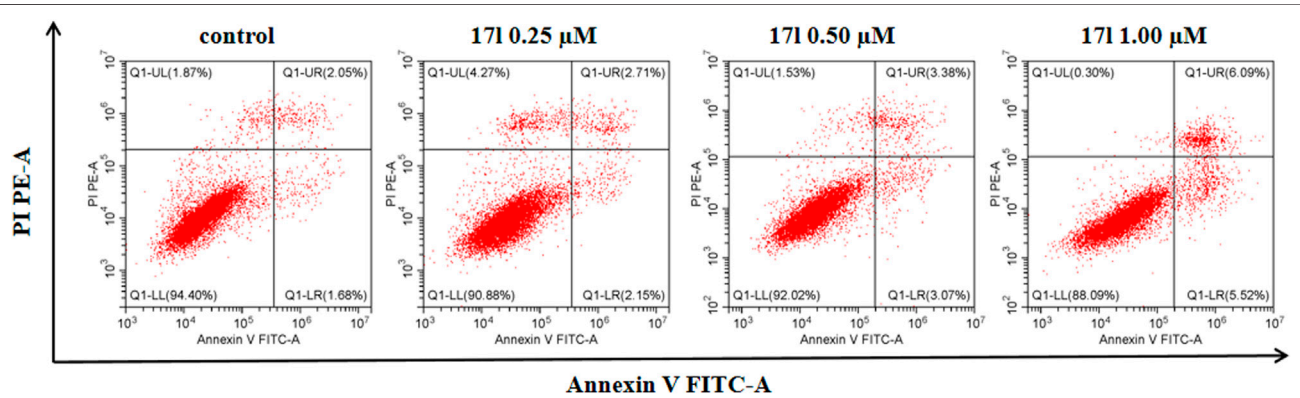


**FIGURE 5 |** The analyses of compound **17l** induces apoptosis of A549 cells.

foretinib as positive control. **Table 1** shows the results, and all the values were averages of two independent experiments. As shown from the chart, most of the compounds exhibited favorable antiproliferative activities against A549, MCF-7, and Hela cell lines, and most of them exhibited more excellent antiproliferative activities against A549 than that of MCF-7 and Hela. Among them, compound **17l** showed a wonderful antiproliferative activity against A549, MCF-7, and Hela cell lines, and their $IC_{50}$ values were 0.98 ± 0.08, 1.05 ± 0.17, and 1.28 ± 0.25 μM, respectively, which was similar to that of the reference compound foretinib. Overall result of antiproliferative activity showed that the introduction of triazolo [4,3-*a*] pyrazine core could improve the antitumor effect of target compounds, which indicated that triazolo [4,3-*a*] pyrazine core was an active pharmacophore.

Moreover, compared with compounds **16a–f** (X = H) without a substituent, the introduction of an F atom on the phenoxy group in compound **16g–l** is favorable for antiproliferative activity. The same trend had also been observed between compounds **17a–f** and **17g–m**. By comparing with compounds **16a–l** and **17a–m**, it was found that compounds with methyl substitution ($R_1$ = H) had higher antiproliferative activity against

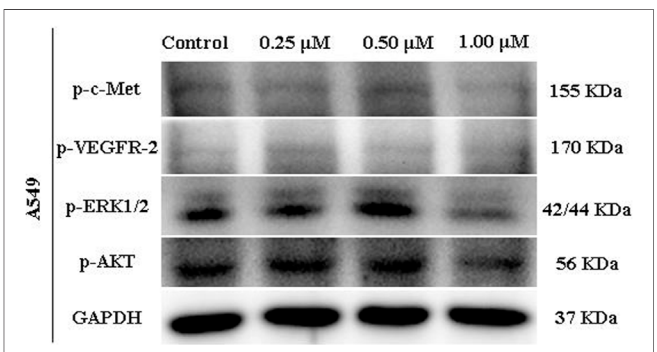


**FIGURE 6 |** c-Met biomarker modulation by compound **17l** (Evaluated by Western blot).

three tumor cell lines. Comparing compounds **17a** and **17d** (or **17g** and **17k**), compound **17a** without an F atom substitution on the benzene ring had higher antiproliferative activity against the three tumor cell lines. Compounds **17b–17c** and **17h–17j** showed that the introduction of the 2-pyridine group into the 5-methylthiazole ring had better antiproliferative activity on the

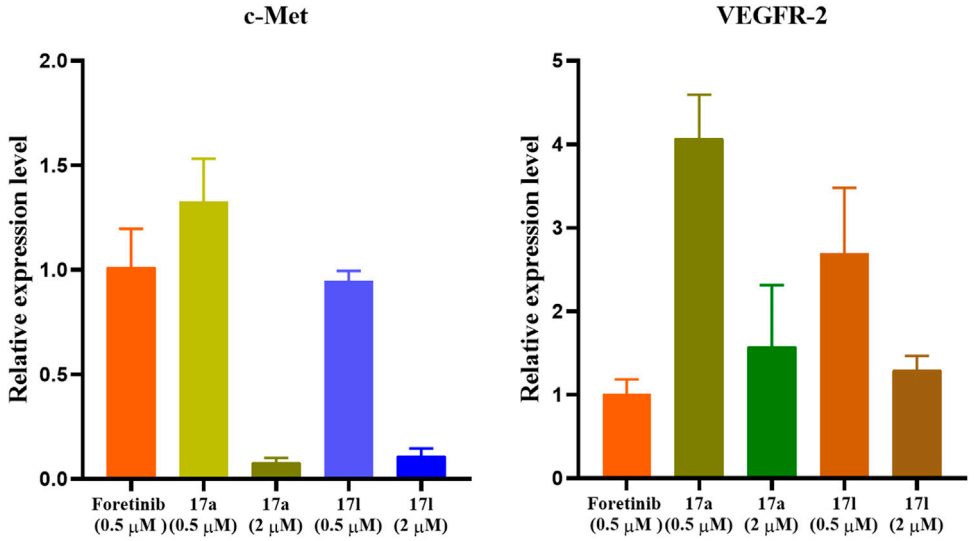


**FIGURE 7 |** Gene expression pattern of c-Met and vascular endothelial growth factor receptor (VEGFR)-2 in A549 cells treated with foretinib, **17a**, and **17l**.

three kinds of tumor cells. Compounds **17e** and **17l** showed better antiproliferative activity and kinase activity when the five-atom part was 5-(trifluoromethyl)-1*H*-pyrazole.

Furthermore, taking foretinib as positive control, we tested the c-Met inhibitory activities of target compounds. Most target compounds exhibited moderate inhibitory activities of c-Met kinase according to experimental results (**Table 1**). Specifically, compounds **17a**, **17e**, and **17l** showed excellent activity against c-Met kinase at the nanomolar level, with the $IC_{50}$ values of 55, 77, and 26 nM, respectively. It is worth noting that the activity against c-Met kinase of compound **17l** was equal to positive control foretinib (19.00 nM). The most active compound **17l** was selected to further test the inhibitory activities against VEGFR-2 and $EGFR^{wt}$ kinases, and also test the antiproliferative activity against three cell lines using sorafenib (multitarget inhibitors through inhibiting VEGFR and PDGFR) as positive control, including human non-small cell lung cancer cells (H460), human lung adenocarcinoma cell line harboring a deletion in exon 19 of EGFR (PC-9), and non-small-cell lung cancer cells harboring T790M-targeted epidermal growth factor receptor mutation to the tyrosine kinase inhibitor gefitinib cell line (H1975). The results indicated that the inhibitory activity of compound **17l** against H1975 and H460 cells was similar with positive control, while the antiproliferative activity against PC-9 cells was worse than it. The inhibitory activities (**Table 2**) demonstrated that **17l** was a potential dual c-Met/VEGFR-2 inhibitor with high selectivity to $EGFR^{wt}$.

Additionally, we also selected the optimal compound **17l** to explore the relationship between antiproliferative activity and compound concentration. Three cell lines (A549, MCF-7, and Hela) were treated with compound **17l** at different concentrations for 72 h. **Figure 3** illustrates that with the increase in compound **17l** concentration, its inhibitory ratio against the three cell lines increased gradually, presenting dose dependency. Furthermore, the antiproliferative activity of compound **17l** on A549 cells was better than that on MCF-7 and Hela cells.

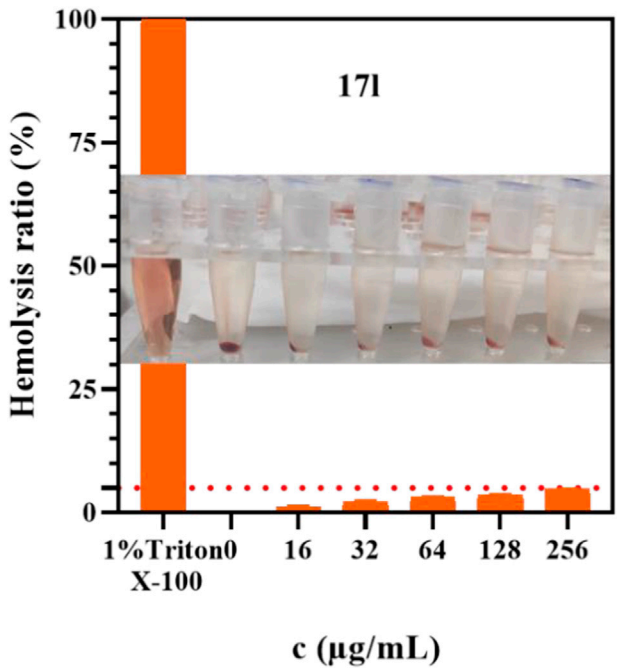


**FIGURE 8 |** The hemolysis rate of compound **17l** with different concentrations.

## 3.3 Effect on Cell Cycle Progression

We treated A549 cells with 1.0 μM compound **17l** for 72 h and determined its effect on cell cycle by flow cytometry to further reveal the growth inhibition mechanism of the target compound on tumor cells. The results are shown in **Figure 4**. Compared with the control group, A549 cells cultured with compound **17l** had a significant inhibitory effect on cell growth in G0/G1 phase, and the cell block rate increased from 61.14% to 76.14%. At the same

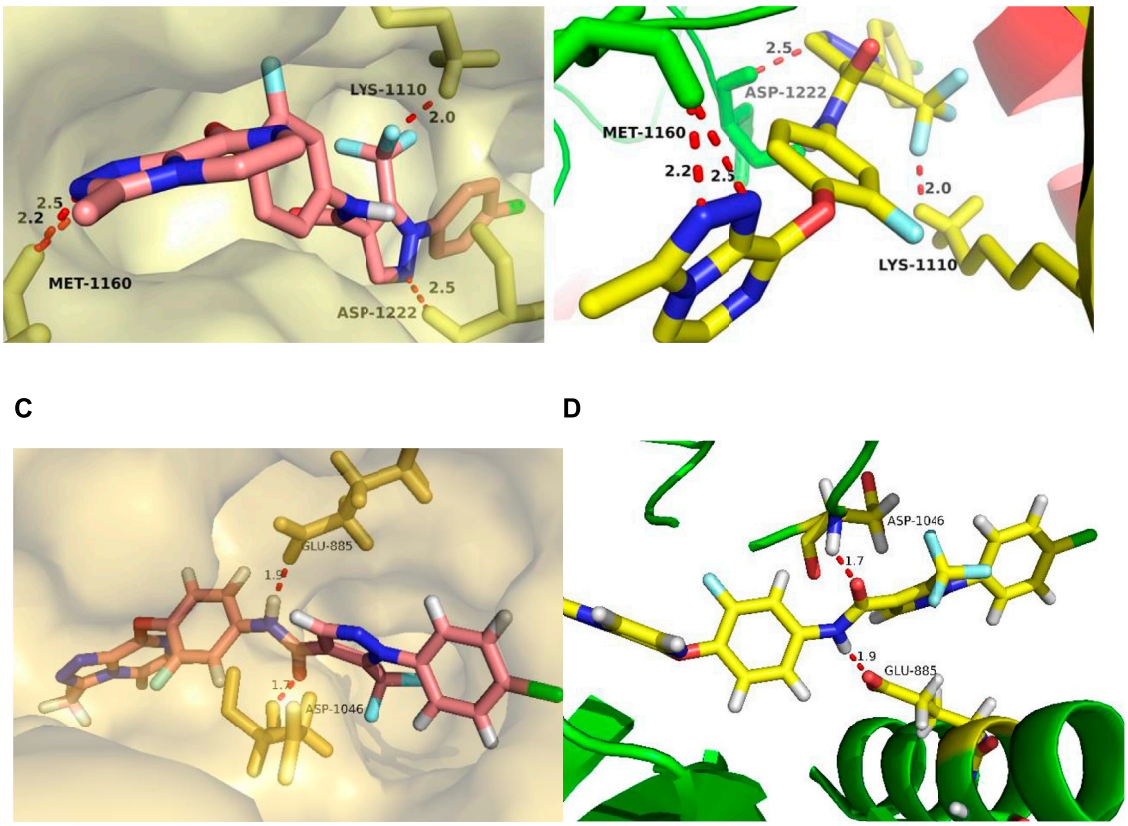


**FIGURE 9 |** The docking mode of compound **17l** with c-Met (PDB code 3LQ8) and VEGFR-2 (PDB code 4ASD). **(A,B)** showed three major hydrogen bond interactions formed between the **17l** and c-Met protein. **(C,D)** showed two hydrogen bond interactions between the **17l** and VEGFR-2 protein.

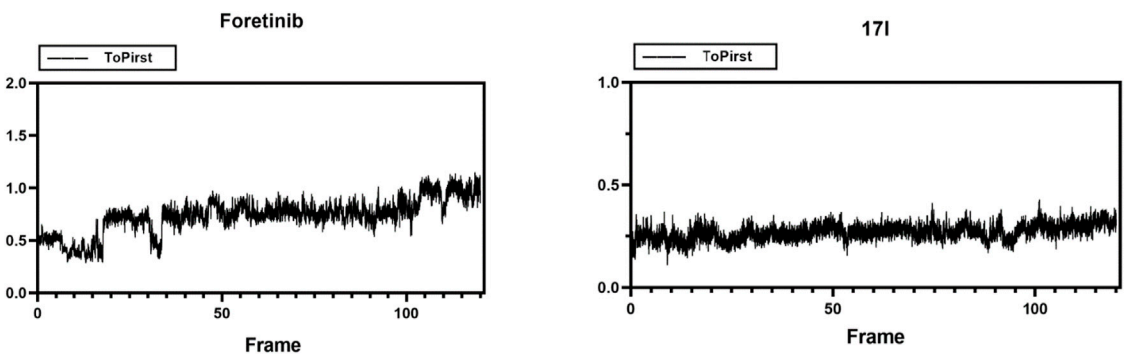


**FIGURE 10 |** Root-mean-squared deviation (RMSD) plots for the backbone atoms and foretinib or **17l** during 120-ns MD simulations. The *X* axis is the frame number. The *Y* axis is the RMSD value.

time, the content of cell block rate decreased in S phase, but the change in G2/M phase was not obvious. In conclusion, compound **17l** could inhibit the growth of A549 cells in the G0/G1 phase.

## 3.4 Effect on Apoptosis

The assay of annexin V/PI staining was performed to deeper research the mechanism of apoptosis induced by compound **17l** in A549 cells. **Figure 5** shows the analysis results of A549 cells cultured with compound **17l** for 72 h. In comparison with the control group (the total apoptosis rate was 3.73%), A549 cells were treated with 0.25, 0.50, and 1.00 μM, the total apoptosis rates of compound **17l** were 4.86%, 6.45%, and 11.61%, respectively. In conclusion, compound **17l** induced apoptosis of A549 cells in a dose-dependent manner, and the effect of late apoptosis was obvious.

**TABLE 3 |** Predicted free energies (kcal/mol) for binding of foretinib and **17l** to c-Met kinase.

| Energy terms (kcal/mol) | Foretinib | 17l |
|---|---|---|
| VDW energy[a] | −56.890 ± 1.764 | −58.850 ± 0.765 |
| EE energy[b] | −10.453 ± 1.081 | −9.239 ± 0.510 |
| Polar energy[c] | 41.902 ± 2.074 | 39.615 ± 0.624 |
| Apolar energy[d] | −6.008 ± 0.132 | −5.470 ± 0.058 |
| Delta total[e] | −31.448 ± 1.414 | −33.944 ± 0.961 |

*Note.* [a]*Van der Waal energy.*
[b]*Electrostattic energy.*
[c]*Polar solvation energy.*
[d]*SASA, energy.*
[e]*Binding energy.*

## 3.5 Modulation of C-Met Activity in A549 Cell Line by Compound 17l

We further verified the effect of compound **17l** on c-Met and downstream signaling pathways. We treated A549 cell line with different doses of compound **17l** for 24 h to measure its phosphorylation inhibition in different pathways. At different concentrations, compound **17l** inhibited the protein levels of p-c-Met (Tyr1003) (**Figure 6**) and *p*-VEGFR-2 (Tyr1059) (**Figure 6**), indicating that it can inhibit phosphorylation protein of c-Met and VEGFR-2, but the inhibitory effect on *p*-VEGFR-2 is not obvious. At the same time, we observed that at a concentration of 1.00 μM, compound **17l** significantly inhibited the phosphorylation protein of c-Met's downstream biomarker signals ERK1/2 and AKT. This result further indicates that compound **17l** may be an effective c-Met inhibitor.

## 3.6 Fluorescence Quantitative PCR Analysis

Different amounts of apoptosis cells resulted in different gene expression levels. Therefore, compounds **17a** and **17l** with the best antiproliferation activity were selected as representatives to investigate c-Met/VEGFR-2 gene expression level in tumor cells for further verifying the results of anti-proliferation activity. Compounds **17a** and **17l** with the best antiproliferative activity were selected as representatives. The expression patterns of c-Met and VEGFR-2 kinases in the signal pathway were analyzed by fluorescent quantitative PCR. In the results shown in **Figure 7**, the expression of c-Met gene in A549 cells treated with compound **17a** was higher than that of foretinib at 0.5 μM, while the expression of c-Met gene in A549 cells treated with compound **17l** was comparable with foretinib. However, VEGFR-2 gene expression was higher in both **17a**- and **17l**-treated A549

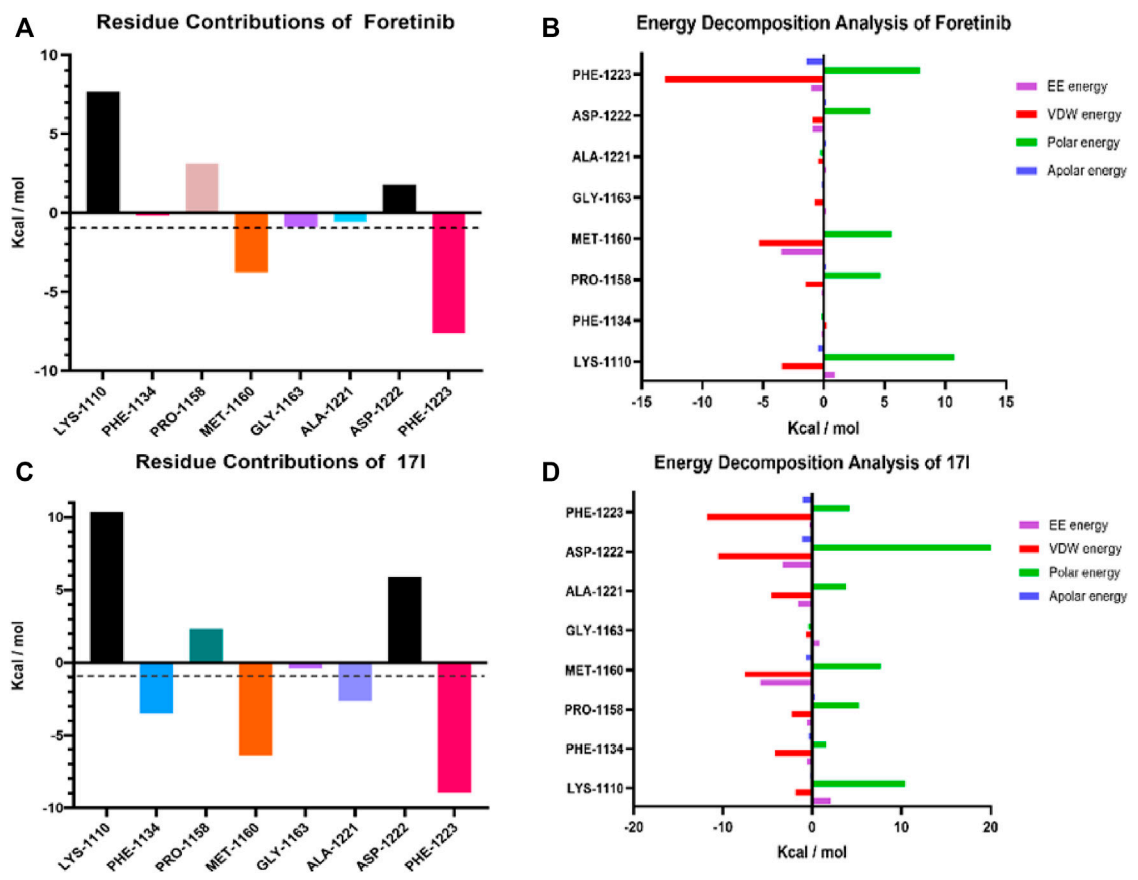


**FIGURE 11 |** Molecule dynamic stimulation results of foretinib-3LQ8 and **17l**–3LQ8. Residue contributions of potential hot residues of **(A)** and **(C)**. Energy decomposition of potential hot residues of **(B)** and **(D)**. The unit of energy is kcal/mol.

cells than in foretinib cells at 2 μM. The results were consistent with the antiproliferative activity of our compounds.

## 3.7 Hemolytic Test

The best compound **17l** with antiproliferative activity and kinase inhibition activity was selected to detect its hemolytic toxicity at a gradient concentration of 16–256 μg/ml, and the safety of intravenous administration was preliminarily investigated. In the results shown in **Figure 8**, the hemolytic rate of compound **17l** was still less than 5% even at the highest concentration within the study range, which proved that compound **17l** had low hemolytic toxicity to red blood cells. Its hemolytic toxicity meets the requirements of intravenous administration, which provides a basis for further *in vivo* research.

## 3.8 Molecular Docking Study

Taking comprehensive consideration of c-Met and VEGFR-2 inhibitory activities and antiproliferative activities, compound **17l** was chosen as a representative in exploring the binding model of target compounds with c-Met and VEGFR-2 protein. Compound **17l** was docked with c-Met protein (PDB code 3LQ8) and VEGFR-2 protein (PDB code 4SAD), respectively, which used the AutoDock 4.2 software (The Scripps Research Institute, USA), and the PyMOL 1.8 x software (https://pymol.org) was used to modify the docking results. The entire heterocyclic skeleton of compound **17l** was closely embedded into the hydrophobic cavity of c-Met protein in **Figure 9A** and as shown in **Figure 9C**, the compound was also tightly embedded in the hydrophobic cavity of VEGFR-2 protein. In addition, there were two N atoms on the triazolopyrazine ring of compound **17l**, which formed a bidentate hydrogen bond with MET-1160 that was the key amino acid residue in the hinge region of the protein. The result indicated that the introduction of triazolopyrazine ring was the key to guarantee the activity of target compounds (**Figure 9B**). Meanwhile, the oxygen atom of the pyridazinone group of the five-atom linker formed a hydrogen bond with LYS-1110, and the two nitrogen atoms on the pyridazinone group constituted a bidentate hydrogen bond with residue ASP-1222, which also indicated that the target compounds had strong binding ability with c-Met protein. In **Figure 9D**, the result indicated that the amide fragment of the five-atom linker of **17l** formed hydrogen bonds with GLU-885 and ASP-1046 of VEGFR-2 kinase, respectively, improving the binding ability of the compound to the kinase to a certain extent. The results of molecular docking illustrated that compound **17l** might be a potential dual inhibitor of c-Met/VEGFR-2.

## 3.9 Molecular Dynamic Simulation

Molecular dynamic simulations were performed in Gromacs 2019.3 in order to assess the stability of a system of protein with small molecules. Compound **17l** and c-Met protein (3LQ8) systems were selected as representatives for the simulation, and the whole process lasted for 120 ns. MD simulations trajectories were utilized for data extracting and binding free energy calculating. As shown in **Figure 10**, the root-mean-squared deviation (RMSD) values, of the protease backbone atoms relative to their crystal structures during the MD simulation, indicated that the ligand–receptor system of foretinib-3LQ8 as control tended to be stable at 3.5 ns and the distribution of the **17l**–3LQ8 system also tended to be stable quickly. The results indicated that the intramolecular system was stable, and the dynamic simulation was meaningful.

The MM-PBSA method was utilized to calculate the total binding free energy of **17l**, which were −58.850 ± 0.765, −9.239 ± 0.510, 39.615 ± 0.624, −5.470 ± 0.058, and −33.944 ± 0.961 kcal/mol for the complexes of **17l**–3LQ8, respectively (**Table 3**). The results show that the total free energy of compound **17l** was close to that of foretinib. As the docking studies demonstrated, the energies of van der Waal energy (−58.850 ± 0.765 kcal/mol) and binding energy (−33.944 ± 0.961 kcal/mol) of compound **17l** were lower than those of foretinib, which may interpret its higher binding free energy.

The g_mmpbsa method was used to calculate residue contributions of potential hot residues of foretinib and compound **17l** in order to evaluate the contribution of residues in the binding model of c-Met protein. In addition, to explore dominated interactions in the ligand–protein system, energy decomposition of potential hot residues was performed. For foretinib (**Figure 11A**), the results demonstrated that the residues may be significant for inhibitory effect: MET-1160 (−3.771 kcal/mol) and PHE-1223 (−7.607 kcal/mol). For compound **17l** (**Figure 11C**), the results suggest that PHE-1134 (−3.5073 kcal/mol), MET-1160 (−6.3982 kcal/mol), ALA-1221 (−2.6418 kcal/mol), and PHE-1,223 (−8.9509 kcal/mol) may be important residues. Among these residues, MET-1160 and PHE-1223 was the most desirable for the total binding free energies, and the interaction with LYS-1,110, PRO-1,158, and ASP-1,222 seemed like unfavorable. The results show that the docking result of compound **17l** was better than that of foretinib. The binding of ligand–receptor by EE energy and VDW energy was necessary (**Figures 11B, D**).

# 4 CONCLUSION

This study reports the synthesis and antiproliferative activities of [1,2,4]triazolo [4,3-a]pyrazine derivatives **16a–17m**. Most derivatives performed moderate to significant potency, and the most promising compound **17l** (c-Met kinase $IC_{50}$ = 0.026 μM) exhibited excellent antiproliferative activities against A549, MCF-7, and Hela cancer cell lines with $IC_{50}$ values of 0.98 ± 0.08, 1.05 ± 0.17, and 1.28 ± 0.25 μM, respectively. Compound **17l** could arrest A549 cell cycle in the G0/G1 phase and induce apoptosis in A549 cells in a dose-dependent manner. The docking study indicated that the introduction of 4-methyl-5-(trifluoromethyl)-1*H*-pyrazole as the five-atom linker between moiety A and moiety B maintained the potent cytotoxicity. Therefore, compound **17l** may be a potential dual c-Met/VEGFR-2 kinase inhibitor, which can be further studied in the hope of producing more effective anticancer drugs.

# DATA AVAILABILITY STATEMENT

The raw data supporting the conclusion of this article will be made available by the authors, without undue reservation.

# AUTHOR CONTRIBUTIONS

ZB and WZ contributed to the conception and design of the study. XL, YL, QZ, QP, and XD performed the experiments. XL, YL, and QZ performed the statistical analysis. XL and YL wrote the first draft of

the manuscript together. PZ made partial revision and provided guidance for the supplementary trials and the data analysis. All authors contributed to the manuscript revision, and read and approved the submitted version. l.

## FUNDING

We gratefully acknowledge the generous support provided by The National Natural Science Funds (Nos. 82060629 and 81903642), Natural Science Foundation of Jiangxi, China (20212BBG73033), Science and Technology Project Founded by the Education Department of Jiangxi Province, China (GJJ201103), and Key Research and Development of General Projects of Jiangxi Province (20212BBG73033), the China Postdoctoral Science Foundation (No. 2020M681528), the Postdoctoral Science Foundation of Jiangsu Province (No. 2021K369C), the Jiangsu Cancer Hospital Postdoctoral Science Foundation (No. SZL202015).

## SUPPLEMENTARY MATERIAL

The Supplementary Material for this article can be found online at: https://www.frontiersin.org/articles/10.3389/fchem.2022.815534/full#supplementary-material

## REFERENCES

Albrecht, B. K., Harmange, J.-C., Bauer, D., Berry, L., Bode, C., Boezio, A. A., et al. (2008). Discovery and Optimization of Triazolopyridazines as Potent and Selective Inhibitors of the C-Met Kinase. *J. Med. Chem.* 51, 2879–2882. doi:10.1021/jm800043g

Alsahafi, E., Begg, K., Amelio, I., Raulf, N., Lucarelli, P., Sauter, T., et al. (2019). Clinical Update on Head and Neck Cancer: Molecular Biology and Ongoing Challenges. *Cell Death Dis.* 10 (8), 1–7. doi:10.1038/s41419-019-1769-9

Boezio, A. A., Copeland, K. W., Rex, K., Albrecht, K. B., Bauer, D., Bellon, S. F., et al. (2016). Discovery of (R)-6-(1-(8-Fluoro-6-(1-methyl-1 H-Pyrazol-4-Yl)-[1, 2, 4] Triazolo [4, 3-a] Pyridin-3-Yl) Ethyl)-3-(2-Methoxyethoxy)-1, 6-naphthyridin-5 (6 H)-one (AMG 337), a Potent and Selective Inhibitor of MET with High Unbound Target Coverage and Robust *In Vivo* Antitumor Activity. *J. Med. Chem.* 59 (6), 2328–2342. ACS Publications. doi:10.1021/acs.jmedchem.5b01716

Buchanan, S. G., Hendle, J., Lee, P. S., Smith, C. R., Bounaud, P.-Y., Jessen, K. A., et al. (2009). SGX523 Is an Exquisitely Selective, ATP-Competitive Inhibitor of the MET Receptor Tyrosine Kinase with Antitumor Activity *In Vivo*. *Mol. Cancer Ther.* 8, 3181–3190. doi:10.1158/1535-7163.mct-09-0477

Cui, J. J., McTigue, M., Nambu, M., Tran-Dubé, M., Pairish, M., Shen, H., et al. (2012). Discovery of a Novel Class of Exquisitely Selective Mesenchymal-Epithelial Transition Factor (C-MET) Protein Kinase Inhibitors and Identification of the Clinical Candidate 2-(4-(1-(Quinolin-6-Ylmethyl)-1h-[1,2,3]triazolo[4,5-B]pyrazin-6-Yl)-1h-Pyrazol-1-Yl)ethanol (PF-04217903) for the Treatment of Cancer. *J. Med. Chem.* 55, 8091–8109. doi:10.1021/jm300967g

Cui, J. J., Tran-Dubé, M., Shen, H., Nambu, M., Kung, P.-P., Pairish, M., et al. (2011). Structure Based Drug Design of Crizotinib (PF-02341066), a Potent and Selective Dual Inhibitor of Mesenchymal-Epithelial Transition Factor (C-MET) Kinase and Anaplastic Lymphoma Kinase (ALK). *J. Med. Chem.* 54, 6342–6363. doi:10.1021/jm2007613

Darden, T., York, D., and Pedersen, L. (1993). Particle Mesh Ewald: AnN·Log(N) Method for Ewald Sums in Large Systems. *J. Chem. Phys.* 98, 10089–10092. doi:10.1063/1.464397

Eder, J. P., Vande Woude, G. F., Boerner, S. A., and LoRusso, P. M. (2009). Novel Therapeutic Inhibitors of the C-Met Signaling Pathway in Cancer. *Clin. Cancer Res.* 15, 2207–2214. doi:10.1158/1078-0432.ccr-08-1306

Fujiwara, Y., Senga, T., Nishitoba, T., Osawa, T., and Nakamura, K. (2004). *Quinoline Derivative and Quinazoline Derivative Inhibiting Self-Phosphorylation of Hepatocytus Proliferator Receptor and Medicinal Composition Containing the Same.* EP2088141A3.

Furge, K. A., Zhang, Y.-W., and Vande Woude, G. F. (2000). Met Receptor Tyrosine Kinase: Enhanced Signaling through Adapter Proteins. *Oncogene* 19, 5582–5589. doi:10.1038/sj.onc.1203859

Giordano, S., and Petrelli, A. (2008). From Single- to Multi-Target Drugs in Cancer Therapy: When Aspecificity Becomes an Advantage. *Cmc* 15, 422–432. doi:10.2174/092986708783503212

Guo, Q., Zhao, Y., Dai, X., Zhang, T., Yu, Y., Zhang, X., et al. (2017). Functional Silver Nanocomposites as Broad-Spectrum Antimicrobial and Biofilm-Disrupting Agents. *ACS Appl. Mater. Inter.* 9, 16834–16847. doi:10.1021/acsami.7b02775

He, B., Tu, Y., Jiang, C., Zhang, Z., Li, Y., and Zeng, B. (2019). Functional Genomics of Aspergillus oryzae: Strategies and Progress. *Microorganisms* 7, 103. doi:10.3390/microorganisms7040103

Inai, T., Mancuso, M., Hashizume, H., Baffert, F., Haskell, A., Baluk, P., et al. (2004). Inhibition of Vascular Endothelial Growth Factor (VEGF) Signaling in Cancer Causes Loss of Endothelial Fenestrations, Regression of Tumor Vessels, and Appearance of Basement Membrane Ghosts. *Am. J. Pathol.* 165, 35–52. doi:10.1016/s0002-9440(10)63273-7

Jemal, A., Murray, T., Samuels, A., Ghafoor, A., Ward, E., and Thun, M. J. (2003). Cancer Statistics, 2003. *CA: A Cancer J. Clinicians* 53, 5–26. doi:10.3322/canjclin.53.1.5

Korcsmáros, T., Szalay, M. S., Böde, C., Kovács, I. A., and Csermely, P. (2007). How to Design Multi-Target Drugs. *Expert Opin. Drug Discov.* 2, 799–808. doi:10.1517/17460441.2.6.799

Kumari, R., Kumar, R., Lynn, A., and Lynn, A. (2014). g_mmpbsa-A GROMACS Tool for High-Throughput MM-PBSA Calculations. *J. Chem. Inf. Model.* 54, 1951–1962. doi:10.1021/ci500020m

Li, C., Shan, Y., Sun, Y., Si, R., Liang, L., Pan, X., et al. (2017). Discovery of Novel Anti-angiogenesis Agents. Part 7: Multitarget Inhibitors of VEGFR-2, TIE-2 and EphB4. *Eur. J. Med. Chem.* 141, 506–518. doi:10.1016/j.ejmech.2017.10.030

Lindahl, E., Abraham, M., Hess, B., and van der Spoel, D. (2019). GROMACS 2019.3 Manual (Version 2019.3). Available at: Zenodo.org.

Liu, X., Newton, R. C., and Scherle, P. A. (2010). Developing C-MET Pathway Inhibitors for Cancer Therapy: Progress and Challenges. *Trends Mol. Med.* 16, 37–45. doi:10.1016/j.molmed.2009.11.005

Maeda, H., and Khatami, M. (2018). Analyses of Repeated Failures in Cancer Therapy for Solid Tumors: Poor Tumor-Selective Drug Delivery, Low Therapeutic Efficacy and Unsustainable Costs. *Clin. Transl. Med.* 7, 11–20. doi:10.1186/s40169-018-0185-6

Moustakas, A., and Heldin, C.-H. (2007). Signaling Networks Guiding Epithelial? mesenchymal Transitions during Embryogenesis and Cancer Progression. *Cancer Sci.* 98, 1512–1520. doi:10.1111/j.1349-7006.2007.00550.x

Organ, S. L., and Tsao, M.-S. (2011). An Overview of the C-MET Signaling Pathway. *Ther. Adv. Med. Oncol.* 3, S7–S19. doi:10.1177/1758834011422556

Parikh, P. K., and Ghate, M. D. (2018). Recent Advances in the Discovery of Small Molecule C-Met Kinase Inhibitors. *Eur. J. Med. Chem.* 143, 1103–1138. doi:10.1016/j.ejmech.2017.08.044

Pasquini, G., and Giaccone, G. (2018). C-MET Inhibitors for Advanced Non-small Cell Lung Cancer. *Expert Opin. Investig. Drugs* 27, 363–375. doi:10.1080/13543784.2018.1462336

Prins, P. A., Al-Hajeili, M. R., Kim, K. S., Hwang, J., Hartley, M. L., and He, A. R. (2016). MET Inhibition and Merestinib (LY-2801653) for Cancer Treatment. *Drugs Fut* 41, 607–615. doi:10.1358/dof.2016.041.10.2524678

Ribatti, D. (2005). The Crucial Role of Vascular Permeability Factor/vascular Endothelial Growth Factor in Angiogenesis: a Historical Review. *Br. J. Haematol.* 128, 303–309. doi:10.1111/j.1365-2141.2004.05291.x

Schirrmacher, V. (2019). From Chemotherapy to Biological Therapy: A Review of Novel Concepts to Reduce the Side Effects of Systemic Cancer Treatment (Review). *Int. J. Oncol.* 54, 407–419. doi:10.3892/ijo.2018.4661

Shibuya, M. (2001). Structure and Function of VEGF/VEGF-receptor System Involved in Angiogenesis. *Cell Struct. Funct.* 26, 25–35. doi:10.1247/csf.26.25

Tarver, T. (2012). *Cancer Facts & Figures 2012*. Atlanta, GA: American Cancer Society, 66. Available from. Taylor & Francis.

Wang, J., Wang, W., Kollman, P. A., and Case, D. A. (2006). Automatic Atom Type and Bond Type Perception in Molecular Mechanical Calculations. *J. Mol. Graphics Model.* 25, 247–260. doi:10.1016/j.jmgm.2005.12.005

Wang, J., Wolf, R. M., Caldwell, J. W., Kollman, P. A., and Case, D. A. (2004). Development and Testing of a General Amber Force Field. *J. Comput. Chem.* 25, 1157–1174. doi:10.1002/jcc.20035

Yakes, F. M., Chen, J., Tan, J., Yamaguchi, K., Shi, Y., Yu, P., et al. (2011). Cabozantinib (XL184), a Novel MET and VEGFR2 Inhibitor, Simultaneously Suppresses Metastasis, Angiogenesis, and Tumor Growth. *Mol. Cancer Ther.* 10, 2298–2308. doi:10.1158/1535-7163.mct-11-0264

Zhang, B., Liu, X., Xiong, H., Zhang, Q., Sun, X., Yang, Z., et al. (2020a). Discovery of [1,2,4] triazolo[4,3-A]pyrazine Derivatives Bearing a 4-Oxo-Pyridazinone Moiety as Potential C-Met Kinase Inhibitors. *New J. Chem.* 44, 9053–9063. doi:10.1039/d0nj00575d

Zhang, Q., Liu, X., Gan, W., Wu, J., Zhou, H., Yang, Z., et al. (2020b). Discovery of Triazolo-Pyridazine/-Pyrimidine Derivatives Bearing Aromatic (Heterocycle)-Coupled Azole Units as Class II C-Met Inhibitors. *ACS Omega* 5, 16482–16490. doi:10.1021/acsomega.0c00838

Zhang, Q., Zheng, P., and Zhu, W. (2020c). Research Progress of Small Molecule VEGFR/c-Met Inhibitors as Anticancer Agents (2016-Present). *Molecules* 25, 2666. doi:10.3390/molecules25112666

Zhao, B., Zhao, C., Hu, X., Xu, S., Lan, Z., Guo, Y., et al. (2020). Design, Synthesis and 3D-QSAR Analysis of Novel Thiopyranopyrimidine Derivatives as Potential Antitumor Agents Inhibiting A549 and Hela Cancer Cells. *Eur. J. Med. Chem.* 185, 111809. doi:10.1016/j.ejmech.2019.111809

Zillhardt, M., Park, S.-M., Romero, I. L., Sawada, K., Montag, A., Krausz, T., et al. (2011). Foretinib (GSK1363089), an Orally Available Multikinase Inhibitor of C-Met and VEGFR-2, Blocks Proliferation, Induces Anoikis, and Impairs Ovarian Cancer Metastasis. *Clin. Cancer Res.* 17, 4042–4051. doi:10.1158/1078-0432.ccr-10-3387

**Conflict of Interest:** The authors declare that the research was conducted in the absence of any commercial or financial relationships that could be construed as a potential conflict of interest.

**Publisher's Note:** All claims expressed in this article are solely those of the authors and do not necessarily represent those of their affiliated organizations, or those of the publisher, the editors, and the reviewers. Any product that may be evaluated in this article, or claim that may be made by its manufacturer, is not guaranteed nor endorsed by the publisher.

frontiers | Frontiers in Oncology

ORIGINAL RESEARCH
published: 21 April 2022
doi: 10.3389/fonc.2022.870636

# Meclofenamic Acid Restores Gefinitib Sensitivity by Downregulating Breast Cancer Resistance Protein and Multidrug Resistance Protein 7 *via* FTO/m6A-Demethylation/c-Myc in Non-Small Cell Lung Cancer

*Hui Chen*, Bin Jia, Qiang Zhang and Yu Zhang*

*Department of Lung Cancer, Tianjin Medical University Cancer Institute and Hospital, National Clinical Research Center for Cancer, Key Laboratory of Cancer Prevention and Therapy, Tianjin's Clinical Research Center for Cancer, Tianjin Lung Cancer Center, Tianjin, China*

OPEN ACCESS

**Edited by:**
*Qingbin Cui,*
*University of Toledo, United States*

**Reviewed by:**
*Peng Xu,*
*Shanghai Jiao Tong University, China*
*Amin Huang,*
*The First Affiliated Hospital of Sun Yat-sen University, China*

***Correspondence:**
*Hui Chen*
*13820968001@163.com*

**Specialty section:**
*This article was submitted to Pharmacology of Anti-Cancer Drugs, a section of the journal Frontiers in Oncology*

**Received:** *07 February 2022*
**Accepted:** *11 March 2022*
**Published:** *21 April 2022*

**Citation:**
*Chen H, Jia B, Zhang Q and Zhang Y (2022) Meclofenamic Acid Restores Gefinitib Sensitivity by Downregulating Breast Cancer Resistance Protein and Multidrug Resistance Protein 7 via FTO/m6A-Demethylation/c-Myc in Non-Small Cell Lung Cancer. Front. Oncol. 12:870636. doi: 10.3389/fonc.2022.870636*

**Background and Objective:** Gefitinib (GE) is a first-line epidermal growth factor receptor (EGFR) tyrosine kinase inhibitor (TKI) for patients with advanced non-small cell lung cancer (NSCLC) carrying EGFR activating mutations. However, drug resistance limits the clinical efficacy of gefitinib and ultimately leads to extremely poor clinical benefit. Meclofenamic acid (MA) is a non-steroidal anti-inflammatory drug (NSAID) that relieves moderate and severe pain. In the present study, we aim to determine the MA sensibilization of GE in NSCLC.

**Methods:** MTT assay was conducted to determine the synergistic effect of MA with GE in GE-sensitive and -resistant cell lines based on the Chou–Talalay method. The Annexin V-PI flow cytometry analysis was conducted to evaluate apoptosis. Western blot assay was used to detect alterations of EGFR downstream molecules. Tritium-labeled GE accumulation analysis was used to determine the efflux activity of GE. Dot blot assays were conducted to determine m6A levels after the MA and GE co-administration. Western blot evaluated the expression of FTO, c-Myc, MRP7, BCRP, and apoptotic proteins.

**Results:** MA showed a significant synergistic effect with GE in GE-resistant NSCLC cells; co-administration of MA with GE induced caspase-related apoptosis in resistant NSCLC cells. Moreover, EGFR downstream molecules, including Akt and MAPKs pathways, were significantly inhibited by the MA-GE combination. Short-term incubation of MA did not alter the efflux of GE; however, after incubation for 24 h, the accumulation of tritium-labeled GE significantly increased. A mechanism study showed that co-administration of MA and GE significantly downregulated BCRP and MRP7 expression in GE-resistant cells; increased N6-methylation was also observed after co-administration. The FTO/c-Myc was determined as target pathways on MA and GE co-administration mechanisms.

**Conclusion:** Our findings provide novel therapeutic approaches for GE-resistant NSCLC by combination use with MA through FTO-mediated N6-demethylation.

**Keywords: meclofenamic acid, gefitinib, M$^6$A, non-small cell lung cancer (NSCLC), drug resistance**

## INTRODUCTION

Though crucial progress for the management of non-small cell lung cancer (NSCLC) has been made in the last 20 years, the overall survival rates of NSCLC are still reasonably low. The 5-year overall survival of NSCLC is only 15% (1). One of the most significant factors for the poor prognosis of NSCLC is the treatment resistance for multiple small molecules, including chemotherapeutic and targeted drugs (2, 3).

As an oncogene, epidermal growth factor receptor (EGFR) is frequently mutated and abnormally activated among non-smoking NSCLC patients, driving the progression of NSCLC (4, 5). Hence, the EGFR tyrosine kinase inhibitors (EGFR-TKIs) have been investigated. The representative drug is gefitinib (GE), which is currently used as the first-line targeted therapy drug for NSCLC patients carrying EGFR mutations (6). The initial high efficacy of GE could be observed in specific NSCLC patients. Regrettably, nearly three-quarters of GE-sensitive NSCLC patients ultimately evolve inevitable treatment resistance in a year, resulting in high mortality rates (7). Therefore, overcoming the resistance of GE in NSCLC is becoming a crucial issue and a significant project in NSCLC management.

A few studies have identified the potential mechanisms for GE primary or acquired resistance in NSCLC, including KRAS mutations as well as mutations on EGFR kinase activity sites, ultimately inducing gain of function of such an oncogene, in which the transformation of T790M and C797S in EGFR are the top two forms (8). Moreover, the downstream and bypass signaling aberrant activation, including BRAF fusion and PIK3CA mutation, and cell phenotype transformation, including epithelial–mesenchymal transition (EMT), could also contribute significantly to the GE resistance in NSCLC (9, 10). More recently, the ATP-binding cassette (ABC) transporters family have been discovered to mediate GE treatment sensitivity, in which the breast cancer resistance protein (BCRP) and multidrug resistance protein-7 (MRP-7) play a significant role in GE resistance (11–13). The mechanisms of action on BCRP- and MRP-7-induced GE resistance involve the intrinsic characteristic of the transporter excretion, which relies on the energy of ATP hydrolysis (14, 15). Hence, the discovery of molecules that could inhibit the function or decrease the expression of BCRP and MRP-7 is a potential approach to overcome GE resistance in NSCLC (13, 16).

Meclofenamic acid (MA) is a non-steroidal anti-inflammatory drug (NSAID) that has been reported to promote platinum-mediated kidney injury (17). In our tentative exploration, we found that MA and GE in combination showed synergistic effects on NSCLC cells. Hence, in the present study, we aimed to study the novel effect of MA on GE resistance induced by BCRP and MRP-7. Our findings may provide unexplored therapeutic potentials for the solution of GE drug resistance in NSCLC cells.

## MATERIALS AND METHODS

### Cell Lines and Cell Culture

The GE-sensitive PC9 cell line and H292 cell line were purchased from the Cellular Institute (Cell Bank) of the Chinese Academy of Science (Shanghai, China). The GE-resistant cells PC9-GR and H292-GR were established by exposing them to increasing concentrations of GE. When the cells could not sustain growth similarly to the parental cell lines under GE treatment, the GE was discarded before the cells restored the growth rate. After over 12 months of GE exposure, the PC9-GR and H292-GR cell lines were successfully generated and maintained in 2 μM of GE. MTT assays were conducted to confirm the resistance characteristic of PC9-GR and H292-GR cells. All the above cell lines were cultured in RPMI 1640 medium containing 10% fetal bovine serum (FBS) incubated in a humid atmosphere containing 5% $CO_2$. The resistant sublines were cultured in a GE-free complete medium for at least 2 weeks to eliminate the interference of GE before all the experiments.

### Cell Proliferation Evaluation

Cell proliferation detections were conducted by MTT assays. The PC9, PC9-GR, H292, and H292-GR cells ($5\times10^3$) were seeded into 96-well plates overnight. Then, different concentrations of GE and MA were treated alone or in combination for 48 h. After incubation, MTT (final concentration: 5 mg/ml) was added to the 96-well plates and incubated at 37°C in the dark for 4 h. The supernatants were discarded, and the formazan was dissolved by DMSO and measured by an iMark microplate reader (Bio-Rad, Hercules, CA, United States). The viabilities were calculated by a percentage relative to the DMSO-treated control group. A GraphPad 8.01 software calculated the median inhibitory concentration ($IC_{50}$) values. The synergistic effects of GE and MA in different NSCLC cells were evaluated by the Chou–Talalay method described previously (18).

### Apoptosis Analysis

Annexin V-FITC and PI synchronous staining were conducted to evaluate apoptotic cells after GE and MA co-administration in GE-resistant NSCLC cell lines. In brief, cells at a density of $5\times10^5$ were seeded into 6-well plates; after incubation overnight, different concentrations of GE and MA were co-administrated for 48 h at 37°C. Subsequently, the cells were collected and stained with Annexin V-FITC and PI (5% respectively) for 30 min at RT in the dark. Then, the cells were centrifuged and resuspended in 250 μl of detection buffer and analyzed by MACS

Verse flow cytometer (BD Biosciences, San Jose, CA, United States). The qualification of apoptotic cells was analyzed by FlowJo VX software (Tristar, CA, United States).

## GE Accumulation Study

The accumulation of GE in resistant NSCLC cells was evaluated by tritium-labeled GE [GE-T (G), 10 Ci/mmol], purchased from Energy Chemical (Shanghai, China). The cells were plated into 6-well plates overnight and co-administrated with GE-T (G) and MA for 2 h, 24 h, and 48 h. Then, the cells were collected and the liquid scintillation was detected by a Quantulus™ GCT spectrometer (Perkin-Elmer, Waltham, MA, United States). The accumulation rates of GE were calculated *via* a custom standard curve.

## Western Blot

The expression level of EGFR-related downstream pathway molecules, the BCRP and MRP-7 expression level, and FTO and its downstream molecules were evaluated by Western blot assay. Specifically, cells were plated into a 6-well plate overnight and co-administrated with GE and MA. The Triton-X 100 lysis buffer was used to extract the total protein. The concentrations of proteins were qualified by BCA protein Assay Kit (Pierce™, Thermo Fisher Scientific, Waltham, MA, United States). Equal amounts of proteins (20–60 μg) were subjected to 8% to 12% sodium dodecyl sulfate-polyacrylamide gel electrophoresis (SDS-PAGE) before being transferred onto polyvinylidene fluoride (PVDF) membranes (Millipore, Billerica, MA, United States). Non-fat milk (5%) was used as a blocking agent to block the non-specific binding sites of PVDF membranes. The primary antibodies of total EGFR, p-EGFR, p-Akt, p-ERK1/2, BCRP, MRP-7, FTO, and c-Myc were incubated as recommended concentrations with the membrane at 4°C for overnight. Then, the membranes were washed with TBST buffer and incubated with HRP-conjugated secondary antibodies at RT for 1 h. After washing with TBST buffer, the ECL was added to the membrane and an Invitrogen iBright (Thermo Fisher Scientific, Waltham, MA, United States) was used to visualized the protein bands. The relative intensity was calculated by catching the gray level using ImageJ software.

## Quantitative Real-Time PCR

The mRNA expression levels of BCRP, MRP7, FTO, and MYC were determined by qPCR. In brief, the total RNA was extracted from the cells in the presence or absence of MA using TRIzol reagent (Invitrogen, Carlsbad, CA, United States) according to the manufacturer's instructions. The concentration of total RNA was measured by ultraviolet spectrophotometry. According to the manufacturer's instructions, complementary DNAs (cDNAs) were transcribed using RevertAid RT (Thermo Fisher Scientific, Waltham, MA, United States). PCR was performed on Real-Time PCR Detection System (Bio-Rad, Hercules, CA, USA) with SYBR™ Green PCR from Thermo Fisher Scientific (Waltham, MA, United States). The $2^{-\Delta\Delta Ct}$ methods calculated the copy number, and samples were run in triplicate and normalized to GAPDH. Then, the expression levels of mRNAs were reported as fold changes versus control. The primers were as follows: For BCRP, the forward primer (5'-3') was GCTACACCA CCTCCTTCTGT, and the reverse primer (5'-3') was GGAA GAAGAGAACCCCAGCT. For MRP7, the forward primer (5'-3') was AGAGTACACCTGTGACCTGC, and the reverse primer (5'-3') was GAGCACCAACAACAGGGAAG. For GAPDH, the forward primer (5'-3') was GCACCGTCAAGGCTGAGAAC, and the reverse primer (5'-3') was TGGTGAAGACGCCAGTGGA.

## Tritium-Labeled GE Accumulation Analysis

The parental and drug-resistant cell lines were seeded into 6-well plates overnight. The cells were incubated with tritium-labeled GE (GE-T) in the presence or absence of MA for 2 h, 24 h, 48 h, or 72 h, respectively, at 37°C containing 5% $CO_2$. Then, the cells were lysed by Triton X-100 lysis buffer (Beyotime, Shanghai, China). The radioactivity of the total lysis product was measured by a Tri-Card 4910 liquid scintillation analyzer (PerkinElmer, Waltham, MA, United States).

## Cell Membrane Protein Extraction

A membrane and cytoplasm protein isolation kit isolated the cell membrane protein from Beyotime (Shanghai, China). In brief, $5\times10^7$ cells were seeded into a 6-$cm^2$ dish, then were incubated in the presence or absence of GE and MA for 24 h. The cells were collected after treating with EDTA buffer, centrifuged, and homogenized. The nucleus was discarded by centrifuging at 700*g* for 10 min at 4°C, and the supernatants were collected. The cell membrane was collected by centrifuging at 14,000*g* for 30 min at 4°C. Then, the manufactured lysis buffer was used to extract membrane proteins. The composed membrane proteins were subjected to SDS-PAGE subsequently as aforementioned.

## Dot Blot Assays for $m^6A$ Level Detection

The dot blot assays for detecting $m^6A$ levels were conducted as previously described (19). In brief, according to the manufacturer's instructions, the total RNAs were isolated from the cells in the presence or absence of GE and MA using TRIzol reagent (Invitrogen, Carlsbad, CA, United States). PolyATtract® mRNA Isolation Systems (Promega, Madison, WI, United States) was then used to extract mRNA. The ultraviolet spectrophotometry method was used to determine the concentration of mRNA. Subsequently, the mRNAs were denatured for 3 min at 95°C, followed by cooling in ice directly. The mRNAs were UV cross-linked after being spotted on an Amersham Biosciences Hybond-N+ membrane optimized for nucleic acid transfer (GE Healthcare, Little Chalfont, United Kingdom). The membranes were shed with TBST buffer, followed by blocking with 5% non-fat milk, and hybridized with anti-m6A antibody (Abcam, Cambridge, MA, United States) overnight at 4°C. Then, the membranes were washed with TBST buffer and incubated with HRP-conjugated secondary antibodies at RT for 1 h. After washing with TBST buffer, the ECL was incubated and an Invitrogen iBright (Thermo Fisher Scientific, Waltham, MA, United States). The relative intensity was calculated by catching the gray level using ImageJ software.

## Me-RIP

The methylated RNA immunoprecipitation (Me-RIP) was conducted to detect the $m^6A$ modification of MYC as

previously described (20). In brief, total RNAs were isolated, then the mRNA was further isolated and purified using the TIANSeq mRNA Capture Kit (TIANGEN Biotech, Beijing, China). The anti-$M^6A$ or anti-IgG (1:100, Abcam, Cambridge, UK) were added and incubated with protein A/G agarose beads (Santa Cruz Biotechnology, Santa Cruz, CA, United States) in IP buffer overnight at 4°C. The eluent buffer was conducted to elute RNA. The phenol-chloroform was used to purify the RNAs. The qPCR was performed to determine the mRNA level of $m^6A$ MYC.

## Statistical Analysis

Data are expressed as mean ± SD in at least three independent experiments. The significance was determined using one-way ANOVA. GraphPad 8.00 software was used to determine the statistical analysis. $p < 0.05$ was considered statistically significant.

# RESULTS

## The Synergistic Anti-Viability Effects of MA and GE on GE-Resistant Sublines

The potential synergistic anti-proliferation effects of MA and GE were determined by MTT assays and fitted using Chou–Talalay methods as previously described (18). We first detected the antiproliferation characters of MA and GE on parental and resistant NSCLC cells. As illustrated in **Figures 1A–D**, the $IC_{50}$ values of GE on PC9 and PC9/GR cells were 0.32 and 3.45 μM, respectively. In H292 and H292/GR cells, the $IC_{50}$ of GE was 0.51 and 5.03 μM, indicating the confirmed resistance profile of PC9/GR and H292/GR cells. The $IC_{50}$ of MA, in all cell lines, was 4–8 μM.

Next, the drug combination of GE and MA was conducted, and the combination index (CI) was calculated. As shown in **Figures 1E–H**, the different $IC_{50}$ value fractions were undertaken in the combined administration of GE and MA. The CI value calculation results indicated that GE and MA showed potent synergistic effects in GE-resistant cells (PC9/GR and H292/GR). In contrast, no significant synergistic effects of GE and MA were observed in parental cells (**Figures 1I–L**). Based on the results of the drug combination, we chose related concentrations for the following experiments: for PC9/GR cells, 2.5 μM GE and 4 μM MA were adopted; for H292/GR cells, 4 μM GE and 6 μM MA were conducted.

## The Combination of GE and MA Significantly Induces Resistant NSCLC Cell Apoptosis

Based on the combination of GE and MA results, different concentrations of GE and MA were co-administrated in PC9/GR and H292/GR cells to evaluate the apoptotic cell population by flow cytometry. As illustrated in **Figures 2A, B**, though single use of GE or MA in PC9/GR and H292/GR cells induced poor

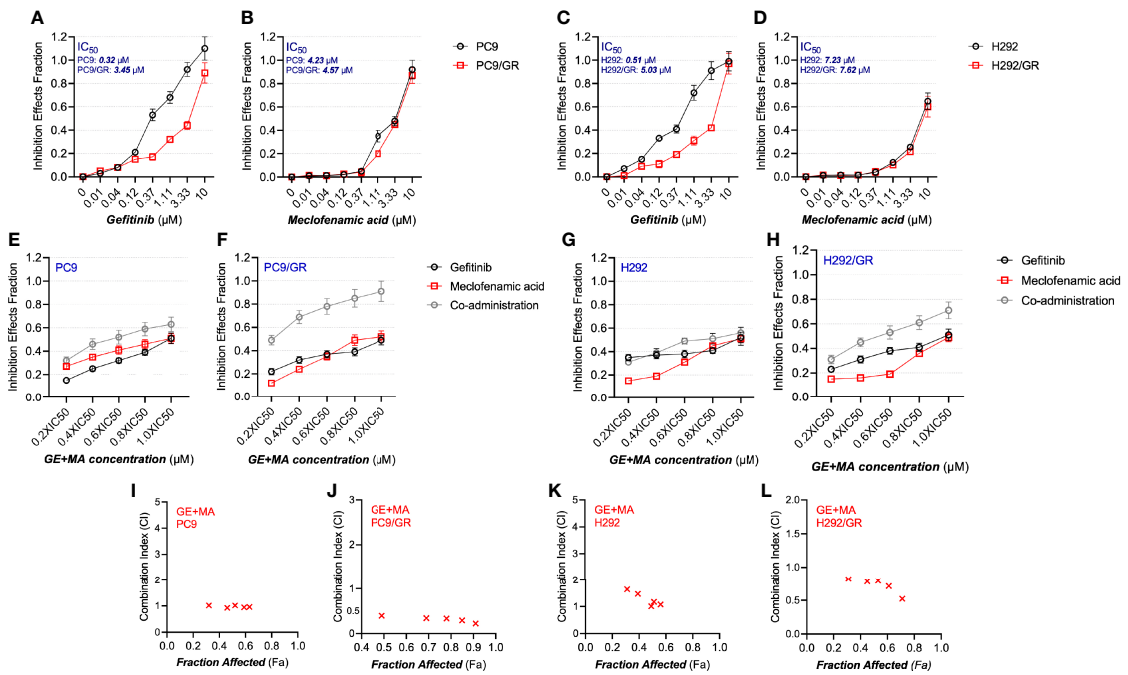


**FIGURE 1** | The antiproliferative effects of MA and/or GE on gefitinib-resistant NSCLC cells. **(A–D)** The parental PC9 and H292 as well as gefitinib-resistant PC9/GR and H292/GR cells were treated with various concentrations of GE or MA; the antiproliferative effects were determined by MTT assay following 48 h of incubation. Cells were treated with GE and MA as a single agent or in combination for 48 h, and MTT assays were used to analyze the cell viability. The Chou–Talalay method was conducted to calculate the combination index (CI); a CalcuSyn software were used to analyze the data. **(E–H)** illustrate the combination ratio/viability, while **(I–L)** show the fraction affected/combination index. Data are presented for at least three independent repetitions and were illustrated as mean ± SD.

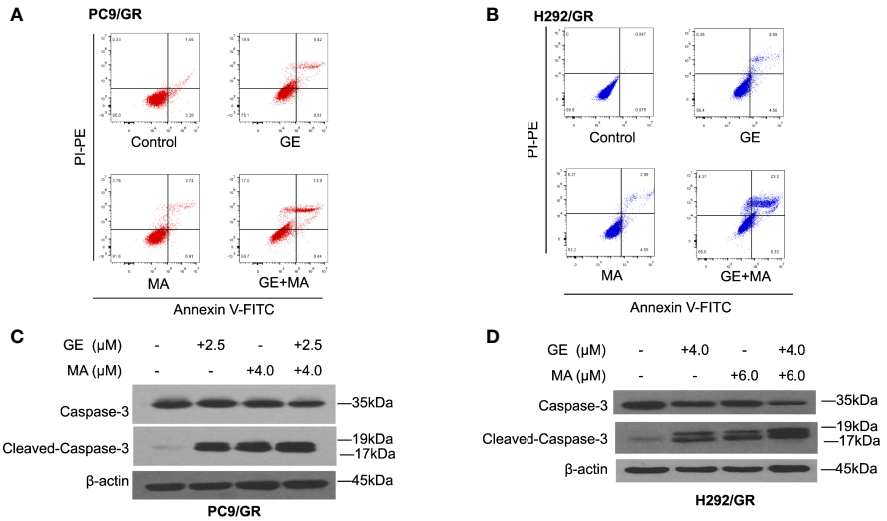


**FIGURE 2** | MA and GE synergistically induced caspase-3-associated apoptosis in gefitinib-resistant NSCLC cells. Apoptotic cells in PC9/GR **(A)** and H292/GR **(B)** exposed to the single drugs or combination are presented in dot blot. Western blot results show dynamic caspase-3 face after PC9/GR **(C)** or H292/GR **(D)** exposed to single or combination drugs.

apoptosis, the co-administration significantly induced cell apoptosis potently, indicating the potential combined effects of GE and MA. Furthermore, Western blot results showed that the apoptotic effects of GE combination of MA were caspase-3-dependent (**Figures 2C, D**).

## GE-MA Co-Administration Significantly Inhibited EGFR Downstream Pathways

We next evaluated the potential mechanisms of action on the synergistic effects of GE and MA. As shown in **Figure 3A**, in PC9/GR cells, the EGFR-related downstream key molecules were detected by Western blot. GE or MA single use did not significantly induce inactivation of EGFR downstream molecules. However, the combination-treated GE and MA significantly inhibited the phosphorylation of EGFR, Akt, and ERK1/2, which indicated that the synergistic effects of GE and MA might be related to the inactivation of the EGFR molecule pathway. In addition, the co-administration of GE and MA in H292/GR cells also induced a potent decrease of phosphorylated modification of EGFR signaling pathways molecules, which further indicated that the EGFR signaling is related to the synergistic effects of GE and MA on drug-resistant NSCLC cells (**Figure 3**).

## MA Significantly Induced GE Accumulation in GE-Resistant NSCLC Cells

Considering the impaired cytotoxicity of GE in resistant NSCLC cells, the synergistic effects may be related to the increased accumulation of GE. Hence, the tritium-labeled GE-based accumulation assays were conducted. As shown in **Figures 4A, B**, short-term incubation of MA (2 h) did not significantly alter GE accumulation in either PC9/GR or H292/GR cells. Interestingly, more prolonged incubation of MA (24 h, 48 h, and 72 h) potently increased the intracellular tritium-labeled GE in PC9/GR and H292/GR cells, but not in their corresponding parental cells.

## MA and the Combination of GE Significantly Decrease the Expression Level of Membrane Drug Efflux Proteins

We next evaluated whether MA or combination with GE could alter the membrane drug pumps in GE-resistant NSCLC cells. As illustrated in **Figure 5**, the cell membrane of both PC9/GR and H292/GR cells was isolated, and SDS-PAGE detected the expression of MRP7 and BCRP. As illustrated in **Figure 5A**, the expression of MRP7 and BCRP in PC9/GR significantly decreased in MA and MA/GE co-administrated group compared with the control or GE treatment group. In addition, similar results were found in H292/GR cells, where both the BCRP and MRP7 were downregulated by MA or MA/GE co-administrated.

## Co-Administration of MA and GE Downregulated BCRP and MRP7 Expression by Increasing the M6A Modification of MYC

The total M6A modification in PC9/GR and H292/GR cells was detected by dot blot assays of M6A. As shown in **Figures 6A, B**, the M6A modification of mRNA in the MA- or MA/GE-treated group significantly increased, indicating that MA or MA/GE co-administration may affect the activity of M6A-related proteins. Moreover, demethylase FTO was significantly downregulated in both PC9/GR and H292/GR cells in MA- and MA/GE-treated groups (**Figures 6C, D**). Furthermore, the transcription factor MYC was significantly decreased in the MA or MA/GE co-treatment group. The Me-RIP results indicated that both MA alone and in combination with the GE group significantly increased the M6A modification of MYC (**Figures 6E, F**).

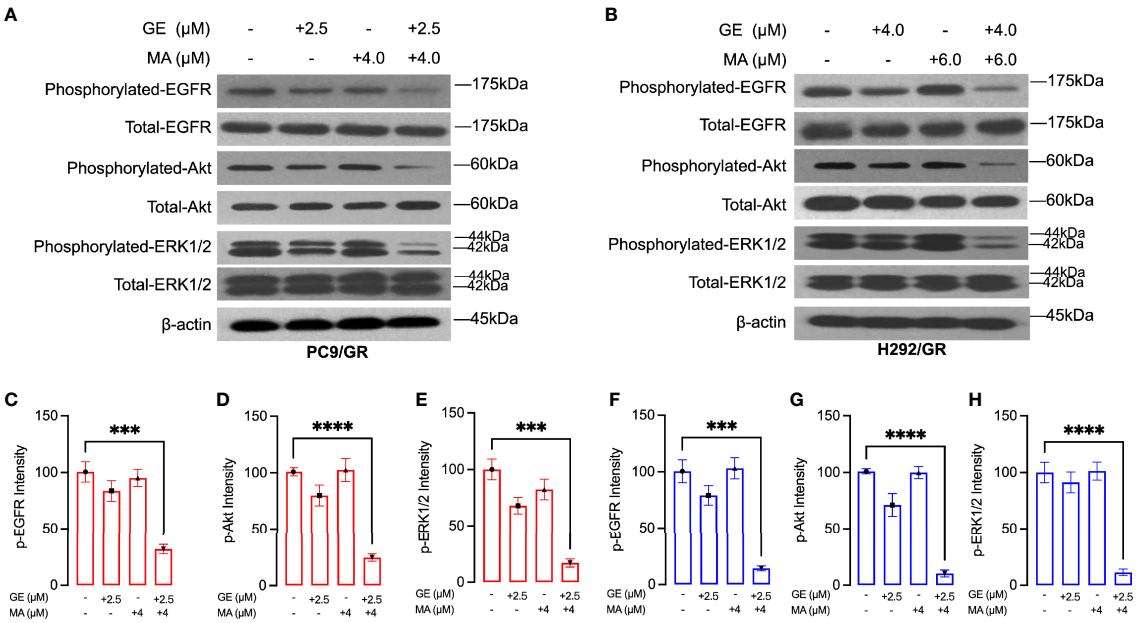


**FIGURE 3** | MA and GE synergistically inhibited the activity of the EGFR-related signaling pathway. Western blot results showed the expression of p-EGFR, p-Akt, and p-ERK1/2 in PC9/GR **(A)** and H292/GR **(B)** cells exposed to MA and GE for single or combination use. **(C–H)** showed the statistical analysis of the Western blot results **(A, B)**. Data are presented for at least three independent repetitions and were illustrated as mean ± SD. ***$p < 0.001$, ****$p < 0.0001$.

## DISCUSSION

As a first-line drug for patients with NSCLC, GE has shown great application value in the clinics, but its acquired resistance is a massive obstacle for the further benefits of NSCLC patients (21). The elucidated mechanisms of action on GE-resistant cells are complicated, including EGFR T790M mutation and MET amplification (22). In addition, the increased efflux of GE by BCRP and MRP7 is also responsible for the GE resistance in NSCLC (11, 23). Hence, BCRP and MRP7 are potential targets for reversing GE resistance in NSCLC.

The present study found that MA, an NSAID, showed significant synergistic effects with GE in GE-resistant NSCLC cell lines. Using the Chou–Talalay combination equation, we confirmed that MA and GE showed significantly synergistic effects in GE-selected resistant cells but not in normal NSCLC cells. The caspase-related apoptosis was found after being co-administrated with MA and GE in GE-resistant cell lines. Moreover, the downstream molecules of EGFR pathways were significantly inactivated after combination use, indicating that the administration of MA might enhance the effects of GE. Hence, we further detected whether the accumulation of GE in GE-resistant cell lines increased after MA treatment. The results indicated that MA could significantly enhance the intracellular GE concentration, suggesting that MA may act as a sensitizer of GE in GE-resistant NSCLC cells.

As mentioned above, overexpression of BCRP and MRP7 may be responsible for the resistance of gefitinib in NSCLC cells. Hence, the expression levels of BCRP and MRP7 were detected by Western blot in both cell membrane and total cell lysate. MA

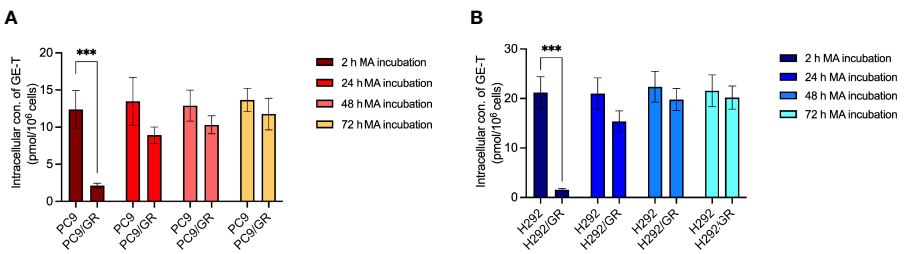


**FIGURE 4** | MA significantly enhanced the accumulation of GE in gefitinib-resistant cells. **(A)** The collection of GE in parental PC9 and PC9/GR cells exposed to MA. **(B)** The accumulation of GE in parental H292 and H292/GR cells exposed to MA. Data are presented for at least three independent repetitions and were illustrated as mean ± SD. ***$p < 0.001$.

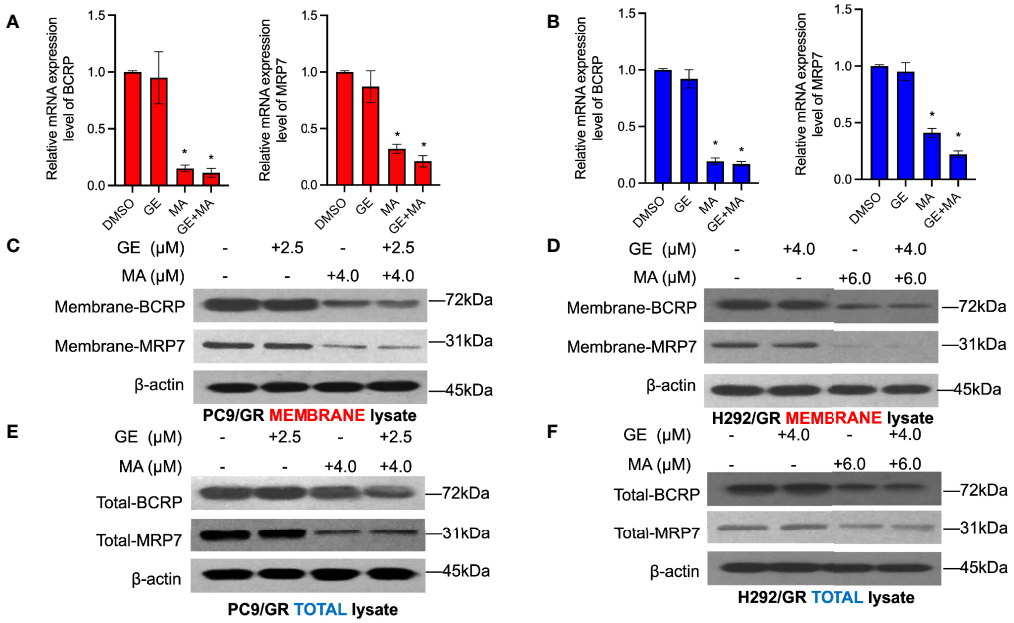


**FIGURE 5** | MA and GE synergistically inhibited the expression of BCRP and MRP7. BCRP and MRP7 in PC9/GR **(A)** and H292/GR **(B)** cells. **(C, D)** The membrane protein expression of BCRP and MRP7 in PC9/GR and H292/GR cells after MA and GE for single or in combination exposed. **(E, F)** The total cell lysate protein expression of BCRP and MRP7 in PC9/GR and H292/GR cells after MA and GE for single or in combination exposed. Data are presented for at least three independent repetitions and were illustrated as mean ± SD. *$p < 0.05$.

and MA/GE coadministration significantly decreased both membrane and whole cell lysate expression of BCRP and MRP7, which explained that MA could increase the accumulation of GE in GE-resistant NSCLC cell lines.

The downregulatory effects of BCRP and MRP7 may be related to the alteration of mRNA; we evaluated the mRNA expression level of both BCRP and MRP7. Our results indicated that MA and MA/GE coadministration significantly decreased

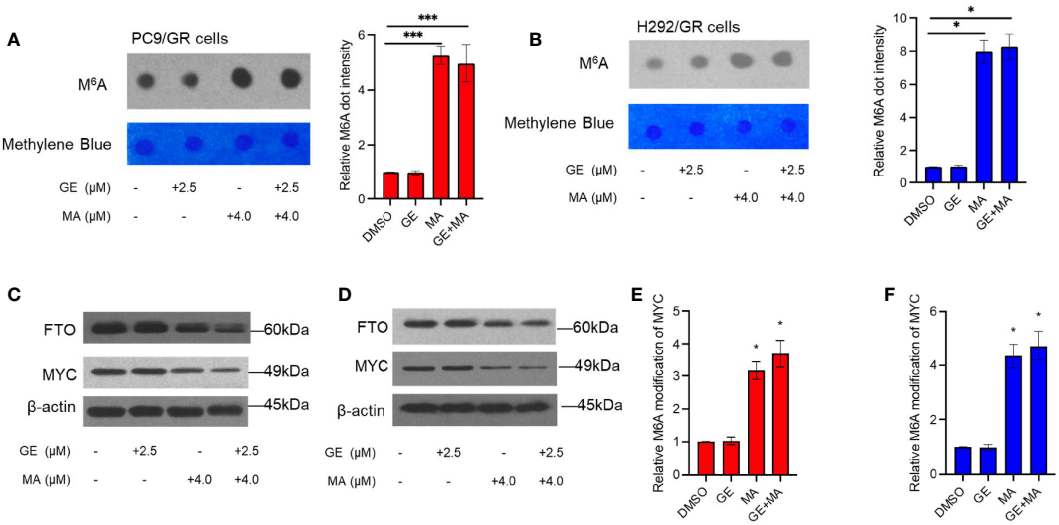


**FIGURE 6** | MA and GE in combination upregulated FTO-mediated MYC M6A modification. **(A, B)** Dot blot shows the M6A modification level in PC9/GR and H292/GR cells exposed to MA and GE for a single drug or combination. **(C, D)** Expression of FTO and MYC determined by Western blot assays in PC9/GR and H292/GR cells. **(E, F)** The m6A modification level of MYC cells was assessed by Me-RIP assay in PC9/GR and H292/GR cells exposed to MA and GE for a single drug or in combination. Data are presented for at least three independent repetitions and were illustrated as mean ± SD. *$p < 0.05$, ***$p < 0.001$.

the mRNA expression level of BCRP and MRP7. The M6A modification is a hot spot of mRNA modification, which will reduce mRNA stability (24). We hypothesized that the M6A modification might be involved in decreasing BCRP and MRP7 mRNA levels. The results for dot blot assays indicated that the M6A modification level was significantly upregulated. As the main M6A eraser, FTO has been widely accepted to have a significant role in cancers (25, 26). In addition, FTO was also documented to be correlated with the expression of ABC transporters (27). In our Western blot results, we observed that FTO expression significantly decreased after MA or GE/MA co-administration, indicating that the upregulation of global M6A modification may be related to the decreasing of FTO. Myc is a key transcription factor that regulates a series of gene expressions, including BCRP and MRP7 (28, 29). In addition, mRNA of MYC was also documented to be influenced by FTO (30). We used Me-RIP assay to detect the effects of MA or coadministration with GE on M6A modification on MYC mRNA. The results indicated that the M6A modification level was significantly increased after MA or MA/GE co-administration. These results suggest that MA acts as a reversal agent that can enhance resistant NSCLC cells sensitive to the EGFR inhibitor, GE, through FTO/M6A/MYC axis-mediated downregulation of BCRP and MRP7.

ABC transporters have been shown to have a significant role in GE resistance in NSCLC cells. In contrast to active site mutation of EGFR, overexpression of ABC transporters potently decreases the intracellular concentration of substrate drugs, ultimately inducing drug resistance (31). In NSCLC cells, BCRP and MRP7 are two central identified efflux pumps that confer the GE resistance, and GE was also proved to be a substrate of BCRP and MRP7 (13), which makes these two pumps potential targets for overcoming GE resistance in NSCLC. Our findings suggest novel approaches to overcome GE resistance in NSCLC by impeding the expression level of BCRP and MRP7 *via* the FTO/M6A/MYC axis. Nevertheless, further studies need to unfold because the downregulation of efflux pumps could also be influenced by posttranslational modification, including glycosylation and ubiquitination; whether such changes also participate in the synergistic effects of MA and GE remains to be determined.

## DATA AVAILABILITY STATEMENT

The original contributions presented in the study are included in the article/**Supplementary Material**. Further inquiries can be directed to the corresponding author.

## AUTHOR CONTRIBUTIONS

HC performed the main experiments and analyzed the data. BJ and QZ drafted the manuscript, which HC revised. HC and YZ designed the study and revised the final version of the manuscript. All authors contributed to the article and approved the submitted version.

## ACKNOWLEDGMENTS

We appreciate Wordvice for English editing work.

## SUPPLEMENTARY MATERIAL

The Supplementary Material for this article can be found online at: https://www.frontiersin.org/articles/10.3389/fonc.2022.870636/full#supplementary-material

## REFERENCES

1. Herbst RS, Morgensztern D, Boshoff C. The Biology and Management of Non-Small Cell Lung Cancer. *Nature* (2018) 553:446–54. doi: 10.1038/nature25183
2. Lim ZF, Ma PC. Emerging Insights of Tumor Heterogeneity and Drug Resistance Mechanisms in Lung Cancer Targeted Therapy. *J Hematol Oncol* (2019) 12:134. doi: 10.1186/s13045-019-0818-2
3. Liu WJ, Du Y, Wen R, Yang M, Xu J. Drug Resistance to Targeted Therapeutic Strategies in Non-Small Cell Lung Cancer. *Pharmacol Ther* (2020) 206:107438. doi: 10.1016/j.pharmthera.2019.107438
4. Maemondo M, Inoue A, Kobayashi K, Sugawara S, Oizumi S, Isobe H, et al. Gefitinib or Chemotherapy for Non-Small-Cell Lung Cancer With Mutated EGFR. *N Engl J Med* (2010) 362:2380–8. doi: 10.1056/NEJMoa0909530
5. Rosell R, Carcereny E, Gervais R, Vergnenegre A, Massuti B, Felip E, et al. Erlotinib Versus Standard Chemotherapy as First-Line Treatment for European Patients With Advanced EGFR Mutation-Positive Non-Small-Cell Lung Cancer (EURTAC): A Multicentre, Open-Label, Randomised Phase 3 Trial. *Lancet Oncol* (2012) 13:239–46. doi: 10.1016/S1470-2045(11)70393-X
6. Nagasaka M, Zhu VW, Lim SM, Greco M, Wu F, Ou SI. Beyond Osimertinib: The Development of Third-Generation EGFR Tyrosine Kinase Inhibitors For Advanced EGFR+ NSCLC. *J Thorac Oncol* (2021) 16:740–63. doi: 10.1016/j.jtho.2020.11.028
7. Liu S, Li Q, Li G, Zhang Q, Zhuo L, Han X, et al. The Mechanism of M(6)A Methyltransferase METTL3-Mediated Autophagy in Reversing Gefitinib Resistance in NSCLC Cells by β-Elemene. *Cell Death Dis* (2020) 11:969. doi: 10.1038/s41419-020-03148-8
8. Westover D, Zugazagoitia J, Cho BC, Lovly CM, Paz-Ares L. Mechanisms of Acquired Resistance to First- and Second-Generation EGFR Tyrosine Kinase Inhibitors. *Ann Oncol* (2018) 29:i10–9. doi: 10.1093/annonc/mdx703
9. Tulchinsky E, Demidov O, Kriajevska M, Barlev NA, Imyanitov E. EMT: A Mechanism for Escape From EGFR-Targeted Therapy in Lung Cancer. *Biochim Biophys Acta Rev Cancer* (2019) 1871:29–39. doi: 10.1016/j.bbcan.2018.10.003
10. Suda K, Murakami I, Yu H, Kim J, Tan AC, Mizuuchi H, et al. CD44 Facilitates Epithelial-To-Mesenchymal Transition Phenotypic Change at Acquisition of Resistance to EGFR Kinase Inhibitors in Lung Cancer. *Mol Cancer Ther* (2018) 17:2257–65. doi: 10.1158/1535-7163.MCT-17-1279
11. Zhao H, Huang Y, Shi J, Dai Y, Wu L, Zhou H. ABCC10 Plays a Significant Role in the Transport of Gefitinib and Contributes to Acquired Resistance to Gefitinib in NSCLC. *Front Pharmacol* (2018) 9:1312. doi: 10.3389/fphar.2018.01312
12. Huang L, Fu L. Mechanisms of Resistance to EGFR Tyrosine Kinase Inhibitors. *Acta Pharm Sin B* (2015) 5:390–401. doi: 10.1016/j.apsb.2015.07.001
13. Beretta GL, Cassinelli G, Pennati M, Zuco V, Gatti L. Overcoming ABC Transporter-Mediated Multidrug Resistance: The Dual Role of Tyrosine Kinase Inhibitors as Multitargeting Agents. *Eur J Med Chem* (2017) 142:271–89. doi: 10.1016/j.ejmech.2017.07.062
14. Yang Y, Ji N, Cai CY, Wang JQ, Lei ZN, Teng QX, et al. Modulating the Function of ABCB1: *In Vitro* and *In Vivo* Characterization of Sitravatinib, A

Tyrosine Kinase Inhibitor. *Cancer Commun (Lond)* (2020) 40:285–300. doi: 10.1002/cac2.12040
15. Cui Q, Cai CY, Gao HL, Ren L, Ji N, Gupta P, et al. Glesatinib, a C-MET/SMO Dual Inhibitor, Antagonizes P-Glycoprotein Mediated Multidrug Resistance in Cancer Cells. *Front Oncol* (2019) 9:313. doi: 10.3389/fonc.2019.00313
16. Sakamoto S, Sato K, Takita Y, Izumiya Y, Kumagai N, Sudo K, et al. ABCG2 C421A Polymorphisms Affect Exposure of the Epidermal Growth Factor Receptor Inhibitor Gefitinib. *Invest New Drugs* (2020) 38:1687–95. doi: 10.1007/s10637-020-00946-x
17. Zhou P, Wu M, Ye C, Xu Q, Wang L. Meclofenamic Acid Promotes Cisplatin-Induced Acute Kidney Injury by Inhibiting Fat Mass and Obesity-Associated Protein-Mediated M(6)A Abrogation in RNA. *J Biol Chem* (2019) 294:16908–17. doi: 10.1074/jbc.RA119.011009
18. Chou TC. Drug Combination Studies and Their Synergy Quantification Using the Chou-Talalay Method. *Cancer Res* (2010) 70:440–6. doi: 10.1158/0008-5472.CAN-09-1947
19. Jia G, Fu Y, Zhao X, Dai Q, Zheng G, Yang Y, et al. N6-Methyladenosine in Nuclear RNA Is a Major Substrate of the Obesity-Associated FTO. *Nat Chem Biol* (2011) 7:885–7. doi: 10.1038/nchembio.687
20. Yue C, Chen J, Li Z, Li L, Chen J, Guo Y. microRNA-96 Promotes Occurrence and Progression of Colorectal Cancer *via* Regulation of the Ampkα2-FTO-M6a/MYC Axis. *J Exp Clin Cancer Res* (2020) 39:240. doi: 10.1186/s13046-020-01731-7
21. Gandara DR, Li T, Lara PN, Kelly K, Riess JW, Redman MW, et al. Acquired Resistance to Targeted Therapies Against Oncogene-Driven Non–Small-Cell Lung Cancer: Approach to Subtyping Progressive Disease and Clinical Implications. *Clin Lung Cancer* (2014) 15:1–6. doi: 10.1016/j.cllc.2013.10.001
22. Morgillo F, Della Corte CM, Fasano M, Ciardiello F. Mechanisms of Resistance to EGFR-Targeted Drugs: Lung Cancer. *ESMO Open* (2016) 1: e000060. doi: 10.1136/esmoopen-2016-000060
23. Huang Y, Dai Y, Wen C, He S, Shi J, Zhao D, et al. Circsetd3 Contributes to Acquired Resistance to Gefitinib in Non-Small-Cell Lung Cancer by Targeting the miR-520h/ABCG2 Pathway. *Mol Ther Nucleic Acids* (2020) 21:885–99. doi: 10.1016/j.omtn.2020.07.027
24. Liu ZX, Li LM, Sun HL, Liu SM. Link Between M6a Modification and Cancers. *Front Bioeng Biotechnol* (2018) 6:89. doi: 10.3389/fbioe.2018.00089
25. Tao L, Mu X, Chen H, Jin D, Zhang R, Zhao Y, et al. FTO Modifies the M6a Level of MALAT and Promotes Bladder Cancer Progression. *Clin Transl Med* (2021) 11:e310. doi: 10.1002/ctm2.310
26. Shi H, Zhao J, Han L, Xu M, Wang K, Shi J, et al. Retrospective Study of Gene Signatures and Prognostic Value of M6a Regulatory Factor in Non-Small Cell Lung Cancer Using TCGA Database and the Verification of FTO. *Aging (Albany NY)* (2020) 12:17022–37. doi: 10.18632/aging.103622
27. Xiao P, Liu YK, Han W, Hu Y, Zhang BY, Liu WL. Exosomal Delivery of FTO Confers Gefitinib Resistance to Recipient Cells Through ABCC10 Regulation in an M6a-Dependent Manner. *Mol Cancer Res* (2021) 19:726–38. doi: 10.1158/1541-7786.MCR-20-0541
28. Ouyang L, Yan B, Liu Y, Mao C, Wang M, Liu N, et al. The Deubiquitylase UCHL3 Maintains Cancer Stem-Like Properties by Stabilizing the Aryl Hydrocarbon Receptor. *Signal Transduct Target Ther* (2020) 5:78. doi: 10.1038/s41392-020-0181-3
29. Porro A, Haber M, Diolaiti D, Iraci N, Henderson M, Gherardi S, et al. Direct and Coordinate Regulation of ATP-Binding Cassette Transporter Genes by Myc Factors Generates Specific Transcription Signatures That Significantly Affect the Chemoresistance Phenotype of Cancer Cells. *J Biol Chem* (2010) 285:19532–43. doi: 10.1074/jbc.M109.078584
30. Su R, Dong L, Li C, Nachtergaele S, Wunderlich M, Qing Y, et al. R-2hg Exhibits Anti-Tumor Activity by Targeting FTO/m(6)A/MYC/CEBPA Signaling. *Cell* (2018) 172:90–105.e23. doi: 10.1016/j.cell.2017.11.031
31. Locher KP. Mechanistic Diversity in ATP-Binding Cassette (ABC) Transporters. *Nat Struct Mol Biol* (2016) 23:487–93. doi: 10.1038/nsmb.3216

**Conflict of Interest:** The authors declare that the research was conducted in the absence of any commercial or financial relationships that could be construed as a potential conflict of interest.

**Publisher's Note:** All claims expressed in this article are solely those of the authors and do not necessarily represent those of their affiliated organizations, or those of the publisher, the editors and the reviewers. Any product that may be evaluated in this article, or claim that may be made by its manufacturer, is not guaranteed or endorsed by the publisher.

frontiers | Frontiers in Pharmacology

ORIGINAL RESEARCH
published: 25 April 2022
doi: 10.3389/fphar.2022.871259

# Novel MDM2 Inhibitor XR-2 Exerts Potent Anti-Tumor Efficacy and Overcomes Enzalutamide Resistance in Prostate Cancer

*Meng Wu[1,2†], Jingyi Cui[3,4†], Huimin Hou[1†], Ying Li[3,4], Shengjie Liu[1], Li Wan[5,2], Lili Zhang[5], Wei Huang[5], Gaoyuan Sun[5], Jingchao Liu[1], Pengfei Jin[6]*, Shunmin He[2]* and Ming Liu[1]**

[1]Department of Urology, Beijing Hospital, National Center of Gerontology, Institute of Geriatric Medicine, Chinese Academy of Medical Sciences, Beijing, China, [2]Key Laboratory of RNA Biology, Center for Big Data Research in Health, Institute of Biophysics, Chinese Academy of Sciences, Beijing, China, [3]Graduate School of Peking Union Medical College, Beijing, China, [4]The Key Laboratory of Geriatrics, Beijing Institute of Geriatrics, Institute of Geriatric Medicine, Chinese Academy of Medical Sciences, Beijing Hospital/National Center of Gerontology of National Health Commission, Beijing, China, [5]Clinical Biobank, Beijing Hospital, National Center of Gerontology, National Health Commission, Institute of Geriatric Medicine, Chinese Academy of Medical Sciences, Beijing, China, [6]Department of Pharmacy, Beijing Hospital, National Center of Gerontology, Institute of Geriatric Medicine, Chinese Academy of Medical Science, Beijing Key Laboratory of Assessment of Clinical Drugs Risk and Individual Application (Beijing Hospital), Beijing, China

**Background:** The inactivation of tumor-suppressor p53 plays an important role in second generation anti-androgens (SGAs) drug resistance and neuroendocrine differentiation in castration-resistant prostate cancer (CRPC). The reactivation of p53 by blocking the MDM2–p53 interaction represents an attractive therapeutic remedy in cancers with wild-type or functional p53. Whether MDM2-p53 inhibitor could overcome SGAs drug resistance in CRPC is still needed further research. Here, we investigated the anti-tumor efficacy and mechanisms of a novel MDM2-p53 inhibitor XR-2 in CRPC.

**Methods:** To investigate the functions and mechanisms of XR-2 in prostate cancer, *in vitro* and *in vivo* biofunctional assays were performed. Western blot and qRT-PCR assay were performed to detect the protein and mRNA expression levels of indicated genes. CCK8, colony formation, flow cytometry and senescence assays were performed for cell function identifications. RNA-sequencing and bioinformatics analysis were mainly used to identify the influence of XR-2 on prostate cancer cells transcriptome. Subcutaneous 22Rv1 derived xenografts mice model was used to investigate the *in vivo* anti-tumor activity of XR-2. In addition, the broad-spectrum anti-tumor activities *in vivo* of XR-2 were evaluated by different xenografts mice models.

**Results:** XR-2 could directly bind to MDM2, potently reactivate the p53 pathway and thus induce cell cycle arrest and apoptosis in wild-type p53 CRPC cell lines. XR-2 also suppresses the AR pathway as p53 regulates AR transcription inhibition and MDM2 participates in AR degradation. As a result, XR-2 efficiently inhibited CRPC cell viability,

**Abbreviations:** MDM2, modification murine double minute-2; qRT-PCR, quantitative reverse-transcriptase polymerase chain reaction; GAPDH, glyceraldehyde 3-phosphate dehydrogenase. DHT, dihydrotestosterone; CRPC, castration-resistant prostate cancer Contributions.

OPEN ACCESS

**Edited by:**
Qingbin Cui,
University of Toledo, United States

**Reviewed by:**
Eswar Shankar,
The Ohio State University, United States
Qingmei Ye,
Hainan General Hospital, China

***Correspondence:**
Ming Liu
liumingbjh@126.com
Shunmin He
heshunmin@ibp.ac.cn
Pengfei Jin
jinpengfei3674@bjhmoh.cn

†These authors have contributed equally to this work

**Specialty section:**
This article was submitted to Pharmacology of Anti-Cancer Drugs, a section of the journal Frontiers in Pharmacology

**Received:** 08 February 2022
**Accepted:** 01 April 2022
**Published:** 25 April 2022

**Citation:**
Wu M, Cui J, Hou H, Li Y, Liu S, Wan L, Zhang L, Huang W, Sun G, Liu J, Jin P, He S and Liu M (2022) Novel MDM2 Inhibitor XR-2 Exerts Potent Anti-Tumor Efficacy and Overcomes Enzalutamide Resistance in Prostate Cancer. Front. Pharmacol. 13:871259. doi: 10.3389/fphar.2022.871259

showed a synergistic effect with enzalutamide and overcame enzalutamide resistance both *in vitro* and *in vivo*. Moreover, results illustrated that XR-2 possesses broad-spectrum anti-tumor activities *in vivo* with favourable safety.

**Conclusion:** MDM2-p53 inhibitor (XR-2) possesses potently prostate cancer progresses inhibition activity both *in vitro* and *in vivo*. XR-2 shows a synergistic effect with enzalutamide and overcomes enzalutamide resistance.

**Keywords: MDM2 inhibitor, enzalutamide resistance, combination therapy, castration-resistant prostate cancer, p53**

## INTRODUCTION

Globally, prostate cancer (PCa) is one of the most common malignancies and the fifth leading cause of cancer-related death in men. (Sung et al., 2021). Despite initial response to surgical, radiation and androgen ablation therapies, advanced localised PCa finally progresses to incurable metastatic castration-resistant PCa (CRPC). (Harris et al., 2009; Niu et al., 2010). Although second-generation anti-androgens (SGAs), which included abiraterone, enzalutamide, apalutamide and darolutamide, increased the overall survival time and decreased the prostate-specific antigen (PSA) level in patients with CRPC, (de Bono et al., 2011; Penson et al., 2016; Chi et al., 2019; Fizazi et al., 2020), 20–40% of these patients did not respond to abiraterone and enzalutamide. The remaining responders also inevitably developed acquired resistance, resulting in a limited survival improvement. (Chi et al., 2015; Wyatt et al., 2016). Many studies have confirmed that genomic aberrations, such as alterations of the androgen receptor (AR), DNA repair, p53 and Rb1, PI3K/AKT/mTOR pathway and Wnt/β-catenin pathway confer resistance to SGAs. (Watson et al., 2015; Ciccarese et al., 2017; Ku et al., 2017; Antonarakis et al., 2018; Isaacsson Velho et al., 2020). Based on molecular stratification, poly ADP-ribose polymerase (PARP) inhibitor prolongs survival time of advanced CRPC with certain DNA repair defects, leading to regulatory approvals in 2020. (Hussain et al., 2020). However, the BRCA1/2 mutation most sensitive to PARP inhibitor accounts for only a minority of CRPC cases with ATM mutations, comprising <10% of CRPC cases. (Neeb et al., 2021). Therefore, developing novel agents for men with fatal SGA-resistant CRPC is imperative.

The p53 is one of the most important tumor suppressors encoded by the *TP53* gene; p53 regulates some fundamental cellular processes under cellular stress, DNA damage or oncogene activation. (Wade et al., 2013; Levine, 2020). The transactivation of target genes by p53 induces cell cycle arrest, DNA repair and even apoptosis, and these downstream responses lead to the repair or culling of damaged and potentially tumorigenic cells. E3 ligase murine double minute-2 (MDM2) is a negative regulator of wild-type p53, which can promote p53 degradation through the proteasome pathway. The inactivation of p53 caused by p53 mutation or MDM2 overexpression in tumor cells is considered the main cause of tumor formation and progression. (Wade et al., 2013). Thus, the reactivation of p53 by blocking the MDM2–p53 interaction represents an attractive therapeutic remedy in cancers with wild-type or functional p53.

Inspiringly, a series of active small molecules have been developed by inhibiting MDM2–p53 interaction, with some currently being investigated in clinical trials regarding haematologic and solid malignancies. (Skalniak et al., 2019; Duffy et al., 2022). However, none of these inhibitors reached regulatory approval because gastrointestinal and bone marrow-related toxicities may restrict the clinical application of these drugs. (Konopleva et al., 2020). As a result, efforts to look for new-generation MDM2 inhibitors with stronger efficacy and acceptable toxicities are still worthwhile. Polyethylene glycol (PEG) modification is a well-known chemical modification strategy to increasing drug water solubility and reducing toxicities. Spirooxindole-containing compound is one of the most important MDM2 inhibitor types. By investigating different isomers of spirooxindole-containing compounds, Zhao et al. found that *cis-cis* isomers which contains *cis-cis* substitution pattern on the pyrrolidine ring showed high MDM2 binding affinity and complete long-lasting tumor regression in an animal model of human cancer, which shed light on MDM2 inhibitor development. (Zhao et al., 2013).

Previously, MDM2 inhibitor nutlin-3 and MI-219 were reported induced radiosensitization and enhanced androgen deprivation therapy (ADT) efficacy *in vitro* and *in vivo*. (Tovar et al., 2011; Feng et al., 2016). While, the influences of MDM2 inhibitor on SGAs therapeutic effect are still unanswered. Recent clinical studies have demonstrated that p53 inactivation was associated with poor response to SGAs. (Maughan et al., 2018; De Laere et al., 2019). In addition, *TP53* and *Rb1* play key roles in suppressing PCa lineage plasticity and anti-androgen resistance. (Mu et al., 2017; Nyquist et al., 2020). Therefore, we hypothesised that targeting p53 reactivation using MDM2 inhibitor could produce a synergistic effect with SGAs and potentially overcome SGAs resistance in PCa. In this study, we developed XR-2, which is a *cis-cis* isomer spirooxindole-based PEGylation MDM2 inhibitor, by specifically blocking MDM2–p53 interaction; XR-2 inhibits PCa proliferation in a p53-dependent manner. XR-2 displays a synergistic effect with enzalutamide and overcomes enzalutamide resistance both *in vitro* and *in vivo*. Furthermore, XR-2 possesses broad-spectrum anti-tumor activity *in vivo* in different cancer types with favourable safety.

# METHODS

## Cell Lines and Reagents

The LNCaP (ATCC, CRL-1740), 22Rv1 (ATCC, CRL-2505), DU145 (ATCC, HTB-81), C4-2 (ATCC, CRL-3314), MCF7 (ATCC, HTB-22) and SJSA1 (ATCC, CRL-2098) cell lines were purchased from American Type Culture Collection (ATCC, VA, United States). The HepG2 (SCSP-510) and NCI-H460 (TCHu205) cell lines were purchased from the National Collection of Authenticated Cell Cultures of China. LNCaP, C4-2, 22Rv1, SJSA1 and NCI-H460 cell lines were cultured with Roswell Park Memorial Institute (RPMI)-1,640 supplemented with 10% foetal bovine serum (FBS, Gibco, Thermo Fisher Scientific, MA, United States). DU145 and HepG2 cell lines were cultured with DMEM supplemented with 10% FBS. MCF7 was cultured with Eagle's minimum essential medium supplemented with 10% FBS. LNCaP-R cells were derived from LNCaP cells, as LNCaP cells were cultured with RPMI-1640 supplemented with 10% FBS and 5 μM enzalutamide for 2 months, and then these 5 μM enzalutamide-treated LNCaP cells were cultured with RPMI-1640 supplemented with 10% FBS and 10 μM enzalutamide for another 6 months.

XR-1, XR-2 and XR-3 (all produced in house) were dissolved in dimethyl sulfoxide (DMSO, Sigma-Aldrich, MO, United States) for *in vitro* experiments, and XR-2 was dissolved in Cremophor EL (Shanghai Aladdin Bio-Chem Technology Co., LTD., China), 95% ethanol (Shanghai Aladdin Bio-Chem Technology Co., LTD.) and saline solution (1.5:1.5:7) for *in vivo* experiments. Enzalutamide and RG7388 (idasanutlin) were purchased from Selleck (Houston, TX, United States).

## Western Blot Analysis

Logarithmic growth-phase cells were seeded at a density of ~4 × $10^5$ cells per well in a 6-well plate and incubated for 48 h. Then, DMSO (Sigma-Aldrich) or test compounds were added to each well at the designated concentrations. After another 24 h of incubation, cells were collected and lysed with radioimmunoprecipitation assay lysis buffer supplemented with protease inhibitor and phosphatase inhibitor on ice for 30 min. Then, the protein lysis buffer was treated with 10% sodium dodecyl sulphate–polyacrylamide gel electrophoresis and transferred onto polyvinylidene difluoride membranes for Western blot analysis. The following antibodies were used for the detection of proteins: rabbit anti-MDM2 (1:1,000, Abways, Tracxn Technologies Limited, India), rabbit anti-p53 (1:1,000, Abways), mouse anti-PARP1 (1:1,000, Santa Cruz, United States), rabbit anti-cleaved PARP1 (1:1,000, Selleck), mouse anti-AR (441, 1:1,000, Santa Cruz, United States) and rabbit anti-PSA (1:1,000, Abways). Mouse anti-actin (1:5,000, Abcam) was used as a loading control. Proteins were visualised using anti-mouse, anti-rabbit or anti-rabbit HRP-conjugated secondary antibodies (1: 5,000, Zhongshan Jinqiao Biotechnology Company, China) and ECL-Plus (Millipore, MA, United States). The resulting bands were analysed and quantified using ImageJ® 1.49 g software (National Institutes of Health, MD, United States). Each experiment was repeated at least twice.

## Cell Viability Assay

PCa cells were seeded at a density of 1 ×$10^4$ cells per well in a 96-well plate. LNCaP and 22Rv1 cells were cultured in a complete RPMI-1640 growth medium. DU145 cells were cultured in DMEM growth medium. After 24 h incubation, 1 μL of DMSO (Sigma-Aldrich) or 1 μl of the indicated concentrations of XR-2 were added to each well. After 72 h of incubation, 20 μl of MTT (Invitrogen, MA, United States) solution (5 mg/ml in phosphate-buffered saline (PBS)) was added per well and incubated for another 4 h. The MTT formazan formed by metabolically viable cells was dissolved in 100 μl of isopropanol. The absorbance was measured at 570 nm wavelength on a plate reader (EnSpire 2,300, PerkinElmer, MA, United States). Experiments were performed in triplicates. The value of the DMSO group was 100%.

## Colony Formation Assay

Logarithmic growth phase cells were seeded at a density of ~1 ×$10^4$ cells per well in 6-well plates (n = 3) and treated with the required drugs/compounds or vehicle for 12–14 days. The culture media were changed every 3 days. After removal of the culture media, cells were washed by PBS twice and colonies were fixed by methanol for 10 min. Thereafter, colonies were stained using 1% (w/v) crystal violet (Sigma, MO, United States) for 10 min. Each well was washed with distilled deionised water until the background was clean; after another 30 min of airing, colony pictures were generated. To quantify staining, the stained wells were washed with 1 ml of 10% acetic acid, and absorbance at 590 nm wavelength was detected on a plate reader (EnSpire 2,300, PerkinElmer).

## Quantitative Reverse-Transcriptase Polymerase Chain Reaction

All kinds of cells were seeded at a density of ~4 × $10^5$ cells per well in a 6-well plate and incubated for 48 h. Then, cells were treated with vehicles (DMSO) or test compounds at designated concentrations. After another 24 h of incubation, total RNA was extracted by TRIzol (Invitrogen, MA, United States) according to the manufacturer's instructions. Complementary cDNA synthesis was performed using a cDNA reverse transcription kit (AGbio, Inc.) and total mRNA templates. Relative mRNA levels of AR, PMMA, p53 and p21 were quantified by qRT-PCR using a SYBR Green Premix Pro Taq HS qPCR Kit (AGbio) on the qPCR instrument (Bio-Rad, CA, United States). The mRNA expression levels were normalised to glyceraldehyde 3-phosphate dehydrogenase (GAPDH). All reactions were performed in triplicates. The gene-specific primers are listed in **Supplementary Table S1**.

## Gene Knocking Down Assay

The Small interfering RNAs (siRNAs) of *TP53* were designed and synthesized by Sangon Biotech (Shanghai, China). siRNA stocks (20 μM) and Lipofectamine™ RNAiMAX Transfection Reagent (ThermoFisher, 13778100) were diluted in opti-MEM, the mix was incubated for 20 min and then added to cells according to the instruction. After another 24 h, cells were treated with indicated

compounds. The siRNA primers are listed in **Supplementary Table S2**.

## Flow Cytometry Analysis of Cell Cycle and Apoptosis

Logarithmic growth phase cells were seeded at a density of ~4 $\times 10^5$ cells per well in a 6-well plate and incubated for 48 h. Then, DMSO (Sigma-Aldrich) or test compounds were added to each well at designated concentrations. For the cell cycle analysis, after compounds were treated for 24 h, cells were harvested and fixed with ice-cold 70% (v/v) ethanol for 24 h. Then, cells were centrifuged at 1,000 rpm for 5 min. Cell pellets were then washed once with phosphate-buffered saline (PBS) and stained with propidium iodide. A total of 30,000 events were acquired by flow cytometer (BDC6, BD Biosciences, United States), and proportions of cells in each phase of the cell cycle were calculated using FlowJo software (BD Biosciences). For apoptosis analysis, after compound treatment for 24 h, cells were harvested and washed once with cold PBS. Then, cells were incubated for 15 min at room temperature with Annexin V-FITC-PI in a binding buffer. Cells were then analysed on a flow cytometer (BDC6, BD Biosciences) using FlowJo software. Results were expressed as percentages of Annexin V+ cells. Experiments were performed in duplicate.

## Dual-Luciferase Reporter System Assay

As previously described, plasmid PSA-luc was a reporter gene plasmid in which the firefly luciferase expression is dependent on the PSA promoter; plasmid Renilla was a Ranilla luciferase reporter gene plasmid. These two plasmids were kindly provided by Dr Cen (Peking Union Medical College, China). LNCaP cells were seeded at a density of 6–7 $\times 10^4$ cells per well in 24-well plates. After incubation for 24 h, cells in each well were co-transfected with 100 ng of PSA-luc and 3 ng of Renilla plasmids using Lipofectamine 2000 reagent (Invitrogen) following the manufacturer's protocol. After 24 h from the transfection, the medium was changed to phenol red-free RPMI-1640 supplemented with 10% charcoal-stripped FBS, containing 5 nM of DHT (1 μl) and 1 μl of test compounds at designated concentrations. After 24 h, the cells were lysed in 100 μl of passive lysis buffer per well, and 20 μl of the cell lysates were used for the detection of the luciferase activity using a dual-luciferase assay system (Promega, WI, United States) on a plate reader (Centro XS3 LB 960, Berthold Technologies, Germany). All experiments were run in triplicates.

## RNA Sequencing

LNCaP cells were treated by compounds at designated concentrations for 24 h. Total RNA was extracted from approximately 1 $\times 10^6$ cells using Invitrogen TRIzol® RNA Isolation Reagent. Sequencing libraries were generated using VAHTS Universal V6 RNA-seq Library Prep Kit for Illumina® (NR604-01/02, CA, United States), following the manufacturer's recommendations. Index codes were added to attribute sequences to each sample. Then, the library was examined successively. The clustering of the index-coded samples was performed on a cBot cluster generation system using HiSeq PE Cluster Kit v4-cBot-HS (Illumina, CA, United States) according to the manufacturer's instructions. After cluster generation, the libraries were sequenced on an Illumina platform and 150 bp paired-end reads were generated. The passed raw reads were aligned and assembled by STAR (https://github.com/alexdobin/STAR). Differentially expressed genes were analysed by HTseq-count (https://pypi.org/project/HTSeq) and edgeR (https://bioconductor.org/packages/edgeR). The KEGG analysis was performed by EnrichR (https://cran.rproject.org/). Heatmaps were generated by Hiplot website (https://hiplot.com.cn/). Original data is available in The Genome Sequence Archive for Human (https://ngdc.cncb.ac.cn/gsa-human/; Accession code: HRA001434).

## Senescence Assay

Cells were seeded at a density of ~1 $\times 10^5$ cells per well in 6-well plates and incubated for 24 h. Then, DMSO or test compounds were added to each well at designated concentrations. After another 72 h of incubation, cell senescence was evaluated by visualising β-galactosidase activity using senescence β-galactosidase staining kit (C0602, Beyotime Technology, China) according to the manufacturer's instructions. Three fields of each well were photographed for each of the three independent replicates for each treatment condition.

## *In vivo* Xenograft Studies

All animal experimental procedures were conducted in the animal facility of KeyGEN BioTECH (Nanjing, China). All experimental procedures involving the care and use of mice were approved by the KeyGEN BioTECH Institutional Animal Care and Use Committee. The mice were housed five per cage in an environmentally controlled SPF room (temperature 20–26°C; relative humidity 40–70%) on a 12-h light/dark cycle. The mice were fed commercial rodent chow (Beijing Keao Xieli Feed, Beijing, China) and received filter-purified water ad libitum. All studies utilised 4–6-week-old mice purchased from the Shanghai Laboratory Animal Center (Shanghai, China). 22Rv1 cells (2 $\times 10^6$ cells with Matrigel at a ratio of 1:1) were injected subcutaneously in the flank of the male SCID mice. SJSA-1 cells (2 $\times 10^6$ cells with Matrigel at a ratio of 1:1), NCI-H460 cells (2 $\times 10^6$ cells with Matrigel at a ratio of 1:1), or HepG2 cells (2 $\times 10^6$ cells with Matrigel at a ratio of 1:1) were injected subcutaneously in the flank of female BALB/c nude mice. When the average tumor volume reached 100–150 $mm^3$, the mice were randomised and divided into the indicated groups (n = 8/group). XR-2 was administered once per day intraperitoneally. RG7388 and enzalutamide were administered once per day by oral gavage. Combination therapy studies were performed in a blinded manner. The tumor volume and mice bodyweight were monitored every other day, and the tumor volume was calculated according to the formula $W^2 \times L/2$ ($mm^3$), wherein W was the short diameter and L was the long diameter. Data are expressed as mean ± SD. Whole blood was collected 24 h later after the last administration from the orbit. Blood cell analysis was performed using a haematology analyser (XS-800I, Sysmex Corporation, Japan).

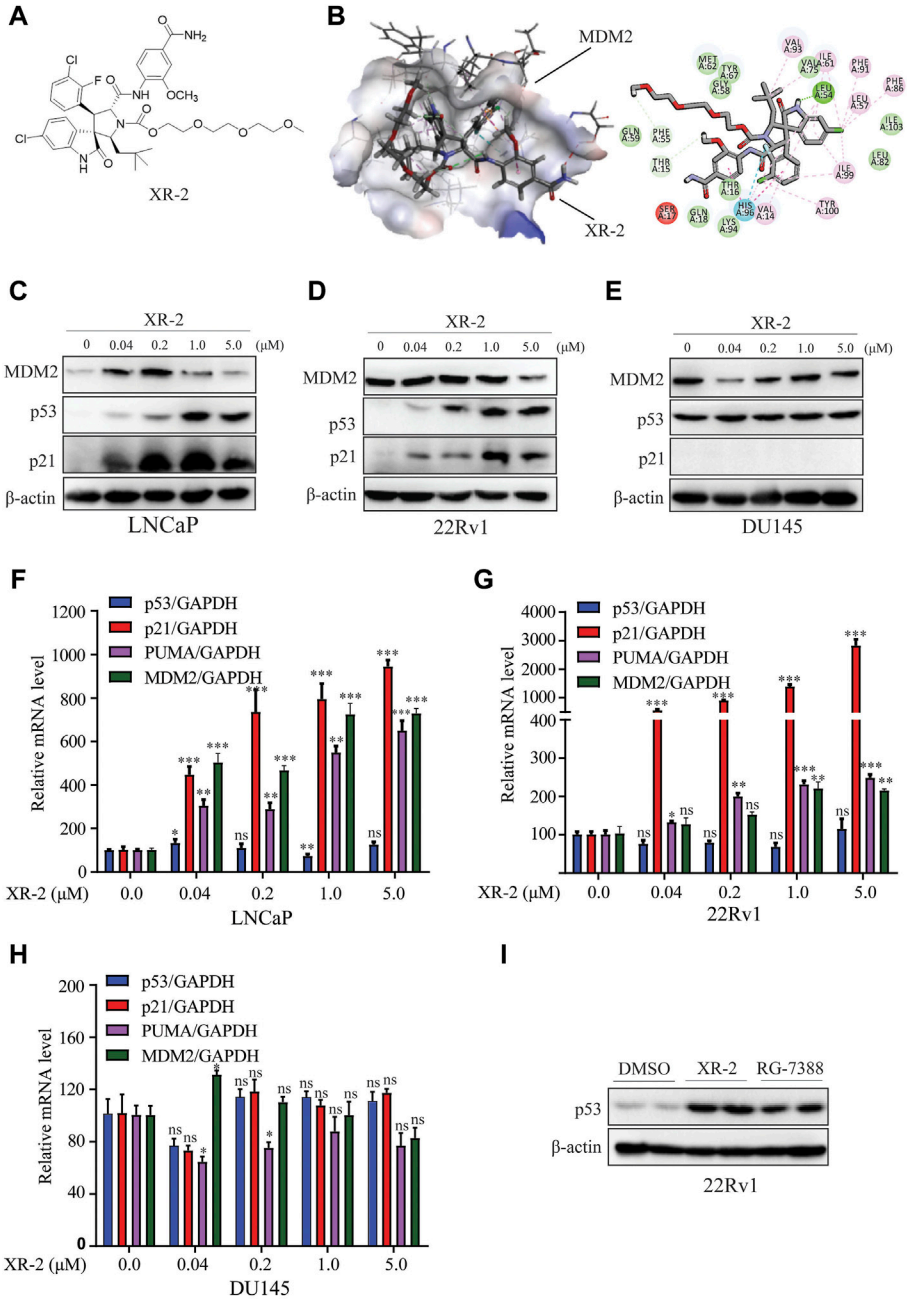


**FIGURE 1 |** XR-2 effectively reactivates the p53 pathway. **(A)** Chemical structure of XR-2. **(B)** Predicted binding mode of XR-2 with MDM2. **(C)** Cells were treated with the indicated concentrations of XR-2 for 24 h. MDM2, p53, p21 and β-actin protein levels were measured by Western blot analysis in LNCaP, **(D)** 22Rv1 and **(E)** DU145 cells. **(F)** Cells were treated with the indicated concentrations of XR-2 for 24 h, and the mRNA levels of p53, *p21*, *PUMA* and *MDM2* were measured by qRT-PCR and normalised to GAPDH in LNCaP, **(G)** 22Rv1 and **(H)** DU145 cells. **(I)** 22Rv1 cells were treated with 1 μM XR-2 and 1 μM RG-7388 for 24 h; p53 and β-actin protein levels were measured by Western blot analysis. Experiments were performed in triplicates. All results are shown as mean ± SD. $^{*}p < 0.05$, $^{**}p < 0.01$, $^{***}p < 0.001$ vs. control group.

## Immunohistochemical Staining

Antibodies to Ki67 (abcam, ab16667) and cleaved caspase 3 (CST, 9,661) were used for immunostaining on formalin-fixed paraffin-embedded xenograft tumor tissues. Generally, the rehydrated slides were microwave-heated for 20 min in citrate buffer (10-mM, pH 6.0) for antigen retrieval. Then incubated in 1% $H_2O_2$ for 10 min, after blocking with serum-free protein block, slides were incubated with the primary antibodies (Ki67, 1: 200; Cleaved caspase 3, 1: 100) for 2 h at room temperature, followed by incubation with HPR-conjugated secondary antibody for 1 h at room temperature. The immunoreaction products were visualized with 3, 3-diaminobenzidine (DAB)/H2O2 solution.

## In Silico Docking

The MDM2 protein crystal structure (PDB code: 5TRF) was downloaded from the PDB database (https://www.rcsb.org). Chain A of the MDM2 crystal structure remained and was modified by the "protonate 3D" module of Discovery Studio 3.5. The 2D chemical structure of XR-2 drawn by the Chemdraw 18.1 software was generated in 3D structure using the "prepare ligands" module by Discovery Studio 3. 5. As described previously, (Li et al., 2019), the binding site was centred at Ile99 in MDM2 with a radius of 10 Å to cover the binding pocket of MDM2. Then, the prepared XR-2 has docked into the MDM2 chain A binding site by the 'CDOCKER' module of Discovery Studio 3.5 by default. After analysing the 10 binding poses of XR-2 to MDM2, we selected the highest-ranked pose for the MDM2 structure as the binding model of XR-2.

## Chemistry Synthesis

**2-(2-methoxyethoxy)ethyl-(2′S,3R,4′S,5′R)-5'-((4-carbamoyl-2-methoxyphenyl)carbamoyl)-6-chloro-4'-(3-chloro-2-fluorophenyl)-2′-neopentyl-2-oxospiro[indoline-3,3′-pyrrolidine]-1′-carboxylate (XR-1)**:Compound 2 was synthesized as previous explained. (Shu et al., 2013). Compound 2 (612 mg, 1.0 mmol) was dissolved in DMF (100 ml), then anhydrous KCO3 (4.0 mmol) was added and 1-chloroethyl (2- (2-methoxyethoxy) ethyl) carbonate (904 mg, 4.0 mmol) was added and stirred overnight at room temperature. After the reaction, water (20 ml) was added and extracted by ethyl acetate. The organic phase was separated, washed with brine, 1M hydrochloric acid and water successively, and then concentrated through the column to obtain the target product (644 mg, yield: 85%), which was a white solid. 1H NMR (CDCl3,400 MHz): 10.59 (s, 1H), 8.47 (d, J = 8.4 Hz, 1 H),7.80 (d, J = 1.6 Hz, 1 H), 7.55 (d, J = 1.3 Hz, 1 H), 7.48 (t, J = 6.8 Hz, 1 H), 7.28–7.36 (m, 2 H), 7.19–7.26 (m, 2 H), 7.04 (t, J = 8.0 Hz), 6.05–6.55 (bs, 1 H), 5.30–5.80 (bs, 1 H), 4.70 (t, J = 9.62 Hz, 1 H), 4.40–4.54 (m, 3 H), 3.94 (s, 3 H), 3.83 (t, J = 4.7 Hz, 2 H), 3.62–3.74 (m, 3 H), 3.60 (t, J = 4.6 Hz, 2 H), 1.24–1.35 (m, 1 H), 0.96 (s, 9 H); HRMS (ESI-TOF): m/z calculated for C37H41Cl2FN4NaO8+ [M + Na]+: 781.2183, found: 781.2190.

**2-(2-(2-methoxyethoxy)ethoxy)ethyl-(2′S,3R,4′S,5′R)-5'-((4-carbamoyl-2-methoxyphenyl)carbamoyl)-6-chloro-4'-(3-chloro-2-fluorophenyl)-2′-neopentyl-2-oxospiro[indoline-3,3′-pyrrolidine]-1′-carboxylate (XR-2):** Compound 2 (612 mg, 1.0 mmol) was dissolved in DMF (100 ml), then anhydrous KCO3 (4.0 mmol) was added with drops of 2- (2- (2-methoxyethoxy) ethane-1-ol (1.08 g, 4.0 mmol), and stirred overnight at room temperature. After the reaction, water (20 ml) was added and extracted by ethyl acetate. The organic phase was separated and washed with brine, 1M hydrochloric acid and water successively, and then concentrated through the column to obtain the target product (Yield: 80%), which was a white solid. 1H NMR (CDCl3,400 MHz): 10.6 (s, 1H), 8.45 (d, J = 8.0 Hz, 1H), 7.8 (s, 1 H), 7.55 (s, 1 H), 7.48 (t, J = 8.0 Hz, 1 H), 7.35 (t, J = 8.0 Hz, 2 H), 7.20–7.40 (m, 2 H), 7.04 (t, J = 8.0 Hz, 1 H), 6.1–6.6 (bs, 1 H), 5.4–5.8 (bs, 1 H), 4.69 (t, J = 10, 1 H), 4.40–4.55 (m, 3 H), 3.04 (s, 3 H), 3.83 (t, J = 4, 2 H), 3.69–3.77 (m, 4 H), 3.62–3.69 (m, 4 H), 3.50–3.58 (m, 2 H), 3.36 (s, 3 H), 3.18–3.30 (m, 1 H), 1.24–1.36 (m, 1 H), 0.95 (s, 9 H); 13C NMR (CDCl3,100 MHz): 174.41, 171.63, 168.82, 157.69, 155.21, 149.52, 148.46, 140.10, 134.91, 130.57, 130.01, 128.73, 127.35, 125.51, 124.81 (Jc-F = 4.3 Hz), 123.62, 123.36, 121.40 (d, J = 19 Hz), 119.95, 118.22, 116.15, 109.98, 72.01, 70.83, 70.81, 70.68, 68.61, 68.06, 66.60, 66.57, 65.51, 59.12, 55.76, 50.96, 42.79, 30.45, 29.89; HRMS (ESI-TOF): m/z calculated for C39H45Cl2FN4NaO9+ [M + Na]+: 825.2445, found: 825.2456.

**2,5,8,11,14-pentaoxahexadecan-16-yl-(2′S,3R,4′S,5′R)-5'-((4-carbamoyl-2-methoxyphenyl)carbamoyl)-6-chloro-4'-(3-chloro-2-fluorophenyl)-2′-neopentyl-2-oxospiro[indoline-3,3′-pyrrolidine]-1′-carboxylate (XR-3):** Compound 2 (306 mg, 0.5 mmol) was dissolved in DMF (50 ml), followed by the addition of anhydrous KCO3 (2.0 mmol) and the addition of 1-chloroethyl (2,5,8,11, 14-pentaxyhexadecane-16-yl) carbonate (720 mg, 2.0 mmol), stirred overnight at room temperature. After the reaction, water (20 ml) was added and extracted by ethyl acetate. The organic phase was separated, washed with brine, 1M hydrochloric acid and water successively, and then concentrated through the column to obtain the target product (Yield: 79%), which was a white solid. 1H NMR (CDCl3,400 MHz): 10.56 (s, 1 H), 8.41 (d, J = 8.4 Hz, 1 H), 7.79 (d, J = 1.7 Hz, 1 H), 7.54 (d, J = 1.3 Hz, 1 H), 7.49 (t, J = 6.8 Hz, 1 H), 7.20–7.40 (m, 4 H), 7.00–7.15 (m, 1 H), 6.30–6.60 (m, 1 H), 5.19 (bs, 1 H), 4.71 (t, J = 9.4 Hz, 1 H), 4.40–4.60 (m, 2 H), 4.25–2.34 (m, 1 H), 3.93 (s, 3 H), 3.83 (t, J = 4.6 Hz, 2 H), 3.78 (s, 1 H), 3.60–3.75 (m, 16 H), 3.50–3.58 (m, 2 H), 3.35–3.40 (m, 4 H), 1.20–1.37 (m, 1 H), 0.86–1.08 (m, 10 H); HRMS (ESI-TOF): m/z calculated for C43H53Cl2FN4NaO11 [M + Na]+: 913.2970, found: 913.2975.

## Data Analysis

Statistical analysis was performed using GraphPad Prism (version 5.01; GraphPad Software). Comparisons between groups were performed with a two-tailed Student's t-test, except where specified, and differences were considered significant at $p < 0.05$.

# RESULTS

## XR-2 as a Potent MDM2 Inhibitor

To develop a more potently selective MDM2 inhibitor with acceptable toxicity, we synthesised some of PEGylation spirooxindole derivatives (PSD) based on previous reported spiroindolinone pyrrolidinecarboxamide compound 2 (**Supplementary Figure S1**). (Shu et al., 2013). Then, we evaluated the primary tumor inhibition activity of some of these compounds in SJSA1-derived xenografts. The results indicated that the 2-weeks treatment with the *cis-cis* isomer of PSD XR-2 (**Figure 1A**) led to the highest suppression rate of tumor progression, which was higher than treatment with its *trans-cis* isomer and both isomers mixture. XR-2 was also proven to be more potent than its non-PEGylation initial analogue compound 2 (**Supplementary Figure S2**). Therefore, we chose XR-2 for further investigation.

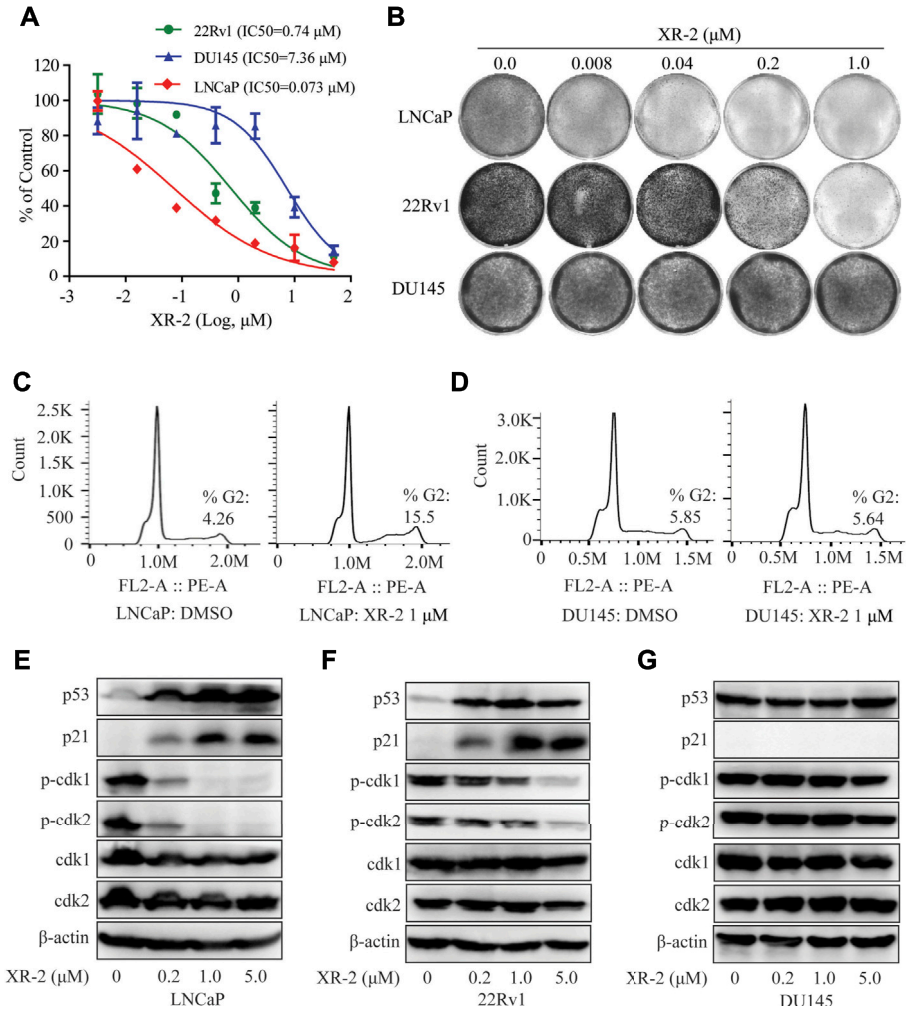


**FIGURE 2 |** Influence of XR-2 on the cellular proliferation and cell cycle of CRPC cell lines. **(A)** CRPC cells, namely, LNCaP, 22Rv1 and DU145, were treated with different concentrations of XR-2 for 72 h, and cell proliferation was detected with the CCK8 assay. **(B)** Crystal violet staining of LNCaP, 22Rv1 and DU145 cells treated with different concentrations of XR-2 for 12–14 days **(C)** Flow cytometry assay was performed to detect cell cycle distribution of LNCaP cells treated with or without XR-2 for 24 h. **(D)** Flow cytometry assay was performed to detect cell cycle distribution of DU145 cells treated with or without XR-2 for 24 h. **(E)** Cells were treated with the indicated concentrations of XR-2 for 24 h; levels of p53, p21, p-CDK1, CDK1, p-CDK2, CDK2 and β-actin were measured by Western blot analysis in LNCaP, **(F)** 22Rv1 and **(G)** DU145 cells. Experiments were performed in triplicates. All results are shown as mean ± SD. $^{*}p < 0.05$, $^{**}p < 0.01$, $^{***}p < 0.001$ vs. control group.

To predict the binding mode of XR-2 to the MDM2 protein, molecular docking was performed based on the protein structure of MDM2 (PDB code: 5TRF) using Discovery Studio software. We found that XR-2 could suitably locate into the p53 binding site of MDM2 and form hydrogen bond interactions with Leu54 and His96 (**Figure 1B**). The homogeneous time-resolved fluorescence binding assay proved that XR-2 directly inhibited MDM2–p53 interaction (**Supplementary Figure S3**). Mechanistically, through competitive binding to the p53 pocket in MDM2, an MDM2 inhibitor could block MDM2–p53 interaction and subsequently led to p53 accumulation and transcriptional activation in wild-type p53 cells. Herein, we analysed the activity and specificity of XR-2 to activate p53 in PCa cells. In LNCaP cells with wild-type p53, Western blot analysis results indicated that XR-2 significantly induced p53 protein accumulation in a dose-dependent manner. In addition, we detected p21 protein upregulation, which further proved the activation of the p53 pathway (**Figure 1C**). In 22Rv1 cells, another wild-type p53 cells, XR-2 induced similar p53 activation (**Figure 1D**). However, in p53-mutated DU145 cells, XR-2 did not influence the levels of both p53 and p21 (**Figure 1E**). Moreover, quantitative reverse-transcriptase polymerase chain reaction (qRT-PCR) analysis revealed that XR-2 caused a dose-dependent upregulation of p53 downstream target genes *p21*, *PUMA* and *MDM2* but not p53 mRNA expression levels in both LNCaP and 22Rv1 cells (**Figures 1F,G**). Not surprisingly, XR-2 could not increase *p21*, *PUMA* and p53 mRNA levels in DU145 cells (**Figure 1H**). Notably, XR-2 demonstrated comparable p53

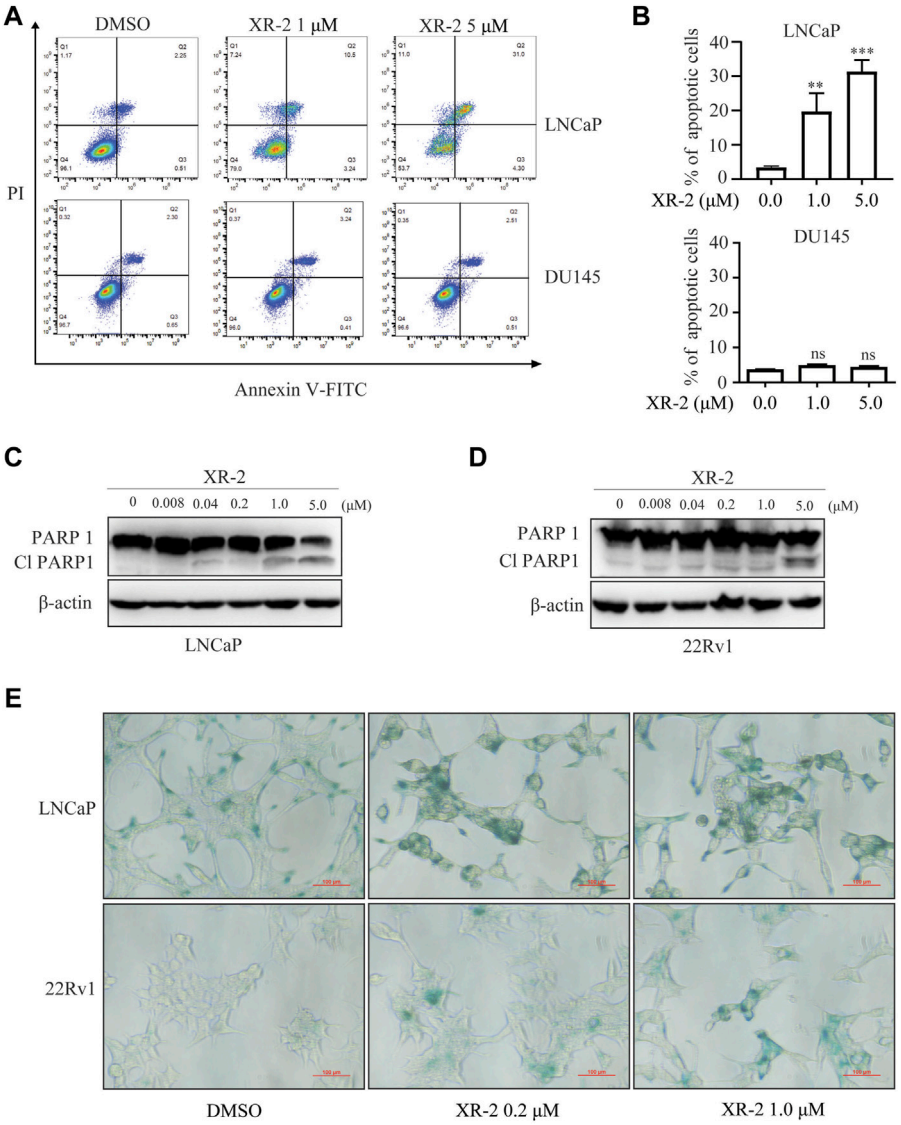


**FIGURE 3 |** Influence of XR-2 on CRPC cell line apoptosis and senescence. **(A)** Flow cytometry assay to detect apoptosis levels of LNCaP and DU145 cells treated with different concentrations of XR-2 for 24 h. **(B)** Quantitative analysis of flow cytometry assay results. **(C)** Cells were treated with the indicated concentrations of XR-2 for 24 h, and PARP1 and β-actin protein levels were measured by Western blot analysis in LNCaP, and **(D)** 22Rv1 cells. **(E)** LNCaP and 22Rv1 cells were treated with the indicated concentrations of XR-2 for 72 h, and β-galactosidase staining was performed. Experiments were performed in triplicates. All results are shown as mean ± SD. $^{*}p < 0.05$, $^{**}p < 0.01$, $^{***}p < 0.001$ vs. control group.

induction activity with the well-known MDM2 inhibitor RG7388 (**Figure 1I**). Taken together, our data provide clear evidence that XR-2 is a potent and specific MDM2 inhibitor.

## XR-2 Inhibits Cellular Proliferation and Induces Cell Cycle Arrest in Wild-Type p53 CRPC Cell Lines.

The p53 key downstream target genes *p21* and *PUMA* could regulate cell cycle arrest, apoptosis and senescence in various cancer cells. Subsequently, we investigated the CRPC inhibition activity of XR-2; as shown in **Figure 2A**, XR-2 selectively inhibited the proliferation of wild-type p53 LNCaP and 22Rv1 cells in a dose-dependent manner with $IC_{50}$ of 0.073 and 0.74 μM, respectively. Conversely, p53-mutated DU145 cells were quite less sensitive to XR-2. Furthermore, to estimate the effects of XR-2 on CRPC cell clonogenic activity, we exposed LNCaP, 22Rv1 and DU145 cells to different concentrations of XR-2 for about 2 weeks. As a result, XR-2 strongly decreased the number of LNCaP and 22Rv1 cell colonies in a dose-dependent manner compared with the

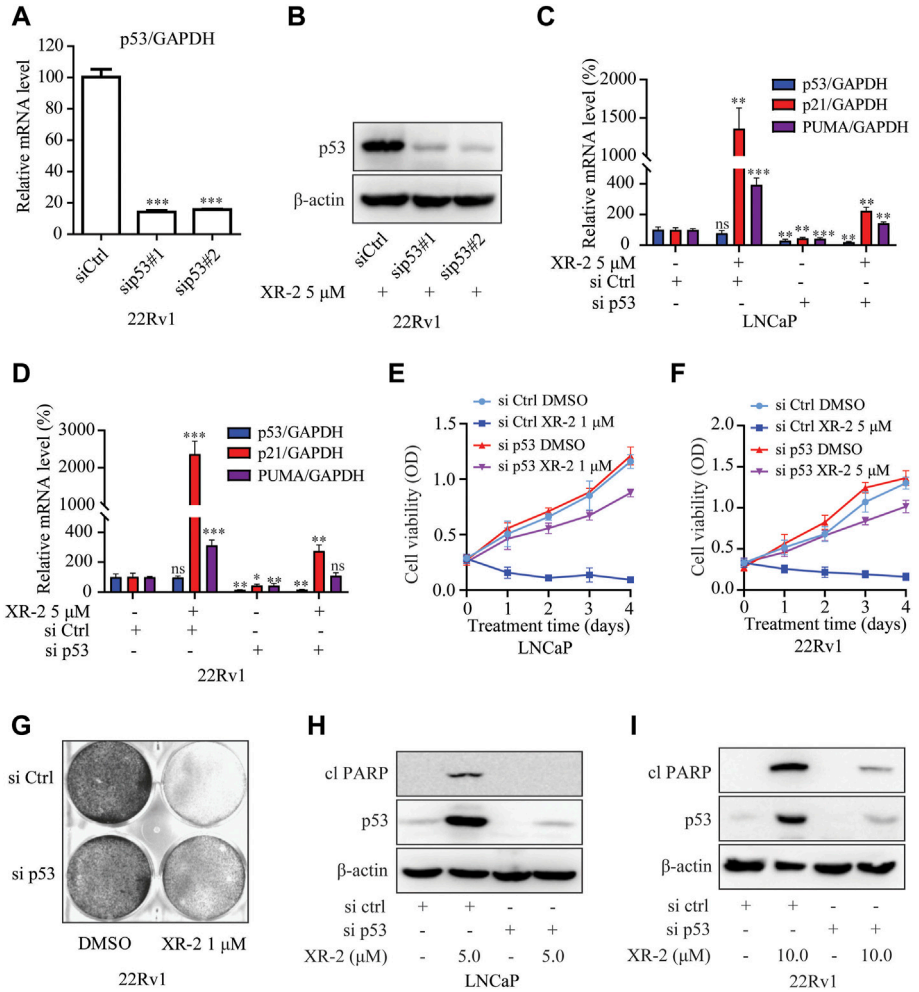


**FIGURE 4 |** XR-2 inhibits CRPC cell viability through the p53 pathway. **(A)** 22Rv1 cells were treated with sip53 or siCtrl for 24 h, and the mRNA levels of p53 were measured by qRT-PCR and normalised to GAPDH. **(B)** 22Rv1 cells were treated with sip53 and XR-2 5 μM for 24 h, and p53 and β-actin protein levels were measured by Western blot analysis. **(C)** LNCaP cells were treated with sip53 and XR-2 1 μM for 24 h, and the mRNA levels of p53, p21 and *PUMA* were measured by qRT-PCR and normalised to GAPDH. **(D)** 22Rv1 cells were treated with sip53 and XR-2 5 μM for 24 h, and the mRNA levels of p53, *p21* and *PUMA* were measured by qRT-PCR and normalised to GAPDH. **(E)** LNCaP cells were treated with or without sip53 and XR-2 1 μM for different days, and cell proliferation was detected with the CCK8 assay. **(F)** 22Rv1 cells were treated with or without sip53 and XR-2 5 μM for different days, and cell proliferation was detected with the CCK8 assay. **(G)** Crystal violet staining of 22Rv1 cells treated with or without sip53 and XR-2 with 1 μM for 12–14 days **(H)** LNCaP cells were treated with or without sip53 and XR-2 with 5 μM for 24 h, and protein levels of cleaved PARP1, p53 and β-actin were measured by Western blot analysis. **(I)** 22Rv1 cells were treated with or without sip53 and XR-2 with 10 μM for 24 h, and protein levels of cleaved PARP1, p53 and β-actin were measured by Western blot analysis. Experiments were performed in triplicates. All results are shown as mean ± SD. $^{*}p < 0.05$, $^{**}p < 0.01$, $^{***}p < 0.001$ vs. control group.

untreated group, while specific treatment concentrations did not influence the number of DU145 cell colonies (**Figure 2B**).

Furthermore, flow cytometry analysis revealed that XR-2 therapy selectively increased the proportion of G2/M phase cells than the control group in LNCaP cells rather than in DU145 cells (**Figures 2C,D**). To further confirm the mechanisms of cell cycle arrest, we evaluated the influence of XR-2 on the protein levels of different cell cycle-related proteins in LNCaP, 22Rv1 and DU145 cells. XR-2 increased CDK suppressor p21 protein levels as mentioned above in LNCaP and 22Rv1 cells and thus dose-dependently reduced the cell cycle regulated protein levels of phosphorylation of CDK1 and CDK2 (**Figures 2E,F**). In DU145 cells, XR-2 could not upregulate p21 protein; thus, it cannot reduce the protein levels of activated phosphorylation CDK1 and CDK2 (**Figure 2G**). Collectively, these findings demonstrated that XR-2 effectively inhibited cell proliferation and induced cell cycle arrest of CRPC cells by activating the p53 pathway.

## XR-2 Promotes CRPC Cell Apoptosis and Senescence

Moreover, we examined whether XR-2 influences CRPC cell apoptosis by flow cytometry assay. As shown in **Figures 3A,B**,

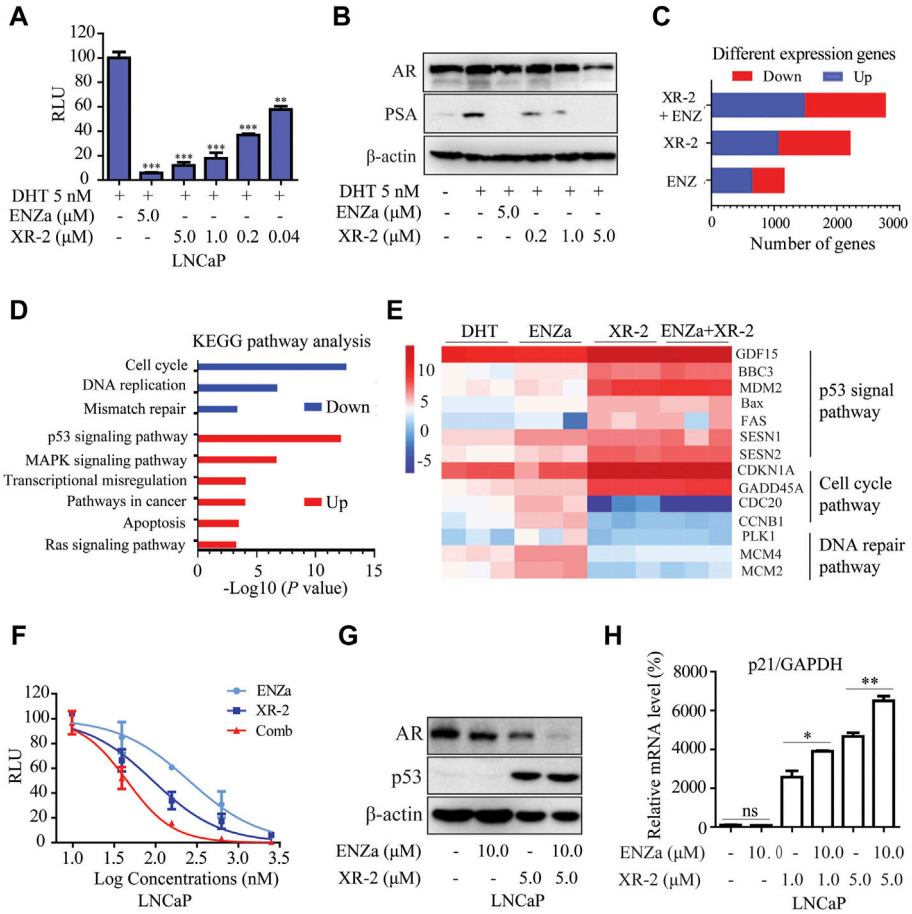


**FIGURE 5 |** XR-2 blocks the AR pathway and demonstrates synergistic effects with enzalutamide. **(A)** A dual-luciferase reporter assay was performed to measure PSA-luc reporter luciferase activities stimulated by 5 nM DHT and treated with different concentrations of XR-2 for 24 h in LNCaP cells co-transfected with the Renilla and PSA promoter expression vector plasmids. **(B)** LNCaP cells were treated with the indicated concentrations of XR-2 in the presence of 5 nM DHT for 24 h, cells were then lysed, and PSA and AR protein levels were measured by Western blot analysis. **(C)** LNCaP cells were treated with XR-2 (1 μM), enzalutamide (5 μM), alone or in combination for 24 h in triplicate experiments. Cells were collected for RNA-seq analysis after treatment. The number of differentially expressed genes after each treatment was shown. **(D)** The Kyoto Encyclopedia of Genes and Genomes pathway analysis of the most significantly enriched biological processes upregulated or downregulated in response to combined treatments compared with control groups. **(E)** Representative differentially expressed genes in response to XR-2, enzalutamide and combination treatments. **(F)** A dual-luciferase reporter assay was performed to measure PSA-luc reporter luciferase activities stimulated by 5 nM DHT and treated with different concentrations of XR-2, enzalutamide or both agents combined for 24 h in LNCaP cells co-transfected with the Renilla and PSA promoter expression vector plasmids. **(G)** LNCaP cells were treated with XR-2, enzalutamide or both agents combined for 24 h, cells were then lysed and p53 and AR protein levels were measured by Western blot analysis. **(H)** LNCaP cells were treated with XR-2, enzalutamide or both agents combined for 24 h, and the mRNA levels of *p21* were measured by qRT-PCR and normalised to GAPDH. Experiments were performed in triplicates. All results are shown as mean ± SD. $^{*}p < 0.05$, $^{**}p < 0.01$, $^{***}p < 0.001$ vs. control group.

XR-2 significantly induced apoptosis of LNCaP cells rather than of DU145 cells. Western blot analysis further proved that XR-2 promoted the accumulation of apoptotic marker cleaved PARP protein in LNCaP and 22Rv1 cells (**Figures 3C,D**). The mRNA levels of apoptotic markers Bax and growth arrest and DNA damage-inducible 45 (GADD45A) were also upregulated in LNCaP and 22Rv1 cells rather than in DU145 cells (**Supplementary Figure S4A,B**). As we confirmed that XR-2 increased the expression of the senescence marker p21, we examined the mechanism of cell senescence by detecting senescence-associated β-galactosidase. We observed a significant increase in β-galactosidase staining in LNCaP and 22Rv1 cells treated with XR-2 for 72 h compared with vehicle treatment.

## XR-2 Inhibits CRPC Cell Viability in a p53-dependent Manner

To further confirm whether XR-2 inhibits CRPC cell viability through p53 activation, we performed *TP53* gene knockdown assay by siRNA. The results demonstrated that p53 knockdown reduced p53 mRNA expression levels in 22Rv1 cells (**Figure 4A**). Not surprisingly, XR-2 therapy was unable to promote p53 accumulation in p53 knockdown cells (**Figure 4B**). Efficient

knockdown of p53 in LNCaP and 22Rv1 cells also potently attenuated XR-2 induced upregulation of *p21* and *PUMA* mRNA expression levels (**Figures 4C,D**). Furthermore, p53 knockdown forcefully reduced the cell proliferation inhibition potency of XR-2 in LNCaP and 22Rv1 cells (**Figures 4E,F**). We also found that XR-2-induced colony formation inhibition activity in 22Rv1 cells was blocked by p53 knockdown (**Figure 4G**). Finally, we found that p53 knockdown diminished XR-2-induced cell apoptosis indicated by the expression levels of the cleaved PARP protein in LNCaP and 22Rv1 cells (**Figures 4H,I**). These data firmly established that XR-2 inhibits CRPC cell viability through the p53 pathway.

## XR-2 Inhibits the AR Pathway and Shows Synergistic Effects With Enzalutamide

As p53 overexpression was reported to diminish the androgen response, (Cronauer et al., 2004), we investigated whether p53 inducer XR-2 could block the AR pathway in PCa cells. The results of dual-luciferase reporter assay in LNCaP cells indicated that XR-2 inhibited dihydrotestosterone (DHT)-induced transcriptional activities of endogenous AR in a dose-dependent manner (**Figure 5A**). Moreover, Western blot analysis revealed that XR-2 downregulated DHT-activated PSA protein expression levels in a dose-dependent manner; surprisingly, XR-2 could also downregulate AR protein levels (**Figure 5B**).

RNA sequencing assay was performed to evaluate the gene expression status of LNCaP cells under XR-2 and enzalutamide treatment. Compared with single agents, XR-2 plus enzalutamide in LNCaP cells resulted in more differentially expressed genes, implicating that combined treatment had more remarkable effects (**Figure 5C**). The Venn analysis indicated that the largest number of differentially upregulated and downregulated genes appeared to be induced by XR-2 plus enzalutamide compared with either single-agent treatment. Interestingly, the proportion of overlapped genes between XR-2 monotherapy and combination therapy appeared higher than that between enzalutamide monotherapy and combination therapy (**Supplementary Figure S5A,B**). The Kyoto Encyclopedia of Genes and Genomes (KEGG) analysis demonstrated that XR-2 plus enzalutamide upregulated the expression of genes encoding constituents of the P53 signalling pathway and downregulated those involved in DNA replication, mismatch repair and cell cycle progression (**Figure 5D**). As shown in **Figure 5E**, the main p53-target genes were upregulated in XR-2 monotherapy and combination therapy, such as growth differentiation factor 15 (GDF15), which is a surrogate for p53 activation, and apoptogenic genes *BBC3*, *PUMA*, *MDM2*, *Bax* and *FAS*. XR-2 monotherapy and combination therapy also upregulated the expressions of negative regulators of cell cycle progression genes, including *cyclin-dependent kinase inhibitor 1A* and *GADD45*. In addition, the combination therapy enhanced AR pathway inhibition compared with the control and enzalutamide groups, which were characterised by lower expression levels of key AR-target genes including *FKBP5*, *PMEPA1*, *KLK3*, *NKX3-1* and *KLK2* (**Supplementary Figure S5C**). Altogether, these findings suggest that XR-2 plus enzalutamide induced enhanced p53 pathway reactivation and AR pathway inhibition.

To further confirm the synergistic effects between XR-2 and enzalutamide, we examined the influences of XR-2 plus enzalutamide on AR and p53 pathways. We found that XR-2 plus enzalutamide demonstrated enhanced AR transcriptional inhibition activity than either monotherapy in different concentrations (**Figure 5F**). Similarly, as demonstrated in **Figure 5G**, the XR-2 plus enzalutamide reduced AR protein levels more efficiently than monotherapy in both LNCaP, 22Rv1 and C4-2 cells (**Supplementary Figure S5D,F**). By contrast, by detecting the *p21* mRNA levels in LNCaP, 22Rv1 and C4-2 cells, we found that enzalutamide could enhance XR-2-induced p53 pathway activation (**Supplementary Figure S5G,H,E**). Together, these findings indicate that XR-2 could inhibit the AR pathway, and XR-2 plus enzalutamide synergistically inhibits AR and p53 pathways.

## XR-2 Overcomes Enzalutamide Resistance *in vitro*

To evaluate whether XR-2-induced p53 reactivation and AR inhibition could inhibit enzalutamide-resistant CRPC cell viability, we constructed enzalutamide-resistant LNCaP (LNCaP-R) cells through long-term enzalutamide treatment (**Figure 6A**). Compared with LNCaP cells, LNCaP-R cells demonstrated a more robust cell proliferation activity with 5 μM enzalutamide treatment (**Figure 6B**). Nevertheless, XR-2 potently blocked LNCaP-R cell proliferation and colony formation activity in a dose-dependent manner (**Figures 6C,D**). In enzalutamide-resistant 22Rv1 cells, XR-2 similarly suppressed the proliferation of 22Rv1 cells and demonstrated synergistic effects with enzalutamide (**Figures 6E,F**). Western blot analysis revealed that XR-2 also induced apoptosis marker protein cleaved PARP1 expression and demonstrated synergistic effects with enzalutamide in LNCaP-R cells (**Figure 6G**). Subsequently, we found that the proportion of β-galactosidase-positive cells were significantly increased in both XR-2 monotherapy and combination therapy compared with that in the control or enzalutamide group. These results proved that XR-2 could overcome enzalutamide resistance *in vitro*.

## XR-2 Inhibits Enzalutamide-resistant CRPC Xenograft Progress

As previous study proved that XR-2 could activate the p53 pathway and inhibit PCa cell viability *in vitro*. Then, we investigated the tumor inhibition efficacy of XR-2, enzalutamide and XR-2 plus enzalutamide *in vivo* by using 22Rv1 xenografts in male SCID mice. In this study, $5 \times 10^6$ 22Rv1 cells were injected into the left flank of each male mouse, and the tumor volume was allowed to increase to approximately 100 $mm^3$. Then, the tumor-bearing mice received intraperitoneal injection of the vehicle control, 30 mg/kg of XR-2, 30 mg/kg of enzalutamide and 30 mg/kg of XR-2 plus 30 mg/kg of enzalutamide once a day for 4 weeks. The

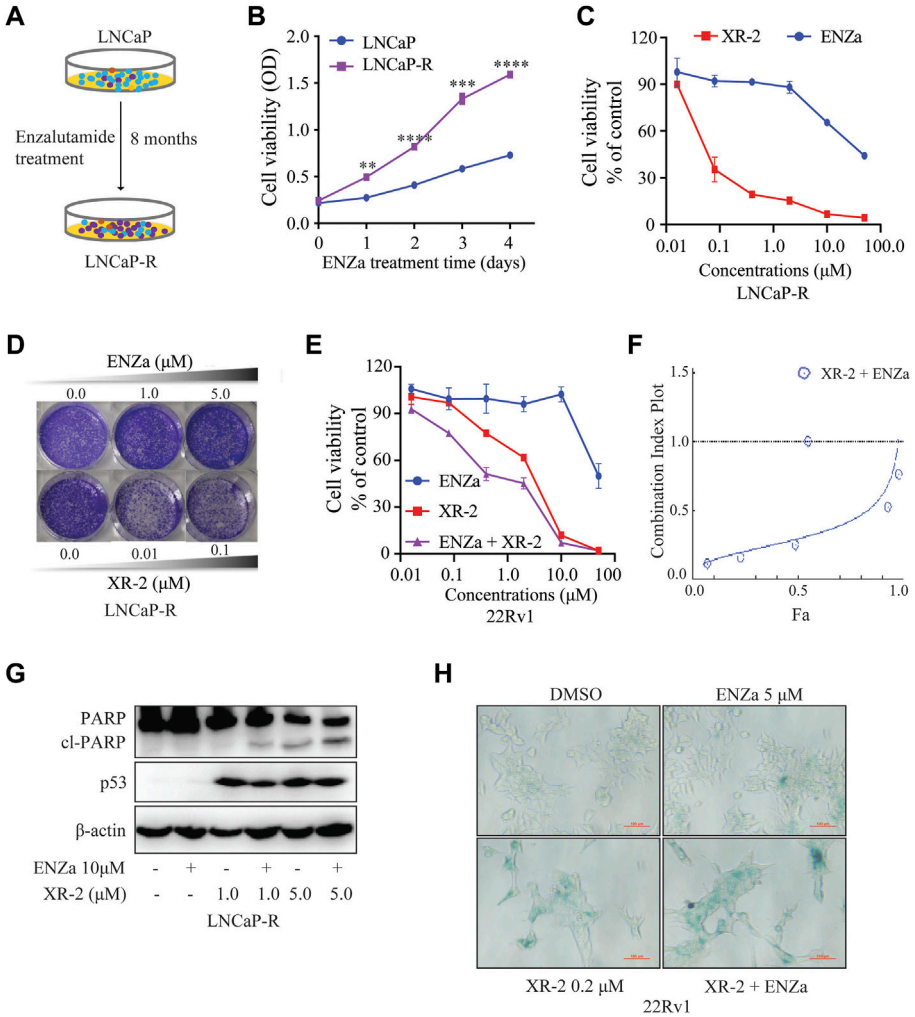


**FIGURE 6 |** XR-2 inhibits the viability of enzalutamide-resistant CRPC cells. **(A)** Sketch map about the construction of LNCaP-R cells. **(B)** LNCaP and LNCaP-R cells were treated with enzalutamide 5 μM for days, and cell proliferation was examined with the CCK8 assay. **(C)** LNCaP-R cells were treated with different concentrations of XR-2 and enzalutamide for 72 h, and cell proliferation was assessed with the CCK8 assay. **(D)** Crystal violet staining of LNCaP-R cells treated with different concentrations of XR-2 and enzalutamide for 12–14 days **(E)** 22Rv1 cells were treated with different concentrations of XR-2, enzalutamide or both agents combined for 72 h, and cell proliferation was evaluated with the CCK8 assay. **(F)** The combination index of XR-2 and enzalutamide was calculated by CompuSyn software. **(G)** LNCaP-R cells were treated with XR-2, enzalutamide or both agents combined for 24 h, and PARP1, p53 and β-actin protein levels were measured by Western blot analysis. **(H)** 22Rv1 cells were treated with the indicated concentrations of XR-2, enzalutamide or both agents combined for 72 h, and β-galactosidase staining was performed. Experiments were performed in triplicates. All results are shown as mean ± SD. $^{*}p < 0.05$, $^{**}p < 0.01$, $^{***}p < 0.001$ vs. control group.

results indicated that enzalutamide could only inhibit 22Rv1 tumor growth weakly, mainly due to ARV7 overexpression, while both XR-2 monotherapy and combination therapy suppressed 22Rv1 tumor progression and decreased tumor weight significantly (**Supplementary Figure S6A, S7A,B**). Interestingly, the combination therapy revealed a more effective tumor inhibition activity than XR-2 or enzalutamide monotherapy. We also evaluated whether XR-2 treatment activated p53 protein levels *in vivo*; as shown in **Supplementary Figure S6B**, the tumor p53 protein levels were remarkably accumulated in both XR-2 monotherapy and combination therapy groups. Moreover, XR-2 was tolerable to the SCID mice, as the mice bodyweight of the XR-2 monotherapy and combination therapy groups nearly had no change compared with the vehicle group (**Figure 7C**). Further analysis revealed that both XR-2 monotherapy and combination therapy did not influence the weight of the critical organs and blood neutrophil counts of mice, which reminded the favourable *in vivo* safety of XR-2 (**Figures 7D,E**). Moreover, immunohistochemistry assay results proved that XR-2 reduced Ki-67 protein levels and induced cleaved caspase3 protein accumulation compared with the vehicle group. Compared with monotherapy, the combination therapy enhanced these changes in protein levels (**Figure 7F**). Taken together, our data indicated that XR-2 could inhibit the growth of CRPC both *in vitro* and *in vivo*.

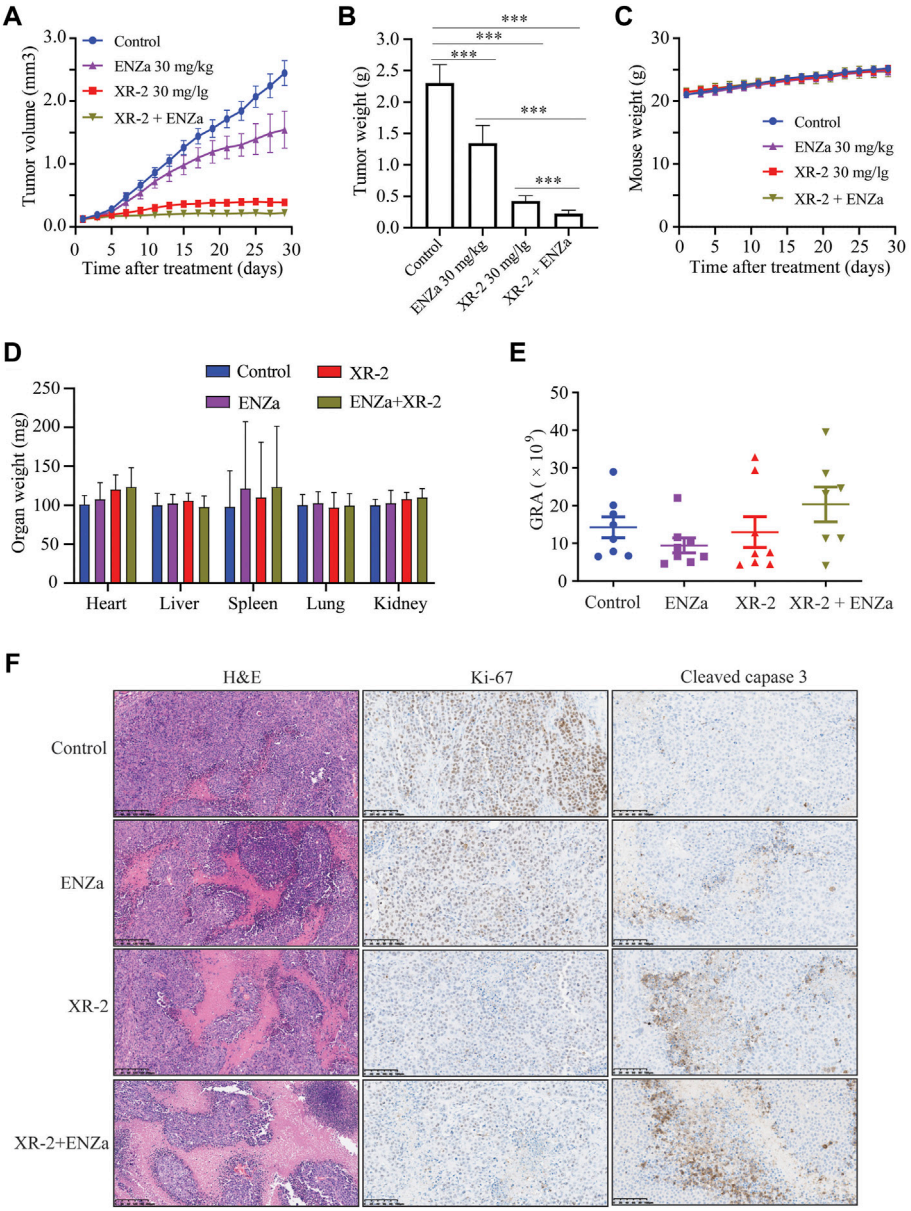


**FIGURE 7 |** XR-2 suppresses 22Rv1 cell-derived xenograft progress *in vivo*. **(A)** Xenografts arising from 22Rv1 cells were treated with blank control, 30 mg/kg of XR-2, 30 mg/kg of enzalutamide and 30 mg/kg of XR-2 plus 30 mg/kg enzalutamide once a day for 4 weeks, and tumor growth was monitored every other day. **(B)** Tumor weight at the last observation day. **(C)** Mice were weighed by electronic scale every other day. **(D)** Critical organs of the mice were weighed at the last observation day. **(E)** Blood neutrophil counts of the mice at the last observation day. **(F)** Immunohistochemical analysis of Ki67 and cleaved caspase 3 levels in harvested tumor s. All results are shown as mean ± SD. $^{*}p < 0.05$, $^{**}p < 0.01$, $^{***}p < 0.001$ vs. control group.

## DISCUSSION

Drug resistance such as AR pathway alterations, oncogene activation and lineage plasticity have been widely reported to restrict the clinical benefits of SGAs. (Watson et al., 2015; Ge et al., 2020; Isaacsson Velho et al., 2020). Studies have demonstrated that the inactivation of the tumor suppressor p53 was associated with poor response to SGAs and lineage plasticity in PCa. (De Laere et al., 2019; Nyquist et al., 2020). In this work, we identified a compound XR-2 that effectively inhibits MDM2–p53 interaction and selectively reactivates the p53 pathway. XR-2 could suppress the proliferation activity of CRPC cells in a p53-dependent manner. Besides, XR-2 induces cell cycle arrest and apoptosis in wild-type p53 CRPC cell lines. Further study proves that XR-2 could also block the AR pathway and shows a synergistic effect with enzalutamide through p53 pathway reactivation and AR pathway inhibition. Moreover, XR-2 could overcome enzalutamide resistance both *in vitro* and *in*

*vivo*. These results tend to support the potential of XR-2 monotherapy and XR-2 plus enzalutamide in the treatment of SGA-resistant CRPC.

MDM2 overexpression and p53 mutation in PCa is associated with worse clinical outcomes. MDM2 overexpression was a prognostic of the development of metastatic disease as well as overall mortality. (Khor et al., 2009; Venkatesan et al., 2018). *TP53* inactivation was established as a biomarker to predict abiraterone or enzalutamide resistance in metastatic CRPC. (Maughan et al., 2018; De Laere et al., 2019). Therefore, the above observations suggest that MDM2 inhibition in PCa may have a dual suppressive effect by blocking MDM2 function and activating p53 functions. Thus, the inhibition of MDM2 represents an attractive strategy for the treatment of PCa with wild type p53, especially in combination with the current standard of care therapies. Efforts had been made to evaluate the effects of MDM2–p53 inhibitors in PCa treatment. The first-generation MDM2 inhibitor Nutlin-3 could inhibit androgen receptor-driven c-FLIP expression, resulting in apoptosis of PCa cells and enhancing the curative effect of chemotherapy. Another MDM2 inhibitor MI-219 showed the sensitisation of PCa cells to radiotherapy and androgen deprivation therapy. (Chappell et al., 2012; Feng et al., 2016; Logan et al., 2016). However, whether MDM2-p53 inhibitor could combine SGAs to treat CRPC is still unanswered. Previous work has proved that p53 could inhibit AR expression levels through combining with p53 DNA-binding site of *AR* gene. (Alimirah et al., 2007; Chopra et al., 2018). Our work indicates that XR-2 is able to induce p53 accumulation in wild-type p53 PCa cells, as a result, accumulated p53 downregulates the AR protein expression levels. Moreover, MDM2 E3 ligase activity is reported to play vital role in proteasome-mediated AR ubiquitylation and degradation. (Lin et al., 2002). Many researches have demonstrated that MDM2-p53 inhibitors could upregulate MDM2 expression levels in wild-type p53 cancer cells, our work also finds XR-2 upregulates MDM2 levels in PCa cells, therefore, promoting MDM2-regulated AR and ARV7 degradation through proteasome pathway. Theoretically, these mechanisms may explain the combination of MDM2-p53 inhibitor XR-2 and AR antagonist enzalutamide induces enhanced AR pathway inhibition. All in all, the AR downregulating effects of XR-2 combine with the AR antagonizing effects of enzalutamide contribute to the role of the combination in overcoming AR pathway alterations such as AR mutation, AR overexpression and AR splice variants induced by SGA drug resistance.

Despite clinical trials of some MDM2–p53 inhibitors in haematologic and solid malignancies, none of these inhibitors reached regulatory approval and mainly imputed gastrointestinal and bone marrow-related toxicities. (Konopleva et al., 2020). In this study, we develop a novel *cis-cis* isomer of spirooxindole-based PEG modification MDM2 inhibitor XR-2, which has favourable water solubility, so that parenteral administration partially reduced irritation to the gastrointestinal tract. Blood cell analysis also proves that XR-2 does not affect the neutrophil count. MDM2–p53 inhibitors have broad-spectrum anti-tumor activity in many other studies. (Yi et al., 2018; Fang et al., 2020). XR-2 also demonstrated anti-tumor activity *in vivo* in various tumor types. In NCI-H460, which is a p53 wild-type lung cancer cell line model, XR-2 suppressed NCI-H460 tumor progression effectively, and XR-2 did not delay the weight gain of mice that received the therapeutic dose. Similarly, XR-2 could significantly inhibit the progression of liver cancer cell line HepG2-derived tumor *in vivo* with acceptable safety. More importantly, in a p53 wild-type osteosarcoma cell line SJSA1-derived xenograft model, XR-2 shows stronger tumor inhibition activity than RG-7388, which is under clinical investigation. (Ding et al., 2013). XR-2 nearly lost its influence on mouse weight even under treatment with 100 mg/kg dose, which converts to a human equivalent dose of approximately 500 mg for a 60-kg patient. These data illustrate the safety and effectiveness of XR-2 in cancer treatment.

## CONCLUSION

MDM2 inhibitor (XR-2) possesses potently prostate cancer progresses inhibition activity both *in vitro* and *in vivo*. XR-2 shows a synergistic effect with enzalutamide and overcomes enzalutamide resistance. This is the first report on MDM2-p53 inhibitor overcoming SGAs resistance which provide convincing clues for further clinical trial of the combination therapy of SGAs with MDM2 inhibitor in prostate cancer.

## DATA AVAILABILITY STATEMENT

The datasets presented in this study can be found in online repositories. The names of the repository/repositories and accession number(s) can be found in the article/ **Supplementary Material**.

## ETHICS STATEMENT

The animal study was reviewed and approved by KeyGEN BioTECH Institutional Animal Care and Use Committee.

## AUTHOR CONTRIBUTIONS

ML, SH, and PJ designed the study and wrote the paper. MW, JC, HH, YL, and LW performed the major part of the experimental study. ML, SH, MW, JC, HH, SL, JL, LZ, WH, and GS contributed to data analysis. All authors analyzed the results and approved the final version of the manuscript.

## FUNDING

This work was in part supported by National Natural Science Foundation of China. (Grant number. 82104231); Project funded by China Postdoctoral Science Foundation (Grant number. 2021M700504); Beijing Hospital Clinical Research 121 Project (Grant number. BJ-2018-090); Beijing Municipal

Science and Technology Project (Grant number. Z201100005620007); Discipline Construction Project of Peking Union Medical College (Grant number. 201920202101).

## SUPPLEMENTARY MATERIAL

The Supplementary Material for this article can be found online at: https://www.frontiersin.org/articles/10.3389/fphar.2022.871259/full#supplementary-material

**Supplementary Figure S1 |** The procedure for the synthesis of compound XR-2 and its analogues.

**Supplementary Figure S2 |** Primary evaluation of pegylation spirooxindole derivatives (PSD) tumor inhibition activity *in vivo*. **(A)** The stereochemical structure of *cis-cis* isomer XR-2 and its *trans-cis* isomer XR-2-2. **(B)** Xenografts arising from SJSA1 cells were treated with blank control, 30 mg/kg compound 2, 30 mg/kg XR-2 (racemic), XR-2 (laevo) and XR-2 (dextro) once a day for 14 days, tumour growth was monitored every other day. **(C)** Mice image at the last monitor day. **(D)** Tumour image at the last monitor day.

**Supplementary Figure S3 |** The effects of XR-2 on MDM2-p53 binding activity were detected by HTRF assay. Experiments were in triplicates. All results are shown as mean ± s.d.

**Supplementary Figure S4 |** The influence of XR-2 on CRPC cell lines apoptosis. **(A, B)** LNCaP, 22Rv1 and DU145 cells were treated with DMSO and XR-2 5 μM for 24 h, the mRNA levels of *Bax* and *GADD45A* were measured by quantitative-PCR and normalized to GAPDH. Experiments were in triplicates. All results are shown as mean ± s.d. $^{*}P < 0.05$, $^{**}P < 0.01$, $^{***}P < 0.001$ vs. control group.

**Supplementary Figure S5 |** XR-2 blocks AR pathway and shows synergistic effects with enzalutamide. **(A)** Venn Diagram about up-regulated numbers of differentially expressed genes after each treatment. **(B)** Venn Diagram about down-regulated numbers of differentially expressed genes after each treatment. **(C)** Representative AR pathway genes in response to enzalutamide, and combination treatment. **(D)** 22Rv1 cells were treated with XR-2, enzalutamide or both agents combined for 24 h, then cells were lysed, p53 and AR protein levels were measured by western blot analysis. **(E)** 22Rv1 cells were treated with XR-2, enzalutamide or both agents combined for 24 h, the mRNA levels of *p21* were measured by quantitative-PCR and normalized to GAPDH. **(F)** C4-2 cells were treated with XR-2, enzalutamide or both agents combined for 24 h, then cells were lysed, p53 and AR protein levels were measured by western blot analysis. **(G)** C4-2 cells were treated with XR-2, enzalutamide or both agents combined for 24 h, the mRNA levels of *p21* were measured by quantitative-PCR and normalized to GAPDH. Experiments were in triplicates. All results are shown as mean ± s.d. $^{*}P < 0.05$, $^{**}P < 0.01$, $^{***}P < 0.001$ vs. control group.

**Supplementary Figure S6 |** XR-2 suppresses 22Rv1 cells derived xenografts progress *in vivo*. **(A)** Xenografts arising from 22Rv1 cells were treated with blank control, 30 mg/kg XR-2, 30 mg/kg enzalutamide and 30 mg/kg XR-2 combined with 30 mg/kg enzalutamide once a day for 4 weeks, tumor image at the last monitor day was photographed. **(B)** 22Rv1 cells derived tumors were lysed by RIPA buffer, p53 and GAPDH protein levels were measured by western blot analysis.

**Supplementary Figure S7 |** XR-2 suppresses wide types cancer cells derived xenografts progress *in vivo*. **(A)** Xenografts arising from NCI-H460 cells were treated with blank control and 30 mg/kg XR-2 once a day for 31 days, tumor growth was monitored every other day. **(B)** Mice image at the last monitor day. **(C)** Mice weight was weighed by electronic scale every other day. **(D)** Xenografts arising from HepG2 cells were treated with blank control and 30 mg/kg XR-2 once a day for 28 days, tumor growth was monitored every other day. **(E)** Mice image at the last monitor day. **(F)** Mice weight was weighed by electronic scale every other day. **(G)** Xenografts arising from SJSA1 cells were treated with blank control, 50 mg/kg XR-2, 100 mg/kg XR-2 and 50 mg/kg RG-7388 once a day for 14 days, tumor growth was monitored every other day. **(H)** Mice image at the last monitor day. **(I)** Mice weight was weighed by electronic scale every other day. All results are shown as mean ± s.d. $^{*}P < 0.05$.

## REFERENCES


Alimirah, F., Panchanathan, R., Chen, J., Zhang, X., Ho, S. M., and Choubey, D. (2007). Expression of Androgen Receptor Is Negatively Regulated by P53. *Neoplasia* 9 (12), 1152–1159. doi:10.1593/neo.07769

Antonarakis, E. S., Lu, C., Luber, B., Liang, C., Wang, H., Chen, Y., et al. (2018). Germline DNA-Repair Gene Mutations and Outcomes in Men with Metastatic Castration-Resistant Prostate Cancer Receiving First-Line Abiraterone and Enzalutamide. *Eur. Urol.* 74 (2), 218–225. doi:10.1016/j.eururo.2018.01.035

Chappell, W. H., Lehmann, B. D., Terrian, D. M., Abrams, S. L., Steelman, L. S., and McCubrey, J. A. (2012). p53 Expression Controls Prostate Cancer Sensitivity to Chemotherapy and the MDM2 Inhibitor Nutlin-3. *Cell Cycle* 11 (24), 4579–4588. doi:10.4161/cc.22852

Chi, K., Hotte, S. J., Joshua, A. M., North, S., Wyatt, A. W., Collins, L. L., et al. (2015). Treatment of mCRPC in the AR-axis-targeted Therapy-Resistant State. *Ann. Oncol.* 26 (10), 2044–2056. doi:10.1093/annonc/mdv267

Chi, K. N., Agarwal, N., Bjartell, A., Chung, B. H., Pereira de Santana Gomes, A. J., Given, R., et al. (2019). Apalutamide for Metastatic, Castration-Sensitive Prostate Cancer. *N. Engl. J. Med.* 381 (1), 13–24. doi:10.1056/NEJMoa1903307

Chopra, H., Khan, Z., Contreras, J., Wang, H., Sedrak, A., and Zhu, Y. (2018). Activation of P53 and Destabilization of Androgen Receptor by Combinatorial Inhibition of MDM2 and MDMX in Prostate Cancer Cells. *Oncotarget* 9 (5), 6270–6281. doi:10.18632/oncotarget.23569

Ciccarese, C., Massari, F., Iacovelli, R., Fiorentino, M., Montironi, R., Di Nunno, V., et al. (2017). Prostate Cancer Heterogeneity: Discovering Novel Molecular Targets for Therapy. *Cancer Treat. Rev.* 54, 68–73. doi:10.1016/j.ctrv.2017.02.001

Cronauer, M. V., Schulz, W. A., Burchardt, T., Ackermann, R., and Burchardt, M. (2004). Inhibition of P53 Function Diminishes Androgen Receptor-Mediated Signaling in Prostate Cancer Cell Lines. *Oncogene* 23 (20), 3541–3549. doi:10.1038/sj.onc.1207346

de Bono, J. S., Logothetis, C. J., Molina, A., Fizazi, K., North, S., Chu, L., et al. (2011). Abiraterone and Increased Survival in Metastatic Prostate Cancer. *N. Engl. J. Med.* 364 (21), 1995–2005. doi:10.1056/NEJMoa1014618

De Laere, B., Oeyen, S., Mayrhofer, M., Whitington, T., van Dam, P. J., Van Oyen, P., et al. (2019). TP53 Outperforms Other Androgen Receptor Biomarkers to Predict Abiraterone or Enzalutamide Outcome in Metastatic Castration-Resistant Prostate Cancer. *Clin. Cancer Res.* 25 (6), 1766–1773. doi:10.1158/1078-0432.CCR-18-1943

Ding, Q., Zhang, Z., Liu, J. J., Jiang, N., Zhang, J., Ross, T. M., et al. (2013). Discovery of RG7388, a Potent and Selective P53-MDM2 Inhibitor in Clinical Development. *J. Med. Chem.* 56 (14), 5979–5983. doi:10.1021/jm400487c

Duffy, M. J., Synnott, N. C., and O'Grady, S. (2022). Targeting P53 for the Treatment of Cancer. *Semin. Cancer Biol.* 79, 58–67. doi:10.1016/j.semcancer.2020.07.005

Fang, Y., Liao, G., and Yu, B. (2020). Small-molecule MDM2/X Inhibitors and PROTAC Degraders for Cancer Therapy: Advances and Perspectives. *Acta Pharm. Sin B* 10 (7), 1253–1278. doi:10.1016/j.apsb.2020.01.003

Feng, F. Y., Zhang, Y., Kothari, V., Evans, J. R., Jackson, W. C., Chen, W., et al. (2016). MDM2 Inhibition Sensitizes Prostate Cancer Cells to Androgen Ablation and Radiotherapy in a P53-dependent Manner. *Neoplasia* 18 (4), 213–222. doi:10.1016/j.neo.2016.01.006

Fizazi, K., Shore, N., Tammela, T. L., Ulys, A., Vjaters, E., Polyakov, S., et al. (2020). Nonmetastatic, Castration-Resistant Prostate Cancer and Survival with Darolutamide. *N. Engl. J. Med.* 383 (11), 1040–1049. doi:10.1056/NEJMoa2001342

Ge, R., Wang, Z., Montironi, R., Jiang, Z., Cheng, M., Santoni, M., et al. (2020). Epigenetic Modulations and Lineage Plasticity in Advanced Prostate Cancer. *Ann. Oncol.* 31 (4), 470–479. doi:10.1016/j.annonc.2020.02.002

Harris, W. P., Mostaghel, E. A., Nelson, P. S., and Montgomery, B. (2009). Androgen Deprivation Therapy: Progress in Understanding Mechanisms of Resistance and Optimizing Androgen Depletion. *Nat. Clin. Pract. Urol.* 6 (2), 76–85. doi:10.1038/ncpuro1296

Hussain, M., Mateo, J., Fizazi, K., Saad, F., Shore, N., Sandhu, S., et al. (2020). Survival with Olaparib in Metastatic Castration-Resistant Prostate Cancer. *N. Engl. J. Med.* 383 (22), 2345–2357. doi:10.1056/NEJMoa2022485

Isaacsson Velho, P., Fu, W., Wang, H., Mirkheshti, N., Qazi, F., Lima, F. A. S., et al. (2020). Wnt-pathway Activating Mutations Are Associated with Resistance to First-Line Abiraterone and Enzalutamide in Castration-Resistant Prostate Cancer. *Eur. Urol.* 77 (1), 14–21. doi:10.1016/j.eururo.2019.05.032

Khor, L. Y., Bae, K., Paulus, R., Al-Saleem, T., Hammond, M. E., Grignon, D. J., et al. (2009). MDM2 and Ki-67 Predict for Distant Metastasis and Mortality in Men Treated with Radiotherapy and Androgen Deprivation for Prostate Cancer: RTOG 92-02. *J. Clin. Oncol.* 27 (19), 3177–3184. doi:10.1200/JCO.2008.19.8267

Konopleva, M., Martinelli, G., Daver, N., Papayannidis, C., Wei, A., Higgins, B., et al. (2020). MDM2 Inhibition: an Important Step Forward in Cancer Therapy. *Leukemia* 34 (11), 2858–2874. doi:10.1038/s41375-020-0949-z

Ku, S. Y., Rosario, S., Wang, Y., Mu, P., Seshadri, M., Goodrich, Z. W., et al. (2017). Rb1 and Trp53 Cooperate to Suppress Prostate Cancer Lineage Plasticity, Metastasis, and Antiandrogen Resistance. *Science* 355 (6320), 78–83. doi:10.1126/science.aah4199

Levine, A. J. (2020). p53: 800 Million Years of Evolution and 40 Years of Discovery. *Nat. Rev. Cancer* 20 (8), 471–480. doi:10.1038/s41568-020-0262-1

Li, Y., Yang, J., Aguilar, A., McEachern, D., Przybranowski, S., Liu, L., et al. (2019). Discovery of MD-224 as a First-In-Class, Highly Potent, and Efficacious Proteolysis Targeting Chimera Murine Double Minute 2 Degrader Capable of Achieving Complete and Durable Tumor Regression. *J. Med. Chem.* 62 (2), 448–466. doi:10.1021/acs.jmedchem.8b00909

Lin, H. K., Wang, L., Hu, Y. C., Altuwaijri, S., and Chang, C. (2002). Phosphorylation-dependent Ubiquitylation and Degradation of Androgen Receptor by Akt Require Mdm2 E3 Ligase. *EMBO J.* 21 (15), 4037–4048. doi:10.1093/emboj/cdf406

Logan, I. R., McClurg, U. L., Jones, D. L., O'Neill, D. J., Shaheen, F. S., Lunec, J., et al. (2016). Nutlin-3 Inhibits Androgen Receptor-Driven C-FLIP Expression, Resulting in Apoptosis of Prostate Cancer Cells. *Oncotarget* 7 (46), 74724–74733. doi:10.18632/oncotarget.12542

Maughan, B. L., Guedes, L. B., Boucher, K., Rajoria, G., Liu, Z., Klimek, S., et al. (2018). p53 Status in the Primary Tumor Predicts Efficacy of Subsequent Abiraterone and Enzalutamide in Castration-Resistant Prostate Cancer. *Prostate Cancer Prostatic Dis.* 21 (2), 260–268. doi:10.1038/s41391-017-0027-4

Mu, P., Zhang, Z., Benelli, M., Karthaus, W. R., Hoover, E., Chen, C. C., et al. (2017). SOX2 Promotes Lineage Plasticity and Antiandrogen Resistance in TP53- and RB1-Deficient Prostate Cancer. *Science* 355 (6320), 84–88. doi:10.1126/science.aah4307

Neeb, A., Herranz, N., Arce-Gallego, S., Miranda, S., Buroni, L., Yuan, W., et al. (2021). Advanced Prostate Cancer with ATM Loss: PARP and ATR Inhibitors. *Eur. Urol.* 79 (2), 200–211. doi:10.1016/j.eururo.2020.10.029

Niu, Y., Chang, T. M., Yeh, S., Ma, W. L., Wang, Y. Z., and Chang, C. (2010). Differential Androgen Receptor Signals in Different Cells Explain Why Androgen-Deprivation Therapy of Prostate Cancer Fails. *Oncogene* 29 (25), 3593–3604. doi:10.1038/onc.2010.121

Nyquist, M. D., Corella, A., Coleman, I., De Sarkar, N., Kaipainen, A., Ha, G., et al. (2020). Combined TP53 and RB1 Loss Promotes Prostate Cancer Resistance to a Spectrum of Therapeutics and Confers Vulnerability to Replication Stress. *Cell Rep* 31 (8), 107669. doi:10.1016/j.celrep.2020.107669

Penson, D. F., Armstrong, A. J., Concepcion, R., Agarwal, N., Olsson, C., Karsh, L., et al. (2016). Enzalutamide versus Bicalutamide in Castration-Resistant Prostate Cancer: The STRIVE Trial. *J. Clin. Oncol.* 34 (18), 2098–2106. doi:10.1200/JCO.2015.64.9285

Shu, L., Li, Z., Gu, C., and Fishlock, D. (2013). Synthesis of a Spiroindolinone Pyrrolidinecarboxamide MDM2 Antagonist. *Org. Process. Res. Dev.* 17 (2), 247–256. doi:10.1021/op3003213

Skalniak, L., Surmiak, E., and Holak, T. A. (2019). A Therapeutic Patent Overview of MDM2/X-Targeted Therapies (2014-2018). *Expert Opin. Ther. Pat* 29 (3), 151–170. doi:10.1080/13543776.2019.1582645

Sung, H., Ferlay, J., Siegel, R. L., Laversanne, M., Soerjomataram, I., Jemal, A., et al. (2021). Global Cancer Statistics 2020: GLOBOCAN Estimates of Incidence and Mortality Worldwide for 36 Cancers in 185 Countries. *CA Cancer J. Clin.* 71 (3), 209–249. doi:10.3322/caac.21660

Tovar, C., Higgins, B., Kolinsky, K., Xia, M., Packman, K., Heimbrook, D. C., et al. (2011). MDM2 Antagonists Boost Antitumor Effect of Androgen Withdrawal: Implications for Therapy of Prostate Cancer. *Mol. Cancer* 10, 49. doi:10.1186/1476-4598-10-49

Venkatesan, T., Alaseem, A., Chinnaiyan, A., Dhandayuthapani, S., Kanagasabai, T., Alhazzani, K., et al. (2018). MDM2 Overexpression Modulates the Angiogenesis-Related Gene Expression Profile of Prostate Cancer Cells. *Cells* 7 (5). doi:10.3390/cells7050041

Wade, M., Li, Y. C., and Wahl, G. M. (2013). MDM2, MDMX and P53 in Oncogenesis and Cancer Therapy. *Nat. Rev. Cancer* 13 (2), 83–96. doi:10.1038/nrc3430

Watson, P. A., Arora, V. K., and Sawyers, C. L. (2015). Emerging Mechanisms of Resistance to Androgen Receptor Inhibitors in Prostate Cancer. *Nat. Rev. Cancer* 15 (12), 701–711. doi:10.1038/nrc4016

Wyatt, A. W., Azad, A. A., Volik, S. V., Annala, M., Beja, K., McConeghy, B., et al. (2016). Genomic Alterations in Cell-free DNA and Enzalutamide Resistance in Castration-Resistant Prostate Cancer. *JAMA Oncol.* 2 (12), 1598–1606. doi:10.1001/jamaoncol.2016.0494

Yi, H., Yan, X., Luo, Q., Yuan, L., Li, B., Pan, W., et al. (2018). A Novel Small Molecule Inhibitor of MDM2-P53 (APG-115) Enhances Radiosensitivity of Gastric Adenocarcinoma. *J. Exp. Clin. Cancer Res.* 37 (1), 97. doi:10.1186/s13046-018-0765-8

Zhao, Y., Liu, L., Sun, W., Lu, J., McEachern, D., Li, X., et al. (2013). Diastereomeric Spirooxindoles as Highly Potent and Efficacious MDM2 Inhibitors. *J. Am. Chem. Soc.* 135 (19), 7223–7234. doi:10.1021/ja3125417

**Conflict of Interest:** The authors declare that the research was conducted in the absence of any commercial or financial relationships that could be construed as a potential conflict of interest.

**Publisher's Note:** All claims expressed in this article are solely those of the authors and do not necessarily represent those of their affiliated organizations, or those of the publisher, the editors and the reviewers. Any product that may be evaluated in this article, or claim that may be made by its manufacturer, is not guaranteed or endorsed by the publisher.

frontiers | Frontiers in Oncology

REVIEW
published: 06 May 2022
doi: 10.3389/fonc.2022.866154

# Research Advances on Anti-Cancer Natural Products

*Meng Guo[1†], Jie Jin[1†], Dong Zhao[2†], Zheng Rong[1], Lu-Qi Cao[2], Ai-Hong Li[3], Xiao-Ying Sun[1], Li-Yi Jia[1], Yin-Di Wang[1], Ling Huang[1], Yi-Heng Li[4], Zhong-Jing He[4], Long Li[2], Rui-Kang Ma[2], Yi-Fan Lv[2], Ke-Ke Shao[2] and Hui-Ling Cao[1,2,3,4*]*

[1] College of Pharmacy, Shaanxi University of Chinese Medicine, Xianyang, China, [2] Xi'an Key Laboratory of Basic and Translation of Cardiovascular Metabolic Disease, Shaanxi Key Laboratory of Ischemic Cardiovascular Disease, Institute of Basic and Translational Medicine, Xi'an Medical University, Xi'an, China, [3] Shaanxi Key Laboratory of Chinese Herb and Natural Drug Development, Medicine Research Institute, Shaanxi Pharmaceutical Holding Group Co., LTD, Xi'an, China, [4] College of Life Sciences, Northwest University, Xi'an, China

Malignant tumors seriously threaten people's health and life worldwide. Natural products, with definite pharmacological effects and known chemical structures, present dual advantages of Chinese herbs and chemotherapeutic drug. Some of them exhibit favorable anti-cancer activity. Natural products were categorized into eight classes according to their chemical structures, including alkaloids, terpenoids and volatile oils, inorganic salts, phenylpropanoids, flavonoids and isoflavones, quinone, saponins and polysaccharides. The review focused on the latest advances in anti-cancer activity of representative natural products for every class. Additionally, anti-cancer molecular mechanism and derivatization of natural products were summarized in detail, which would provide new core structures and new insights for anti-cancer new drug development.

**Keywords: natural product, anti-cancer, core structure, derivatization, molecular mechanism**

OPEN ACCESS

***Edited by:***
*Leli Zeng,*
*Sun Yat-sen University, China*

***Reviewed by:***
*Bin Yu,*
*Zhengzhou University, China*
*Xiao Jun Yao,*
*Macau University of Science and Technology, Macao SAR, China*

****Correspondence:***
*Hui-Ling Cao*
*caohuiling_jzs@xiyi.edu.cn*

*[†]These authors have contributed equally to this work*

***Specialty section:***
*This article was submitted to Pharmacology of Anti-Cancer Drugs, a section of the journal Frontiers in Oncology*

***Received:*** *30 January 2022*
***Accepted:*** *07 March 2022*
***Published:*** *06 May 2022*

***Citation:***
*Guo M, Jin J, Zhao D, Rong Z, Cao L-Q, Li A-H, Sun X-Y, Jia L-Y, Wang Y-D, Huang L, Li Y-H, He Z-J, Li L, Ma R-K, Lv Y-F, Shao K-K and Cao H-L (2022) Research Advances on Anti-Cancer Natural Products. Front. Oncol. 12:866154. doi: 10.3389/fonc.2022.866154*

## 1 INTRODUCTION

Malignant tumors, as the second leading death cause, seriously threaten people's health and life worldwide. It was estimated that there were approximately19.3 million new cancer cases and 10 million cancer deaths worldwide in 2020 (1). Chemotherapeutic drugs are the major therapy, which includes cytotoxic drugs, hormonal drugs, biological response regulators, monoclonal antibodies, adjuvants and others. Although they suppress tumor growth, their adverse toxic effects frequently affect patients' health and life quality. For instance, renal or liver injury, myocardial cell contractile dysfunction, abnormal blood coagulation, serious gastrointestinal reactions and so on. New target drugs significantly promote survival rate of cancer patients, but they are susceptible to drug resistance (2).

There are about 11,146 medical plants in China and 200 ones exhibit anti-cancer activity, such as Radix Sophorae Subprostratae, Black Nightshade, Taxus mairei, etc (3, 4). Natural products are pharmacological components extracted and separated from medical plants, animals or minerals and identified chemical structures by chemical and physical techniques. On the one hand, as major active components in Chinese herbs, they exhibit definite pharmacological effects and high security based on thousands of clinical practice. On the other hand, they have known chemical structure to facilitate new

drug development (5, 6). As a result, natural products present dual advantages of Chinese herbs and Chemotherapeutic drugs. Some of them exhibit favorable anti-cancer activity and would provide new core structures and new insights anti-cancer new drug development. Natural products were divided into eight categories according to their chemical structures, including alkaloids, terpenoids and volatile oils, inorganic salts, phenylpropanoids, flavonoids and isoflavones, quinone, saponins, polysaccharides (3–6). The review summarized research advances in anti-cancer activity of representative natural products for every class and focused on their anti-cancer molecular mechanism and derivatization, which would provide new core structures and new insights for anti-cancer new drug development.

## 2 ANTI-CANCER FUNCTIONS OF NATURAL PRODUCTS

Many natural products exhibit anti-cancer activity, which are divided into eight categories according to their chemical structures. (1) Alkaloids, such as harringtonine, camptothecin, vincristine, matrine, evodiamine and evodiamine. (2) Terpenoids and volatile oils, such as artemisinin, paclitaxel and triptolide. (3) Inorganic salts, such as $As_2O_3$. (4) Phenylpropanoids, such as podophyllotoxin. (5) Flavonoids and isoflavones, such as genistein, apigenin, and baicalein. (6) Quinones, such as tanshinone and emodin. (7) Saponins, such as ginsenoside. (8) Polysaccharides, such as lycium barbarum polysaccharide and lentinan (3–6). The review focused on research advances in anti-cancer activity of representative natural products for every category, which was expected to provide new core structures and new insights for anti-cancer new drug development.

### 2.1 Alkaloids

Alkaloids refer to a class of natural products with N-atom in the chemical structure, such as harringtonine, camptothecin, vincristine, matrine, evodiamine and rutaecarpine. The alkaloids are divided into eight categories according to their structures, as shown in **Table 1** (6–8).

#### 2.1.1 Harringtonine

Cephalotaxus herbs has been used for anti-cancer clinical practice in ancient China. Harringtonine (**Figure 1A**), an alkaloid monomer, was extracted from Torreya Grandis in 1963. In 1973, it was demonstrated that homoharringtonine had an apparent inhibition on mouse lymphocytic leukemia cell line P388 and leukemia cell line L1210. Homoharringtonine has been used clinically since 1974 and has shown favorable curative effects on acute and chronic myeloid leukemia, non-lymphocytic leukemia, acute promyelocytic leukemia, acute monocytic leukemia, malignant lymphoma, and others. It was added to the Chinese Pharmacopoeia in 1990. In 2012, Harringtonine was approved by FDA (American Food and Drug Administration) for the treatment of acute myeloid leukemia in 2012 (9, 10).

It was indicated that Harringtonine exhibited favorable anti-cancer activity (11–14). It inhibited cervical cancer cell line HeLa proliferation and promoted cell apoptosis by down-regulating the expression of CenpB (centromeric protein) to prevent cell cycle progression from G2 to G1 phase (11). Harringtonine induced L1210 cell cycle arrest in G1 phase and induced HL60 cell cycle arrest in G2/M phase by down-regulating the expression of cycle related proteins such as cyclinB1 and Cdc2 (12). It promoted acute promyelocytic leukemia cell line NB4 apoptosis, which was related to the down-regulation of Mcl-1 expression in NB4 cells, had nothing with apoptosis proteins Bcl-2 or Bax (13).

Cancer cell produced drug resistance attributed to overexpression of MDR1 (multidrug resistance gene1). Harringtonine reversed drug resistance of doxorubicin-resistant human gastric cancer cell line SGC-7901/ADM [relative reversal rate, (72.44±2.92)%] by inhibiting MDR1 expression to promote cell apoptosis (14).

#### 2.1.2 Camptothecin

Camptothecin (**Figure 1B**), a pentacyclic dipoly-indole alkaloid, was first extracted from Camptothecus in 1966. It was indicated that Camptothecin had a broad-spectrum anti-cancer activity and was used for the treatment of gastric cancer, rectal cancer, and leukemia. Irinotecan, a camptothecin derivative, was launched in Japan in 1994 and was approved by US FDA two years later. It has remarkable curative effects on advanced colorectal cancer. Currently, irinotecan is the first-line clinical therapy for colorectal cancer, lung cancer, breast cancer, etc (15–20).

It was indicated that combining Camptothecin or its derivatives with other drugs established favorable anti-tumor activity, such as inhibiting the energy metabolism of tumor cells, inducing cell cycle arrest, and promoting apoptosis. The mechanism was related to the up-regulation of phosphorylation of associated proteins, such as Akt (protein kinase B), p38MAPK (mitogen-activated protein kinases), and ERK (extracellular regulated protein kinases). It is also related to the activation of the caspase-dependent pathway, downregulating the expression of anti-apoptotic protein Bcl-2, and upregulating the expression of pro-apoptotic protein Bax and cleaved caspase-3 (15–20). Combining Bufalin and Hydroxycamptothecin reduced the cell cycle arrest in G2/M and S phases in human prostate cancer cell line DU145, increasing the expression of caspase-3 and caspase-9 and inhibiting cell proliferation (15). The inhibitory effects of Hydroxycamptothecin on HeLa cells transfected with P53 gene was significantly enhanced, and the P53 gene could promote the pro-apoptosis effects of Hydroxycamptothecin on HeLa cells (16). The combination of Hydroxycamptothecin (0.625 μmol/L) and Celecoxib (30 mg/L) could promote cell apoptosis of human hepatoma cell line SMMC-7721 by down-regulating the expression of Bcl-2 and COX-2, up-regulating the expression of Bax (17). Hydroxycamptothecin combined with 2-DG (2-deoxy-D-glucose, 5 mmol/L) could inhibit the energy metabolism and promote cell apoptosis of human breast cancer cell lines MDA-MB-231 and MCF-7 by up-regulating the expression of pro-apoptotic protein caspase-3 (18). The combination of Camptothecin and Chonglou Saponin II could promote cell apoptosis of cell lines H460 and H446 by up-regulating the phosphorylation of Akt, P38MAPK, ERK to

**TABLE 1** | Classification of anti-tumor alkaloids and representative natural products.

| Category | | Representative natural products |
|---|---|---|
| Ornithine alkaloids | Pyrrolidines | Orcosine |
| | Scopolanes | Scopolamine |
| | Pyrrolizidine | Senecioine |
| Lysine alkaloids | Piperidines | Piperine |
| | Quinolizidine | Matrine |
| | Indolizidines | Monophylline |
| Phenylalanine and tyrosine alkaloids | Amphetamines | Ephedrine |
| | Isoquinolines | Berberine |
| | Benzyl phenethylamines | Lycoline |
| Tryptophan alkaloids | Simple indoles | Indigoside |
| | Dimeric indoles | Camptothecin, vincristine |
| | Other indoles | Evodiamine |
| Anthranilic acid alkaloids | Quinolines | Dicerine |
| | Acridones | Caprinine |
| Histidine alkaloids | | Pilocarpine |
| Terpenoid alkaloids | | Gentioline, Aconitine |
| Steroidal alkaloids | | Solanine |

down-regulate the expression of anti-apoptotic protein Bcl-2 (19). The treatment with different concentration Camptothecin could affect cell morphology and increase the cell early apoptosis rate of human prostate cancer cell line PC-3 ($IC_{50}$, 23.25 μM) by affecting the expressions of Bax, cleaved caspase-3 and Bcl-2 (20).

### 2.1.3 Vincristine

Vincristine (**Figure 1C**), a dimeric indole alkaloids extracted from Catharanthus roseus, was approved by US FDA in 1963 as a microtubule inhibitor. It is mainly used for the treatment of acute lymphoblastic leukemia and Hodgkin lymphoma. It is also used in the treatment of germ cell tumors, small cell lung cancer and breast cancer (21–26).

The combination of Vincristine or its derivatives with other drugs showed favorable anti-tumor activities. The combination of Vincristine and pantoprazole could reverse drug resistance of KB/VCR-resistant cells by inhibiting the drug efflux of P-gp, inhibit cell invasion and metastasis by down-regulating the expression of MMP2 and MMP9, induce cell cycle arrest in G2/M phase by up-regulating P21expression to inhibit the phosphorylation of CyclinB1 and CDC2, promote cell apoptosis by down-regulating Bcl-2 and Bcl-xL and up-regulating PARP (poly ADP-ribose polymerase), caspase-3 and Bax (21). Vincristine combined with DDP (cisplatin) or quercetin could increase the inhibitory rate on human colorectal adenocarcinoma vincristine-resistant cell line HCT-8/V from 24.3% to 55.3% and 45.4% (22). They reversed the drug resistance of HCT-8/V cells by down-regulating the expression of P-gp to inhibit its drug efflux function and inhibited the proliferation of HCT-8/V cells and promoted apoptosis by regulating autophagy (23). Vincristine combined with Celecoxib could significantly inhibit the proliferation and migration (24) and promote cell apoptosis of oral cancer drug-resistant cell KB/VCR by down-regulating the expression of the

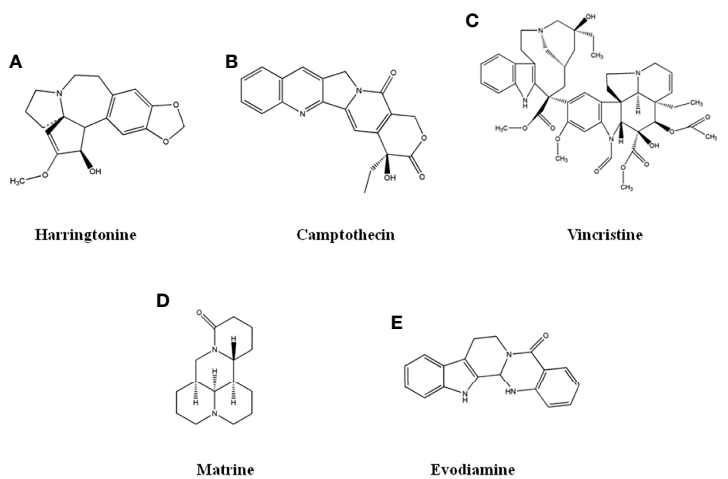


**FIGURE 1** | The structure of Alkaloid compounds. **(A)** Harringtonine. **(B)** Camptothecin. **(C)** Vincristine. **(D)** Matrine. **(E)** Evodiamine.

anti-apoptotic protein Bcl-2 and up-regulating the expression of the pro-apoptotic protein Bax (25, 26).

### 2.1.4 Matrine

Matrine (**Figure 1D**), a quinolizidine alkaloids, was extracted from the dried root of Sophora flavescens, a leguminous plant. Matrine has many pharmacological activities, such as anti-tumor, anti-virus, immune regulation, etc. It is used as an auxiliary anti-tumor drug in clinics (27).

Both Matrine or Oxymatrine presented a favorable anti-tumor activity (28–32). Phosphorylation of Histone H2AX (γH2AX) at ser139 site was essential for tumor cell proliferation and migration. Matrine or Oxymatrine could inhibit the proliferation and migration of human cervical cancer cell lines SiHa and c33a (28), which was related to the activation of p38 signaling pathway, up-regulation of the phosphorylation level of H2AX (28). Promoting EMT (epithelial-mesenchymal transition) can promote the invasion and migration of tumor cells. Oxymatrine could inhibit the invasion and metastasis of human pancreatic cancer cell line Panc-1 by inhibiting EMT, which was related to up-regulation of E-cadherin, down-regulation of vimentin, mucin 1, Snail (full-length protein) and Gli2 (core transcription factor) in Twist and hedgehog signaling pathways (29). Matrine or Oxymatrine induced cell cycle arrest, which was related to up-regulation of the expression of p21 gene, and inhibition of cell DNA synthesis and proliferation. Mucin 1 is highly expressed in tumor cells and a marker protein for normal cells to turn to tumor cells. Matrine combined with radiotherapy could down-regulate the mRNA and protein expression of mucin 1 in HepG2 cells, and significantly increase apoptosis rate of HepG2 cells (30). Matrine could induce cell cycle arrest at the G1 phase in human endometrial carcinoma cell line Ishikawa ($IC_{50}$, 20.66 μg/mL) (31). P21 gene is the upstream gene of CDKs (cell cycle-dependent kinases), which is closely related to the cell division. Oxymatrine could up-regulate the expression of the p21 gene in human gastric cancer cell line SGC-7901 to inhibit cell DNA synthesis and proliferation, and could induce SGC-7901 cell cycle arrest in G0/G1 phase (32).

### 2.1.5 Evodiamine and Rutaecarpine

Evodiamine and rutaecarpine (**Figure 1E**), indole alkaloids extracted from Evodia rutaecarpa, are used in clinical treatment for anti-cancer, gastric ulcer and oral ulcer. Evodiamine had inhibitory activity on various tumor cells with few toxicity (33–38).

Cyclin cdc25c is a key molecule in cell cycle regulation, promoting cells to enter the M phase. Evodiamine could down-regulate the expression of cyclin cdc25c and up-regulating the expression of p53 to induce human gastric cancer cell line BGC-823 cell cycle arrest in G2/M phase. It could promote cell apoptosis by up-regulating the expression of apoptosis-related proteins cleaved caspase-3, 8, 9 and cleaved PARP-1 (33). Evodiamine could inhibit cell proliferation, induce cell cycle arrest in the G2/M phase and promote cell apoptosis of SW1990 cell by up-regulating the expression of active caspase-3 and 8 (34). Evodiamine could promote cell apoptosis of human osteosarcoma cell line HOS by up-regulating the expression of caspase-3 and down-regulating the expression of Bcl-2 (35). Evodiamine could exhibited better inhibitory activity on the proliferation of human lung adenocarcinoma cell line A549 than cisplatin at 24 h and reached the best effects at 72 h (36). Rutaecarpine exhibited the best inhibitory effects on hepatoma cell line H22 cells at 24 h ($IC_{50}$, 24.81 μg/ml), on sarcoma cell line S180 cells at 48 h ($IC_{50}$, 19.35 μg/ml), on HepG2 at 72 h ($IC_{50}$,14.52 μg/ml) (37). Rutaecarpine could inhibit the proliferation of S180 cells and H22 cells *in vivo*, and it induced thymus and spleen injury of nude mice was less than that of cyclophosphamide (38).

## 2.2 Terpenoids and Volatile Oils

Terpenoids, in the form of volatile oil, were synthesized by methylpentanedioic acid pathway, including monoterpenes and sesquiterpenes, such as artemisinin, paclitaxel and triptolide (6–8).

### 2.2.1 Artemisinin

Artemisinin (**Figure 2A**), a sesquiterpene lactone with a peroxy group, was extracted from the leaves of Artemisia annua L. by Chinese scholars in 1971. Artemisinin and its derivatives are well-known anti-malarial drugs and have anti-tumor activity. The artemisinin discovery is a successful example of new drug development from natural products. Youyou Tu, a Chinese pharmacologist, won the 2015 Nobel Prize in Physiology or Medicine for artemisinin discovery.

Artemisinin and Dihydroartemisinin exhibited favorable anti-tumor activity in inhibiting proliferation, migration, and invasion of tumor cells, which was attributed to up-regulating the expression of RECK (reversion inducing cysteine rich protein with Lazal motif) and down-regulating the expression of MMP-2 and N-Cadherin (39). Artemisinin inhibited the proliferation and promote apoptosis of hepatocellular carcinoma cell lines Huh7 and SMMC-7721 by inhibiting the phosphorylation of Akt and S6 in mTOR signaling pathway of Huh7 cells and the phosphorylation of C-myc and S6 in mTOR signaling pathway of SMMC-7721 cells (40). Artemisinin induced cell cycle arrest in G/2M phase in HepG2 cells (41) or induced cell cycle arrest in G0/G1 phase in human breast cancer cell line MT40 (42) by regulating the mitochondrial pathway to inhibit cell proliferation and promote apoptosis (41).

Dihydroartemisinin, an artemisinin derivative, could inhibit tumor cell proliferation, migration, and invasion and promote apoptosis (43–46). Dihydroartemisinin could inhibit the proliferation and promote apoptosis of human pancreatic cancer cell line PANC-1, which was related to the mitochondrial pathway (43). Dihydroartemisinin could inhibit the proliferation of cutaneous T-cell lymphoma cells and promote cell apoptosis (44). Dihydroartemisinin also inhibited activity on ovarian cancer cells (45) and liver cancer cells SMMC-7721 (46).

### 2.2.2 Paclitaxel

Paclitaxel (**Figure 2B**), a diterpenoid monomer from the bark of Taxus mairei, is mainly used in the first-line clinical treatment of ovarian cancer and non-small cell lung cancer, as well as the follow-up treatment of breast cancer. It was approved by US FDA in 1992 and listed in China in 1995. Docetaxel, a drug with

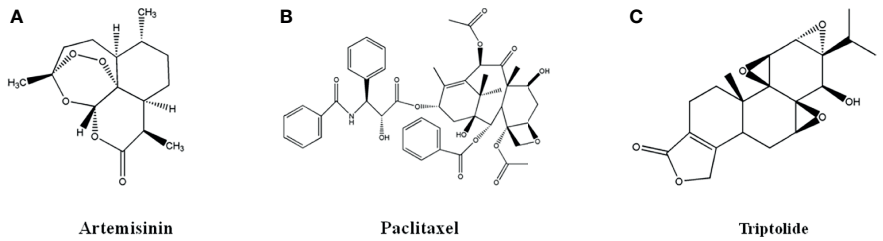


**FIGURE 2** | The structure of Terpenoids and Volatile oils. **(A)** Artemisinin. **(B)** Paclitaxel. **(C)** Triptolide.

Paclitaxel as major ingredient, was approved by US FDA in 2004 for the treatment of breast cancer, ovarian cancer and non-small cell lung cancer. Paclitaxel exerted anti-tumor activity by inhibiting tubulin depolymerization to inhibit cell mitosis to inhibit proliferation and promote cell apoptosis (47, 48).

Paclitaxel showed favorable inhibitory activity on a variety of tumor cells (47, 48). Combined with various drugs, paclitaxel could inhibit the proliferation and migration of tumor cells through promoting the secretion of immune factors, regulating the expression of EMT-related proteins, down-regulating the expression of N-Cadherin, β-Catenin and Vimentin, and up-regulating the expression of epithelial marker proteins E-Cadherin, Claudin-1 and ZO-1 (47, 48). Paclitaxel combined with luteolin could inhibit the proliferation and migration, promote apoptosis of human esophageal cancer cell lines EC109 and TE-1, which was attributed to expression changes of EMT-related proteins, down-regulation of N-Cadherin, β-Catenin and Vimentin, and up-regulation of E-Cadherin, Claudin-1 and ZO-1 (47). The curative effects *in vivo* of paclitaxel combined with PD1 antibody was better than that of single drug therapy in xenograft nude mice model with D2F2 breast cancer (48).

### 2.2.3 Triptolide

Triptolide (**Figure 2C**), epoxy diterpene lactones from the root bark of Tripterygium wilfordii, had effects of anti-tumor, anti-rheumatoid and anti-oxidation (49–52). Triptolide had inhibitory activity on human colorectal cancer, endometrial cancer, breast cancer, A549/Taxol lung cancer, thyroid cancer, mouse lymphoma cells, which was attributed to the expression of p53 gene, nucleus transcription factor and tumor necrosis factor, heat shock proteins, and estrogen receptor, the regulation of PI3K-Akt-mTOR, MAPK, Wnt-β-catenin signal pathways (49). Triptolide could promote apoptosis of human colon cancer cell line HCT116 cells by inhibiting Akt phosphorylation to promote autophagy (50). Triptolide could induce cell cycle arrest in G2/M phase of human endometrial cancer cell line Ishikawa, which was closely associated with the down-regulation of Akt and mTOR protein phosphorylation and mRNA in PI3K-Akt-mTOR pathway (51). Triptolide could significantly promote cell apoptosis and inhibit cell proliferation of human ovarian cancer cell line SKOV3 by increasing ROS and up-regulating the expression of cleaved caspase-9 and cleaved caspase-3, and down-regulating the expression of bcl-2 (52).

## 2.3 Inorganic Salt

Arsenic trioxide ($As_2O_3$), inorganic monomer, is highly toxic. $As_2O_3$ was another successful example for new drug development from natural products. Chen Zhu's team treated acute promyelocytic leukemia with all-trans retinoic acid and $As_2O_3$ and the 5-year disease-free survival rate jumped to more than 90% to reach the cure level. Dr. Chen Zhu was awarded the Ernest Butler Award of the American Society of Hematology in 2015 (8).

$As_2O_3$ could inhibit cell proliferation and promote cell apoptosis in hepatoma stem cell MHCC97H by down-regulating Bcl-2 expression (53). $As_2O_3$ could promote the apoptosis of mouse melanoma cell line B16 by up-regulating the expression of p53 and Bax, down-regulating the expression of Bcl-2 (54). APC (adenomatous polyposis coli) is a tumor suppressor gene associated with colon adenomatous polyps, colon and rectal cancer and other diseases. $As_2O_3$ (2-8 μmol/L) could up-regulate the mRNA and protein expression of APC gene, therefore, effectively inhibit the proliferation of T24 cells and promote apoptosis (55). FOXO1 (forkhead boxO1) gene is a transcription factor regulating cell growth and a tumor suppressor gene. $As_2O_3$ could up-regulate the expression of FOXO1 gene mRNA and protein, thus, inhibit cell proliferation, migration and invasion, and promote cell apoptosis of human breast cancer cell line MCF-7 (56). $As_2O_3$ could inhibit cell proliferation and promote cell apoptosis of human uterine sarcoma cells by down-regulating the level of ERK phosphorylation, up-regulating the expression of caspase-3 (57).

## 2.4 Phenylpropanoids

Phenylpropanoid compounds, whose primary core structure is C6-C3 connected by a benzene ring and a 3-chain carbon. The representative compounds of Lignans are Podophyllotoxin, Isotaxol, Schisandrin, Magnolol and Phillyrin (58–60).

Podophyllotoxin (**Figure 3**), a lignin monomer extracted from the rhizome of Common Dysosma Rhizome, had anti-tumor effects (58–60). Podophyllotoxin could inhibit tumor cell proliferation and promote apoptosis, which was attributed to inhibiting tubulin polymerization to prevent the formation of a mitotic spindle, therefore, affecting cell division, and inducing cell arrest in metaphase (58). Podophyllotoxin, Picropodophyllotoxin and 4-demethylpodophyllotoxin could inhibit the cell proliferation of human hepatoma cell lines QSG7701 and SMMU7721 and HeLa

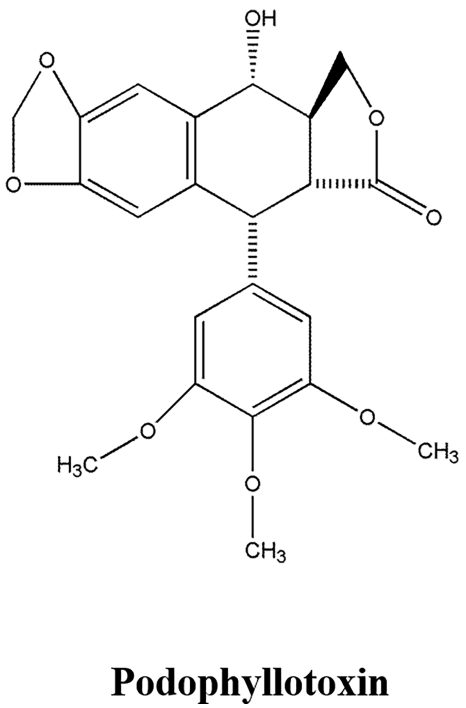


**FIGURE 3** | The structure of Phenylpropanoid compound. Podophyllotoxin.

cells. Among them, Podophyllotoxin performed the best activity. Podophyllotoxin, with broad-spectrum of anti-tumor activity, had favorable inhibitory activity on human leukemia cell line Jurkat, pleomorphic glioma cell line T98G and Glioma cell line SH-SY5Y. Podophyllotoxin showed excellent inhibitory activity on HeLa cells, promoted the formation of apoptotic bodies in the nucleus, and apoptosis occurred in 48 h, and induced cell cycle arrest in G2/M phase, which was attributed to down-regulation of calreticulin and Bcl-2, up-regulation of nucleolar phosphate protein and Bax to induce cell cycle arrest and promote apoptosis (59). Deoxypodophyllotoxin could inhibit the proliferation of human ovarian cancer cell line SKOV3, which was attributed to the down-regulation of ERK1/2 protein expression (60).

## 2.5 Flavonoids and Isoflavones

Flavonoids and isoflavones, 2-phenylchromone as the core structure, include a variety of structural types, such as Flavonoids, Dihydroflavonoids, Isoflavones, Dihydroisoflavones, Chalcone, Hesperidone and so on. The representative monomers have Genistein and Apigenin (61–67).

### 2.5.1 Genistein

Genistein (**Figure 4A**), a flavonoid from the rhizome of Leguminosae Genistin. It has anti-tumor, anti-bacterial, anti-oxidant, hypolipidemic and estrogen-like effects. It could inhibit angiogenesis, induce tumor cell programmed death, therefore, exhibit favorable anti-tumor activity (61–63). Genistein could reverse drug resistance of 5-fluorouracil-resistant hepatoma cell line Bel-7402/5Fu by up-regulating the expression of Akt and mTOR in PI3K/Akt/mTOR pathway, down-regulating the expression autophagy-related genes of Beclin and LC3 to promote cell autophagy (61). Genistein could inhibit the proliferation of human colon cancer cell line HCT116, which was related to the up-regulation of the ratio of LC3 II/I, the formation of autophagosome to promote cell autophagy (62). Genistein derivative WH-20 could inhibit the proliferation, migration and invasion of human breast cancer cell line MCF-7 and induce cell cycle arrest in G1 phase, which was attributed to down-regulated expression of related proteins in Notch pathway, such as Notch1, Jagged1, NF- κB, p65 and IκBa. Additionally, it inhibited the proliferation, migration and induced cell cycle arrest of MCF-7 cells by binding to Er β receptor, down-regulating the expression of MMP9, VEGF and CyclinD1 (63).

### 2.5.2 Apigenin

Apigenin (**Figure 4B**), Flavonoid monomer widely found in plants, has anti-tumor, anti-bacterial, anti-viral, and cardio-cerebrovascular protective effects (64–67). Apigenin could significantly inhibit the proliferation and invasion of human esophageal cancer cell line Eca-109 (65) and human lung cancer cell line PC9GR (66) by up-regulating the expression of E-cadherin, and down-regulating the transcription factor Snail, MMP-9 and VEGF. Apigenin could inhibit the growth of 3D tumor sphere of human hepatocellular carcinoma cell line MHCC97H by up-regulating the protein expression of SHP-1, down-regulating the phosphorylation level of STAT3 protein (67).

## 2.6 Quinonoid

The quinonoid monomers had favorable anti-cancer activity, such as Tanshinone and Emodin (68–76).

### 2.6.1 Tanshinone

Tanshinone, phenanthrenequinones derived from Salvia Miltiorrhiza, included Tanshinone IIA, Isocryptotanshinone, and Dihydrotanshinone, which exhibited anti-cancer, anti-bacterial, anti-inflammatory activities (68–73).

Tanshinone monomers could inhibit the proliferation of human colorectal cancer and gastric cancer cells, induce cell cycle arrest, and promote cell apoptosis, which was related to downregulating the expression level of HIF-1 (hypoxia inducible factor-1), VEGFR, bFGF (68), inhibiting tumor angiogenesis, suppressing the expression level of transcription related protein, down-regulating anti-apoptotic protein Bcl-2, while upregulate the pro-apoptotic proteins p53, Bax, cleaved caspase-3, and p21. They could reverse the doxorubicin drug resistance in gastric cancer cells by downregulating the expression of MRP1 and p62, while upregulating the autophagy-related gene LC3B-II to promote cell autophagy (69).

Tanshinone IIA inhibited the proliferation of HCT-116 cells by downregulating the expression of HIF-1α, VEGFR, and bFGF to inhibit angiogenesis (68). Combination of Tanshinone IIA and $As_2O_3$ synergistically inhibited the proliferation of SW620 cells

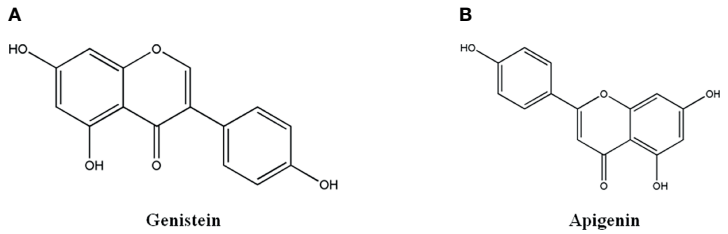


**FIGURE 4** | The structure of Flavonoids. **(A)** Genistein. **(B)** Apigenin.

by downregulating the expression of MMP9, VEGF, CD44v6, and upregulating the nm23-H1 (69). Phosphorylation of STAT3 promoted the progression of gastric cancer. Tanshinone IIA inhibited the proliferation and promoted apoptosis of human gastric cancer cell lines SNU-638, MKN1, and AGS cells, which was attributed to inhibiting the phosphorylation of STAT3 to downregulate Bcl-2, and upregulate Bax, and cleaved caspase-3 (70). Tanshinone IIA reversed the doxorubicin resistance in SNU-719R and SNU-610R cells by decreasing the expression of MRP1, inducing cell cycle arrest in G2/M phase, downregulating the expression of Bcl-2, while upregulating the level of p53 and Bax to promote cancer cell apoptosis, upregulating the autophagy-related protein LC3B-II and downregulate p62 to facilitate cell autophagy (71). Dihydrotanshinone inhibited the cell proliferation of SW480 by downregulating the β-catenin downstream protein c-Myc to inhibit the Wnt/β-catenin signaling pathway (72). Isocryptotanshinone could inhibit BGC-823 cells and SGC-7901 cells, induce cell cycle arrest in G0/G1 phase and promote cell apoptosis by upregulating p53 and p21, while downregulating Cyclin D1 and Bcl-2 (73).

### 2.6.2 Emodin

Emodin (**Figure 5**), an anthraquinone from Rhubarb, had anti-cancer, diarrhea, anti-bacterial, anti-spasmodic, cough relief, and diuretic activity (74–76). Emodin inhibited the proliferation, migration, and invasion, suppressed the cellular glycolysis and promoted apoptosis of endometrial cancer cell line HEC-1-B and gastric cancer cell lines BGC-823 and AGS, inhibited the xenograft growth of human colon cell line CT26 in nude mice model, which was attributed to downregulating the expression of CD44 and carbonic anhydrase IX protein (74), peroxidase Prx V, increasing intracellular ROS (75), downregulating anti-apoptosis proteins Bcl-2 and Pro-caspase 3, upregulating pro-apoptosis proteins Caspase3, Bax and HIF-α (76).

## 2.7 Saponin

Saponin, foaming and hemolysis properties, included triterpenoid saponin and steroid saponin. The former included Ginesnoside and Pachymic acid, the later included Diosgenin and Polyphyllin (77–83).

Ginsenoside, derived from Panax ginseng, comprised of a wide range of saponins with anti-cancer effects such as Rh1, Rh2, Rh3, Rg3, and Rg5. Ginsenoside could reverse multidrug resistance cancer cells by regulating MDR expression (77–80). Ma et al. (77) established a multidrug resistance biliary cancer cell line QBC939/ADM using cyclophosphamide, mitomycin, and 5-fluorouracil. Ginsenoside Rg3 reversed drug resistance to inhibit cell proliferation by upregulating the expression of MDR. Wan et al. (78) established a cisplatin resistant SGC7901/DDP cell line and found that Ginsenoside Rg3 could sensitize drug resistant cells to cisplatin by downregulating the mRNA and protein level of PD-L1. Hu et al. (79) constructed a doxorubicin-resistant SGC7901/ADR cell line and found that Ginsenoside Rh2 could sensitize the cells to doxorubicin by downregulating the expression of P-glycoprotein and Bcl-2, resulting in G2/M phase arrest and apoptosis. Ginsenoside Rg3 reversed the drug resistance of Lovo/5-Fu cells by upregulating the expression of NM23 and caspase-8 without affecting the drug resistance-related protein LRP (80)..

Ginesnoside inhibited the proliferation, migration, and invasion of breast cancer, colorectal cancer, lung cancer, ovarian cancer, and glioblastoma cells by inhibiting VEGF, angiogenesis, and downregulating MMP-9 (81–83). Ginsenoside Rh1 inhibited cell migration and invasion of SW480 cells by downregulating the expression of MMP-9 (82). Ginsenoside Rh3 promoted cell apoptosis in ovarian cancer cell line SKOV-3 cells (83).

## 2.8 Polysaccharides

Polysaccharides, widely distributed in plants, animals, and microorganisms, exhibited anti-cancer activity. On the one hand, they directly inhibited cell proliferation and migration, induce cell apoptosis of cancer cells. On the other hand, they were used for anti-cancer adjuvants by activating body immune cells and complement and increasing cytokine secretion to improve the immune function (84–88).

### 2.8.1 Lycium Barbarum Polysaccharide

Lycium barbarum polysaccharide, from medicinal and edible homologous herb wolfberry, presented anti-cancer activity. They could inhibit the proliferation, induce cell cycle arrest and promote cell apoptosis of human breast cancer cells MCF-7 (84), bladder cancer DU145 cells (85), liver cancer HepG2 cells (86), and tongue squamous carcinoma CAL-27 cells (87), which was attributed to activating the expression of ERK in p53 signaling pathway (84) and PI3K/Akt signaling pathway (85), downregulating the expression of anti-apoptotic protein Bcl-2, upregulating the expression of pro-

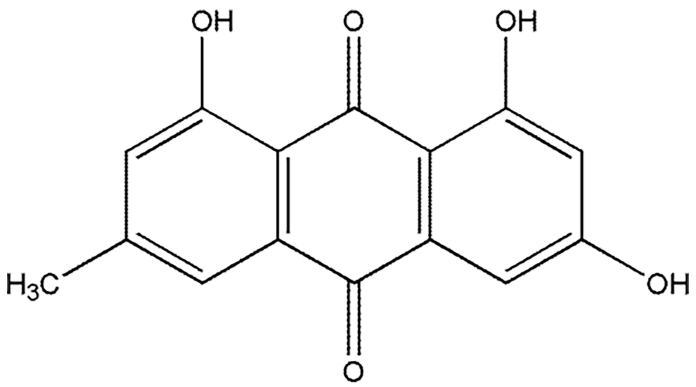


**FIGURE 5** | The structure of Quinone compound. Emodin.

apoptotic proteins Bax, Caspase-3 and Caspase-9, downregulating the expression of cyclinD, cyclinE and CDK2 (86), and promoting autophagy-related protein LC3 from type I to type II to promote autophagy (87). Lycium barbarum polysaccharide combined with chemotherapeutic drugs such as DDP could improve anti-cancer effects by activating body immune cells and complement and increasing cytokine secretion to improve the immune function. Additionally, they could relieve side effects of chemotherapeutic drugs (88).

### 2.8.2 Lentinan

Lentinan, extracted from Lentinus edodes, has anti-cancer activity and improve the immune function of the body. Clinically, it has been used as adjunct therapy for advanced lung cancer and gastric cancer treatment (89–92). Lentinan could *in vivo* inhibit the growth of murine sarcoma S-180 cells, human cervical cancer HeLa cells, breast cancer MCF-7 cells, liver cancer HepG2 cells, and squamous cell carcinoma SCC-7 cells in tumor xenograft models, which was attributed to regulation of tumor suppressor p53, caspase and Era genes (89), inhibition of PI3K/Akt/mTOR signaling pathway, and inhibition of angiogenesis (90). Lentinan could inhibit the proliferation, migration, induce cell cycle arrest and promote cell apoptosis of human glioma SHG-44 cells (91), oral squamous cell carcinoma HN4 cells (92).

## 3 ANTI-CANCER MOLECULAR MECHANISM OF NATURAL PRODUCTS

The anti-cancer molecular mechanism of natural products can be attributed to the regulation of (1) inhibiting the cell proliferation, migration, and invasion, inducing cell cycle arrest and apoptosis to inhibit or kill cancer cells by regulating related cell signaling pathways; (2) inhibiting angiogenesis by regulating related signaling pathway; (3) inhibiting tumor by regulating suppressor gene, autophagy, or intracellular ROS level; and (4) reversing drug resistance in cancer cells by regulating the expression level of drug resistance associated genes or transporters.

### 3.1 Regulation of Cell Proliferation, Migration, Invasion, Cell Cycle and Apoptosis by Signaling Pathways

Natural products, such as Matrine or Oxymatrine, could inhibit the proliferation and migration of cancer cells by upregulating p38 signaling pathway and phosphorylation level of H2AX (28–32). Artemisinin inhibited the proliferation of tumor cells by inhibiting the phosphorylation of Akt and S6 in mTOR signaling pathway (40–42).

EMT is a biologic process in which the polarized epithelial cells transform to a mesenchymal cell phenotype under certain conditions, leading to enhanced capability of migration and invasion. Low expression level of TGF-β was able to crosstalk with other signaling molecules and promote EMT. Cadherin, especially E-cadherin, is actively involved in the regulation of EMT and promotes cell migration. Downregulation of E-cadherin decreased the adhesiveness of cancer cells and allowed them to migrate to distal tissues (64). Paclitaxel (47), Artemisinin (39), Dihydroartemisinin, and Apigenin (66), could induce Wnt, Notch, and P38 signaling pathways, upregulate the expression of SH2-containing protein tyrosine phosphatase 1 (SHP-1) (67), RECK, β-Catenin, Vimentin, Claudin-1, ZO-1, downregulate the level of E-cadherin, p-STAT3, mucin1, Gli2, Vimentin, Snail, and Twist, therefore, inhibiting EMT to suppress cancer cell proliferation, migration and invasion.

Natural products could induce cell cycle arrest to inhibit cancer cell growth and proliferation by regulating signaling pathways to affect the cyclin expression. Paclitaxel (47) could stabilize polymerized microtubules during mitosis, leading to cell cycle arrest. The cyclin Cdc25C is an important mediator for entering mitosis and regulates G2/M. Harringtonine (13), Vincristine (21, 22), Matrine and Oxymatrine (32) and Lycium barbarum

polysaccharide (84–86), could downregulate the phosphorylation of PI3K, Akt and mTOR in PI3K/Akt/mTOR signaling pathway and the protein expression in Notch pathway, inhibit the binding to Estrogen receptor β, upregulate p53, p21, and downregulate CDK2, cyclinA, cyclinB1, cyclinD1, cyclinE, Cdc2, Cdc25C, thus leading to cell cycle arrest and inhibit cancer cell growth.

Natural products could promote cancer cell apoptosis by regulating signaling pathways to affect the expression of apoptosis related proteins. Apoptosis is a process of programmed cell death, including mitochondria pathway, death receptor pathway, and endoplasmic reticulum pathway. The apoptosis related proteins include Cyto-C, Caspase3, 7, 8, 9, 12, and anti-apoptotic genes (Bcl-2, Bcl-x), and pro-apoptotic gene Bax (93). Homoharringtonine, Camptothecin, Vincristine, Artemisinin, Dihydroartemisinin and Tanshinone could downregulate Ras-MAPK, PI3k-Akt, Wnt-β-catenin, STAT3 (72), ATAD2, and Notch1, while upregulate of P53, P21, IGFBP3, NDRG1 to activate mitochondrial mediated endogenous apoptotic caspase pathway, therefore, downregulate the level of anti-apoptotic gene Bcl-2, Bcl-xL, survivin, livin (48, 76), as well as upregulate the pro-apoptotic gene Bax, cleaved caspase-3, 8, 9, AIF, and cleaved PARP1 to promote cancer cell apoptosis (33).

## 3.2 Regulation of Angiogenesis by Related Signaling Pathways

Angiogenesis is a crucial process in the development and progression of tumors, which provides essential nutrients for tumor tissues (94). Therefore, inhibiting angiogenesis has been established as an effective strategy for cancer treatment including direct ways and indirect ways. Direct angiogenesis inhibition can be achieved by downregulation of VEGF, FGF, and TNF-α, and upregulation of angiostatin, endostatin, and IF-α. VEGF is a downstream protein in the PI3K/Akt signaling pathway. Inhibiting the levels of VEGF and MMPs can decrease the degradation of extracellular matrix, which indirectly inhibits tumor angiogenesis. Ginsenosides (81–83), Tanshinones (68) and Lentinan (95) could inhibit Akt phosphorylation and the corresponding PI3K/Akt/mTOR pathway, inhibit phosphorylation of IκBα, NF-κB-p65, upregulate the expression of SHP-1, downregulate the protein level of angiogenesis-associated HIF-1α, MMP-2, MMP-9, VEGF, bFGF and Cyc-D1 to inhibit angiogenesis and the proliferation of tumor cells.

## 3.3 Regulation of Tumor Suppressor Gene, Autophagy, or Intracellular ROS Level

Natural products such as $As_2O_3$ (53–56) and Triptolide (49) could upregulate tumor suppressor genes PTEN, p53 (54), APC (55), FOXO1 (56), and miR-145, and downregulate MMP2 and MMP9 to inhibit tumor angiogenesis, migration, and invasion. Furthermore, natural products could downregulate the expression of CDK2, cyclin A, cyclin B1, cyclin D1, and cyclin E, leading to cell cycle arrest. They also induce cancer cell apoptosis by upregulating the cytochrome C, AIF, caspase-3, caspase-9, Bax and the ratio of Bax/Bcl-2 and downregulating the expression of Bcl-2.

Vincristine (23), Genistein (61), Lycium barbarum polysaccharide (87) would upregulate the expression of Akt and mTOR in PI3K/Akt/mTOR signaling pathway (61, 85, 87), while downregulating the autophagy related Beclin1, thereby promoting the transition of LC3 I to LC3 II, and mediating the formation of autophagosome. Hence, Chinese herb monomers could facilitate cancer cell autophagy, inhibit cell growth (87).

Paclitaxel (47) and Emodin (74) could promote cancer cells apoptosis *via* increasing cellular ROS level by upregulating the expression level of JNK, MAPK4, and ASK1 (47), decreasing the level of CD44 and CAIX (74), and downregulating the expression of peroxidase PrxV.

## 3.4 Regulation of Drug Resistance Associated Genes or Transporters

MDR refers to the phenomenon that cancer cells become resistant to multiple drugs that shares similar chemical structure, leading to ineffective of the drugs and increase the therapeutic burden of patients. Therefore, it is essential to sensitize cancer cells to therapeutic drugs and reverse drug resistance (96). Overexpression of MDR1 gene may lead to the MDR phenotype of cancer cells, which allows the cells to pump out chemotherapeutic drugs using the energy derived from ATP hydrolysis. Harringtonine (14), Vincristine (21) and Tanshinone (71) could downregulate the expression of MDR1 gene as well as the protein level of P-gp (21) and MRP1 (71), thereby inhibiting the drug efflux activity and reverse MDR.

# 4 DERIVATIZATION OF NATURAL PRODUCTS

Although a wide variety of natural products exhibit anti-cancer activity, the effect is not enough to use for clinical treatment. Through structural optimization, some natural products have been advanced as effective anti-cancer drugs. For example, Homoharringtonine, a derivative of Harringtonine, was the first anti-cancer natural product in China used as a first-line treatment for acute myeloid leukemia in combination with chemotherapy. It was also used for the treatment of malignant lymphoma, choriocarcinoma, malignant mole, lung cancer, and others. Irinotecan and Topotecan, the water-soluble derivatives of Camptothecin, were used for metastatic colorectal cancer. The structural derivative of Vinblastine, Isovinblastine, was approved in France in 1991 for late-stage lung cancer treatment with low neurotoxicity compared to Vinblastine. The Paclitaxel derivative Docetaxel was the first marketed Taxane drug with 2-3-fold anti-tumor efficacy than Paclitaxel. Etoposide was the first marketed anti-tumor drug of Podophyllotoxin derivatives. Many of these structural optimized monomers are still used in the first-line treatment, which is encouraging for natural products research.

## 4.1 Harringtonine Derivatives

A wide range of Harringtonie derivatives have been developed to enhance the anti-cancer efficacy since its discovery. Homoharringtonine, a derivative of Harringtonine, was the first anti-cancer Chinese herb monomer drug in China as a first-line treatment for acute myeloid leukemia, which was used in

combination with chemotherapy. It was also used to treat malignant lymphoma, choriocarcinoma, malignant mole, lung cancer, and others (97–99).

Zhong et al. (97) synthesized 10 amino acid Harringtonines, which showed inhibitory effect against promyelocytic leukemia HL-60 cells. The anti-cancer activity of compound 6 showed an 75.2% inhibitory effect, suggesting the anti-cancer effects may be dependent on the compound. Ye et al. (98) synthesized 6 new ester base compounds by linking the side chain of Paclitaxel and its enantiomer to the C3 position of Harringtonine. The MTT cell viability assay showed that compound VIIIa, VIIIb, IXa and IXc showed potential anti-proliferative effects toward oral epithelial squamous cell carcinoma KB cells, CRC HCT-8 cells, and liver cancer BEL-7402 cells. Compound VIIIa has the most significant effect against HCT-8 and BEL-7402 cells. Wu et al. (99) synthesized 17 compounds by modifying Homoharringtonine at different positions. The *in vitro* data showed that the cycloheptatrienone and lactone structure of Homoharringtonine was important for the anti-cancer effects against HCT-116, A375, A549 and Huh-7 cells. Compound 6 had the most significant effects with $IC_{50}$ values below 10 μM in cancer cells, and 67.20 μM in normal cell L-02, suggesting a good selectivity and safety for cancer treatment.

## 4.2 Camptothecin Derivatives

Camptothecins are potential anti-cancer drugs, the derivatives of which have been approved in clinical use, including 10-hydroxycamptothecin, Belotecan, Irinotecan, Topotecan. Irinotecan and Topotecan are water-soluble derivatives of Camptothecins that are used for metastatic colorectal cancer (100). Studies reported that the modification of Camptothecin is mainly focused on the ring structures, and substitution on C-9 and C-10 positions increase the anti-cancer activity of the compounds (101).

The derivative 7-ethyl-10-hydroxycamptothecin, also known as SN-38 (**Figure 6A**), has the strongest anti-cancer effects. Irinotecan (**Figure 6B**) is a derivative of SN-38 which is metabolized into SN-38 after administration. SN-38 showed optimal effects against metastatic colorectal cancer, small cell and non-small cell lung cancer, and breast cancer (102, 103). It is reported that the combination of SN-38 and other anti-cancer drug has no observed side effect to fetus when treating breast cancer during pregnancy (104). Guerrant et al. (105) synthesized a novel camptothecin-like histone deacetylase and topoisomerase I dual inhibitor, which demonstrated enhanced cytotoxicity against liver cancer Hela cells. Lee et al. (106) designed some novel 7-(N-substituted-methyl)-camptothecin derivatives that show significant cell killing effects towards MDA-MB-231, KB, A549, and drug resistant Kbvin cells. Wang et al. (107) synthesized a new compound with seven-membered lactone ring, which exhibited better *in vitro* anti-tumor effects than SN-38.

## 4.3 Vinblastine Derivatives

Both Vinblastine and Vincristine have significant anti-tumor activity, and the derivatives that have been approved for clinical use include Vinorelbine, Vindesine, and Vinflunine. The structural derivative of Vinblastine, Isovinblastine, was approved in France in 1991 for late-stage lung cancer treatment with low neurotoxicity compared to vinblastine. Hu et al. (108) synthesized 30 lead compounds by modifying the C-3 and C-4 position of Vinorelbine. The *in vitro* data showed that C-3 substitution has significant impact on the cytotoxicity in Hela and A549 cells. Among them, the derivatives with N25 substituent had the strongest *in vitro* anti-cancer activity, and the $IC_{50}$ value was one third of that of the positive control. The A549 tumor xenograft model results showed that N25 substituent derivative had higher inhibitory rate than Vinorelbine and other compounds (N8, N11, N18). Li et al. (109) optimized the synthesis and separation process of 3-phenethyl ester-6'-oxyvinblastine nitrogen oxide, and the MTT assay showed promising *in vitro* anti-cancer efficacy in HepG2, Hela, MCF-7, and A549 cells. Compared to Vinorelbine, the compound had $IC_{50}$ values lower than 10 μg/mL. Cell-penetrating peptides can covalently transport compounds into cells. Studies reported that the combination of Vinblastine with Oligoarginine had better efficacy against leukemia cell HL-60 *in vitro*, and the combination of Vinblastine and tryptophan Br-vind-(L)-Trp-Arg8 had significant inhibitory effects against leukemia cell P388.

## 4.4 Taxane Derivatives

Paclitaxel has strong anti-cancer effects, and the most successful derivative is Docetaxel, which is the first marketed semi-synthetic Paclitaxel derivative. Docetaxel (**Figure 7A**) has 2-3-fold stronger effects compared to Paclitaxel, with long retention time in cells, high bioavailability, and few side effects (110). Later, researchers have synthesized new compound by modifying the structure of Docetaxel. Che et al. (111) synthesized larotaxel (**Figure 7B**) by modifying the C-7 and C-8 position of Docetaxel, which showed promising inhibitory effects against breast cancer and pancreatic cancer. Iimura et al. (112) introduced methoxy group to the C-7 and C-10 position of Docetaxel to obtain a new compound named Carbazitaxel (**Figure 7C**). It has been approved for the treatment of hormone-resistant metastatic prostate cancer, and had favorable anti-cancer effects towards colorectal cancer, lung cancer, and cervical cancer. Roh EJ et al. (113) performed structural modification on the C-3 position of Paclitaxel, and the new compounds (**Figure 7D**) exhibited 20 times higher inhibitory effects to A549 and SK-OV3 cells than Paclitaxel.

## 4.5 Podophyllotoxin Derivatives

The structure-optimized derivatives of Podophyllotoxin showed favorable anti-tumor activity, and Etoposide was the first podophyllotoxin derivatives approved for use. Wu et al. (114) synthesized 23 derivatives by esterification and amidation of Podophyllotoxin with Ligustrazine and different amino acids. The *in vitro* experiments showed that compound P-02 had the highest inhibitory effects and induced early apoptosis in A549 and L-02 cells. Gao et al. (115) examined the anti-cancer activity of ZM-10, a derivative of Podophyllotoxin, on oral squamous cell carcinoma KB cells. The results suggested that ZM-10 could induce G2/M phase arrest and promote cell apoptosis. PCR data showed that ZM-10 downregulated the mRNA level of anti-apoptotic gene Bcl-2 and upregulated the mRNA level of pro-apoptotic gene P53, caspase-3, and Bax. Leng et al. (116) reported

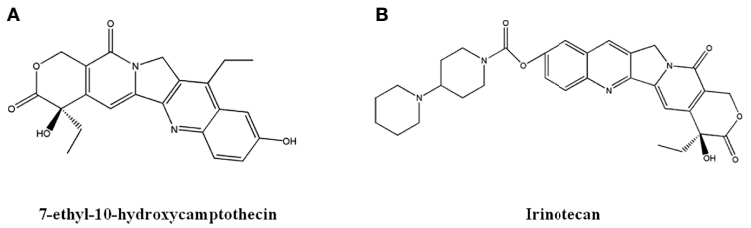


**FIGURE 6** | The structure of Camptothecin derivatives. **(A)** 7-ethyl-10-hydroxycamptothecin. **(B)** Irinotecan.

that QW-83 could concentration-dependently inhibit the proliferation of ovarian cancer He-La cells and induce cell apoptosis. Tian et al. (117) showed that the synthetic compound 4b, 4e, and 4f from Podophyllotoxin and indoles showed more significant cytotoxic effects on HeLa and K562 cells than Etoposide.

## 4.6 Matrine Derivatives

Matrine is a potential anti-cancer drug. Matrine injection has been used as an adjuvant therapy in clinics since 2003. However, Matrine has a short duration of activity due to its high solubility and rapid elimination. In order to optimize the therapeutic effects, researchers performed structural medication on matrine. Wang et al. (118) obtained two types of Matrine derivatives by esterification to 13-hydroxyethyl Matrine (**Figures 8A, B**). The results showed that the derivatives parabens and 4-chlorobenzoates had more significant inhibitory effects than Matrine in HepG2 cells. Another group synthesized three 14-aroylmatrine compounds (**Figure 8C**) by introducing benzylidene derivatives to the C-14 position of matrine by Claisen-Schmidt reaction (119). The new compounds have potential anti-cancer effects to melanoma B16-F10 cells. He et al. (120) obtained Deoxymatrine (**Figure 8D**) by reducing the C-15 position of Matrine with lithium aluminum tetrahydrogen. The synthesized deoxymatrine showed concentration-dependent inhibitory effects to liver cancer HepG2 and SMMC7721 cells, and the effects was stronger than Matrine. Zhang et al. (121) synthesized glycyrrhetinic acid Matrine complex (**Figure 8E**) through esterification of 18α-glycyrrhetinic acid, 18β-glycyrrhetinic acid and 13-hydroxyethoxymatrine. The compound had better inhibitory effects than Matrine in MCF-7 and SMMC-7221 cells.

## 4.7 Evodiamine Derivatives

Several novel derivatives of Evodiamine exhibited favorable anti-tumor activity. Dong et al. (122, 123) reported that compounds with hydroxy group substitution on the C-10 position of A ring (**Figure 9A**) and chloride group substitution on C-3 position of E rings (**Figure 9B**) had significant anti-cancer activity. The compounds showed better effects than Evodiamine in A549, MDA-MB-435, and HCT116 cells, with $IC_{50}$ values lower than 0.003 μM. Studies also identified that compound A with simultaneous introduction of -$NO_2$ from C-10 and C-12 on the A ring of Evodiamine (**Figure 9C**) and compound B with p-chlorobenzoyl group introduced to N-13 on ring B (**Figure 9D**) had significant anti-tumor effects. In MDA-MB-435 cells, the $GI_{50}$

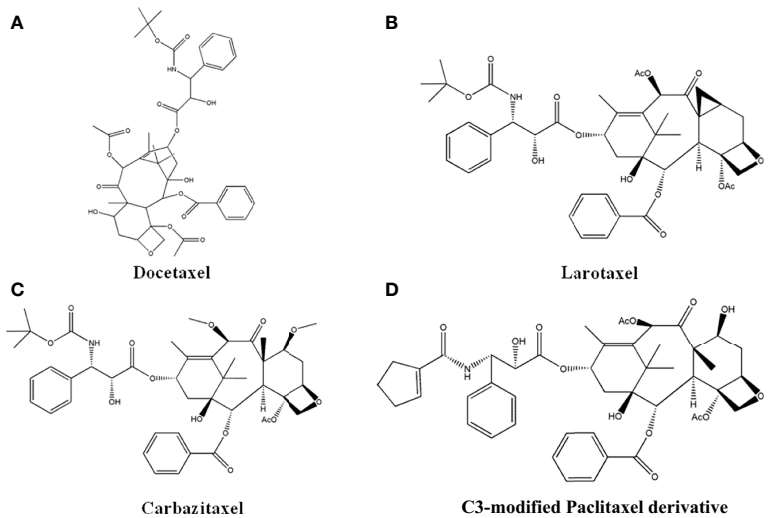


**FIGURE 7** | The structure of Taxol derivatives. **(A)** Docetaxel. **(B)** Larotaxel. **(C)** Carbazitaxel. **(D)** C3-modified Paclitaxel derivative.

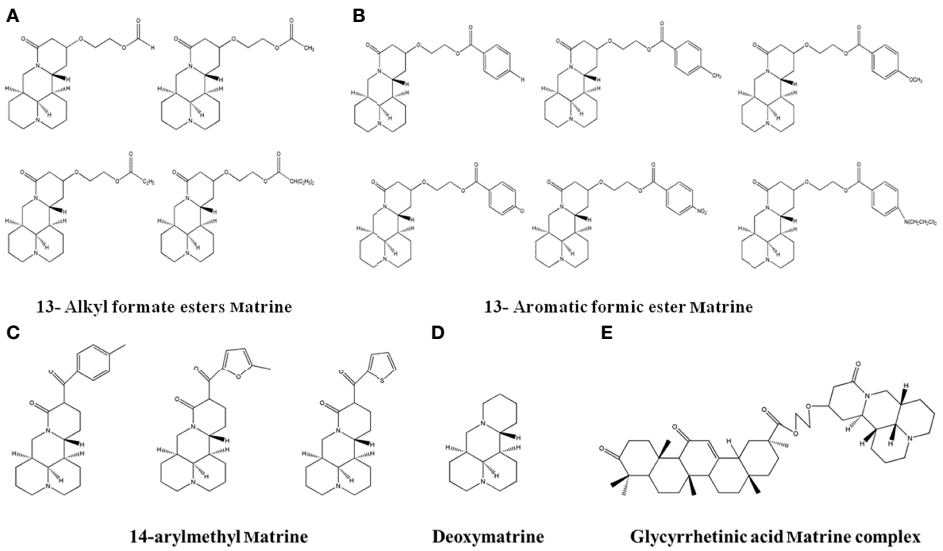


**FIGURE 8** | The structure of Matrine derivatives. **(A)**13-Alkylformate esters Matrine. **(B)** 13-Aromatic ester Matrine. **(C)** 14-arylmethyl Matrine. **(D)** Deoxymatrine. E. Glycyrrhetinic acid matrine complex.

values were 0.16 μmol/L and 0.049 μmol/L, respectively. It was also suggested that compound with chloride substitution on C-12 on A ring (**Figure 9E**) had optimal inhibitory effects against MDA-MB-435 cells, with $GI_{50}$ value less than 0.003 μM (122, 123).

## 4.8 Apigenin Derivatives

Apigenin has good anti-tumor activity, but its water solubility and intestinal absorption are poor, which limits its therapeutic application. Therefore, it is structurally modified to improve its anti-tumor activity. Xiang et al. (124) performed structural modifications on Apigenin to generate 6 new Apigenin derivatives. The results suggested that methyl etherification and bromination derivatives (**Figure 10A**) have optimal water solubility and intestinal absorption, with 12.09-fold stronger anti-cancer effects than Apigenin. Chen et al. (125) synthesized 4 new Apigenin derivatives by reacting 4'-O-benzylapigenin with bromoacetylglucose and bromogalactose, respectively. The apigenin-7-O-β-D-acetylgalactoside (**Figure 10B**) has the most significant antiproliferation effects against MCF-7 and HL-60 cells. Han et al. (126) reported that derivatives with leucine, alanine and valine as substituents (**Figures 10C-E**) have potential anti-cancer effects to HeLa cells. Daskiewicz et al. (127) introduced isoprenyl group to the 5-position of the Apigenin molecule, and after molecular rearrangement, 8-prenyl Apigenin

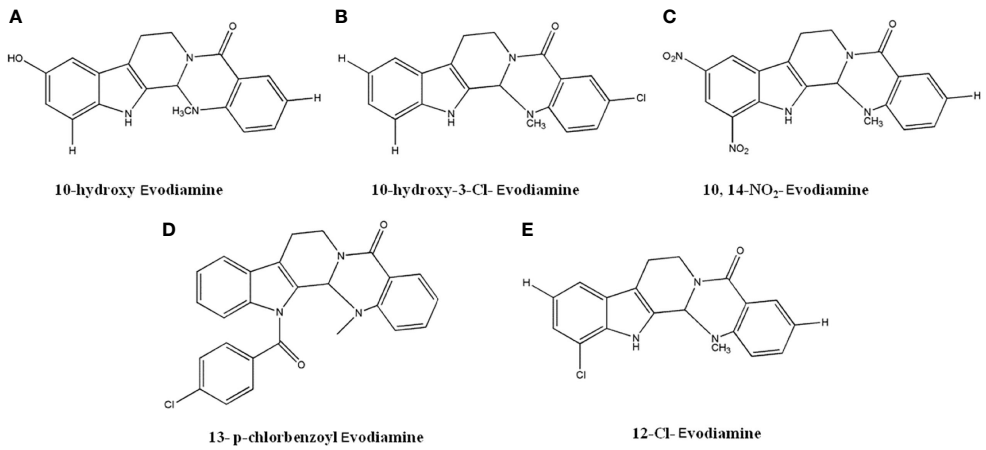


**FIGURE 9** | The structure of Evodiamine derivatives. **(A)** 10-hydroxy Evodiamine. **(B)** 10-hydroxy-3-Cl-Evodiamine. **(C)** 10,14-NO2-Evodiamine. **(D)** 13-p-chlorbenzoyl Evodiamine. **(E)** 12-Cl-Evodiamine.

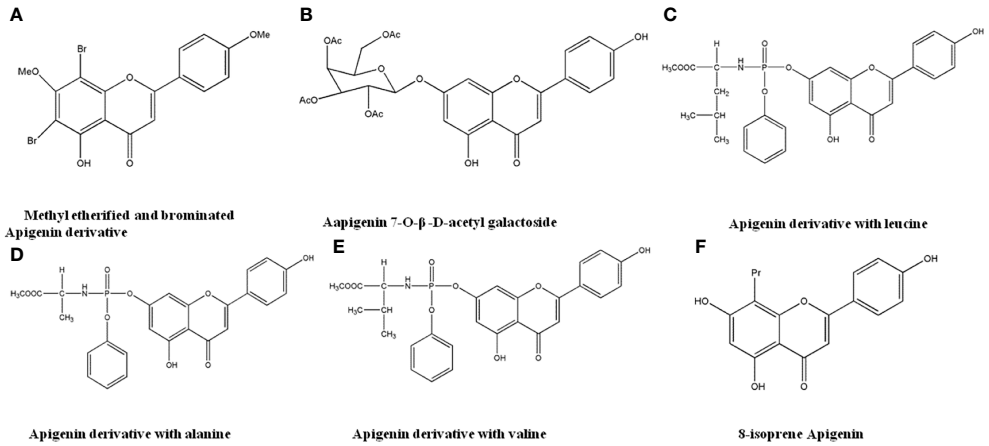


**FIGURE 10** | The structure of Apigenin derivatives. **(A)** Methyl etherified and brominated Apigenin derivative. **(B)** Apigenin 7-O-β-D-acetyl galactoside. **(C)** Apigenin derivative with leucine. **(D)** Apigenin derivative with alanine. **(E)** Apigenin derivative with valine. **(F)** 8-isoprene Apigenin.

(**Figure 10F**) was obtained. The compound had significant anti-proliferative effects and induced apoptosis in HT-29 cells.

## 4.9 Artemisinin Derivatives

As an anti-malarial drug, Artemisinin exhibits anti-tumor activity, but its clinical application was limited by poor water solubility and bioavailability. Several Artemisinin derivatives, after structural optimization, showed enhanced anti-cancer effects. Researchers have combined the short-chain ubiquinone compounds Thymoquinone, with Artemisinin, and found that the resulting Artemisinin-Thymoquinone hybrid (**Figure 11A**) was effective against colorectal cancer. The inhibitory activity of HCT-116 and HT29 cells was better than 5-Fu treatment with less cytotoxicity (128). It was reported that the cinnamic acid-dihydroartemisinin ester hybrid (**Figure 11B**) had selective cytotoxic effects to lung cancer cells (129). Mitochondria play an important role in tumorigenesis and development. The synthetic product of triphenylphosphine and Artemisinin (**Figure 11C**) can introduce Artemisinin into mitochondria and enhance its anti-tumor activity (130). The new Artemisinin ester compounds synthesized by the reaction of acid chloride or acid anhydride (**Figure 11D**) have enhanced anti-tumor activity with good safety and thermal stability.

# 5 CONCLUDING REMARKS

A variety of natural products have shown favorable anti-tumor activity, providing new insights and core structures for anti-cancer new drug development. While natural products have low anti-cancer activity, poor water solubility, and poor absorption,

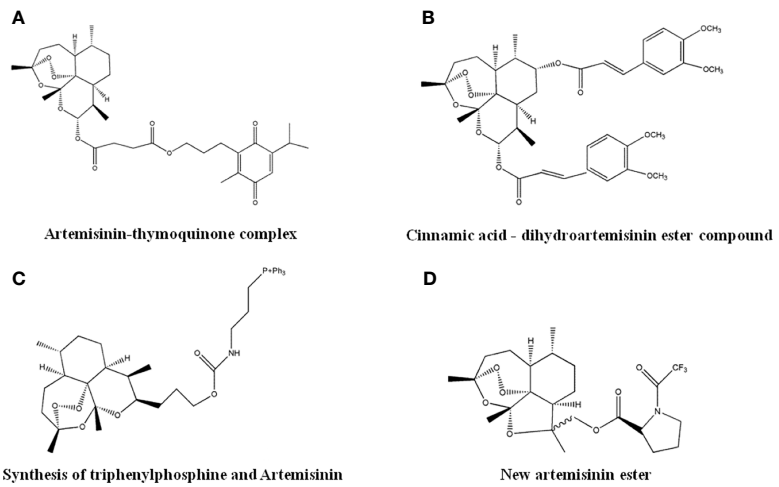


**FIGURE 11** | The structure of Artemisinin derivatives. **(A)** Artemisinin-thymoquinone complex. **(B)** Cinnamic acid-dihydroartemisinin ester compound. **(C)** Synthesis of triphenylphosphine and Artemisinin. **(D)** New artemisinin ester.

structural optimization allows the development of lead compounds with high anti-cancer efficacy. The anti-cancer molecular mechanism of natural products and their derivatives are still not well understood, which hinders their clinical application. With the progress of in-depth research on natural products, more potential derivatives will be developed and will have broad application in cancer treatment.

## AUTHOR CONTRIBUTIONS

H-LC designed the research study. MG, JJ, and DZ wrote the manuscript. ZR, X-YS, L-YJ, Y-DW, LH, and Y-HL collected the references. L-QC, Z-JH, LL, R-KM, Y-FL, and K-KS analyzed the data. A-HL and H-LC revised the paper. All authors contributed to editorial changes in the manuscript. All authors read and approved the final manuscript.

## FUNDING

This work was supported by the National Natural Science Foundation of China (U1932130); the Key Program of Shaanxi Provincial Science and Technology Department (2022ZDLSF05-15, 2021SF-303); the Key Program of Shaanxi Provincial Education Department (20JS134); the Program of Shaanxi Administration of Traditional Chinese Medicine (2019-ZZ-ZY009); the Key Program of Weiyang District Bureau of Science, Technology and Industry Information Technology (201928).

## REFERENCES

1. Sung H, Ferlay J, Siegel RL, Laversanne M, Soerjomataram I, Jemal A, et al. Global Cancer Statistics 2020: Globocan Estimates of Incidence and Mortality Worldwide for 36 Cancers in 185 Countries. *A Cancer J Clin* (2021) 71(03):209–49. doi: 10.3322/caac.21660
2. Zhu SS, Chen X, Yan QY, Lin Z. Progress in Clinical Application of Antitumor Drugs. *Chin Modern Doctor (Chinese)* (2019) 57(09):164–8.
3. Zhang LD, Gong JY. Conservation and Sustainable Reuse of Traditional Chinese Medicine Resources. *World Latest Med Inf Abstracts (Chinese)* (2016) 16(18):203–4.
4. Yang MH, Liu Y, Kong LY. Study on New Drugs Based on Effective Monomer Components of Traditional Chinese Medicine. *World Sci Technol – Modern Traditional Chin Med (Chinese)* (2016) 18(03):329–36. doi: 10.11842/wst.2016.03.001
5. Chen YQ, Wang M. Analysis of Common Anticancer Traditional Chinese Medicines. *Chin Med Guide (Chinese)* (2015) 13(10):233–4.
6. Xu QP, Liu JH, Liu BR. Research Progress in Antitumor Activity of C_(19)-, C_(20) -Diterpenoid Alkaloids. *Prog Pharm (Chinese)* (2016) 40(01):3–10.
7. Su XY, Xue JP, Wang CX. Advances in Synthetic Biology of Functional Components of Traditional Chinese Medicine. *Chin J Chin Materia Med (Chinese)* (2016) 41(22):4150–7. doi: 10.4268/cjcmm20162211
8. Shuang XW. Chen Zhu was Awarded the Ernest Beutler Prize. *China Sci Technol Transl (Chinese)* (2017) 30(01):63.
9. Zhang YY, Han T, Wu LS, Ming GL, Qin LP. Research Progress of Origin, Pharmacological Action and Clinical Application of Trichotaxine Compounds. *Modern Med Clin Med (Chinese)* (2011) 26(05):370–4.
10. Li ZR, Han R. Research Progress of New Antitumor Drugs – Harringtonine and Harringtonine. *Chin Traditional Herbal Med (Chinese)* (1986) 17(03):39–45.
11. Liang QJ, Zhang S, Zheng YB, Wang C, Wang YC. Effects of Harringtonine on Hela Cell Proliferation and its Relationship With Cenpb Gene. *Chin J Biophysics (Chinese)* (2005) 21(01):26–32. doi: 10.3321/j.issn:1000-6737.2005.01.003
12. Wu CX, Shen HQ, Xia DJ. Harringtonine Induces Apoptosis of NB4 Cells by Down-Regulating Mcl-1 Protein. *J Zhejiang Univ (Med) (Chinese)* (2013) 42 (04):431–6. doi: 10.3785/j.issn.1008-9292.2013.04.010
13. Liang SH, Peng A, Wang YC. Effect of Harringtonine on L-1210 Cell Proliferation. In: *The 7th Conference of Chinese Society for Cell Biology (Chinese)*. Zhengzhou, China: Chinese Society of Cell Biology (1999).
14. Zhang C, Shao SL, Li XY, Zhang ZZ, Zhang WW, Yun DZ. Silencing MDR1 Gene Enhances Apoptosis of SGC7901/ADM Cells Induced by Harringtonine. *Genomics Appl Biol (Chinese)* (2018) 37(08):3631–4. doi: 10.13417/j.gab.037.003631
15. Zhang QC, Gu ZZ. Effects of Low Dose Bufalin Combined With Hydroxycamptothecin on the Growth of Human Prostate Cancer Cell Line Du145 In Vitro. In: The 14th National Academic Conference of Urology Professional Committee of Chinese Association of Integrated Traditional and Western Medicine and the 2016 Academic Annual Conference of Urology Professional Committee of Guangdong Association of Integrated Traditional and Western Medicine (Chinese) Guangzhou. Guangdong, China. *Proceedings of the 16th Andrology Academic Conference of Chinese Society of Traditional Chinese Medicine (2016)*.
16. Qi QX, Pan Y, He QZ, Sun L, Liu PP. Effect of Hydroxycamptothecin on Wild-Type P53 Transfection in Cervical Carcinoma Cells. *Oncol Pharm (Chinese)* (2019) 9(01):40–4.
17. Liu LZ, Wu JB, Huang DH, Jian J, Zhang Y. Effects of Celecoxib Combined With Hydroxycamptothecin on Hypoxia-Induced Proliferation and Apoptosis of Human Hepatocarcinoma Cells. *Modern Oncol (Chinese)* (2019) 27(17):3000–5. doi: 10.3969/j.issn.1672-4992.2019.17.005
18. Liu YM, Ge XM, Zhang P, Sun XJ, Zhen YN, Li JH, et al. The Synergistic Effect of 2-Deoxy-D-Glucose Combined With Hydroxycamptoctin on Apoptosis of Breast Cancer Cells. *J Sichuan Univ (Medl Ed) (Chinese)* (2019) 50(04):527–32.
19. Guo HM, Li YL, Liu Z. Effects of Saponins ii Combined With Camptothecin on Apoptosis and Signaling Pathway of Lung Cancer H460 and H446 Cells. *Tianjin Traditional Chin Med (Chinese)* (2019) 36(02):165–70. doi: 10.11656/j.issn.1672-1519.2019.02.19
20. Zhao XY, Zhao R, Tian FY, Hou JC, Zhang WS, Zhang W. Apoptosis of Pc-3 Cells Induced by Camptothecin and its Mechanism in Prostate Cancer. *Chin J Toxicol (Chinese)* (2018) 32(04):264–7.
21. Lu ZN. *Effect of Pantoprazole on Chemosensitivity of KB/V Drug-Resistant Cells to Vincristine in Human Oral Epithelial Carcinoma*. Jinan: Shandong University (Chinese (2018).
22. Sun LN, Zhang T, Guo JJ, Yu YY, Yao XS, Sun WB. Effect of Cisplatin Combined With Vincristine on Drug Resistance Reversal of HCT-8/V Tumor Cells by Real-Time Dynamic Living Cell Imaging. *Chin J Immunol (Chinese)* (2019) 35(09):1085–90.
23. Sun LN. *Effect of Vincristine Combined With DDP, Rhil-24 and Que on Drug Resistance of HCT-8/V Cells*. Zunyi: Zunyi Medical University (Chinese (2019).
24. Zhang HB, Huang YQ, Sun H, Wen YH, Zhu DW, Shi XF, et al. Celecoxib Enhances the Inhibitory Effect of Vincristine on the Proliferation and Migration of KB/VCR Cells. *J Clin Exp Pathol (Chinese)* (2018) 34 (05):498–502. doi: 10.13315/j.cnki.cjcep.2018.05.006
25. Huang YQ. *Celecoxib Enhances the Sensitivity of KB/VCR Cells to Vincristine and Induces Apoptosis*. Guangzhou: Southern Medical University (Chinese (2013).
26. Yan YX, Li WZ, Huang YQ, Liao WX. The COX-2 Inhibitor Celecoxib Enhances the Sensitivity of KB/VCR Oral Cancer Cell Lines to Vincristine by Down-Regulating P-Glycoprotein Expression and Function. *Prostaglandins Other Lipid Mediat* (2012) 97(1-2):29–35. doi: 10.1016/j.prostaglandins.2011.07.007
27. Li H. Research Progress of Matrine Antitumor Activity. *World Latest Med Inf Digest (Chinese)* (2019) 19(46):96–8. doi: 10.19613/j.cnki.1671-3141.2019.46.041
28. Zhao ST, Lei L, Cheng JX. Matrine Inhibits the Proliferation and Migration of Cervical Cancer Cells by Regulating H2AX Phosphorylation Through P38 Pathway. *J Tongji Univ (Med Sci) (Chinese)* (2018) 39(04):22–8.
29. Liu BQ, Zhang B, Xu W, Zhang WC, Xia SH. Effect of Oxymatrine on Epithelial Mesenchymal Transformation and Gli2 Expression in Pancreatic

Cancer Cells. *J Zunyi Med Coll (Chinese)* (2018) 41(06):705–9.
30. Ding MN. *Effects of Matrine on the Proliferation and Radiosensitivity of Human Hepatocellular Carcinoma Cells*. Wuhan: Hubei University of Traditional Chinese Medicine (Chinese (2019).
31. Zhang XL, Chen Z, Shao AN. Study on the Mechanism of Matrine Inhibiting Proliferation of Human Endometrial Cancer Cells. *J Clin Exp Med (Chinese)* (2018) 17(08):822–5. doi: 10.3969/j.issn.1671-4695.2018.08.012
32. Li L, Sun YF, Li S, Wang QC. Effect of Oxymatine on Proliferation of Gastric Cancer Cell Line SGC 7901. *J Taishan Med Univ (Chinese)* (2018) 39(01):6–9.
33. Zhang HN, Zhu WH, Wang HR, Guo YL, Ge KL, Wang YN. Effects of Brucine on the Proliferation of Human Gastric Cancer Cells and its Molecular Mechanism. *Asia-pacific Traditional Med (Chinese)* (2019) 15 (04):19–23. doi: 10.11954/ytctyy.201904006
34. Chen H, Wang ZH, Chen L, Fan HW, Zhou B, Xu LB, et al. Effects of Rucoridine on Proliferation and Apoptosis of Human Pancreatic Cancer SW1990 Cell Line *In Vitro* and In Vivo. *J Wenzhou Med Univ (Chinese)* (2017) 47(06):431–4. doi: 10.3969/j.issn.2095-9400.2017.06.009
35. Su WZ, Zhu JW, Xu HH, Wang Y, Liu SH, Luo SY, et al. Evodogine Inhibited the Proliferation and Promoted Apoptosis of Human Oste Osarcoma HOS Cells. *J Anatomical Res (Chinese)* (2019) 41(02):135–9.
36. Cai KH, Zhang S, Guo H, Wang JB, Yang RL, Yang HY. Effect of Rutadiine on the Proliferation of Human Lung Adenocarcinoma Cell Line A549. *Chem Biol Eng (Chinese)* (2018) 35(10):16–20. doi: 10.3969/j.issn.1672-5425.2018.10.004
37. Guo H, Wang ZZ, Yang Q, Liu DM, Yang YY, Wang CL. Study on the Inhibitory Effect of Rucordinine on the Proliferation of Three Kinds of Tumor Cells In Vitro. *Pharmacol Clin Of Chin Materia Med (Chinese)* (2015) 31(05):44–7.
38. Guo H, Yang YY, Yu DL, Wang CL, Zhang S. Synthesis, Structural Characterization and *In Vivo* Antitumor Activity of Rucornidine. *Chem Biol Eng (Chinese)* (2010) 27(10):37–40.
39. Shao YY. *Effects of Dihydroartemisinin on Apoptosis, Migration and Invasion of Glioma Cells and its Mechanism*. Chongqing: Chongqing Medical University (Chinese) (2018).
40. Wang HG, Li YT, Cai K, Han XL, Yuan LX, Yang JS, et al. Artemisinin Inhibits the Proliferation of Human Hepatocellular Carcinoma Cells Huh7 and SMMC-7721 and its Mechanism. *West China J Pharm (Chinese)* (2019) 34(06):1–4. doi: 10.13375/j.cnki.wcjps.2019.06.007
41. Li YW, Zhang W, Li Y, Xu JJ, Zhang H, Lv SJ, et al. Molecular Mechanism of Artemisinin Induced Apoptosis of Human Hepatoma Hepg2 by Mitochondrial Pathway. *Chin J Toxicol (Chinese)* (2018) 32(03):194–8. doi: 10.16421/j.cnki.1002-3127.2018.03.004
42. Yu HP, Cui L, Wang BR, Liu JH, Wang K. Effects of Artemisinin on Growth Inhibition and CD71 Expression in Breast Cancer MT40 Cells. *J Huazhong Univ Sci Technol (Med Ed) (Chinese)* (2018) 47(03):295–9. doi: 10.3870/j.issn.1672-0741.2018.03.008
43. Zhu WH, Xu N, Xu JJ, Zhang H, Li Y, Lv SJ, et al. Effects of Dihydroartemisinin on the Proliferation and Apoptosis of Human Pancreatic Cancer Cell Lines. *Acta Anatomic Sin (Chinese)* (2018) 49(01):70–4.
44. Zhang Q, Wang YM, Jiang WW, Gu XG, Zhang CL. Antitumor Effects of Dihydroartemisinin Alone and in Combination With Methotrexate in Cutaneous T-Cell Lymphoma Cell Line. *Chin J Dermatol Venereol Integrated Traditional Western Med (Chinese)* (2018) 17(02):112–7. doi: 10.3969/j.issn.1672-0709.2018.02.005
45. Liu YM, Gao SJ, Sun H. Research Progress of Artemisinin and its Derivatives Against Ovarian Cancer. *Prog Modern Obstet Gynecol (Chinese)* (2018) 27 (04):305–7. doi: 10.13283/j.cnki.xdfckjz.2018.04.014
46. Jin T, Li TJ, Wu T, Wang Y, Zhou DP. Antitumor Mechanism and Toxicity of Paclitaxel. *J Northeast Agric Univ (Chinese)* (2005) 06):816–9. doi: 10.3969/j.issn.1005-9369.2005.06.026
47. Qin TT. *of Luteolin Combined With Paclitaxel on Esophageal Cancer In Vivo and In Vitro*. Zhengzhou: Zhengzhou University (Chinese) (2019).
48. Zhang FM, Zhu CK, Sun XF, Xu PS. PD1 Antibody Combined With Paclitaxel Chemotherapy Enhances Anti-Tumor Efficacy in Breast Cancer Mice. *Chin J Immunol (Chinese)* (2019) 35(10):874–8.
49. Wang HF, Chen J, Li LQ. Research Progress in Antitumor Mechanism of Triptolide. *J Med Philosophy (B) (Chinese)* (2018) 39(11):68–71. doi: 10.12014/j.issn.1002-0772.2018.11b.22
50. Xin Y, Gu YH. Effects of Triptolide on Autophagy in Colon Cancer Cells by Inhibiting P13K/AKT Signaling. *Chin J Clin Pharmacol (Chinese)* (2019) 35 (16):1798–801. doi: 10.13699/j.cnki.1001-6821.2019.16.022
51. Guan CL, Zheng J, Wang HL. Effect of Triptolide on Ishikawa Cells of Endometrial Carcinoma. *Chin Traditional Med (Chinese)* (2019) 41 (07):1706–10. doi: 10.3969/j.issn.1001-1528.2019.07.044
52. He BY. *Effect of Tripterine on Apoptosis of Human Ovarian Cancer SKOV3 Cells Induced by Reactive Oxygen Species*. Jinzhou: Jinzhou Medical University (Chinese) (2018).
53. Cui Y. *Effects of Arsenic Trioxide on MHCC97H Liver Cancer Stem Cells*. Hengyang: University of South China (Chinese) (2017).
54. Huang Y, Zhu H, Gao J. Effects of Arsenic Trioxide on the Expression of P53, Bax and Bcl-2 Proteins in Mouse B16 Cells. *J Binzhou Med Coll (Chinese)* (2019) 42(06):411–4. doi: 10.19739/j.cnki.issn1001-9510.2019.06.003
55. Sun JP, Liu JH, Du DL, Yang XD, Zhang Y. Effects of Arsenic Trioxide on T24 Cell Proliferation and APC Gene Expression in Bladder Carcinoma. *J Bengbu Med Coll (Chinese)* (2018) 43(08):989–92.
56. Shi Y, Lin CQ, Zeng FP, Cao T, Zhang J. The Inhibition of Arsenic Trioxide in Human Breast Cancer Mcf-7 Cells and its Effect on FOXO1 Expression. *Genomics Appl Biol (Chinese)* (2018) 37(07):3238–44. doi: 10.13417/j.gab.037.003238
57. Wang SX, Yu L, He XJ, Wang HJ, Zhang YL, Zhao YY. Effect of As2O3 on Xenograft Tumor of Human Uterine Sarcoma in Nude Mice. *Qilu Med J (Chinese)* (2017) 32(06):656–9.
58. Xu Y. Progress in Antitumor Drugs Targeted by Tubulin Polymerization. *Chin Hosp Drug Eval Anal (Chinese)* (2015) 15(09):1271–3. doi: 10.14009/j.issn.1672-2124.2015.09.052
59. Wang BC. *Antitumor Activity and Mechanism of Podophyllotoxin In Vitro*. Shanghai: East China University of Science and Technology (Chinese) (2013).
60. Xia WZM, Ga ZDJ, Gong QJZ, Lin DY, Miao LY, Zhang LY. Inhibitory Effect of Deoxypodophyllotoxin on SKOV3 Proliferation of Human Ovarian Cancer Cells. *Chin J Gerontol (Chinese)* (2019) 39(07):1689–91. doi: 10.3969/j.issn.1005-9202.2019.07.053
61. Liu B. Effect of Genstein on Resistance of Hepatocellular Carcinoma BEL-7402/5Fu Cells. *Chin J Modern Gen Surg (Chinese)* (2019) 22(02):90–5. doi: 10.3969/j.issn.1009-9905.2019.02.00
62. Tang LJ. *Inhibition and Mechanism of Genistein Derivatives on Proliferation, Migration and Invasion of Breast Cancer Cells*. Hengyang: University of South China (Chinese (2016).
63. Sun J, Shi L, Ji Q, Wang YY, Zhang J. The Role of Autophagy in Inhibiting the Proliferation of Colon Cancer Cell Line HCT116. *J Shanghai Univ Traditional Chin Med (Chinese)* (2018) 32(01):60–4.
64. Chen TT, Yang PW, Zhang SH. Research Progress of Apigenin Anti-Tumor Mechanism. *Chin J Modern Appl Pharm (Chinese)* (2019) 36(04):507–10. doi: 10.13748/j.cnki.issn1007-7693.2019.04.026
65. Yu M, Yuan L, Jiang FJ. Effect of Apigenin on the Proliferation and Invasion of Human Esophageal Carcinoma Eca109 Cells. *J Jining Med Coll (Chinese)* (2019) 42(05):341–4.
66. Li B, Cai Y, Chen H. Effects of Apigenin on the Invasion and Migration of PC9GR Cells in Lung Cancer. *Modern Distance Educ Chin Med (Chinese)* (2019) 17(17):91–4.
67. Cui YH, Chen A, Xu C, Cao JG, Xiang HL, Zhang JS. Apigenin Upregulates SHP-1 Protein Expression and Inhibits STAT3 Phosphorylation and Globulogenesis in Hepatocellular Carcinoma MHCC97H Cells. *J Hunan Normal Univ (Med Ed) (Chinese)* (2018) 15(05):1–4.
68. Zhou LH, Li Y, Sui H, Feng YY, Liu NN, Ji Q, et al. Effects of Tanshinone ii a on Angiogenesis in Human Colon Cancer Cells. *Chin J Traditional Chin Med (Chinese)* (2019) 34(03):947–51.
69. Cheng XZ, Huang FC, Chen JT. Effects of Dihydrotanshinone on Wnt/β-Catenin Signaling Pathway in Colorectal Cancer Cells. *Chin J Clin Pharmacol (Chinese)* (2019) 35(15):1633–5. doi: 10.13699/j.cnki.1001-6821.2019.15.025
70. Chen L. *Tanshinone ii a Reverses Doxorubicin Resistance in Gastric Cancer*

*Cells*. Wuhu: Wannan Medical College (Chinese) (2018).
71. Zhang YJ, Peng BJ, Cao TS, Lu XS, Guo SG. Tanshinone ii a Regulates the Proliferation and Apoptosis of Gastric Cancer Cells by Inhibiting STAT3 Activation. *Chongqing Med (Chinese)* (2019) 48(04):559–63.
72. Wang XY, Zhang GR, Zhao C, Cao WY, Liang YJ, Chu HY, et al. Molecular Mechanism of As2O3 Combined With Tansinone ii a on Colon Cancer Cells. *Chin J Modern Med (Chinese)* (2018) 20(05):5–8. doi: 10.3969/j.issn.1672-9463.2018.05.002
73. He JJ, Li M, Tang GF, Li HZ, Qi XL. Effect of Isocryptotanshinone on Cell Proliferation, Cell Cycle and Apoptosis of Gastric Cancer Cells. *J Clin Oncol (Chinese)* (2019) 24(02):129–32.
74. Hu JX, Shi XW. Study on the Antitumor Effect of Emodin on the Expression of Carbonic Anhydrase ix in Colon Cancer Transplanted Mice. *Chin J Clin Pharmacol (Chinese)* (2019) 35(18):2082–4.
75. Jiao BY, Wang C, Liu Y, Gong YX, Han YH, Jin CH, et al. Emodin Induces Apoptosis of AGS Gastric Cancer Cells by Down-Regulating Prx V Protein Level. *J Heilongjiang Bayi Agric Univ (Chinese)* (2018) 30(01):24–8.
76. Pan SY, Tian L, Li WH. Effects of Aloe Emodin on the Migration and Invasion of Human Endometrial Carcinoma Cells. *World Latest Med Inf Abstracts (Chinese)* (2019) 19(24):108–10.
77. Ma HB, Lin T, Liu XF. Effect of Ginsenoside Rg3 on Multidrug Resistance of Human Bile Duct Cancer Cells. *Guangming Traditional Chin Med (Chinese)* (2018) 33(23):3492–5.
78. Wan PW, Wang Q, Wan C. Ginsenoside Rg3 Reverses Cisplatin Resistance in Gastric Cancer Cells by Down-Regulating PD-L1. *J Med Res (Chinese)* (2018) 47(12):120–5. doi: 10.11969/j.issn.1673-548X.2018.12.028
79. Hu SS, Yan KM, Wang JJ, Guo M, Tie J, Nie YZ, et al. Effect of Ginsenoside Rh_2 on the Sensitivity of Gastric Cancer Cells SGC7901/ADR. *Chin Herbal Med (Chinese)* (2018) 49(17):4313–117. doi: 10.7501/j.issn.0253-2670.2018.17.022
80. Yang MP, Wang Y, Wang XH, Liu JL. Effects of Ginsenoside Rg3 on the Invasion and Drug Resistance of Colorectal Cancer Cell Line Lovo/5-FU. *J Harbin Med Univ (Chinese)* (2018) 52(01):24–8. doi: 10.3969/j.issn.1000-1905.2018.01.006
81. Wei R, Xiao YH, Xu W, Zeng F. Effect of Ginsenoside Rh1 on Invasion and Metastasis of Human Colon Cancer Cells. *Chongqing Med (Chinese)* (2019) 48(12):1996–2000. doi: 10.3969/j.issn.1671-8348.2019.12.004
82. Wei WG, Zhu BC, Jin HM. Study on the Inhibitory Effect of Ginsenoside Rh3 on Human Ovarian Cancer Cell Line SKOV-3. *J Harbin Med Univ (Chinese)* (2018) 52(01):15–8.
83. Chen DY, Shen ZQ, He B. Research Progress in Pharmacological Action and Mechanism of Ginsenoside Active Monomer -20(R) -Ginsenoside Rg3. *Natural Products Res Dev (Chinese)* (2019) 31(07):1285–90. doi: 10.16333/j.1001-6880.2019.7.024
84. Shen LL, Du G. Lycium Barbarum Polysaccharide Stimulates Proliferation of MCF-7 Cells by the ERK Pathway. *Life Sci* (2012) 91:9–10. doi: 10.1016/j.lfs.2012.08.012
85. Chen F. *Effects of Lycium Barbarum Pollen Polysaccharides on PI3K/AKT Signaling Pathway in Prostate Cancer Cells*. Yinchuan: Ningxia Medical University (Chinese (2019).
86. Huang X, Xiao BX, Zhao JW, Mao F, Yao J, Guo JM. Effects of Lycium Barbarum Polysaccharide (LBP) on the Growth of Human Hepatoma Cell Line Hepg2 and its Molecular Mechanism. *Chin Herbal Med (Chinese)* (2010) 41(09):1501–3.
87. Jiang M, Li ZN. Lycium Barbarum Polysaccharide Induces Autophagy to Inhibit Proliferation of Human Tongue Squamous Carcinoma Cells. *Chin J Clin Stomatol (Chinese)* (2017) 33(11):656–9. doi: 10.3969/j.issn.1003-1634.2017.11.006
88. Zhang HL, Gao LP, Leng HT, Li Z. Effects of Lycium Barbarum Polysaccharide Extract on Renal Toxicity Induced by Cisplatin in Rats. *Food Sci (Chinese)* (2012) 33(05):268–71.
89. Xu H. *Antitumor Activity and Potential Mechanism of Lentinan*. Wuhan: Wuhan University (Chinese (2016).
90. Ma L, Rong F, Wang JB, Zhang NP, Liu H. Effects of Lentinan on Apoptosis and PI3K/AKT Signaling Pathway of Leukemia HL-60 Cells In Vitro. *Chin J Pathophysiol (Chinese)* (2019) 35(06):1069–74. doi: 10.3969/j.issn.1000-4718.2019.06.017
91. Wan QL, Ren YH, Lu RN, Li Y, Chen CB, Liu SY. Effects of Lentinan on Proliferation, Cycle, Apoptosis and Migration of Glioma SHG-44 Cells. *Chin Patent Med (Chinese)* (2019) 41(11):2614–9.
92. Yan YN, Wang JJ, Yuan Y, Wan LZ. Effects of Lentinus Edodes Polysaccharide on the Proliferation of Oral Squamous Cell Carcinoma Cells. *J Oral Biomed (Chinese)* (2018) 9(02):79–81.
93. Xu BY, Hu J, Liu J, Dai N, Hu M, He YC. Effect of Antitumor Traditional Chinese Medicine on Apoptosis of Tumor Cells. *Famous Doctor (Chinese)* (2018) 10):25.
94. Liu ZM, Zhang JL, Mou ZY, Lv JT. Antitumor Angiogenesis of Chinese Herbal Monomer and its Mechanism. *Chin J Traditional Chin Med (Chinese)* (2019) 25(08):44–7.
95. Zhou M, Song X, Huang Y, Wei L, Li Z, You Q, et al. Wogonin Inhibits H2O2-Induced Angiogenesis *via* Suppressing PI3K/Akt/NF-κb Signaling Pathway. *Vasc Pharmacol (Chinese)* (2014) 60(3):110–9. doi: 10.1016/j.vph.2014.01.010
96. Yu HT, Fu MJ. Chinese Herbal Medicine Reverses Multidrug Resistance in Tumor. *Clin Res Traditional Chin Med (Chinese)* (2019) 11(27):71–4.
97. Zhong SB, Liu WQ, Li RL, Ling YZ, Li ZH, Tu GZ, et al. Biosynthesis and Antitumor Activity of Taxyl Alkaloids. *Chin J Pharmacol (Chinese)* (1994) 29(01):33–8.
98. Ye XR, Chai YH, Li XN, Wu KM. Synthesis and Antitumor Activity of Harringtonine Derivatives. *Acta Pharm Sin (Chinese)* (2004) 39(06):429–33. doi: 10.3321/j.issn:0513-4870.2004.06.007
99. Wu X, Gong L, Chen C, Tao Y, Zhou W, Kong L, et al. Semi-Synthesis of Harringtonolide Derivatives and Their Antiproliferative Activity. *Molecules (Chinese)* (2021) 26(5):1380. doi: 10.3390/molecules26051380
100. Huang KD, Gao SY, Liu KK, Wang YL, Cao T, Wang J, et al. Progress in Structural Modification of Anticancer Drug Camptothecin Derivatives. *Guangzhou Chem Industry (Chinese)* (2018) 46(15):17–9.
101. Garciacarbonero R, Supko JG. Current Perspectives on the Clinical Experience. *Pharmacol Continued Dev Camptothecins* (2002) 08(03):641–61. doi: 10.2307/1994032
102. Ito S, Takagawa R, Minami Y, Watanabe J, Masui H. Clinical Efficacy of Low-Dose CDDP and CPT-11 Therapy as Second- or Third-Line Chemotherapy for Advanced and Recurrent Gastric Cancer. *Gan to Kagaku Ryoho Cancer Chemother* (2014) 41(09):1107–11.
103. Mathijssen RH, Alphen RJV, Verweij J, Loos WJ, Nooter K, Stoter G, et al. Clinical Pharmacokinetics and Metabolism of Irinotecan (CPT-11). *Clin Cancer Res Official J Am AssocCancer Res* (2001) 7(8):2182–94. doi: 10.1093/carcin/22.8.1327
104. Taylor J, Amanze A, Di Federico E, Verschraegen C. Irinotecan Use During Pregnancy. *Obstet Gynecol* (2009) 114:451–2. doi: 10.1097/AOG.0b013e3181a1d478
105. Guerrant W, Patil V, Canzoneri JC, Yao LP, Hood R, Oyelere AK. Dual-Acting Histone Deacetylase-Topoisomerase I Inhibitors. *Bioorganic Medicinal Chem Lett* (2013) 23(11):3283–7. doi: 10.1016/j.bmcl.2013.03.108
106. Zhao X, Goto M, Song ZL, Morrisnatschke SL, Zhao Y, Wu D, et al. Design and Synthesis of New 7-(N-Substituted-Methyl)-Camptothecin Derivatives as Potent Cytotoxic Agents. *Bioorg Med Chem Lett* (2014) 24(16):3850–3. doi: 10.1016/j.bmcl.2014.06.060
107. Wang L. *Structural Modification of Camptothecin*. Shanghai: East China Normal University (Chinese (2016).
108. Hu LJ. *Design, Synthesis and Antitumor Structural-Activity Relationship of Vinorelbine Derivatives*. Hangzhou: Zhejiang University of Technology (Chinese (2013).
109. Li FN. *Semi-Synthesis and Antitumor Activity Evaluation of 3-Phenylethyl-6 '-Epoxy-Nitro Vinblastine*. Wuhan: China University of Science and Technology (Chinese (2012).
110. Wei Q, Sun T. Research Progress on Antitumor Active Constituents and Derivatives of Taxus Chinensis. *Nat Products Res Dev (Chinese)* (2016) 28 (10):1664–75.
111. Che X, Shen L, Xu H, Liu K. Isolation and Characterization of Process-Related Impurities and Degradation Products in Larotaxel. *J Pharm Biomed Anal* (2011) 55(5):1190–6. doi: 10.1016/j.jpba.2011.03.036
112. Shin I, Kouichi U, Satoru O, Jun CB, Toshiharu Y, Michio I, et al. Orally Active Docetaxel Analogue: Synthesis of 10-Deoxy-10-C-Morpholinoethyl Docetaxel Analogues. *Bioorg Med Chem Lett* (2001) 11(3):407–10. doi:

10.1016/S0960-894X(00)00682-X
113. Roh EJ, Song CE, Kim D, Pae HO, Chung HT, Lee KS, et al. Synthesis and Biology of 3'-N-Acyl-N-Debenzoylpaclitaxel Analogues. *Bioorganic Medicinal Chem* (1999) 7(9):2115–9. doi: 10.1016/S0968-0896(99)00173-X
114. Wu GR. *Derivatives: Design, Synthesis and In Vitro Antitumor Activity Evaluation*. Beijing: Beijing University of Chinese Medicine (Chinese (2019).
115. Gao YT, Cao S, Peng Y, Wang H, Wang YZ, Chen H. Effect and Mechanism of Podophyllotoxin Derivative ZM-10 on Oral Squamous Cell Carcinoma KB Cell Line. *J Armed Police Logistics Coll (Med Ed) (Chinese)* (2017) 26(06):466–9.
116. Leng L, Gao CG, Chen H, Niu C, Cao B. Effect of Podophyllotoxin Derivative QW-83 on Apoptosis of Human Cervical Carcinoma Hela Cells and its Mechanism. *Chin Pharm (Chinese)* (2016) 27(07):892–5. doi: 10.6039/j.issn.1001-0408.2016.07.09
117. Tian DL, Liang CP, Liang J, Chen H. Synthesis and Anticancer Activity of Novel Indolepodophyllotoxin Derivatives. *China J Traditional Chin Med (Chinese)* (2019) 44(12):2532–7. doi: 10.19540/j.cnki.cjcmm.20190321.207
118. Wang P, Tao ZW, Zheng XH, Liu TT. Synthesis and *In Vitro* Antitumor Activity of Novel Ester Matrine Derivatives. *China J N Drugs (Chinese)* (2012) 21(21):2547–51.
119. Wang L, You Y, Wang S, Liu X, Liu B, Wang J, et al. Synthesis, Characterization and *In Vitro* Anti-Tumor Activities of Matrine Derivatives. *Bioorg Med Chem Lett* (2012) 22(12):4100–2. doi: 10.1016/j.bmcl.2012.04.069
120. He LQ, Huang P, Wang XS. Synthesis and Antitumor Activity of Matrine Derivatives. *Chem World (Chinese)* (2011) 52(09):523–5. doi: 10.3969/j.issn.0367-6358.2011.09.004
121. Zhang N, Cui XY, Zhao XM, Li DD, Dai LL, Tao ZW. Synthesis and Antitumor Activity of Glycyrrhetinic Acid-Matrine Complex. *Modern Med Clin (Chinese)* (2014) 29(11):1199–202. doi: 10.7501/j.issn.1674-5515.2014.11.026
122. Dong G, Wang S, Miao Z, Yao J, Zhang Y, Guo Z, et al. New Tricks for an Old Natural Product: Discovery of Highly Potent Evodiamine Derivatives as Novel Antitumor Agents by Systemic Structure–Activity Relationship Analysis and Biological Evaluations. *J Med Chem* (2012) 55(17):7593–613. doi: 10.1021/jm300605m
123. Dong G, Sheng C, Wang S, Miao Z, Yao J, Zhang W. Selection of Evodiamine as a Novel Topoisomerase I Inhibitor by Structure-Based Virtual Screening and Hit Optimization of Evodiamine Derivatives as Antitumor Agents. *J Med Chem* (2010) 53(21):7521–31. doi: 10.1021/jm100387d
124. Xiang HL, Geng YJ, Zhi-Juan WU, Zhao XF, Cao JG. Synthesis and Anti-Hepatoma Activities of Apigenin Etherified and Brominated Derivatives. *J Hunan Normal Univ* (2009) 6(03):26–9. doi: 10.3969/j.issn.1673-016X.2009.03.008
125. Chen L. *Synthesis of Bioactive Apigenin and Acacia Glycosides and Flavonoid Glycoconjugates*. Changsha: Hunan University (Chinese (2012).
126. Han TJ. *Design and Synthesis of Six Flavonoid 7-Aminophosphate Derivatives*. Dalian: Dalian University of Technology (Chinese (2012).
127. Daskiewicz JB, Depeint F, Viornery L, Bayet C, Comte-Sarrazin G, Comte G, et al. Effects of Flavonoids on Cell Proliferation and Caspase Activation in a Human Colonic Cell Line HT29: An SAR Study. *J Med Chem* (2005) 48 (8):2790–804. doi: 10.1021/jm040770b
128. Frhlich T, Ndreshkjana B, Muenzner JK, Reiter C, Hofmeister E, Mederer S, et al. Synthesis of Novel Hybrids of Thymoquinone and Artemisinin With High Activity and Selectivity Against Colon Cancer. *Chemmedchem* (2017) 12(3):226–34. doi: 10.1002/cmdc.201600594
129. Xu CC, Deng T, Fan ML, Lv WB, Yu BY. Synthesis and *In Vitro* Antitumor Evaluation of Dihydroartemisinin-Cinnamic Acid Ester Derivatives. *Eur J Med Chem* (2015) 107:192–203. doi: 10.1016/j.ejmech.2015.11.003
130. Zhang CJ, Wang JG, Zhang JB, Lee YM. Mechanism-Guided Design and Synthesis of a Mitochondria-Targeting Artemisinin Analogue With Enhanced Anticancer Activity. *Angew Chem Int Ed* (2016) 55(44):13770–4. doi: 10.1002/anie.201607303

**Conflict of Interest:** Author A-HL is employed by Shaanxi Pharmaceutical Holding Group Co., LTD, China. Author H-LC previously acted as an advisor for Shaanxi Pharmaceutical Holding Group Co., LTD, China.

The remaining authors declare that the research was conducted in the absence of any commercial or financial relationships that could be construed as a potential conflict of interest.

**Publisher's Note:** All claims expressed in this article are solely those of the authors and do not necessarily represent those of their affiliated organizations, or those of the publisher, the editors and the reviewers. Any product that may be evaluated in this article, or claim that may be made by its manufacturer, is not guaranteed or endorsed by the publisher.

frontiers | Frontiers in Oncology

ORIGINAL RESEARCH
published: 13 May 2022
doi: 10.3389/fonc.2022.873649

# DHW-221, a Dual PI3K/mTOR Inhibitor, Overcomes Multidrug Resistance by Targeting P-Glycoprotein (P-gp/ABCB1) and Akt-Mediated FOXO3a Nuclear Translocation in Non-small Cell Lung Cancer

*Mingyue Liu[1], Chang Xu[1], Xiaochun Qin[1], Wenwu Liu[1], Deping Li[1], Hui Jia[2], Xudong Gao[3], Yuting Wu[1], Qiong Wu[3], Xiangbo Xu[1], Bo Xing[1], Xiaowen Jiang[1], Hongyuan Lu[4], Yingshi Zhang[1]*, Huaiwei Ding[5,6]* and Qingchun Zhao[1,3]**

[1] Department of Life Science and Biochemistry, Shenyang Pharmaceutical University, Shenyang, China, [2] School of Traditional Chinese Medicine, Shenyang Pharmaceutical University, Shenyang, China, [3] Department of Pharmacy, General Hospital of Northern Theater Command, Shenyang, China, [4] School of Pharmacy, China Medical University, Shenyang, China, [5] Key Laboratory of Structure-Based Drug Design and Discovery of Ministry of Education, Shenyang Pharmaceutical University, Shenyang, China, [6] State Key Laboratory of Chemical Oncogenomics, Tsinghua Shenzhen International Graduate School, Shenzhen, China

Multidrug resistance (MDR) is considered as a primary hindrance for paclitaxel failure in non-small cell lung cancer (NSCLC) patients, in which P-glycoprotein (P-gp) is overexpressed and the PI3K/Akt signaling pathway is dysregulated. Previously, we designed and synthesized DHW-221, a dual PI3K/mTOR inhibitor, which exerts a remarkable antitumor potency in NSCLC cells, but its effects and underlying mechanisms in resistant NSCLC cells remain unknown. Here, we reported for the first time that DHW-221 had favorable antiproliferative activity and suppressed cell migration and invasion in A549/Taxol cells *in vitro* and *in vivo*. Importantly, DHW-221 acted as a P-gp inhibitor *via* binding to P-gp, which resulted in decreased P-gp expression and function. A mechanistic study revealed that the DHW-221-induced FOXO3a nuclear translocation *via* Akt inhibition was involved in mitochondrial apoptosis and G0/G1 cell cycle arrest only in A549/Taxol cells and not in A549 cells. Interestingly, we observed that high-concentration DHW-221 reinforced the pro-paraptotic effect *via* stimulating endoplasmic reticulum (ER) stress and the mitogen-activated protein kinase (MAPK) pathway. Additionally, intragastrically administrated DHW-221 generated superior potency without obvious toxicity *via* FOXO3a nuclear translocation in an orthotopic A549/Taxol tumor mouse model. In conclusion, these results demonstrated that DHW-221, as a novel P-gp inhibitor, represents a prospective therapeutic candidate to overcome MDR in Taxol-resistant NSCLC treatment.

**Keywords: NSCLC, P-glycoprotein, FOXO3a nuclear translocation, Multidrug resistance, DHW-221, paraptosis**

OPEN ACCESS

***Edited by:***
*Qingbin Cui,*
*University of Toledo, United States*

***Reviewed by:***
*Ning Ji,*
*Tianjin Medical University Cancer Institute and Hospital, China*
*Yingbo Huang,*
*University of Minnesota, United States*

***Correspondence:**
*Qingchun Zhao*
*zhaoqingchun1967@163.com*
*Huaiwei Ding*
*dinghuaiwei627@163.com*
*Yingshi Zhang*
*zhangyingshi526@163.com*

***Specialty section:***
*This article was submitted to Pharmacology of Anti-Cancer Drugs, a section of the journal Frontiers in Oncology*

***Received:*** *11 February 2022*
***Accepted:*** *23 March 2022*
***Published:*** *13 May 2022*

***Citation:***
*Liu M, Xu C, Qin X, Liu W, Li D, Jia H, Gao X, Wu Y, Wu Q, Xu X, Xing B, Jiang X, Lu H, Zhang Y, Ding H and Zhao Q (2022) DHW-221, a Dual PI3K/mTOR Inhibitor, Overcomes Multidrug Resistance by Targeting P-Glycoprotein (P-gp/ABCB1) and Akt-Mediated FOXO3a Nuclear Translocation in Non-small Cell Lung Cancer. Front. Oncol. 12:873649. doi: 10.3389/fonc.2022.873649*

## INTRODUCTION

Non-small cell lung cancer (NSCLC) has become one of the most prevalent malignant tumors with a high incidence and fatality rate worldwide (1–3). Most NSCLC patients are diagnosed at an unresectable stage (3). Despite continuous efforts to develop efficient treatment strategies, the intrinsic and acquired resistance of chemotherapeutic agents, especially for multidrug resistance (MDR), is still a limitation for improving the efficiency of chemotherapeutics (4). Paclitaxel, a microtubule stabilizer, has become the first-line chemotherapeutic drug in the fight against advanced and metastatic NSCLC, yet acquired resistance to Taxol, including MDR, is frequently encountered, thereby leading to treatment failure and relapse (5, 6). Therefore, developing alternative therapeutic approaches is important to better understand the molecular mechanism of Taxol resistance and improve the prognosis of patients with Taxol-resistant NSCLC.

MDR in cancer is induced by various mechanisms, including the overexpression of ATP-binding cassette (ABC) transporters, enhancement of damaged DNA self-repair capacity, elevation of xenobiotics metabolisms, change of genetic factors, and abnormal activation of related signaling pathways (7, 8). P-Glycoprotein (P-gp), an ABC transporter, is encoded by ABC subfamily B member 1 (ABCB1) and is highly expressed in MDR cells, and it is responsible for decreasing drug accumulation to confer drug resistance to chemotherapeutic agents, especially to Taxol (9, 10). Therefore, it is extremely urgent to develop a novel P-gp inhibitor or antitumor drug that is not a P-gp substrate to avoid the efflux of chemotherapeutic agents and increase drug sensitivity, thereby preventing P-gp-mediated MDR.

Phosphatidylinositol-3-kinase, a lipid kinase, plays a vital role in cell proliferation, cell survival, cell cycle progression, migration, and invasion (11). More importantly, the PI3K/Akt signaling pathway is activated in cancers, including MDR tumors, and is directly involved in controlling growth regulatory transcription factors (12, 13). Forkhead box O3a (FOXO3a), a tumor suppressor in the FOXO transcription factor family (FOXO1, FOXO3, FOXO4, and FOXO6), is particularly important due to its unique role in cell apoptosis, cell cycle arrest, and longevity (14). In addition, FOXO3a, a direct downstream target of Akt, is phosphorylated by Akt at Thr32, Ser253, and Ser315, which releases it from the nucleus into the cytoplasm in an inactive form where it undergoes subsequent protease-dependent degradation (14, 15). Recently, overexpression of FOXO3a has been shown to overcome or reverse drug resistance in ovarian (16), luminal breast (17), pancreatic (18), lung (19), and colorectal (20) cancers. Consequently, blockade of the PI3K/Akt signaling pathway contributes to the activation the FOXO3a-mediated cell death progress in treating Taxol-resistant NSCLC.

Given the important role of the PI3K/Akt/mTOR signaling pathway in cancer, it has been reported that CMG002, a PI3K/mTOR dual-target inhibitor, overcomes chemoresistance in ovarian cancer (21). Additionally, studies have shown that inhibition or knockout of PI3K 110α contributes to overcome P-gp-mediated MDR in cancer (22). In a previous study, we designed and synthesized a novel PI3K/mTOR dual inhibitor, 2,4-difluoro-*N*-(5-(1-(4-(2-hydroxyethoxy)phenyl)-1*H*-benzo[*d*]imidazol-6-yl)-2-methoxypyridin-3-yl)benzenesulfonamide (DHW-221), and we demonstrated that it exerts a remarkable antitumor activity in NSCLC cells (23, 24). However, the effect of DHW-221 in Taxol-resistant NSCLC cells remains unclear. In the present study, we aimed to elucidate the molecular mechanisms of DHW-221 in overcoming MDR in A549/Taxol cells *in vitro* and *in vivo*.

**Abbreviations:** NSCLC, non-small cell lung cancer; MDR, multidrug resistance; Taxol, Paclitaxel; ABC, ATP-binding cassette; P-gp, P-glycoprotein; ABCB1, ABC subfamily B member 1; PI3K, phosphatidylinositol-3-kinase; FOXO3a, Forkhead box O3a; MTT, 3-(4,5-dimethylthiazol-2-yl)-2,5-diphenyltetrazolium bromide; Rho-123, Rhodamine; DAPI, 4,6-diamino-2-phenyl indole; HE, hematoxylin and eosin; IHC, immunohistochemistry; EMT, epithelial–mesenchymal transition; μM, micromolar; μm, micrometer; IC50, 50% inhibitory concentration; p-FOXO3a, phosphorylated FOXO3a; p-Akt, phosphorylated Akt.

## MATERIALS AND METHODS

### Compounds and Reagents

DHW-221 was synthesized and purified as described previously (23). GDC-0980 and MG132 were obtained from Bide Pharmtech Ltd. (Shanghai, China). Taxol, docetaxel, vincristine, cisplatin, verapamil, and cycloheximide (CHX) were purchased from MedChem Express (NJ, USA). Rhodamine (Rho-123) and crystal violet were obtained from Shanghai Maclin Biochemical Co., Ltd. (Shanghai, China). Hoechst 33342 and 4,6-diamino-2-phenyl indole (DAPI) were obtained from Beyotime Biotechnology (Nanjing, China). The Annexin-V fluorescein isothiocyanate (FITC)/PI-double staining apoptosis detection kit and propidium iodide (PI) were obtained from Becton, Dickinson and Company (NJ, USA). P-gp antibody (CST, #13978; Rabbit, AF5185), PI3Kp110α antibody (rabbit, AF5112), p-FOXO3a (Ser253) antibody (rabbit, AF3020), and Bim antibody (Rabbit, AF0121) were purchased from Affinity Biosciences Pty Ltd. (Melbourne). Lactic dehydrogenase (LDH) detection kit (WL03271) and other primary antibodies were purchased from Wanlei Biotechnology Co., Ltd. (Shenyang, China)

### Cell Culture

Taxol-sensitive A549 cells and Taxol-resistant A549 (A549/Taxol) cells were generously gifted by Prof. Yang at Shenyang Pharmaceutical University. Cells were cultured in Roswell Park Memorial Institute (RPMI) 1640 medium supplemented with 10% fetal bovine serum (FBS) and 1% penicillin-streptomycin at 37°C and 5% $CO_2$. To maintain resistant characteristics, A549/Taxol cells were cultured in medium containing 300 nM Taxol, which was replaced with drug-free culture medium for 7 days during the experiment.

### Cell Viability Assay

A 3-(4, 5-dimethylthiazol-2-yl)-2, 5-diphenyltetrazolium bromide (MTT) assay and LDH assay were selected to evaluate the effects of DHW-221 and other drugs on cell viability. First, cells were seeded into 96-well plates at $6 \times 10^3$ cells/well. After

cell adherence, cells were treated with various concentrations of DHW-221 and other drugs for the indicated times. For the MTT assay, cells were cultured with MTT (5 mg/ml) for 4 h. The supernatant was discarded, and the formed formazan crystals were dissolved by dimethylsulfoxide (DMSO). Absorbance was recorded at 490 nm using a microplate reader (Elx 800, Bio-Tek, Winooski, Vermont, USA ). The half-maximal inhibitory concentration ($IC_{50}$) values were calculated by GraphPad Prism 7.0 software (San Diego, CA, USA). Importantly, the resistance index (RI) was calculated using the following formula: RI = ($IC_{50}$ of A549/Taxol cells)/($IC_{50}$ of A549 cells). For the LDH assay, the cell supernatant was collected from each well and incubated with the reagent mixture according to the manufacturer's instructions. LDH release was measured as an indicator of cytotoxicity at 450 nm by a microplate reader (Elx 800, Bio-Tek, Winooski, Vermont, USA).

## Colony Formation Assay

To evaluate the long-term antiproliferative activity of DHW-221, colony formation assay was performed as previously described (25). First, cells were seeded into six-well plates at approximately $1.5\times10^3$ cells/well. After adherence, cells were treated with various concentrations of DHW-221 and GDC-0980. After 48 h, the medium was replaced with drug-free medium followed by incubation for an additional 10 days. The colonies were fixed with methanol for 10–s20 min and then stained with 0.1% (w/v) crystal violet for 30 min. Finally, 30% glacial acetic acid was used to dissolve the crystal violet, and the absorbance was measured at 570 nm by a microplate reader (Elx 800, Bio-Tek, Winooski, Vermont, USA).

## Hoechst 33342 Staining, Mitochondrial Membrane Potential (MMP) Assay, and Annexin-FITC/PI Assay

Hoechst 33342 staining, a mitochondrial membrane potential (MMP) assay, and an Annexin-FITC/PI assay were used to detect cell apoptosis. First, cells were seeded into six-well plates at $1.0 \times 10^5$ cells/well and cultured overnight. Cells were then treated with various concentrations of DHW-221 and GDC-0980 for 48 h. For Hoechst 33342 staining and the MMP assay, cells were washed twice with cold phosphate-buffered saline (PBS), then stained with Hoechst 33342 or JC-1 staining solution for 15 min in the dark and then imaged using a confocal microscope (Olympus Corp., Tokyo, Japan). After Hoechst 33342 staining, normal and necrotic cells showed weak blue fluorescence, while apoptotic cells showed strong blue fluorescence. After JC-1 staining, the appearance of red and green fluorescence represented normal and decreased mitochondrial membrane potential, respectively. Of note, decreased MMP is a hallmark event in the early stages of apoptosis. For the Annexin-FITC/PI double staining assay, cells were collected, washed twice with cold PBS, and suspended in 1× binding buffer. Cells were then stained with FITC-conjugated Annexin V for 5 min, and PI was added to the cells for 15 min in the dark. Cells were then analyzed using a FACSCalibur flow cytometer (BD Biosciences, San Jose, CA, USA).

## Cell Cycle Assay

To determine the effect of DHW-221 on cell cycle distribution, PI staining was performed as described previously (25). Cells were seeded into the six-well plates at $1.0 \times 10^5$ cells/well and incubated overnight. After adherence, cells were treated with various concentrations of DHW-221 and GDC-0980. After 48 h, cells were harvested and fixed in 70% cold ethanol at −20°C overnight. Next, cells were washed twice with cold PBS and stained with PI for 15 min in the dark. Finally, cells were analyzed using a FACSCalibur flow cytometer (BD Biosciences, CA, USA).

## Western Blot Analysis

Western blot analysis was used to investigate the effect of drugs on the expression levels of different proteins. First, cells were seeded into 100-mm culture dishes and incubated overnight. After treatment with various concentrations of DHW-221 and other drugs for a specified time, cells were harvested, lysed in radioimmunoprecipitation assay buffer (RIPA) buffer with 0.1 M phenylmethylsulfonyl fluoride (PMSF) and centrifuged at 13,000 rpm for 10 min at 4°C. The total protein concentration was detected using a BCA protein assay kit (Beyotime, China). The cell lysates were mixed with sample dye and boiled at 100°C for 10 min. The proteins were then resolved by sodium dodecyl sulfate–polyacrylamide gel electrophoresis (SDS-PAGE) and transferred onto polyvinylidene fluoride (PVDF) membranes. Subsequently, the PVDF membranes were blocked with 5% non-fat milk dissolved in Tris-buffered saline solution with Tween® 20 (TBST) buffer for 2 h at room temperature followed by incubation with the following primary antibodies overnight at 4°C: rabbit anti-P-gp (1:1,000), anti-PI3Kp110α (1:1,000), and anti-FOXO3a (1:1,000). After incubation with peroxidase-conjugated secondary antibodies (1:12,000) for 1 h at room temperature, the protein bands were visualized with an ultrasensitive ECL chemiluminescence detection kit and analyzed by ImageJ software (National Institute of Health, MD).

## Nuclear and Cytoplasmic Fractionation

To investigate the subcellular localization of FOXO3a, the subcellular fractionation of cells was conducted with a Nuclear and Cytoplasmic Protein Extraction Kit (Wanlei, WLA020a, Shenyang, China) according to the manufacturer's instructions. Cells were harvested, and cytoplasmic protein extraction reagent A was added followed by vortexing. Cytoplasmic protein extraction reagent B was then added. Cells were centrifuged at 12,000 rpm for 5 min at 4°C, and the resulting supernatant was the cytoplasmic protein fraction. Subsequently, the insoluble precipitates were dissolved with nuclear protein extraction reagent C and vortexed vigorously every 2 min for 30 s for eight cycles. After centrifugation at 12,000 rpm for 10 min at 4°C, the resulting supernatant was the nuclear protein fraction.

## Immunofluorescence Staining

To examine the cellular localization of certain proteins, immunofluorescence staining was performed. Cells were seeded into 24-well plates at $5 \times 10^4$ cells/well and incubated overnight.

After treatment with various concentrations of DHW-221 and GDC-0980, cells were fixed with 4% paraformaldehyde, permeabilized with 0.01% (v/v) Triton X-100, incubated with immune staining blocking buffer for 1 h, and then incubated at 4°C overnight with the following primary antibodies: FOXO3a, vimentin, or occludin (1:100). Cells were then incubated with FITC- or Cy3-conjugated (diluted 1:150) goat anti-rabbit IgG (H + L) for 1 h in the dark. DAPI was used to stain cell nuclei for 10 min. Finally, images were obtained with the same confocal microscope (Olympus Corp., Tokyo, Japan) and microscope settings throughout capturing of images. The fluorescence intensities of protein or fluorescent markers in the control and treatment samples were compared at the same threshold. Images were converted into grayscale images with ImageJ software, and positive pixel area (PPA) was analyzed by applying the same threshold to measure the mean fluorescence intensity.

## Wound-Healing Assay and Transwell Assay

A wound-healing assay and a Transwell assay were performed to assess the effect of DHW-221 treatment on the migration and invasion capability of A549/Taxol cells. For the wound-healing assay, cells were seeded into six-well plates at $2.0 \times 10^5$ cells/well and incubated overnight. A 200-μl pipette tip was used to scratch a straight line through the monolayer on the bottom of the six-well plate. After treatment with various concentrations of DHW-221 and GDC-0980 for 24 h, images were acquired using a microscope and subsequently imported into ImageJ software to evaluate the wound area. For the Transwell assay, serum-free medium containing $1.0 \times 10^5$ A549/Taxol cells (200 μl) was placed into the upper chamber of a 24-well Transwell plate (Corning Life Sciences, Bedford, MA, USA) with or without Matrigel, and cells were treated with DHW-221 (0.05, 0.10, and 0.15 μM) and GDC-0980 (0.10 μM). Medium containing 10% FBS (600 μl) was used as a chemoattractant in the lower chamber. After 24 h, the invaded cells in the lower chamber were fixed with methanol, stained with 0.1% crystal violet solution, and imaged using a microscope. Finally, 33% glacial acetic acid solution was added to the lower chamber, which was shaken for 10 min. Absorbance was then measured at 570 nm using a microplate reader (Elx 800, Bio-Tek, Winooski, Vermont, USA).

## Molecular Docking

To predict the potential binding mode of DHW-221 and ABCB1, molecular docking was performed. The crystal structures of the human ABCB1-tariquidar complex (PDB code: 7A6E) and ABCB1-ATP complex (PDB code: 6C0V) were downloaded from Protein Data Bank (http://www.rcsb.org). The Protein Preparation Wizard in Maestro (version 11.5) was utilized to remove water, add hydrogenation, and prime. The DHW-221 was drawn, saved as a "mol." format by ChemDraw14.0 Ultra software, and optimized with the LigPrep module. The Grid Generation Tool was then used to define the binding pocket (20 Å radius) of ABCB1. Finally, the predicted binding conformations of ABCB1-DHW-221 were generated to select the optimal binding mode using the Ligand Docking module and PYMOL 2.5 software. The co-crystallized tariquidar ligand and ATP were selected as templates for molecular docking.

## Cellular Thermal Shift Assay

Cellular Thermal Shift Assay (CETSA) was conducted to explore target engagement of DHW-221 to ABCB1 in A549/Taxol cells. Cells were seeded into 100-mm cultural dishes. After reaching 80%–90% confluency, cells were treated with DMSO, DHW-221 (0.60 μM), or verapamil (0.60 μM) for 3 h. Cells were harvested with a cell scraper, resuspended in cold PBS, and equally divided into six parts into 0.2-ml PCR tubes (80 μl/tube). To lyse cells, six repeated cycles of freeze–thawing (37°C and 57°C) were performed using liquid nitrogen. After centrifugation at 14,000*g* for 30 min at 4°C, 50 μl of the soluble fraction was removed, mixed with SDS-sample buffer (5′), and heated in boiling water for 10 min. The samples were then evaluated by Western blot analysis.

## Intracellular Rho-123 Uptake

Intracellular Rho-123 uptake was performed to evaluate the effect of DHW-221 on P-gp function. Cells were seeded into six-well plates at $1.0 \times 10^5$ cells/well and incubated overnight. After treatment with DHW-221 or verapamil for 48 h, Rho-123 (15 μM) was added into the medium for co-treatment with DHW-221 or verapamil for 3 h in the dark. Cells were then washed twice with cold PBS, fixed with 4% paraformaldehyde for 30 min, permeabilized with 0.1% Triton X-100, and incubated with DAPI for 15 min. Images were acquired using a confocal microscope (Olympus Corp., Tokyo, Japan). Cells were then harvested, washed twice with cold PBS, and resuspended to detect Rho-123 accumulation by FACSCalibur flow cytometer (BD Biosciences, San Jose, CA, USA).

## Human Orthotopic A549/Taxol Mouse Tumor Model

To evaluate the antitumor activity of DHW-221 in Taxol-resistant lung neoplasm, we established a human orthotopic nude mouse model for Taxol-resistant lung cancer *via* tail vein injection. Male nude mice (4–6 weeks old and 18–20 g) were obtained from Beijing Weitonglihua Laboratory Animal Technology Co., Ltd. (Beijing, China, and USA) and fed in specific pathogen-free (SPF) conditions. Specifically, A549/Taxol cells ($2.0 \times 10^6$/200 μl, per mice) were resuspended in cold PBS and inoculated into nude mice *via* tail vein injection. After 7 days, the tumor-bearing nude mice were randomly divided into six groups as follows: model (vehicle, CMC-Na + 1% Tween-80 + 0.3% DMSO), Taxol (10 mg/kg, Taxol injection diluted in saline), DHW-221 (10, 20, and 40 mg/kg, dissolved in the same vehicle as the model group), and GDC-0980 (10 mg/kg, dissolved in the same vehicle as the model group). The nude mice in the Taxol group were intraperitoneally administered with Taxol every 2 days, while the nude mice in the model, DHW-221, and GDC-0980 groups were intragastrically administered daily for 2 weeks. The body weights of the mice in each group were monitored every day. Finally, the mice were sacrificed, and the visceral organs (heart, liver, spleen, lung, and kidney) were removed, weighed, and used for further experiments. Bouin's

solution was used to stain the lung tissues. The other visceral organs were fixed with 4% paraformaldehyde and stored at room temperature for subsequent experiments. The structure of compound DHW-221 was shown in **Figures 1A**.

## Hematoxylin and Eosin Staining and Immunohistochemistry

To examine the histological and pathological changes of DHW-221 in Taxol-resistant lung neoplasm, HE staining and immunohistochemistry (IHC) were performed. All tissues were fixed with 4% paraformaldehyde, dehydrated in a graded ethanol solution (70%, 80%, 90%, 95%, and 100%, v/v), incubated in xylene until transparent, and embedded in paraffin. Subsequently, the tissues were cut into approximately 5-μm-thick sections for further study. For pathological examination, paraffin sections were sequentially deparaffinized in a xylene (xylene I, xylene II, and xylene III) and graded alcohol solution (90%, 80%, and 70%, v/v). Paraffin sections were stained with hematoxylin and eosin (HE) to distinguish tumorous metastatic foci and normal tissues. For IHC, the paraffin sections were incubated with the following primary antibodies: anti-Ki67, anti-FOXO3a, and anti-p-FOXO3a. The sections were then incubated with the appropriate secondary antibody according to the DAB kit. Finally, images were acquired using a Keyence BZ-X700 microscope and BZ-X analyzer software (Osaka, Japan). Brown granules were considered as positive staining in the cytoplasm or nucleus.

## Evaluation of Serum Biochemical Parameters

Serum biochemical parameters were used to evaluate drug toxicity according to the manufacturer's protocols using the corresponding kits obtained from Nanjing Jiancheng Biochemical Co., Ltd. (Nanjing, China). Creatine kinase (CK),

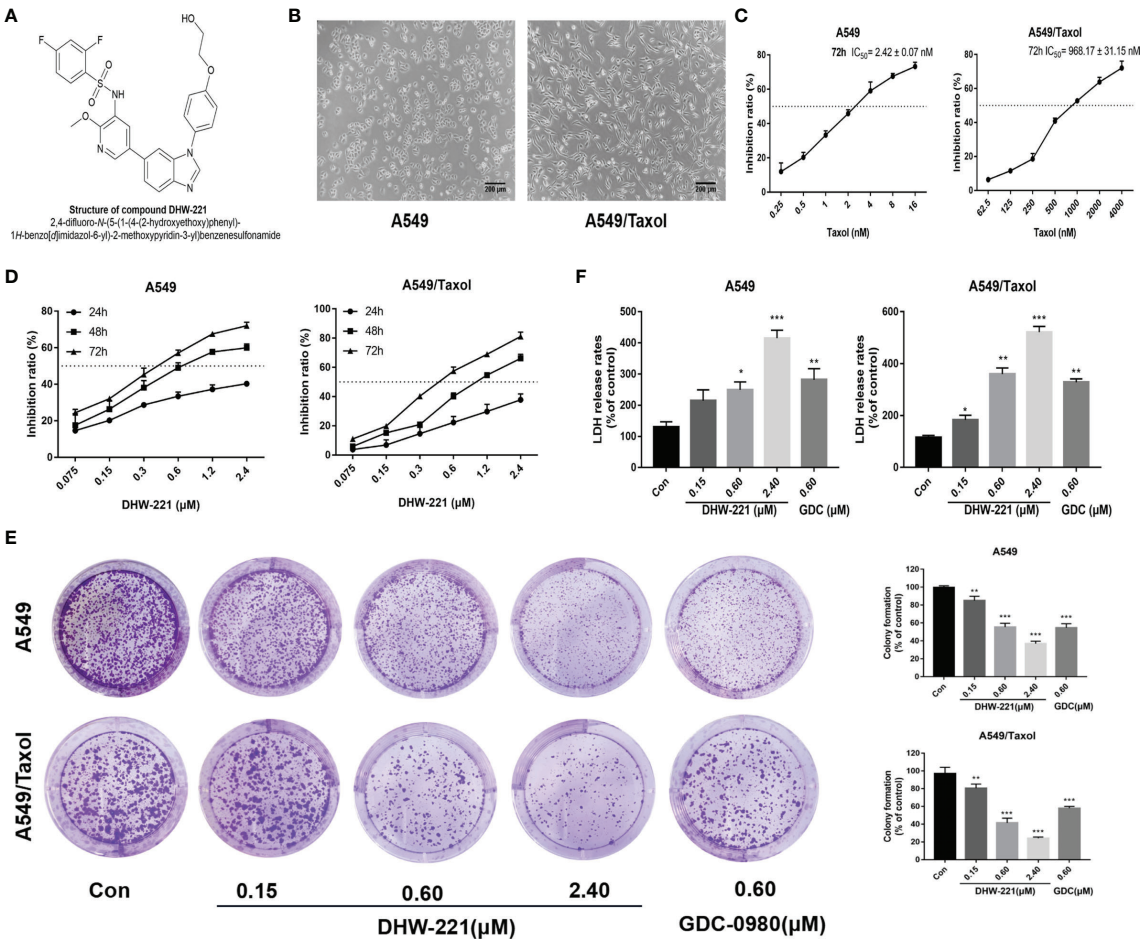


**FIGURE 1** | DHW-221 inhibits cell viability in A549 and A549/Taxol cells. **(A)** The chemical structure of DHW-221h. **(B)** Representative morphology of parental and Taxol-resistant NSCLC cells (A549 and A549/Taxol cells). Scale bar = 200 μm. **(C)** Inhibition effect of A549 and A549/Taxol cells after exposure to Taxol for 72 h. **(D)** Cell viability of A549 and A549/Taxol cells treated with various concentrations of DHW-221 for 24,48, and 72 h. **(E)** The growth-inhibitory effect of DHW-221 on A549 and A549/Taxol cells was measured by colony formation assay; the quantitative results were illustrated as the right panel. **(F)** Cytotoxicity of DHW-221 was examined by LDH release assay for 48 h. Statistical comparisons were performed with one-way ANOVA followed by Dunnett's *post-hoc* test for multiple comparisons (n = 3). Data were expressed as mean ± SD. *p < 0.05, **p < 0.01, ***p < 0.001 versus control.

creatinine (CRE), alanine aminotransferase (ALT), and aspartate aminotransferase (AST) were evaluated to analyze heart, kidney, and liver functions, respectively. Blood was collected from the mouse eye socket and incubated for 1 h at 37°C. After centrifugation twice at 3,500 rpm for 15 min at 4°C, the supernatant (serum) was collected and stored at −80°C. Next, the serum (5 μl) was added to 96-well plates, mixed with different reagents, and incubated for the indicated time according to the manufacturer's instructions. The absorbance was measured at 510 nm using a microplate reader. The ALT, AST, CRE, and CK values in serum were calculated using a standard curve in the manufacturer's instructions.

## Statistical Analysis

All experiments were repeated in triplicate. Data are presented as mean ± SD. Statistical analysis was performed using GraphPad Prism 7.0 software (San Diego, CA, USA). Data were analyzed with one-way ANOVA followed by Dunnett's *post-hoc* test for multiple comparisons. Unpaired Student's t-test was used to compare the difference between two experimental groups. $p < 0.05$ was considered as statistically significant.

# RESULTS

## DHW-221 Exerts Significant Inhibitory Activity in MDR Cancer Cells

Previously, we reported that DHW-221 exerts a remarkable antitumor activity in NSCLC cells (24), but the effect of DHW-221 in MDR NSCLC cells remains unclear. To determine whether A549/Taxol cells are MDR, we compared the cellular morphological changes in A549/Taxol and A549 cells. As depicted in **Figures 1B, C**, A549/Taxol cells were fibrous and elongated with a clear boundary, while A549 cells were cobblestone-like and clustered. In addition, the MTT assay indicated that A549/Taxol cells were resistant to Taxol, docetaxel, vincristine, and cisplatin with the resistance index (RI) values of 403.4, 392.2, 20.5, and 14.2, respectively (**Table 1**). These findings indicated that the A549/Taxol cells were MDR. Next, to evaluate the effect of DHW-221 on the cell viability of A549/Taxol and A549 cells, an MTT assay was performed. Our results showed that DHW-221 exhibited significant cytotoxicity in a concentration- and time-dependent manner in A549/Taxol and A549 cells with an RI of 1.2 (**Figure 1D** and **Table 1**). Of note, the $IC_{50}$ values are shown in **Supplementary Table S1**. Although there was significant inhibitory activity of DHW-221 between 48 and 72 h in both cells (**Supplementary Figure S1**), the tumor cells within 48 h were in the optimal stage of logarithmic growth phase. Hence, we selected the 0.15, 0.60, and 2.40 μM concentrations and 48 h as the optimized conditions for subsequent experiments in A549/Taxol and A549 cells. In addition, colony formation assay was performed to assess the long-term antiproliferative activity of DHW-221. The results demonstrated that DHW-221 decreased the colony formation ability of A549/Taxol and A549 cells in a concentration-dependent manner (**Figure 1E**). Furthermore, an LDH release assay was used to evaluate the cell toxicity of DHW-221, and the results showed that DHW-221 treatment resulted in severe cellular damage as compared to control group in both cells (**Figure 1F**). The above results demonstrated a better antiproliferative activity of DHW-221 (48 h—A549: $IC_{50}$ = 0.631 ± 0.072 μM; A549/Taxol: $IC_{50}$ = 0.874 ± 0.056 μM) than that of GDC-0980 (48 h—A549: $IC_{50}$ = 0.864 ± 0.033 μM; A549/Taxol: $IC_{50}$ = 0.975 ± 0.026 μM), which is a dual PI3K/mTOR inhibitor and was used as a positive control (**Figure 1F** and **Supplementary Figure S1**). These results revealed that DHW-221 exerts a significant inhibitory activity in MDR cancer cells.

## DHW-221 Acts as a P-gp Inhibitor in A549/Taxol Cells Through Inhibiting P-gp Function and Expression

Overexpression of P-gp is the most common cause of MDR in cells, and it causes a decrease in the intracellular concentration of chemotherapeutic drugs (9). To confirm whether A549/Taxol cells exhibit clinically relevant drug resistance, Western blot analysis was performed to detect P-gp expression in A549/Taxol cells. Western blot analysis showed that A549/Taxol cells exhibited a higher expression of P-gp than A549 cells (**Figure 2A**). As a yellow-green fluorescence substrate of P-gp, Rhodamine 123 (Rho-123) directly reflects P-gp function according to cellular accumulation (26). To determine whether DHW-221 affects P-gp function, FACS analysis was performed to detect the intracellular accumulation of Rho-123. As shown in **Figure 2B**, the intracellular accumulation of Rho-123 in A549/Taxol cells was significantly lower than that in A549 cells. Verapamil (VRP), a known first-generation P-gp inhibitor, was used as a positive control. Cotreatment with DHW-221 and verapamil significantly enhanced the intracellular Rho-123 accumulation in A549/Taxol cells without affecting A549 cells. Furthermore, fluorescence microscopy analysis demonstrated that the green fluorescence intensity was significantly increased in A549/Taxol cells, further confirming that DHW-221 increases intracellular Rho-123 accumulation in a concentration-

**TABLE 1** | The resistance index (RI) for various compounds at 72 h in A549/Taxol cells (mean ± SD, n = 3).

| Comp. | $IC_{50}$ (μM) | | RI |
|---|---|---|---|
| | A549 | A549/Taxol | |
| Docetaxel | 0.0012 ± 0.0002 | 0.4706 ± 0.0891 | 392.2 |
| Vincristine | 0.0021 ± 0.0008 | 0.0430 ± 0.0011 | 20.5 |
| Cisplatin | 5.6645 ± 1.1759 | 80.2240 ± 1.0672 | 14.2 |
| DHW-221 | 0.4242 ± 0.0238 | 0.5274 ± 0.0339 | 1.2 |

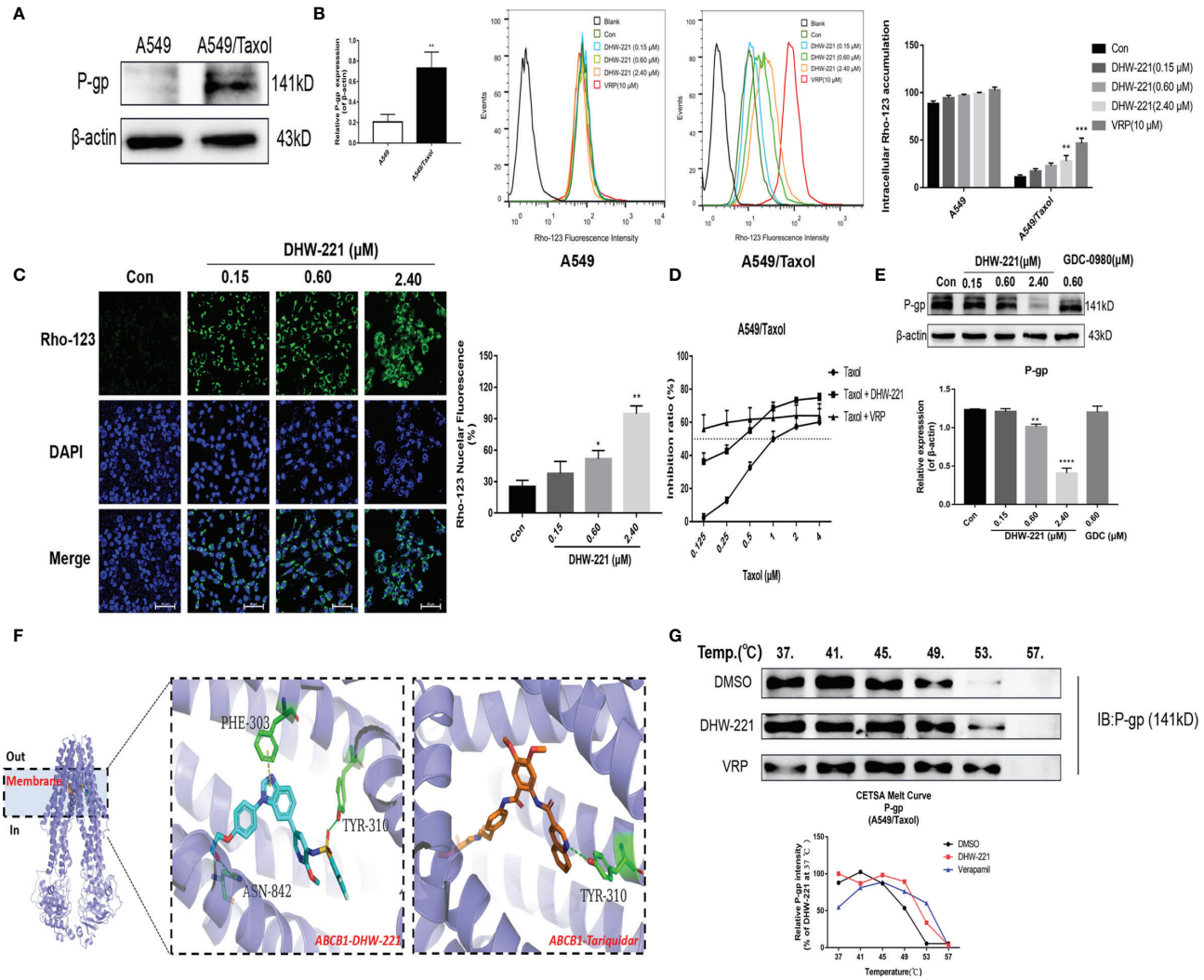


**FIGURE 2** | DHW-221 accelerates intracellular Rho-123 accumulations and inhibits P-gp expression by binding to P-gp. **(A)** Comparison of P-gp in A549 and A549/Taxol cells. Statistical comparisons were performed with unpaired Student's t-test (n = 3). **p < 0.01 versus A549. **(B, C)** After treatment of DHW-221 or verapamil for 48 h, Rho-123 (15 μM) was added into the mediums to co-incubate with DHW-221 or verapamil for 3 h in dark. The intracellular accumulation of Rho-123 was evaluated by flow cytometry and confocal microscope, respectively. Verapamil (VRP, 10 μM) was used as a positive control. Green fluorescence indicated Rho-123, and blue fluorescence indicated DAPI. Scale bar = 100 μm. Nuclear mean fluorescence intensity of Rho 123 was measured by ImageJ and analyzed using FlowJo 10 software. Statistical comparisons were performed with one-way ANOVA followed by Dunnett's *post-hoc* test for multiple comparisons (n = 3). *p < 0.05, **p < 0.01, ***p < 0.001 versus control. **(D)** Effect of DHW-221 or verapamil to reverse Taxol resistance for 48 h in A549/Taxol cells. **(E)** Western blot analysis of DHW-221 inhibited P-gp expression in A549/Taxol cells. **(F)** Ribbon diagram of human ABCB1 (PDB code: 7A6E, purple spiral) bound to drug (membrane region) and predicted binding modes for DHW-221 (blue stick) and tariquidar (orange stick, a known third-generation P-gp inhibitor) with ABCB1. Hydrogen bonds were shown as green dashed lines. Key residues for DHW-221 and tariquidar interaction were highlighted. **(G)** Effect of DHW-221 on the thermal stability of ABCB1 was quantitatively detected by a cellular thermal shift assay (CETSA). Statistical comparisons were performed with one-way ANOVA followed by Dunnett's *post-hoc* test for multiple comparisons (n = 3). Data are presented as mean ± SD. **p < 0.01, ****p < 0.0001versus control.

dependent manner in A549/Taxol cells (**Figure 2C**). These results suggested that DHW-221 inhibits P-gp function through increasing the intracellular accumulation of Rho-123 in A549/Taxol cells.

In recent years, the development of novel P-gp inhibitors has been regarded as a promising strategy to overcome MDR (27, 28). To explore whether DHW-221 acts as a P-gp inhibitor, we examined the cell growth inhibitory effect of Taxol alone and in combination with DHW-221 or verapamil in A549/Taxol cells. Here, we selected 50 nM DHW-221 and 10 μM verapamil, which had no significant cytotoxicity in A549/Taxol cells (**Figure 1D**). The cell viability assay showed that cotreatment with DHW-221 and Taxol enhanced the cytotoxic effect of A549/Taxol cells, which was similar to the effects of verapamil, suggesting that DHW-221 functions as a P-gp inhibitor and may be a MDR reversal agent (**Figure 2D**). Moreover, the

expression of P-gp was significantly downregulated in DHW-221-treated A549/Taxol cells (**Figure 2E**). These results demonstrated that DHW-221 acts as a P-gp inhibitor through inhibiting P-gp function and protein expression.

Based on the inhibitory activity of DHW-221 on P-gp, we performed molecular docking and CETSA to further elucidate whether DHW-221 binds to P-gp. The active pocket of P-gp mainly contains the transmembrane (TM, including the drug-binding site) and ATP-binding domains (29). In order to determine whether DHW-221 bind to the drug binding site of P-gp, molecular docking was performed. As shown in **Figure 2F**, DHW-221 fitted well into the drug-binding site of P-gp with a relatively higher binding affinity than tarquidar (a third-generation P-gp inhibitor), and it formed H-bonds with Phe303, Asn842, and Tyr310 residues. The glide scores of DHW-221 and tarquidar were −12.246 and −11.482 kcal/mol, respectively. These results suggested that DHW-221 binds to P-gp in the TM region, thereby reducing drug efflux. Meanwhile, 6C0V protein model was selected to evaluate whether DHW-221 bind to the ATP binding pocket of P-gp. We found that DHW-221 possessed a weaker affinity (−5.646 kcal/mol) compared to the drug-binding site (data not shown). Additionally, CETSA demonstrated that DHW-221 treatment enhanced the thermal stability of ABCB1 protein, similar to the effect of verapamil (**Figure 2G**). Taken together, these results suggested that DHW-221 inhibits P-gp function and expression through binding to the TM region of P-gp.

## DHW-221 Triggers Apoptosis and Paraptosis Through the Mitochondrial Pathway, ER Stress, and MAPK Signaling Pathway in A549/Taxol Cells

Previous studies have shown that DHW-221 has a pro-apoptotic effect in NSCLC cells (24). Therefore, we investigated whether DHW-221 triggers apoptosis in A549/Taxol cells. Hoechst 33342 staining was performed to detect the cellular morphological changes in each group. We observed condensed chromatin and smaller nuclei accompanied with strong blue fluorescence in both A549/Taxol and A549 cells (**Figure 3A**). Next, A549/Taxol and A549 cells were treated with various concentrations of DHW-221 and GDC-0980, and cell apoptosis was assessed by FACS analysis. Compared to the control group, the rates of early and late apoptosis were significantly increased in the DHW-221-treated group in both A549/Taxol and A549 cells (**Figure 3B**). At a concentration of 2.4 μM, the pro-apoptotic ability of DHW-221 in A549/Taxol cell was stronger than that of A549 cells (**Figure 3B**), which agreed with previous results (**Figure 1D**). These results demonstrated that DHW-221 triggers apoptosis in A549/Taxol and A549 cells in a concentration-dependent manner. To elucidate the underlying mechanism of DHW-221-triggered apoptosis in A549/Taxol cells, we examined the MMP by JC-1 staining. A decrease in the MMP is a landmark event in the early stage of apoptosis. After treatment with DHW-221 and GDC-0980, JC-1 did not exist in the mitochondrial matrix in the form of polymers, resulting in significantly reduced red fluorescence intensity in the mitochondria and significantly enhanced green fluorescence in the cytoplasm (**Figure 3C**), which indicated that the intracellular MMP was decreased by DHW-221 in A549/Taxol cells. These results implied that cell apoptosis induced by DHW-221 may occur *via* the mitochondrial pathway. We next investigated the expression of mitochondrial apoptosis pathway-related proteins by Western blot analysis. In a concentration-dependent manner, DHW-221 upregulated the expression levels of apoptosis-related proteins [cytochrome C, cleaved caspase 3, and cleaved poly(ADP-ribose) polymerase (PARP)] and downregulated the expression levels of the anti-apoptotic protein, Bcl-2, in A549/Taxol cells (**Figure 3D**). These results demonstrated that apoptosis induced by the mitochondrial pathway participates in DHW-221-induced cell death in A549/Taxol cells.

Interestingly, we observed that high-concentration DHW-221 exacerbated the formation of massive vacuoles in A549/Taxol cells (**Figure 4A**). As cytoplasmic vacuolization is strongly linked to paraptosis-like cell death (30), we hypothesized that DHW-221 may induce paraptosis in A549/Taxol cells. Paraptosis is a non-apoptotic and caspase-independent form of programmed cell death that is completely different from apoptosis and requires protein synthesis (31). To test our hypothesis, the protein synthesis inhibitor, cycloheximide (CHX), was added to DHW-221-treated A549/Taxol cells. Cotreatment with CHX and DHW-221 attenuated cytoplasmic vacuolation compared to treatment with 2.4 μM DHW-221 alone (**Figure 4A**). Furthermore, Western blot analysis showed that DHW-221 significantly inhibited the expression of Alix, a well-known paraptosis regulator that inhibits the onset of paraptosis (**Figure 4B**). Some studies have shown that paraptosis-like cell death induced by Zika virus (ZIKV) or $^{125}$I radioactive seeds is regulated by the PI3K/Akt signaling pathway (32, 33). In addition, the mTOR inhibitor, everolimus, triggers cell paraptosis in childhood acute lymphoblastic leukemia (34). Based on these studies, our findings suggested that DHW-221 increases the pro-paraptotic ability of A549/Taxol cells. Because the process of paraptosis is inseparable from the involvement of endoplasmic reticulum (ER) stress and mitogen-activated protein kinase (MAPK) signaling pathway (35), we evaluated the protein expression of key regulatory proteins in ER stress and the MAPK signaling pathway by Western blot analysis. As shown in **Figure 4B**, the expression levels of ATF4, CHOP (key regulator in ER stress), p-JNK, p-ERK, and p-p38 were significantly upregulated after treatment with DHW-221. These findings indicated that activated ER stress and the MAPK signaling pathway lead to DHW-221-triggered paraptosis in A549/Taxol cells.

## DHW-221 Induces Cell Cycle Arrest at the G0/G1 Phase in A549/Taxol Cells

Considering that PI3K inhibitors eliminate tumor cells by inducing G0/G1 phase arrest in various solid tumors (36, 37), we investigated whether DHW-221 exerts a similar effect in A549/Taxol cells by evaluating the effect of DHW-221 on cell cycle distribution by FACS analysis. Our results showed that

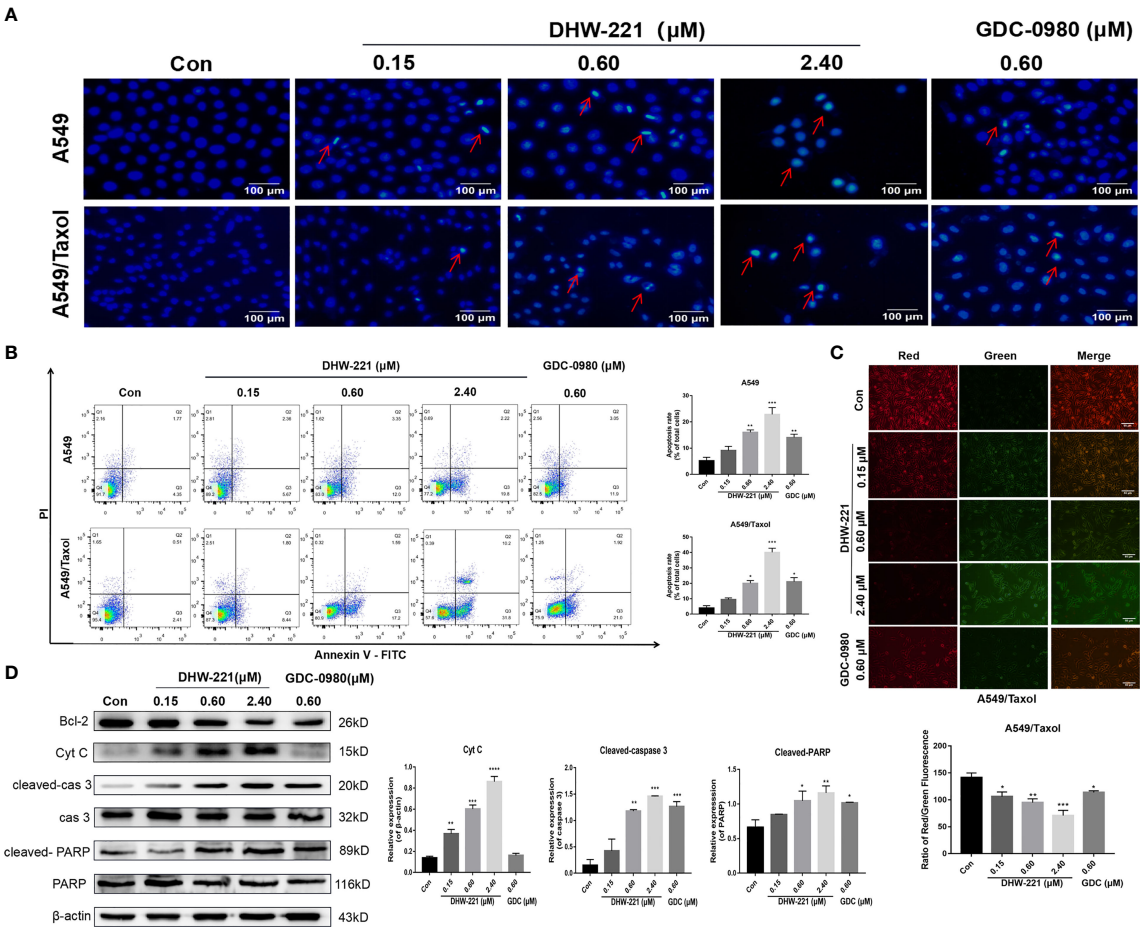


**FIGURE 3** | DHW-221 exerts an evident pro-apoptotic effect through the mitochondrial pathway in A549/Taxol cells. **(A)** Hoechst 33342 staining results for 48 h in A549 and A549/Taxol cells. Strong blue fluorescence indicated apoptotic cells, scale bar = 100 μm. **(B)** Induction of apoptosis by various concentrations of DHW-221 in A549 and A549/Taxol cells were evaluated by Annexin-V-FITC/PI staining for 48 h. **(C)** The changes of mitochondrial membrane potential in A549/Taxol cells were detected by JC-1 staining after exposure to DHW-221 and GDC-0980. Green and red fluorescence represented decreased and normal mitochondrial membrane potential, respectively. Scale bar = 100 μm. The red and green mean fluorescence intensity were measured by ImageJ software, and the relative radio was analyzed using GraphPad Prism 7.0 software. Statistical comparisons were performed with one-way ANOVA followed by Dunnett's *post-hoc* test for multiple comparisons (n = 3). *p < 0.05, **p < 0.01, ***p < 0.001 versus control. **(D)** Western blot analysis of apoptosis-related proteins in A549/Taxol cells. Cells were treated with various concentrations of DHW-221 (0.15, 0.60, and 2.40 μM) and GDC-0980 (0.60 μM) for 48 h. Statistical comparisons were performed with one-way ANOVA followed by Dunnett's *post-hoc* test for multiple comparisons (n = 3). Data were expressed as mean ± SD. *p < 0.05, **p < 0.01, ***p < 0.001, ****p < 0.0001 versus control.

DHW-221 treatment for 48 h significantly reduced the proportion of cells in S phase and increased the proportion of cells in G0/G1 phase, indicating that DHW-221 arrests the cell cycle at the G0/G1 phase in A549/Taxol and A549 cells (**Figure 4C**). To further elucidate the potential mechanism of DHW-221-induced cell cycle arrest, we examined the expression levels of key G0/G1 phase-related proteins by Western blot analysis. The cyclin D1-CDK4 complex activity is regulated by p21 and is the key to block cancer cells entering into S phase (38). **Figure 4D** shows that DHW-221 treatment decreased the expression levels of cyclin D1, CDK4, and CDK6 and increased the expression levels of p21 in a concentration-dependent manner. These data suggested that G0/G1 cell cycle arrest is involved in DHW-221-induced cell death in A549/Taxol cells.

## Akt-Mediated FOXO3a Nuclear Translocation Is Involved in Mitochondrial Apoptosis and G0/G1 Cell Cycle Arrest Induced by DHW-221 in A549/Taxol Cells

Aberrant activation of some signaling pathways, including the PI3K/Akt signaling pathway, has been recognized as a common cause of MDR (39). Western blot analysis demonstrated that the PI3K/Akt/FOXO3a signaling pathway was hyperactivated in A549/Taxol cells compared to A549 cells (**Figure 5A**). Extensive studies have shown that blocking the PI3K/Akt signaling pathway enhances the sensitivity of various drug-resistant human cancer cells to several drugs, including cisplatin, oxaliplatin, and gemcitabine (39–41). Thus, we assessed the effect of DHW-221 on the PI3K/Akt signaling

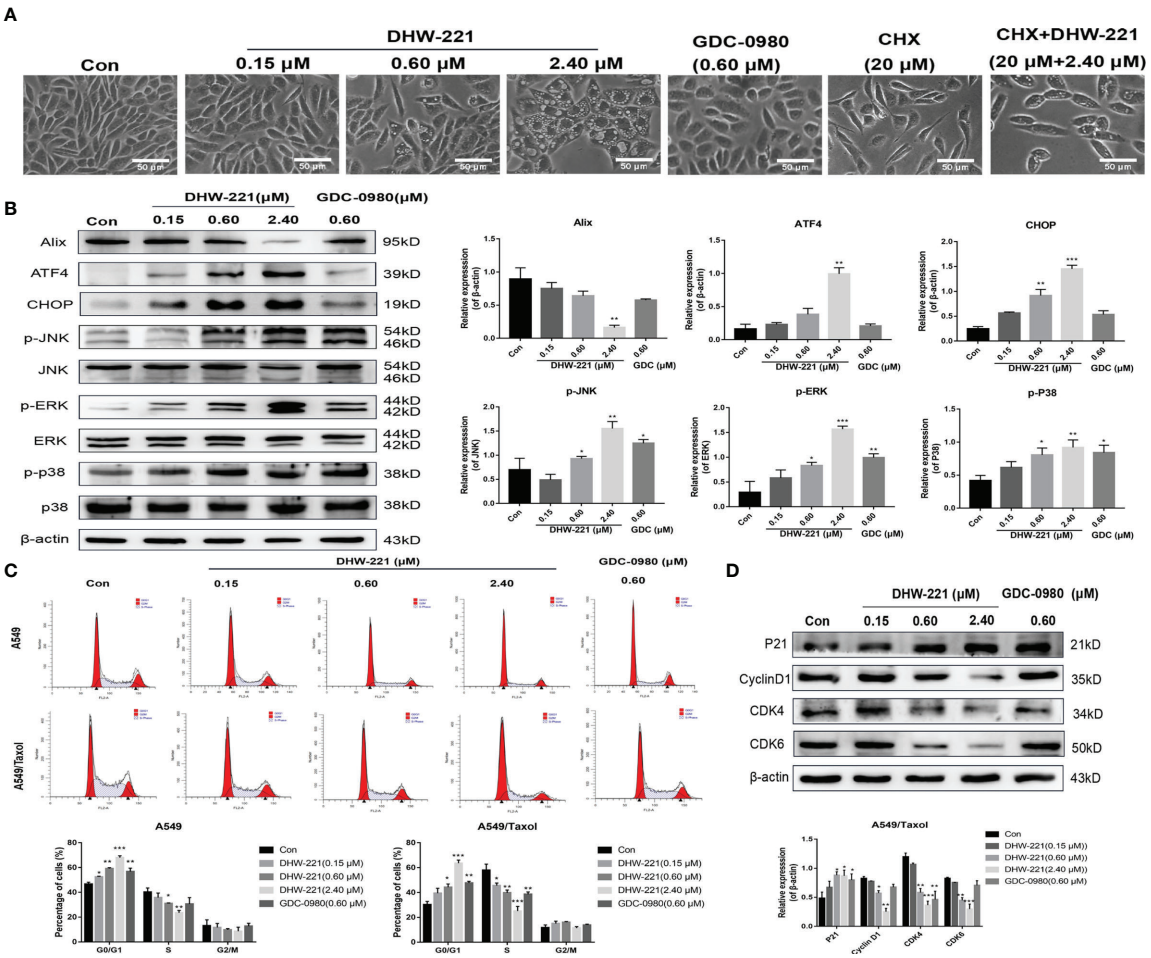


**FIGURE 4** | DHW-221 induces paraptosis and cell cycle arrest in A549/Taxol cells. **(A)** Representative microscope images of DHW-221-incubated A549/Taxol cells. Cells were pretreated with cycloheximide (CHX, 20 μM) followed by DHW-221 (2.40 μM) treatment for 12 h. Scale bar = 50 μm. **(B)** The expression levels of Alix, ER stress (ATF4 and CHOP) and MAPK signaling pathway related proteins (p-ERK, p-JNK, and p-P38) in A549/Taxol cells were measured by Western blot. The histogram (below) indicated the relative band intensity ratio of each protein for three independent experiments. (h) **(C)** The cell cycle distribution followed by DHW-221 and GDC-0980 treatment for 48 h in A549/Taxol cells was illustrated by FACS analysis. **(D)** The expression levels of cell cycle-associated proteins were measured by Western blot. The relevant quantitative results were shown in the figure below. Statistical comparisons were performed with one-way ANOVA followed by Dunnett's *post-hoc* test for multiple comparisons (n = 3). Data are presented as mean ± SD. *p < 0.05, **p < 0.01, ***p < 0.001 versus control.

pathway in A549/Taxol and A549 cells by Western blot analysis. Treatment with various concentrations of DHW-221 and GDC-0980 significantly decreased the expression levels of PI3Kp110α and p-Akt in a concentration-dependent manner, while no obvious change was observed in the total Akt level, which suggested that DHW-221 blocked the PI3K/Akt signaling pathway in both A549/Taxol and A549 cells (**Figure 5B**), agreeing with a previous study (24). FOXO3a, a direct downstream target of Akt, is directly phosphorylated by Akt at the Ser253 site, which allows it to bind to its chaperone protein, 14-3-3, resulting in transfer from the nucleus to the cytoplasm; this process is an important tumorigenic mechanism for evading cancer cell apoptosis (14). In addition, the pro-apoptotic protein, Bim, is regulated by FOXO3a at the transcriptional level (42). To investigate whether DHW-221-induced cell apoptosis is mediated *via* the Akt/FOXO3a/Bim pathway, we utilized Western blot analysis. In A549/Taxol cells, DHW-221 treatment significantly downregulated p-FOXO3a (Ser253) expression and upregulated FOXO3a expression, and these changes were accompanied by an increase in Bim expression. In contrast, no significant changes in FOXO3a and Bim expression levels were observed in DHW-221-treated A549 cells, indicating that DHW-221-induced cell apoptosis is unrelated to FOXO3a expression in A549 cells. However, these findings need to be further confirmed by substantial experiments in future work.

To further investigate the relocalization of FOXO3a in DHW-221-treated A549/Taxol cells, Western blot analysis and immunofluorescence staining were performed to examine the subcellular localization of FOXO3a. As shown in **Figures 5C, E**, DHW-221 increased nuclear FOXO3a protein and decreased

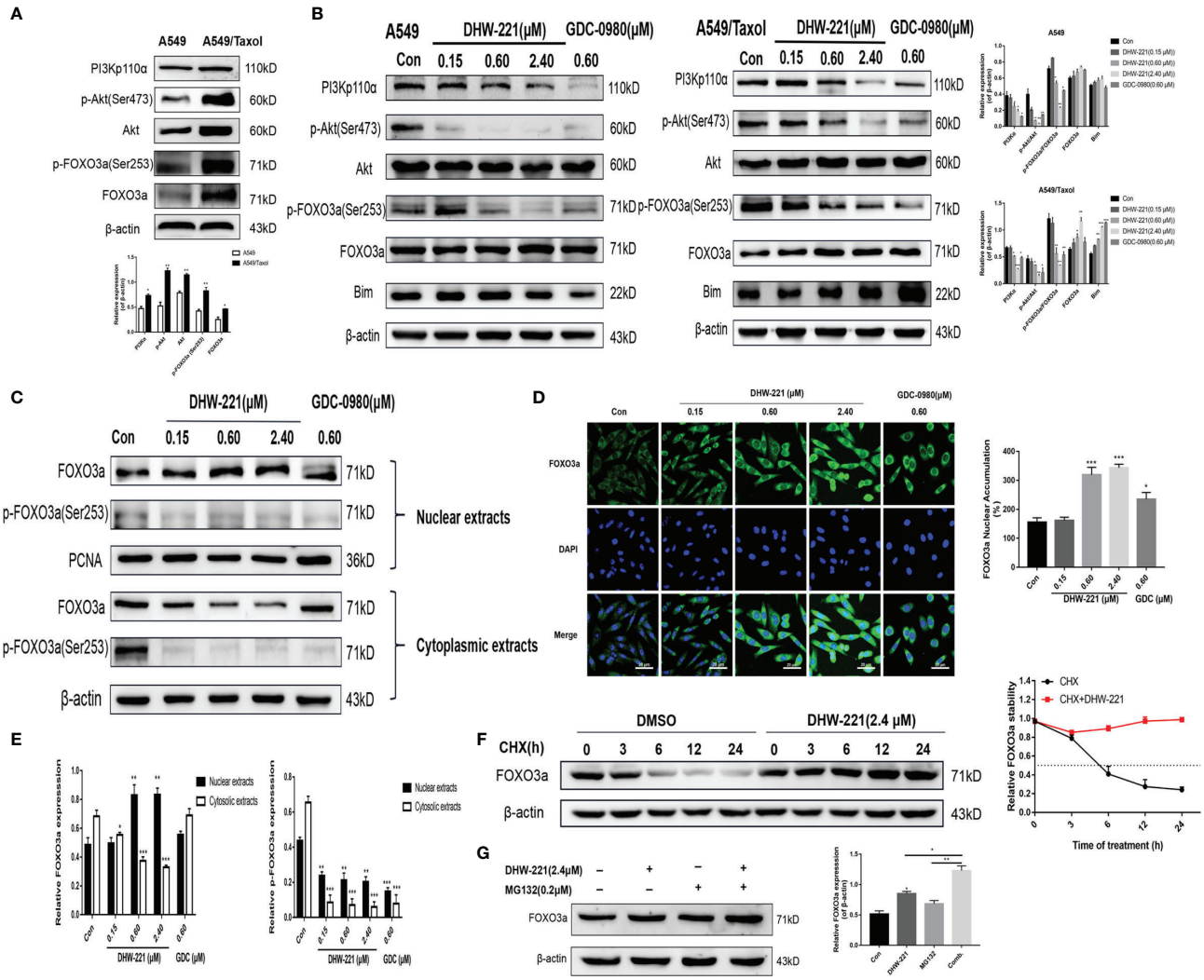


**FIGURE 5** | DHW-221-triggered mitochondrial apoptosis is linked to Akt-mediated FOXO3a nuclear translocation in A549/Taxol cells. **(A, B)** Comparison and the expression levels of PI3K/Akt/FOXO3a signaling pathway related proteins in A549 and A549/Taxol cells were determined by Western blot, in the presence and absence of DHW-221 and GDC-0980. Statistical comparisons were performed with unpaired Student's t-test (n = 3) in Panel **(A)**. *p < 0.05, **p < 0.01 versus A549. Statistical comparisons were performed with one-way ANOVA followed by Dunnett's *post-hoc* test for multiple comparisons in Panel **(B)** (n = 3). *p < 0.05, **p < 0.01, ***p < 0.001 versus control. **(C, E)** The FOXO3a and p-FOXO3a expressions in the nuclear and cytoplasmic fractions of A549/Taxol cells were detected by Western blot. Proliferating cell nuclear antigen (PCNA) was selected as nucleoprotein internal control. The quantitative results were shown in Panel **(E)**. **(D)** Immunofluorescence staining of FOXO3a in A549/Taxol cells was carried out to evaluate the effect of DHW-221 on FOXO3a nuclear translocation. Scale bar = 20 μm. The histograms indicated the percentage of the cells in each condition exhibiting FOXO3a nuclear mean fluorescence intensity (positive cells, green fluorescence) by ImageJ. **(F)** FOXO3a degradation in A549/Taxol cells with or without DHW-221 co-treatment in different time spot when protein biosynthesis was blocked with 20 μM cycloheximide (CHX). FOXO3a stability was analyzed relative to control by ImageJ software. **(G)** FOXO3a proteins levels in the presence of MG132 (0.20 μM) or 2.40 μM DHW-221-treated A549/Taxol cells at 24 h. Statistical comparisons were performed with one-way ANOVA followed by Dunnett's *post-hoc* test for multiple comparisons (n = 3). Data were presented as mean ± SD. *p < 0.05, **p < 0.01, ***p < 0.001 versus control.

cytoplasmic phosphorylated FOXO3a at the Ser253 site, which indicated that FOXO3a was predominantly transferred from the cytoplasm to the nucleus by DHW-221 in A549/Taxol cells. Furthermore, DHW-221 caused nuclear translocation of FOXO3a, which was manifested by a gradual increase in green fluorescence intensity in the nucleus (**Figure 5D**). These results suggested that DHW-221 induces Akt-mediated FOXO3a nuclear translocation. Studies have shown that FOXO3a directly affects the expression of the downstream target genes, p21 and cyclin D1 (42), which was in agreement with the results of the present study (**Figure 4D**). These results suggested that DHW-221-induced mitochondrial apoptosis and cell cycle arrest are closely related to Akt-mediated FOXO3a nuclear translocation in A549/Taxol cells.

To elucidate the mechanism of the DHW-221-mediated increase in FOXO3a expression, CHX and the proteasome inhibitor, MG132, were added into culture media to inhibit

protein synthesis. We first measured the half-life of FOXO3a after exposure to CHX alone and in combination with DHW-221 at various time points in A549/Taxol cells by Western blot analysis. As shown in **Figure 5F**, FOXO3a expression was attenuated by CHX in the DMSO group, whereas cotreatment of DHW-221 and CHX restored FOXO3a expression, which indicated that DHW-221 prevents FOXO3a degradation, thus increasing FOXO3a stability. **Figure 5G** shows that FOXO3a expression was slightly enhanced upon MG132 treatment, which suggested that FOXO3a was instable, indicating that the combination of DHW-221 and MG132 unexpectedly promoted FOXO3a accumulation in A549/Taxol cells. These results demonstrated that DHW-221 interferes with FOXO3a degradation in a proteasome-independent manner.

## DHW-221 Suppresses Migration and Invasion Through Inhibiting Epithelial-Mesenchymal Transition Phenotypic Changes

Based on the inhibitory effect of DHW-221 on the migration and invasion ability of NSCLC cells (24), we hypothesized that DHW-221 may also have a similar effect in A549/Taxol cells. A wound-healing assay was performed to verify the effects of DHW-221 on the migration capability of A549/Taxol cells. To exclude the effect of cell proliferation, we selected the concentration of DHW-221 that had no evident cytotoxic effect on A549/Taxol cells for subsequent experiments. As shown in **Figure 6A**, the wound-healing rate of DHW-221-treated A549/Taxol cells was significantly decreased compared to the control group, and similar results were found in A549 cells. In addition, the effect of DHW-221 on the cell invasion capability was further determined with or without Matrigel-coated Transwell membranes. After 24 h of DHW-221 treatment, the number of cells that migrated and invaded through the chamber was significantly reduced compared to the control group in DHW-221-treated A549/Taxol cells. These results suggested that DHW-221 inhibits the migration and invasion capabilities of A549/Taxol cells in a concentration-dependent manner (**Figures 6A, C**).

Extensive studies have shown that FOXO3a is involved in regulating the epithelial–mesenchymal transition (EMT) process in numerous cancers (43, 44). To verify whether A549/Taxol cells acquire the EMT phenotype, we examined the expression levels of epithelial markers (E-cadherin and occludin) and a mesenchymal marker (N-cadherin) in A549/Taxol and A549 cells. In A549/Taxol cells, the expression levels of E-cadherin and occludin were decreased compared to A549 cells, but the expression levels of N-cadherin were increased compared to A549 cells (**Figure 6B**), indicating that A549/Taxol cells have a stronger capacity for cell motility than A549 cells. The slender and fibrous morphology change in A549/Taxol cells (**Figure 1B**), which is a typical characteristic of a mesenchymal cells, suggested that A549/Taxol cells possess an EMT phenotype. To determine whether DHW-221 inhibits cell migration and invasion *via* the EMT process, the effect of DHW-221 on the expression of EMT-related proteins was examined by Western blot analysis. As shown in **Figure 6D**, DHW-221 treatment increased the expression levels of E-cadherin and occludin but significantly decreased the expression levels of mesenchymal markers, including vimentin and slug. Moreover, DHW-221 treatment decreased the expression of snail, which is a key transcription factor in regulating EMT (45). Matrix metalloproteinase (MMP) family proteins, such as MMP2 and MMP9, are of vital importance in cancer metastasis, and MMPs are highly expressed in cancers (46). Moreover, the expression levels of MMP2 and MMP9 were significantly downregulated by DHW-221 in A549/Taxol cells (**Figure 6D**). To further determine whether DHW-221 reverses EMT phenotypic changes, the expression of occludin and vimentin was visualized by immunofluorescence staining. With the increasing concentration of DHW-221, the green fluorescence intensity of vimentin was gradually weakened, whereas the red fluorescence intensity of occludin was enhanced in A549/Taxol cells (**Figure 6E**). Collectively, these findings suggested that DHW-221 suppresses the migration and invasion capabilities of A549/Taxol cells through reversing EMT phenotypic changes.

## DHW-221 Has Superior Antitumor Effects With no Obvious Toxicity in an Orthotopic A549/Taxol Tumor Mouse Model

To further assess whether DHW-221 has antitumor activity in Taxol-resistant lung neoplasms, A549/Taxol cells were injected into nude mice *via* the tail vein to establish an orthotopic lung tumor model. After 1 week, DHW-221 (10, 20, and 40 mg/kg) and GDC-0980 (10 mg/kg) were intragastrically administered daily for 2 weeks, whereas Taxol (10 mg/kg) was intraperitoneally administered every 2 days (47, 48) (**Figure 7A**). Compared to the model and Taxol groups, the number of lung nodules was significantly decreased in the DHW-221-treated group (**Figures 7B, C**). To observe the pathological changes of mouse lung tissues, HE staining was performed. Compared to the blank group, the alveoli of the model and Taxol groups were covered by nodules, while the lung nodule formation in the DHW-221 and GDC-0980 group was slower than that of the model and Taxol groups (**Figure 7E**). Of note, we observed sparse pink cytoplasm and densely stained round or oval vesicular nuclei in tumor cells in the model and Taxol groups (**Figure 7E**). Additionally, to verify whether DHW-221 induces FOXO3a translocation *in vivo*, we examined the expression levels of FOXO3a and p-FOXO3a by IHC. After DHW-221 treatment, p-FOXO3a expression was downregulated, and FOXO3a expression was upregulated (**Figure 7F**). Ki67 is an indicator of proliferative capacity in cancers, and Ki67 expression is closely associated with tumor invasion and metastasis; thus, Ki67 expression affects the prognosis of cancer patients (49). In the present study, we examined Ki67 expression by IHC. Compared to the blank group, Ki67 expression was increased in the model and Taxol groups, but there was no change in Ki67 expression in the DHW-221 and GDC-0980 groups (**Figure 7F**). These findings suggested that DHW-221 inhibits tumor growth through FOXO3a translocation in A549/Taxol cell-bearing mice.

Although some chemotherapeutic drugs have high efficacy in clinic, many are limited due to their toxicity. In the present study, we evaluated the toxicity of DHW-221 *in vivo*. During treatment, there

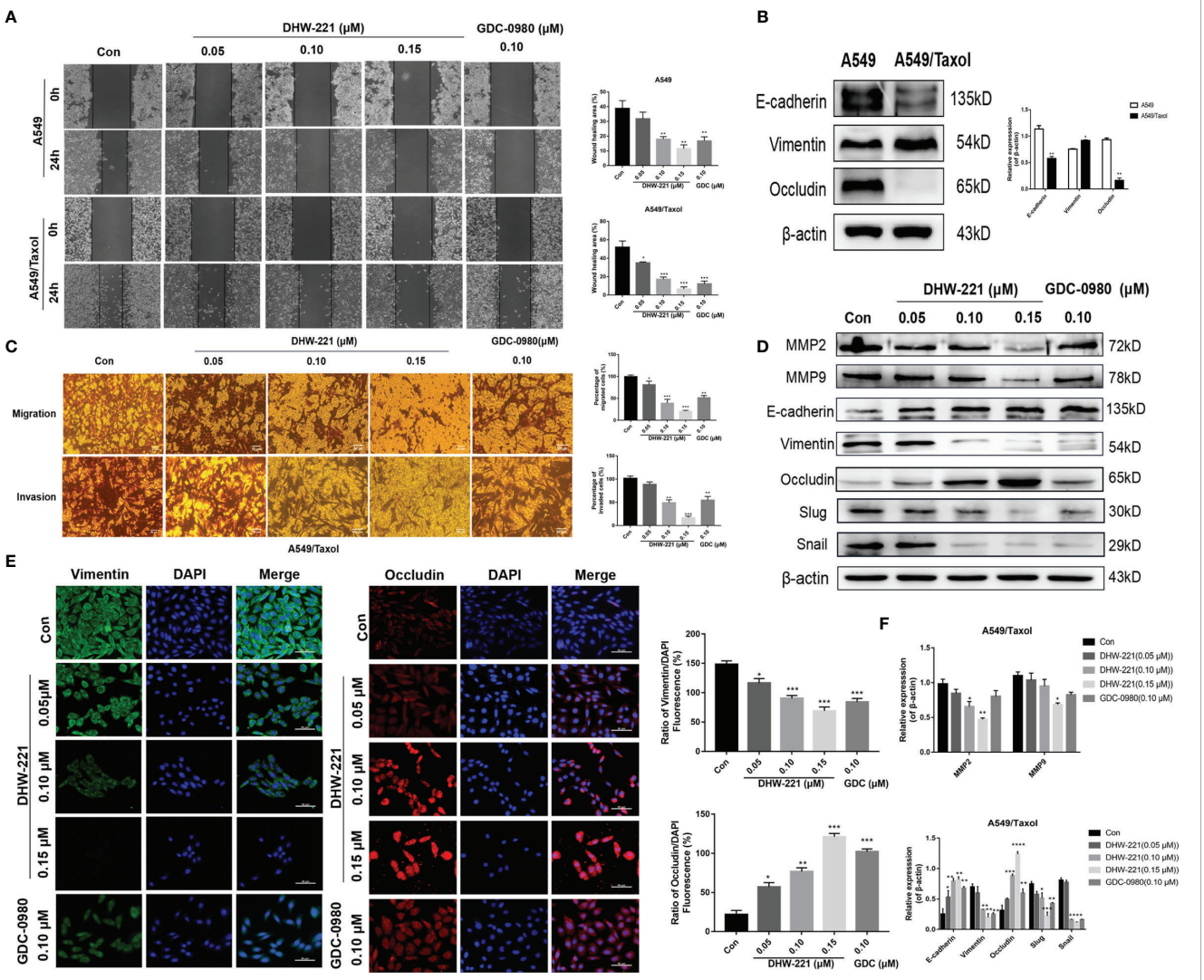


**FIGURE 6** | Cell migration and invasion caused by EMT phenotype are inhibited by DHW-221 in A549/Taxol cells. **(A, C)** The effects of various concentrations of DHW-221 on the migration and invasion of A549/Taxol cells were studied by the wound healing assay and Transwell assays, respectively. The corresponding quantitative statistical graphs were attached to the side. **(B)** The changes of EMT markers (E-cadherin, vimentin, and occludin) in A549 and A549/Taxol cells. Statistical comparisons were performed with unpaired Student's t-test (n = 3). *p < 0.05, **p < 0.01 versus A549. **(D, F)** The expression levels and quantitative analysis results of MMP2, MMP9, and EMT markers after exposure to DHW-221 at 48 h were tested by Western blot. **(E)** Immunofluorescence staining of vimentin and occludin in A549/Taxol cells were observed by a confocal microscopy, scale bar = 100 μm. Green, red, and blue fluorescence separately represented vimentin, occludin, and DAPI. The mean fluorescence intensity of vimentin and occludin were measured by ImageJ, and the relative fluorescence (green or red/DAPI ratio) were analyzed using GraphPad Prism 7.0. Statistical comparisons were carried out with one-way ANOVA followed by Dunnett's *post-hoc* test for multiple comparisons (n = 3). Data are presented as mean ± SD. *p < 0.05, **p < 0.01, ***p < 0.001, ****p < 0.0001 versus control.

were no significant differences in the body weight and viscera index between the DHW-221 and GDC-0980 groups in A549/Taxol cell-bearing mice (**Figures 7D**, **8B**). Moreover, after DHW-221 treatment, the model mice did not show any behavioral abnormalities or loss of appetite. Intriguingly, a mouse in the model, Taxol, and 10 mg/kg DHW-221 A549/Taxol group died of hind limb paralysis after being treated with drugs for 14 days, which may have been caused by overburden of the tumor compressing the nerves in the hind limbs. Evaluation of the histological changes in the visceral organs due to DHW-221 treatment in A549/Taxol cell-bearing mice by H&E staining demonstrated that there were no evident histological abnormalities in myocardial tissue, hepatocyte morphology, glomeruli, and splenic corpuscles (**Figure 8A**). To further determine the toxicity of DHW-221, biochemical parameters, including CK, ALT, AST, and CRE, were evaluated in the heart, liver, and kidney. After DHW-221 treatment, there were no abnormal toxicity signs in the CK, ALT, AST, and CRE levels in A549/Taxol cell-bearing mice (**Figure 8B**). Taken together, these results suggested that DHW-221 suppresses tumor growth without body weight change and toxicity through FOXO3a translocation *in vivo*.

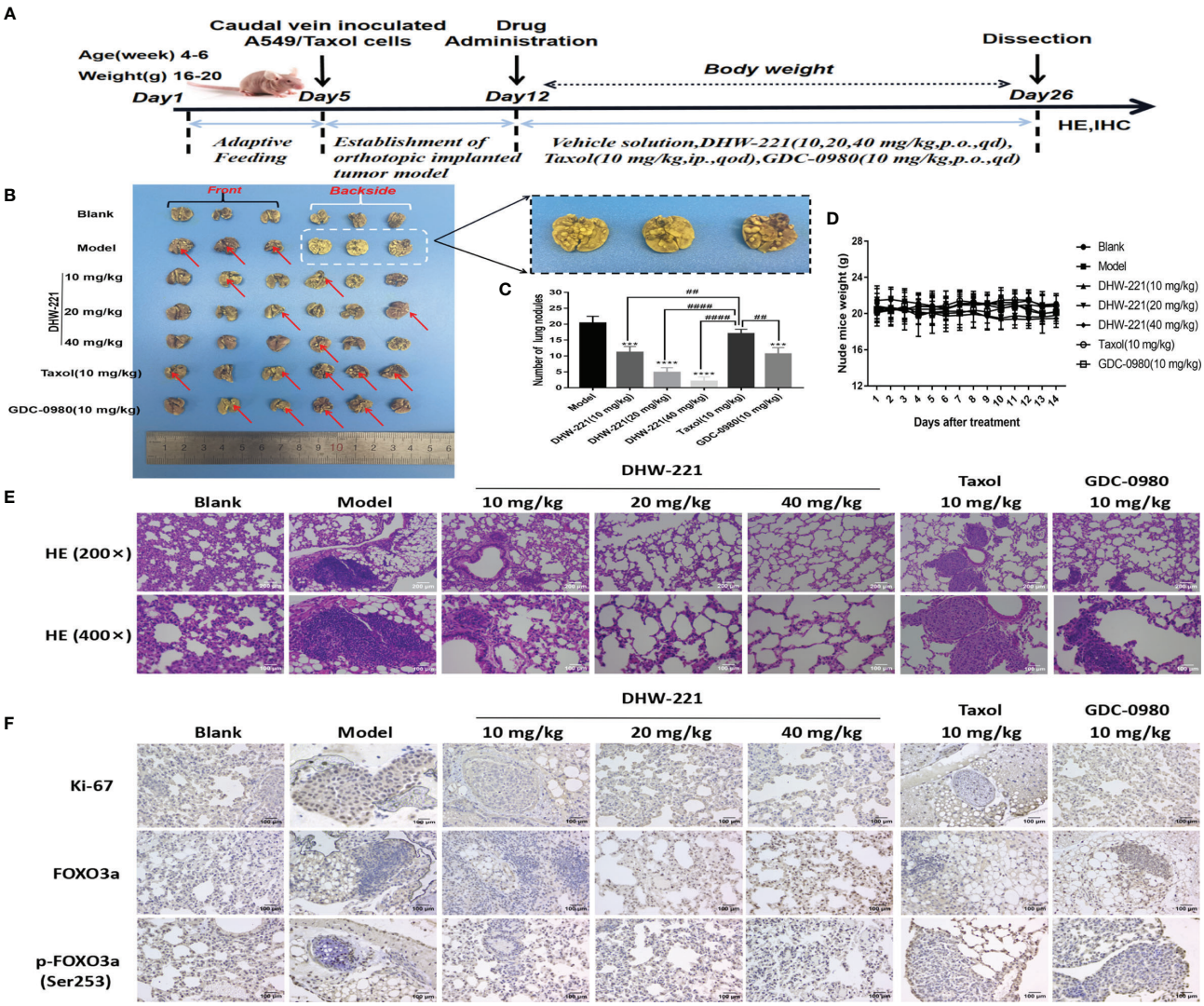


**FIGURE 7** | DHW-221 inhibits tumor growth in an orthotopic A549/Taxol nude mice model by tail vein. **(A)** The schematic figure of tumor modeling nude mice and drug administration. **(B)** Front and back images of orthotopic A549/Taxol lung samples in nude mice based on the Bouin's staining (n = 6). Arrows and enlarged parts indicated nodules formed in the lungs. **(C)** Statistical analysis of the number of lung nodules in mice in each group (n=6). Statistical comparisons were performed with one-way ANOVA followed by Dunnett's *post-hoc* test for multiple comparisons. Data were presented as mean ± SD. ***$p < 0.001$, ****$p < 0.0001$ versus control. $^{\#\#}p < 0.01$, $^{\#\#\#\#}p < 0.0001$ versus taxol. **(D)** Body weight change curve of nude mice after DHW-221, GDC-0980, and Taxol administrations. **(E)** Hematoxylin and eosin (HE) staining of lung tissues in each group under different magnifications (200× and 400×). Scale bar = 200 and 100 μm. **(F)** The expressions of Ki67, FOXO3a, and p-FOXO3a in lung tissues were detected by immunohistochemistry. Scale bar = 100 μm.

## DISCUSSION

Lung cancer has been a serious threat to human health worldwide due to high morbidity and mortality, especially for NSCLC (50). Paclitaxel, as a first-line chemotherapeutic drug, is widely used to treat NSCLC in the clinic (5). However, acquired resistance to Taxol greatly affects its clinical efficacy and patient prognosis during treatment, especially due to the emergence MDR (51). MDR in cancer continues to be an inevitable phenomenon that limits the efficacy of chemotherapeutical drugs against NSCLC (52), in which cancer cells gain the capacity to develop cross-resistance to a wide range of structurally and functionally irrelevant drugs. Therefore, it is important to understand how to overcome MDR.

Previously, we designed and synthesized DHW-221, as a dual PI3K/mTOR inhibitor, and we showed that it exerts a potent antitumor activity against NSCLC cells ***in vitro*** and ***in vivo*** (23, 24). In the present study, we found that A549/Taxol cells gained cross-resistance to Taxol, docetaxel, vincristine, and cisplatin, resulting in elongated and fibroid morphology (**Figure 1B**). We also demonstrated that DHW-221 suppressed cell proliferation and colony formation in a concentration- and time-dependent

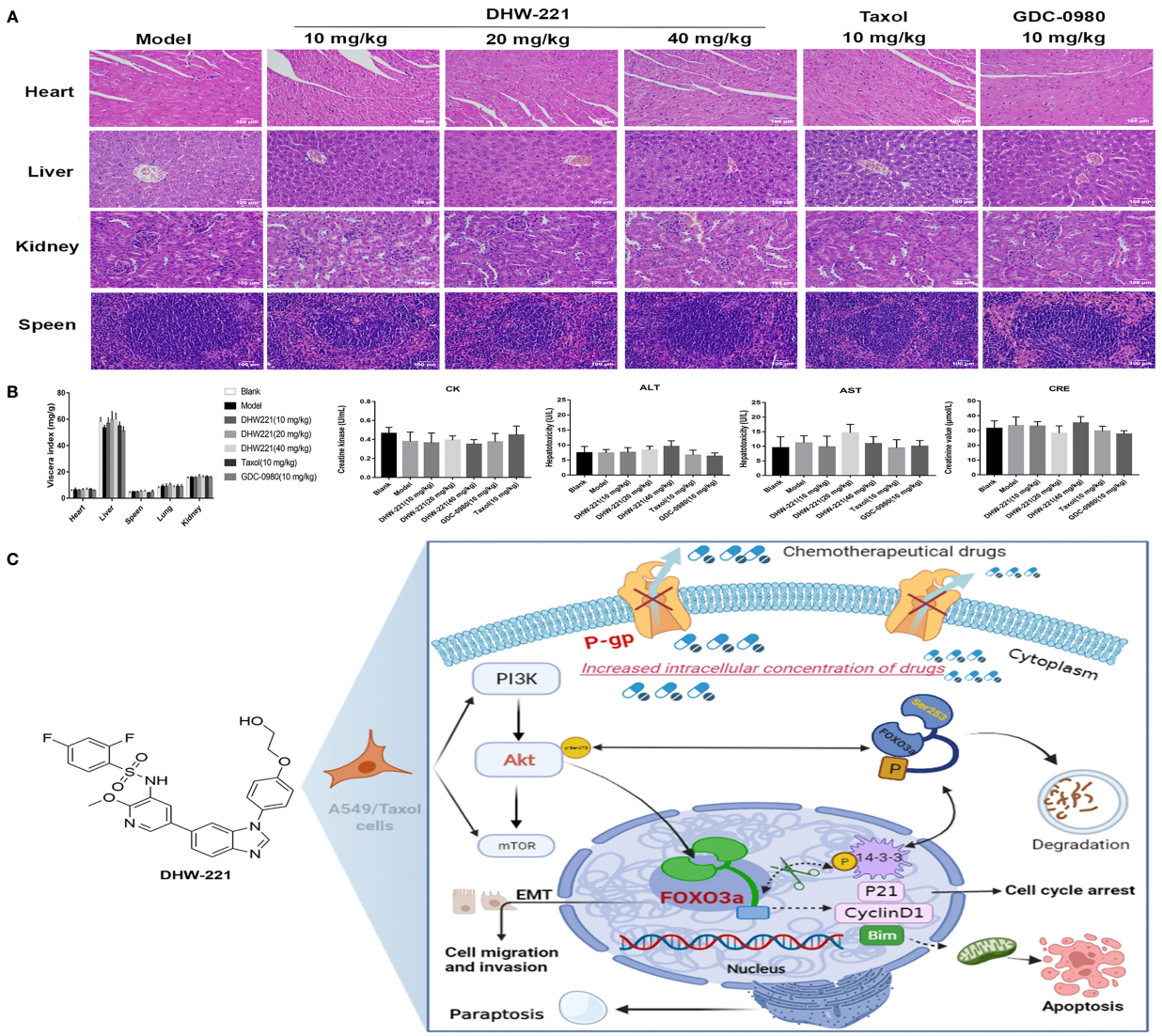


**FIGURE 8** | DHW-221 has no obvious toxicity in DHW-221-administered nude mice. **(A)** HE staining of the heart, liver, kidney, and speen from orthotopic nude mice. Scale bar = 100 μm. **(B)** The viscera index of organs (heart, liver, speen, lung, and kidney) and the biochemical parameters of heart (CK), liver (ALT, AST), and kidney (CRE) from the serum of each group in orthotopic nude mice. Data were presented as mean ± SD. Statistical comparisons were carried out with one-way ANOVA followed by Dunnett's *post-hoc* test for multiple comparisons (n = 6). **(C)** Molecular mechanism underlying the anticancer effects of DHW-221 on the P-gp and PI3K/Akt/FOXO3a signaling pathway in A549/Taxol cells.

manner in A549/Taxol cells compared to A549 cells and that this affect was superior to that of GDC-0980 (a dual PI3K/mTOR inhibitor) (**Figures 1D, E**). Therefore, we speculated that DHW-221 may represent a valuable therapeutic agent in Taxol-sensitive and Taxol-resistant NSCLC therapy. We identified the underlying molecular mechanisms by which DHW-221 exhibits an excellent inhibitory potency to conquer MDR in A549/Taxol cells.

P-gp is considered as an energy-dependent drug discharge pump that mediates MDR by decreasing intracellular drug accumulation (9). Previous studies have shown that P-gp is overexpressed in several MDR cancer cells (9, 53), which prompted us to develop a novel P-gp inhibitor to successfully avoid the risks of drug efflux (13, 54). Rhodamine 123 (Rho-123) acts as a P-gp substrate and is used to measure P-gp function (26). In the present study, we found that DHW-221 and verapamil (a known first-generation P-gp inhibitor) significantly increased the intracellular accumulation of Rho-123 in A549/Taxol cells (**Figure 2B**). Additionally, chemotherapeutics in combination with a P-gp inhibitor is also an alternative approach to achieve more durable therapeutic effects in MDR cancer cells (55, 56). Treatment with 50 nM DHW-221 significantly potentiated the efficacy of Taxol in A549/Taxol cells (**Figure 2D**). Moreover, the overexpression of P-gp was significantly reversed by DHW-221 in A549/Taxol cells (**Figure 2E**), implying that DHW-221 may be a P-gp inhibitor and a MDR reversal agent to inhibit P-gp

expression and function. These results supported the results of previous studies wherein BZML inhibits P-gp function, thereby conferring A549/Taxol cell MDR; however, it remains unclear whether BZML binds to ABCB1 (47). In contrast, the present study further verified that DHW-221 enhanced ABCB1 protein stability to inhibit its expression and function ***via*** binding to ABCB1 (**Figures 2F, G**). Furthermore, Zhang et al. reported that inhibition or knockout of PI3K 110α or 110β overcomes P-gp-mediated MDR in cancer (22). Therefore, these characteristics may contribute, at least in part, to the ability of DHW-221 to overcome MDR.

Apoptosis induced by the mitochondrial endogenous pathway and mitotic arrest has become a common cell death mode of many anticancer drugs in clinic. As expected, DHW-221 augmented the pro-apoptotic effect through activating the caspase-dependent mitochondrial pathway and inducing cell cycle arrest at the G0/G1 phase in A549/Taxol cells (**Figures 3A–D**, **4C**), which agreed with a previous study (24). However, apoptosis evasion tends to make tumor cells to be more resistant to chemotherapy drugs (57, 58), which is frequently caused by overexpression of antiapoptotic Bcl-2 family proteins (59, 60). Su et al. demonstrated that a Bcl-2 inhibitor may represent a promising and alternative agent for the treatment of Bcl-2 overexpressed refractory or recurrent hematological malignancies when conventional chemotherapy fails (61). In the present study, DHW-221 significantly downregulated Bcl-2 expression in a concentration-dependent manner (**Figure 3D**), suggesting that DHW-221 triggers cell apoptosis through the activating caspase-dependent mitochondrial pathway in a manner dependent on Bcl-2 expression.

Accumulating evidence has shown that reactivating cell apoptosis and cell cycle arrest are not efficient strategies to improve the efficacy of chemotherapeutics (31). Thus, it is highly desirable to develop novel anticancer agents that are independent of cell apoptosis to overcome chemoresistance in cancers (31, 62). Paraptosis is a non-apoptotic and caspase-independent form of programmed cell death, and it is typically characterized by cytoplasmic vacuolation derived from the ER (30, 63). Emerging evidence has highlighted that paraptosis is an important and alternate cell death pathway for overcoming chemoresistance, including MDR, in human cancer cells (31, 64). Chen et al. reported that curcuminoid B63 induces paraptosis-like cell death in 5-fluorouracil (5-FU)-resistant gastric cancer cells. Moreover, Li et al. found that honokiol reverses Taxol resistance by inducing paraptosis in H1650 cells (65). Interestingly, the present study demonstrated that high-concentration DHW-221 (2.4 μM) significantly triggered cell paraptosis *via* activating ER stress and the MAPK signaling pathway in A549 cells (data not shown). These findings were consistent with previous studies showing that high concentration of Taxol induces paraptosis-like cell death *via* an ER vacuolization-mediated pathway in A549 cells (66). Taken together, these findings indicated that DHW-221 triggers three diverse cell death modes, namely, apoptosis, paraptosis, and cell cycle arrest, which may amplify the cytotoxic effect of DHW-221 in MDR A549 cells.

Abnormal activation of the PI3K/Akt signaling pathway is strongly linked to the MDR in cancer (67), including Taxol-resistant breast (68) and prostate cancers (69). Our results demonstrated that abnormal activation of the PI3K/Akt signaling pathway was significantly inhibited by DHW-221 in A549/Taxol cells (**Figures 5A, B**). In addition, Forkhead box O3a (FOXO3a), an important tumor transcription factor in the FOXO family and a direct downstream target of Akt, is essential for regulating multiple physiological processes, including cell proliferation, cell apoptosis, migration, and longevity (14). In the clinic, the cytostatic and cytotoxic effects of various anticancer drugs, including paclitaxel, doxorubicin, lapatinib, imatinib, and cisplatin, are mediated by FOXO3a activation (70). Borris et al. revealed that the involvement of FOXO3a activity in regulating P-gp activity response involves doxorubicin-induced PI3K/Akt signaling (71). The present study demonstrated that PI3K/Akt-mediated FOXO3a overactivation caused MDR in A549/Taxol cells (**Figure 5B**). Cytoplasmic translocation of Akt-dependent FOXO3a has emerged as a key process in carcinogenesis for evading cancer cell apoptosis (15, 72). The Bcl-2 subfamily member and BH3-only protein, Bim, is activated when cells receive intrinsic apoptosis signals, which inhibits the activity of the antiapoptotic protein, Bcl-2, thereby inducing the release of proapoptotic proteins and ultimately leading to permeabilization of the mitochondrial outer membrane (73). Furthermore, FOXO3a regulates Bim expression at the transcriptional level (42). In the present study, DHW-221 significantly increased the expression levels of FOXO3a and Bim but inhibited the expression levels of Bcl-2 in A549/Taxol cells (**Figures 3D**, **5B**). Methylseleninic acid has been reported to induce cell apoptosis *via* Akt-mediated nuclear FOXO3a translocation in A549 cells (74). In the present study, we demonstrated that DHW-221 increased FOXO3a expression and transferred it from the cytoplasm to the nucleus in A549/Taxol cells (**Figures 5C–E**). Previous studies have reported that Akt activation stimulates FOXO3a degradation *via* the proteasome pathway (17). The present study further confirmed that DHW-221 interfered with FOXO3a degradation in a proteasome-dependent manner (**Figures 5F, G**). Consistent with *in vitro* studies, DHW-221 significantly suppressed tumor growth without significant toxicity and body weight changes through FOXO3a nuclear translocation *in vivo* (**Figures 7**, **8A, B**). Collectively, these findings suggested that mitochondrial apoptosis induced by DHW-221 is regulated by Akt-mediated FOXO3a nuclear translocation in A549/Taxol cells.

In addition, nuclear translocation of FOXO3a also contributes to cell cycle arrest through activating transcriptional targets, such as $p21^{Cip1}$ (p21) and cyclin D1 (75). The cyclin D1-CDK4/6 complex plays a key role in the cell cycle process, as it phosphorylates and inactivates Rb protein, thereby blocking the cell proliferation cycle in S phase (38, 76). Song et al. found that Tic10 arrests at the G0/G1 phase by decreasing the expression levels of FOXO3a-dependent CDK4/6 proteins in 5-FU-resistant

breast cancer cells (77). The present study demonstrated that DHW-221 upregulated p21 protein expression and downregulated cyclin D1, CDK4, and CDK6 protein expression *via* FOXO3a-mediated mechanisms, thereby inducing cell cycle arrest at the G0/G1 phase and apoptosis in A549/Taxol cells (**Figures 4C, D**). These findings indicated that the DHW-221-induced G0/G1 phase arrest participates in the cell death process in A549/Taxol cells.

EMT is highly involved in tumor invasion and metastasis during tumorigenesis and development. Studies have suggested that EMT is one of most common causes of chemotherapy drug resistance (78). Li et al. reported that acquired drug resistance is related to EMT and that drug-resistant cells exhibit stem cell-like properties (79). In the present study, we found that the A549/Taxol cells showed morphological changes with a mesenchymal-like phenotype and higher cell motility (**Figures 1B**, **6B**), which was consistent with our previous study (80). EMT is characterized by loss of the epithelial cell adhesion markers, E-cadherin and occludin, and the upregulation of mesenchymal cell-associated proteins, such as N-cadherin, vimentin, and snail. Previous studies have reported that blockade of the PI3K/Akt/mTOR signaling pathway alleviates ovarian cancer chemoresistance through reversing the EMT process. The present study demonstrated that DHW-221 significantly suppressed the invasion and metastasis of A549/Taxol cells by regulating the expression of EMT-related proteins *in vitro* (**Figures 6A–F**). Ki67, a nuclear proliferation-related protein, is closely associated with tumor invasion and metastasis in cancers (49). In the present study, Ki67 expression was reduced after DHW-221 treatment in the MDR A549 nude mouse model, further confirming the role of DHW-221-induced inhibition of invasion and migration *in vitro* and *in vivo*. Taken together, these results provided molecular evidence that the PI3K/mTOR dual inhibitor, DHW-221, overcomes MDR *via* targeting P-gp and Akt-mediated FOXO3a nuclear translocation in NSCLC.

The present study had several limitations. First, FOXO3a has been widely acknowledged to affect cell invasion and metastasis through regulating the EMT process in numerous cancer cells (14, 81), but the relationship between the two is rarely reported in drug-resistant cells (82). Unfortunately, the present study lacked experimental evidence to clarify the molecular mechanism of the DHW-221-mediated regulation of the EMT process *via* FOXO3a nuclear translocation in A549/Taxol cells. Second, there was no significant difference in FOXO3a expression and Bim expression in A549 cells (**Figure 5B**), implying that cell apoptosis triggered by DHW-221 is not regulated by Akt-mediated FOXO3a in A549 cells. However, this mechanism needs to be further confirmed by experiments in future work. Third, in an established human orthotopic A549/Taxol mouse tumor model *via* tail vein, the initial randomization of mice does not base on the tumor volume/size of each mouse, although we count the number of lung nodules to evaluate tumor growth in each group; the tumor growth inside the lung is possibly ignored. We think that it may not be the optimal way to assess tumor growth of mice *in vivo*. Thus, our future studies will further clarify the underlying mechanisms of DHW-221 as a MDR reversal agent in MDR A549 cells by the *in vivo* imaging technology of small animals to provide more evidence for reversal of Taxol-resistance to help solve the drug-resistance problem.

In conclusion, the present study for the first time demonstrated that DHW-221, as a PI3K/mTOR dual inhibitor and novel P-gp inhibitor, exerts potent cytotoxic activity and induces cell apoptosis to overcome MDR through Akt-mediated FOXO3a nuclear translocation in NSCLC (**Figure 8C**, made in https://app.biorender.com/) both *in vitro* and *in vivo*. Moreover, DHW-221 induces cell cycle arrest and paraptosis *via* activating ER stress and MAPK signaling. In addition, DHW-221 suppresses cell migration and invasion by reversing the EMT process. Therefore, DHW-221 represents a prospective therapeutic candidate for further investigation in drug-resistant NSCLC therapy. The present study provided information for a PI3K/mTOR dual inhibitor, which may aid in solving the drug resistance in NSCLC.

## DATA AVAILABILITY STATEMENT

The original contributions presented in the study are included in the article/**Supplementary Material**. Further inquiries can be directed to the corresponding authors.

## ETHICS STATEMENT

The animal study was reviewed and approved by Ethics Committee for Animal Experiments of Shenyang Pharmaceutical University.

## AUTHOR CONTRIBUTIONS

ML: conceptualization, methodology, investigation, formal analysis, writing—original draft. CX and XQ: resources, validation, supervision, writing—review and editing. WL, DL, HJ, and XG: resources, software, writing—review and editing. YW, QW, XX, and BX: resources and validation. XJ and HL: validation and supervision. YZ and HD: supervision. QZ: conceptualization, data curation, writing—review and editing, project administration, and funding acquisition. All authors contributed to the article and approved the submitted version.

## FUNDING

This study was supported by Liaoning Natural Fund Guidance Plan (Number 2019-ZD-0446) and State Key Laboratory of Chemical Oncogenomics, Tsinghua Shenzhen International Graduate School.

## SUPPLEMENTARY MATERIAL

The Supplementary Material for this article can be found online at: https://www.frontiersin.org/articles/10.3389/fonc.2022.873649/full#supplementary-material

## REFERENCES


1. Zhang H, Jiang H, Zhu L, Li J, Ma S. Cancer-Associated Fibroblasts in non-Small Cell Lung Cancer: Recent Advances and Future Perspectives. *Cancer Lett* (2021) 514:38–47. doi: 10.1016/j.canlet.2021.05.009
2. Bray F, Ferlay J, Soerjomataram I, Siegel RL, Torre LA, Jemal A. Global Cancer Statistics 2018: GLOBOCAN Estimates of Incidence and Mortality Worldwide for 36 Cancers in 185 Countries. *CA Cancer J Clin* (2018) 68:394–424. doi: 10.3322/caac.21492
3. Arbour KC, Riely GJ. Systemic Therapy for Locally Advanced and Metastatic Non-Small Cell Lung Cancer: A Review. *JAMA - J Am Med Assoc* (2019) 322:764–74. doi: 10.1001/jama.2019.11058
4. Cui Q, Wang JQ, Assaraf YG, Ren L, Gupta P, Wei L, et al. Modulating ROS to Overcome Multidrug Resistance in Cancer. *Drug Resist Update* (2018) 41:1–25. doi: 10.1016/j.drup.2018.11.001
5. Wu Z-X, Wang J-Q, Cui Q, Xu X-X, Chen Z-S. Paclitaxel and Chemoresistance. *Paclitaxel* (2022). doi: 10.1016/b978-0-323-90951-8.00002-3
6. Alqahtani FY, Aleanizy FS, El Tahir E, Alkahtani HM, AlQuadeib BT. Paclitaxel. *Profiles Drug Subst Excipients Relat Methodol* (2019) 44:205–38. doi: 10.1016/bs.podrm.2018.11.001
7. Assaraf YG, Brozovic A, Gonçalves AC, Jurkovicova D, Linē A, Machuqueiro M, et al. The Multi-Factorial Nature of Clinical Multidrug Resistance in Cancer. *Drug Resist Update* (2019) 46:100645. doi: 10.1016/j.drup.2019.100645
8. Garcia-Mayea Y, Mir C, Masson F, Paciucci R, LLeonart ME. Insights Into New Mechanisms and Models of Cancer Stem Cell Multidrug Resistance. *Semin Cancer Biol* (2020) 60:166–80. doi: 10.1016/j.semcancer.2019.07.022
9. Waghray D, Zhang Q. Inhibit or Evade Multidrug Resistance P-Glycoprotein in Cancer Treatment. *J Med Chem* (2018) 61:5108–21. doi: 10.1021/acs.jmedchem.7b01457
10. Liu X. ABC Family Transporters. *Adv Exp Med Biol* (2019) 1141:13–100 doi: 10.1007/978-981-13-7647-4_2
11. Yang J, Nie J, Ma X, Wei Y, Peng Y, Wei X. Targeting PI3K in Cancer: Mechanisms and Advances in Clinical Trials. *Mol Cancer* (2019) 18:26. doi: 10.1186/s12943-019-0954-x
12. Xu F, Na L, Li Y, Chen L. Roles of the PI3K/AKT/mTOR Signalling Pathways in Neurodegenerative Diseases and Tumours. *Cell Biosci* (2020) 10:54. doi: 10.1186/s13578-020-00416-0
13. Chen M, Lu J, Wei W, Lv Y, Zhang X, Yao Y, et al. Effects of Proton Pump Inhibitors on Reversing Multidrug Resistance*Via* Downregulating V-ATPases/PI3K/AKt/mTOR/HIF-1α Signaling Pathway Through TSC1/2 Complex and Rheb in Human Gastric Adenocarcinoma Cells *In Vitro* and *In Vivo*. *Onco Targets Ther* (2018) 11:6705–22. doi: 10.2147/OTT.S161198
14. Liu Y, Ao X, Ding W, Ponnusamy M, Wu W, Hao X, et al. Critical Role of FOXO3a in Carcinogenesis. *Mol Cancer* (2018) 17:104. doi: 10.1186/s12943-018-0856-3
15. Chen J, Gomes AR, Monteiro LJ, Wong SY, Wu LH, Ng TT, et al. Constitutively Nuclear FOXO3a Localization Predicts Poor Survival and Promotes Akt Phosphorylation in Breast Cancer. *PloS One* (2010) 5:e12293. doi: 10.1371/journal.pone.0012293
16. Lu M, Chen X, Xiao J, Xiang J, Yang L, Chen D. FOXO3a Reverses the Cisplatin Resistance in Ovarian Cancer. *Arch Med Res* (2018) 49:84–8. doi: 10.1016/j.arcmed.2018.04.014
17. Pellegrino M, Rizza P, Donà A, Nigro A, Ricci E, Fiorillo M, et al. FoxO3a as a Positive Prognostic Marker and a Therapeutic Target in Tamoxifen-Resistant Breast Cancer. *Cancers (Basel)* (2019) 11:1858. doi: 10.3390/cancers11121858
18. Chen YR, Lai YL, Da LS, XT L, YC F, Xu WC. SIRT1 Interacts With Metabolic Transcriptional Factors in the Pancreas of Insulin-Resistant and Calorie-Restricted Rats. *Mol Biol Rep* (2013) 40:3373–80. doi: 10.1007/s11033-012-2412-3
19. Han R, Hao S, Lu C, Zhang C, Lin C, Li L, et al. Aspirin Sensitizes Osimertinib-Resistant NSCLC Cells *In Vitro* and *In Vivo via* Bim-Dependent Apoptosis Induction. *Mol Oncol* (2020) 14:1152–69. doi: 10.1002/1878-0261.12682
20. Prabhu VV, Allen JE, Dicker DT, El-Deiry WS. Small-Molecule ONC201/TIC10 Targets Chemotherapy-Resistant Colorectal Cancer Stem-Like Cells in an Akt/Foxo3a/TRAIL-Dependent Manner. *Cancer Res* (2015) 75:1423–1432. doi: 10.1158/0008-5472.CAN-13-3451
21. Choi HJ, Heo JH, Park JY, Jeong JY, Cho HJ, Park KS, et al. A Novel PI3K/mTOR Dual Inhibitor, CMG002, Overcomes the Chemoresistance in Ovarian Cancer. *Gynecol Oncol* (2019) 153:135–48. doi: 10.1016/j.ygyno.2019.01.012
22. Zhang L, Li Y, Wang Q, Chen Z, Li X, Wu Z, et al. The PI3K Subunits, P110α and P110β are Potential Targets for Overcoming P-Gp and BCRP-Mediated MDR in Cancer. *Mol Cancer* (2020) 19:1–18. doi: 10.1186/s12943-019-1112-1
23. Ding HW, Yu L, Bai MX, Qin XC, Song MT, Zhao QC. Design, Synthesis and Evaluation of Some 1,6-Disubstituted-1H-Benzo[D]Imidazoles Derivatives Targeted PI3K as Anticancer Agents. *Bioorg Chem* (2019) 93:103283. doi: 10.1016/j.bioorg.2019.103283
24. Qin X, Liu M, Wu Y, Wang S, Lian S, Jia H, et al. Dual Blocking of PI3K and mTOR Signaling by DHW-221, a Novel Benzimidazole Derivative, Exerts Antitumor Activity in Human Non-Small Cell Lung Cancer. *Clin Transl Med* (2021) 11:e514. doi: 10.1002/ctm2.514
25. Lu HY, Zu YX, Jiang XW, Sun XT, Liu TY, Li RL, et al. Novel ADAM-17 Inhibitor ZLDI-8 Inhibits the Proliferation and Metastasis of Chemo-Resistant Non-Small-Cell Lung Cancer by Reversing Notch and Epithelial Mesenchymal Transition *In Vitro* and *In Vivo*. *Pharmacol Res* (2019) 148:104406. doi: 10.1016/j.phrs.2019.104406
26. Netsomboon K, Laffleur F, Suchaoin W, Bernkop-Schnürch A. Novel *In Vitro* Transport Method for Screening the Reversibility of P-Glycoprotein Inhibitors. *Eur J Pharm Biopharm* (2016) 100:9–14. doi: 10.1016/j.ejpb.2015.11.019
27. Dong J, Qin Z, Zhang WD, Cheng G, Yehuda AG, Ashby CR, et al. Medicinal Chemistry Strategies to Discover P-Glycoprotein Inhibitors: An Update. *Drug Resist Update* (2020) 49:100681. doi: 10.1016/j.drup.2020.100681
28. Zhang H, Xu H, Ashby CR, Assaraf YG, Chen ZS, Liu HM. Chemical Molecular-Based Approach to Overcome Multidrug Resistance in Cancer by Targeting P-Glycoprotein (P-Gp). *Med Res Rev* (2021) 41:525–55. doi: 10.1002/med.21739
29. Alam A, Kowal J, Broude E, Roninson I, Locher KP. Structural Insight Into Substrate and Inhibitor Discrimination by Human P-Glycoprotein. *Sci (80- )* (2019) 363:753–6. doi: 10.1126/science.aav7102
30. Kessel D. Paraptosis and Photodynamic Therapy: A Progress Report. *Photochem Photobiol* (2020) 96:1096–100. doi: 10.1111/php.13242
31. Lee D, Kim IY, Saha S, Choi KS. Paraptosis in the Anti-Cancer Arsenal of Natural Products. *Pharmacol Ther* (2016) 162:120–33. doi: 10.1016/j.pharmthera.2016.01.003
32. Monel B, Compton AA, Bruel T, Amraoui S, Burlaud-Gaillard J, Roy N, et al. Zika Virus Induces Massive Cytoplasmic Vacuolization and Paraptosis-Like Death in Infected Cells. *EMBO J* (2017) 36:1653–68. doi: 10.15252/embj.201695597
33. Hu L, Wang H, Zhao Y, Wang J. 125i Seeds Radiation Induces Paraptosis-Like Cell Death *via* PI3K/AKT Signaling Pathway in HCT116 Cells. *BioMed Res Int* (2016) 2016:8145495. doi: 10.1155/2016/8145495
34. Baraz R, Cisterne A, Saunders PO, Hewson J, Thien M, Weiss J, et al. mTOR Inhibition by Everolimus in Childhood Acute Lymphoblastic Leukemia Induces Caspase-Independent Cell Death. *PloS One* (2014) 9:e102494. doi: 10.1371/journal.pone.0102494
35. Wang S, Guo Y, Yang C, Huang R, Wen Y, Zhang C, et al. Swainsonine Triggers Paraptosis *via* ER Stress and MAPK Signaling Pathway in Rat Primary Renal Tubular Epithelial Cells. *Front Pharmacol* (2021) 12:715285. doi: 10.3389/fphar.2021.715285
36. Wang J, Liang D, Zhang XP, He CF, Cao L, Zhang SQ, et al. Novel PI3K/Akt/mTOR Signaling Inhibitor, W922, Prevents Colorectal Cancer Growth *via* the Regulation of Autophagy. *Int J Oncol* (2021) 58:70–82. doi: 10.3892/ijo.2020.5151
37. Dan S, Yoshimi H, Okamura M, Mukai Y, Yamori T. Inhibition of PI3K by ZSTK474 Suppressed Tumor Growth Not *via* Apoptosis But G0/G1 Arrest. *Biochem Biophys Res Commun* (2009) 379:104–9. doi: 10.1016/j.bbrc.2008.12.015
38. Montalto FI, De Amicis F. Cyclin D1 in Cancer: A Molecular Connection for Cell Cycle Control, Adhesion and Invasion in Tumor and Stroma. *Cells* (2020) 9:2648. doi: 10.3390/cells9122648
39. Chen C, Chen J, Zhao K-N. Editorial (Thematic Issue: Signalling Pathways in Anti-Cancer Drug Resistance). *Curr Med Chem* (2014) 21:3007–8. doi: 10.2174/0929867321261408041604 43
40. Chen X, Xu H, Yu X, Wang X, Zhu X, Xu X. Apigenin Inhibits *In Vitro* and *In Vivo* Tumorigenesis in Cisplatin-Resistant Colon Cancer Cells by Inducing Autophagy, Programmed Cell Death and Targeting M-TOR/PI3K/Akt Signalling Pathway. *J BUON* (2019) 24:488–93.

41. Wang Y, Kuramitsu Y, Baron B, Kitagawa T, Tokuda K, Akada J, et al. PI3K Inhibitor LY294002, as Opposed to Wortmannin, Enhances AKT Phosphorylation in Gemcitabine-Resistant Pancreatic Cancer Cells. *Int J Oncol* (2017) 50:606–12. doi: 10.3892/ijo.2016.3804
42. Guo Y, Zhao Y, Zhou Y, Tang X, Li Z, Wang X. LZ-101, a Novel Derivative of Danofloxacin, Induces Mitochondrial Apoptosis by Stabilizing FOXO3a *via* Blocking Autophagy Flux in NSCLC Cells. *Cell Death Dis* (2019) 10. doi: 10.1038/s41419-019-1714-y
43. Zhang N, Hua X, Tu H, Li J, Zhang Z, Max C. Isorhapontigenin (ISO) Inhibits EMT Through FOXO3A/METTL14/VIMENTIN Pathway in Bladder Cancer Cells. *Cancer Lett* (2021) 520:400–8. doi: 10.1016/j.canlet.2021.07.041
44. Luo M, Wu C, Guo E, Peng S, Zhang L, Sun W, et al. FOXO3a Knockdown Promotes Radioresistance in Nasopharyngeal Carcinoma by Inducing Epithelial-Mesenchymal Transition and the Wnt/β-Catenin Signaling Pathway. *Cancer Lett* (2019) 455:26–35. doi: 10.1016/j.canlet.2019.04.019
45. Wang Y, Shi J, Chai K, Ying X, Zhou B. The Role of Snail in EMT and Tumorigenesis. *Curr Cancer Drug Targets* (2014) 13:963–72. doi: 10.2174/1568009613136660102
46. Cabral-Pacheco GA, Garza-Veloz I, Rosa CCD La, Ramirez-Acuña JM, Perez-Romero BA, Guerrero-Rodriguez JF, et al. The Roles of Matrix Metalloproteinases and Their Inhibitors in Human Diseases. *Int J Mol Sci* (2020) 21:9739. doi: 10.3390/ijms21249739
47. Bai Z, Gao M, Zhang H, Guan Q, Xu J, Li Y, et al. BZML, a Novel Colchicine Binding Site Inhibitor, Overcomes Multidrug Resistance in A549/Taxol Cells by Inhibiting P-Gp Function and Inducing Mitotic Catastrophe. *Cancer Lett* (2017) 402:81–92. doi: 10.1016/j.canlet.2017.05.016
48. Bai Z, Gao M, Xu X, Zhang H, Xu J, Guan Q, et al. Overcoming Resistance to Mitochondrial Apoptosis by BZML-Induced Mitotic Catastrophe is Enhanced by Inhibition of Autophagy in A549/Taxol Cells. *Cell Prolif* (2018) 51:e12450. doi: 10.1111/cpr.12450
49. Yang C, Zhang J, Ding M, Xu K, Li L, Mao L, et al. Ki67 Targeted Strategies for Cancer Therapy. *Clin Transl Oncol* (2018) 20:570–75. doi: 10.1007/s12094-017-1774-3
50. Thandra KC, Barsouk A, Saginala K, Aluru JS, Barsouk A. Epidemiology of Lung Cancer. *Wspolczesna Onkol* (2021) 25:45–52. doi: 10.5114/wo.2021.103829
51. Wu H, Chen S, Yu J, Li Y, Zhang Xy, Yang L, et al. Single-Cell Transcriptome Analyses Reveal Molecular Signals to Intrinsic and Acquired Paclitaxel Resistance in Esophageal Squamous Cancer Cells. *Cancer Lett* (2018) 420:156–67. doi: 10.1016/j.canlet.2018.01.059
52. Li YJ, Lei YH, Yao N, Wang CR, Hu N, Ye WC, et al. Autophagy and Multidrug Resistance in Cancer. *Chin J Cancer* (2017) 36:52. doi: 10.1186/s40880-017-0219-2
53. Bukowski K, Kciuk M, Kontek R. Mechanisms of Multidrug Resistance in Cancer Chemotherapy. *Int J Mol Sci* (2020) 21:3233. doi: 10.3390/ijms21093233
54. Ganesan M, Kanimozhi G, Pradhapsingh B, Khan HA, Alhomida AS, Ekhzaimy A, et al. Phytochemicals Reverse P-Glycoprotein Mediated Multidrug Resistance *via* Signal Transduction Pathways. *BioMed Pharmacother* (2021) 139:111632. doi: 10.1016/j.biopha.2021.111632
55. Liu W, Meng Q, Sun Y, Wang C, Huo X, Liu Z, et al. Targeting P-Glycoprotein: Nelfinavir Reverses Adriamycin Resistance in K562/ADR Cells. *Cell Physiol Biochem* (2018) 51:1616–31. doi: 10.1159/000495650
56. Zhang Y, Sriraman SK, Kenny HA, Luther E, Torchilin V, Lengyel E. Reversal of Chemoresistance in Ovarian Cancer by Co-Delivery of a P-Glycoprotein Inhibitor and Paclitaxel in a Liposomal Platform. *Mol Cancer Ther* (2016) 15:2282–93. doi: 10.1158/1535-7163.MCT-15-0986
57. Thoma C. Prostate Cancer: Targeting Apoptosis Resistance in CRPC. *Nat Rev Urol* (2016) 13:631. doi: 10.1038/nrurol.2016.200
58. Bolkun L, Grubczak K, Schneider G, Zembko P, Radzikowska U, Singh P, et al. Involvement of BAFF and APRIL in Resistance to Apoptosis of Acute Myeloid Leukemia. *J Cancer* (2016) 7:1979–83. doi: 10.7150/jca.15966
59. Mohammad RM, Muqbil I, Lowe L, Yedjou C, Hsu HY, Lin LT, et al. Broad Targeting of Resistance to Apoptosis in Cancer. *Semin Cancer Biol* (2015) 35: S78–S103. doi: 10.1016/j.semcancer.2015.03.001
60. Jullien M, Gomez-Bougie P, Chiron D, Touzeau C. Restoring Apoptosis With BH3 Mimetics in Mature B-Cell Malignancies. *Cells* (2020) 9:717. doi: 10.3390/cells9030717
61. Su Y, Zhang X, Sinko PJ. Exploitation of Drug-Induced Bcl-2 Overexpression for Restoring Normal Apoptosis Function: A Promising New Approach to the Treatment of Multidrug Resistant Cancer. *Cancer Lett* (2007) 253:115–23. doi: 10.1016/j.canlet.2007.01.018
62. Fontana F, Raimondi M, Marzagalli M, Di Domizio A, Limonta P. The Emerging Role of Paraptosis in Tumor Cell Biology: Perspectives for Cancer Prevention and Therapy With Natural Compounds. *Biochim Biophys Acta - Rev Cancer* (2020) 1873:188338. doi: 10.1016/j.bbcan.2020.188338
63. Sang J, Gan L, Zou MF, Lin ZJ, Fan RZ, Huang JL, et al. Jolkinolide B Sensitizes Bladder Cancer to mTOR Inhibitors *via* Dual Inhibition of Akt Signaling and Autophagy. *Cancer Lett* (2022) 526:352–62. doi: 10.1016/j.canlet.2021.11.014
64. Wang Y, Wen X, Zhang N, Wang L, Hao D, Jiang X, et al. Small-Molecule Compounds Target Paraptosis to Improve Cancer Therapy. *BioMed Pharmacother* (2019) 118:109203. doi: 10.1016/j.biopha.2019.109203
65. Li XQ, Ren J, Wang Y, Su JY, Zhu YM, Chen CG, et al. Synergistic Killing Effect of Paclitaxel and Honokiol in Non-Small Cell Lung Cancer Cells Through Paraptosis Induction. *Cell Oncol* (2021) 44:135–50. doi: 10.1007/s13402-020-00557-x
66. Wang C, Chen T. Intratumoral Injection of Taxol *In Vivo* Suppresses A549 Tumor Showing Cytoplasmic Vacuolization. *J Cell Biochem* (2012) 113:1397–406. doi: 10.1002/jcb.24012
67. Liu R, Chen Y, Liu G, Li C, Song Y, Cao Z, et al. PI3K/AKT Pathway as a Key Link Modulates the Multidrug Resistance of Cancers. *Cell Death Dis* (2020) 11:797. doi: 10.1038/s41419-020-02998-6
68. Zhang W, Cai J, Chen S, Zheng X, Hu S, Dong W, et al. Paclitaxel Resistance in MCF-7/PTX Cells is Reversed by Paeonol Through Suppression of the SET/phosphatidylinositol 3-Kinase/Akt Pathway. *Mol Med Rep* (2015) 12:1506–14. doi: 10.3892/mmr.2015.3468
69. Byun WS, Jin M, Yu J, Kim WK, Song J, Chung HJ, et al. A Novel Selenonucleoside Suppresses Tumor Growth by Targeting Skp2 Degradation in Paclitaxel-Resistant Prostate Cancer. *Biochem Pharmacol* (2018) 158:64–94. doi: 10.1016/j.bcp.2018.10.002
70. Wilson M SC, Brosens J J, Schwenen H DC, Lam E. FOXO W-F. And FOXM1 in Cancer: The FOXO-FOXM1 Axis Shapes the Outcome of Cancer Chemotherapy. *Curr Drug Targets* (2011) 12:1256–66. doi: 10.2174/138945011796150244
71. Hui RCY, Francis RE, Guest SK, Costa JR, Gomes AR, Myatt SS, et al. Doxorubicin Activates FOXO3a to Induce the Expression of Multidrug Resistance Gene ABCB1 (MDR1) in K562 Leukemic Cells. *Mol Cancer Ther* (2008) 7:670–8. doi: 10.1158/1535-7163.MCT-07-0397
72. Hong ZY, Lee HJ, Shin DY, Kim SK, Seo MR, Lee EJ. Inhibition of Akt/FOXO3a Signaling by Constitutively Active FOXO3a Suppresses Growth of Follicular Thyroid Cancer Cell Lines. *Cancer Lett* (2012) 314:34–40. doi: 10.1016/j.canlet.2011.09.010
73. Zhang LN, Li JY, Xu W. A Review of the Role of Puma, Noxa and Bim in the Tumorigenesis, Therapy and Drug Resistance of Chronic Lymphocytic Leukemia. *Cancer Gene Ther* (2013) 20:1–7. doi: 10.1038/cgt.2012.84
74. Tarrado-Castellarnau M, Cortés R, Zanuy M, Tarragó-Celada J, Polat IH, Hill R, et al. Methylseleninic Acid Promotes Antitumour Effects *via* Nuclear FOXO3a Translocation Through Akt Inhibition. *Pharmacol Res* (2015) 102:218–34. doi: 10.1016/j.phrs.2015.09.009
75. Pellegrino M, Rizza P, Nigro A, Ceraldi R, Ricci E, Perrotta I, et al. FoxO3a Mediates the Inhibitory Effects of the Antiepileptic Drug Lamotrigine on Breast Cancer Growth. *Mol Cancer Res* (2018) 16:923–34. doi: 10.1158/1541-7786.MCR-17-0662
76. Hamilton E, Infante JR. Targeting CDK4/6 in Patients With Cancer. *Cancer Treat Rev* (2016) 45:129–38. doi: 10.1016/j.ctrv.2016.03.002
77. Song Y, Lu M, Qiu H, Yin J, Luo K, Zhang Z, et al. Activation of FOXO3a Reverses 5-Fluorouracil Resistance in Human Breast Cancer Cells. *Exp Mol Pathol* (2018) 105:57–62. doi: 10.1016/j.yexmp.2018.05.013
78. Ramesh V, Brabletz T, Ceppi P. Targeting EMT in Cancer With Repurposed Metabolic Inhibitors. *Trends Cancer* (2020) 6:942–50. doi: 10.1016/j.trecan.2020.06.005
79. Sharma SV, Lee DY, Li B, Quinlan MP, Takahashi F, Maheswaran S, et al. A Chromatin-Mediated Reversible Drug-Tolerant State in Cancer Cell Subpopulations. *Cell* (2010) 141:69–80. doi: 10.1016/j.cell.2010.02.027
80. An L, Li DD, Chu HX, Zhang Q, Wang CL, Fan YH, et al. Terfenadine Combined With Epirubicin Impedes the Chemo-Resistant Human non-Small Cell Lung Cancer Both *In Vitro* and *In Vivo* Through EMT and Notch Reversal. *Pharmacol Res* (2017) 124:105–15. doi: 10.1016/j.phrs.2017.07.021

81. Liu H, Yin J, Wang H, Jiang G, Deng M, Zhang G, et al. FOXO3a Modulates WNT/β-Catenin Signaling and Suppresses Epithelial-to-Mesenchymal Transition in Prostate Cancer Cells. *Cell Signal* (2015) 27:510–8. doi: 10.1016/j.cellsig.2015.01.001
82. Deng J, Bai X, Feng X, Ni J, Beretov J, Graham P, et al. Inhibition of PI3K/Akt/mTOR Signaling Pathway Alleviates Ovarian Cancer Chemoresistance Through Reversing Epithelial-Mesenchymal Transition and Decreasing Cancer Stem Cell Marker Expression. *BMC Cancer* (2019) 19:618. doi: 10.1186/s12885-019-5824-9

**Conflict of Interest:** The authors declare that the research was conducted in the absence of any commercial or financial relationships that could be construed as a potential conflict of interest.

**Publisher's Note:** All claims expressed in this article are solely those of the authors and do not necessarily represent those of their affiliated organizations, or those of the publisher, the editors and the reviewers. Any product that may be evaluated in this article, or claim that may be made by its manufacturer, is not guaranteed or endorsed by the publisher.

# Advantages of publishing in Frontiers

**OPEN ACCESS**
Articles are free to read for greatest visibility and readership

**FAST PUBLICATION**
Around 90 days from submission to decision

**HIGH QUALITY PEER-REVIEW**
Rigorous, collaborative, and constructive peer-review

**TRANSPARENT PEER-REVIEW**
Editors and reviewers acknowledged by name on published articles

**Frontiers**
Avenue du Tribunal-Fédéral 34
1005 Lausanne | Switzerland

**Visit us:** www.frontiersin.org
**Contact us:** frontiersin.org/about/contact

**REPRODUCIBILITY OF RESEARCH**
Support open data and methods to enhance research reproducibility

**DIGITAL PUBLISHING**
Articles designed for optimal readership across devices

**FOLLOW US**
@frontiersin

**IMPACT METRICS**
Advanced article metrics track visibility across digital media

**EXTENSIVE PROMOTION**
Marketing and promotion of impactful research

**LOOP RESEARCH NETWORK**
Our network increases your article's readership